

Risk assessment with regard to the
occurrence of malaria in Africa under
the influence of observed and
projected climate change



Inaugural - Dissertation
zur
Erlangung des Doktorgrades
der Mathematisch-Naturwissenschaftlichen Fakultät
der Universität zu Köln
vorgelegt von

Volker Ermert

aus Kirchen/Sieg

Köln 2010

Berichterstatter (Gutachter): Prof. Dr. A. H. Fink
Prof. Dr. M. Kerschgens
Dr. A. P. Morse

Tag der mündlichen Prüfung: 23. November 2009

Abstract

Malaria is one of the most serious health problems in the world. The projected climate change will probably alter the range and transmission potential of malaria in Africa. In this study, potential changes in the malaria transmission are assessed by forcing three malaria models with bias-corrected data from ensemble scenario runs of a state-of-the-art regional climate model.

The *Liverpool Malaria Model* (LMM) from the Geography Department of the University of Liverpool is utilised. The LMM simulates the spread of malaria at a daily resolution using daily mean temperature and 10-day accumulated precipitation. The simulation of some key processes has been modified in the model, in order to reflect a more physical relationship. An extensive literature survey with regard to entomological and parasitological malaria variables enables the calibration and validation of a new LMM version. Comparison of this version with the original model exhibits marked improvements. The new version demonstrates a realistic simulation of entomological variables and of the malaria season, as well as correctly reproduces the epidemic potential at fringes of endemic malaria areas. Various sensitivity experiments reveal that the LMM is fairly sensitive to values of its required parameters. Effects of climatic changes on the malaria season are additionally verified by the *MARA Seasonality Model* (MSM). The Garki model finally enables the completion of the malaria picture in terms of the immune status and the infectiousness of different population groups, as well as relative to the age-dependent prevalence structure.

In every case three ensemble runs were performed on a 0.5° grid. The LMM was driven for the present-day climate (1960-2000) by bias-corrected data from the *REgional MModel* (REMO), with a land use and land cover specified by the *Food and Agriculture Organization* (FAO). Malaria projections were carried out for 2001-2050 according to the climate scenarios A1B and B1 as well as FAO land use and land cover changes. Garki model runs were subsequently forced by the *Entomological Inoculation Rate* (EIR) from the LMM. Finally, additional results relative to the malaria season were produced by MSM.

For the present-day climate (1960-2000), the highest biting rates are simulated for Equatorial Africa. The malaria runs show a decrease in the malaria spread from Central Africa towards the Sahel. The length of the malaria season is closely related to monsoon

rainfall. The model simulations show a marked influence of mountainous areas causing a complex pattern of the spread of malaria in East Africa. The malaria infected population reveals the expected peak in children below an age of about five years. Regions of epidemic malaria occurrence, as defined by the coefficient of variation of the annual parasite prevalence maximum, are found along a band in the northern Sahel. Farther south, malaria occurs more regularly and is therefore characterised as endemic. Epidemic-prone areas are additionally identified at various highland territories, as well as in arid and semi-arid zones of the Greater Horn of Africa. No adequate immune protection of the population was found for these areas.

Largely due to land surface degradation, REMO simulates a prominent surface warming and a significant reduction in the annual rainfall amount over most of tropical Africa in either climate change scenario. Assuming no future human-imposed constraints on malaria transmission, changes in temperature and precipitation will alter the future geographic distribution of malaria. In the northern part of sub-Saharan Africa, the precipitation decline will force significant decreases of the malaria transmission in the Sahel. In addition to the withdrawal of malaria transmission along the fringe of the Sahara, the frequency of malaria occurrence will be reduced for several grid boxes of the Sahel. As a result, epidemics in these more densely populated areas will become more likely, in particular as adults lose their immunity. The level of malaria prevalence farther south will remain stable for most areas. However, the start of the malaria season will be delayed and the transmission is expected to cease earlier.

Most pronounced changes in Africa are found for East Africa. Significantly higher temperatures and slightly higher rainfall cause a substantial increase in the season length and parasite prevalence in formerly epidemic-prone areas. Territories formerly unsuitable for malaria will become suitable under the warmer future climate. The simulations indicate changes in the highland epidemic risk. At most grid boxes malaria transmission will stabilise below about 2000 m. At these altitudes the population will improve their immune status. In contrast, malaria will climb to formerly malaria-free zones above these levels enforcing the probability of malaria epidemics.

Zusammenfassung

Die Malaria stellt eine der gefährlichsten Krankheiten der Welt dar. Höchstwahrscheinlich werden sich die Ausbreitung und das Übertragungspotenzial der Malaria in Afrika unter dem Einfluss des projizierten Klimawandels verändern. Aus diesem Grund versucht die vorliegende Studie potenzielle Veränderungen in der Malariaübertragung abzuschätzen. Drei unterschiedliche Malariamodelle werden hierzu mit korrigierten Ensembleläufen eines auf dem Stand der Wissenschaft befindlichen regionalen Klimamodells betrieben.

Verwendung findet zunächst das sog. „Liverpool Malaria Model (LMM)“ vom Geographischen Department der Universität Liverpool. Das LMM simuliert die Verbreitung der Malaria auf Tagesbasis und wird lediglich durch die Tagesmitteltemperatur und die 10-tägig akkumulierte Niederschlagsmenge angetrieben. Um Vorgänge in der Natur besser widerzuspiegeln wurde im LMM die Simulation einiger wichtiger Prozesse verändert. Eine intensive Literaturrecherche in Bezug auf entomologische und parasitologische Malariavariablen ermöglicht die Kalibrierung und die Validierung einer neuen LMM Version. Der Vergleich dieser neuen Version mit dem ursprünglichen Modell offenbart deutliche Verbesserungen. Die neue Modellversion zeigt eine realistische Simulation von entomologischen Variablen, der Malariasaison und reproduziert korrekt das Epidemiepotenzial am Rande endemischer Malariagebiete. Zahlreiche Sensitivitätsstudien zeigen, dass das LMM sensitiv bzgl. unterschiedlichen Modelleinstellungen reagiert. Zusätzlich wird der Effekt der Klimaänderung auf die Malariasaison mit Hilfe des sog. „MARA Seasonality Models (MSM)“ überprüft. Durch die Berücksichtigung des Immunstatus und der Infektiösität von unterschiedlichen Bevölkerungsgruppen als auch der altersabhängigen Struktur der Malariaprävalenz durch das sog. Garki Modell wird schließlich das Malariabild vervollständigt.

Die Modelle wurden jeweils für drei Ensembleläufe auf einem 0.5° Gitter betrieben. Für das heutige Klima (1960-2000) wurde das LMM hierbei mit korrigierten Daten des REgionalen MOdells (REMO) laufen gelassen, die wiederum auf einer Landnutzung und Landoberfläche der „Food and Agriculture Organization (FAO)“ beruhen. Malariaprojektionen wurden anschließend für den Zeitraum 2001-2050 mit REMO-Daten der Klimaszenarien A1B und B1 berechnet. In diesem Fall sind die Klimaszenarien durch FAO-Szenarien der Landnutzung und Landoberflächen entstanden. Danach wurde das

Garki Modell mit Hilfe der entomologischen Inokulationsrate des LMM betrieben. Zusätzliche Ergebnisse bezüglich der Malariasaison wurden schließlich durch das MSM produziert.

Für das heutige Klima (1960-2000) werden die höchsten Stechraten für das äquatoriale Afrika simuliert. Die Malarialäufe zeigen einen Abfall in der Malariaverbreitung von Zentralafrika bis zum Sahel. Hierbei steht die Länge der Malariasaison im engen Zusammenhang mit dem Auftreten des Monsuns. Die ostafrikanischen Hochländer verursachen außerdem ein komplexes Muster in der Malariaverbreitung. Wie erwartet treten in den ersten fünf Lebensjahren die höchsten Malariaprävalenzen auf. Epidemieregionen werden durch den Variationskoeffizienten der maximalen jährlichen Malariaprävalenz definiert. Solche Gebiete sind entlang eines Streifens im nördlichen Sahel zu finden. Weiter südlich tritt die Malaria regelmäßiger auf und ist deshalb als endemisch charakterisiert. Epidemiegebiete werden ebenso für zahlreiche Hochländer sowie für aride und semi-aride Regionen des Großen Horns von Afrika identifiziert. Für diese Gebiete konnte kein angemessener Immunschutz in der Bevölkerung gefunden werden.

In den REMO-Simulationen verursacht hauptsächlich die Degradation der Landoberfläche in beiden Klimaszenarien einen deutlichen Temperaturanstieg und eine signifikante Reduzierung der Jahresniederschläge über großen Teilen tropischen Afrikas. Falls der Mensch die Malariaverbreitung in der Zukunft nicht merklich beeinflusst wird der Klimawandel die zukünftige Malariaübertragung stark verändern. Der Niederschlagsrückgang wird eine signifikante Reduzierung der Malariaübertragung im Sahel verursachen. Zusätzlich zum Rückzug der Malaria entlang der Grenze zur Sahara wird an einigen Gitterpunkten im Sahel die Häufigkeit des Malariaauftretens herabgesetzt. Diese bevölkerungsreicheren Gebiete werden somit häufiger mit Epidemien rechnen müssen, da in diesen Regionen vor allem Erwachsene ihre Immunität verlieren werden. Weiter südlich bleibt das Malarianiveau für die meisten Gebiete stabil, allerdings wird sich der Start der Malariasaison verzögern und es wird ein früheres Ende der Malariaübertragung erwartet.

In Afrika werden die stärksten Veränderungen für Ostafrika projiziert. In früheren Epidemiegebieten verursachen signifikant höhere Temperaturen und leicht erhöhte Niederschläge einen beträchtlichen Anstieg in der Länge der Saison und in der Prävalenz des Malariaparasiten. In Regionen die zuvor für die Malaria ungeeignet waren kann sich die Malaria in einem wärmeren zukünftigen Klima verbreiten. Die Simulationen offenbaren deutliche Veränderungen des Epidemierisikos der Hochländer. Für die meisten Gitterboxen stabilisiert sich unterhalb von etwa 2000 m die Malariaübertragung. In diesen Höhenbereichen wird die Bevölkerung eine bessere Immunität aufweisen. Das Risiko für Malariaepidemien steigt jedoch oberhalb dieses Niveaus, da die Malaria in diese Höhenlagen zukünftig erstmals vordringen kann.

Contents

Abstract	i
Zusammenfassung	iii
Abbreviations	xi
Symbols	xiii
1 Introduction	1
2 State of research, objectives, and overview	5
2.1 The Climate of Africa	5
2.1.1 The climate of West Africa	6
2.1.2 The climate of the Greater Horn of Africa	7
2.1.3 Interannual variability of precipitation	10
2.2 IPCC SRES scenarios	14
2.3 Climate change projections	16
2.3.1 Global climate projections	16
2.3.2 Regional climate projections for Africa	17
2.4 Malaria biology	21
2.4.1 The parasite cycle	21
2.4.2 Immunity	23
2.4.3 Superinfection	25
2.4.4 Parasite clearance	25
2.4.5 Detectability of malaria parasites	25
2.4.6 Heterogeneous biting	26
2.5 Distribution of malaria transmission	26
2.6 Malaria factors	28

2.6.1	Climatic factors	28
2.6.2	Other factors	30
2.7	Malaria modelling	32
2.7.1	Classic malaria models and successors	32
2.7.2	Malaria models related to environmental variables	33
2.7.3	Climate- and weather-driven malaria models	35
2.8	Changes in malaria occurrence	37
2.8.1	Observed malaria changes	37
2.8.2	Projected malaria changes	38
2.9	Objectives and Overview	41
3	Data	45
3.1	DMN precipitation data	45
3.2	Synoptic station data	45
3.3	GSOD	47
3.4	CLImatological NOrmals (CLINO)	47
3.5	GHCN	48
3.6	The ‘Institut de Recherche pour le Développement’ data set (IRD)	49
3.7	PREC/L	50
3.8	The Climatic Research Unit data set (CRU)	51
3.9	The ECMWF 40-year ReAnalysis data set (ERA40)	52
3.10	Present-day runs and climate projections from REMO	53
3.10.1	REMO simulations	53
3.10.2	Land use and land cover changes	54
3.11	Entomological and parasitological data	55
3.12	Data overview	56
4	Validation of meteorological model data	57
4.1	REMO precipitation versus IRD	57
4.1.1	Monthly and annual rainfall	57
4.1.2	Frequency distribution of 10-day accumulated precipitation	60
4.2	REMO precipitation versus CRU	62
4.3	ERA40 temperatures vs. station data	64
4.4	REMO temperatures vs. station data	66
4.5	REMO temperatures vs. ERA40	67
5	Malaria modelling	69

5.1	Liverpool Malaria Model (LMM)	69
5.1.1	Gonotrophic cycle	70
5.1.2	Egg deposition	73
5.1.3	Mosquito Mature Age (<i>MMA</i>)	76
5.1.4	Survival of immature mosquitoes	76
5.1.5	Survival probability of adult mosquitoes (p_d)	78
5.1.6	Dry season survival of the mosquito population	82
5.1.7	Sporogonic cycle	83
5.1.8	Human blood index (a)	84
5.1.9	Mosquito-to-human transmission efficiency (b)	85
5.1.10	Human Infectious Age (<i>HIA</i>)	86
5.1.11	Recovery rate (r)	87
5.1.12	Gametocyte prevalence (sPR)	88
5.1.13	Human-to-mosquito transmission efficiency (c)	89
5.1.14	Issues regarding the age-dependence of malaria	89
5.2	Garki model	90
5.3	MARA Seasonality Model (MSM)	95
6	Calibration, validation, and sensitivity tests of the LMM	97
6.1	LMM calibration and validation	97
6.1.1	Calibration of the LMM	98
6.1.2	Validation of the final LMM _n setting	103
6.2	LMM sensitivity tests	105
6.3	LMM _n versus LMM _o	112
7	Malaria simulations for the present-day and future climate	117
7.1	REMO climate projections for Africa	117
7.2	Present-day malaria distribution	119
7.2.1	LMM _n runs based on IRD/ERA40 (1968-1990)	119
7.2.2	Evaluation of LMM _n runs based on REMO (1960-2000)	122
7.2.3	Garki model simulations based on LMM _n runs (1960-2000)	131
7.2.4	Malaria seasonality from the MSM (1960-2000)	134
7.3	Malaria projections for 2001-2050	137
7.3.1	LMM _n projections based on REMO	137
7.3.2	Garki model projections based on LMM _n	146
7.3.3	MSM projection of the malaria seasonality	151
7.3.4	A1B versus B1	152

8	Summary, discussion, and future prospects	153
8.1	Summary	153
8.2	Discussion and future prospects	155
8.2.1	Calibration and sensitivity of the LMM _n	156
8.2.2	Performance of the malaria models	157
8.2.3	Uncertainty of the applied climate projections	159
8.2.4	Evaluation of the malaria projections	160
8.2.5	Neglected factors and future extensions of the LMM	162
8.2.6	Final remarks	164
	Appendices	I
C	Data processing	I
C.1	Configuration of GSOD time series	I
C.2	Generation of time series at synoptic stations	III
C.3	Bias-correction of REMO precipitation	IV
C.4	Bias-correction of REMO temperatures	VI
C.5	The ensemble mean	VI
C.6	The 360-day year	VII
C.7	Grid transformation	VII
C.8	The Wilcoxon-Mann-Whitney rank-sum test	VIII
D	Entomological and parasitological malaria variables	XI
D.1	Human biting ratio (<i>HBR</i>)	XII
D.2	Circumsporozoite protein rate (<i>CSPR</i>)	XII
D.3	Entomological inoculation rate (<i>EIR</i>)	XII
D.4	Asexual parasite ratio (<i>PR</i>)	XIII
D.5	Malaria seasonality	XIII
D.6	Data table convention	XV
D.7	Entomological and parasitological data	XVII
D.8	Parasitological data assigned to synoptic stations	XXVIII
D.9	Entomological data assigned to synoptic stations	XXIX
D.10	Duration of the gonotrophic cycle (n_g)	XXX
D.11	Produced eggs per female mosquito ($\#E_p$)	XXXI
D.12	Development of immature mosquitoes	XXXII
D.13	Daily survival probability of adult mosquitoes (p_d)	XXXIV
D.14	Sexual Parasite Ratio (<i>sPR</i>)	XXXVII
D.15	Human-to-mosquito transmission efficiency (<i>c</i>)	XLI

D.16	Mosquito-to-human transmission efficiency (b)	XLII
D.17	Human Blood Index (a)	XLIII
D.18	Human Infectious Age (HIA)	XLIV
E	LMM validation and settings	XLV
E.1	Definition of the validation	XLV
E.2	Figures and tables with regard to the LMM calibration	XLVII
E.3	Figures in terms of the LMM _n validation	LII
E.4	Figures in terms of the LMM ₀ validation	LIV
E.5	Spin-up period of the LMM	LVII
F	Supplementary figures	LVIII
F.1	Data from CRU	LVIII
F.2	Standardised rainfall anomalies	LVIII
F.3	Monthly REMO temperature and precipitation data	LIX
F.4	Present-day malaria seasonality	LXVII
F.5	Malaria projections	LXIX
G	Geographical information	LXXXVII
Glossary		LXXXIX
References		XCVII
Acknowledgements		CXI
Erklärung		CXIII
Lebenslauf		CXV

Abbreviations

<i>p_d</i>	daily survival probability of female mosquitoes [%]
<i>An.</i>	<i>Anopheles</i>
<i>P.</i>	<i>Plasmodium</i>
AEJ	African Easterly Jet
AEW	African Easterly Wave
AOGCM	Atmospheric Ocean General Circulation Model
CH ₄	methane
CLIMAT	monthly CLIMATological data, i.e. the WMO format 71
CLIMEX	CLIMatic indEX
CLINO	CLIMatological NOrmals for the period 1961-1990
CO ₂	carbon dioxide
CRU	Climatic Research Unit
DDT	Dichlor-Diphenyl-Trichloroethane
DMN	National Weather Service (French: ‘Direction de la Météorologie Nationale’)
DWD	German Weather Service (German: „Deutscher WetterDienst“)
ECHAM4	European Centre HAmбург Model, 4th generation
ECHAM5/MPI-OM	European Centre HAmбург Model, 5th generation/Max-Planck-Institute-Ocean Model
ECMWF	European Centre for Medium-Range Weather Forecasts
EEA	Equatorial East Africa
ERA40	ECMWF 40-year ReAnalysis
FAO	Food and Agriculture Organization
GCM	General Circulation Model
GFDL-CM2.0	Geophysical Fluid Dynamics Laboratory Climate Model, version 2.0
GHCN	Global Historical Climatology Network version 2
GHG	GreenHouse Gas
GSOD	Federal climate complex Global Surface Summary of Day version 7

IMPETUS	Integrated Approach to the Efficient Management of Scarce Water Resources in West Africa, German: „Integratives Management Projekt für Einen Tragfähigen Umgang mit Süßwasser“
IOD	Indian Ocean Dipole
IPCC	Intergovernmental Panel on Climate Change
IPCC-AR4	Fourth Assessment Report of the IPCC
IRD	‘Institut de Recherche pour le Développement’
ITCZ	InterTropical Convergence Zone
ITF	InterTropical Front
LMM	Liverpool Malaria Model
LMM _n	new Liverpool Malaria Model (see Sec. 5.1)
LMM _o	original Liverpool Malaria Model (Hoshen and Morse 2004)
LUC	Land Use and land Cover
MARA	mapping MAlaria Risk in Africa
MDM	MARA Distribution Model
MIASMA	Modelling framework for the health Impact ASsessment of Man-induced Atmospheric changes
MIROC3.2 medres	Model for Interdisciplinary Research on Climate, medium-resolution version 3.2
MOZ	Malaria potential Occurrence Zone
MRI	Meteorological Research Institute
MRR	Mark-Release Recapture
MSM	MARA Seasonality Model
N ₂ O	nitrous oxide
NDVI	Normalised Difference Vegetation Index
NeA	Northeast Africa
PCR	Polymerase Chain Reaction
PREC/L	Precipitation REConstruction over Land
QT-NASBA	QuanTitative-Nucleic Acid Sequence-Based Amplification
RCM	Regional Climate Model
REMO	REgional MOdel
REMO(cor)	bias-corrected REMO data
REMO(raw)	raw (uncorrected) REMO data
RT-PCR	Reverse Transcriptase-Polymerase Chain Reaction
SO _x	sulphur oxides
SRES	Special Report on Emission Scenarios
SST	Sea-Surface Temperature
SYNOP	surface SYNOptic observation, i.e. the WMO format 12
TEJ	Tropical Easterly Jet
VC	Vectorial Capacity
WHO	World Health Organization
WMO	World Meteorological Organization

Symbols

$\#E_o$	number of oviposited eggs per female mosquito [eggs]
$\#E_p$	number of produced eggs per female mosquito [eggs]
$\#RR_{\geq 1,m}$	monthly number of days with at least 1 mm precipitation
Δx	difference with regard to variable x between different periods or scenarios
$\eta_{d,-RR}$	rainfall independent daily survival probability of immature mosquitoes [%]
η_d	daily survival probabilities of immature mosquitoes (field conditions) [%]
$\sigma(x)$	standard deviation in terms of variable x
θ	potential temperature [$^{\circ}\text{C}$]
θ_{850}	potential temperature at 850 hPa [$^{\circ}\text{C}$]
a	Human Blood Index [%]
b	mosquito-to-human transmission efficiency [%]
c	human-to-mosquito transmission efficiency [%]
$c_{a \rightarrow c}$	adult-to-child conversion rate
$c_v(x)$	coefficient of variation in terms of variable x
CAP	CAP on the number of fertile mosquitoes
$CSPR$	CircumSporozoite Protein Rate [%]
$CSPR_a$	annual mean circumsporozoite protein rate [%]
D_{gH}	degree days of the gonotrophic cycle (humid conditions) [$^{\circ}\text{days}$]
D_{gL}	degree days of the gonotrophic cycle (dry conditions) [$^{\circ}\text{days}$]
D_s	degree days of the sporogonic cycle [$^{\circ}\text{days}$]
E_{2Seas}	End month of the second malaria Season
EIR	Entomological Inoculation Rate, i.e. the number of infectious mosquito bites per human per time [infective bites time^{-1}]
EIR_a	annual Entomological Inoculation Rate [infective bites year^{-1}]
EIR_m	monthly Entomological Inoculation Rate [infective bites month^{-1}]
$EIRc$	Entomological Inoculation Rate for children between 2-10 years [infective bites time^{-1}]
$ESeas$	End month of the malaria Season

f	fuzzy suitability (fuzzy distribution model)
GF	Gametocyte Fraction
HBR	Human Biting Rate, i.e. the number of mosquito bites per human and per time period [bites time ⁻¹]
HBR_a	annual Human Biting Rate [bites year ⁻¹]
HBR_c	Human Biting Rate for children between 2-10 years [bites time ⁻¹]
HIA	Human Infectious Age [days]
I	proportion of immune individuals
I_a	annual mean proportion of immune individuals
MMA	Mosquito Mature Age [days]
$MSeas$	length of the Main malaria Season, i.e. the number of months in which 75% of EIR_a is recorded
$n_{\sigma\varphi}$	duration of gametocytogenesis [days]
n_f	number of female mosquitoes
n_g	duration of the gonotrophic cycle [days]
n_m	duration of gametocyte maturation
n_p	duration of the prepatent period [days]
n_s	duration of the sporogonic cycle [days]
pd_{\downarrow}	shift off relative to the dry season mosquito survival probability [%]
PR	asexual Parasite Ratio [%]
PR_{2-10}	annual mean asexual parasite ratio of children aged 2-10 years [%]
PR_a	annual mean asexual parasite ratio [%]
$PR_{max,a}$	annual maximum of the asexual parasite ratio [%]
$PR_{min,a}$	annual minimum of the asexual parasite ratio [%]
R	daily larval development Rate [day ⁻¹]
r	daily human recovery rate [day ⁻¹]
R_0	basic Reproduction rate
RR_{-}	10-day accumulated rainfall threshold [mm]
RR_{3m}	three-month moving averaged monthly precipitation (two preceding and the actual month are used) [mm]
RR_{\bullet}	rainfall laying multiplier
$RR_{\Sigma 10d}$	10-day accumulated precipitation, i.e. the decadal precipitation amount [mm]
RR_a	annual precipitation amount [mm]
RR_c	catalyst month of precipitation
RR_m	monthly precipitation amount [mm]
S	most suitable rainfall condition in terms of egg deposition and survival of immature mosquitoes (fuzzy distribution model) [mm]
S_2Seas	Start month of the second malaria Season
SAR	Ratio between the Sexual and Asexual parasite prevalence, i.e. the proportion of gametocytaemic parasite positive humans [%]

SAR_a	annual mean ratio between the sexual and asexual parasite prevalence [%]
$SC(x)$	skill score with regard to variable x
$Seas$	length of the malaria Season, i.e. the number of months suitable for malaria transmission
sPR	sexual parasite ratio, i.e. the gametocyte prevalence, which is the percentage of humans with gametocytes in their blood [%]
sPR_a	annual mean sexual parasite ratio [%]
$SSeas$	Start month of the malaria Season
T	daily mean temperature [$^{\circ}\text{C}$]
T_{3m}	three-month moving average temperature (two preceding and the actual month are included)[$^{\circ}\text{C}$]
T_a	annual mean temperature [$^{\circ}\text{C}$]
T_{gH}	temperature threshold of the gonotrophic cycle (humid conditions) [$^{\circ}\text{C}$]
T_{gL}	temperature threshold of the gonotrophic cycle (dry conditions) [$^{\circ}\text{C}$]
$T_{min,m}$	monthly minimum temperature [$^{\circ}\text{C}$]
T_m	monthly mean temperature [$^{\circ}\text{C}$]
T_s	sporogonic temperature threshold [$^{\circ}\text{C}$]
T_w	water temperature [$^{\circ}\text{C}$]
tr_{im}	trickle of the number of added infectious mosquitoes [infectious females (ten days) $^{-1}$]
U_1	lower threshold of unsuitable rainfall conditions for egg deposition and survival of immature mosquitoes (fuzzy distribution model) [mm]
U_2	upper threshold of unsuitable rainfall conditions for egg deposition and survival of immature mosquitoes (fuzzy distribution model) [mm]
X_2Seas	second identified month of maximum transmission (only available for a timeframe)
$XSeas$	month of maXimum transmission, i.e. the month with the largest <i>EIR</i> value
y	proportion of malaria positive individuals, i.e. the ‘true’ parasite prevalence
$y_{1,a}$	annual mean proportion of malaria positive, infectious, non-immune individuals
y_1	proportion of malaria positive, infectious, non-immune individuals
y_a	annual mean proportion of malaria positive individuals
$y_{max,a}$	annual maximum proportion of malaria positive individuals
z	altitude [m]

1 Introduction

The climate system of the Earth strongly affects human life and has a wide range of health impacts. Humans strongly affect the climate by *GreenHouse Gas* (GHG) emissions leading to anthropogenic global warming. It is well known that a warm and humid climate triggers several water-associated diseases such as malaria (e.g., Githeko et al. 2000). *Vector*-borne diseases are highly sensitive to global warming and associated changes in precipitation (Martens et al. 1997). Malaria is particularly strongly influenced by warm and moist tropical atmospheric conditions (e.g., Patz et al. 1998). Temperatures in Africa lie above the threshold for parasite development and rainy seasons lead to a rapid increase of the *mosquito* population (e.g., Hay et al. 2000a). The *International Panel on Climate Change* (IPCC) expects that *climate change* will have a mixed effect on the spread of malaria (Confalonieri et al. 2007). Like in the Sahel the geographical range will probably contract, elsewhere like in highlands it will expand, and the transmission season might be significantly altered. Populations at margins of current distribution are estimated to be particularly vulnerable to changes (Confalonieri et al. 2007).

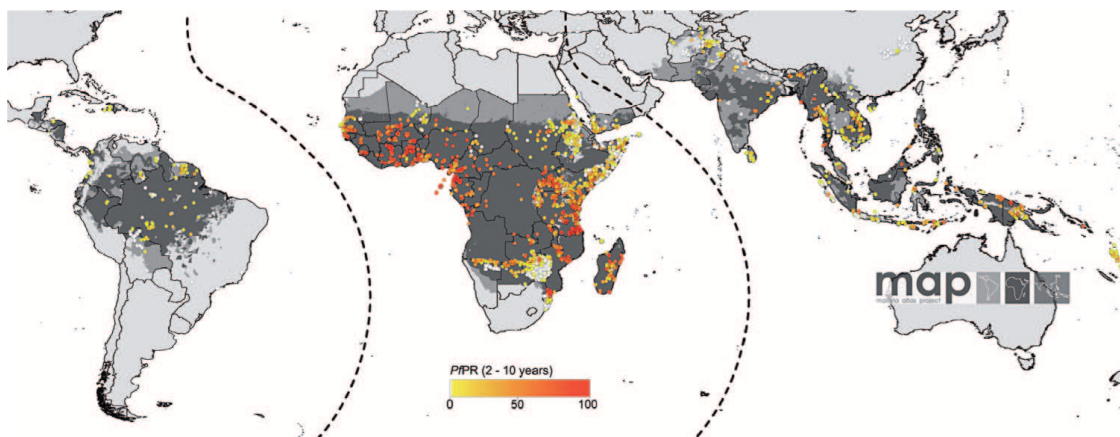


Fig. 1.1: Spatial limits of *P. falciparum* malaria risk. Areas are defined as stable (dark grey areas), unstable (medium grey areas), or malaria-free (light grey). Single dots display standardised community surveys of *P. falciparum* prevalence in children aged 2-10 years between January 1985 and July 2008 (for further information cf. Hay et al. 2009).

Malaria (Italian: ‘mal’=bad, ‘aria’=air) is caused by a parasitic *protozoa* of genus *Plasmodium* (*P.*) and is one of the world’s most serious health problems (e.g., De Sav-

igny and Binka 2004). The *World Health Organization* (WHO) estimated that about two billion people, that is more than 40% of the total world population, are exposed to this mosquito-borne disease (WHO 1997; cp. Fig. 1.1). Estimates revealed that malaria causes about 273 million clinical cases and 1.12 million deaths annually. At least 90% of worldwide malaria deaths occur in sub-Saharan Africa (Greenwood and Mutabingwa 2002; Greenwood et al. 2005). This life-threatening disease is mostly restricted to young children as immunity to severe malaria is later developed (Gupta et al. 1999; Snow et al. 1999a). Pregnant women are especially prone to malaria causing an increased risk of infant low birth weight and infant *mortality* (Menendez 1999; Steketee and Mutabingwa 1999; D'Alessandro 1999).

Anopheles (*An.*) is a genus of mosquito from the family Culicidae comprising several hundred recognised species. Female *Anopheles* require proteins for their egg production. Some of these species prefer to blood-feed on humans (*anthropophily*), while others preferentially feed on animals (*zoophily*). A few tens of *Anopheles* species are commonly malaria vectors and transmission takes place when either the mosquito female or the human *host* is carrying malaria agents. Primarily responsible for malaria in Africa is the clinically meaningful and most dangerous pathogen *P. falciparum* (e.g., Snow et al. 1997).

Most important malaria vectors in sub-Saharan Africa are found in the *An. gambiae* complex, also termed *An. gambiae sensu lato* (*s.l.*). Distribution of these vectors like that of *An. gambiae sensu stricto* (*s.s.*) and *An. arabiensis* is strongly governed by atmospheric conditions (Lindsay and Birley 1996; Lindsay et al. 1998). *An. arabiensis*, for example, was predominantly found in dry areas such as the Sahel, whereas *An. gambiae sensu stricto* (*s.s.*) tends to favour more humid environments such as in the tropical rainforest zone.

Malaria is a severe human disease with a striking positive correlation to poverty. *Endemic* malaria countries have lower rates of economic growth than non-malaria countries (Nabarro and Tayle 1998; Sachs and Malaney 2002; Greenwood et al. 2005). Malaria impedes development, is related to lack of work, and forces income loss. People suffering from malaria often struggle to earn their living. Secondary damage, in addition, may have profound effects on quality of life and functioning of the person concerned.

Likewise, non-climatic factors serve as drivers of increased malaria transmission across the African continent (Small et al. 2003). The increase in highland malaria in the 20th century is in certain parts attributed to a rise in antimalarial drug resistance, to breakdowns in health service provision and vector control operations, as well as land use changes (Shanks et al. 2000). Especially in the Sahelian and Sudanian zone, man-made alterations of the landscape have caused changes in transmission of malaria. Agriculture is supposed to ameliorate human nutrition by the growing cultivation of rice via large-scale irrigation. In arid and semi-arid areas, rice production has more than doubled during the last three decades (Sissoko et al. 2004) and markedly modified the seasonality and the transmission intensity of malaria (Dolo et al. 2004).

In middle of the 20th century, elimination of malaria was considered an achievable goal. Development of highly effective, residual insecticide *Dichloro-Diphenyl-Trichloroethane* (DDT) initiated a global eradication programme initially succeeding in many Asian countries (Greenwood and Mutabingwa 2002). The aspiration of global eradication was abandoned in 1969. The main reason for failure were technical challenges of executing the strategy especially in Africa (Tanner and de Savigny 2008). At present, eradication of malaria still remains elusive due to various reasons. There is, for instance, lack of adequate funding of control measures and the establishment of broad-based health systems. Insecticide resistance and development of resistance of *P. falciparum* to cheap and effective drugs (Greenwood and Mutabingwa 2002) finally led to an increase in malaria mortality and *morbidity* at the end of the 20th century (Nabarro and Tayle 1998; Hay et al. 2002b). However, eradication of malaria transmission is back on the global health agenda (Tanner and de Savigny 2008).

Malaria is an extremely climate-sensitive tropical disease and hence climate exerts a strong impact upon the distribution of the malaria transmission in space and time. Assessment of the potential change in malaria risk caused by present and projected anthropogenic global warming is one of the most important topics in the field of climate change and health (Patz et al. 2005). For this reason, the present study considers the malaria risk of the African population for the next few decades. The information provided here might serve as an important contribution for strategic planning of malaria control in the future (cp. Thomas et al. 2004).

2 State of research, objectives, and overview

2.1 The Climate of Africa

The climate of most parts of the African continent is tropical or subtropical, with the central phenomenon being the seasonal migration of the tropical rain belts. The northern and southern boundaries of the continent are affected by winter rainfall regimes which are governed by the passage of mid-latitude fronts.

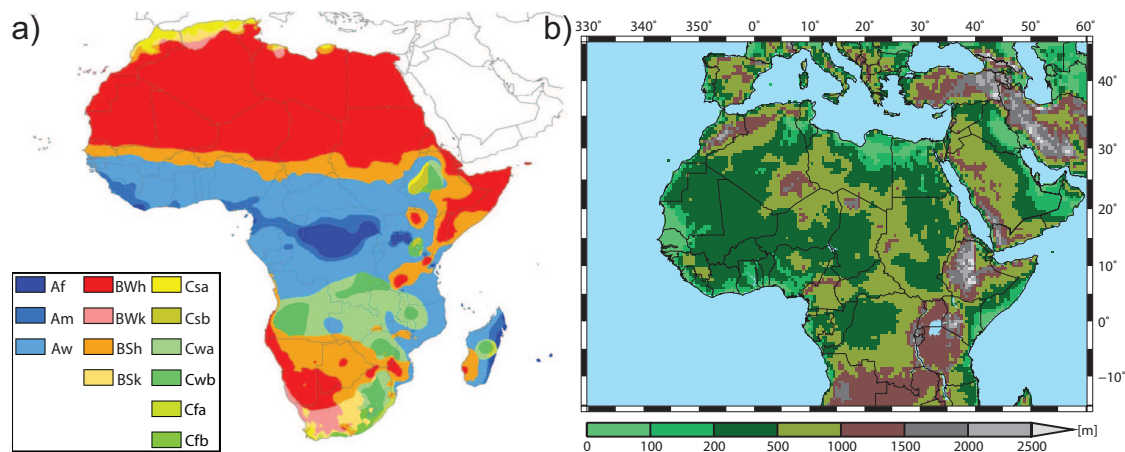


Fig. 2.1: (a) Köppen climate classification of Africa (Peel et al. 2007, their Fig. 4). A: tropical, B: arid, C: temperate climate; f: rainforest, m: monsoon, w: savannah; W: desert, S: steppe; h: hot, k: cold; s: dry summer, w: dry winter, f: without dry season; a: hot summer, b: warm summer. (b) Orography of Africa as used by REMO (cp. Paeth et al. 2009) including national boundaries and major lakes.

According to the Köppen climate classification, Africa is dominated by three main climate types, namely an arid, a tropical, and a temperate climate (Peel et al. 2007). Due to the subtropical high pressure belts in the Northern and Southern Hemisphere more than half of the continent (i.e. in the area and vicinity of the Sahara and Namib Deserts), is characterised by arid conditions (see Fig. 2.1a). In contrast, the central part of Africa exhibits a semi-humid or humid tropical climate. A temperate climate is partially found in southern Africa and to some extent in the Ethiopian Highlands. Parts of the north of Africa have a Mediterranean climate.

Individual rainfall-producing weather systems account for the variability in the climatological precipitation amount in tropical Africa (e.g., Le Barbé and Lebel 1997; Shinoda et al. 1999; Le Barbé et al. 2002). During the rainy season there is a high frequency of rainfall events due to the short duration of the water vapour discharge-loading cycle (e.g., Peters and Tetzlaff 1988). Several types of precipitation systems were found to cause rainfall over tropical Africa (cf. Fink et al. 2006 and references therein). These comprise, for example, organised mesoscale convective systems, monsoon rains, and local showers or instability storms.

Due to the close relation of malaria with climate and weather conditions (cp. Sec. 2.6.1) the following sections provide further information on the climate of West Africa and the Greater Horn of Africa (see Fig. G.3).

2.1.1 The climate of West Africa

The climate of West Africa transitions between an equatorial tropical climate in the south and a warm desert climate in the north. During boreal summer the climate is largely controlled by the West African monsoon circulation, which produces the bulk of annual precipitation. During boreal winter the dry season is characterised by dry and dusty northeasterly Harmattan winds that originate from the Sahara Desert (e.g., Buckle 1996).

The climate of West Africa is affected by both cool and humid monsoon air masses as well as hot and dry Saharan air masses. The *InterTropical Front* (ITF), also termed monsoon trough in the literature, defines the border between these two air masses (e.g., Hamilton and Archbold 1945; see Fig. 2.2). In contrast, the *InterTropical Convergence Zone* (ITCZ) is defined by the maximum water vapour convergence in a tropospheric column (Fink 2006). The ITCZ is generally located between 6° and 10° latitude south of the ITF and is associated with strong precipitation amounts (e.g., Ermert and Brücher 2008).

Due to the wedge-shaped penetration of the monsoon air under the Saharan air mass, the atmospheric layering becomes baroclinic (e.g., Fig. 3 in Pytharoulis and Thorncroft 1999). The result of this temperature contrast is a westward thermal wind, the so-called *African Easterly Jet* (AEJ), that maximises at a height of about 650 hPa where the north-south temperature gradient reverses (e.g., Burpee 1972, his Fig. 2). The AEJ maximum is located between about 10-15°N (e.g., Parker et al. 2005) at the time of the northernmost position of the ITF at about 20°N during August (e.g., Flohn 1965).

The baroclinic and barotropic instability of the AEJ is leading to westward-propagating low-level *African Easterly Waves* (AEWs; e.g., Thorncroft and Hoskins 1994), which are the dominant synoptic-scale features of the West African monsoon during boreal summer (e.g., Carlson 1969b,a). There is an interaction of AEWs with rainfall bearing systems (e.g., Reed et al. 1977; Payne and McGarry 1977). AEWs primarily trigger cloud clusters ahead of an AEW trough and west of the Greenwich meridian (Fink and Reiner 2003).

The atmospheric conditions above West Africa are continuously changing throughout the year. Between November and March during the dry season, the Sahelian and Sudanian zone are located north of the ITF (Fig. 2.2). The northeasterly trade winds, known as the Harmattan, prevail. The Harmattan blows across the Sahara Desert and is therefore dry and dusty (e.g., Hamilton and Archbold 1945). During the first part of the dry season between November and January, the Harmattan airflow is cool, causing the cool dry season. From February to May the Harmattan air mass is increasingly heated due to the higher sun angles, a longer length of day, and the dominance of sensible heat fluxes in the heat budget of the near surface layer. During this hot dry season the highest annual temperatures are observed, with maximum temperatures well above 40°C. Strong daytime insolation as well as clear and dry nights lead to a large mean daily temperature range.

During boreal spring the increasing solar radiation over the Sahel and Sahara regions causes a strengthening and northward progression of the continental heat low (cp. Pedgley 1972). In its wake, the relatively cool, moist, and convectively unstable monsoon air penetrates farther into the continent (cp. Thorncroft et al. 2003; their Fig. 6). During the pre-onset of the monsoon the depth of the monsoon layer increases and short-term northward excursions of the ITCZ cause first substantial rainfalls along the Guinean coast. Farther north in the Sudanian zone the start of the rainy season is delayed until May or June (cp. Le Barbé et al. 2002). At the end of June, during the main onset of the monsoon system, the ITCZ abruptly jumps from 5°N to approximately 10°N, resulting in abundant rainfall and cloudier conditions in the Sahel (cp. Sultan et al. 2003; Sultan and Janicot 2003). During this time, the coast is affected by the ‘little dry season’, which is directly related to coastal upwelling, a colder *Sea-Surface Temperature* (SST), and the resulting drop of rainfall (Vollmert et al. 2003). The swift retreat of the monsoon system and the ITCZ toward the equator from September to November causes a second and less intense rainy season in the south (cp. Omotosho 1985). By the end of November, the ITCZ is situated far from the coast and the dry season is again set in place over West Africa (e.g., Le Barbé et al. 2002).

2.1.2 The climate of the Greater Horn of Africa

The dynamics and variability of the climate of the Greater Horn of Africa are quite complex. The large-scale circulation is superimposed upon regional factors associated with lakes, orography, and maritime influences (see Fig. 2.1b). Various spatial and temporal processes determine the geographical distribution of diverse climatic zones. Climate ranges from desert to tropical rain forest with a transition over relative small distances (cp. Fig. 2.1a). Areas with a uni-, bi-, or trimodal annual rainfall are located within distances of markedly less than 100 km (e.g., Davies et al. 1985, their Figs. 3 & 4). Despite this diversity, large parts of East Africa, such as the equatorial zone, experience a fairly similar interannual variability of precipitation, primarily linked to large-scale atmospheric and oceanic changes (e.g., Nicholson 1996; see Sec. 2.1.3). Due to the great

latitudinal extension of the Greater Horn of Africa, the following analysis will separate between climate conditions of *Equatorial East Africa* (EEA; southern Ethiopia, Kenya, western Somalia, Uganda, Rwanda, Burundi, and Tanzania) and *Northeast Africa* (NeA; eastern Sudan, Eritrea, Ethiopia, and Djibouti; see Figs. G.1 & G.3).

The climate of the Greater Horn of Africa is predominantly affected by three main air streams and three convergence zones (see Fig. 2.2). During high and low sun seasons this area is affected by a southeastern and northeastern monsoon flow, respectively. These airflows are representing in part the western edge of the Asian monsoon, are parallel to the coast, and are strongly meridional. They do not represent a classical monsoon which moves moist air on- and dry air offshore (Buckle 1996). By contrast to the West African monsoon, both the southeasterly and the northeasterly monsoon flow are associated with relatively dry conditions. The third stream represents a west, southwesterly flow that transports humid, convergent, and thermally unstable Congo air and is associated with rainfall. The air streams are separated by the monsoon trough and the Congo Air Boundary. A third convergence zone in the middle troposphere borders the dry and stable northerly air from the Sahara and the more humid southerly air mass (Nicholson 1996).

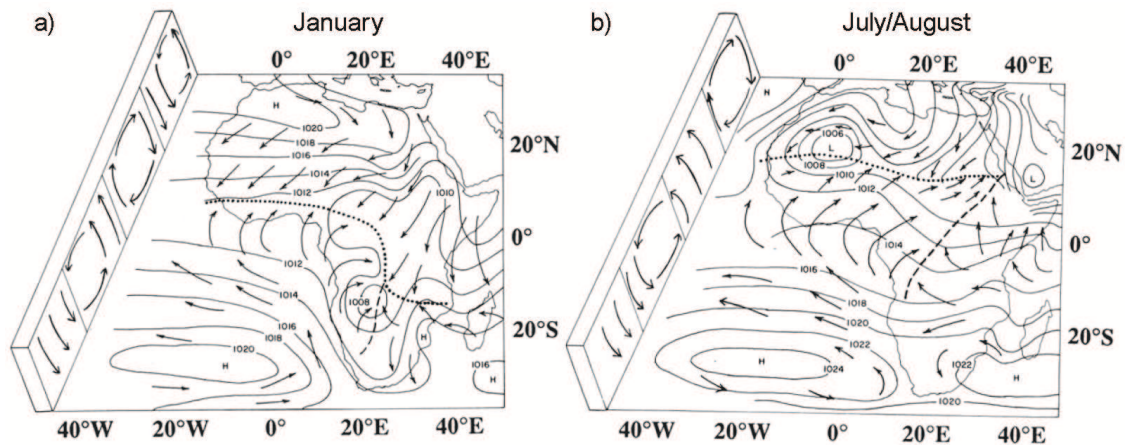


Fig. 2.2: Schematic pattern of general winds (arrows), pressure systems (solid lines), convergence zones (dashed lines), as well as the monsoon trough (dotted lines) for (a) the January and (b) the July/August circulation over Africa (after Nicholson 1996).

EEA is affected by two distinct equinoctial rainy seasons. Main rain-bearing systems commonly occur during transition seasons, when the meridional flow is interrupted between March and May as well as between October and December (see Gatebe et al. 1999, their Tab. 1). Semiannual precipitation is therefore basically related to the migration of the ITCZ (e.g., Behera et al. 2005) corresponding to the movement of the belt of maximum solar insolation (Marchant et al. 2006). During these periods the flow is often onshore and is forced to ascend by topography and coastal friction (Nicholson 1996). Maximum rainfall generally lags the position of the overhead sun by approximately one month (Black et al. 2003). Double peaks in rainfall are usually termed long and short rains (e.g., Hastenrath et al. 1993). Between March and May the northward passage of the ITCZ causes the more abundant long rains. During boreal summer the

persistent southerly monsoonal flow leads to active coastal upwelling that produces cold SSTs along the eastern coast of the Greater Horn of Africa (see Behera et al. 2005, their Fig. 1). This fact as well as the swift retreat of the monsoon system in boreal autumn (see Leroux 1983) explains the shorter duration of heavy rainfall and lower intensity of the short rains in October and November. Although, most precipitation is associated with the long rains, the short rains experience a larger degree of interannual variability (Hastenrath et al. 1993). An accurate prediction of the strength of short rains is therefore of considerable importance for agriculture and *epidemic* diseases like malaria (Clark et al. 2003). Outside of the transition seasons, rainfall is mostly linked to the humid Congo air mass and occurs especially over the Western Rift Valley (Fig. G.1)¹. A third rainfall season is limited to parts of western Kenya and Uganda, is most pronounced in July-August and contributes significantly to annual precipitation (Davies et al. 1985).

NeA is also affected by the migration of the monsoon system causing uni- and bimodal rainfall patterns. During the dry season from October to December/January (locally known as the *Bega*), rainfall is restricted to tropical-extratropical interactions and to occasional developments of the Red Sea Convergence Zone at the coastal plains and eastern escarpment of Eritrea (Seleshi and Zanke 2004). Between February and April converging northeast and southeast winds produce a brief period of rainfall, known as the *Belg* rains (e.g., Diro et al. 2009). During this time, precipitation falls in southern, central, and eastern parts of Ethiopia. In May, rainfall decreases due to the strengthening of the Egyptian High (Conway 2000). The bulk of precipitation (65-95% of total annual rainfall) in NeA falls in the so-called *Kiremt* season between June and September, when the ITCZ moves over the area (Segele and Lamb 2005; see Fig. 2.2). The southwesterly air stream transports moisture from the Atlantic and Indian Ocean into the region (e.g., Diro et al. 2009). The mean airflow as well as orographic lifting produce abundant precipitation in the western parts of the Ethiopian Highlands (Segele and Lamb 2005, their Fig. 1). Precipitation decreases to the north toward Eritrea to about 600 mm of rain in June-August mainly due to weaker upper level forcings (Segele et al. 2008). In general, *Kiremt* rainfall is influenced by the Arabian and Sudan thermal lows, which determine the position of the ITCZ, as well as upper level features such as the AEJ and TEJ. Moreover, the strength of Sankt Helena and Mascarene Highs as well as the low-level Somali jet are affecting the southwesterly flow (Seleshi and Zanke 2004; Diro et al. 2009).

Some local effects play a role in the distribution of rainfall and temperature in East Africa. For example, elevation differences and other topographical characteristics greatly influence the climate of East Africa. The highlands of the Western Rift Valley block the moist and unstable westerly airflow from the Atlantic. Likewise, the Ethiopian Highlands provide leeward rain shadows leading to a complex pattern of rainfall and aridity along the Great Rift Valley, down to the Afar Depression, as well as in the Ogaden (cp. Nicholson 1996; Conway 2000). Highland territories exhibit zones with relatively low temperatures. During the wet season, temperature decreases by about

¹See App. G for the geographical positions of various territories, highlands, mountains, lakes, as well as towns.

5.3°C per 1000 m of elevation in Ethiopia for example. Mean annual temperatures in the Ethiopian *Woina Dega* (*Dega*) climate zone are 16–20°C at an altitude between 1800 and 2400 m and only 6–16°C above 2400 m (Conway 2000). In northern Kenya, divergence in the airflow is associated with the low-level Lake Turkana Jet, which is channelled by the Ethiopian and East African highlands (Kinuthia 1992; Camberlin 1997, his Fig. 3). Large water bodies significantly alter the convective activity (cp. Ogallo 1989). The rainfall over Lake Victoria, for example, is dramatically enhanced by a nocturnal lake-breeze circulation (Ba and Nicholson 1998). In contrast, the upwelling of cold water along the Somali coast suppresses moist convection along the coast (cp. Halpern and Woiceshyn 1999; Hodges 1998).

2.1.3 Interannual variability of precipitation

Africa is known for its variable climate, often exceeding the range of variation of many other places on Earth. In Africa, climate variability is mainly manifested as changes in rainfall. One striking feature are the overall drier conditions in the Sahel since the 1970s, even though the Central Sahel recently exhibits an upward trend (e.g., Nicholson 2005; Ali and Lebel 2009; Lebel and Ali 2009). In Africa, rainfall distributions in space and time have been studied extensively due to their importance for economy, agriculture, and epidemic diseases. Anomalously low or high rainfall amounts can give rise to drought or floods, respectively, both with disastrous economic and humanitarian consequences (Washington et al. 2006). In November–December 1997, for example, unusual high rainfall gave rise to a major malaria epidemic in northeastern Kenya (Brown et al. 1998).

Oceans markedly influence the characteristics and circulation of the atmosphere. The atmospheric boundary layer of the tropical Atlantic, for example, is enriched by moisture from the Atlantic Ocean, feeding the West African summer monsoon (cp. Cadet and Nnoli 1987). The temperature contrast between oceans and adjacent continental land masses determines the flow of air (cp. Haarsma et al. 2005). Cold (warm) SSTs suppress (enhance) the formation of deep convection and hence rainfall (e.g., Vollmert et al. 2003). Due to the migration of atmospheric features, the impact of an SST anomaly depends on season. SST anomalies may enhance rainfall in one season, but reduce it in another (cp. Balas et al. 2007). On a larger scale, oceans influence the generation of the Walker circulation. This equatorial feature is able to link local processes to the large-scale. Ascending and descending branches of the Walker cell directly influence the thermal static stability of the troposphere. For these reasons, natural or anthropogenic changes in oceans have a strong influence on Earth's climate.

West Africa

The Sahel has attracted special interest because of its drought conditions in the 1970s and 1980s. Research has moved steadily away from explanations for rainfall variations in this region as primarily due to land use changes and more towards explanations based

on SST changes (Christensen et al. 2007a). On interannual and interdecadal time scales Sahel rainfall is largely determined by fluctuations in SSTs. Atmospheric simulations using *General Circulation Models* (GCMs) show that the north-south interhemispheric SST gradient is most important. Colder oceans in the Northern Hemisphere and warmer low-latitude SSTs around Africa weaken the continental convergence associated with the summer monsoon (cp. Giannini et al. 2003; Hoerling et al. 2006). In particular, cold (warm) SSTs in the Atlantic Ocean in the region south of West Africa favour a strong (weak) monsoon circulation and lead to wet (dry) conditions in the Sahel (cp. Lamb 1978; Eltahir and Gong 1996). Warm SSTs in the equatorial Atlantic favour an anomalously southerly ITCZ location (cp. Balas et al. 2007) that leads to increased precipitation along the Guinean coast (cp. Ruiz-Barradas et al. 2000). Bader and Latif (2003) suggested that the warming trend in the Indian Ocean played a crucial role for the drying trend over the Sahel (see also Palmer 1986; Giannini et al. 2003; Lu and Delworth 2005; Hoerling et al. 2006). A warm Indian Ocean enhances convection over the tropical Indian Ocean resulting in upper tropospheric divergence. This divergence induces an unusual east-west circulation and upper level convergence over West Africa, which ultimately suppresses rainfall. In addition, Rowell (2003) concluded that a warmer Mediterranean Sea tends to moisten the Sahel. In such a situation, a higher moisture content of the lower troposphere, which is advected southward across the eastern Sahara, produces additional precipitation. Finally, there seems to be a Pacific-Sahel teleconnection (e.g., Janicot et al. 1996). A warm *El Niño/Southern Oscillation* (ENSO) might generate interacting stationary equatorial waves enhancing large-scale subsidence over the Sahel (see Rowell 2001). Janicot et al. (2001) proposed that moisture advection over West Africa is reduced during El Niño years through induced changes in pressure gradients.

Atmospheric conditions are also markedly influenced by surface conditions of land masses. Vegetation partly determines the surface albedo, recycles precipitable water via transpiration, and affects various other processes (see Christensen et al. 2007a, their Box 11.4). Charney's hypothesis, for example, points to a positive albedo-precipitation feedback (Charney 1975). An increase in surface albedo due to an anthropogenic reduction in vegetation could cause a decrease in precipitation that, in turn, would lead to a decrease in vegetation cover and thus a further enhancement of albedo. Indeed, Giannini et al. (2003) argued that the response of the West African summer monsoon to oceanic forcing is amplified by land-atmosphere interactions (cp. also Taylor et al. 2002). The variance of rainfall in the GCM is weaker in absence of a feedback between the atmospheric circulation and land surface processes. However, the sign of rainfall anomalies in the Sahel is still determined by SST variability.

Recent research indicated that changes in SST have probably the dominant influence on Sahel rainfall (cf. Hegerl et al. 2007; Christensen et al. 2007a). A spatially varying, anthropogenic sulphate aerosol forcing is found to provide an important feedback on the cooling at high latitudes and changes in the interhemispheric SST gradients result in a southward shift of the ITCZ (Williams et al. 2001; Biasutti and Giannini 2006). Aerosols seem to have a key role in the determination of lifetime and albedo of clouds (Rotstayn

and Lohmann 2002). Effects of clouds on Sahel rainfall were further demonstrated by Haarsma et al. (2005). Their climate *scenarios* led to an increase in low-level clouds over oceans contributing to less warming over oceans than over the Sahara. This again induces a stronger summer monsoon and therefore a wetter Sahel.

Greater Horn of Africa

A strong interannual variability of rainfall in EEA has been found for the short rains and is mainly influenced by the Indian Ocean. In Kenya and Tanzania, for example, the October-November rainfall is highly correlated to annual rainfall despite its lower amounts (Nicholson 1996).

EEA rainfall in boreal autumn seems to depend on the strength of a Walker cell. In the interval between the northeast and southwest monsoons in boreal autumn, a closed zonal circulation materialises above the Indian Ocean equator (Hastenrath 2000; cp. Fig. 2.3a). This circulation accelerates equatorial surface westerlies driving the oceanic Eastward Equatorial Jet (cp. Wyrski 1973) in the upper part of the Indian Ocean (Luyten et al. 1980; Hastenrath et al. 1993). The formation of the jet in the tropical ocean is accompanied by a flattening of the thermocline at its western origin (Wyrski 1973). The regime of a weak atmospheric zonal circulation entails slow westerlies, a decreased subsidence, and abundant rainfall in EEA (Hastenrath 2001; see also Jury et al. 2002). It also seems to be found preferably under El Niño conditions (cp. Hastenrath 2000).

More recently, the atmospheric fluctuation described above has been associated with the so-called *Indian Ocean Dipole* (IOD; first described by Saji et al. 1999). IOD events show large-scale SST anomalies producing enhanced EEA rainfall. SST anomalies in the Indian Ocean had traditionally been viewed as an outcome of the ENSO system (e.g., Nicholson and Nyenzi 1990; Nicholson 1996) that is forced under El Niño and suppressed under La Niña conditions, but there is increasing evidence that it is a separate and distinct phenomenon (Marchant et al. 2006). Behera et al. (2005) showed that the IOD influence on short rains in EEA is overwhelming as compared to that of ENSO (see also Saji and Yamagata 2003a, their Fig. 1). In particular, 1961 – the second largest IOD event of the 20th century – was not an El Niño year (e.g., Black et al. 2003). Moreover, Saji and Yamagata (2003b) found that the strength of ENSO events might actually depend on the IOD mode. They noted that ENSO events co-occurring with IOD events are much stronger compared to unrelated events. However, other studies concluded that in some occasions ENSO can force IOD events (e.g., Black et al. 2003; Clark et al. 2003).

During boreal autumn a positive dipole mode of the IOD is associated with a distinct dipole-like SST pattern in the tropical Indian Ocean (e.g., Saji and Yamagata 2003b, their Fig. 2). Such events show cool (warm) SST anomalies in the east (west) Indian Ocean (e.g., Webster et al. 1999; Fig. 2.3b). The troposphere above the Indian Ocean shows a strong variability during a positive IOD event, which is characterised by following

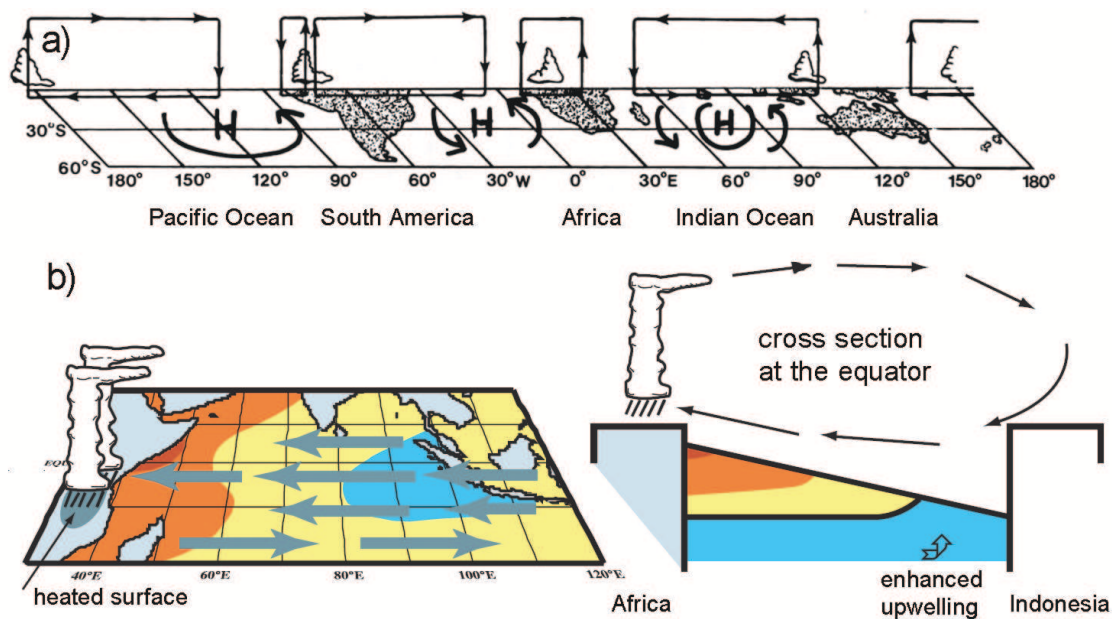


Fig. 2.3: (a) Illustration of the usual Walker circulation along the equator (after Nicholson 1996). (b) Schematic of the IOD event in 1997 (from Webster et al. 1999). A cool (warm) SST anomaly occurred in the eastern (western) Indian Ocean in the second half of 1997. In autumn 1997, the heating anomaly off the East African coast changed the usually weak climatological equatorial westerlies to surface easterlies (left panel). The SST anomalies came along with anomalies in the sea surface height, which was decreased (increased) in the eastern (western) basin of the Indian Ocean (right panel).

structures: (i) Walker cell anomaly over the equator; (ii) deep modulation of monsoon westerlies; and (iii) an anomalous Hadley cell over the Bay of Bengal (Saji and Yamagata 2003a). A positive dipole mode weakens the westerly flow that normally transports moisture away from the African continent out over the Indian Ocean (Black et al. 2003; Fig. 2.3). The normal convection patterns situated over the eastern Indian Ocean warm pool are shifted westward and bring abundant short rains over EEA as well as drought conditions causing forest fires over the Indonesian region (Marchant et al. 2006). Positive IOD events therefore result in significant rain variability in surrounding land masses (see also Fig. 2.3) and unusual high (low) temperatures over countries west (east) of the Indian Ocean.

The climate of NeA also exhibits a large interannual variability. Much like the Sahel, droughts in the 1970s and 1980s in Ethiopia resulted in low agricultural production and affected millions of people (e.g., Seleshi and Zanke 2004). Atmospheric features significantly influencing rainfall of NeA include ENSO, SSTs in the Indian Ocean, and pressure systems, which steer moisture advection.

A large-scale teleconnection with ENSO markedly influences *Kiremt* (June–September) precipitation in NeA. It was found that El Niño years are typically associated with lower rainfall amounts and drought years. A late onset and short *Kiremt* season is likely to be connected with El Niño conditions. In contrast, La Niña conditions usually lead to higher precipitation quantities (e.g., Beltrando and Camberlin 1993; Segele and Lamb 2003, 2005; Seleshi and Zanke 2004; Block and Rajagopalan 2007; Korecha and

Barnston 2007; Segele et al. 2008). As previously noted, ENSO events seem to alter zonal Walker-type circulations. Westerly (easterly) anomalies in lower (upper) levels cause an increased moisture flow towards the area and hence abundant summer rainfall years (Camberlin 1995). A different response was detected for the *Belg* season, when El Niño can produce excess rainfall (cp. Diro et al. 2009).

Interannual *Kiremt* rainfall variability is also linked to pressure patterns. Anomalous low pressure in India triggers a west-east pressure gradient near the equator intensifying the monsoon flow over the Indian Ocean and Africa. An enhanced Indian monsoon leads to a stronger moisture advection from the Congo Basin toward NeA (Camberlin 1995, 1997). Moreover, an intensification of pressure over the Gulf of Guinea in the Atlantic enhances the westerly/southwesterly monsoon flow across the continent and produces wetter conditions over the Horn of Africa (Segele and Lamb 2005; Segele et al. 2008).

Rainfall in NeA is also correlated with SSTs near Africa. Warm SSTs in the western Indian Ocean and the Arabian Sea are associated with a delayed *Kiremt* cessation and hence prolonged rainfall (Segele and Lamb 2003, 2005). It is interesting to note that *Kiremt* rainfall does not seem to depend on IOD conditions (see above). Saji and Yamagata (2003a) found that in the southern part of Ethiopia (3–7°N, 32–46°E) *Kiremt* rainfall is significantly correlated with ENSO but not with the IOD. Segele et al. (2008) established that warm (cool) SSTs in the southern Indian Ocean leads to reduced (enhanced) Ethiopian monsoon rainfall. They argued that a warm (cool) southern Indian Ocean weakens (intensifies) the Mascarene high and hence the flow. Furthermore, the number of tropical depressions over the southwest Indian Ocean predominantly affects precipitation of the *Belg* season. Shanko and Camberlin (1998) showed that a high (low) number of tropical depressions is negatively (positively) correlated with *Belg* rainfall. During boreal winter the presence of tropical depressions reduces the moisture advection toward Ethiopia due to an enhanced flow into the systems.

2.2 IPCC SRES scenarios

Greenhouse gases reduce the loss of heat of the Earth's atmosphere. GHGs include *carbon dioxide* (CO₂), *nitrous oxide* (N₂O), *methane* (CH₄), *sulphur oxides* (SO_x), and various other gases such as halocarbons. Increased anthropogenic GHG emissions since the industrial revolution have changed the natural balance and led to a rise of global surface temperatures of 0.74°C between 1906 and 2005 (Trenberth et al. 2007). For this reason, impressions of the future evolution of GHG concentrations are essential for Earth's climate projections. Already at the start of the 1990s, the IPCC developed six alternative scenarios (Houghton et al. 1992). These scenarios were finally superseded by the IPCC *Special Report on Emissions Scenarios* (SRES; see Nakićenović et al. 2000). Some basic information with an emphasis on A1B and B1 climate scenarios is presented below.

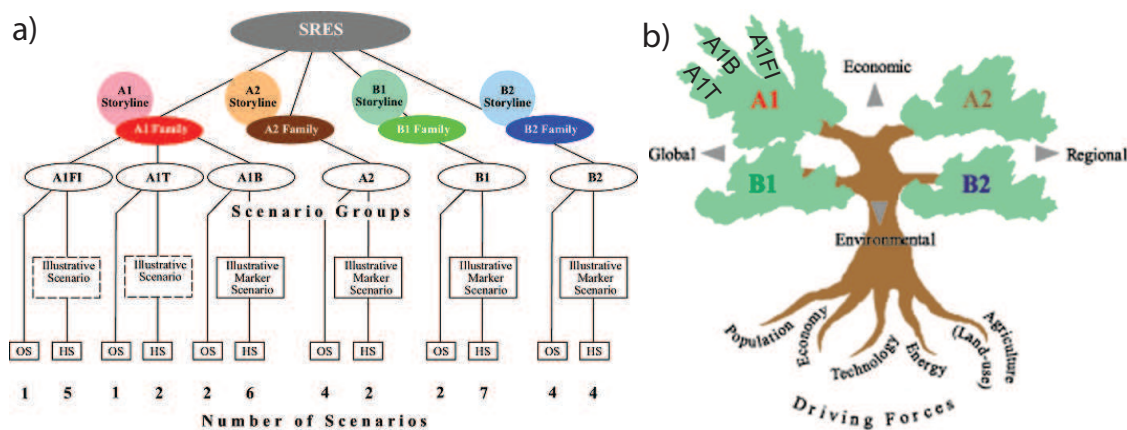


Fig. 2.4: Schematic illustration of SRES scenarios (after Nakićenović et al. 2000). In (a) HS denotes scenarios with ‘harmonised’ assumptions on global population, gross world product, and finite energy, whereas OS scenarios explore uncertainties in driving forces beyond those of harmonised scenarios. Under (b) the four scenario ‘families’ are depicted as branches of a tree. Further details see text.

Driving forces of GHGs are mainly the demographic and socio-economic development as well as changes in technology and the environment. Nakićenović et al. (2000) presented four different narrative storylines (the so-called ‘families’ are A1, A2, B1, and B2) that estimate future progression of emissions. Six scenario groups are drawn from the four families (cp. Fig. 2.4). One group each in A2, B1, and B2 as well as three groups within A1 characterised by different energy technology developments: A1FI describes a fossil fuel (including coal, oil, and gas) intensive, A1B follows a balanced energy supply mix, and A1T is a predominantly non-fossil fuel scenario.

The level of economic activity by 2100 ranges between ten and 26 times the gross world product values of 2000. By 2100 the A1 scenario family represents the upper bound of the gross domestic product, whereas the B1 scenario family is intermediary. Alternative pathways are explored to describe a convergent world. The A1 scenario family is characterised by capacity building, and increased cultural as well as social interactions. Alternatively, rapid changes in economic structures towards a service and information economy take place under B1.

Technology change will strongly impact future GHG emissions of the 21st century. B1 and to some extent also A1B follow a trend toward an increase of renewable and nuclear energies in the long term. A1 and B1 scenarios expect significant innovations in energy technologies and drastic reductions in costs for solar, wind, and other renewable energies. Clean and resource-efficient technologies are introduced in the B1 scenario, whereas A1B has a balanced emphasis on all energy sources.

The population growth until 2050 as well as dietary changes result in a global expansion of grassland and pasture at the expense of forest area under the A1 storyline. An increased productivity largely compensates the growing food demand under B1. By 2100, B1 and B2 scenario families include a considerable ‘greening’ of the planet, due

to demographic and dietary shifts. In general, methane and nitrous oxide emissions peak in the mid-century and decline thereafter.

2.3 Climate change projections

The projection of future conditions of the Earth's atmosphere is essential for the analysis of the possible evolution of climate change and its impact on mosquito-borne diseases such as malaria. Climate projections are based on GCMs, which are dynamically coupled to *Ocean Models* (OMs), the so-called *Atmospheric Ocean General Circulation Models* (AOGCMs).

Various uncertainties are associated with climate modelling. The horizontal and vertical resolution of state-of-the-art AOGCMs are limited (cp. Rall et al. 2007, their Tab. 8.1). Small-scale processes are therefore not explicitly represented in current climate models and their certainty is limited to continental scales. The parameter setting of the models are also not perfect due to limitations in scientific understanding or lack of observations of physical processes. Feedbacks from vegetation are not included in actual global climate models and future modifications of the land surface were not considered in the *Fourth Assessment Report of the IPCC* (IPCC-AR4; Solomon et al. 2007). Also the aerosols forcing, such as the feedback from dust aerosol production, are not fully represented by AOGCMs (e.g., Christensen et al. 2007a).

A source of confidence in climate models is the ability of models to simulate most general features of the current atmospheric circulation (see FAQ 8.1 in Rall et al. 2007). Nevertheless, difficulties still remain with the simulation of tropical precipitation amounts in association with monsoon systems (see Sec. 2.3.2), ENSO, and the Madden-Julian Oscillation (cp. Madden and Julian 1971).

Single runs of AOGCMs are not able to produce definitive climate projections because of the uncertainty of the initial state as well as due to the simplification of atmospheric physics in model formulations. Climate projections are therefore performed by means of *ensemble runs*. Uncertainties and weaknesses of single climate models are partially overcome by analysing a *multi-model* data set comprising ensemble runs of various AOGCMs (cp. Palmer et al. 2004a,b; Hagedorn et al. 2005).

2.3.1 Global climate projections

The physical science basis of the IPCC-AR4 consists of future climate scenarios projected from 23 AOGCMs (Solomon et al. 2007). Continued GHG emissions will probably cause a further warming of the globe and will induce many changes in the global climate system throughout the 21st century. The global mean temperature increase until 2100 for all scenarios ranges from 1.1-6.4°C (Fig. 2.5; e.g., B1: +1.8°C (1.1-2.9°C) and A1B: +2.8°C (1.7-4.4°C)). Note, the feedback of the carbon cycle causes greater uncertainties with regard to higher temperature increases. Efficiency of the Earth's system

to absorb anthropogenic CO₂ is reduced under future climate change conditions and a larger fraction of CO₂ will remain airborne (Meehl et al. 2007).

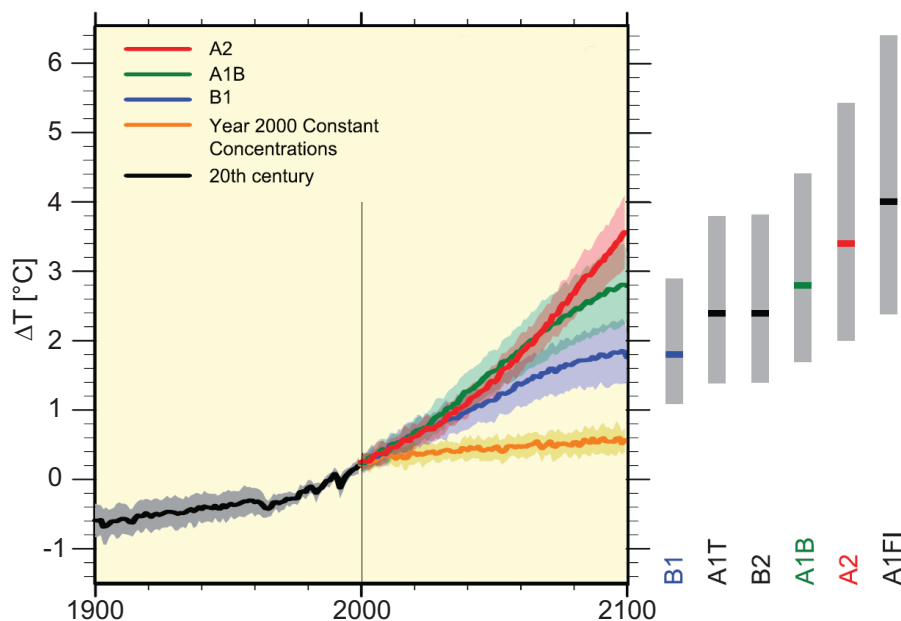


Fig. 2.5: Multi-model averages (solid lines) and standard deviation ranges of individual model annual averages (shading) for the projected surface warming (ΔT ; relative to 1980-1999) of A2, A1B, and B1 scenarios (after Solomon et al. 2007). Also included is the experiment where GHG concentrations were held constant at the year 2000 values (orange line). The best estimate (solid line in the grey bars) and range (grey bars) of the temperature increase is assessed for six SRES marker scenarios (for details see Meehl et al. 2007).

The multi-model mean shows a pronounced global warming over land and at high northern latitudes (cp. Meehl et al. 2007, their Fig. 10.8) and precipitation is projected to increase in various parts of the world since the global hydrological cycle generally intensifies (see Meehl et al. 2007, their Fig. 10.12a). A decrease in precipitation is suggested for the subtropics, in particular around the Mediterranean Sea. There is no indication of discernible changes in ENSO except for model dependent changes in the interannual variability.

2.3.2 Regional climate projections for Africa

Based on the multi-model data set the IPCC-AR4 provides a regional perspective of the projected climate change (Christensen et al. 2007a). A closer look onto the African continent reveals that the whole of Africa is expected to warm (cp. the top row of Fig. 2.6) with a temperature increase exceeding that of the globe's average. The drier subtropical regions are projected to warm more strongly than the wetter tropical areas. The median temperature rises between 3 and 4°C, about 1.5 times the response of the global mean temperature increase. The largest temperature intensification is found in the western Sahara (above 4°C). The projected rise in temperature is smallest in equatorial and coastal

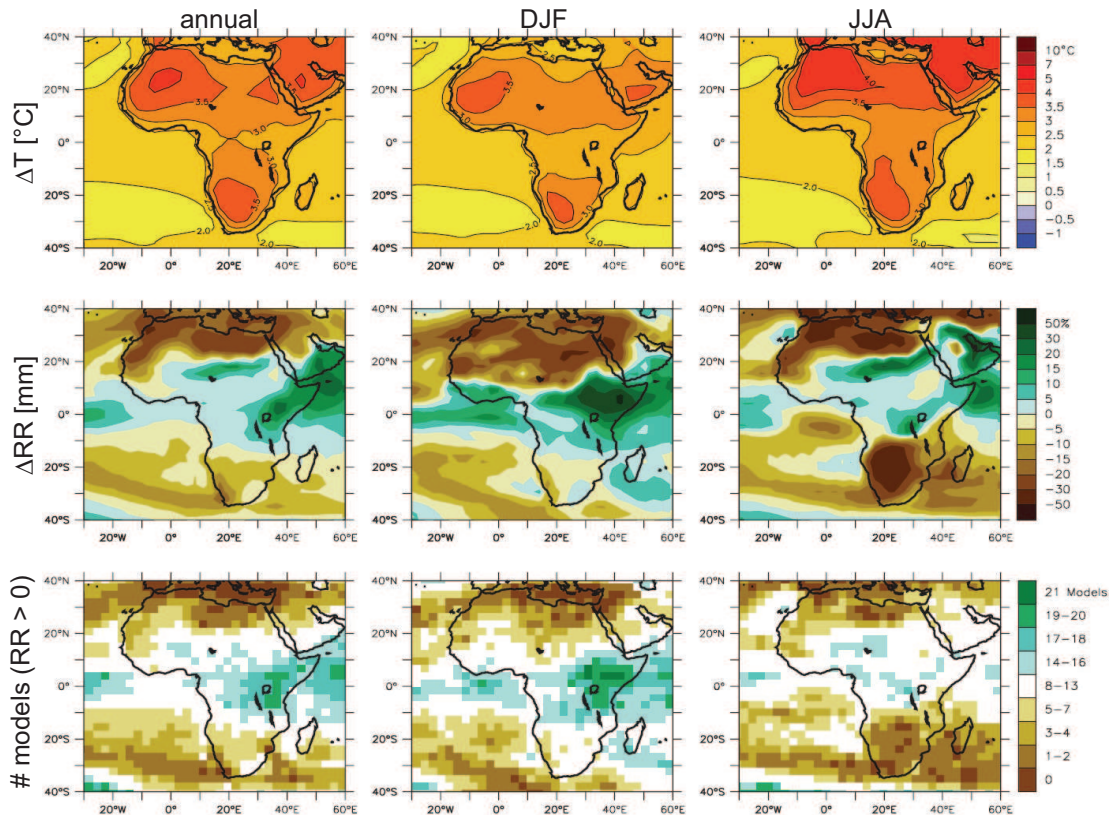


Fig. 2.6: Changes in temperature (ΔT ; top row) and precipitation (ΔRR ; middle row) over Africa between 1980-1999 and 2080-2099 averaged over 21 AOGCMs (from Christensen et al. 2007a). Also illustrated is the number (#) of models that project increases in precipitation (bottom row).

areas (lower than 3°C in some subdomains). Compared to extra-tropical regions there is only a small amplitude of change relative to the seasonal temperature cycle.

The projection of the hydrological cycle is hampered by significant systematic errors of AOGCMs in the simulation of precipitation. Cook and Vizzy (2006) found that six out of 18 AOGCMs generate no realistic West African monsoon. During boreal summer (June-September) these models are not moving ITCZ rainfall onto the African continent. In various climate models such as *ECHAM5/MPI-OM* (European Centre Hamburg Model, 5th generation/Max-Planck-Institute-Ocean Model), the ITCZ is displaced toward the equator and is found over the Atlantic (see Cook and Vizzy 2006, their Fig. 5). Dipolar rainfall variations in the Sahel and the Guinean coast, associated with a fairly realistic interannual SST variability in the Gulf of Guinea, are only present in four of 18 models. Additionally, AOGCMs generally simulate higher than observed ocean temperatures in the Gulf of Guinea. Clearly, models underforecast the upwelling leading to partly 3°C higher ocean temperatures along the coast.

The global pattern of precipitation decrease in the subtropics is also found for the African continent (cp. the middle row of Fig. 2.6). In comparison with 1980-1999 most AOGCMs show an annual rainfall reduction for 2080-2099 in much of Mediterranean Africa, the northern Sahara, as well as southern Africa (see bottom part of Fig. 2.6). In

northern Africa, probability of a rainfall reduction increases with latitude, as part of a larger-scale drying pattern and to a certain extent due to a poleward shift of storm tracks bearing winter rains. Similar processes are also found in southern Africa where rainfall is likely to decline during winter rainfall periods particularly at the west coast of South Africa.

The great majority of AOGCMs foresee higher rainfall amounts in the equatorial tropics of Africa, predominantly in East Africa (see also Christensen et al. 2007a, their Fig. S11.13). East of the Great Lakes rainfall projection is most robust and 18 out of 21 models depict positive rainfall signals. These higher rainfall amounts are part of the large-scale picture with drying in much of the subtropics and an increase in precipitation in most parts of the tropics. Christensen et al. (2007a) argued that this is a plausible hydrological response to a warmer atmosphere. Higher temperatures increase the water vapour content of the atmosphere resulting in an enhanced water vapour transport.

Evolution of rainfall in the 21st century for West Africa and especially that for the Sahel is fairly uncertain. About half (8-13) of the 21 models show either higher or lower annual amounts of precipitation. Four climate models predict an overall drier West Africa; six AOGCMs simulated a dipole rainfall pattern for West Africa with a drier Sahel and a wetter Guinean coast; eight models project higher amounts of rainfall for the Sahel and three of which reveal a reversed dipole pattern; and three models show some mixed rainfall patterns (Christensen et al. 2007a, their Fig. S11.13). Hoerling et al. (2006) found a wet signal over the Sahel for 2000-2049. They attributed this increase to the projected warming of the North Atlantic compared with the South Atlantic (cp. Sec. 2.1.3). Moreover, Cook and Vizzy (2006) analysed the 21st century integration of three AOGCMs, showing the simulations of the 20th century over West Africa of the best quality. The *version 2.0 of the Geophysical Fluid Dynamics Laboratory Climate Model* (GFDL-CM2.0) projects a very strong drying in the Sahel and throughout the Sahara in the second half of the century. By contrast, the *medium-resolution version 3.2 of the Model for Interdisciplinary Research on Climate* (MIROC3.2(medres)) simulates fairly wet conditions during the 21st century. A doubling of the number of anomalously dry years by the end of the century causes a modest drying in the Sahel in the *Japanese Meteorological Research Institute* (MRI) model. Cook and Vizzy (2006) concluded that the third model provides the most reasonable scenario of Sahelian precipitation throughout the 21st century.

A major limitation of state-of-the-art AOGCMs is their coarse horizontal resolution. Regional details of climate are not detectable by AOGCMs. However, information of local scales is required to impact on political measures and practical planning in terms of food security, water supply, and health (e.g., Paeth et al. 2009). Finer resolutions are usually achieved by applying so-called *Regional Climate Models* (RCMs). RCMs are embedded into AOGCMs and in principle such a dynamical downscaling is more consistent than empirical downscaling (e.g., Hewitson and Crane 2006). Nevertheless, this model-into-model approach can be problematic. Firstly, potential model errors in AOGCMs and RCMs are superimposed. Secondly, a RCM depends strongly on AOGCM runs

since the simulation largely depends on lateral boundary conditions. Thirdly, grid points close to the border of the model domain are not representative due to lateral boundary effects.

Several regional climate simulations were performed for various parts of the African continent. For example, RCMs were used for the simulation of the short rains in East Africa (e.g., Sun et al. 1999; Song et al. 2004). Such RCMs are able to simulate large-scale circulation characteristics as well as local features such as the Lake Turkana Jet and the diurnal reversal of the lake/land breeze circulation over Lake Victoria (cp. Sec. 2.1.2). More recently, climate change scenarios for Africa were performed by time slice simulations of RCMs. Most of these models, focusing on tropical Africa, are accurately simulating the seasonality of rainfall. Several RCM time slice experiments project a wetter Sudan-Sahel region for the late 21st century (e.g., Oouchi et al. 2006; Coppola and Giorgi 2005; Kamga et al. 2005; Kunstmann and Jung 2005; Caminade et al. 2006; Jung 2006). Moreover, an increase in the interannual variability of rainfall is detected either due to land-atmosphere feedbacks (Coppola and Giorgi 2005) or induced by shifts in Atlantic SST gradients (Caminade et al. 2006).

Land use change is a potential contributor to climate change in the 21st century (Christensen et al. 2007a). For example, Taylor et al. (2002) found a drying over the Sahel of 4% from 1996-2015 due to a change in land use. They also suggested that climatic impacts of land use change are likely to increase rapidly in future. By contrast, Maynard and Royer (2004) projected that land use changes only have a small regional effect on future climate. Paeth et al. (2009) presented several ensemble experiments with the *REgional MOdel* (REMO) forced with increasing GHG concentrations as well as land use changes until 2050. REMO predicts a significant weakening of the hydrological cycle over most parts of tropical Africa. It was found that land use changes are primarily responsible for the simulated climate response.

Empirical downscaling was used to provide projections for daily precipitation on the basis of six AOGCM simulations for the SRES A2 scenario. By means of various meteorological variables, the technique from Hewitson and Crane (2006) defined atmospheric states which are associated with certain rainfall probabilities. The downscaling version shows more common features in projected changes of precipitation than raw data from AOGCMs (cp. Christensen et al. 2007a, their Fig. 11.3). The ensemble mean of the downscaling reveals increased precipitation in East Africa and a strong drying in the core of the Sahel during boreal summer. Additionally, the downscaling results in local-scale variation of projected changes. For example, by contrast to the Sahel an increase in rainfall is indicated for stations along the Guinean coast.

In summary, the above-mentioned statements underline that rainfall projections for West Africa, in particular for the Sahel, are fairly uncertain. Various studies predict higher rainfall amounts for the Sahelian region mainly due to enhanced warming of the northern Atlantic. However, regional climate modelling as well as empirical downscaling suggests that the modest increase in Sahel rainfall in the multi-model data set should

be viewed with caution. A rainfall surplus, however, in the area of East Africa is predicted with some confidence.

2.4 Malaria biology

Malaria is one of the most dangerous *infectious* and widespread diseases found in tropical and subtropical regions. Every year this vector-borne disease causes worldwide about 273 million clinical cases and more than one million deaths (Touré and Oduola 2004). Particularly in sub-Saharan Africa where *P.falciparum* causes high morbidity and mortality rates (e.g., Snow et al. 1999a,b). Malaria is caused by protozoan parasites of the genus *Plasmodium*. The two most serious forms of this genus are *P.falciparum* and *P.vivax*. People suffering from malaria may experience fever, headache, malaise, severe anaemia, coma, impaired consciousness, convulsions, hypoglycaemia, and high parasitaemia (Colwell and Patz 1998; Gay-Andrieu et al. 2005). Deaths predominantly occur in young children and may result from neurological damage and progressive coma, pulmonary edema, kidney failure, or shock caused by the collapse of the vascular system (Colwell and Patz 1998).

2.4.1 The parasite cycle

The cycle of the malaria parasite starts when the parasite within the insect is transmitted by a female mosquito to the human host whilst feeding (e.g., Price et al. 1996; Phillips 2001; see Fig. 2.7). A blood meal is required by the insect to produce eggs which are laid and then develop in standing water. During the blood-meal of a female *Anopheles* mosquito *sporozoites*, the infective form of the malaria parasite within mosquitoes, are injected into the human host. Sporozoites then invade hepatocytes (liver cells) where they increase in numbers. In liver, sporozoites subsequently mature into schizonts, which rupture and release numerous *merozoites* after 5-6 days (Price et al. 1996). When these merozoites enter the bloodstream the so-called erythrocyte stage starts, the beginning of an asexual cycle. In the erythrocyte stage merozoites attach themselves to specific red blood cell receptors where the asexual reproduction of the parasite (schizogony) leads to the development of immature *trophozoites*. This stage is the so-called ring stage as parasitised red blood cells of an infected host are identifiable under the microscope. Mature trophozoites finally evolve again into schizonts. The erythrocytic cycle takes about 48 hours to complete (Rosenberg et al. 1990a) and results in the rupture of schizonts, which liberate on average 16 merozoites (Eichner et al. 2001). The malaria parasite therefore cannot be identified before schizonts have ruptured after about 7 days (e.g., Schneider et al. 2005; see Tab. D.15).

The blood stage of the parasite is responsible for clinical manifestations of the disease (Talman et al. 2004). Mature, asexual stages of *P.falciparum* are mostly absent from the peripheral circulation and are detectable under microscope. This is due to the

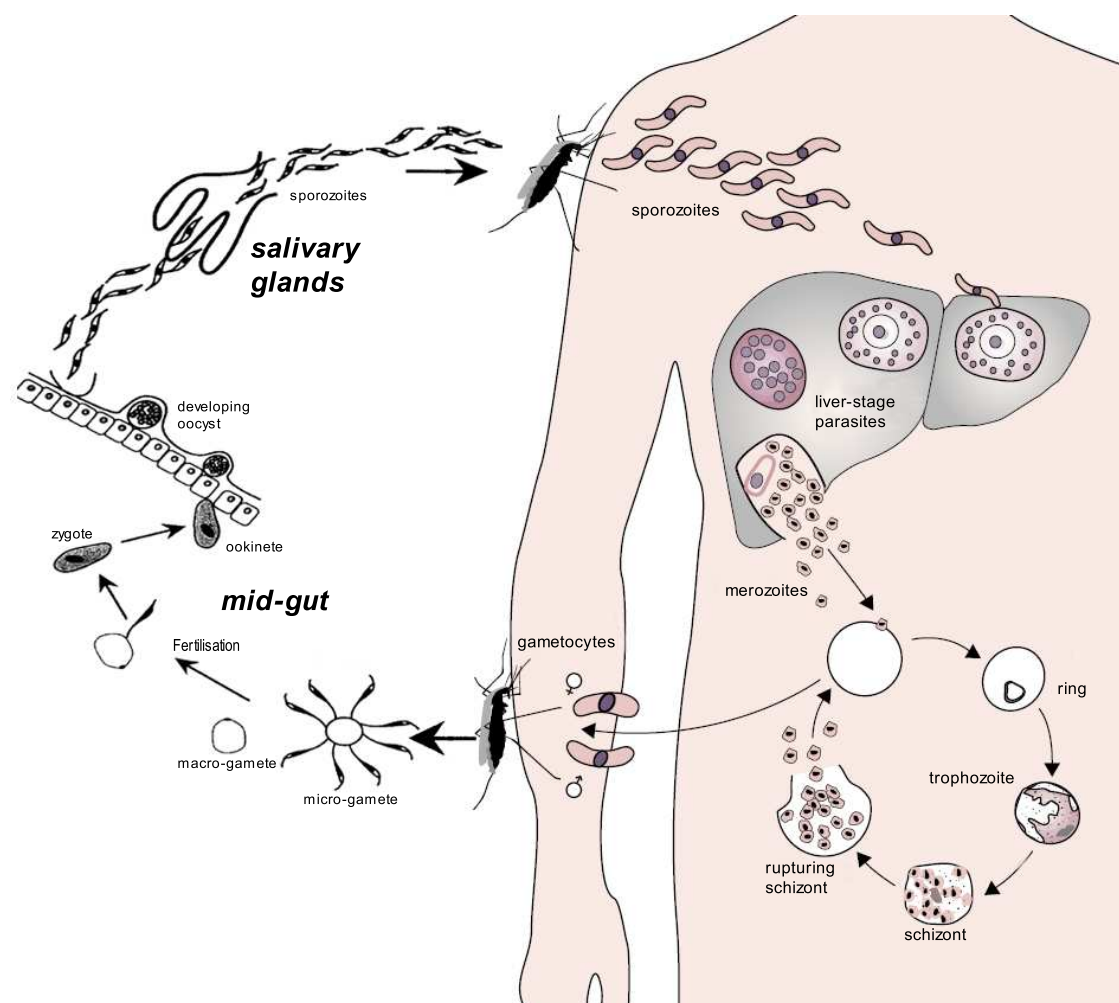


Fig. 2.7: Cycle of the malaria parasite in the human and mosquito host (after Greenwood et al. 2005 and Phillips 2001).

sequestration of asexual parasites, that is the adherence of infected erythrocytes to the microvascular endothelia of many organs and tissues such as heart, lung, liver, skin, and brain (MacPherson et al. 1985). The process often leads to a severe affection of the body (e.g., cerebral malaria). On the other hand bursting erythrocytes cause malaise and fever. Prolonged *infection* sometimes leads to severe anaemia.

Sexual stages of the parasite play a minor role in terms of morbidity, but are essential for the transmission of the parasite. Production of the sexual form of the parasites also begins in the erythrocyte stage when merozoites either go into another round of schizogony or develop male and female *gametocytes*. Maturing gametocytes are preferentially sequestered in the bone marrow and spleen (Thomson and Robertson 1935; Smalley et al. 1981). Gametocyte maturation lasts about 8-11 days and after initial infection this form is detectable after approximately 11-28 days in blood (see Sec. 5.1.10). Male and female gametocytes are finally released into the bloodstream and might be picked up by an *Anopheline* vector.

The development of the malaria parasite within the mosquito denotes the so-called *sporogonic cycle* or extrinsic incubation period (see, e.g., Price et al. 1996; see Sec. 5.1.7). This cycle starts when gametocytes are ingested by the biting mosquito vector. Male and female gametocytes first fuse to form a zygote. These become mobile and transform into elongated ookinetes, which invade the mid-gut wall and turn into oocysts. Those oocysts increase in size, rupture, and finally release sporozoites. In the end, these sporozoites reach the salivary glands of mosquitoes and the life cycle of the malaria parasite is perpetuated.

2.4.2 Immunity

Various biological processes influence the transmission of the malaria parasite and the malaria *prevalence*. In areas where malaria is *endemic*, humans usually go through various states of immunity. At birth, infants are partially protected from infection due to the transfer of antibodies from mother (Wernsdorfer and McGregor 1988). This passive maternal immunity is lost after few months. Young children lack functional immunity, but can quickly develop protection against non-cerebral severe malaria infections (see Gupta et al. 1999). The *asexual Parasite Ratio (PR)* rises quickly to almost 100% in early childhood and declines slowly on the way to adulthood due to progressive immunisation (Aron 1988). This partial host immunity does not completely prevent infection (Aron 1988), but reduces asexual parasite densities (e.g., Buckling and Read 2001). Adolescents between 12 and 15 years of age or older usually acquire an immune status that prevents disease outbreak (Kun et al. 2002).

Acquisition and loss of immunity

Sexual reproduction (i.e., genetic recombination) through female and male gametocytes assures the genetic diversity of the malaria parasite (e.g., Nassir et al. 2005). As the human host can develop immunity against a strain, continuous generation of new strains is essential to the transmission success of malaria. Malaria infections usually involve more than one parasitic genotype (De Roode et al. 2004). Individuals living in endemic malaria areas are mostly infected with multiple parasite clones (Cole-Tobian et al. 2007). Repeated exposure to malaria infections can produce semi-immunity against for instance *P. falciparum*. A clinical case of malaria typically arises from infection by a novel strain to which the host has not yet mounted an efficient protective immune response or to a strain with greater virulence (Kun et al. 2002). Strain-specific immunity increases prevalence of *asymptomatic* parasite carriers with age (Kun et al. 2002). For this reason, development and loss of functional immunity is a key determinant for frequency and severity of clinical symptoms (e.g., Brinkmann and Brinkmann 1991).

Vulnerability of a population with regard to the malaria pathogen also depends on its ethnic affiliation. A different response to the malaria parasite was found in sympatric ethnic groups, which reside in a Sudanese savanna area northeast of Ouagadougou (Burkina

Faso). Modiano et al. (1996) detected interethnic differences in infection rates, malaria morbidity, prevalence, and levels of antibodies to various *P. falciparum* antigens. The ethnic group Fulani was, for example, less parasitised and affected by the disease than the Mossi and Rimaibé groups.

Most deaths from malaria are infants and children under five, as well as pregnant women (e.g., Martin and Lefebvre 1995). Immunity is generally found in malaria-endemic areas with high and stable transmission rates (cp. Sutherst 2004). Areas which are prone to epidemic malaria do not necessarily have stable transmission rates leading to lower immunity in the population and increasing the risk of sudden malaria outbreaks of epidemic proportions (cp. Kiszewski and Teklehaimanot 2004). Any increase in irrigation can, for example, lead to a dramatic increase in malaria (Lindsay and Birley 2004). Highland populations generally lack a functional immunity and are in particular vulnerable to this mosquito-borne disease (e.g., Minakawa et al. 2002a). The effect of topography on the reduced risk of malaria infection was, for example, shown in the Usambara Mountains (see Balls et al. 2004). Due to a non-immune response death can occur in all age groups and is not restricted to young children in this region.

When individuals do not receive repeated *inoculations* of various parasite clones, for example, during the dry season, they lose at least parts of their immunity. Hence in endemically unstable areas, several years of drought may lead to a population with low levels of malaria immunity (Connor et al. 1998). By contrast, during the course of the rainy season humans usually acquire or increase an effective protective immunity. Such a situation was reported from a typical savannah village in Burkina Faso by Boudin et al. (1991a). It was shown that from the mid to the end of the malaria transmission season the parasite prevalence and density decreased in children, probably due to an immune response.

Infectiousness

Immunity significantly affects the infectiousness of human hosts (see also Sec. 5.1.13). Partial host immunity reduces infectivity of human blood to mosquitoes during the blood meal. Infectiousness decreases in general with age, but also highly immune hosts can infect *Anopheles* females (Ross et al. 2006). Firstly, immunised hosts show lower asexual parasite and gametocyte densities than non-immune individuals (cp. Buckling and Read 2001), influencing transmission success (cp. Day et al. 1998). Secondly, the so-called *transmission-blocking immunity* reduces the infectivity of gametocytes to mosquitoes. In this case, gametocyte infectivity is reduced through inactivation of gametocytes and/or of resulting gametes in the mosquito mid-gut (Buckling et al. 1999; Boudin et al. 2005). This mechanism seems to be a strain-specific infectivity-reducing immunity that does not affect the density of gametocytes circulating in peripheral blood (Buckling and Read 2001). Thirdly, immunity decreases the infectivity from mosquitoes to humans by clearing an infection before red blood cells are infected (cp. Smith et al. 2007).

2.4.3 Superinfection

Superinfection is an important component of malaria *epidemiology*. It denotes the existence of two or more broods of parasite strains that flourish simultaneously in the blood stream (e.g., Smith et al. 2005). This condition is reached by multiple infectious bites that result in several infective inoculations (Anderson and May 1991). An existing infection is no barrier to superinfection (e.g., Dietz et al. 1974). It was, for instance, found that many children in some hyperendemic communities are continuously infected (Rosenberg et al. 1990a). It is generally assumed that an infection by one strain is not changed by the fact that other strains may infect the same host at the same time. Different parasite broods are cleared by the immune system independently of one another (e.g., Struchiner et al. 1989). The duration of disease of superinfected individuals, battling more than one strain, is therefore likely to be longer. Superinfection might also play an important role for the development of immunity (cp. Struchiner et al. 1989). Without exposure to repeated infection with different parasite clones immunity is not maintained (cp. Boudin et al. 1991a; see Sec. 2.4.2).

2.4.4 Parasite clearance

Production of mosquito-infective gametocytes is important for the transmission of malaria. In areas with limited seasonal transmission, long-lasting sub-patent malaria infections are needed to sustain transmission. This mechanism is guaranteed by slow recovery rates of malaria infections. Such a situation was observed in Asar (Sudan; 13°30'N, 35°30'E), where malaria transmission is limited to a short rainy season and pauses for 7-9 months during subsequent dry seasons (Hamad et al. 2002). Most controlled patients retained asexual infection for at least seven months. Genetic multiplicity of *P. falciparum* increased the longevity of asexual infection and related production of gametocytes (cp. Secs. 2.4.2 & 2.4.3). Gametocyte infections from mixed clones persisted three times longer than those from single clones (Nassir et al. 2005). Note that the rate of recovery from a malaria infection is also a function of exposure history reflecting effects of immunity (e.g., Gu et al. 2003b; see Sec. 2.4.2). Parasite clearance is therefore closely related to the age of individuals as well as to the intensity of transmission. In fact, immune individuals who control their peripheral parasitaemia clear infections faster by a factor of up to ten (Bekessy et al. 1976).

2.4.5 Detectability of malaria parasites

Malaria parasites are usually detected by means of blood films and microscopes. However, the probability of detecting parasites depends on the density of trophozoites. Parasite densities below the detection level of microscopy (1-20 parasites per μl of blood) might play an important role in *Plasmodium* population dynamics and epidemiology of malaria. In adults, parasite densities are usually comparatively low and are often reduced

to sub-microscopic levels (Ouédraogo et al. 2007). These individuals are hence more likely to return false negative microscopy reports (Smith et al. 2005). This fact is also valid for the detection of gametocytes. There is a problem of enumerating gametocytes patterns, gametocytes are prone to be missed by microscopy examination (Nedelman 1989; Drakeley et al. 2006). Studies have shown that the *Polymerase Chain Reaction* (PCR) as well as the *Reverse Transcriptase-Polymerase Chain Reaction* (RT-PCR) are efficiently detecting sub-microscopic levels of *P.falciparum* gametocytes (see Babiker et al. 1999; Menegon et al. 2000; Nwakanma et al. 2008; Sec. 5.1.12).

2.4.6 Heterogeneous biting

Some individuals are more likely to be bitten than others. Such a heterogeneous biting pattern was found in a village close to Brazzaville (Congo). Nightly captures of *Anopheles* were performed directly on legs of volunteers sleeping in their houses. The number of bites increased regularly in infants (age: < 2 years), children (2-10 years), adolescents (10-20 years), and adults, in proportions of 1:1.93:2.53:3.00 (Carnevale et al. 1978) implying a child-to-adult conversion factor of 1.43^2 . Similar observations were made in two villages in The Gambia. Port et al. (1980) found that proportions of feeds upon an individual are associated with the body surface of the host. Results from The Gambia revealed a child-to-adult conversion factor of 3.57 (cf. Hay et al. 2000b). On this account, adults experience a greater risk factor of infection due to an increased biting exposure (cp. Smith et al. 2006a). Proximity to larval habitats (Trape et al. 1992), differential attractiveness to mosquitoes (Lindsay et al. 1993a), and other reasons furthermore lead to inhomogeneous biting behaviours of malaria vectors.

2.5 Distribution of malaria transmission

In sub-Saharan Africa, the spread of malaria disease is predominantly influenced by environmental and meteorological conditions. Of great importance is the impact of weather and climate on the transmission and distribution of malaria (e.g., Craig et al. 1999). Global environmental changes are therefore expected to affect transmission of parasites causing malaria (Guerra et al. 2006).

Biological parameters of malaria are directly influenced by meteorological variables such as rainfall, temperature, and humidity (Thomson et al. 1997), thus cause an unevenly distributed burden of malaria around the globe. Malaria is mainly centred in the tropics, reaching into subtropical regions on five continents (cp. Fig. 1.1). Warm and moist conditions in the tropics lead to a stable transmission of the malaria parasite. The malaria belt in Africa is bounded by the dry Sahara as well as the colder temperate zone of South Africa. In Africa, malaria endemicity is classified as (Connor et al. 1999): (i) rainfall-limited seasonal transmission, as found in the Sahel (e.g., Babiker

²Note that averaged proportions of adolescents and adults were used ($1.93 \cdot 1.43 \approx 2.765 = \frac{2.53+3.00}{2}$).

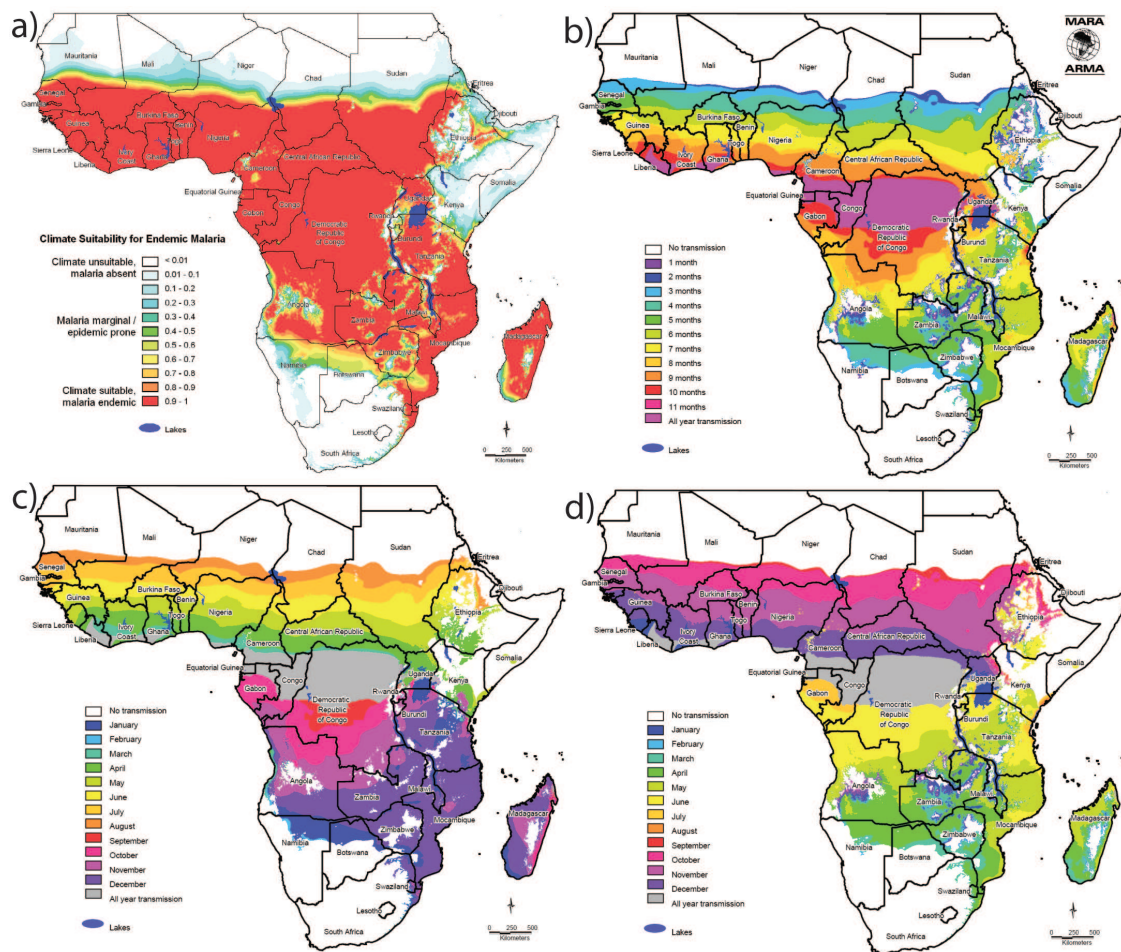


Fig. 2.8: (a) Distribution of endemic malaria, (b) length, (c) onset month, and (d) end month of the malaria transmission season in Africa (for more details cp. Craig et al. 1999; Tanser et al. 2003; source: MARA, <http://www.mara.org.za>). In the regions with two seasons each year, the maps in (c) and (d) refer to the first season in the year.

et al. 1998); (ii) temperature-limited seasonal malaria, as seen in East African highlands (e.g., Balls et al. 2004); and (iii) unconstrained perennial transmission, as observed in parts of Central and Coastal Africa (e.g., Trape and Zoulani 1987; Bockarie et al. 1995).

In West Africa, transmission of malaria is mainly limited by rainfall. In most areas, suitable mosquito breeding sites are only sustained during the rainy season and therefore annual transmission follows seasonal rains (Kovats et al. 2001). The length of the malaria season is often determined by the length of the rainy season (cp. Fig. 2.8). In Niger, for example, malaria is not transmitted in the northern part of the Sahel. Only valleys of the Air Massif provide favourable cooler conditions for malaria vectors (Stafford Smith 1981). A definite malaria season is observed south from Agadez (Niger; 16°58'N, 7°59'E) corresponding approximately with the wet season. In Ndiop (Senegal; 13°41'N, 16°23'W), transmission starts between July and September and ends between September and October (Fontenille et al. 1997a). To some extent presence of permanent streams causes year-round malaria transmission, for instance, in Dielmo (Senegal; 13°43'N, 16°25'W), which is situated on a marshy bank of the Nema stream

(cp. Konaté et al. 1994; Trape et al. 1994; Fontenille et al. 1997b). In the Sudanian zone, in Karangasso (Burkina Faso; 11°13'N, 4°38'W) as well as in the Kassena Nankana district (Ghana; 10°30'-11°00'N, 1°-1°30'W), malaria transmission starts approximately at June and the length of the season adds up to almost six months. Observations closer to the Gulf of Guinea reveal even earlier onsets and longer transmission seasons. In the area of Bouaké (Côte d'Ivoire; 7°41'N, 5°02'W), transmission starts between March and May and ends in October or November (Dossou-Yovo et al. 1998). Malaria transmission is often year-round for the African equatorial zone due to abundant rainfall and the presence of permanent rivers and/or marshes (e.g., Quakyi et al. 2000). In contrast to degraded forests, ancient forest blocks, however, might be even malaria-free during certain years (cp. Manga et al. 1997a).

Malaria epidemic events were frequently found in East African highlands. For example, in 1958 in Ethiopia an epidemic was responsible for estimated 150,000 deaths amongst a largely non-immune population (Cox et al. 2007). In the Sahel, in Sudan, and northern Mali, dramatic malaria outbreaks were recorded in 1986 after prolonged periods of drought (Brinkmann and Brinkmann 1991). Risk of epidemics has been associated with short malaria seasons at geographical margins of stable malaria transmission. More than 124 million Africans live in such areas and experience epidemics causing about 12 million malaria episodes and partially 310,000 deaths annually (Worrall et al. 2004).

2.6 Malaria factors

2.6.1 Climatic factors

Principal climatic factors influencing malaria transmission are temperature and rainfall (Mouchet et al. 1998). Temperature affects malaria through various biological mechanisms. Firstly, egg production of female mosquitoes, that is the so-called *gonotrophic cycle*, only takes place when temperature exceeds about 10°C (cp. Fig. 5.2). Moreover, speed of egg development is steered by temperature conditions (Detinova 1962). Secondly, there is a direct relationship between environmental temperatures and the duration of parasite development within vectors (Detinova 1962). Completion of the sporogonic cycle is only possible above the minimum temperature for malaria parasite development (about 16°C) that is the so-called *sporogonic temperature threshold* (T_s). In Africa, the extrinsic *incubation period* of *P. falciparum* typically lasts 9-14 days (Garrett-Jones and Grab 1964). Thirdly, the ambient air temperature affects the survival of mosquitoes. For example, temperatures in excess of 40°C markedly reduce the duration of survival (e.g., Kirby and Lindsay 2004). Note, that malaria is only transmitted, when the *Anopheles* vector outlives the sporogonic cycle. Fourthly, larval development of mosquitoes depends on water temperatures. For instance, *An. gambiae s.s.* emerge as adults only between water temperatures of 18 and 34°C and most larvae develop between 22 and 26°C (Bayoh and Lindsay 2003). For all these reasons, there is a remarkable influence

of temperature on vector densities (Minakawa et al. 2002a). Small temperature changes can trigger severe malaria epidemics in areas such as highlands.

The second principal climatic factor regarding the spread of malaria is precipitation. Rainfall alters the abundance of aquatic habitats available to mosquitoes for oviposition. Open water surfaces are created after rainfall events and persist for approximately ten days (Shaman and Day 2007). Mosquitoes deposit their eggs in ponds, puddles, or even hoof prints (e.g., Fontenille et al. 1997a). However, excessive rainfall can negatively influence mosquito breeding. Paaijmans et al. (2007) noted unexpected high losses of *An. gambiae* larvae due to rainfall. Heavy rainfall can therefore lead to a paradoxical decrease in malaria transmission (Drakeley et al. 2005) because of flushing of breeding sites, which has a detrimental effect on larval numbers (e.g., Charlwood et al. 1995) and decreases the nutrient availability. Provided that appropriate breeding places persist, mosquito numbers rapidly increase short after the beginning of the rainy season (Lindsay and Birley 1996; Omer and Cloudsley-Thompson 1970). In a West African Sudanian savanna village, the mosquito population size, for example, represented about 150,000–350,000 *An. gambiae s.l.* females at the end of the summer monsoon (Costantini et al. 1996). During the following dry season mosquito populations commonly drop to such low levels that malaria transmission cannot be sustained (e.g., MARA 1998). For this reason, malaria is mostly seasonal in Africa. Malaria occurs outside of rainy seasons only along riverbeds, oases, and other man-made surface water sites (Hay et al. 2000a). However, drought malaria is a common feature in many parts of the world. In such situations, malaria arises when streams and ponds dry up (cp. Charlwood and Alecrim 1989; Shaman and Day 2007; Reiter 2000). For example, in 1934 in Sri Lanka drought was leading to pool formation in dried-out riverbeds (Wijesundera 1988). To sum up, literature suggests that moderate rainfall events stimulate growth of mosquito populations, whereas strong rainfall leads to the flushing of breeding habitats. Except for highland areas precipitation plays a more important role for the spread of malaria in Africa than temperature (Morse et al. 2005).

Atmospheric humidity likewise affects behaviour and biological processes of *Anopheles* vectors. Firstly, increased near-surface humidity directly enhances the flight activity and host seeking behaviour of mosquitoes (Shaman and Day 2007). Secondly, longevity of vector species seems to be influenced by humidity conditions. According to Wernsdorfer and McGregor (1988) relative humidities of at least 60% are most comfortable for mosquitoes. Also laboratory data of *An. gambiae s.s.* suggests that humidity at least slightly impacts mosquito survival (Bayoh 2001; cp. Fig. 5.5). Thirdly, the range and relative abundance of certain mosquito species depends on rainfall and humidity conditions. For example, *An. gambiae s.s.* had the highest prevalence in humid domains and *An. arabiensis* predominated in sites subject to desiccation (Lindsay et al. 1998; Léong Pock Tsy et al. 2003). Fourthly, data from *An. maculipennis* showed that higher relative humidities resulted in shorter gonotrophic cycles and therefore a greater frequency of feeding (Detinova 1962). Fifthly, onset and termination of aestivation (cp. Sec. 5.1.6) are probably controlled by humidity conditions (Wernsdorfer and McGregor 1988). In

summary, lack of rainfall and associated reduced near-surface humidity are important limiting factors for malaria in many arid and semi-arid areas (cp. Kovats et al. 2001).

2.6.2 Other factors

Human activities are crucial for the transmission and prevention of malaria across Africa. For example, humans are strongly changing the earth's environment, leading to an altered abundance and species composition of the mosquito population. Environmental conditions can promote vector-borne disease transmission. Deforestation as well as cultivation of natural swamps increase solar insolation, which usually elevates local temperatures by several degrees (e.g., Githeko et al. 2000). Future land cover change in the tropics may increase the diurnal temperature range by decreasing evaporative cooling during the day (Defries et al. 2002; Paeth et al. 2009, their Fig. 7). Forest replacements provide open sunlit pools that are preferred by important vectors (e.g., Lindsay and Birley 1996). In Western Kenyan highlands, land cover, for example, strongly impacted the survival of mosquito larvae. Different land cover types affected the duration of larval development through its effects on water temperature (Munga et al. 2006; see also Sec. 2.6.1). For these reasons, larvae of *An. gambiae s.l.* were more frequent in pools of cultivated areas than in forested areas and natural swamps (Minakawa et al. 2005).

The development of crop irrigation in Africa has a great prospect for economic development and self-sufficiency in food production (Ijumba and Lindsay 2001). Agricultural practices strongly influence mosquito breeding via an increase in surface water availability (cp. Haines and Fuchs 1991). In Africa, irrigated rice cultivation is associated with higher densities of main vectors of malaria and with an extension of the breeding season (e.g., Briët et al. 2003). The malaria situation might be worsened by irrigation schemes in unstable malaria areas (e.g., Carnevale et al. 1999; Keiser et al. 2005). For example, development of irrigation systems in the Sahel created favourable conditions for the reestablishment of *An. funestus* in Senegal (Konaté et al. 2001). However, for most areas of sub-Saharan Africa, where malaria is endemic, introduction of irrigation has only a minor impact on transmission rates. In Tanzania, irrigated crop production can, for instance, be associated with less malaria than traditional agricultural practices (Ijumba et al. 2002). Reasons for this include improvement of the living standard that results, for example, in a greater use of bed nets and a better access to health. Such a reduced burden of malaria might also be caused by an improved immune protection due to more frequent mosquito bites or by reduced mosquito longevities (Klinkenberg et al. 2002).

Africa is the most rapidly urbanising region of the world (McMichael 2000) and by 2030 more than 50% of the population is expected to live in urban settlements (cp. Hay et al. 2005). A shift in human populations from rural to urban areas will change global patterns of disease and mortality (e.g., Phillips 1993). It is generally assumed that urban areas reduce frequency and transmission dynamics of malaria. An urban environment usually exhibits a great variation of malaria risk. City centres usually experience lower

levels of malaria transmission and severe disease than surrounding locations (e.g., Hay et al. 2005; Kelly-Hope and McKenzie 2009). For example, longitudinal entomological and parasitological malaria surveys from 1984 revealed remarkably lower biting and transmission rates in urban Ouagadougou (Burkina Faso; 12°21'N, 1°31'W) than in nearby rural villages (Rossi et al. 1986; Sabatinelli et al. 1986). However, urbanisation is also a main source of poverty and inequality. Poor housing as well as a lack of sanitation and drainage of surface water can increase vector breeding (Keiser et al. 2004). Dense populations in satellite settlements of cities often promote conditions that are ideal for transmission (Reiter 2001). In highlands, urban heat islands are able to amplify heat waves. Urban populations furthermore increase the pressure on the natural environment leading to a rise in land clearing (McMichael 2000).

Species composition of the mosquito population is also crucial for the level of malaria transmission. For instance, *An. funestus* can extend malaria transmission at the end of the rainy season and at the beginning of the following dry season. This may explain why malaria transmission was about twice as high in locations where both *An. gambiae s.l.* and *An. funestus* were present, compared with locations which only comprised *An. gambiae s.l.* (Kelly-Hope and McKenzie 2009). Such a situation was observed in the 1990s in Senegal. *An. funestus* was abundant in Dielmo, whereas this species was rarely identified in the neighbouring Ndiop. At the same time malaria transmission was about four times higher in Dielmo than in Ndiop (Fontenille et al. 1997b,a; see Tab. D.3; cp. Sec. 2.5).

The *incidence* and geographic distribution of malaria is further influenced by many socio-economic and political factors. These factors comprise the socio-economic status, cultural inflexibility, political rigidity, available resources, technical infrastructure, availability of efficient malaria drugs, preventive measures, and vector control programs. Of great importance for the malaria distribution is the socio-economic development of a community (e.g., Epstein 1998). An analysis between per capita income and malaria incidence indicated a cut-off limit of about \$3100 above which a population is no more vulnerable to malaria (Tol and Dowlatabadi 2001). Gallup and Sachs (2001) showed that income grows more slowly in countries where malaria is present. In the 1950s and 1960s, economic development played an enormous role in eradicating malaria from many areas of the world (e.g., Grover-Kopec et al. 2006). However, attempts to eradicate disease failed in sub-Saharan Africa (e.g., Connor et al. 1998) and this is partly due to the low economic development. Vulnerability of a population is furthermore determined by the nutritional condition (McMichael and Haines 1997). Poor countries or those suffering from natural disasters, conflicts, and civil wars often lack an adequate food supply and public health infrastructure. Factors responsible for the emergence or resurgence of malaria therefore include deterioration or even breakdown of the public health service as well as reduced training programs for medical staff (e.g., Gubler 1998). Moreover, drug and insecticide resistance are driving forces behind malaria resurgences, for example, chloroquine resistance emerged in Senegal in the late 1980s and early 1990s (Bremner et al. 2001) and resistance to DDT slowly appeared in the 1960s in response to intensive

agricultural use (Roberts et al. 2000). Prevention and vector control operations are reliant on financial support and therefore depend on political decisions. However, preventive measures such as impregnated bed net usage are able to diminish malaria morbidity (cp. Lindsay et al. 1993c,b; Akogbéto and Nahum 1996; Cuzin-Ouattara et al. 1999). For instance, a trial with insecticide treated bed nets in Mbébé (Cameroon; 4°09'N, 11°00'E) exhibited a noteworthy reduction of both transmission and parasitaemia (Le Goff et al. 1992).

Various other factors like the construction of roads (see Stafford Smith 1981), migration (e.g., Martens 1999), international trade (cp. van Lieshout et al. 2004), and increased global mobility (cp. Mouchet 2000) are able to change the geographical range of malaria by carrying the pathogen outside the current limit of transmission. For instance, the Trans-Sahara Highway enables a carriage of malaria vectors into northern Niger and hence a seasonal colonisation from the south (Stafford Smith 1981).

2.7 Malaria modelling

2.7.1 Classic malaria models and successors

At the beginning of the 20th century Ross was the pioneer who developed the first mathematical model of malaria transmission. Ross (1911) formulated two differential equations describing the transmission of malaria from mosquito vectors to human hosts and vice versa. This model is based on calculation of transition rates between compartments within the host population and describes the temporal relationship between the *Entomological Inoculation Rate* (*EIR*; i.e., the number of infective bites per person per time period) and *PR* (Ross 1911). Ross (1928) led to the conclusion that malaria would be eradicated, when numbers of *Anopheles* are reduced below a certain figure.

Since Ross' work numerous mathematical malaria models were developed. Reviews of such biological or process-based models can be found for instance in Aron and May (1982), Nedelman (1985), and Dietz (1988). Relevant biological processes usually have been arranged in a set of differential equations. For example, in the 1950s, Macdonald improved the basic model of Ross (e.g., Macdonald 1957). Several factors involved in the transmission of malaria were added to the equations, for example, factor *b*, that is the proportion of biting *Anophelines* with sporozoites in their glands which are actually infective (cp. Macdonald 1955). The model was, for instance, criticised in terms of ignoring immunity.

One of the most accepted models of malaria transmission dynamics and immunity to date is that of the Garki project (Dietz et al. 1974) and variants of it (Nedelman 1985; Struchiner et al. 1989). The Garki model includes acquisition of immunity as well as presence of superinfection (for details see Sec. 5.2). Struchiner et al. (1989) further modified the Garki model for areas of unstable malaria transmission. One of the major changes in this version is that immune individuals can lose their immunity and mainte-

nance of immunity depends on boosting. Cancré et al. (2000) further refined Struchiner's version by means of a Bayesian calibration using parasitological data (Senegal). According to their simulations, during the course of the dry season about 60% of immune subjects lose their immunity in Ndiop (Senegal).

A major disadvantage of classic differential-equation malaria models is the unrealistic assumption of quasi-static vector numbers and constant parasite development rates (Hoshen and Morse 2004). These mathematical systems are constructed without any dynamical equations for the number of mosquitoes (Nedelman 1985). These models are, for example, driven by *EIR* observations. Some of the models were calibrated to specific field sites and might therefore not be transferable to other areas. The development of malaria models is hampered where key parameter values are uncertain. For example, so far no general value or satisfying functional relation has been found for the mosquito survival probability in nature.

2.7.2 Malaria models related to environmental variables

Numerous studies were conducted relating the distribution of malaria and *Anopheles* vectors to various kinds of environmental data. Even simple analysis of proxy ecological variables derived from satellite measurements can indicate variation in environmental factors affecting indices of malaria transmission (Thomson et al. 1996). These environmental variables are often climatic variables or they are closely related to climate conditions. Climate factors generally include temperature, rainfall, and humidity data. Related to rainfall is, for example, the cold-cloud duration as well as the *Normalised Differenced Vegetation Index* (NDVI). Information from environmental covariates is used as predictors for the malaria distribution. Various analysis techniques like logistic regression, the maximum likelihood method, or geo-statistical tools are applied for malaria mapping.

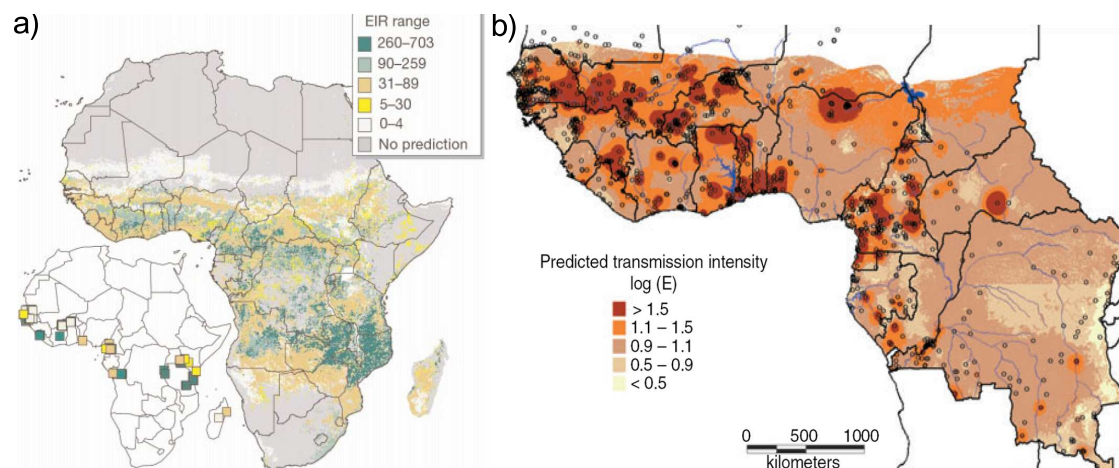


Fig. 2.9: (a) Satellite-derived predictions of the annual *EIR* in Africa (Rogers et al. 2002, their Fig. 3) and (b) predicted logarithmic transmission intensity for West and Central Africa (Gemperli et al. 2006b, their Fig. 6).

Geostationary and polar orbiting meteorological satellites collect meaningful ecological information where surveillance of arthropod vectors are inferable (reviews are provided by Washino and Wood 1994; Hay et al. 1996, 1997; Thomson et al. 1996,

1997; Hay 2000; Goetz et al. 2000). Multitemporal meteorological satellite sensor data, for example, is able to predict the malaria seasonality in Kenya (Hay et al. 1998). In The Gambia, environmental greenness measured by NDVI can forecast seasonal changes of *PR* among children (Thomson et al. 1999; Diggle et al. 2002). Rogers et al. (2002) applied satellite data to predict values of *EIR* (cp. Fig. 2.9) as well as presence and absence of five mosquito species in the *An. gambiae* complex.

Vector-based approaches are used for the construction of distribution maps for malaria vector species. Lindsay et al. (1998) related known occurrences of *An. gambiae* s.s. and *An. arabiensis* to annual precipitation, as well as annual and wet season temperature. Moffett et al. (2007) constructed ecological niche models for ten malaria vectors, which produce relative malaria risk maps. A global malaria risk map was computed by the distribution of dominant *Anopheline* vectors (Kiszewski et al. 2004).

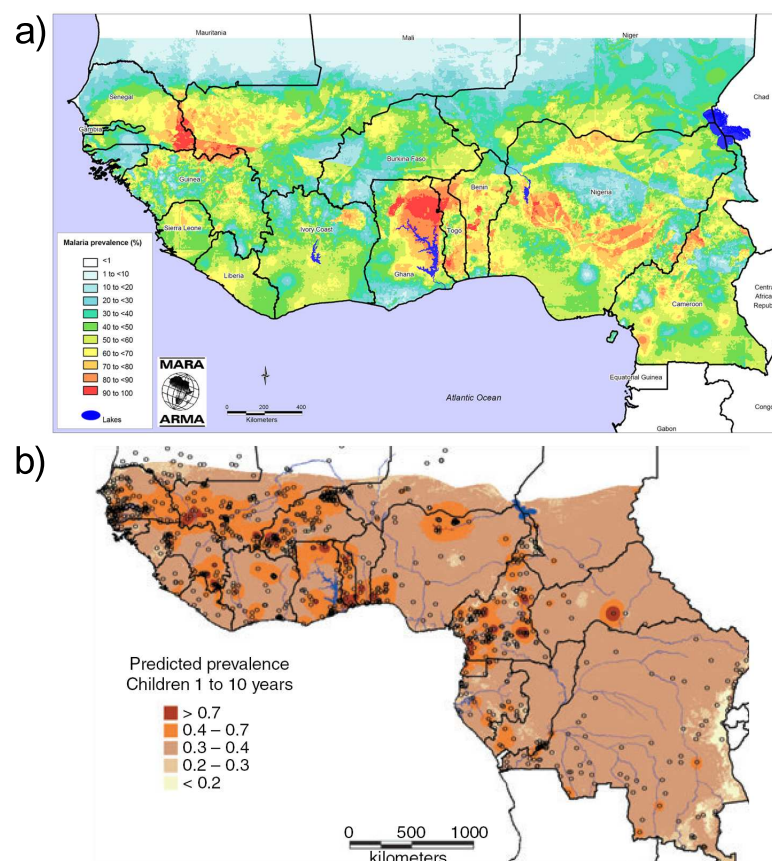


Fig. 2.10: Predicted malaria prevalence of (a) 2-10 years (cp. Kleinschmidt et al. 2001; source: MARA, <http://www.mara.org.za>) and (b) 1-10 years old children (Gemperli et al. 2006b, their Fig. 10).

Statistical approaches are applied for empirical malaria mapping purposes. Rogers and Randolph (2000) constructed a multivariate empirical-statistical model, established current multivariate climatic constraints of the present-day global distribution of malaria, and finally predicted malaria transmission under future climate scenarios. Hay et al. (2001) and Thomson et al. (2006) exploited a simple quadratic relationship between

malaria incidence and precipitation to obtain predictions in epidemic-prone areas. Kleinschmidt et al. (2000) used logistic regression modelling in combination with geo-statistical ('kriging') methods for the distribution of *PR* in Mali. For West Africa, a similar approach was presented by Kleinschmidt et al. (2001) and was based on bio-physical environmental factors. Gemperli et al. (2006a,b) used the Garki model to standardise heterogeneous age *PR* data by means of a single estimate of transmission intensity. The final Bayesian geo-statistical model calculates the two-dimensional parasite transmission intensity on basis of various environmental variables (cp. Fig. 2.10). More recently, the Malaria Atlas Project used a large set of nationally reported case-incidence data, medical intelligence, and biological temperature- and rainfall-dependent rules of transmission exclusion for the generation of a global spatial distribution of *P. falciparum* malaria (Guerra et al. 2008; cp. Fig. 1.1).

Common to all *PR* maps is the implicit assumption that malaria endemicity remains stable over the data survey period. The consequence is that interannual variability is not taken into account (cp. Gemperli et al. 2006b). Seasonal variation of *PR* is also not considered in most studies (cp. Kleinschmidt et al. 2001).

2.7.3 Climate- and weather-driven malaria models

Meteorological variables turn out to be useful explicative variables for the simulation of malaria (e.g., Chalvet-Monfray et al. 2007). Various biological processes depend on temperature, rainfall, and humidity conditions (see Sec. 2.6.1). Climate- or weather-driven malaria models therefore allow for a better understanding of dynamics of malaria transmission.

Already, Sutherst and Maywald (1985) related climatic variables with the abundance and distribution of animals in the computerised CLIMEX (*CLIMatic indEX*) system (also cp. Sutherst 1993, 1998). The *Malaria potential Occurrence Zone* (MOZ) model of Martin and Lefebvre (1995) was one of the first climate-driven malaria models. Lindsay and Birley (1996) applied a simple mathematical model to examine the effect of temperature on the ability of *An. maculipennis* to transmit *P. vivax*. *Vectorial Capacity* (VC; see Glossary) was found sensitive to small increases in temperature in relatively cold climates.

Martens et al. (1995a,b, 1997, 1999), Jetten et al. (1996), Martens (1997), as well as Lindsay and Martens (1998) linked climate data with a module simulating the relationship between climate variables and the *basic Reproduction rate* (R_0 ; cp. Glossary) of malaria. The MIASMA (*Modelling framework for the health Impact ASsessment of Man-induced Atmospheric changes*) model computed the 'transmission' or 'epidemic potential' of the vector population. However, this model does not have a dynamical size of the mosquito population (see also Jetten et al. 1996). The results of the MIASMA model are integrated into a dynamic integrated assessment model, which quantifies the role of economic and social development in limiting malaria occurrence (cp. Tol and Dowlatabadi 2001).

The *Mapping Malaria Risk in Africa* (MARA) project (cp. MARA 1998) offered a simple climate-based distribution model of malaria transmission (hereafter referred as MDM: *MARA Distribution Model*) for sub-Saharan Africa (Craig et al. 1999). The MDM is based on rainfall and temperature determinants of the parasite development and mosquito survival. On basis of monthly temperature and precipitation data the MDM assesses the likelihood that stable transmission could occur (Fig. 2.8a). The MARA project (especially Tanser et al. 2003) additionally provided a model for the malaria seasonality (after this termed MSM: *MARA Seasonality Model*). Different monthly and yearly temperature and precipitation criteria are used to discriminate between suitable and unsuitable months for malaria transmission (Fig. 2.8b-d; for details cf. Sec. 5.3).

More recently, the development of dynamic vector models enabled the simulation of a time-dependent mosquito population. Depinay et al. (2004) designed a complex simulation model of African *Anopheles* ecology and population dynamics that incorporates basic biological requirements for *Anopheles* development and is using local environmental input data. Pascual et al. (2006) introduced a mosquito population model, which is run by daily temperature and rainfall time series. In this dynamical model, temperature controls the development and mortality of larvae as well as mosquito survival. Increase in larval mortality is simulated as a function of accumulated days with no rain to represent desiccation of breeding sites.

Hoshen and Morse (2004) introduced a weather-driven, mathematical-biological model of malaria parasite dynamics, the so-called *Liverpool Malaria Model* (LMM). The LMM comprises weather-dependent within-vector stages as well as weather-independent within-host stages (for more details see Sec. 5.1). On a daily basis, size and behaviour of the total mosquito population and malaria prevalence within human hosts are simulated. Morse et al. (2005) described the integration of the LMM into a probabilistic multi-model seasonal forecast system (also cp. Thomson et al. 2000; Palmer et al. 2004a,b), which was used in the national malaria control programme in Botswana and surrounding countries (Hagedorn et al. 2006).

Outputs of the above described climate- and weather-driven malaria models are very sensitive and depend heavily on a complex range of assumptions. These models are difficult to quantify because of many uncertainties (Lindsay and Birley 1996). Because of limitations some of the models are not able to give accurate descriptions of the current situation of global malaria, so they have a limited value for assessing the impact of long-term climate change (Rogers and Randolph 2000; Reiter 2001).

2.8 Changes in malaria occurrence

2.8.1 Observed malaria changes

Changes in malaria distribution in Africa were observed during the second half of the 20th century. Particularly vulnerable to such changes is the Sahel which is the northern limit of malaria transmission in Africa. In this area, precipitation limits the spread of mosquitoes and consequently that of malaria (e.g., Ndiaye et al. 2001). Since the 1970s the Sahel experienced a marked decrease in annual rainfall amounts. Drought conditions occurred particularly in 1983 and 1984 and at the beginning of the 1990s. These drought conditions deeply altered the health situation in the Sahel (Besancenot et al. 2004). A decrease in malaria transmission was, for example, observed in Senegal and Niger (Mouchet et al. 1996; Julvez et al. 1997b). Faye et al. (1995c) compared entomological and parasitological surveys from the Niayes region (Senegal; about 30 km to the northeast of Dakar) before 1970 with that from 1991-1993. The predominant vector *An.funestus* disappeared and the seasonal presence of remaining vectors was reduced. As a result, the *Human Biting Rate* (HBR; i.e., the number of mosquito bites per human per time) and the *CircumSporozoite Protein Rate* (CSPR; i.e., the proportion of malaria infected mosquitoes) fell significantly. This faded into a strong decrease of *PR* in children (2-9 years) from 40-80% to about 10%. The reasons for these shifts were the dryness as well as human activities (e.g., Faye et al. 1995c; Julvez et al. 1997a,b). Kovats et al. (2001) concluded that in this area malaria transmission used to be endemic seasonally and was expanded to an epidemic risk in a 'desert fringe' malaria zone. However, development of irrigation systems and probably also the return of near-normal rainfall conditions created favourable conditions for the reestablishment of malaria vector *An.funestus* in Sahelian Senegal (cp. Konaté et al. 2001).

In the East African highlands, a significant increase in malaria cases was recorded in the second half of the 20th century. Ethiopia experienced historically the most intensive and widespread recurrent malaria epidemics. Densely populated highland fringes and semi-arid lowlands of the Afar and Somali regions are particularly prone to seasonal and unstable malaria transmission. Occasional massive outbreaks affected most of the country and localised malaria epidemics occur almost every year. Besides the aforementioned catastrophic malaria outbreak in 1958 another countrywide epidemic of similar intensity affected Ethiopia in 1998 (Kiszewski and Teklehaimanot 2004).

In Gikonko (Rwanda), between 1976 and 1990 annual malaria incidence grew from 160 to 260 cases per 1,000 per year and was linked to warmer temperatures (Loevinsohn 1994). In Muhanga (northern Burundi), an unusual increase in malaria cases was observed in March 1991. This epidemic likely resulted from hydro-agricultural environmental changes or from a light rise in temperature at high altitudes (cp. Marimbu et al. 1993). Between altitudes of 1200-1800 m a fourfold increase in microscopic diagnosis of malaria was recorded at Kiremba (Burundi). Bonora et al. (2001) argued that

higher temperatures above 1450 m were responsible for the introduction of the disease into previously malaria-free areas.

In Kabale (southwestern Uganda), an epidemic of malaria was observed in 1998 and was associated with altered rainfall conditions during an El Niño event (Kilian et al. 1999; Lindblade et al. 1999). Also Mouchet et al. (1998) argued that abnormally heavy rainfall in Uganda favoured the severe epidemic of 1994. Conversely, Lindsay et al. (2000) found strikingly less malaria cases in the Usambara Mountains (Tanzania) though El Niño led to 2.4 times more precipitation than normal, suggesting a negative influence of heavy rainfall on mosquito breeding.

In Tanzania, the Eastern Arc Mountains and particularly the Usambara Mountains are usually considered the most significant areas of epidemic risk (see Cox et al. 1999). Already, Matola et al. (1987) recognised a changed pattern of malaria endemicity and transmission at the Amani hills in the eastern Usambara Mountains. In this area temperature is not always the only significant transmission factor. Spread of malaria is often limited by the availability of breeding sites due to the aridity of the highland zone (e.g., Cox et al. 1999; cp. Figs. 2.1a & 4.3a). The mean altitude at which epidemics occur in Tanzania is significantly lower than corresponding altitudes in other countries. Cox et al. (1999) attributed this to the heterogeneity of the environment in the Tanzanian highlands. Malaria epidemics have also been reported outside of the Eastern Arc Mountains. Epidemic-prone districts in Tanzania are additionally clustered in the Kagera district near the Rwanda border (cp. Jones et al. 2007).

An upsurge in epidemic outbreaks was reported for Western Kenyan highlands in the 1980s and 1990s (Hay et al. 2002d). Tea estates of Kericho (Kenya; 0°22'S, 35°17'E), for example, encountered between 1986 and 1998 a rise of severe malaria cases from 16 to 120 cases per 1,000 per year (Malakooti et al. 1998; Shanks et al. 2000). In Kenya, also arid areas in the lowland experienced occasional malaria outbreaks. In the region of Wajir (northeastern Kenya; 1°45'N, 40°04'E), abnormal rainfall and floods in November-December 1997 caused a major epidemic (Brown et al. 1998). A tenfold increase in daily death rates was recorded during the start of 1998 (Brown et al. 1998).

Various researchers argued that climate warming appears not to be responsible for an increase in malaria suitability over Africa (e.g., Hay et al. 2002a,c; Shanks et al. 2002; Small et al. 2003). However, this statement remains controversial. Pascual et al. (2006) raised the point that mosquito population dynamics might have been significantly amplified by observed temperature changes. The debate on the role of climate on malaria epidemics might be resolved by Pascual et al. (2008). Both hypotheses, endogenous disease dynamics and exogenous environmental factors, might play complementary and interacting roles at different temporal scales.

2.8.2 Projected malaria changes

In Africa, malaria is currently only restricted by climate factors in specific arid and highland regions. Climate change is expected to alter transmission rates in this part

of the world. Transmission might become unsustainable in previously endemic areas, sustainable in former epidemic zones, or disease might first occur in antecedent non-malaria areas (Haines et al. 2006). Areas vulnerable to malaria epidemics and future changes are found in regions of fringe transmission (e.g., McMichael and Haines 1997). Communities are and will be particularly vulnerable in usually malaria-free areas or those with unstable malaria (Lindsay and Birley 1996). Areas bordering malaria endemic regions are, for instance, found in the Sahel as well as in East African highlands. By contrast, transmission rates in most malaria endemic zones are so high that a changed climate is expected to have only minor effects on the spread of malaria (e.g., Jetten et al. 1996; Reiter 2001).

Possible changes in the distribution of malaria were provided by various studies. Climate change was projected to be associated with geographical expansions of areas suitable for stable malaria in some regions and with contractions in other regions (e.g., Tanser et al. 2003; Thomas et al. 2004; van Lieshout et al. 2004; Ebi et al. 2005; cp. Tab. 8.2 in Confalonieri et al. 2007). In general, performed malaria projections strongly depended on the applied GCM as well as GHG emission scenarios (e.g., Ebi et al. 2005). Unlike, Rogers and Randolph (2000) found no significant net change by 2050 in the estimated world population living in malaria-transmission zones.

The Sahel

In the Sahel, disease changes are particularly sensitive to an increase in the interannual precipitation variability and extreme events (Thomas 2004; Thomas et al. 2004). However, rainfall is one of the most complex climate variables to project under climate change (Kovats et al. 2001). In arid and semi-arid areas such as the Sahel, prolonged drought conditions may cause malaria to decline (Reiter 2001) and some formerly endemic zones might turn into epidemic-prone areas with a largely non-immune population (cp. Kovats et al. 2001). Such a malaria scenario is simulated for 2100 by the MSM (Tanser et al. 2003). Based on various drier SRES scenarios the MSM predicted a fall in malaria exposure for a host of countries in West Africa. According to MDM runs, higher daily maximum temperatures increasingly reduce mosquito survival and hence malaria transmission during the middle of the 21st century (Thomas et al. 2004).

Highlands

Most malaria projections lead to the conclusion that climate change will increase the spread of malaria in highlands of Africa, where people have some partial or even no malaria immunity (e.g., Martens 1999). Already, Lindsay and Birley (1996) allude to the fact that climate change will increase the likelihood of malaria epidemics in highlands. This argument is followed by various other studies (e.g., Jetten et al. 1996; Lindsay and Martens 1998). Global warming probably results in an increase in altitudes (Kovats and Haines 1995; Reiter 2001; Patz and Olson 2006). An increase in temperature of several degrees might change a normally non-malaria area in one subject to seasonal epidemics

(Jetten et al. 1996). The MDM projected for 2100 an increase in malaria suitability of Zimbabwe highlands using data from 16 climate change projections (Ebi et al. 2005). During the 2050s modest changes from previously malaria-free to stable malaria were projected for highland areas in Ethiopia, Kenya, Rwanda, and Burundi. Thirty years later in the 2080s malaria transmission will become highly suitable in these regions. MSM runs for 2100 predicted a large increase in malaria exposure particularly in highlands of Ethiopia, Kenya, and Zimbabwe (Tanser et al. 2003). An increase in the suitability of malaria in East African highlands by 2050 was also found by Rogers and Randolph (2000). Human populations in highlands might adapt to these changes. Malaria could gradually become stable in parts of African highlands, which would lead to a reduction in epidemic risk (Githeko et al. 2000).

Malaria seasonality

Climate change is projected to alter malaria seasonality. Changes in malaria epidemiology are expected in areas where immunity against malaria is partly lost in the non-transmission season (Jetten et al. 1996). For this reason, lengthening or shortening of vector breeding would affect malaria prevalence (Cook 1992). Small changes in seasonality might be important since transmission rates tend to increase non-linearly through the transmission season (Kovats et al. 2001). Based on data from five atmospheric GCMs the MOZ model predicted an increase in seasonal (unstable) malaria transmission at the expense of perennial (stable) transmission (Martin and Lefebvre 1995). The MIASMA model projected a decrease in suitable malaria months for some African regions (Martens et al. 1999). The MSM simulated, by contrast, 28-42% of new person-months of exposure towards the end of the 21st century in areas of existing transmission (Tanser et al. 2003).

Uncertainties

The currently available malaria projections are criticised in various directions. For example, Martens (1999) stated that climatic effects on public health are mired in a great deal of uncertainty. The dynamic non-linear nature in the biophysical systems, interactions between them, as well as climate scenarios all contribute to this uncertainty (McMichael 1997). A more regional analysis is inevitable necessary (Githeko et al. 2000) since the horizontal resolution of the underlying climate projection is mostly inadequate and neglects local features (McMichael 1997). Models therefore have to be validated on a regional scale, using historical or contemporary data sets (Lindsay and Birley 1996). Setting of parameters in malaria models might entail unverifiable assumptions (cp. McMichael 1997). Models suffer from incomplete parameterisations of key factors that influence the geographical range and intensity of malaria transmission (Confalonieri et al. 2007).

Most studies focused on possible effects of increasing temperatures on disease transmission patterns. However, in future hydrologic changes are also likely to significantly

contribute to rates and efficiency with which mosquito populations grow and transmit pathogens (Shaman and Day 2007). Mosquito breeding must be adequately simulated in relation to hydrological processes instead of precipitation (cp. Sutherst 2004). State-of-the-art malaria projections miss a realistic linkage between environmental conditions and the survival of aquatic mosquito stages (cp. Sec. 2.7.3).

Projections often do not consider the fact that mosquitoes may survive outside their supposed climatic range by exploiting microhabitats with more amenable conditions. Houses are usually more climatically stable than the outside environment (Kovats et al. 2001). Biological processes might be altered under changed climate conditions. Faster desiccation of the mosquito body due to higher temperatures might increase the frequency of blood meals (Kovats and Haines 1995).

Confidence is greater for projected changes in the geographical range of vectors than in changes in malaria incidence because of uncertainties about trends in factors other than climate (Confalonieri et al. 2007). It has to be taken into account that climate is rarely the principal determinant of disease prevalence (cp. Sec. 2.6.2). Human activities and their impact on the spread of malaria are often more significant than climate conditions (Reiter 2001). Global change studies are missing an adequate inclusion of non-climatic variables (Sutherst 2004).

2.9 Objectives and Overview

Strong evidence suggests that human activities alter the earth's climate. Transmission and distribution of various climate- and weather-dependent infectious diseases will probably be changed in the next decades. The main aim of the present study is therefore to assess the risk of malaria in Africa under the influence of the present and modified future climate. Malaria risk is estimated in relation to future climatic-environmental scenarios. Various models are used to dissect uncertainty in malaria models (Sec. 5). Malaria simulations enable the analysis of the influence of atmospheric changes on the malaria distribution up to the years 2050 (Sec. 7).

Firstly, meteorological data is gathered from synoptic weather stations in West Africa and Cameroon for 1973-2006 (Sec. 3). Due to the fact that meteorological data in Africa suffers from numerous data gaps and flawed data, complete and quality checked temperature and precipitation time series are reconstructed by means of monthly and climatological information (App. C.2). Reconstruction of realistic time series is a prerequisite for subsequent malaria simulations. REMO ensemble runs with a horizontal resolution of 0.5° are taken into account for two-dimensional simulations across large parts of Africa. The degree of uncertainty due to emission scenarios of future climate is specified by two different climate projections that are based on the A1B and B1 emission scenarios including land use and land cover changes (Sec. 7.1). Verification of REMO simulations is performed by a gridded observed precipitation data set as well as reanal-

ysed temperatures (Sec. 4). Realistic simulations of the malaria distribution in space and time are assured by the bias correction of REMO data (App. C.3 & C.4).

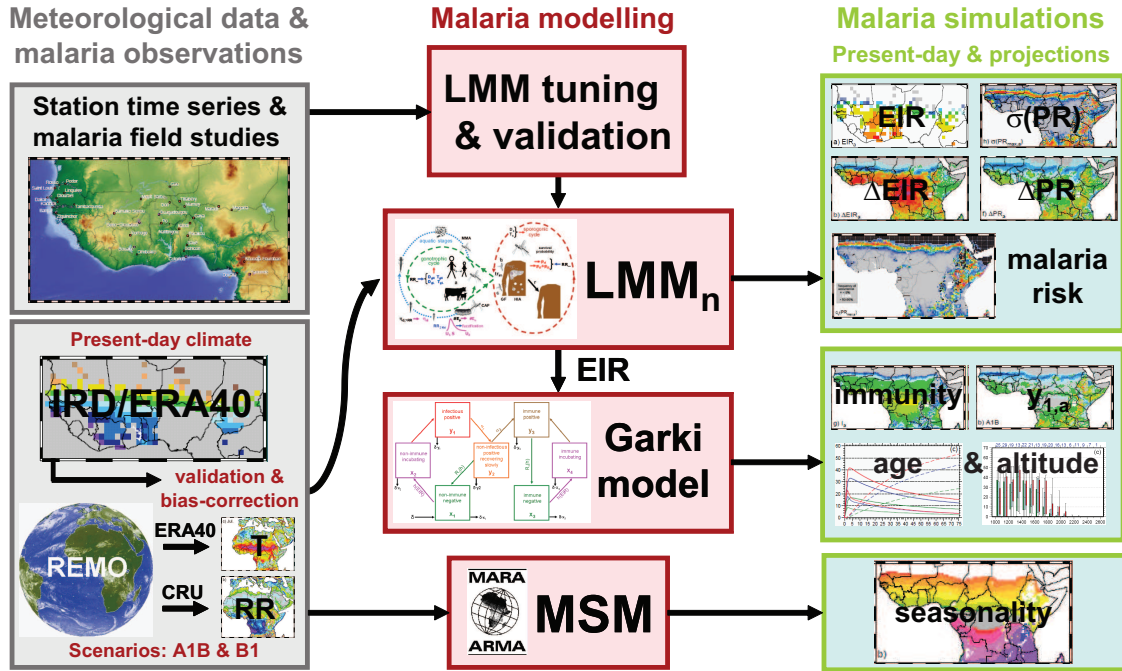


Fig. 2.11: Principle conception of the present malaria study.

Malaria simulations are initially carried out by the LMM. The LMM simulates transmission within the human population on basis of gathered precipitation and temperature data. This dynamical model holds several parameters significantly influencing results of malaria runs (cp. Sec. 6.2). An important step for malaria projections is a realistic setting of the LMM (Sec. 5.1). To ensure a realistic LMM performance the model is validated by means of data from field studies in West Africa and Cameroon. On this account as well as for adjustment of the LMM structure numerous information is extracted from literature (Sec. 5.1 and App. D). The LMM is calibrated by means of observations from eight entomological as well as three parasitological variables (Sec. 6.1). Comparison between the new and the original LMM version finally clarifies the improvement of the model performance (Sec. 6.3).

Scenario-based predictive modelling is applied for the projection of the future malaria distribution. Long-term malaria simulations are performed by the validated LMM version as well as the Garki model (Sec. 7). Malaria projections (2001-2050) are compared to the baseline period of the present-day climate (1960-2000). In a first step, the LMM is driven by means of bias-corrected precipitation and temperature data. Transmission rates of the LMM subsequently serve as data input of the Garki model. These simulations enable consideration of immunity as well as the age-distribution of *PR* and of the immune status.

Identification of malaria-prone areas is of primary importance (Kovats et al. 2001). By means of the interannual variability of *PR* epidemic-prone areas are detected at fringes of malaria transmission. Changes in the epidemic risk are finally discovered by changes in the year-to-year variability of *PR* leading to a risk assessment of malaria.

In Africa, malaria transmission generally follows seasonal rains (e.g., Kovats et al. 2001). Seasonality of malaria is analysed by simulations from the LMM and MSM (Sec. 5.3). Possible changes in the start, end, and length of the malaria season as well as in the maximum transmission month are detected for various parts of Africa.

The study is organised as follows (cp. Fig. 2.11): Details regarding data sources as well as data processing are given in Sec. 3 and in App. C. In Sec. 4, the applied temperature and precipitation data sets are validated against observations and reanalyses. The used malaria models are described in Sec. 5 and additionally the parameterisation and development of a new LMM version is justified (Sec. 5.1). The calibration, final setting, and validation of the LMM is delineated in Sec. 6 and further details are provided in App. E. Sec. 7 describes results of present-day malaria simulations as well as malaria projections of the LMM, Garki model, and MSM. A summary and discussions of main findings follows (Sec. 8). Finally, open questions are raised and information is given for possible future refinements of the LMM. Numerous entomological and parasitological data from literature and supplementary figures are allocated in App. D and App. F, respectively.

3 Data

This section presents detailed information regarding the available data for the purpose of the present study. The LMM is run on a daily time step by two meteorological variables. For this reason, utilised data mainly includes observed, reanalysis-based, and simulated daily average temperatures as well as daily precipitation amounts from various sources. For the construction of a complete time series (App. C.2) also monthly mean temperatures and monthly precipitation data was incorporated. Where and when those values were not available climatological information was used. Two-dimensional meteorological data was gathered for projected malaria changes simulated by the LMM and MSM. Regarding the improved LMM development and validation, malaria data were taken from entomological and parasitological field studies in West Africa.

3.1 DMN precipitation data

Daily precipitation amounts were extracted from a data set allocated by the National Weather Service (DMN; French: '*Direction de la Météorologie Nationale*') of Benin. The original data source covers 69 stations in Benin, including six synoptic weather stations, ten climate, and four agricultural meteorological stations. Precipitation values are available beginning with the year of 1921.

In the present study, data was taken from six synoptic stations for 1960-2005. One advantage in comparison with other sources is the direct access by the DMN to notebooks (French: 'carnet') of observing stations. The DMN performs these observations leading to an almost full data availability.

3.2 Synoptic station data

Meteorological observations permit to study atmospheric weather conditions. Data from observing weather stations can be used for various purposes, for example, for real-time weather warnings at airports, climatological studies, reanalyses, model verifications, or as model input. In the present study, temperature and precipitation measurements were

used as LMM data input. In addition, temperature messages were applied for the verification of two-dimensional temperature data sets.

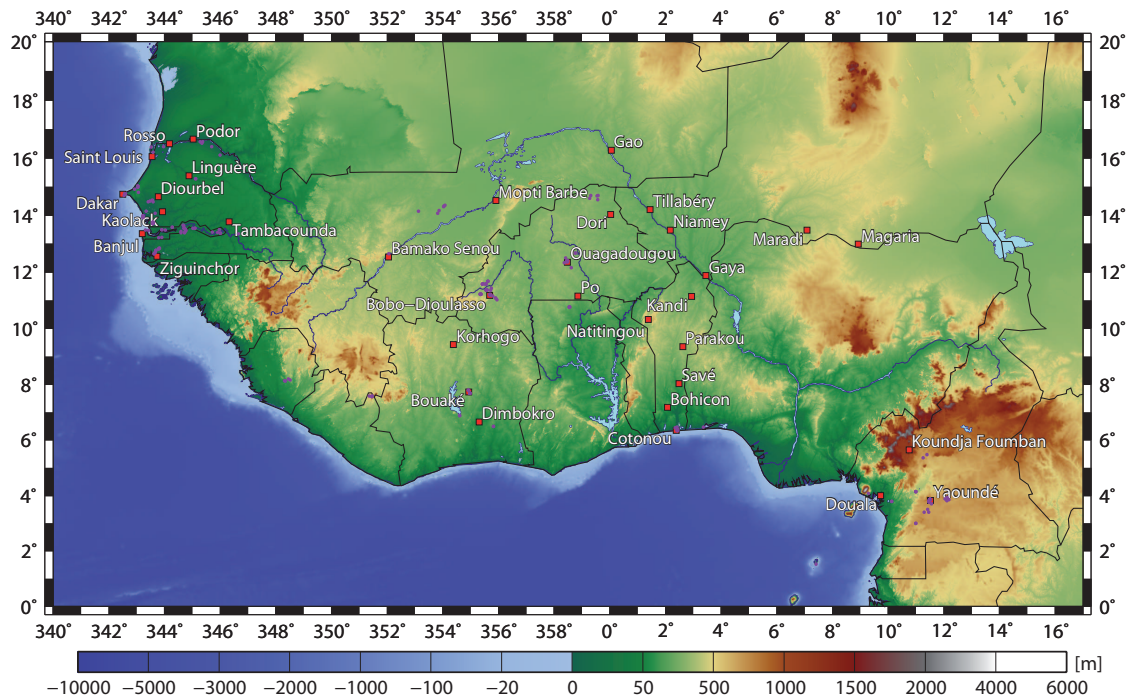


Fig. 3.1: Map showing locations of used synoptic weather stations (Tab. G.1) as well as that from entomological and parasitological field studies (purple dots; cp. Tab. D.3).

The main part of synoptic station data was gathered from the archive of the German Weather Service (DWD; German: „Deutscher WetterDienst“). Since 2000 such data was taken from an archive at the Institute of Geophysics und Meteorology (University of Cologne). The data set comprises ten locations in Benin, Niger, and Mali along a north-south transect at about 2°E (cp. Tab. G.1, Fig. 3.1) and covers a 27 year long time period (1980-2006). Messages include data at main synoptic hours taken at 00, 06, 12, and 18 UTC. For few stations and certain time periods also intermediate messages (03, 09, 15, and 21 UTC) are available. The time step between different messages hence varies between three and six hours.

Unfortunately, *surface SYNOPtic observations* (SYNOPS; *World Meteorological Organization* (WMO) format 12) show numerous data gaps (cp. Fig. 3.2) and also suffer from erroneous messages. Both facts are typical for SYNOP messages coming from West Africa. A time consuming data quality check was carried out for the correction and separation of suspicious values, for example, unrealistic high (low) temperatures or precipitation amounts. To this end SYNOPS were in part compared to the *Federal climate complex Global Surface Summary of Day version 7* (GSOD) data set (see Sec. 3.3). Unrealistic high precipitation values were partially detected by monthly precipitation amounts as provided by the *Global Historical Climatology Network version 2* (GHCN; cp. Sec. 3.5) data set and *monthly CLIMATological data* (CLIMATs; WMO

formate 71) from land stations furnished by the Monthly Climatic Data of the World (<http://www7.ncdc.noaa.gov/IPs/mcdw/mcdw.html>).

3.3 GSOD

In terms of the LMM validation at various locations the above-mentioned synoptic messages represent an insufficient model input. For this reason, GSOD (for further information see <http://www.ncdc.noaa.gov/cgi-bin/res40.pl>) is used as an additional data source. Daily summaries of synoptic messages from all around the world are gathered in GSOD and are administered by the United States National Climatic Data Center. More than 9,000 observing stations are available (accessible through <ftp://ftp.ncdc.noaa.gov/pub/data/globalsod>) that are mainly located in the Northern Hemisphere in North America and Europe. In contrast, the distribution of measurement sites in Africa is much lower (cp. Fig. F.1a).

GSOD comprises 18 meteorological surface variables (e.g., daily mean temperatures and precipitation amounts) taken from synoptic, hourly observations, as exchanged under the WMO World Weather Watch Program. Historical data generally dates back to 1973, for some stations data even starts in 1929. Note that because of the beginning of current synoptic coding in 1982, the data from 1982 to present is the most complete. Because of data restrictions and communication problems, for some stations data gaps occur during certain periods. The quality check as well as configuration of daily temperature and precipitation time series of GSOD data is presented in detail in App. C.1.

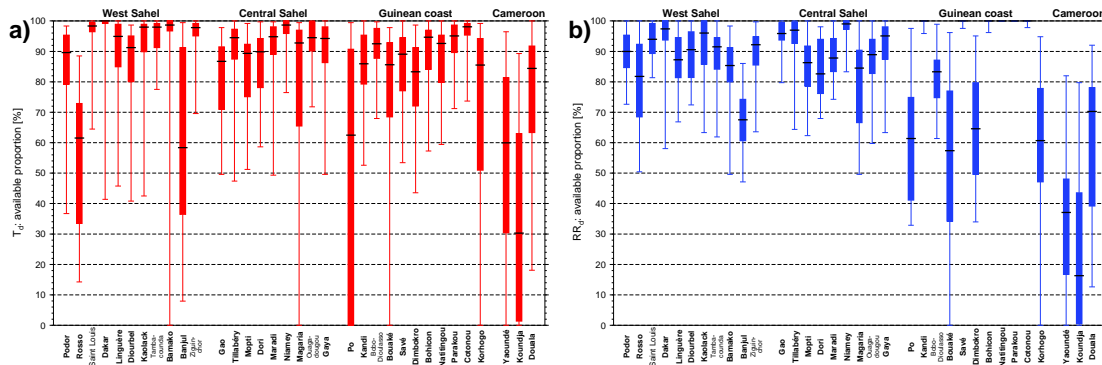


Fig. 3.2: Box-and-whisker plot of yearly availability of (a) daily temperature observations as well as (b) daily precipitation reports from 1973-2006 relative to 34 synoptic stations of West Africa and Cameroon. Availability refers to synoptic messages (Sec. 3.2), GSOD records (Sec. 3.3), as well as additional resources (Sec. 3.1). Stations are grouped for the West Sahel, Central Sahel, Guinean coast, and Cameroon as well as relative to the median of 34 annual rainfall values.

3.4 CLimatological Normals (CLINO)

Climatological information from various weather stations is used for construction of a complete time series of 24-hour precipitation (cp. App. C.2). The utilised *climate* in-

formation is based on WMO *CLimatological NOrmals* (CLINO) for the 30-year average of 1961-1990. For about 4,000 stations in 130 countries climatological data was made available to the WMO by national weather services (WMO 1996). For the present study, monthly mean precipitation amounts and the monthly average number of days with precipitation of at least 1 mm were used for reconstruction of time series of West African synoptic stations (cp. Tab. G.1). For some stations climatological information was taken from the Hong Kong Observatory (http://www.hko.gov.hk/-wxinfo/climat/world/eng/world_climat_e.htm) or the World Weather Information Service (<http://www.worldweather.org>).

3.5 GHCN

Partially large data gaps occur in SYNOP and GSOD data (see Fig. 3.2) that impede malaria modelling. Those data gaps were partly filled and adjusted by means of monthly information from different sources (App. C.2). GHCN data provides monthly surface observations from several thousand stations around the globe since 1701 (Peterson and Vose 1997; see also <http://www.ncdc.noaa.gov/oa/climate/ghcn-monthly>). This century-scaled data base includes mean temperatures, maximum-minimum temperatures, precipitation amounts, as well as sea level pressures. Most stations are distributed in the Northern Hemisphere in North America, Europe, and parts of Asia. However, there are few gauges over central and northern Africa, central Asia, and the Amazon basin (cp. Chen et al. 2002, their Fig. 4). The data set is managed and used operationally by the United States National Climatic Data Center (available online via <ftp://ftp.ncdc.noaa.gov/pub/data/ghcn/v2>). GHCN data storage is updated each month via CLIMAT reports and was applied in several international climate assessments, including the IPCC-AR4 (cp. Trenberth et al. 2007).

The quality of temperature data is ensured by a specialised suite of procedures that incorporate checks for outliers from both a time series and spatial perspective (Peterson et al. 1998). Methods for the quality check for precipitation data is generally comparable to those used in developing temperature data (for details cf. the above-mentioned web page). A major problem of these data sets is that monthly time series for weather stations frequently are obtained from different sources. For this reason, various stations reveal duplicate time series. Regarding the present study in case of temperature duplicates the longest time series were chosen and missing points were filled with duplicates (cp. Peterson and Vose 1997). Duplicates of monthly rainfall were not considered.

Unfortunately, not for every used meteorological station and every required month GHCN data is available. Most used stations show large data gaps during more recent years (e.g., 2000 onward; cf. Chen et al. 2002, their Fig. 3). Comparison with reliable daily precipitation values from the DMN/Benin furthermore shows that some errors remain. Errors for stations in Benin are partly corrected by the DMN precipitation. In terms of 2006 (January-July), digital photos from original CLIMAT messages are avail-

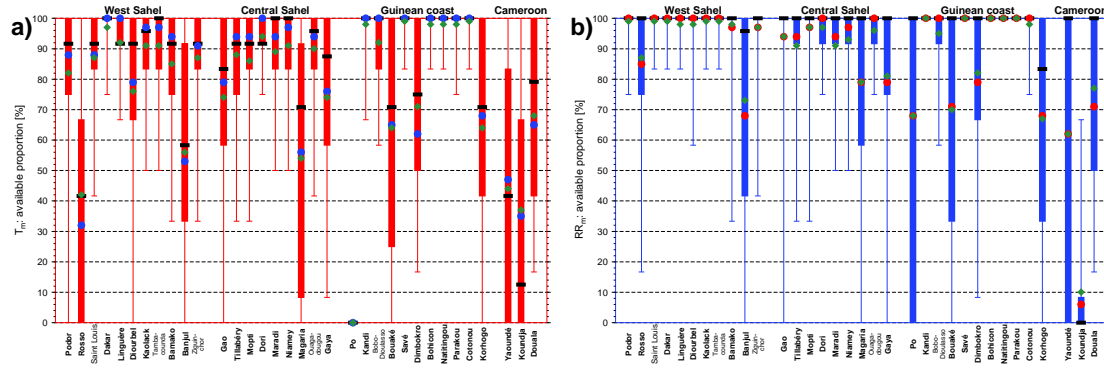


Fig. 3.3: Same as Fig. 3.2, but for yearly availability of monthly GHCN data. Additionally illustrated is the fraction of years with more than six monthly data values (blue and red dots, respectively) as well as the overall proportion of available monthly reports (green diamonds).

able for Parakou and Natitingou (not shown). In addition, some data gaps and doubtful values (as compared to SYNOP messages and GSOD) were replaced by a supplementary data source (A. Niang, personal communication, 2008). However, some data gaps and errors still exist (see Fig. 3.3).

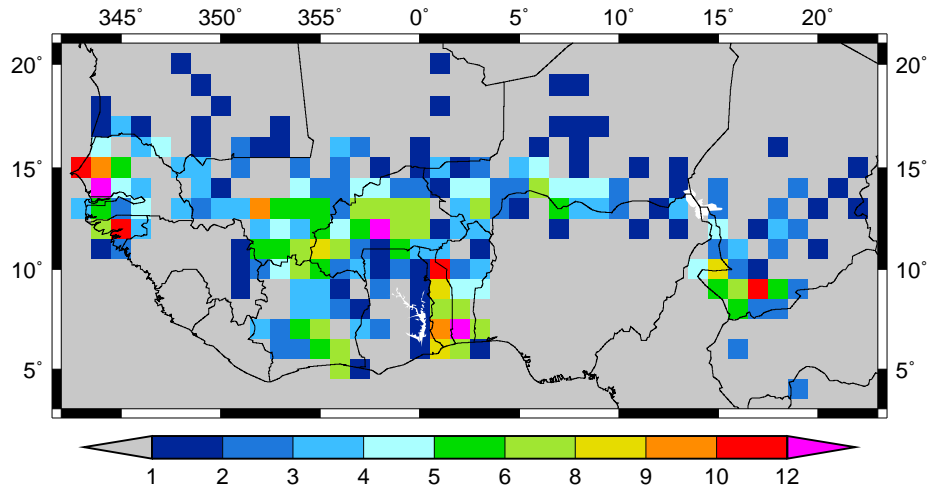


Fig. 3.4: Mean number of daily IRD precipitation observations per grid box for 1968-1990.

3.6 The ‘Institut de Recherche pour le Développement’ data set (IRD)

Evaluation in terms of precipitation is conducted by rainfall observations from the ‘*Institut de Recherche pour le Développement*’ data set (hereafter simply referred to as IRD). Large parts of West Africa are covered by IRD (0-23°N and 20°W-26°E) for the 24 year period from 1968-1991. Precipitation data has a daily resolution and is available on a 1° x 1° grid. Included in the data set are 24-hour precipitation measurements (mostly taken at 06 UTC; cp. Allard 2000), which were interpolated on the aforementioned regular grid. Additionally, the total number of observations available for the particular grid points is given.

Due to the sparse distribution of synoptic weather stations and political reasons the IRD is not available for all grid boxes. No or few data is archived for Guinea, Sierra Leone, Liberia, Ghana, Nigeria, and Cameroon as well as for most parts north of about 15°N (Fig. 3.4). Numerous measurements are only available for large parts of Senegal, Burkina Faso, Togo, and Benin. The number of observations range between zero and 28 observations per day and per grid box. About 72% of all grid points do not show any data. Regarding grid boxes with precipitation measurements (18.2%) mostly only 1-5 observations are available (ratio: 85.1%; cf. Fig. 3.4). In these cases, only a small fraction of grid points shows more than ten observations (3.0%). A lot of grid points do not reveal any data in 1991 (not shown), therefore the data base for malaria modelling is limited to 1968-1990.

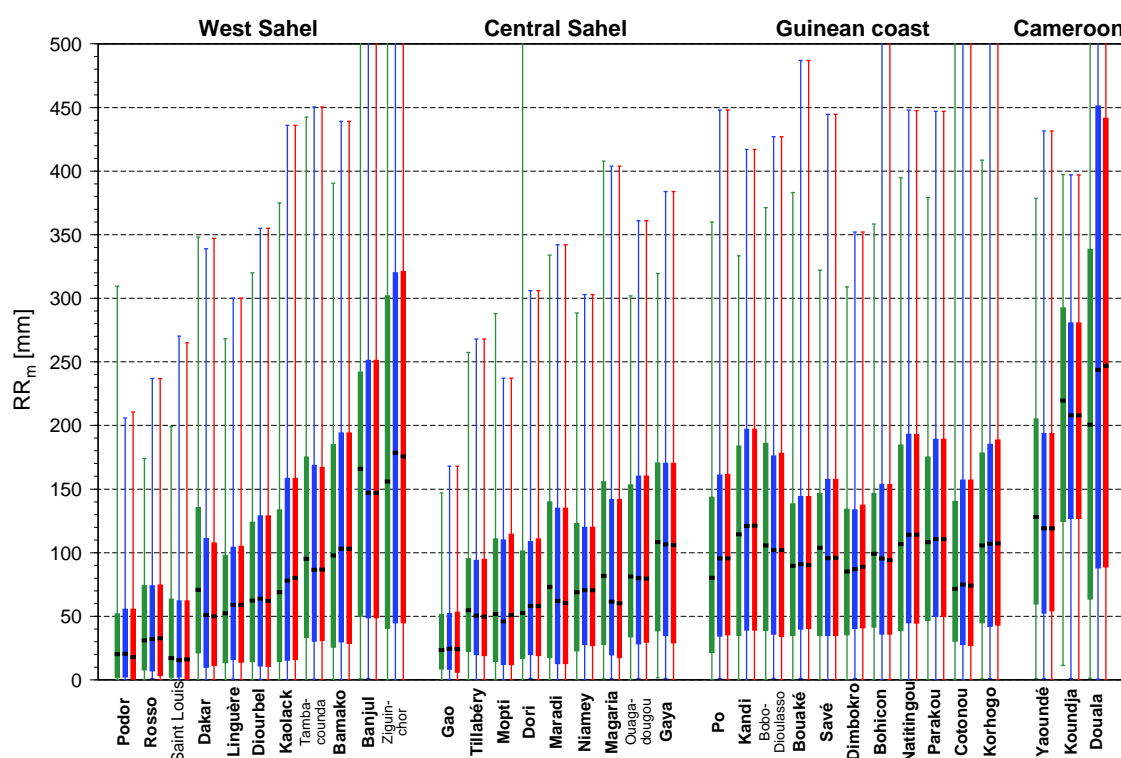


Fig. 3.5: Box-and-whisker plots with regard to monthly precipitation values relative to 1973-2006 and in terms of 34 synoptic stations of West Africa and Cameroon. Displayed are box plots of PREC/L (green), GHCN (blue), and that of reconstructed time series (red box plots), respectively. Note that various monthly values are not available for GHCN (cp. Fig. 3.3b) and that numerous maximum values fall out of the scale of the figure.

3.7 PREC/L

As stated in the previous subsection monthly precipitation is not available for some months and few weather stations. In such cases, adjustment of daily precipitation time series to monthly precipitation is not possible. For this reason, gridded precipitation was taken from the *Precipitation REConstruction over Land* (PREC/L; Chen et al. 2002)

data set. This data is derived from gauge observations from over 17,000 stations that are collected by GHCN (Peterson and Vose 1997) and monthly precipitation reports from the Climate Anomaly Monitoring System. An optimal interpolation method (Gin 1965) is used for creation of monthly gridded analyses of precipitation over global land areas and is available online since 1948 (updated on a quasi-real-time basis on <ftp://ftp.cpc.ncep.noaa.gov/precip/50yr>). Data relative to a regular high resolution latitude-longitude grid of 0.5° was requested for 1960-2006 (M. Chen, personal communication, 2007). The mean distribution and annual cycle of PREC/L agrees well with several published gauge-based data sets (Chen et al. 2002; cp. also Fig. 3.5). PREC/L was hence also utilised for the IPCC-AR4 (see Trenberth et al. 2007).

3.8 The Climatic Research Unit data set (CRU)

Information regarding the monthly variability of various meteorological variables is provided by the *Climatic Research Unit data set* (hereafter named by CRU) and is of particular relevance to a number of applications, for instance, for evaluation of regional climate models (New et al. 2000). CRU has been widely used for different research objectives, for example, the IPCC-AR4 (Trenberth et al. 2007) or evolution of malaria transmission in Great Britain (Kuhn et al. 2002). Various data sets are publicly available (<http://www.cru.uea.ac.uk>) on a regular high-resolution (0.5° or even $10'$) latitude-longitude grid and are representing century-long time series.

CRU represents monthly climate observations from meteorological stations from all around the world and therefore covers the terrestrial surface including oceanic islands but excluding Antarctica. The 1961-1990 mean monthly climatology has been computed as a reference (New et al. 1999). Relative to this climatology monthly climate anomalies are calculated from surface climate data using angular distance-weighted interpolation (New et al. 2000). Anomaly grids of primary variables, these are precipitation, mean temperature, and diurnal temperature range are finally combined with climatology for construction of time series.

The main problem of these data sets is the inadequate spatio-temporal distribution of surface observations. The anomaly interpolation methodology leads to a relaxation of monthly fields towards the 1961-1990 mean in areas of low station coverage. Interpolation errors are increased where the station network is sparsest over cold, dry, and mountainous regions, especially in tropical regions (New et al. 2002). Mountain areas are particularly prone to interpolation errors due to a detailed structured topography.

New et al. (2000) were the first to develop time series for 1901-1995 (termed CRU TS 1.0), which were later extended to 1998 for monthly mean temperatures and precipitation (CRU TS 1.1). However, the data was superseded by CRU TS 2.1 (Mitchell and Jones 2005) that comprises nine climate elements for the period 1901-2002. In the updated version, the existing data base was expanded and improved by refining previous methods.

The present study shows that simulated REMO precipitation is biased against observations (cp. Sec. 4.1). As a consequence, corrected REMO precipitation data has been allocated for the present study (H. Paeth and R. Girmes, personal communication, 2006). At the time of the data correction only CRU TS 1.1 was available and therefore the bias correction is based on 1960-1998 (see App. C.3). However, the raw data and bias-corrected values of REMO precipitation are compared with the more recent CRU TS 2.1 version (cf. Sec. 4.2).

3.9 The ECMWF 40-year ReAnalysis data set (ERA40)

Historical reanalyses such as the *ECMWF 40-year ReAnalysis data set* (ERA40) are essential for climate and atmospheric research (Christensen et al. 2007b). ERA40 temperatures are used here for correction of simulated REMO temperatures (cf. App. C.4). The entire ERA40 archive spans 45 years from September 1957 to August 2002 and comprises various atmospheric variables on 60 model levels. The ERA40 model produced data for the main synoptic hours at 00, 06, 12, and 18 UTC and used a spectral T159 model resolution ('T' indicates triangular truncation of spherical harmonics), corresponding to about 125 km horizontal resolution in the tropics (Cherubini et al. 2006). One additional ERA40 product is a set of analyses such as temperature on screen level (at a height of 2 m) amongst others available on a N80 full Gaussian grid ('N' is, e.g., the number of grid points between the equator and pole), that is equivalent to a 1.125° grid. This analysis was produced as part of the data assimilation and includes observations from weather stations all around the world (Uppala et al. 2005).

The analysis strategy of 2 m temperature is as follows: A primary three-dimensional variational analysis of atmospheric fields is performed on model levels at each particular time step. The 2 m temperature analysis is carried out every six hours, independent of this atmospheric analysis. Analysis of measurements at screen-level is based on a two-dimensional univariate statistical interpolation between a background field and observations (Simmons et al. 2004). This optimum interpolation explicitly includes information on statistics of forecast and observation errors (Douville et al. 2000). The background field used for the optimum interpolation is derived from the six-hour background forecast of the main data assimilation by interpolating between skin temperatures and those at the lowest model level (at a height of about 10 m).

The 2 m temperature analysis is not used to modify atmospheric fields at the model level from which the background forecast for the next analysis in the assimilation sequence is initiated. Instead, temperature analysis at a height of 2 m is used as input to an optimal interpolation analysis of soil temperature for use in the background model (Mahfouf et al. 2000; Douville et al. 2000). Screen-level temperature therefore influences the background forecast through the resulting adjustments to the model's soil temperature fields (Simmons et al. 2004).

ERA40 temperatures are used for the bias-correction of REMO data. Note that a detailed description of the bias correction is provided in App. C.4.

3.10 Present-day runs and climate projections from REMO

At present, climate projections performed by REMO represent the highest atmospheric resolution available for tropical Africa. In this study, REMO simulations are therefore utilised as data input for the LMM and MSM. However, model errors are found with regard to simulated REMO rainfall and temperatures (Sec. 4). For this reason the REMO data is bias-corrected (App. C.3 & C.4). Note that no bias correction was performed for minimum temperatures, which is used for the simulation of the malaria season by the MSM (cp. Secs. 5.3 & 7.3.3). Note that minimum temperatures are except for some high altitudes regions not a limiting factor of malaria transmission in the considered part of Africa.

3.10.1 REMO simulations

REMO originated from the Europa-Modell (Walter et al. 2006) that is the former numerical weather prediction model of the DWD (Majewski 1991). The model was further developed at the Max Planck Institute for Meteorology. Changes of dynamical processes and other physical parameterisations from the *4th generation of the European Centre Hamburg Model* (ECHAM4; Roeckner et al. 1996) were finally introduced into the model (e.g., Jacob 2001). The data used in this study is produced by REMO in version 5.7 that includes a fractional land-sea mask.

REMO is a hydrostatic, limited-area atmospheric model and is designed for applications at the synoptic scale (e.g., Paeth et al. 2009). The space-time resolution of REMO data is 0.5° (i.e., about 55 km at the equator) and 5 minutes (i.e., the integration step), respectively. By means of primitive equations prognostic variables are solved on 20 hybrid atmospheric levels (Jacob et al. 2001). The needed atmospheric forcing data of REMO at lateral and lower boundaries can be either global observations or global climate models. Here, REMO simulations were nested into ECHAM5/MPI-OM global coupled climate model simulations that were forced with different enhanced greenhouse conditions. Each scenario and the twentieth-century simulations are represented by three ensemble members in order to obtain a measure of uncertainty (Paeth et al. 2009; cp. Sec. 2.3). Ensemble members are based on different initial conditions taken from distinct conditions of related ECHAM5/MPI-OM *control runs* (H. Paeth, personal communication, 2006). For the present-day climate (1960–2000) REMO was driven by an observed GHG increase (see Roeckner 2004a; Roeckner et al. 2006a,b). By contrast, the 50 year period (2001–2050) of future climate was forced by enhanced GHGs (see Roeckner 2004b,c; Roeckner et al. 2006c,d,e,f) related to the IPCC SRES A1B and B1 scenarios (Nakićen-

ović et al. 2000; see Sec. 2.2). Additionally, spatially detailed patterns of future *Land Use and land Cover* (LUC) changes are prescribed (see Sec. 3.10.2).

Atmospheric processes at the subgrid-scale such as deep convection and associated convective rainfall are parameterised in REMO. Moist convection is described by the mass flux scheme of Tiedtke (1989). In the used model runs, the moist convection is adapted to tropical Africa, where the atmospheric instability of the monsoon air mass must be adequately considered. On that account, the lower threshold of cloud thickness for the generation of rainfall is set to 1500 instead of 3000 m (Paeth 2005).

The REMO domain covers a limited area of the globe and is set in west-east direction from 30°W-60°E and in south-north direction from 15°S-45°N. The area contains the Mediterranean Sea, the whole subcontinent of West Africa, tropical Africa, and the Arabic Peninsula (see Fig. 2.1b). However, due to the nesting approach errors were introduced by lateral boundary effects. For this reason, data from grid points at the boundary of the REMO domain (e.g., six rows; cp. Paeth et al. 2009) is not interpreted.

3.10.2 Land use and land cover changes

The surface condition of the land area significantly influences atmospheric processes, for instance, the generation of precipitation. Variables with regard to the land surface therefore have to be realistically represented in atmospheric models. REMO contains seasonal-dependent land surface parameters such as the total surface roughness length as well as those induced by vegetation, the fractional vegetation cover, the leaf area index, and the background surface albedo. For the 20th century simulations (1960-2000) these parameters were held constant and were derived from global topographic data with a horizontal grid spacing of 30 arc seconds and National Oceanic & Atmospheric Administration data sets that represent the surface condition for the late 20th century (cp. Hagemann et al. 1999). The data for the late 20th century is the reference for the introduction of a LUC scenario, which is in line with FAO. A detailed description of the applied stochastic land-use change model is given by Paeth et al. (2009). Some basic information with regard to LUC changes is summarised below.

In addition to changing GHGs, REMO is at the lower boundary also forced by LUC changes. Paeth et al. (2009) developed a stochastic land-use change model for Africa that takes into account future population growth as projected by the United Nations report (UN 2006) as well as scattered patterns of urbanisation. The model considers in particular the loss of vegetation due to land degradation processes such as deforestation and uncontrolled settlement. The deforestation projection is taken from a FAO scenario (FAO 2006) and deforestation sums to about 30% until 2050. Changes in the LUC pattern are mainly caused by a population growth of 2% per year and are primarily prescribed in the surrounding area of cities, existing agricultural areas, and traffic axes. It is assumed that the prescribed changes will lead to a plausible structure of LUC in future.

LUC projections were realised in two general steps. Firstly, the stochastic land-use change model is applied to land cover data in 11 km² grid resolution from the United States Geological Survey/Global Land Cover Characteristics classification. The de-

velopment of the stochastic model implicates a random LUC change under three constraints: (i) The projected population prospect of the UN (2006) is valid. (ii) Deforestation is in line with the FAO estimate (FAO 2006). (iii) LUC grid boxes are only affected, when a neighbouring grid box has already been anthropogenically manipulated. In the area of the rain forest, the last constraint ensures that a transformation takes place along boundaries of woodlands. By contrast, natural vegetation is preserved in the central part of rain forests (cp. Paeth et al. 2009, their Fig. 1). Regarding the southern zone of the Sahel, desertification, due to improper agricultural practices and overgrazing, leads to transformation of grassland to bare soil. Secondly, the higher-resolution LUC grid (11 km^2) is adjusted to the REMO grid resolution (0.5°). Furthermore, the different LUC categories are transformed to the five above-mentioned land surface parameters of REMO.

A linear LUC change is assumed for the transient LUC scenario from 2001-2050. Changes are superimposed on the seasonal cycle of vegetation. Compared to the IPCC SRES B1 scenario a stronger LUC scenario is defined under A1B. It is assumed that technological progress under B1 leads to a more efficient agriculture. For this reason, the agricultural area is not as much expanding under the B1 LUC scenario. However, both scenarios do not lead to considerably different LUC projections since population growth is the same under A1B and B1. The spatial mean of forest changes under the A1B scenario is identical to a FAO scenario (Food and Agriculture Organization 2006), which reduces the forest area for about 30% until 2050.

3.11 Entomological and parasitological data

In public literature numerous information with regard to the malaria disease can be found. A lot of published information, which only represents a fragment of all available literature, has been extracted from various articles. The large amount of publications complicated the analysis. For the purpose of the study it was therefore adjutant to archive and summarise relevant data in different tables (see App. D). With regard to malaria modelling entomological and parasitological data is of particular interest since a malaria model has to undergo a certain validation procedure (see Sec. 6). On account of the availability of meteorological data and because of the limitation of time the analysis is restricted to West Africa and Cameroon. When possible the following variables were archived (for details of the procedure and information regarding some variables see App. D). Included in the meta-analysis are the literature references as well as some basic features like the name, geographical position, land-use of the study site, and the time period of the study. Annual averages are provided for *CSPR* and *PR*, annual minima and maxima are indicated for *PR* as well as accumulated annual values are given for *HBR* and *EIR*. The *start*, *end*, and *length of the malaria season* (*SSeas*, *ESeas*, and *Seas*, respectively), as well as the *length of the main transmission season* (*MSeas*; i.e., the number of months in which 75% of *EIR* is recorded) and the *month of the maximum transmission* (*XSeas*; i.e., the month with the highest *EIR* value) are included in the analysis (see Tab. D.3).

Additional information regarding different malaria variables is required for the LMM setting. Data was gathered for the gametocyte prevalence, that is the percentage of humans with gametocytes in their blood (see Sec. 5.1.12 and Tab. D.11). Moreover, articles were reviewed in terms of the mosquito survival probability (see Sec. 5.1.5 and Tab. D.10). Horizontal (*controlled conditions*) and vertical (*field conditions*) life tables from various studies furnish data for the daily survival probability of the aquatic stages of mosquitoes (see Sec. 5.1.4 and Tabs. D.8 & D.9). Furthermore, data is provided for the gonotrophic cycle (see Sec. 5.1.1 and Tab. D.6), the number of eggs per female mosquito (see Sec. 5.1.2 and Tab. D.7), the duration of the immature mosquito stages (see Sec. 5.1.3 and Tabs. D.8 & D.9), the duration until asexual and sexual parasites appear in the blood circulation (see Sec. 5.1.10 and Tab. D.15), and preference of humans by *Anopheles* females (see Sec. 5.1.8 and Tab. D.14). In addition, values for transmission efficiencies of the malaria parasite between human and mosquito hosts are given (see Sec. 5.1.9 & 5.1.13 as well as Tabs. D.13 & D.12).

3.12 Data overview

As previously described various data sets were allocated for the present study. On this account, an overview of the most important data sets might be helpful (see Tab. 3.1). Further details with regard to the generation of time series, the bias correction of REMO precipitation and temperatures, the analysis and conversion of data as well as the Wilcoxon-Mann-Whitney rank-sum test are provided in App. C.

id	name	period	var	resS	resT	note
DMN	Direction de la Météorologie Nationale	1921(1960)-2005	RR	stations	daily	synoptic stations: Kandi, Natitingou, Parakou, Savé, Bohicon, and Cotonou
SYNOPS	surface SYNOptic observations	1980-2006	T, RR	stations	3-6 hourly	ten synoptic stations along about 2°E
GSOD	Federal climate complex Global Surface Summary of Day version 7	1929(1960)-U(2006)	T, RR	stations	daily	synoptic stations
GHCN	Global Historical Climatology Network version 2	1701(1960)-U(2006)	T, RR	stations	monthly	synoptic stations
CLINO	CLImatological NOrmals	1961-1990	$RR, \#RR_{\geq 1}$	stations	monthly	climate values at synoptic stations
IRD	'Institut de Recherche pour le Développement' data set	1968-1991(1990)	RR	1.0°	daily	gridded (number of) rainfall observations
PREC/L	Precipitation REConstruction over Land	1948(1960)-U(2006)	RR	0.5°	monthly	gridded observed rainfall
CRU	Climatic Research Unit data set	1901(1960)-2002(2000)	RR	0.5°	monthly	gridded observed rainfall
ERA40	ECMWF 40-year ReAnalysis data set	1958(1960)-2002(2000)	T, p_s	T159	6 hourly (daily)	-
REMO(raw)	REMO	1960-2000	T, RR, p_s	0.5°	daily	increasing greenhouse gases; constant LUC; three ensemble runs
REMO(cor)	bias-corrected REMO	1960-2000	T, RR	0.5°	daily	increasing greenhouse gases; constant LUC; three ensemble runs; cp. App. C.3 & C.4
A1B: REMO(cor)	A1B: bias-corrected REMO	2001-2050	T, RR	0.5°	daily	SRES: A1B scenario; stochastic LUC changes in line with FAO; three ensemble runs
B1: REMO(cor)	B1: bias-corrected REMO	2001-2050	T, RR	0.5°	daily	SRES: B1 scenario; weaker stochastic LUC changes; three ensemble runs

Tab. 3.1: Overview with regard to used data sets. Columns: id: identifier; name: name of the data set; period: period; var: used variables; resS: spatial resolution; resT: time resolution; note: notes. The 'U' stands for a regular update of the data. Numbers in brackets stand either for the applied time period or for the time resolution. T : temperature; RR : precipitation; $\#RR_{\geq 1}$: number of days with at least 1 mm of precipitation; p_s : surface pressure.

4 Validation of meteorological model data

Data from REMO will be used continually throughout the thesis for initiating rainfall and temperatures in malaria runs. In this section, the *uncorrected REMO* (hereafter referred to as REMO(raw)) and the *bias-corrected REMO data set* (hereafter termed REMO(cor)) are validated against observations and reanalyses. First, the simulated REMO precipitation is compared to IRD in West Africa (Sec. 4.1). REMO precipitation is further verified for other parts of Africa with respect to CRU (Sec. 4.2). Temperatures from reconstructed time series (App. C.2) are compared to those of ERA40 (Sec. 4.3). Finally, REMO temperatures are validated against these reconstructed time series (Sec. 4.4) and ERA40 (Sec. 4.5).

4.1 REMO precipitation versus IRD

4.1.1 Monthly and annual rainfall

Here, the performance of REMO with regard to the simulation of the West African monsoon system is analysed in terms of the spatial distribution as well as the monthly timing of rainfall. Furthermore, the year-to-year variability of precipitation is compared between REMO and IRD.

Observed rainfall is generally decreasing from the Guinean coast toward the Sahara. The *annual precipitation amount* (RR_a) declines from more than 1500 mm in certain parts along the Guinean coast to less than 200 mm in the northern Sahel (see RR_a in Fig. 4.1). The analysis of the seasonal precipitation cycle demonstrates the migration of the West African monsoon system towards the Sahara up till August (see left column in Fig. 4.1). IRD also shows the swift retreat of the monsoon system during October and November.

The comparison of REMO(raw) with IRD reveals major shortcomings in the REMO data. Principally, simulated RR_a is displaced southward. Excessive RR_a is simulated for the Guinean coast and is mostly lower than observed in the Sahel. The further analysis of the seasonal cycle exhibits a delay in the onset of the monsoon in REMO(raw). The first rainfall deficits are found in February at the coastal zone of the Gulf of Guinea

(cp. middle column in Fig. 4.1). During the first half of the rainy season the *monthly precipitation amount* (RR_m) is too low for a strip of about 5° latitudes. The largest differences occur between February and April as well as in July (Fig. 4.1). During those months rainfall at some locations is underestimated in REMO(raw) by more than 100 mm.

In July and August (i.e., the height of the summer monsoon), the largest rainfall deficits are found south of Lake Chad as well as in southern Senegal and The Gambia. In these regions, in REMO(raw) RR_m is in most places more than 100 mm lower than observed. By contrast, between July and October RR_m is often higher (by more than 200 mm) for the Guinean coast as well as the Sudanian zone. Clearly, a bias correction of REMO precipitation was needed (see App. C.3).

In the following analysis, REMO(cor) precipitation is compared to IRD (right column in Fig. 4.1). The correction of REMO precipitation shows major improvements. The deficit of RR_a completely disappears for the Sahel. By contrast, several grid points reveal even higher rainfall amounts. The monthly values are in certain parts more than 100 mm above that of IRD. These differences are expected since REMO(raw) has been bias-corrected for 1960-1998 and not for 1968-1990. During the longer period several wet years are recorded in the 1960s (e.g., Fig. 2 in Fink et al. 2008). A drier period like the one between 1968 and 1990 would therefore result in lower bias-corrected rainfall amounts (cp. App. C.3).

Bias-corrected precipitation at the coast of Senegal and the Gulf of Guinea is considerably reduced. Some grid points exhibit more than 200 mm lower rainfall amounts than IRD. As already stated, the bias correction was not possible for months with no simulated rainfall events (cp. App. C.3). For this reason, the onset of the monsoon still comes a little too late in February and March at the Guinean coast. The deficit of RR_m exceeds 50 mm at some locations. However, the rainfall difference in those months is remarkably reduced by the bias correction. Most significant is the improvement of REMO(raw) between May and August. The aforementioned latitudinal strip vanishes in REMO(cor), which means that rainfall conditions during the main monsoon onset are now comparable to observations. The correction procedure also results in more realistic precipitation amounts during the height of the monsoon. During November and December, however, corrected REMO precipitation is still lower at the coastal area than observed.

In summary, deficiencies in annual precipitation as well as relative to its seasonal distribution are considerably reduced by the bias correction of the REMO data set.

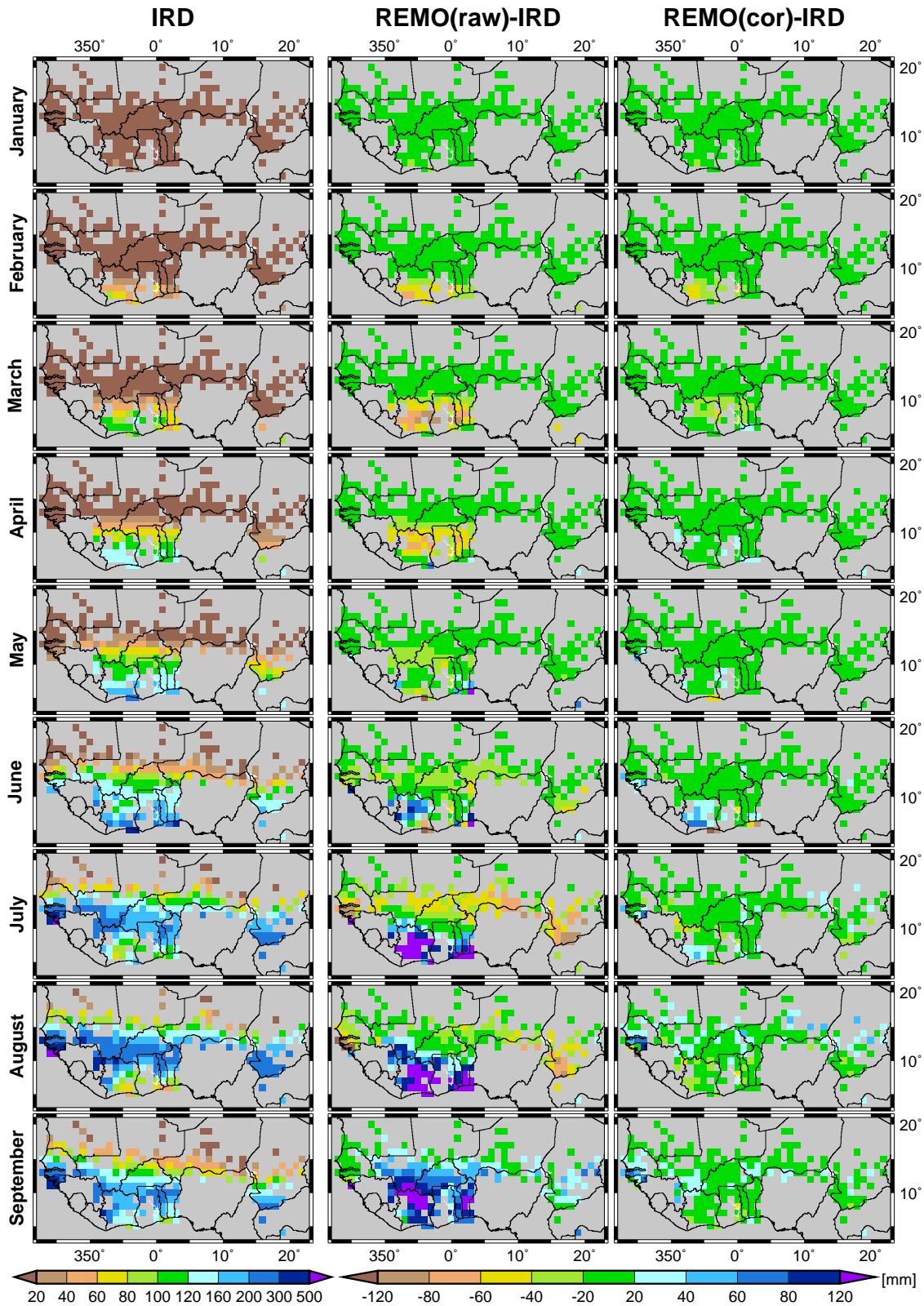


Fig. 4.1: Observed rainfall (in mm) from IRD as well as the difference between IRD and REMO(raw) (REMO(raw)-IRD) as well as REMO(cor) (REMO(cor)-IRD) rainfall (continued on the next page). The first twelve rows depict data with regard to the monthly precipitation amount (RR_m). The penultimate row shows values of the annual precipitation amount (RR_a) and the last row illustrates the standard deviation of RR_a .

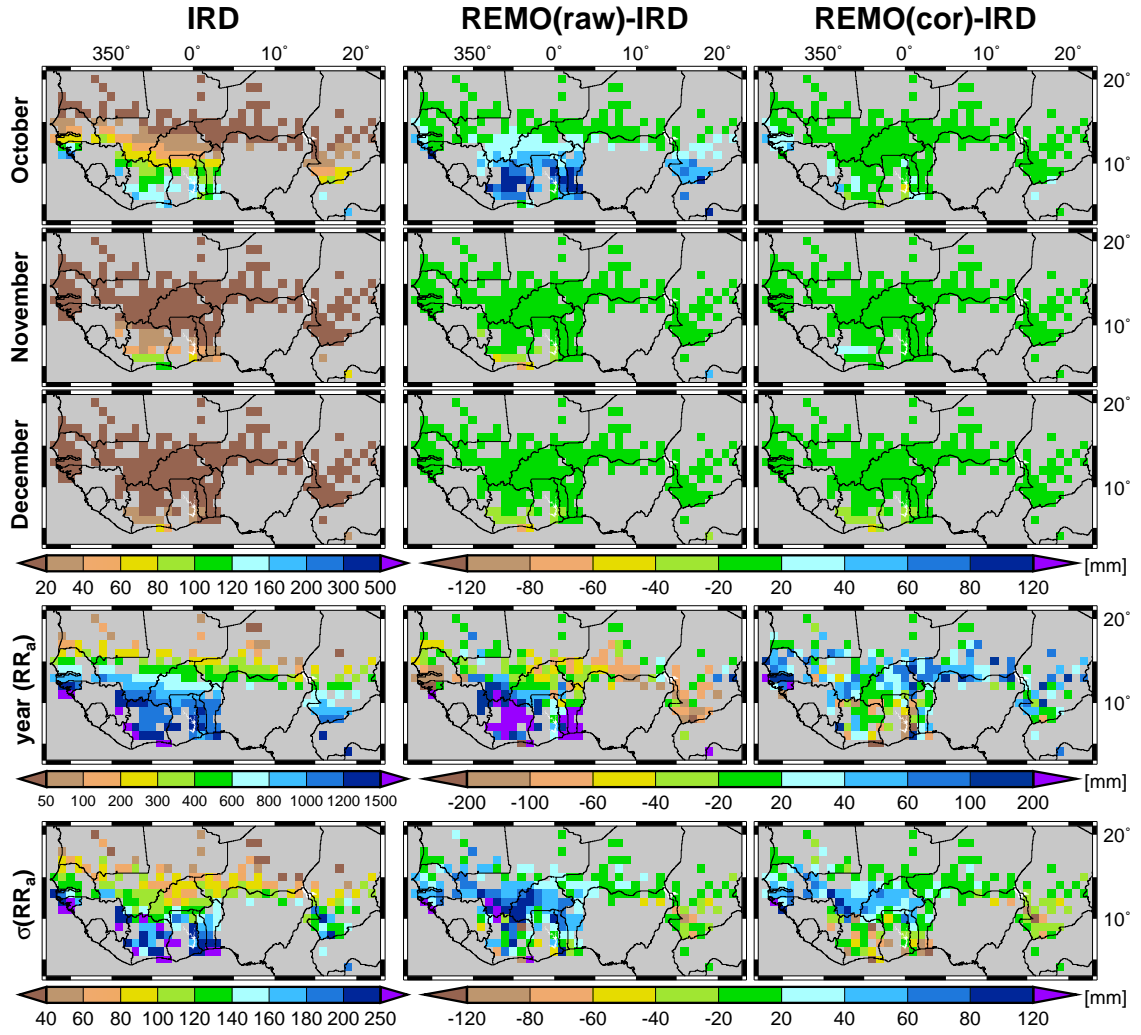


Fig. 4.1: (continued)

4.1.2 Frequency distribution of 10-day accumulated precipitation

In the present study, the LMM is applied for the simulation of malaria transmission. In addition to the temperature input, the model is driven by daily values of the *10-day accumulated precipitation* ($RR_{\Sigma 10d}$). For this reason, the frequency distribution of simulated $RR_{\Sigma 10d}$ values is compared with IRD. It will be shown here for West Africa that the frequency distribution of $RR_{\Sigma 10d}$ values in REMO(cor) compare favourably well with observations.

In principle, it is also possible to check the frequency distribution of daily rainfall. However, this comparison suffers from the fact that simulated REMO precipitation represents average values of a grid box, whereas IRD is based on point measurements. The convective nature of tropical rainfall (see Sec. 2.1) causes a strong mesoscale rainfall variability. For example, Balme et al. (2006) found strong convective scale variability for an area in the region of Niamey. Their rainfall estimation error increases from 3-16% at the annual scale and from 21% to 113% at the event scale, when the number of stations

over a 100 km^2 area decreases from twelve to one. This is a consequence of the high spatial variability of rainfall leading to a single station having behaviour significantly and randomly different from the regional pattern. Another effect of localised convection is an increase in the number of rain events for a grid box when more measuring sites are considered. Hence, the number of rainy days per IRD grid box is expected to increase with the number of available observations. The inclusion of more observations per grid box or by the consideration of longer time periods (e.g., a month) will provide more robust results. In the following, it is assumed that for a period of 10-days the frequency distributions of REMO and IRD are comparable.

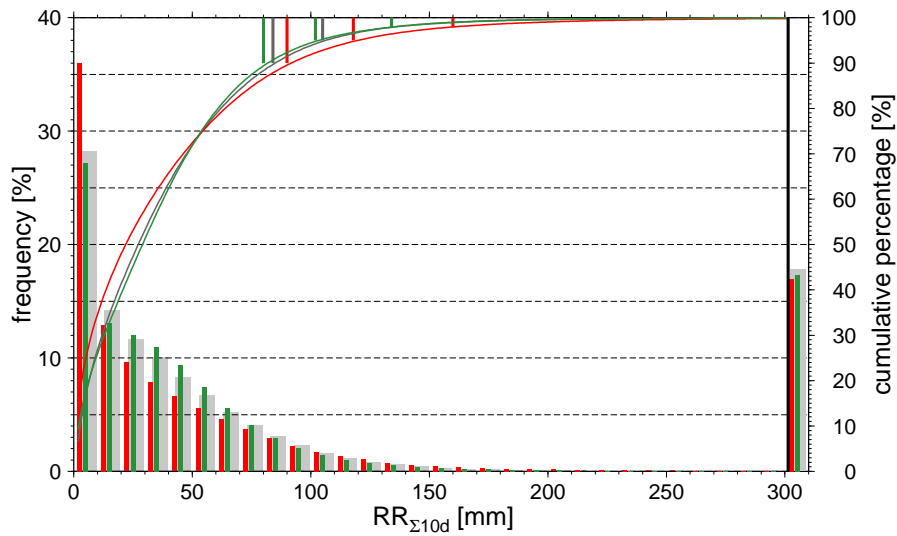


Fig. 4.2: Frequency distribution of daily values of 10-day accumulated precipitation ($RR_{\Sigma 10d}$) for IRD (black line and grey bars) as well as REMO(raw) (red lines and bars) and REMO(cor) (green lines and bars) precipitation with regard to 1968-1990. Note that the frequency distribution is based on 10 mm intervals. Illustrated is also the cumulative percentage (curves; see right scale). In addition, the 90th, 95th, and 98th percentile of daily $RR_{\Sigma 10d}$ values are indicated (small vertical lines). Moreover, to the right of the vertical black line at 300 mm the ratio of 10-day episodes with no rainfall ($RR_{\Sigma 10d} = 0 \text{ mm}$) is given (see right scale).

REMO seems to simulate a correct frequency of dry episodes. The percentage of days with zero $RR_{\Sigma 10d}$ is comparable for all three data sets (right bars in Fig. 4.2 and cp. Fig. 4.1). West Africa is affected by dry conditions for about 45% of the year, which is mainly due to the prominent dry season between October/November and March-May. By contrast, due to the regular occurrence of rain events during the boreal summer monsoon season (e.g., Fink et al. 2006) $RR_{\Sigma 10d}$ is always expected to exceed zero.

Regarding 10-day episodes, REMO(raw) shows a higher frequency of small and excessive rainfall amounts. In contrast, more moderate accumulations are underrepresented in REMO simulations (Fig. 4.2). Between 10 and 90 mm, REMO(raw) values are less frequent than that of IRD. However, excessive rainfall episodes are overrepresented in REMO simulations. Regarding REMO(cor), slightly disproportionate values are only found between 20 and 70 mm.

As a result, cumulative percentages of accumulated frequencies are closer to IRD in REMO(cor) than in REMO(raw). With regard to REMO(raw) below (above) about 50 mm cumulative percentages are higher (lower) than that of IRD and REMO(cor). By contrast, the cumulative percentage of REMO(raw) runs fairly close to that of IRD. This fact is also shown by the 90th, 95th, and 98th percentile of daily $RR_{\Sigma 10d}$ values.

4.2 REMO precipitation versus CRU

In this section, REMO precipitation is validated against CRU for most parts of Africa. CRU provides valuable information with regard to the year-to-year variability and spatial distribution of precipitation. The observed and simulated seasonal cycle of rainfall and its interannual variability are compared for the Sahel, NeA, and EEA.

Due to the long persistence of the ITCZ near the equator, the highest rainfall amounts are in general found at equatorial Africa (Fig. 4.3a). According to CRU, between 1960 and 2000 three rainfall maxima are found. The highest rainfall values are found in the Guinean and Adamawa mountains as well as in the Ethiopian Highlands. Much like IRD (see Fig. 4.1), RR_a strongly decreases towards the Sahara. CRU furthermore shows the presence of the Dahomey Gap between Nigeria and Ghana (Vollmert et al. 2003). Note also that CRU mainly suffers from a shortage of data in Angola, Zaire, Eastern Somali, Saudi Arabia, as well as the Sahara (Fig. F.1a). For this reason, the bias correction of REMO is not as reliable in these areas as in other regions. Fortunately, sufficient data is available for the Sahel as well as for most parts of the Greater Horn of Africa, where major changes in the malaria exposure are expected (cp. Sec. 2.8).

REMO(raw) reveals major differences in comparison with CRU (Fig. 4.3b). REMO simulates much higher precipitation amounts in the Congo Basin. In parts of this area, RR_a is 1000 mm higher in REMO(raw) than in CRU. Again in agreement with IRD (Fig. 4.1), rainfall is often higher for the Guinean coast. However, REMO seems to underestimate RR_a at the windward side of the Guinean mountains as well as in southwestern Nigeria. The comparison with CRU also shows that REMO generally simulates too low RR_a in the Sudanian and Sahelian zones, which is due to the lower RR_m until August (Fig. 4.4a). In contrast, bias-corrected REMO precipitation exhibits realistic RR_a for the Sahel, but reduced amounts of more than 150 mm for certain parts of the area around about 5-10°N (Fig. 4.3c), due to the fixed lower limit of the applied quotient (cp. App. C.3).

A somewhat mixed picture is found for the Greater Horn of Africa. Values for REMO(raw) are too high along the coast of Somalia, Kenya, and parts of Tanzania. Strong rainfall differences are found in Ethiopian Highlands. However, in such regions REMO simulations might represent more realistically elevation effects. As noted in Sec. 3.8, CRU mainly suffers from interpolation errors, particularly in mountainous regions. Unfortunately, this fact also results in a smoothing of bias-corrected precipitation in areas such as the Ethiopian Highlands. In NeA, REMO simulates lower than

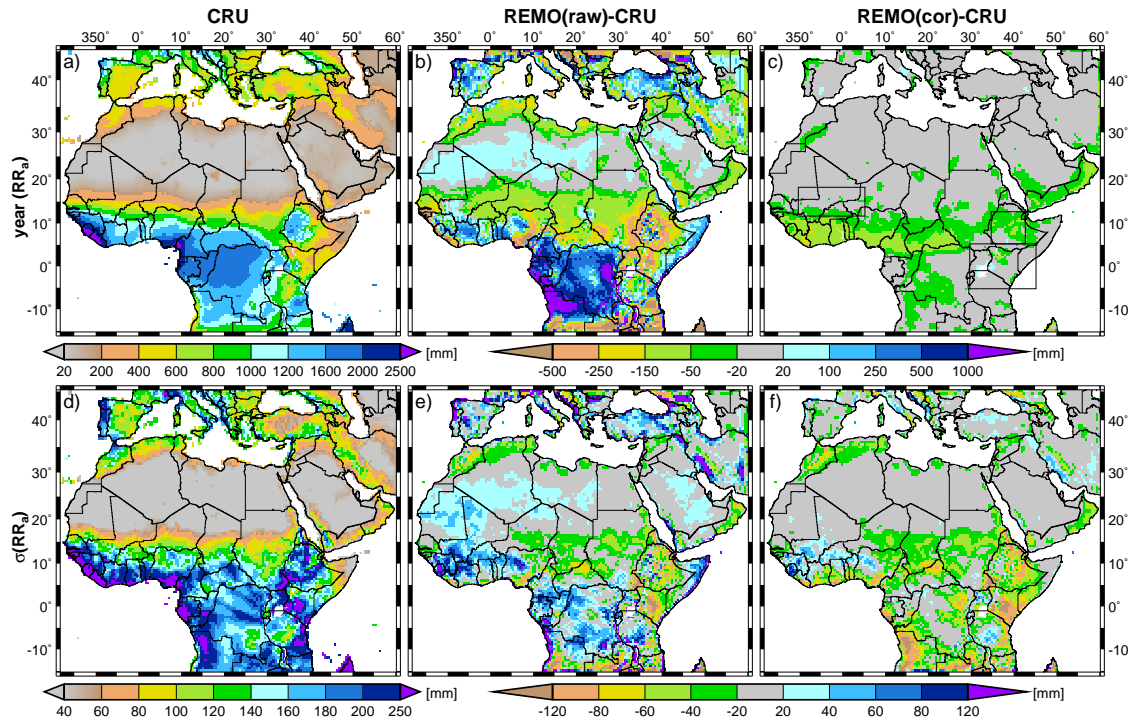


Fig. 4.3: Observed CRU rainfall (in mm) as well as the difference between CRU and REMO(raw) (REMO(raw)-CRU) as well as REMO(cor) (REMO(cor)-CRU) precipitation. (a-c) Annual precipitation amount (RR_a) and (d-f) its standard deviation.

observed RR_m from January-September (Fig. 4.4b). Conversely, rainfall is underrepresented for various parts of East Africa. Here it is interesting to note that for the EEA region REMO simulates only about half of the observed rainfall of the long rains (Fig. 4.4c and cp. Sec. 2.1.2). In fact, the short rains are more abundant in REMO than the long rains, which is the opposite of what is observed. These shortcomings are all overcome by the bias correction.

As expected, CRU exhibits a high *interannual variability* (σ) of annual rainfall in areas of high RR_a (see Fig. 4.3a & d). $\sigma(RR_a)$ is particularly strong along coastal areas, for example, at the Guinean coast. However, in these areas $\sigma(RR_a)$ reaches often less than 20% of RR_a . Remarkable is the strong year-to-year variability in large parts of the Greater Horn of Africa (cp. Sec. 2.1.3), which reaches in certain parts nearly 50% of RR_a (Fig. F.1b).

REMO simulates a higher than observed interannual variability of rainfall for the Congo Basin as well as for West Africa, which is reduced by the bias correction (Fig. 4.3e & f). Note that the result for West Africa contradicts the finding of Paeth et al. (2009), who showed that the year-to-year variability of monthly precipitation is clearly underestimated during the summer monsoon. It is speculated that Paeth et al. (2009) erroneously computed the ensemble mean of $\sigma(RR_m)$ (e.g., the average value of three ensemble runs for single years would result in a much lower value of $\sigma(RR_m)$ rather than the standard deviation with regard to every simulated year of the ensemble runs; see also App. C.5). However, an investigation of time series of RR_a reveals a fairly strong inter-

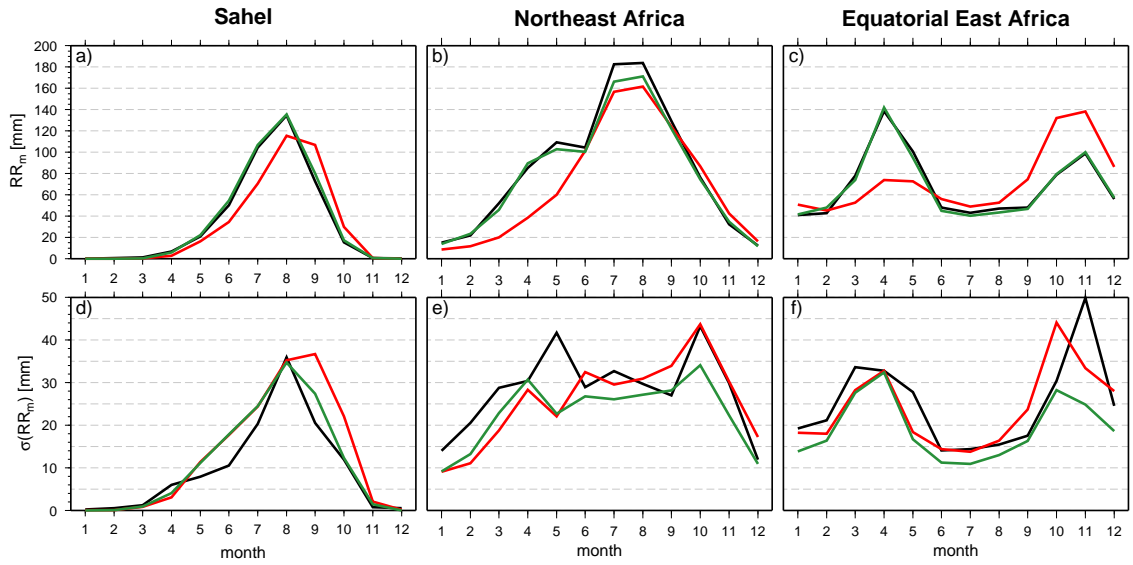


Fig. 4.4: Seasonal cycle of precipitation of the Sahel (12–18°N, 10°W–5°E; a and d), NeA (5.5–12.5°N, 35–42.5°E; b and e), and EEA (5°S–5°N, 30–45°E; c and f) averaged for 1960–2000. Inserted are the CRU (black lines) as well as REMO(raw) (red lines) and REMO(cor) (green lines) values. (a–c) Monthly precipitation (RR_m) and (d–f) its standard deviation ($\sigma(RR_m)$). Note that only data from land grid points is used and for the areas see the inserted boxes in Fig. 4.3c.

annual variability for each single ensemble run (Fig. F.2). Obviously, simulated rainfall is not correlated with observed Sahel rainfall since REMO was not driven by observed SSTs (cp. Sec. 7.1). Also the interannual variability of the seasonal cycle of the REMO simulation is comparable to CRU.

In the area of NeA, REMO simulations reveal both higher and lower interannual variability of rainfall in comparison with CRU (Fig. 4.3e). $\sigma(RR_a)$ is partly higher in REMO(raw) than in CRU, which might again be better captured by REMO simulations (cp. above). Seasonality of $\sigma(RR_m)$ compares fairly well with observed values for the area as a whole (Fig. 4.4e).

REMO is clearly not reproducing the strength of the year-to-year variability in the central part of Kenya and in northwestern Kenya. For EEA as a whole, REMO(raw) mostly underestimates $\sigma(RR_m)$ during the course of the year. Moreover, the timing of the year-to-year variability for the short rains is incorrectly reproduced by REMO(raw) (Fig. 4.4f). The strongest value of $\sigma(RR_m)$ is simulated in October rather than in November. By contrast, the bias correction markedly reduces the interannual variability of the short rains.

4.3 ERA40 temperatures vs. station data

In this section, it will be shown that ERA40 (Sec. 3.9) as well as reconstructed time series (App. C.2) reveal approximately the same seasonal cycle and interannual variability of daily mean screen-level temperatures. On this account, it is concluded that ERA40 as

well as generated station time series form an useful basis for the correction of the REMO temperature bias and the modelling of malaria, respectively.

In contrast to REMO (see Sec. 4.4), the ERA40 temperature analysis correlates well with weather station observations in West Africa (Fig. 4.5a). This is expected since station observations are included in the ERA40 two-dimensional univariate statistical interpolation of screen-level temperatures (Simmons et al. 2004; cp. Sec. 3.9). The seasonal cycle is well captured by ERA40 temperatures. The strength of the two maxima, one during boreal spring and another during boreal autumn, is realistically reflected in the analysis. Also the secondary minimum during the relative cool and humid conditions of the summer monsoon season is well represented by ERA40. In addition, the primary minimum caused by the drop in solar radiation during the cold dry season is reproduced by ERA40 (Ermert and Brücher 2008).

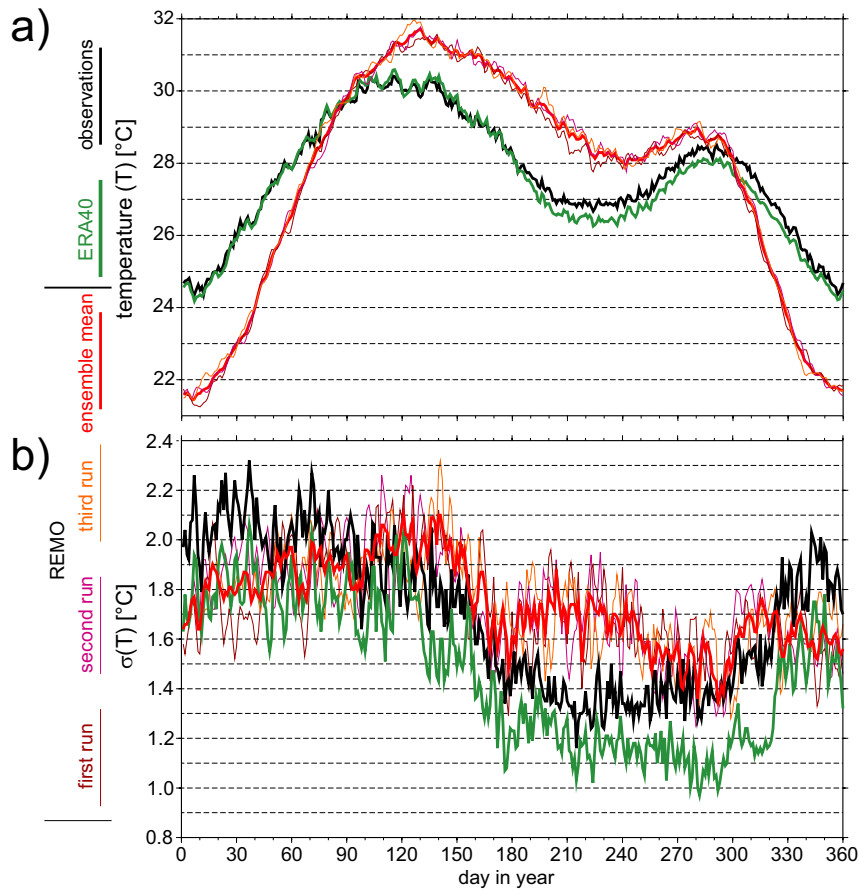


Fig. 4.5: Composite of the annual cycle of (a) daily mean temperatures (T) and (b) their standard deviation ($\sigma(T)$) for 1973-2000 (except for Magaria: 1980-2000 and Po: 1983-2000) of observations at 32 West African synoptic stations (black line; Tab. G.1, but without Douala and Koundja Fomban) as well as related grid point data from REMO (red(dish) lines; including three ensemble runs and their average) and ERA40 (green line).

For the interior of West Africa, ERA40 temperatures are particularly comparable to reported values of synoptic stations. However, ERA40 temperatures are often somewhat lower (often 0-0.5°C) than corresponding observed temperatures (not shown). Differ-

ences between ERA40 and station measurements become larger for stations that are closer to the Atlantic Ocean. The largest differences occur along the coast of Senegal and The Gambia. Between February and June, ERA40 temperatures are up to 8°C higher than recorded measurements at Saint-Louis, Dakar, and Banjul. During this period of the year low observed temperatures might originate from the cold Canary current (Fall et al. 2006). Such small-scale oceanic factors are probably not well captured in ERA40 simulations.

Also the interannual variability of temperatures from the ERA40 model is comparable to that of observations (Fig. 4.5b). However, ERA40 slightly underestimates the year-to-year variability of temperatures. Compared to observations various locations show particularly high standard deviations during spring time between March and May (not shown).

Hoshen and Morse (2004) state that daily mean temperatures from ERA40 compare poorly with observations. They therefore applied daily maximum temperatures with an offset by -5°C to roughly represent daily mean temperatures. At least for West Africa this statement cannot be verified. As shown here, reanalysis-based temperatures correlate well with station data and seem to be a useful tool for verification and modelling purposes. Note finally that statements are based on data from reconstructed temperature time series, which not necessarily represent real atmospheric conditions. However, the agreement between ERA40 and time series also suggests that the generation of a realistic station data base was successful.

4.4 REMO temperatures vs. station data

The validation of atmospheric models is usually performed by the comparison with observations or atmospheric reanalyses such as ERA40. In this section, REMO temperatures are compared for 1973-2000 with reconstructed time series of 34 synoptic stations (Tab. G.1; cp. App. C.2) as well as ERA40. In the following section, REMO(raw) temperatures are additionally verified two-dimensionally by means of ERA40.

The analysis of the mean seasonal cycle of daily mean temperatures shows large differences between REMO temperatures and observed data (Fig. 4.5a). REMO overestimates in general the amplitude of the seasonal cycle, which Paeth et al. (2009) relate to an incorrect simulated cloudiness. The observed seasonal cycle ranges between about 24 and 31°C for the average of the considered stations. However, REMO simulates daily mean temperatures between about 21 and 33°C. During boreal winter, REMO temperatures are about 3°C lower than observed. The negative deviation is the highest in December and January in the interior of West Africa (e.g., 6°C at Natitingou).

REMO simulates the first annual temperature maximum in boreal spring about one month later and its value is about 2-3°C higher in REMO than at the stations. The high temperature excess of up to 3°C at Cotonou and Yaoundé during February-April is

particularly remarkable (not shown). This is probably related to the delay in the onset of the West African summer monsoon in REMO (see Sec. 4.1).

During the summer monsoon temperatures in REMO are up to 3°C higher than measurements in the Sudanian and Sahelian zones. This is linked to underrepresented rainfall amounts (cp. Sec. 4.1), which lead to a reduced evapotranspiration and hence to a diminished evaporative heat loss during the rainy season. By contrast, the second and minor annual temperature maximum is simulated at about the right strength and time of the year. At the end of the rainy season (October/November) the difference between REMO and observations becomes increasingly negative until the turn of the year.

In summary, REMO overestimates the amplitude of the seasonal temperature cycle. Temperatures are too low (high) during the dry (rainy) season.

4.5 REMO temperatures vs. ERA40

In this section, REMO temperatures are validated against ERA40 for the whole REMO domain. As described (App. C.4), the comparison is carried out by the *potential temperature at 850 hPa* (θ_{850}).

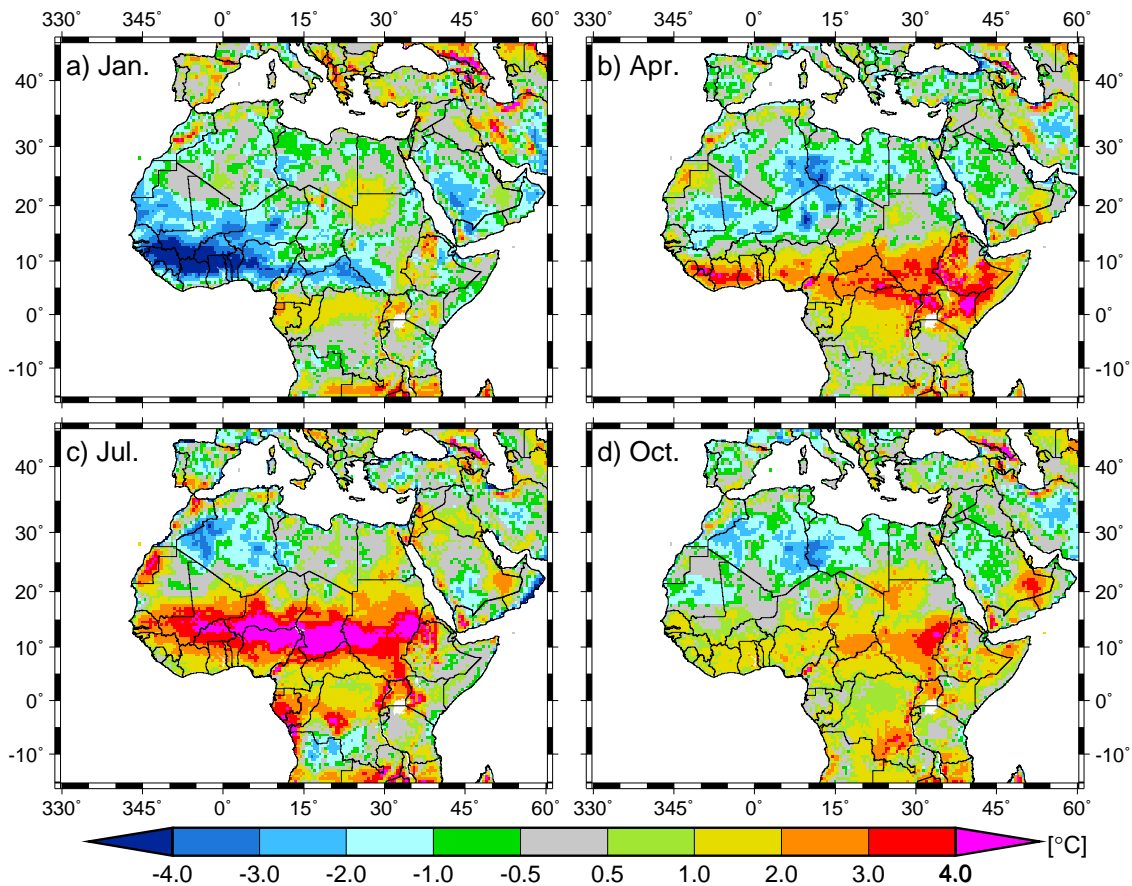


Fig. 4.6: Differences in monthly averaged potential temperatures at 850 hPa ($\Delta\theta_{850}$) between REMO and ERA40 with regard to 1960-2000 (REMO-ERA40) exemplary for (a) January, (b) April, (c) July, and (d) October.

As already noted, REMO overestimates the amplitude of the seasonal cycle in West Africa. The same holds for other parts of Africa, such as East Africa and Central Africa (Fig. 4.6). The most pronounced negative θ_{850} deviations (up to 4°C) occur during boreal winter and are located above the West African subcontinent (Fig. 4.6a). By contrast, higher temperatures are simulated in an expanded zonal strip. Until August this strip covers the whole continent in east-west direction and is pushed towards the Sahara (Fig. 4.6b & c). Again, θ_{850} values are 4°C higher in certain parts in REMO than in ERA40, and the temperature excess is pronounced along the Sudanian and Sahelian zone. About the same is true for the Ethiopian Highlands. Also highland areas of Eastern Kenya reveal higher θ_{850} (Fig. 4.6b & c).

This analysis confirms the findings from station time series (Sec. 4.4). Also the ERA40 data reveals an overrepresented amplitude of the REMO seasonal temperature cycle. REMO temperatures have therefore been bias-corrected (App. C.4) to ensure a realistic data input for malaria simulations.

5 Malaria modelling

The modelling of malaria transmission is a prerequisite for risk assessment of malaria in Africa. In this study, three different malaria models are used to dissect the uncertainty of malaria models. In the first step, the LMM is applied to precipitation and temperature data from REMO (Sec. 5.1). This model produces realistic transmission rates (cp. Sec. 6). However, the LMM suffers, for example, from the fact that it does not account for the immunity status of humans. On this account, the LMM data is subsequently used to run the Garki model (Sec. 5.2), which includes malaria immunity as well as the age-distribution of *PR*. Fully independent of this model chain are results of the MSM (Sec. 5.3), which enable the analysis of the malaria seasonality under climate conditions. Common to all these models is the fact that they do not account for non-climatic malaria factors. This means that besides LUC changes, which are included in REMO data, the present study only accounts for climatic factors affecting the spread of malaria.

5.1 Liverpool Malaria Model (LMM)

The LMM is a weather-driven, mathematical-biological model of malaria parasite dynamics and was originally formulated by Hoshen and Morse (2004). In the present study, this dynamical malaria model is applied for the projection of the spread of malaria under future climate conditions. The LMM is based on full dynamics of the host-vector-parasite triangle (Hoshen and Morse 2004). Different developments of the malaria parasite in the mosquito vector as well as the human host are included in independent sub-models. The LMM simulates the spread of malaria at a daily resolution using *daily mean temperature* (T) and *10-day accumulated precipitation* ($RR_{\Sigma 10d}$). For a detailed mathematical formulation of the *original LMM* (LMM_o) version it is referred to Hoshen and Morse (2004). However, a detailed justification of the setting of various model parameters is missing in their study. For this reason, the results of an extensive literature survey with regard to entomological and parasitological malaria data is presented here. As a consequence of this review, certain parameter ranges are specified for various model variables (cp. Tab. 5.1). The possible range of values provide valuable information for the development of a *new LMM* (LMM_n) setting (this Sec. and Sec. 6). Moreover, the validation of the LMM at locations in West Africa and Cameroon reveals some basic

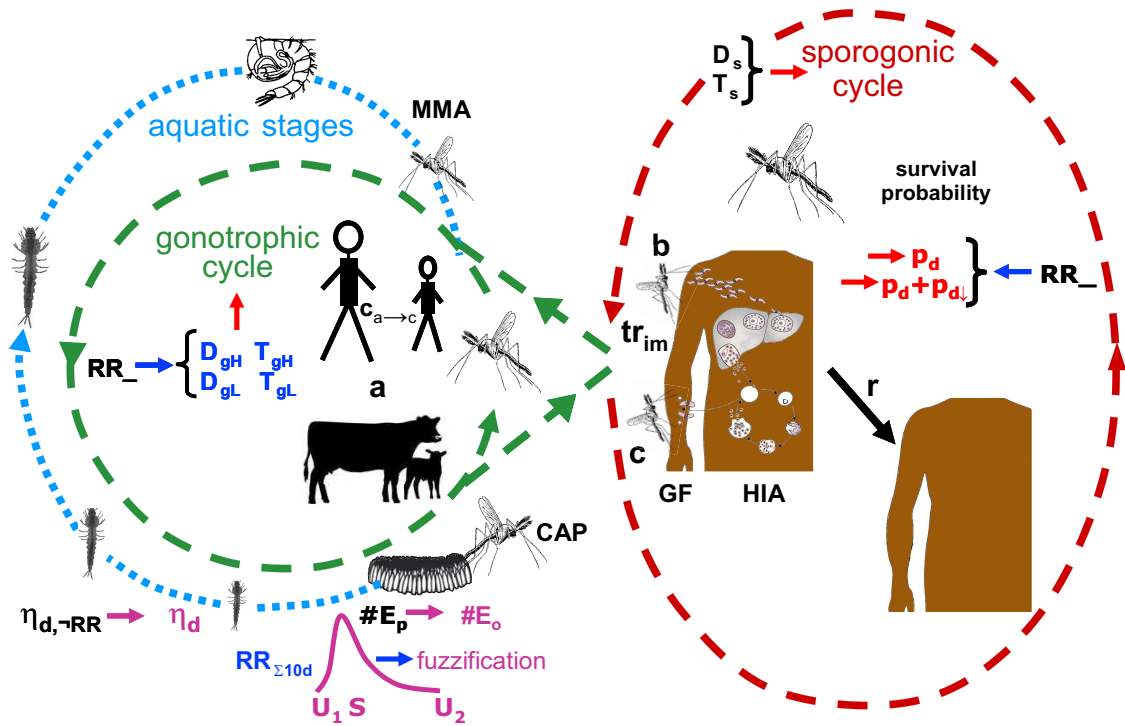


Fig. 5.1: Illustration of various components of the new LMM version. Blue and red arrows depict the rainfall and temperature dependence of various parts of the model, respectively. The fuzzification of the egg deposition as well as the immature mosquito survival is displayed by pink arrows. Note that abbreviations of model parameters are explained in Tab. 5.1.

inadequacies of the original formulation of the model (cf. Sec. 6). On that account, the simulation of some key processes is changed in the LMM_n in order to reflect a more physical relationship. Furthermore, future improvements of the model are proposed, provided that additional knowledge is available.

5.1.1 Gonotrophic cycle

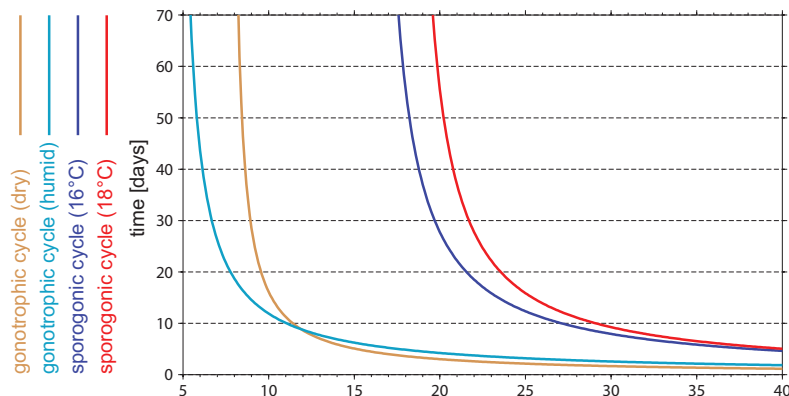


Fig. 5.2: The effect of temperature on the duration of the gonotrophic cycle (n_g) with regard to dry and humid weather conditions. Also illustrated is the impact of temperature on the sporogonic cycle length (n_s) relative to temperature thresholds of 16 and 18°C.

Tab. 5.1: LMM model parameters and their original (Hoshen and Morse 2004) and new settings. Columns: sym: symbol of the model parameter; parameter: name of the parameter; unit: unit; val_o: LMM_o value; ref_o: LMM_o reference; val_n: LMM_n value; ref_n: LMM_n reference; R_{sens}: range of values used for the sensitivity analysis; R_{lit}: literature values. Abbreviations: NU: not used; NA: not available.

sym	parameter	unit	val _o	ref _o	val _n	ref _n	R _{sens}	R _{lit}
D_{gH}	humid degree days of the gonotrophic cycle	°days	37.1	Detinova 1962	37.1	Detinova 1962	37.1	37.1
D_{gL}	dry degree days of the gonotrophic cycle	°days	65.4	Detinova 1962	65.4	Detinova 1962	65.4	65.4
T_{gH}	humid T_g	°C	7.7	Detinova 1962	7.7	Detinova 1962	7.7	7.7
T_{gL}	dry T_g	°C	4.5	Detinova 1962	4.5	Detinova 1962	4.5	4.5
RR_{-}	10-day accumulated precipitation threshold	mm	10	NA	10	NA	10	NA
RR_{\bullet}	rainfall laying multiplier	-	1.0	NA	NU	NA	NA	NA
$\#E_p$	number of produced eggs per female mosquito	-	NU	NU	120	Tab. D.7	50-200	5-290
$\#E_o$	number of oviposited eggs per female mosquito	-	NU	NU	Eq. 5.3	NA	see S/U ₂	NA
U_1	lower threshold of unsuitable rainfall conditions (fuzzy distribution model)	mm	NU	NU	0	Craig et al. 1999	0	0
S	most suitable rainfall condition (fuzzy distribution model)	mm	NU	NU	10	NA	5-50	NA
U_2	upper threshold of unsuitable rainfall conditions (fuzzy distribution model)	mm	NU	NU	500	NA	50-1000	NA
CAP	cap on the number of fertile mosquitoes	-	10,000	NA	400	NA	0-1000	NA
MMA	mosquito mature age	days	15	Jepson et al. 1947	12	Tabs. D.8 & D.9	10-20	11.2-30
$\eta_{d,-RR}$	rainfall independent daily immature mosquito survival	%	NU	NU	82.5	Tab. D.8	50.0-100.0	52.7-99.9
η_d	daily immature mosquito survival	%	Eq. 5.5	NA	Eq. 5.6	NA	-	52.7-89.9

to be continued

Tab. 5.1 – continued

sym	parameter	unit	val ₀	ref ₀	val _n	ref _n	R _{sens}	R _{lit}
p_d	daily mosquito survival	%	Martens I	Martens 1997	Martens II	Martens 1997	Martens II	Sec. 5.1.5, Tab. D.10
$p_{d\downarrow}$	dry season mosquito survival probability shift off	%	NU	NU	-10	NA	-20-0	Sec. 5.1.5, Tab. D.10
D_s	degree-days of the sporogonic cycle	°days	111.0	Detinova 1962	111.0	Nikolaev 1935	111.0	111.0-204.4
T_s	sporogonic temperature threshold	°C	18	Detinova 1962	16	Detinova 1962	18	14.2-19.0
a	human blood index	%	50	NA	80	Tabs. 5.2 & D.14	80	0-100
b	mosquito-to-human transmission efficiency	%	50	NA	30	Tab. D.13	30	1-50
$c_{a \rightarrow c}$	adult-to-child conversion rate	-	NU	NU	0.5	Carnevale et al. 1978; Port et al. 1980	0.5	0.28-0.70
HIA	human infectious age	days	14	NA	20	Tab. D.15	20	12-30
r	daily human recovery rate	day ⁻¹	0.0284	NA	0.0050	e.g. Macdonald and Göckel 1964	0.0010-0.0400	0.0015- 0.0385
GF	fraction of gametocyte carriers	%	NU	NU	50	Tab. D.11	50	10-70
c	human-to-mosquito transmission efficiency	%	50	NA	20	Tab. D.12	20	0-37.9
tr_{im}	trickle of the number of added infectious mosquitoes	-	1.01	NA	1.01	NA	1.01	NA

The model first simulates the gonotrophic cycle, that is the egg development within female mosquitoes (cp. Sec. 2.6.1). The *duration of the gonotrophic cycle* (n_g) is temperature dependent and starts at the *gonotrophic temperature threshold* (T_g), which relies on humidity conditions (Detinova 1962). Since humidity is mostly reliant on precipitation the *10-day accumulated precipitation threshold* (RR_{10d}) distinguishes between dry and humid weather conditions (variables T_{gL} and T_{gH} in Tab. 5.1 for dry and humid conditions, respectively). The LMM uses the *degree-day* concept (cp. Glossary) and calculates the daily progress of egg development within female mosquitoes. The gonotrophic cycle ends in the model when the daily sum of the temperature difference ($T - T_g$) reaches the *degree-days of the gonotrophic cycle* (D_g ; variables D_{gL} and D_{gH} for dry and humid conditions, respectively). Shlenova (1938) performed experiments on the duration of blood digestion and ovarian development in *An. maculipennis*. Various temperature and humidity combinations were used under controlled conditions. Detinova (1962) analysed this data set and found a threshold temperature of 4.5, 9.9, and 7.7°C with regard to relative humidities of 30-40, 70-80, and 90-100%, respectively. The data also reveals values for D_g of 65.4, 36.5, and 37.1°days at the aforementioned humidities. Due to the model construction and since *Anopheles* mosquitoes prefer to feed during night time (e.g., Boyd 1949) one day is added to n_g (Eq. 5.1). For reproduction of *Anopheles*, atmospheric conditions with temperatures above 20°C are ideal. At relatively low temperatures a small rise in temperature shortens the gonotrophic cycle significantly (cp. Fig 5.2). At the end of the gonotrophic cycle mosquitoes finally oviposit at suitable breeding sites and start a new gonotrophic cycle.

$$n_g = 1 + \frac{D_g}{T - T_g} \quad (5.1)$$

5.1.2 Egg deposition

Realistic simulations of the size of the mosquito population are a prerequisite for the simulation of malaria transmission between mosquitoes and humans. Egg deposition is dependent on open water bodies that are mostly filled by precipitation events. However, an accurate simulation of open water bodies is infeasible in the present study. In the LMM₀ version, the process of egg deposition has been simplified. The oviposition rate is roughly assumed to be proportional to both the number of ovipositing mosquitoes and to $RR_{\Sigma 10d}$. The proportionality is the so-called *rainfall laying multiplier* (RR_{\bullet}), which couples $RR_{\Sigma 10d}$ with the oviposition of female mosquitoes. It therefore ultimately determines the size of the mosquito population. As a result, the simulations of the LMM₀ are too sensitive to rainfall conditions in comparison with field observations (cp. Sec. 6.3). Note also that in constant mosquito habitats such as permanent ponds and rice-fields (cp. Dolo et al. 2004; Koudou et al. 2005) rainfall is not a limiting factor of malaria (Hoshen and Morse 2004).

Measurements show that the *number of produced eggs per female mosquito* ($\#E_p$; i.e., the number of eggs/mature oocytes that are found by dissection and/or oviposition of females) depends on the body size of female mosquitoes (Takken et al. 1998b) as well as on the age of females (Lyimo and Takken 1993). In general, $\#E_p$ ranges between 5 and 290 eggs (Lyimo and Takken 1993; Hogg et al. 1996; Takken et al. 1998b; see Tab. D.7). However, due to environmental conditions, not all produced eggs will be (successfully) oviposited. Note that only the last fact is included in the LMM_o version since the *number of oviposited eggs per female mosquito* ($\#E_o$) depends only on $RR_{\Sigma 10d}$. By contrast, the LMM_n version also takes into account a realistic number of eggs per *Anopheles* female (i.e., accounted by $\#E_p$).

The availability of suitable mosquito habitats is not a simple linear function of rainfall (Shaman and Day 2005). Certain rainfall regimes will be most suitable and probably no more breeding sites are provided with increasing rainfall amounts. Various studies have noted that breeding places are washed out by strong rainfall events (e.g., Gimnig et al. 2001; Drakeley et al. 2005; Shaman and Day 2005). In fact, rainfall significantly affects larvae by flushing them out of their aquatic habitat and killing them (Paaajmans et al. 2007). For these reasons, the LMM_n uses a simple fuzzy distribution model (cp. Craig et al. 1999), which has $RR_{\Sigma 10d}$ as input. The general concept is the following: (i) no or a small amount of eggs are oviposited during dry conditions; (ii) more moist conditions lead to a higher proportion of deposited eggs; and (iii) breeding places are washed out by excessive rainfall. The fuzzification therefore differentiates between *dry unsuitable conditions* (threshold U_1), a *most suitable condition* (S), and again *unsuitable conditions for very high rainfall* (threshold U_2). Obviously, U_1 is set to zero since female mosquitoes are not able to produce offspring without water supply. In contrast, even the occurrence of low precipitation values might cause standing water enabling breeding. This fuzzy distribution model might reflect a more physical relationship of the egg laying process than the construction with RR_{\bullet} of the LMM_o.

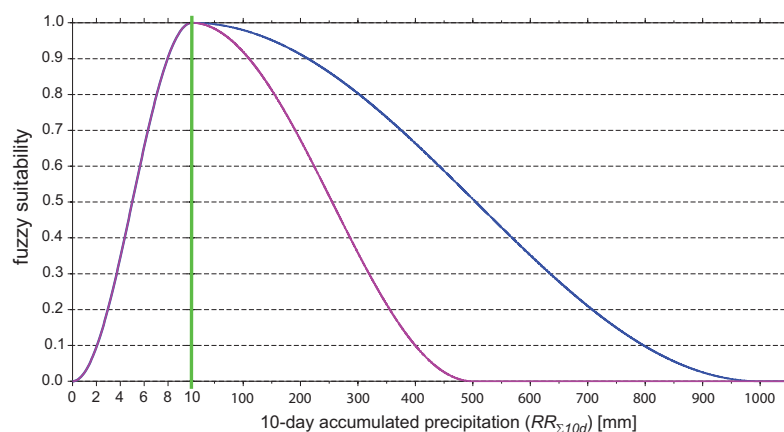


Fig. 5.3: Illustration of the fuzzy function with regard of the influence of $RR_{\Sigma 10d}$ on $\#E_o$ as well as η_d (cp. Sec. 5.1.4). The green vertical line at 10 mm ($=S$) depicts the most suitable rainfall conditions and separates different scales of the abscissa. Pink and blue lines depict two different settings of the fuzzy distribution model. According to these adjustments rainfall conditions are unsuitable for $RR_{\Sigma 10d}$ values of 0 mm ($=U_1$) and above of 500 or 1000 mm ($=U_2$), respectively.

The fuzzy distribution model computes fractions between zero (conditions unsuitable, U_1 and U_2) and one (condition most suitable, S). The *fuzzy suitability* (f) of $RR_{\Sigma 10d}$ is computed by means of a sigmoidal fuzzy membership curve (see also Fig. 5.3):

$$f(RR_{\Sigma 10d}) = \begin{cases} 1 - \cos^2\left(\frac{RR_{\Sigma 10d} - U_1}{S - U_1} \frac{\pi}{2}\right), & \text{if } U_1 < RR_{\Sigma 10d} < S \\ \cos^2\left(\frac{RR_{\Sigma 10d} - S}{U_2 - S} \frac{\pi}{2}\right), & \text{if } S < RR_{\Sigma 10d} < U_2 \\ 0, & \text{else} \end{cases} \quad (5.2)$$

The final $\#E_o$, which are included in the immature mosquito population in the model, is simply determined by multiplication of $\#E_p$ with the respective value of the fuzzy function (Eq. 5.2), that is:

$$\#E_o = \#E_p \cdot f(RR_{\Sigma 10d}) \quad (5.3)$$

Due to the protective effect of houses or usage of mosquito nets only a limited number of mosquitoes are able to contact humans. Humans therefore can only be exposed to a certain amount of biting mosquitoes. The availability of natural resources also has an impact on the growth of the mosquito population. Due to the limited flight range of mosquitoes (e.g., Gillies 1961) only a limited number of breeding sites are available for *Anopheles* females. Also, under optimal hydrological conditions for mosquito breeding, places with standing water will be confined. Provided that there are a large number of fertile mosquitoes larval densities will increase under such circumstances and will hence produce higher larval mortalities (cp. Lyimo et al. 1992; Schneider et al. 2000; Gimnig et al. 2002; Munga et al. 2006). Takken et al. (1998b) showed that high larval densities lead to higher mortality and slower gonotrophic development of adult mosquitoes due to reduced body sizes and therefore small energy resources.

All aforementioned environmental and physical causes are comprised in another model variable limiting the number of fertile mosquitoes. The *cap on the number of fertile mosquitoes* (CAP) simply restricts the size of the mosquito population to a certain level. Without the application of CAP the growth of the mosquito population is often unrealistically strong (cp. Sec. 6.2). Under favourable rainfall conditions the *number of female mosquitoes* (n_f) increases almost exponentially in time ($n_f(t) = \exp(\alpha t)$; $\alpha = \text{const.}$, time: t). A long time period of suitable weather conditions ($\alpha > 1$) therefore leads in some cases to very high mosquito numbers. Note that the size of the number of fertile mosquitoes is also limited in the LMM_o , where CAP has been set to 10,000. However, CAP will be adjusted to a much lower value in the LMM_n (see Sec. 6).

5.1.3 Mosquito Mature Age (*MMA*)

Immature mosquitoes undergo egg, larval, and pupal stages until they mature to adult mosquitoes. In the LMM₀, the *Mosquito Mature Age* (*MMA*; i.e., the time between the egg stage and adult emergence) is fixed at 15 days. However, field studies in Kenya and Mali showed that on average the time between egg deposition and eclosion is about 12 days (cp. Service 1971, 1973, 1977b; Edillo et al. 2004; Mwangangi et al. 2006; Tab. D.9). On this account *MMA* is reduced from 15 to 12 days in the LMM_n.

Development of these aquatic stages, however, depends on *water temperature* (T_w). In Kenya, Munga et al. (2006) found that the larval-to-pupal development time depends on the land cover type, which affects T_w . The mosquito pupation rate in farmland habitats is significantly greater than in swamp and forest habitats, and development times are significantly shorter (see Tab. D.8). Also *An. sergentii* showed a faster development with increased T_w in laboratory. Development from larvae to adults shortens from about 29 days at 17°C to about 11 days at 34°C (Beier et al. 1987, their Tab. 2). This temperature dependence was confirmed in maturation chambers under laboratory conditions (Bayoh and Lindsay 2003). No *An. gambiae* s.s. adults emerged below (above) T_w of 18 (32)°C. Between 18 and 32°C *MMA* was the shortest (longest) with 9.8 (23.3) days at a T_w of 28 (18)°C. Based on the obtained data, Bayoh and Lindsay (2003) computed a *larval development rate* (R) against T_w :

$$R(T_w) = -0.050 + 0.005 T_w - 2.139 \cdot 10^{-16} \exp(T_w) - 281,357.656 \exp(-T_w) \quad (5.4)$$

Similar to the advance in the gonotrophic/sporogonic cycle (Secs. 5.1.1 & 5.1.7) the simulation of immature mosquitoes could be based on T_w . However, this would require information on T_w , which generally depends on the solar insolation as well as shading of water bodies (cp. Depinay et al. 2004). Based on such knowledge a future LMM version could account for the temperature dependence of *MMA*.

5.1.4 Survival of immature mosquitoes

The life cycle of mosquitoes comprises the egg, larval, pupal, and adult stages. The egg, larval, and pupal stages are entirely aquatic and therefore mostly depend on weather conditions. Besides climatic conditions, competition due to overcrowding, water quality, food supply, cannibalism, predators, parasites, as well as pathogens are limiting factors for aquatic stages of mosquitoes (e.g., Service 1973; Koenraadt and Takken 2003; Bayoh and Lindsay 2004; Munga et al. 2006; Paaijmans et al. 2007). In the LMM₀, the *daily survival probability of immature mosquitoes* (η_d) is only subject to $RR_{\Sigma 10d}$ and is calculated as follows:

$$\eta_d = \frac{1 + RR_{\Sigma 10d}}{2 + RR_{\Sigma 10d}} \quad (5.5)$$

This leads to the fact that even under small precipitation amounts a large fraction of larvae outlives the maturation period of 15 days (i.e., MMA of the LMM_o). For example, 27.1 (49.8)% outlive the aquatic stages at a constant value $RR_{\Sigma 10d}$ of 10 (20) mm. However, age distributions from so-called *vertical life tables* reveal that a much smaller fraction (2-15%) of deposited eggs emerge to adults (cp. Service 1971, 1973, 1977b; Weidhaas et al. 1974; Aniedu et al. 1993; Mwangangi et al. 2006; Tab. D.9). By contrast, most laboratory studies prove by means of so-called *horizontal life tables* that under controlled conditions more than 90% of eggs, larvae, and pupae survive one day (e.g., Lyimo et al. 1992; Schneider et al. 2000; Gimnig et al. 2002; Edillo et al. 2004; Munga et al. 2006; Tab. D.8). The higher laboratory survival is because under controlled conditions various natural factors are eliminated. In such experiments, immature mosquitoes are generally only exposed to different temperatures, larval densities, food supply, and water qualities (see Tab. D.8). Note, these studies usually do not account for effects of predation, parasites, and pathogens, but cannibalism is included.

In the LMM_n , the calculation of the survival of immature mosquitoes is separated into two parts. In a first step, it is assumed that survival is independent of hydrological conditions. The *rainfall independent rainfall survival probability of immature mosquitoes* ($\eta_{d,-RR}$) is set to 82.5%. This is due to the fact that in general less than 10% of immature mosquitoes reach the adult stage under field conditions (Tab. D.9) and because MMA is fixed to twelve days ($0.825^{12} \approx 0.099$). In a second step, the dependence to the hydrological stage is included. Under fully dry conditions most breeding habitats will dry up. More humid conditions lead to more suitable breeding places and η_d will therefore increase. However, precipitation events as well as wind gusts result in the flushing of larvae out of, for example, puddles (Paaajmans et al. 2007). Moreover, excessive rainfall destroys larval habitats (cp. Haines and Fuchs 1991; Hay et al. 2000a; Drakeley et al. 2005). For example, Charlwood et al. (1995) observed a detrimental effect on mosquito numbers due to daily heavy rainfall. Flash flooding resulted in a fall of new recruits as the water table rose. These facts are again considered by means of the fuzzy distribution model (Eq. 5.2). Note that, for simplicity, the same parameters are used as for the fuzzification of the egg deposition (U_1 , S , and U_2 ; Tab. 5.1). Finally, the survival probability of immature mosquitoes is realised by multiplication of $\eta_{d,-RR}$ with the fuzzy value:

$$\eta_d = \eta_{d,-RR} \cdot f(RR_{\Sigma 10d}) \quad (5.6)$$

As a consequence, in the LMM_n η_d can only reach 82.5% and no more than 10% of oviposited eggs emerge to adults (i.e., about 5.4% and 0.7% for $f = 0.95$ and $f = 0.8$,

respectively). This modelling again reflects a more physical relationship than the original η_d equation (see Eq. 5.5). However, not considered is the fact that mosquito larvae can benefit from drought conditions such as when streams dry up (e.g., Wijesundera 1988; Reiter 2000; Shaman and Day 2007).

The survival of immature mosquitoes is also temperature dependent, which has been shown by laboratory experiments for *An. sergentii* and *An. gambiae s.s.* (Beier et al. 1987; Bayoh and Lindsay 2003, 2004). No egg hatching has been observed for *An. sergentii* at 34°C (Beier et al. 1987). For *An. gambiae s.s.* survival is with 72.7 (20.7)% the highest (lowest) at T_w of 30 (24)°C. However, as already mentioned (Sec. 5.1.3) at present the dependence of η_d on T_w cannot be considered in the LMM_n version.

5.1.5 Survival probability of adult mosquitoes (p_d)

The age structure of *Anopheles* females and survival rate exerts a strong influence on the reproduction rate of the mosquito population and the spread of the malaria parasite. Hence, vector survivorship is of paramount ecological importance for the distribution of malaria (e.g., Service 1976; Clements and Paterson 1981; Lee et al. 2001; McKenzie et al. 2002; Scholte et al. 2003). The *daily survival probability of female mosquitoes* (p_d) depends on characteristics of mosquito species, activities of individuals, climate, the incidence of parasites, predators (Boyd 1949), and the age of mosquitoes (e.g., Samarawickrema 1967). Most of these factors are elusive and are only indirectly taken into account in malaria models. The LMM only considers the weather impact on vector survivorship. With regard to climate the survival is affected by temperature and the relative humidity (e.g., Macdonald 1956; Hay et al. 1996). At temperatures of about 5°C or even lower mosquitoes seem to disappear (Craig et al. 1999). The entomological study of Kirby and Lindsay (2004) clearly showed that extremely high temperatures above 40°C are often fatal to mosquitoes. The LMM and most other malaria models act on the assumption that in nature few individuals die of senescence and therefore use an exponential model of mortality. This is justifiable when most mosquitoes are killed before they reach old ages (Clements and Paterson 1981). However, entomological studies showed that the mortality rate increases with age (e.g., Nájera 1974; Clements and Paterson 1981; Styler et al. 2007).

An accurate determination of the vector survivorship and its temperature dependence in the field is a matter of great difficulty (Garrett-Jones and Shidrawi 1969). Mosquito survival probabilities are usually estimated by field studies at selected locations (cp. Fig. 5.4; Tab. D.10). In some cases, meteorological data is presented with regard to the study period, at best in terms of mean temperatures or distinguishing between dry and rainy periods. Estimates are determined by inaccurate techniques, these are: captures during a cessation of recruitment (Charlwood et al. 1995), *Mark-Release Recaptures* (MRR), the ratio of different stages of ovarioles, rates of increase in infection, *parous* rates, and the observation of mortality in mosquitoes maintained in labora-

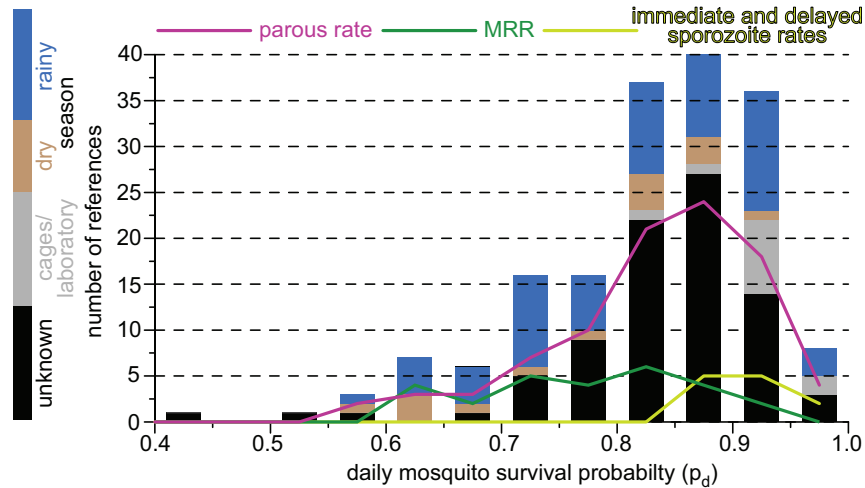


Fig. 5.4: Number of references with regard to p_d values fragmented into intervals of 5% (bars). Observations are partially allocated to humid and dry weather conditions as well as keeping in cages or laboratories. For three ways of p_d determination, the number of references is displayed additionally (lines), these include parous rates (magenta), MRR (turquoise), and immediate and delayed sporozoite rates (light green). Further data and further information are presented in Tab. D.10.

tory (Kiszewski et al. 2004). For example, the proportion parous depends not only on p_d but also on output of breeding places. At start of rainy seasons parous rates and thus p_d values drop due to the great abundance of young *nulliparous* females. By contrast, during dry seasons the p_d estimate increases as a consequence of low ‘birth rates’ (Nájera 1974). Moreover, Kiszewski et al. (2004) found that mark-recaptures reveal the highest mortalities, probably due to damages of mosquitoes when they are first captured. By contrast, the survival of laboratory-reared mosquitoes exceeds those derived in natural settings. This is not surprising since predators and other hazards of the wild take a toll of mosquito life (Clements and Paterson 1981). As previously discussed, the data suggests a higher survival in rainy than in dry seasons (Fig. 5.4). Only few studies reveal probabilities lower than 60%. Most studies derived mosquito survival probabilities of 80-90%. This finding is in agreement with the study of Kiszewski et al. (2004); they applied a median daily survival value of 84.6%.

Various mosquito survival probability schemes (p_d -scheme) were developed with regard to the modelling of malaria. In the LMM, four different p_d -schemes are implemented, these are: the so-called *Lindsay-Birley*, the *Martens I*, the *Martens II*, and the *Bayoh scheme* (Fig. 5.5). Initially, the LMM was set by the Lindsay-Birley scheme (Hoshen and Morse 2004, 2005). Despite the fact that it is not clear if vector survival per gonotrophic cycle is constant (Hoshen and Morse 2004), Lindsay and Birley (1996) assume a constant mosquito survival of 50%, which furthermore separates for humid and dry weather conditions. However, this p_d -scheme is unrealistic at very high temperatures. Experiments performed by Kirby and Lindsay (2004) showed that 50% of *An. arabiensis* and *An. gambiae* s.s. are killed at 40°C within at least two hours. In contrast, above 40°C the Lindsay-Birley scheme shows unrealistic high survivorships (cp. Fig. 5.5).

There is only limited information available in terms of the dependence of mosquito survival on temperatures. Literature (e.g., Craig et al. 1999; Hay et al. 2000a) hence refers to studies published by Martens (Martens et al. 1995a,b; Martens 1997). Martens (1997) states (see also Martens et al. 1995a,b): ‘Relying on data reported by Boyd (1949), Horsfall (1955), and Clements and Paterson (1981), we assume a daily survival probability of 0.82, 0.90, and 0.04 at temperatures of 9, 20, and 40°C, respectively, expressed as:

$$p_d = \exp\left(\frac{-1}{-4.4 + 1.31T - 0.03T^2}\right). \quad (5.7)$$

The so-called Martens I scheme was obviously generated as a polynomial connecting the quoted three data points in the T - p_d -diagram (Fig. 5.5) and is based on the following equation:

$$p_d = -0.0016T^2 + 0.054T + 0.45 \quad (5.8)$$

The formula (Eq. 5.7) provided by Martens (1997) is not considered in the LMM_0 . However, in the LMM_n this formula is introduced and forms the so-called Martens II scheme. The main difference between the Martens I and II schemes is the more smoothly decrease of p_d at temperatures above 25°C in the Martens I scheme.

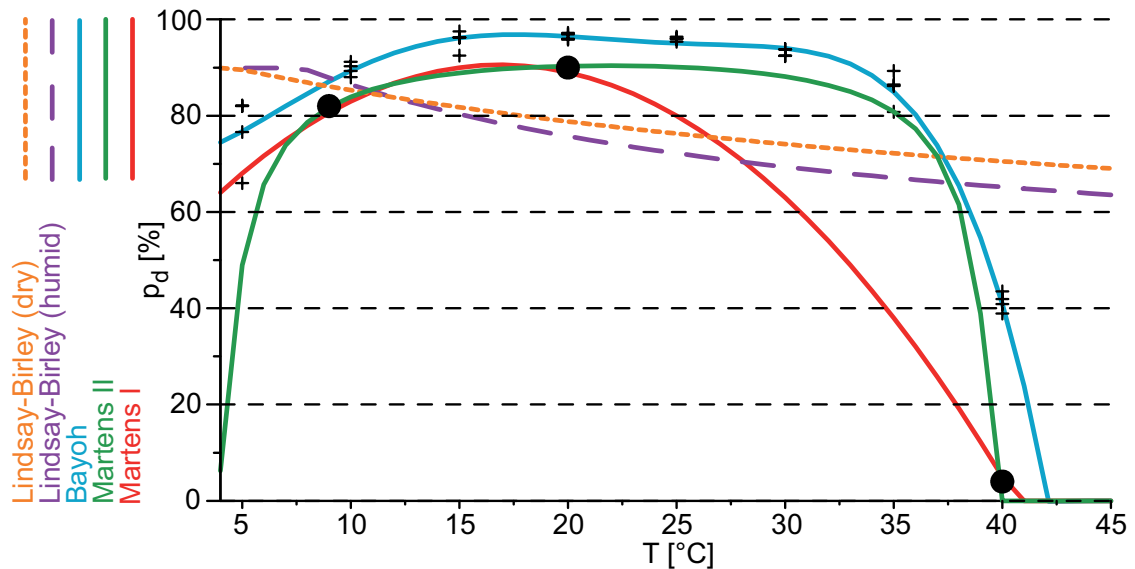


Fig. 5.5: Illustration of different schemes regarding the daily mosquito survival (p_d) against daily mean temperatures (T): the Lindsay-Birley (humid (dry) conditions in dashed purple (orange)), the Martens I (red line; derived from Martens et al. 1995a,b; Martens 1997), the Martens II (green line; given by Martens 1997 and Craig et al. 1999), and the Bayoh scheme (blue line; derived from Bayoh 2001). Crosses (+) denote p_d values with regard to different temperature and humidity conditions (see text). In addition, the data basis of the two Martens schemes are inserted as dots (•).

Taking into account the uncertainty of the so far introduced p_d -schemes, further data is needed. Bayoh (2001) observed survival and mortality rates of *An. gambiae* s.s. in environmental chambers at combinations of temperatures from 0-45°C at 5°C intervals and relative humidity's of 40%, 60%, 80%, and 100%. Using data of these experiments and assuming an exponential model of mortality (cp. the discussion above) it is possible to derive p_d -values. The identified probabilities did not vary considerably with regard to different humidities. For this reason, the probabilities were averaged at each temperature. Finally, the average was used to define a polynomial regarding *An. gambiae* s.s. survivorship in laboratory, the so-called Bayoh scheme (Fig. 5.5):

$$p_d = -2.123 \cdot 10^{-7} T^5 + 1.951 \cdot 10^{-5} T^4 - 6.394 \cdot 10^{-4} T^3 + 8.217 \cdot 10^{-3} T^2 - 1.865 \cdot 10^{-2} T + 7.238 \cdot 10^{-1} \quad (5.9)$$

As previously discussed, vector survival is higher in captivity than in the wild and hence p_d is generally higher in the Bayoh scheme than in both Martens schemes. It is interesting to note that the Bayoh scheme reveals only a slight decrease of p_d between 25 and 35°C. For this reason, the Bayoh scheme agrees better with the Martens II than with the Martens I scheme. On account of these facts the Martens II scheme is utilised for the LMM_n version. However, all presented p_d -schemes are not fully satisfying. Therefore, the incorporation of upcoming new information is essential for future refinements of the LMM.

Various studies point out the importance of the atmospheric humidity on the longevity of adult vectors (e.g., Kovats and Haines 1995; Martens et al. 1995b; Lindsay and Birley 1996; Reiter 2001; Sachs and Malaney 2002; van Lieshout et al. 2004; see Sec. 2.6.1). Relative humidities above 60% seem to be preferred by most vector species. However, it is noted that the crucial factor for the physiology of *Anopheles* females might be the absolute saturation deficit rather than relative humidity (Wernsdorfer and McGregor 1988). The usual dryness of the atmosphere in arid or semi-arid areas such as the Sahel militates against longevity of mosquitoes and so against malaria transmission (cp. Macdonald 1957). In Niger, for example, *Anopheles* populations seem to drop steeply around October, when shifts in prevailing winds drastically reduce humidity. Favourable microclimates become gradually scarcer as the Harmattan conditions establish and the dry season progresses (A. Kiszewsky, personal communication, 2006). In El Salvador, Weidhaas et al. (1974) calculated lower adult survival rates for *An. albimanus* during the dry than during the rainy season. Daily survival was 65-70% and 73-91%, respectively. However, the authors note that occurrence of breeding outside the study area might be in part responsible for the high rainy season survival. On account of the possible influence of humidity on vector survival a *shift off of the dry season mosquito survival probability* ($p_{d\downarrow}$) is introduced in the LMM_n version. To simplify matters, the dry season survival (i.e., the application of $p_{d\downarrow}$) is again steered via RR_{-} (cp. Sec 5.1.1).

5.1.6 Dry season survival of the mosquito population

Existing p_d -schemes (Sec. 5.1.5) would lead to an extinction of the *Anopheles* population in the LMM and thus to the eradication of malaria. However, observations showed that even in the Sahelian zone a sizeable mosquito population survives through the dry season (e.g., Touré et al. 1998). Various processes allow mosquitoes to survive through the long dry season. At several West African villages a rapid recolonisation by few immigrants from dry season refugia was observed (Taylor et al. 1993; Fontenille et al. 1997a; Lindsay et al. 1998). Breeding sites in arid regions are highly localised at permanent springs, open wells, along rivers, or at irrigation sites (Binka et al. 1994; Julvez et al. 1997a; Charlwood et al. 2000; Coetzee 2004). In absence of suitable water for breeding, mosquitoes can survive several months in a state of lowered physiological activity (Omer and Cloudsley-Thompson 1970), or they go into hibernation/aestivation (Garrett-Jones and Shidrawi 1969; Lindsay et al. 1998; Boyd 1949; Lindsay and Birley 1996). At rural sites in eastern Sudan vector numbers increased rapidly shortly after the onset of rains (Hamad et al. 2002) probably due to a retardation of the ovarian cycle (Omer and Cloudsley-Thompson 1970; Boyd 1949). In some circumstances, eggs can survive for weeks without water (Beier et al. 1990). Mosquitoes often also feed during the dry season (Omer and Cloudsley-Thompson 1970; Hamad et al. 2002; Diuk-Wasser et al. 2005). In many cases, the presence of a complementary vector is important. For example, at the coast of Benin and Nigeria *An. melas* and *An. moucheti* maintain transmission during the dry season, when the density of the wet season vector *An. gambiae* s.s. drops (Velema et al. 1991; Awolola et al. 2002).

In the LMM, such processes are represented in a simple way. In the numerical setting, the mosquito population and malaria infection survive by a continuous influx of new infected mosquitoes. Every ten days an infected individual, that is the so-called *trickle of the number of added infectious mosquitoes* (tr_{im}), is added to the mosquito population. This trickle therefore represents breeding during the dry season, the hibernation/aestivation status, or the recolonisation of immigrant individuals from elsewhere. Note, that such a small infected mosquito population is not able to sustain a considerable level of malaria. Substantial malaria transmission is only possible when there is sufficient rain and when temperatures are favourable. However, in case of EIR , HBR , as well as n_f the trickle alone leads to comparatively high values in relatively dry regions. For some areas these levels are as high as measurements in areas of low malaria transmission, even if breeding is not taken into account (i.e., when $\#E_p$ is set to 0.0). In order to get only 'truly' simulated figures, the LMM performs two runs every time. Firstly, the model is run by the standard setting of the LMM_n version (cp. Tab. 5.1). Subsequently, $\#E_p$ is set to 0.0 and breeding due to rainfall is therefore suppressed in the second run. Finally, values of EIR , HBR , and n_f of the second run are subtracted from that of the standard run. In this way, artificial bites and mosquito numbers, which are introduced by tr_{im} are fully eliminated and LMM simulations are comparable to field observations. It is hence possible to divide between malaria and non-malaria areas and to define malaria seasons. Due to the non-linearity of the malaria prevalence PR values cannot be corrected.

5.1.7 Sporogonic cycle

The sporogonic cycle or extrinsic incubation denotes the development of the malaria parasite within the mosquito vector. The cycle starts when gametocytes are ingested by biting *Anopheles* and ends when sporozoites reach the salivary glands. Development of sporozoites is temperature dependent (e.g., Detinova 1962; Snow et al. 1997). The minimum temperature for development of malaria parasites varies experimentally and also among mosquito species (Molineaux 1988), which is mainly due to the applied line-fitting methods (Ikemoto and Takai 2000). For this reason, there is an uncertainty about the value of the *sporogonic temperature threshold* (T_s). Lindsay and Birley (1996) concluded that parasite development ceases below temperatures between 14.5 and 16°C for *P. vivax* and between 16 and 19°C for *P. falciparum*. On that account it is not surprising that T_s data given in literature is inconsistent. Various publications agree that T_s is located within a certain range (e.g., Kovats and Haines 1995; Martens et al. 1995a,b; Lindsay and Birley 1996; Epstein et al. 1998). On the other hand an accurate temperature threshold of 18°C is referred to in various publications (e.g., Bouma et al. 1994; Patz and Lindsay 1999; Githeko et al. 2000; Patz and Reisen 2001; Hoshen and Morse 2004), whereas others quote a value of 16°C or even lower (e.g., Patz et al. 1996; Charlwood et al. 1997; Martens 1997; Craig et al. 1999; Martens 1999; Martens et al. 1999; Snow et al. 1999a; Hay et al. 2000a; Ikemoto and Takai 2000; Reiter 2000; Sachs and Malaney 2002; Hay et al. 2004; Kiszewski et al. 2004).

The course of infection in the mosquito vector is again modelled via the degree-day concept. Nikolaev (1935) showed that the degree-days required for the maturation of sporozoites in an *An. maculipennis* population from Russia are 105 for *P. vivax*, 111 for *P. falciparum* and 144 for *P. malariae*. Note that the duration of sporogony is dependent fundamentally on enzyme kinetics (Sharpe and DeMichele 1977) and thus it is widely assumed to be relatively independent of vector species (cp. Guerra et al. 2008). However, due to an erroneous line-fitting method (see Ikemoto and Takai 2000) the real value of the *degree days of the sporogonic cycle* (D_s) might significantly differ. The *duration of the sporogonic cycle* (n_s) is computed as:

$$n_s = \frac{D_s}{T - T_s} \quad (5.10)$$

The setting of the threshold is particularly important when malaria is modelled in areas with temperatures in the range of T_s (e.g., in highlands of East Africa). For temperatures well above T_s the length of the sporogonic cycle much less depends upon the setting of the minimum temperature (cp. Fig. 5.2). Regarding the sporogonic cycle the LMM₀ was set by a threshold of 18°C (Hoshen and Morse 2004). However, modelled temperatures or data from weather station are unlikely to record conditions in microhabitats where vectors spend most of their time (Hay et al. 1996; Kovats et al. 2001). For example, indoor temperatures in the Usambara mountains (northeast Tanzania) have found

to be 2.6°C higher than atmospheric temperatures (Bødker 2000; Balls et al. 2004). By resting in more climatically stable and warmer houses, vectors may avoid cold temperatures and thus restrictions concerning the progress of parasite development (e.g., Epstein et al. 1998; Reiter 2001; Koenraadt et al. 2006). Therefore, altitude effects might be partly compensated when mosquitoes stay in heated houses (Malakooti et al. 1998). For this reason, the use of 16°C as a temperature threshold for parasite development is decided for the LMM_n. Based on this setting the duration of the sporogonic cycle lasts about 57, 12, and less than 10 days at temperatures of 18, 25, and 28°C, respectively (cp. Eq. 5.10 and Fig. 5.2). This is comparable with field observations from Tanzania, where the extrinsic period lasts 9-11 days at mean temperatures of 25-26°C (Lines et al. 1991).

5.1.8 Human blood index (a)

The rate of malaria transmission directly depends on the degree of the host-vector-pathogen contact. *Anopheles* mosquitoes with a high preference for human blood are considered important vectors of malaria (e.g., Muriu et al. 2008). This fact is expressed in the so-called *human blood index* (a) that is the proportion of blood meals of a mosquito population obtained from man.

Assessment of a is a difficult task as it depends on the feeding preference of each species, accessibility of different potential hosts, as well as on the mosquito sampling technique. The calculation of a is most often performed by captures of indoor resting mosquitoes (*endophilic* females) excluding *exophilic* mosquitoes feeding on humans (Diatta et al. 1998). By contrast, a is best estimated by applying the unweighted mean of a part-sample collected from human dwellings and one from other types of resting-place (Garrett-Jones 1964). Most studies reveal that the most important *Anopheles* species are *anthropophilic* that is they prefer to take blood meals on humans (e.g., for a review cp. Garrett-Jones 1964; Kiszewski et al. 2004; Moffett et al. 2007). However, some species like *An. arabiensis* tend to be more *zoophilic* than other *Anopheles* species. The preferred occurrence of *An. arabiensis* in drier areas such as the Sahel and stronger abundance of cattle in such areas seems to lead to a higher zoophilic behaviour of *An. arabiensis*. *Anopheles* are therefore adaptable to different environments and are not likely to show the same behaviour throughout Africa (Diatta et al. 1998). There are, for example, significant differences between values of a of *An. arabiensis* between East and West Africa (cp. Killeen et al. 2001). These facts underline the importance of the availability of alternative hosts and environmental conditions on the influence of a (Martens 1997).

Kiszewski et al. (2004) and Moffett et al. (2007) presented median and mean values of a from four and ten African *Anopheles* vectors (cp. Tab. 5.2; further data is provided in Tab. D.14), respectively. Major malaria vectors in Africa such as *An. arabiensis*, *An. gambiae* s.s., and *An. funestus* show fairly high values of a . Except for the mean value of a of *An. arabiensis* all median and mean values of these vectors are consistently

Tab. 5.2: Review of values of a from ten African *Anopheles* vectors as provided by Kiszewski et al. (2004) (superscript: k) and Moffett et al. (2007) (superscript: m). Columns: species: name of the mosquito specie; med: median of a ; $\#_{obs}^k$: number of observations; \bar{a} : mean a ; σ : standard deviation of a ; $\#_{ref}^m$: number of references. Columns (ii)-(iii) are taken from Kiszewski et al. (2004) and columns (iv)-(vi) are extracted from Moffett et al. (2007).

species	med ^k [%]	$\#_{obs}^k$	\bar{a}^m [%]	σ^m [%]	$\#_{ref}^m$
<i>An. arabiensis</i>	87.1	32	52.6	24.1	21
<i>An. coustani</i>	-	-	15.7	1.9	2
<i>An. funestus</i>	98.0	30	84.4	19.1	12
<i>An. gambiae</i> s.s.	93.9	36	81.5	15.9	16
<i>An. melas</i>	69.0	6	57.6	26.9	3
<i>An. merus</i>	-	-	100.0	-	1
<i>An. moucheti</i>	-	-	93.1	8.0	3
<i>An. nili</i>	-	-	94.9	5.5	3
<i>An. paludis</i>	-	-	-	-	0
<i>An. quadriannulatus</i>	-	-	1.1	-	1

higher than 80% for these three vectors. For this reason, the LMM_o value of a of 50% seems to be an underestimation. Due to the fact that the *endophily* of major African vectors probably was overestimated (cp. Vercruysse et al. 1983; Diatta et al. 1998) the value for LMM_n is approximated by 80%.

5.1.9 Mosquito-to-human transmission efficiency (b)

Not every biting infectious mosquito is able to pass malaria infection to humans. Unfortunately, the *mosquito-to-human transmission efficiency* (b ; i.e., the proportion of sporozoite-positive mosquito bites infecting susceptible people; Tab. D.13) is a largely undefined variable (Nájera 1974). For this reason, this factor was commonly ignored in most malaria models (cp. Nedelman 1984). However, the proportion of actually infective *Anophelines* is a crucial parameter in the epidemiology and simulation of malaria.

One infectious bite is generally thought to infect about half of immunologically naive people and this level seems to decrease with the level of endemicity and is age dependent (Filion et al. 2006). This transmission efficiency is a function of exposure history, reflecting effects of immunity (Gu et al. 2003b). The study of Rickman et al. (1990) showed that three (two) out of five non-immune subjects developed malaria parasitaemia after exposure to one (two) infected mosquito(es) (that means $b=33\%$). In addition, a total of 44.1% of 68 experimentally infected *An. gambiae* and 49.2% of 63 infectious *An. stephensi* transmitted sporozoites in vitro into a sucrose solution (Beier et al. 1991). By contrast, entomological observations from infants revealed fairly low b values. For example, Pull and Grab (1974) estimated the value of b as between 1.5 and 2.6%. Indeed, such studies generally ignore superinfection (Sec. 2.4.3) and the fact that

adults are bitten more often than children or infants (see Port et al. 1980; Sec. 2.4.6). Superinfection also explains the strong variation of b in children in an urban area of Senegal, where age-corrected HBR values were used for the analysis of b (Vercruysse et al. 1983). Low EIR values in March led to comparatively high b values of about 46%. By contrast, stronger transmission in June resulted in a value of b of only about 8%. In conclusion, the value of b seems to be generally lower than 50% - the original value of the LMM - for most African populations. For this reason, b is approximated as 30% in the LMM_n version.

5.1.10 Human Infectious Age (HIA)

Transmission of the malaria parasite from humans to mosquitoes is made possible by male and female gametocytes. The duration after infection until mature gametocytes appear in blood is termed here as the *Human Infectious Age* (HIA). The period in days after that a human becomes infectious starting from the mosquito bite is longer than the so-called *prepatent period* (n_p ; i.e., the time needed for the detection of asexual parasites in blood after infection of humans). This is due to the *time needed for gametocytogenesis* ($n_{\sigma\varphi}$; i.e., the time needed for production of male and female gametocytes), which is also called *sequestration time* (cp. Sec. 2.4.1), as well as the final *maturation period of gametocytes* (n_m ; meaning that $HIA = n_p + n_{\sigma\varphi} + n_m$).

Asexual parasites are usually detected by blood slides, which are examined under microscopes. According to microscope detection n_p lasts one week or slightly longer (e.g., Collins and Jeffery 1999: eight days). Schneider et al. 2005 compared the microscope with the *Quantitative-Nucleic Acid Sequence-Based Amplification* (QT-NASBA) detection method. They found that microscope detection is delayed by one to two days (n_p : 8.3 versus 6.0-7.0 days). This is in agreement with findings of Murphy et al. (1989), who cultured asexual parasites from blood taken 6.5-7.0 days after exposure. By contrast, Rickman et al. 1990 found a prolonged n_p of 14.0-16.5 days from patients without antimalarial immunity. Moreover, a study comparing the Panama, McLendon, and Santee Cooper strains of *P. falciparum* revealed mean n_p values of 10.3, 13.0 and 9.8 days, respectively (Jeffery et al. 1959).

The duration for gametocytogenesis is derived in vitro or from the delay in vivo between the onset of symptoms (e.g., fever) or detection of asexual parasites and detection of male and female gametocytes (Eichner et al. 2001). Values reported in literature generally (see cp. Tab. D.15) range between 7 and 15 days (Shute and Maryon 1951: about ten days for non-immune subjects; Miller 1958: about twelve days for immune adults; Hawking et al. 1971: nine to twelve days; Day et al. 1998: 7-15 days). Diebner et al. (2000) and Eichner et al. (2001) more recently estimated the sequestration time from fitting a model to malaria therapy data. According to their studies the time needed for transition of asexual blood stages of *P. falciparum* to mature gametocytes amounts to four to twelve days (mean 7.4 days). It is also shown that sequestration time depends on presence of the parasite strain (geometric mean: 4.9 days for Santee Cooper strain (South

Carolina, 1946); 6.2 days for El Limon strain (Panama, 1948); 8.7 days for McLendon strain (South Carolina, 1940)). Eichner et al. (2001) concluded that in former literature the time for sequestration was probably overestimated by the time needed to reach a certain level of *gametocytaemia* that can be detected by microscopy. However, gametocytes of *P. falciparum* do not infect mosquitoes, when mature forms first appear in blood. The time needed for n_m is about one to four days, when these forms of the malaria parasite finally become capacitated (cp. Macdonald 1957; Sinden 1983; Nedelman 1989).

In summary, due to the length of n_p (about six to ten days), $n_{\sigma\varphi}$ (four to twelve days), and n_m (one to four days) *HIA* lasts altogether about 11-28 days. For this reason, *HIA* is approximated as 20 days in the LMM_n version, which is five days longer than the LMM₀ value of 15 days (cp. Tab. 5.1).

5.1.11 Recovery rate (r)

A slow *recovery rate* (r) of malaria infection is a crucial factor for transmission of malaria (cp. Sec. 2.4.4). Recovery is affected by the genetic multiplicity of the malaria parasite (cp. Sec. 2.4.3) and is a function of exposure history, reflecting effects of immunity (see Sec. 2.4.2). Parasite clearance is therefore closely related to the age of an individual as well as to transmission intensity. The former fact was found in longitudinal data from 16 villages in the West African savannah (e.g., Molineaux and Gramiccia 1980, their Fig. 31). Daily recovery rates were 0.0045 in infants (<1 year), fell to a minimum of 0.0016 in young children (1-4 years), and increased again to 0.0194 in the oldest adult age group (≥ 43 years). Dependence of r on transmission intensity was found at 30 sites along coastal Kenya. Gu et al. (2003b) showed that the daily parasite clearance was lower than 0.005 day^{-1} at one or less infectious bites per year and higher at intensities of ten or more.

The LMM structure does not account for an individual immune status. As a result, r is independent from transmission intensity or age of an individual in the model, only one single setting of the recovery rate is possible (cp. Sec. 5.2). For this reason, the applied clearance rate represents an age or transmission intensity average. Due to the fact that the LMM₀ does not include superinfection (Sec. 2.4.3) parasite clearance is related to the elimination of single parasite clones (see Hoshen and Morse 2004). The recovery rate was originally set to 0.0284 day^{-1} enabling about 90% of the infected population to clear their infection after 80 days ($(1 - r)^{80} \approx 0.10$). However, estimates from simple infections of *P. falciparum* induced in immunologically naive patients for malaria therapy revealed often longer persistence. Patterns of recrudescence survived partly longer than 150 days (see Collins and Jeffery 1999, their Fig. 3). In order to further include superinfection, the parasite clearance is significantly decreased in the LMM_n and is now set to 0.005 day^{-1} . In fact, the value of 0.005 day^{-1} was previously assessed by Macdonald and Göckel (1964) and was also applied in various malaria models (e.g., Macdonald et al. 1968; Gu et al. 2003b).

5.1.12 Gametocyte prevalence (sPR)

The presence of male and female gametocytes in the blood of human hosts, that is the so-called *sexual parasite ratio* (sPR ; i.e., gametocytaemia), is a necessary condition for malaria transmission. Gametocytaemia is generally lower than PR (Fig. 5.6a). Only one *annual mean sexual Parasite Ratio* (sPR_a) was found to be higher than 40%, which has been detected by RT-PCR (see Tab. D.11). In most studies using microscopy less than 15% of the population were detected as gametocyte carriers. In contrast, the majority of studies revealed parasite prevalence higher than 30%. The *annual averaged ratio between the asexual and sexual parasite prevalence* (SAR_a ; i.e., the proportion of malaria parasite positive humans that are gametocytaemic) mainly ranges between 10 and 35% (Fig. 5.6b; Tab. D.11).

There is a problem of enumerating gametocytes patterns; gametocytes are prone to be missed by standard microscopy examination (Nedelman 1989; Drakeley et al. 2006; Sec. 2.4.5). For example, RT-PCR revealed in comparison with microscopy a 40% higher sPR (Ali et al. 2006). Ouédraogo et al. (2007) recently found that the QT-NASBA technique provided about 3.3 fold higher estimates of sPR than microscopy. This clearly demonstrates that studies based on the detection of gametocytes by microscopy are rather insensitive and inaccurate in the quantification of gametocytes in blood smears.

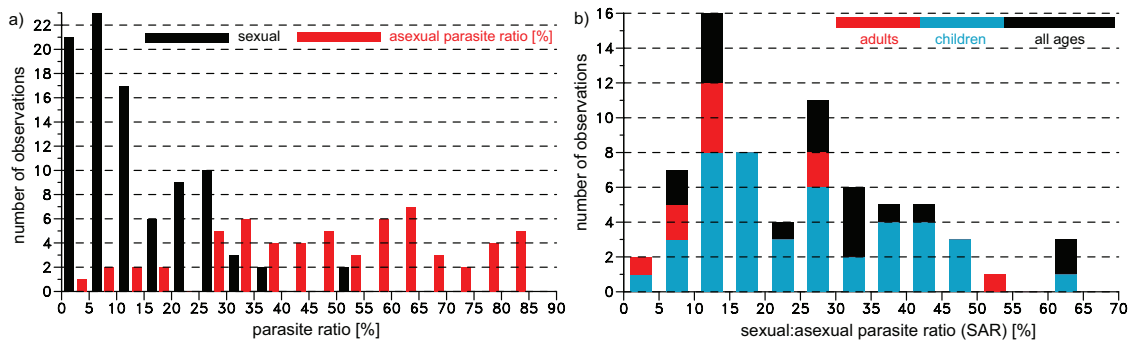


Fig. 5.6: Parasitological observations with regard to PR_a and sPR_a (Tab. D.11). Frequency distribution of (a) PR_a and sPR_a as well as (b) SAR_a . Particular observations have been grouped into 5% intervals. Note that PR values were calculated by $PR = \frac{sPR}{SAR}$.

Sexual and asexual parasite ratios are generally higher in children than in adults (Tab. D.11). That is due to the fact that adults better control asexual and sexual parasite densities, and are therefore more likely to carry gametocytes at the borderline level of detection (Drakeley et al. 2006). Young children are least likely to be able to control malaria infections, and likely more parasites turn into gametocytes. In Kenya, Bousema et al. (2004) found a decrease in the mean duration of gametocyte carriage with increasing age for asymptomatic children.

The fact that not all infected humans actually carry male and female gametocytes is accounted for in the LMM_n version. A *fraction of gametocyte carriers* (GF) is introduced into the model. This fraction stands for the proportion of the population that: (i) is infected by the malaria parasite; (ii) has already passed the length of HIA ; and (iii) is exhibiting a reasonable amount of gametocytes. These humans are therefore the infec-

tors of the human population. Due to the problem of enumerating gametocytes patterns, GF is set in the LMM_n to the comparatively high value of 0.5 (cp. Fig. 5.6).

5.1.13 Human-to-mosquito transmission efficiency (c)

Not all *Anopheles* females feeding on gametocyte-infected hosts get infected. Most malaria transmission models have not used direct field estimates of the *human-to-mosquito transmission efficiency* (i.e., the proportion of mosquito bites on infectious humans, which infect susceptible mosquitoes) that is usually termed parameter c in literature (e.g., Nedelman 1985). Because of practical difficulties of obtaining parameter c most studies rely on the assumption that infectiousness is directly related to the prevalence of blood-stage parasites or gametocytes (Killeen et al. 2006).

One factor reducing infectivity of gametocytes to mosquitoes is transmission blocking immunity that is a specific immunity acquired in humans. Immune factors, ingested with the blood meal, inhibit or block the development of free sexual stages: gamete, zygote, and ookinete, which have common antigens with gametocytes (Boudin et al. 2005).

The infectiousness of mosquitoes can be determined by using blood from gametocyte carriers. It is either measured by direct skin feeding or by membrane feeding (Bonnet et al. 2002). However, the best method for estimating infectiousness of a human population is to feed laboratory-reared *Anopheles* on a representative population sample without regard to the presence of gametocytes (Boudin et al. 1991a). Obviously, not all *Anophelines* feeding on gametocyte-infected hosts become infected. Human-to-mosquito transmission efficiencies are generally lower than 40%, and for the majority of trials infectiousness is higher than 20% (Tab. D.12). Muirhead-Thomson (1954) observed that the ‘best infectors’ infected only about 30% of mosquitoes feeding on them. On the other hand cryptic gametocytaemia can result in mosquito infections (Ross et al. 2006). In the LMM_n version, c is approximated as 20%, which is located amidst observed measurements. This means, in combination with the value of GF , that in the model a fraction of 10% of females feeding potentially malaria-infectious hosts becomes infected with the parasite.

5.1.14 Issues regarding the age-dependence of malaria

Entomological and parasitological studies clearly identified the age-dependence of malaria in areas of year-round and seasonal malaria transmission. The increase of functional immunity from child- to adulthood leads to an age-dependence of PR , sPR , r , b , as well as c . Values are comparatively much higher in children than in adults. Children therefore were found to be most likely to infect mosquitoes (e.g., Bonnet et al. 2003). There is a general decrease with age in the infectiousness but even highly immune hosts contribute to the infectious reservoir (Ross et al. 2006). A large proportion of infections results from feeding on adults since the host-vector contact is higher in adults than in

children (Carnevale et al. 1978; Port et al. 1980). That is due to their greater attractiveness (Sec. 2.4.6) and therefore most blood meals to vector mosquitoes are provided by this age group (Killeen et al. 2006).

Due to the lack of an age-dependence of the LMM it is assumed that *children between 2-10 years (groupC)* and the *rest of the population (groupR)*; these are infants, adolescents, and adults) equally contribute to the infectious reservoir of malaria. On that condition an isolated simulation of the malaria transmission based on *groupC*, *groupR*, or that of the whole population always results in the same infection level of the mosquito population and after age-adjustment also in the same *HBR* and *EIR* values. The LMM simulation is therefore henceforth orientated on *groupC*. For this reason, the host-vector contact is lowered in the LMM_n version by the *adult-to-child conversion rate* ($c_{a \rightarrow c}$). Due to findings of Carnevale et al. (1978) and Port et al. (1980) $c_{a \rightarrow c}$ is approximated as 0.5 (see Sec. 2.4.6), which means that *HBR* and *EIR* for children between 2-10 years (*HBR_c* and *EIR_c*, respectively) is two times lower than that for adults ($HBR_c = c_{a \rightarrow c} \cdot HBR$; $EIR_c = c_{a \rightarrow c} \cdot EIR$). This in turn implies that simulated *HBR* and *EIR* values have to be doubled when they are compared to field observations.

In conclusion, most model variables are set by means of data taken from literature. However, some newly inserted (these are S , U_2 , $\#E_p$, and $p_{d\downarrow}$) and one old variable (i.e., *CAP*) of the LMM_n could not be defined by the literature survey. These values are calibrated by means of entomological and parasitological data from West Africa and Cameroon (cp. Sec. 6). Due to the calibration of model parameters the aforementioned assumption relative to the contribution of different age-groups might not be of particular relevance. The calibration finally enables the LMM_n to simulate realistic entomological data, which will serve as input for the Garki model (cp. Sec. 5.2).

5.2 Garki model

Probably the most widely known and accepted integrated models of malaria transmission dynamics and immunity to date are those of the Garki project (Dietz et al. 1974; Gemperli et al. 2006a,b; for a review cf. Nedelman 1984) and variants of it (Nedelman 1985; Struchiner et al. 1989). The original version of this model was primarily developed for endemic malaria transmission in the Nigerian African savannah (cf. Molineaux and Gramiccia 1980). The Garki model was further modified for areas of unstable malaria transmission (Struchiner et al. 1989). Various other studies utilised the Garki model and its variants. For example, Struchiner's version of the Garki model was refined by Cancr  et al. (2000) using a Bayesian calibration of longitudinal parasitological data gathered from Ndiop (Senegal; 13°41'N, 16°23'W). In addition, Gemperli et al. (2006a,b) applied the original Garki model for standardisation of heterogeneous age *PR* data from field observations.

The Garki model was developed by Dietz et al. (1974). This model is a complex mass action model including the acquisition of immunity as well as the presence of su-

perinfection (cp. Fig. 5.7). It is formulated in seven non-linear difference equations that are iteratively solved by a computer (see Eq. 5.11). In a first step, this model divides the human population, which is set to one, into individuals that have parasites in their blood, the so-called *positives* (y_1 , y_2 , and y_3), and humans not carrying the malaria pathogen, the so-called *negatives* (x_1 and x_2). Those individuals with parasites in the liver are called incubating (x_2 and x_4). The duration of the incubation stage is set to N days.

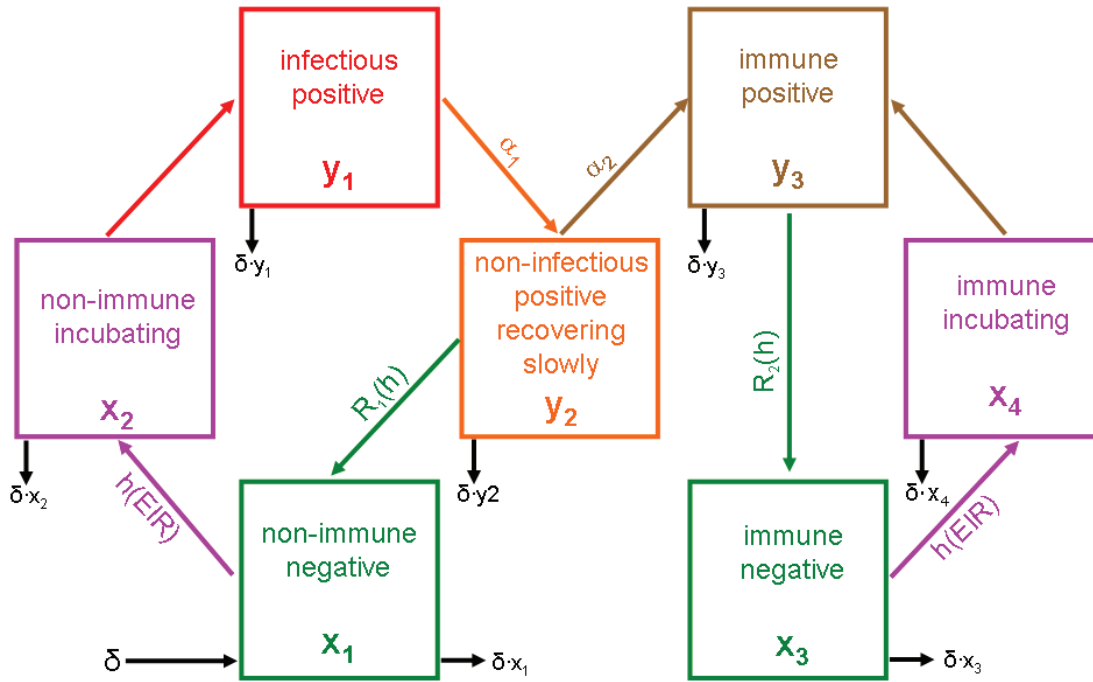


Fig. 5.7: States and transitions of the Garki model (according to Dietz et al. 1974). Included are also model parameters (see text and Eq. 5.11).

Parasitological data from eight villages in the Kano State, Northern Nigeria, revealed that the gametocyte prevalence and density decreases more rapidly with age than *PR* and the density of trophozoites. For this reason, Dietz et al. (1974) concluded that immunity reduces infectivity of humans before recovery is increased and/or detectability is reduced. In the model it is assumed that individuals with a certain parasite load are not able to infect mosquitoes to such an extent that their sporozoites can produce successful infections in humans. On this account, positives are divided into infectious (y_1) as well as non-infectious (y_2 and y_3) individuals. The loss of infectivity is acquired first at a rate α_1 , when humans reach category y_2 . The status of immunity and increase in recovery (the y_3 category) might be later acquired at the rate α_2 .

Longitudinal data from the Kano State showed that parasite clearance of *P. falciparum* depends on age (e.g., Molineaux and Gramiccia 1980, their Fig. 31). In fact, immunity increased the rate of recovery from patent parasitaemia by a factor of up to ten (Bekessy et al. 1976). For this reason, the Garki model further adopts that the acquisition of immunity (individuals x_3 , x_4 , and y_3) is directly associated with quickly recovering infection rates. Non-infectious positives are therefore further separated in y_2

with low recovery rates (r_1) and y_3 with high clearance rates (r_2) of individual malaria clones.

Malaria parasites are usually detected by means of blood films. However, the probability of detecting parasites depends on the density of trophozoites. In adults, parasite densities are usually comparatively low and are reduced to submicroscopic levels (Ouedraogo et al. 2007). Hence, positive immune individuals (y_3) have the lowest probability (q_3) of being detected in the model. Other classes of positives (y_1 and y_2) are assigned to detection probabilities q_1 and q_2 , respectively (it is assumed $q_1 = q_2$). There is furthermore no loss of immunity with respect to the higher recovery rate and lower detectability. However, the whole population loses immunity since dying immune individuals are replaced by non-immune newborn infants. The size of the human population is constant in the model, *birth and death rates* (δ) are equalised. Death rates are independent of age so that the age-distribution of the human population is exponential.

The Garki model is driven by the observed *VC*, which depends only on entomological variables. It follows directly from the definition of *VC* that each mosquito bite on an infectious individual will result in *VC* new inoculations n days later (here n is the duration of the sporogonic cycle). In fact, Dietz et al. (1974) assumed that these mosquito bites happen on day t . Based on this assumption it is possible to compute *EIR* by means of $EIR(t) = VC(t - n)y_1(t - n)$ (cp. Gempferli et al. 2006a). For this reason, a more direct approach would be to run the Garki model by *EIR* instead of *VC* data. In the following, the model defines the *inoculation rate* (h) as the rate at which negatives are transferred to positives. The following relationship is assumed by Dietz et al. (1974) for the inoculation rate: $h(t) = \lambda_{max}[1 - \exp(-EIR(t))]$. The expression in the square brackets is the probability, assuming a Poisson distribution for the number of contacts, that at least one contact is made. The parameter λ_{max} represents the *maximum rate of acquiring infections*¹ (Dietz 1988).

The presence of superinfection (for details cf. Dietz et al. 1974) and acquired immunity are considered by means of two recovery rates (R_1 and R_2). These two rates are related to the inoculation rate (h) and the recovery rate from single clone infections (r_1 and r_2): $R_i = \frac{h}{\exp(\frac{h}{r_i}) - 1}$ ($i=1,2$). Hence, non-immune individuals recover slower than immune individuals ($R_1 < R_2$).

The assumptions listed above lead to a set of differential equations (Eq. 5.11), which are written here for an iteration interval of 1 day. Note that the model operates with a time interval of five days. The Δ symbol refers to the difference operator, for example,

¹Note that this parameter was originally denoted in Dietz et al. (1974) by the misleading term ‘susceptibility (g)’.

$\Delta x_1 = x_1(t+1) - x_1(t)$. The following equations omit the time variable except in those cases, where reference is made to a time different from t :

$$\begin{aligned}
\Delta x_1 &= \delta + R_1(h) y_2 - [h + \delta] x_1 \\
\Delta x_2 &= h x_1 - [1 - \delta]^N h(t-N) x_1(t-N) - \delta \cdot x_2 \\
\Delta x_3 &= R_2(h) y_3 - [h + \delta] x_3 \\
\Delta x_4 &= h x_3 - [1 - \delta]^N h(t-N) x_3(t-N) - \delta \cdot x_4 \\
\Delta y_1 &= [1 - \delta]^N h(t-N) x_1(t-N) - [\alpha_1 + \delta] y_1 \\
\Delta y_2 &= \alpha_1 y_1 - [\alpha_2 + R_1(h) + \delta] y_2 \\
\Delta y_3 &= \alpha_2 y_2 + [1 - \delta]^N h(t-N) x_3(t-N) - [R_2(h) + \delta] y_3
\end{aligned} \tag{5.11}$$

One drawback of the Garki model is the assumption that all individuals are equally exposed to vector feeding. It would be more adequate to include age-dependent factors to accurately describe and predict dynamics of pathogen transmission (Styler et al. 2007). The model also ignores the naturally acquired immunity against pre-erythrocytic stages of the parasite. However, the Garki model was not designed for the assessment of the likely impact of malaria vaccination (cp. Smith et al. 2006b). Another handicap of the Garki model is the constant duration of the sporogonic cycle. In fact, the length of this cycle depends on temperature (Sec. 2.6.1) meaning that this model version does not properly work in highland areas.

Tab. 5.3: Parameters of the Garki model and their setting (cp. Dietz et al. 1974). Columns: sym: symbol of the model parameter; parameter: parameter name; val: value; unit: unit.

sym	parameter	val	unit
α_1	daily rate of losing infectivity	0.002	day ⁻¹
α_2	daily rate of acquiring high recovery rate	0.00019	day ⁻¹
δ	birth and death rates of the human population	36.5	1000 ⁻¹ year ⁻¹
N	incubation period in humans	15	day ⁻¹
n	incubation period in vectors	10	day ⁻¹
r_1	low daily recovery rate	0.0023	day ⁻¹
r_2	high daily recovery rate	0.023	day ⁻¹
λ_{max}	maximum rate of acquiring infections	0.097	(5 days) ⁻¹
h	inoculation rate, i.e. $h(t) = \lambda_{max}[1 - \exp(-EIR(t))]$	-	day ⁻¹
$R_1(h)$	recovery rate of non-immune individuals (function of h)	-	-
$R_2(h)$	recovery rate of immune individuals (function of h)	-	-
x_1	proportion of malaria negative, non-immune individuals	-	-
x_2	proportion of incubating, non-immune individuals	-	-
x_3	proportion of malaria negative, immune individuals	-	-
x_4	proportion of incubating, immune individuals	-	-

to be continued

Tab. 5.3 – continued

sym	parameter	val	unit
y_1	proportion of malaria positive, infectious, non-immune individuals	-	-
y_2	proportion of malaria positive, non-infectious, slowly recovering, non-immune individuals	-	-
y_3	proportion of malaria positive, non-infectious, fast recovering, immune individuals	-	-
q_1	detectability of y_1	1	-
q_2	detectability of y_2	1	-
q_3	detectability of y_3	0.7	-
y	true malaria positive proportion, i.e. $y = y_1 + y_2 + y_3$	-	-
I	proportion of immune individuals, i.e. $y = x_3 + x_4 + y_3$	-	-
\tilde{z}	observed malaria positive proportion, i.e. $\tilde{z} = q_1 y_1 + q_2 y_2 + q_3 y_3$	-	-

Originally the Garki model assumes that the input data repeats itself year after year. For this reason, the Garki model primarily does not account for the interannual variability of malaria transmission. However, the above described setting enables the simulation of malaria transmission in a particular population for a certain time period, although no age-specific values are extractable. During model spin-up (i.e., the period during which equilibrium is reached) the different population categories (see Fig. 5.7) are adjusted to the seasonal distribution of $EIR(t)$ of the first year of the simulation period. After reaching the state of equilibrium the model can be driven by EIR data from the remaining period. During this period seasonal and interannual changes of any output variable can be studied. For example, the daily inoculation rate (h), the proportion of infectious individuals (y_1), the observed positive proportion (\tilde{z} ; $\tilde{z} = q_1 y_1 + q_2 y_2 + q_3 y_3$), the true positive proportion (y ; $y = y_1 + y_2 + y_3$), or the proportion of immune individuals ($I = x_3 + x_4 + y_3$). By contrast, age-specific data can only be simulated under constant entomological conditions that is when $EIR(t)$ is the same year after year. This assumption might be valid for endemic malaria areas such as that for which the Garki model was developed. Age-specific values are produced when running the model with x_1 initialised as one, δ set to zero, and $EIR(t)$ only varies seasonally. The result of this model run is the life history of a cohort of individuals born into the non-immune negative category and in this case the modelled time is interpreted as the age of the cohort.

In the present study the Garki model is driven by EIR instead of VC data. As mentioned before this is a more direct modelling approach since one intrinsic assumption is omitted. Moreover, by using EIR it is possible to run the model in highland areas. This is due to the fact that the sporogonic cycle is no more relevant for the simulation since in the original version of the model only EIR is a function of n . In addition, the interannual variability of malaria has been taken in account. Similar to the procedure of Molineaux et al. (1978), after the production of a steady state, the Garki model was run for a longer

time period (e.g., 1961-2000) with variable *EIR* conditions. Note here that *EIR* values are taken from LMM simulations. This model chain enables the simulation of realistic transmission rates between humans and mosquitoes (via the LMM) and provides a reasonable pattern of malaria epidemiology (by means of the Garki model).

5.3 MARA Seasonality Model (MSM)

One important aspect of malaria is its seasonality. A correct assessment of the effect of changes in transmission patterns therefore also have to include an analysis of changes in the transmission period of malaria exposure. A prolonged transmission season might be as important as a geographical expansion of the disease spread. Tanser et al. (2003) presented the so-called MARA Seasonality Model (MSM) that was exclusively developed for the simulation of the seasonality of malaria.

The basis of the MSM is mean long-term monthly precipitation and temperature data. The MSM is using a Boolean logic approach, defining the monthly occurrence of malaria. Tanser et al. (2003) defined different temperature and precipitation criteria that account for the suitability of this vector-borne disease (cp. Tab. 5.4). The model uses two monthly and three yearly variables. On a monthly basis the *three-month moving average temperature* (T_{3m}) and the *three-month moving average monthly precipitation* (RR_{3m}) is applied (e.g., for July, months May, June, and July are used). That is because a sporadic month is not adequate for the occurrence of malaria. Yearly variables are the *monthly minimum temperature* ($T_{min,m}$), the *standard deviation of the monthly mean temperature* ($\sigma(T_m)$), and existence of a *catalyst month of precipitation* (RR_c).

According to the model every $T_{min,m}$ must exceed 5°C since mosquito populations are reduced at very low temperatures. Tanser et al. (2003) further assumed that vector and parasite populations have to be fully regenerated after relatively cool periods. They analysed stable and seasonal malaria profiles and showed that in stable malaria areas *monthly mean temperatures* (T_m) reveal only small variations during the course of the year. In contrast, T_m is stronger fluctuating in seasonal malaria areas such as regions in higher latitudes and altitudes. It is additionally demonstrated that T_{3m} has only slightly to exceed 19.5° in stable malaria areas, whereas temperatures have clearly to exceed this threshold in seasonal transmission areas. On this account, malaria transmission in the model is only simulated when T_{3m} is higher than the total of 19.5°C and $\sigma(T_m)$.

Rainfall also limits malaria transmission in the MSM. The MSM assumes that vector breeding sites depend on preceding precipitation events and that a certain moisture status has to be reached for an increase of the survival probability of mosquitoes. For all these reasons, also for the precipitation criteria a three-month moving average of 60 mm is used. Tanser et al. (2003) also called for a catalyst month of 80 mm in order to provide adequate vector breeding and the ability for the regeneration of the mosquito population.

A certain month is assigned transmission when the four above described criteria are fulfilled (see Tab. 5.4). However, it is further expected that, despite a predicted one-

month interruption, malaria transmission is maintained. This is justified by the strength of the climatic suitability of bordering months and the persistent parasite reservoir.

Tab. 5.4: Criteria of the MSM to calculate months suitable for malaria transmission in Africa (Tanser et al. 2003). Columns: #: criteria number; sym: symbol of the applied parameter; parameter: name of the parameter; criteria: criteria used to calculate months suitable.

#	sym	parameter	criteria
1	$T_{min,m}$	monthly minimum temperature	every month: $T_{min,m} \geq 5^{\circ}\text{C}$
2	T_{3m}	three-month moving average temperature	$T_{3m} \geq 19.5^{\circ}\text{C} + \sigma(T_m)$
3	RR_{3m}	three-month moving averaged monthly precipitation	$RR_{3m} \geq 60 \text{ mm}$
4	RR_c	catalyst month of precipitation	one month: $RR_c \geq 80 \text{ mm}$
5	-	assigned transmission status	criteria 1-4 (one month interruption is allowed)

The MSM was spatiotemporally validated against parasite surveys of *P. falciparum* malaria transmission in Africa between 1929 and 1994. The validation of the model showed a sensitivity (i.e., the ability to predict areas of transmission to within a month) of 63% and a temporal sensitivity (i.e., the ability to accurately predict malaria occurrence in any month) of 90%. Moreover, specificity within one-month temporal accuracy of 96% was obtained (Tanser et al. 2003).

The basis of the model is climatic and thus has some limitations. Non-climatic factors are hence not considered by the MSM (cp. Sec. 2.6.2). Another disadvantage of the model is the fact that it cannot account for the interannual variability of the malaria season. Hence, epidemic-prone areas are not detectable via this modelling approach.

6 Calibration, validation, and sensitivity tests of the LMM

6.1 LMM calibration and validation

The LMM entails the combination of many separate sub-models, each with its own parameterisation. Numerous parameters could potentially create larger variations than the weather driving force and indeed the output from this malaria model is largely dependent on the choice of the models' parameters (Sec. 6.2). A prerequisite for malaria simulations is ideally an optimal setting of the LMM. The development of such an ideal parameter setting is only possible by means of the validation of every sub-model. So far the validation of the LMM has focused on malaria prevalence as well as incidence data. The LMM₀ was validated for a comparatively small area in Botswana (Hoshen and Morse 2004; Jones 2007). The so far most-sophisticated validation procedure was performed by Jones (2007). This study compared the simulated mosquito population size as well as the modelled incidence with a 20 year time series of standardised malaria anomalies. However, the validation of transmission rates such as *EIR* or malaria seasonality are missing. Because of the saturation of malaria prevalence at high transmission rates the modelling of realistic biting rates should be more challenging than the reproduction of reasonable parasite ratios. The model validation for various climate conditions is also absolutely essential. The LMM has to be verified against a large set of precipitation and temperature conditions.

The present study aims to determine a LMM setting that compares well to field observations. Note that an 'optimum' LMM setting is hampered by the huge degree of freedom in the setting of model parameters as well as uncertainties in meteorological time series and malaria observations. However, the model calibration produces numerous adapted parameter settings. Various versions of the LMM were forced by temperature and rainfall conditions of 34 synoptic stations in West Africa and Cameroon for 1973-2006 (Tab. G.1). The model is hence subject to different climate conditions (Fig. 6.1). The climate of this data set ranges from an arid hot desert to a tropical monsoon climate (see Fig. 2.1a) and therefore evokes various malaria transmission levels. Fairly dry conditions in the Sahel, for example, resulted in no malaria transmission at Diomandou Dieri

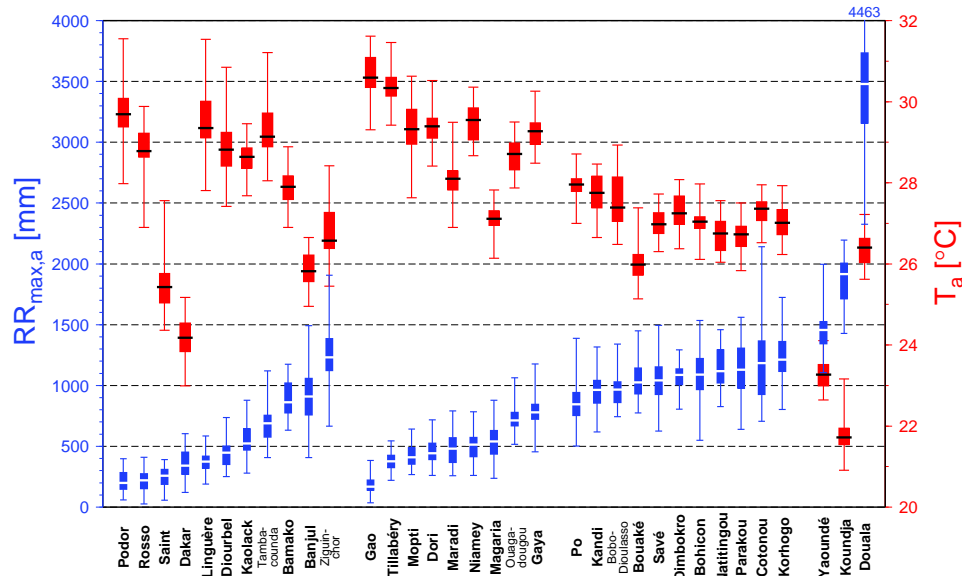


Fig. 6.1: Box-and-whisker plot of annual rainfall (RR_a ; blue box plots & left scale) and annual mean temperatures (T_a ; red box plots & right scale) between 1973 and 2006 relative to 34 synoptic stations of West Africa and Cameroon. Stations are grouped for the West Sahel, Central Sahel, Guinean coast, and Cameroon as well as relative to the median of 34 RR_a values.

(Senegal; $16^{\circ}31'N$; $14^{\circ}39'W$; Faye et al. 1993). In contrast, a continuous rainfall supply caused year-round transmission in Cameroon at Etoa ($3^{\circ}46'N$; $11^{\circ}29'E$; Quakyi et al. 2000). However, temperatures of this data set lie usually well above $20^{\circ}C$ (cp. Fig. 7.1a) inhibiting the model validation for the lower malaria temperature limit (e.g., Fig. 5.2).

Numerous model simulations are validated against eleven observed entomological and parasitological variables (App. D). The validation primarily focuses on the performance of the model with regard to entomological field measurements (i.e., HBR_a and EIR_a). For every single LMM parameter setting a *skill score* ($SC(x)$) is assigned by means of five criteria (Tab. E.1). The reader is referred to App. E.1 for a detailed description of the validation procedure.

6.1.1 Calibration of the LMM

The majority of model parameters has already been fixed (Sec. 5.1). Indeed, some parameters are not allocatable due to different specifications in literature or due to the lack of data (these are: S , U_2 , $\#E_p$, CAP , and $p_{d\downarrow}$). Note that some false estimation of predefined parameters might be undertaken. However, the calibration will largely compensate such inaccurate assessments. A too high human biting index (a), for example, can be compensated by a lower value of $\#E_p$ (Fig. 6.7). In the same way it is found that $\#E_p$ and CAP compensate each other at more humid stations (e.g., in Cameroon; Fig. 6.7a & b).

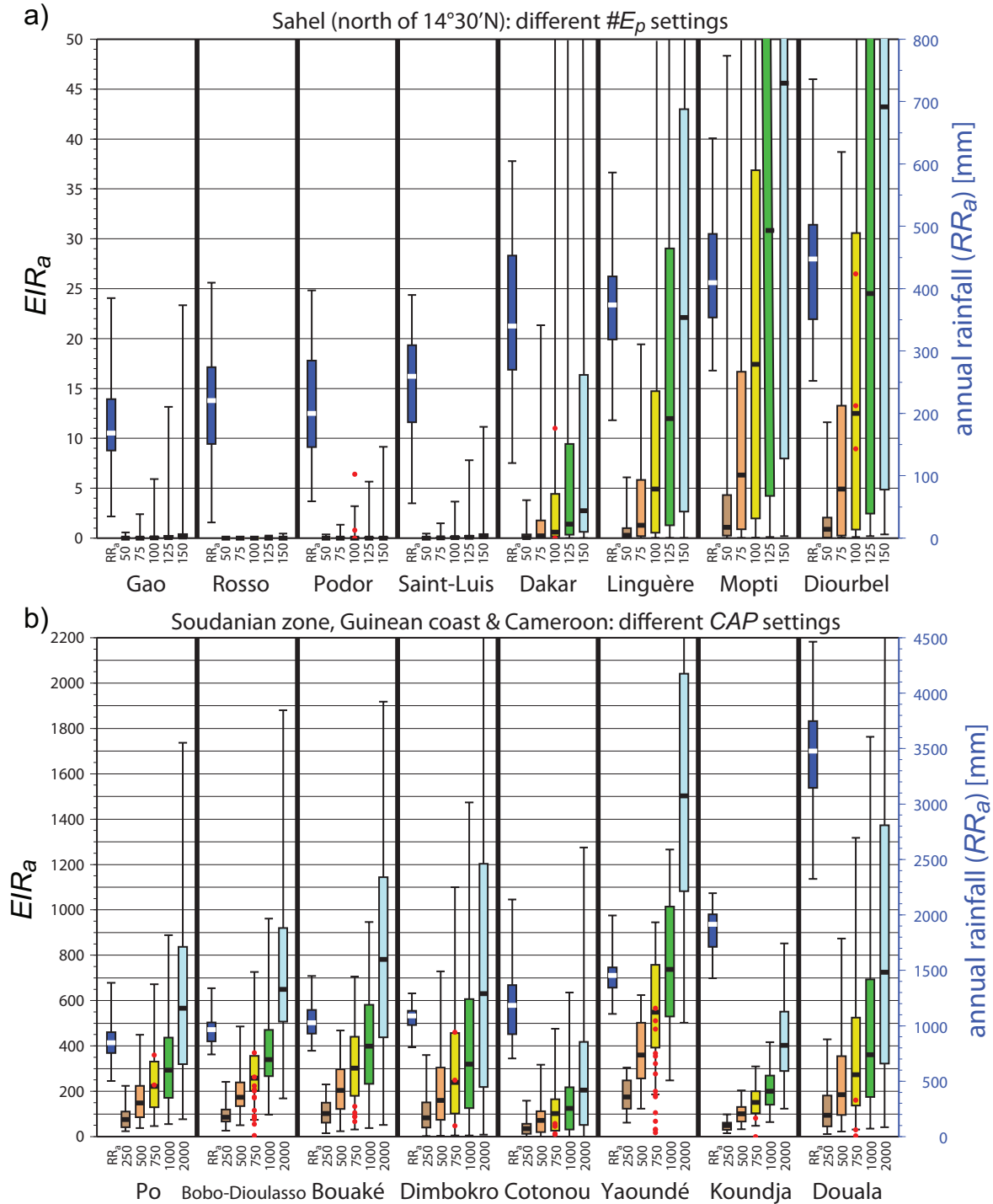


Fig. 6.2: Box-and-whisker plots of five different LMM settings with regard to 34 EIR_a values between 1973 and 2006 relative to eight synoptic stations of (a) the Sahel (north of 14°30'N) and (b) the Sudanian Zone, Guinean coast, and Cameroon (cp. Tab. G.1). Different settings of (a) $\#E_p$ and (b) CAP are represented by varying colours (brown to light blue box plots). Note, various simulated values outrange the scale of figures. LMM setting: cp. val_n in Tab. 5.1, but: (a) $p_{d_l}=0\%$, CAP=500 fertile females, $\#E_p=50, 75, 100, 125$, and 150 eggs; (b) $p_{d_l}=0\%$, $\#E_p=75$ eggs, CAP=250, 500, 750, 1000, and 2000 fertile females. Red dots depict available EIR_a field measurements (cp. Tab. D.3). In addition to EIR_a , the statistic relative to RR_a is illustrated for each station (dark blue box plots; right scale).

The LMM calibration includes two general steps. The initial experiment enables a rough estimate of realistic parameter values. The second set of model runs permits a final adjustment of model settings. In order to simplify the calibration procedure, $p_{d\downarrow}$ is initially set to zero. Altogether three different settings are tried out for U_2 . Ahumada et al. (2004) defined extreme rainfall as more than 255 mm of cumulative rainfall throughout a period of three days. Their model markedly reduces the mosquito population under excessive rainfall. According to a 10-day period this suggests a U_2 value of about 500-1000 mm. In fact, U_2 is either set to 500, 750, or 1000 mm.

For the isolation of particular settings the remaining parameters (S , U_2 , $\#E_p$, and CAP) are varied simultaneously (S : 5-30 mm; U_2 : 500-1000 mm; $\#E_p$: 50-150 mm; CAP : 250-2000 fertile females). The first 300 different LMM settings are ranked with regard to the skill score of all eleven malaria variables ($SC(all)$) and in terms of HRB_a and EIR_a (see also Tab. 6.1).

The ranking with regard to $SC(HBR_a, EIR_a)$ shows that S affects mainly the spread of malaria in the northern part of the Sahel, for example, at various stations in Senegal (Tab. E.2 & Fig. E.1). In these dry areas the growth opportunity of the mosquito population is strongly suppressed by the fuzzy distribution model when S is set to high values (cp. Fig. 5.3). Obviously, S has to be calibrated to relatively low values in order to keep malaria going in the northern Sahelian zone. However, too low S values seem to be unrealistic since the *potential evaporation* in tropical Africa usually exceeds several millimetres per day. S is finally fixed to 10 mm as this value still enables the simulation of malaria in the northern part of the Sahel. This analysis shows the clear need for the validation of the model under different rainfall conditions. Only stations in the northern Sahel enable a proper estimation of S .

exp	variable	area	criteria	result
Exp. 1	$p_{d\downarrow} = 0$	-	-	-
Exp. 1.1	$S \in [5, 30]$	northern Sahel	$SC(HBR_a, EIR_a)$	$\Rightarrow S := 10 \text{ mm}$
Exp. 1.2	$U_2 \in [500, 1000]$	West Africa	$SC(all)$	$\Rightarrow U_2 := 500 \text{ mm}$
Exp. 1.3	$\#E_p \in [50, 150]$	Sahel	$SC(HBR_a, EIR_a)$	$\Rightarrow \#E_p \in [75, 125]$
Exp. 1.4	$CAP \in [250, 2000]$	West Africa	$SC(all)$	$\Rightarrow CAP \in [300, 900]$
Exp. 2	$CAP \in [300, 900]$ $\#E_p \in [70, 130]$ $p_{d\downarrow} \in [0, 10]$	West Africa	$SC(HBR_a, EIR_a)$	$\Rightarrow CAP := 400$ fertile females, $\#E_p := 120$ eggs, $p_{d\downarrow} := -10\%$

Tab. 6.1: Overview in terms of the evaluation of performed calibration experiments (Exp.). Columns: exp: number of the experiment; variable: particular settings of model variables; area: area of interest; criteria: applied criteria; result: result of the experiment.

The evaluation of the 300 model settings also enables a final setting of U_2 since the highest skill scores are exclusively generated by a value of 500 mm (see Tabs. E.2 & E.3). The lowest skill scores are attained by settings with high values of CAP , $\#E_p$, and U_2 as well as low values of S , which apparently evoke large mosquito populations (Tab. E.2).

A closer analysis of data reveals that malaria transmission rates in the Sahel are fairly sensitive to the $\#E_p$ setting (Figs. 6.2a & E.2a). The median HRB_a value rises, for example, at Linguère, Mopti, and Diourbel from less than 100 to several thousand bites per year, when $\#E_p$ increases from 50 to 150 eggs (Fig. E.2a). Unfortunately, only nine field observations of HRB_a and EIR_a are available north of $14^{\circ}30'N$. This fact impedes a proper determination or further confinement of $\#E_p$. However, the LMM underestimates (overestimates) EIR_a , when $\#E_p$ is set to 50 (150) eggs (cp. Fig. 6.2a).

After isolating $\#E_p$ (75-125 eggs) also the value of CAP can be more precisely determined. CAP is only of importance for comparatively large annual rainfall amounts. CAP markedly reduces the number of deposited eggs and hence biting rates under wet conditions. In fact, the reduction is markedly pronounced in the Sudanian zone, along the Guinean coast, and in Cameroon for low CAP values (≤ 750 fertile females). In contrast, large values of CAP (≥ 1000) cause fairly high numbers of non-infectious and infectious mosquito bites (cp. Figs. 6.2b & E.2b). The ranking relative to $SC(all)$ shows that LMM settings come off badly when CAP is set to 250 fertile females (not shown).

Basis of the second iteration of the LMM calibration are conclusions from the initial experiment. Only the setting of CAP , $\#E_p$ and $p_{d\downarrow}$ remain undetermined. $\#E_p$ values are now varied between 70 and 130 eggs and CAP is set between 300 and 900 fertile mosquitoes. Five different values for $p_{d\downarrow}$ are in addition utilised (0.0, -2.5, -5.0, -7.5, and -10.0%). The second set of model runs includes altogether 455 different model sets.

The highest skill score in terms of all eleven malaria variables obtain runs with comparatively low (high) $\#E_p$ and high (low) CAP values (App. E, Tab. E.5). Particularly notable is that various model settings exhibit comparatively high skill scores. This fact and the considerable inherent uncertainties in the used data impede a final objective fixation of remaining parameters. For simplicity, the model setting with the highest skill score in terms of HBR_a and EIR_a is finally chosen (App. E, Tab. E.4). A total of 78 points from 106 possible points (73.6%) is gained by a setting with $\#E_p=120$ eggs, $CAP=400$ fertile females, and $p_{d\downarrow}=-10\%$ ($SC(all) = 279 (440)$; numbers in brackets refer to points that could be theoretically achieved). The value of 120 produced eggs is in the middle of observations (Tab. D.7) and forces a reasonable level of malaria transmission in the northern Sahel. Due to the high $\#E_p$ value CAP is fixed to the relatively low value of 400 fertile females limiting the number of mosquito bites in more humid areas such as Cameroon. The $p_{d\downarrow}$ value of -10% enables the simulation of a realistic season end. The application of $p_{d\downarrow}$ allows a one to two months earlier end of transmission (cp. Fig. 6.3). Correspondence with respect to modelled seasons from the MARA project is improved by the earlier break in transmission (Fig. 2.8c & d).

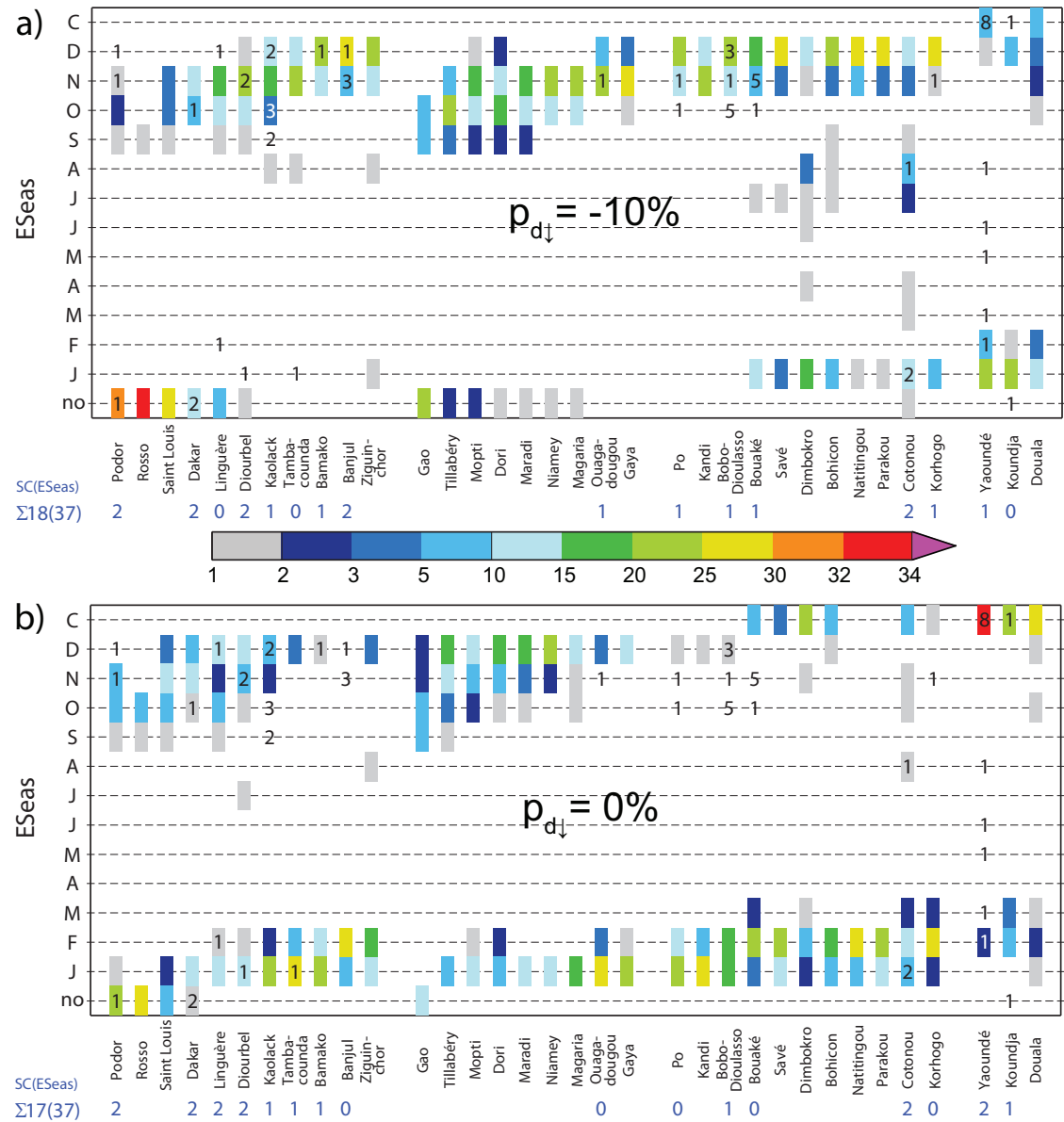


Fig. 6.3: Validation of LMM simulations in terms of $ESeas$ in the area of 34 synoptic stations in West Africa and Cameroon. The simulated data (filled rectangles) is compared to observed values (inserted as a digit). The frequency distribution (in numbers) with regard to simulated 34 values for 1973–2006 is given for each month. The frequency of years with no ('no') and year-round ('C') transmission are also illustrated. In (a) results of the LMM_n simulation ($p_{d1} = -10\%$) are presented. (b) Same as (a) but for $p_{d1} = 0\%$. $SC(ESeas)$ is denoted for every station as blue digits. Stations are grouped for the West Sahel, Central Sahel, Guinean coast, and Cameroon as well as relative to the median value of RR_a .

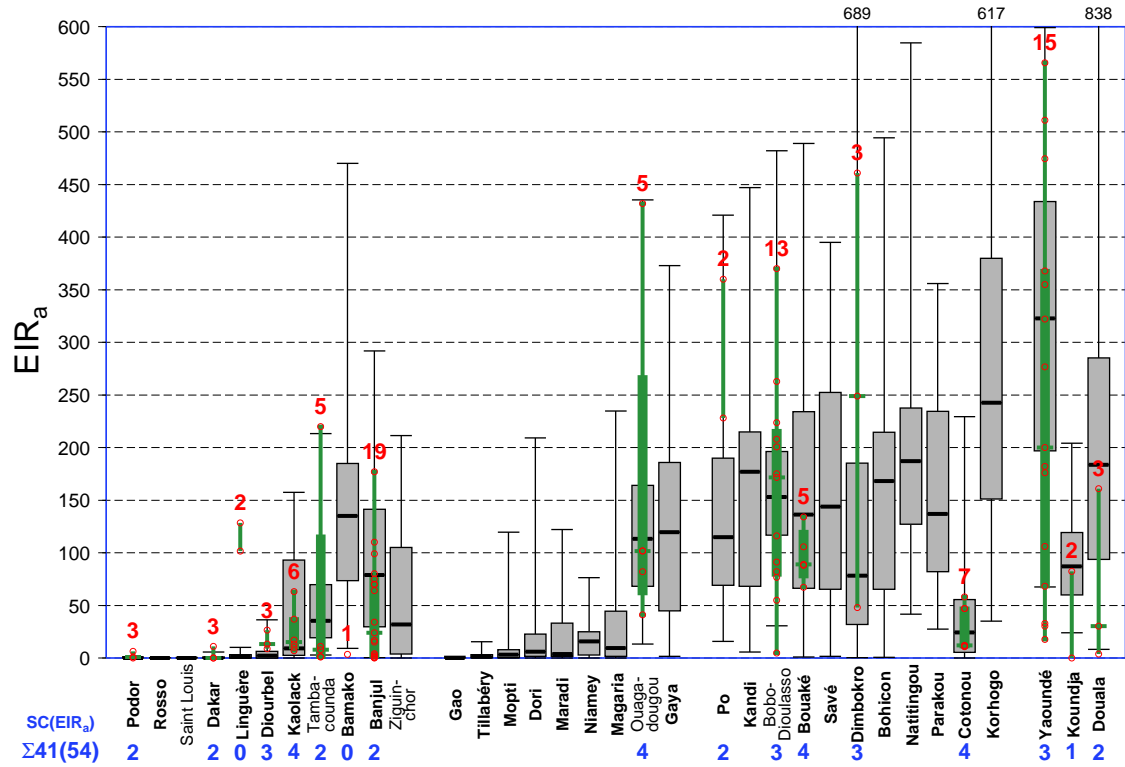


Fig. 6.4: Validation of the LMM_n simulation in terms of EIR_a in the area of 34 synoptic stations of West Africa and Cameroon. Simulated 34 annual EIR_a values between 1973 and 2006 are illustrated as grey box-and-whisker plots (maximum values outranging the figure are inserted above). Field observations of EIR_a (green lines and box plots) are either displayed as a vertical line (two available measurements), a vertical line with the median (three or four values), or as a box-and-whisker plot (\geq five data points). Each observation is furthermore inserted as a red circle and the number of observations is given above entered observations (red digits). $SC(EIR_a)$ is denoted for every station as blue digits. Stations are grouped for the West Sahel, Central Sahel, Guinean coast, and Cameroon as well as relative to the median of 34 RR_a values.

6.1.2 Validation of the final LMM_n setting

Simulations of the final model setting are comparable to all entomological variables. The new model setting leads to the simulation of about the same EIR_a values as observed (Fig. 6.4; $SC(EIR_a) = 41(54)$). Low EIR_a values are modelled under dry conditions in the Sahel. EIR_a values are much higher for annual rainfall of about 1000 mm and again decrease as observed when the model is subject to higher annual rainfall (cp. Fig. 6.1). The LMM_n simulation encompasses observed values in various cases. For some stations with numerous observations even median values are comparable, for example, in the vicinity of Bobo-Dioulasso (13 observations) or in the area of Kaolack (six observations). However, there are also some exceptions, for example, in the vicinity of Barkedji the simulated EIR_a is much lower than two observations (Le Masson et al. 1997). High biting rates in this area are probably a result of special local environmental conditions. Le Masson et al. (1997) and Molez et al. (2006) conjectured that the presence of clay hollows, which collect water as soon as the rains start, caused a long persistence of temporary ponds and hence of malaria transmission. With regard to HBR_a and consequently

also for $CSPR_a$ values about same statements are valid. There is a fair correspondence between the LMM_n simulations of HBR_a as well as $CSPR_a$ and observations from entomological studies (Figs. E.4a & E.4b; $SC(HBR_a) = 37(52)$; $SC(CSPR_a) = 33(55)$).

Another result of the calibration is that the simulations are able to capture the variability of malaria transmission. The interannual variability of EIR_a , for example, is fairly large. For most stations the number of infectious mosquito bites fluctuates between values of less than 100 and several hundred. Such differences are also typical for field observations. Burkot et al. 1988, for instance, found large variations in $CSPR_a$ and EIR_a among villages in Papua New Guinea, despite their close geographic proximity. EIR_a values range from 68-526 infectious mosquito bites within a radius of 20 km. Malaria transmission not only varies in space but also from year to year. Unfortunately, long-term studies are rare and continuous observations from rural sites are only available from Ndiop for four years (Senegal; 13°41'N, 16°23'W). In this Sahelian village malaria transmission varied in the middle of the 1990s between 7 and 63 infective bites (see Fontenille et al. 1997a; Tab. D.3). For this area simulated EIR_a values range from almost zero to about 158 infectious bites. Note that the LMM simulation refers to meteorological data from Kaolack, which is located about 55 km to the northeast of Ndiop (Figs. 3.1 & G.2).

The simulation of malaria seasonality by the LMM_n is fairly consistent with field observations. The length of the season agrees with observations (Fig. E.3a; $SC(Seas) = 31(42)$). In general, the season length shortens with decreasing annual rainfall (cp. Fig. 6.1). Short malaria seasons and no malaria transmission are simulated for the Sahel and year-round transmission is found, for instance, in Cameroon. Also the length of the main transmission season often agrees with observations (Fig. E.3b; $SC(MSeas) = 28(37)$). Interestingly, the timing of maximum transmission is well captured by the LMM_n version (Fig. E.3d; $SC(XSeas) = 23(41)$). The simulated month with maximum transmission often coincide with that of observations, especially in the Sahel. However, model simulations seem to disagree for areas with year-round transmission. Naturally, the match probability decreases the longer the season lasts. Both the start as well as the end of the malaria season seem to be realistically reproduced by the LMM_n version (Figs. E.3c & 6.3a; $SC(SSeas) = 28(41)$; $SC(ESeas) = 18(37)$). At various locations the maximum number of observations and simulations are found in the same month or they either reveal most frequently no or year-round transmission. Observations that fall outside of simulations hardly differ more than one month. Also note that the simulated malaria seasonality might not be directly comparable to field measurements (cp. App. D.5). The comparison is strongly influenced by the definition of the malaria season. The chosen threshold might be too small in comparison with field studies. As previously noted by Morse et al. (2005) and Jones (2007), it is therefore still possible that the onset of the malaria season is a little lagged.

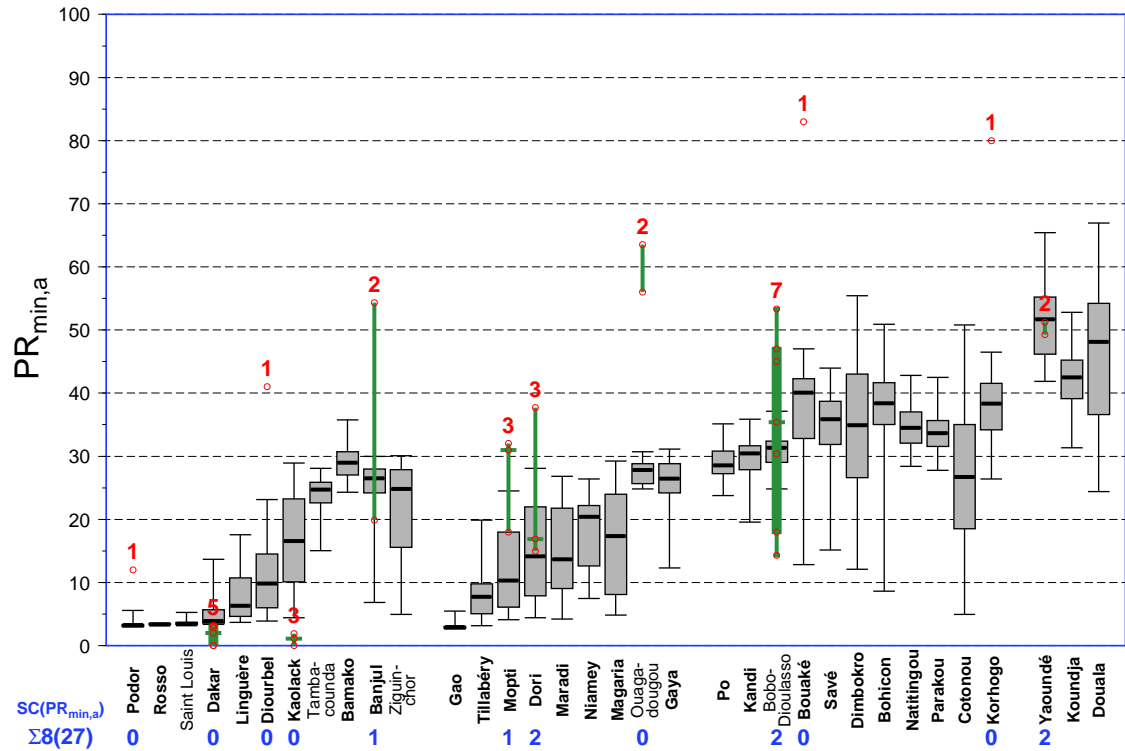


Fig. 6.5: Same as Fig. 6.4, but for $PR_{min,a}$.

The performance of the LMM_n with regard to parasitological variables is somewhat mixed. The main reason for relatively low skill scores are fairly heterogeneous parasitological observations that cannot be reproduced by the LMM. Measurements of $PR_{min,a}$, for example, exhibit a remarkable spread. Nine observations reveal higher values than 50% whereas 23 values are lower than this threshold. These differences suggest that some special factors are strongly affecting PR values. As a consequence, the LMM_n reaches only eight from 27 possible points (Fig. 6.5; $SC(PR_{min,a})$). However, the LMM_n performs somewhat better with regard to the other two parasitological variables (Figs. E.4c & E.4d; $SC(PR_a)=16(29)$; $SC(PR_{max,a})=16(25)$).

In summary, the collected entomological and parasitological data from various locations enabled the calibration of a realistic LMM version. The LMM_n compares reasonably well with entomological observations such as EIR_a . Also, features of the malaria season seem to be captured satisfactorily. The performance with regard to parasitological values is somewhat weaker due to limitations of the LMM as well as the heterogeneous distribution of parasite observations.

6.2 LMM sensitivity tests

Numerous issues are still contestable either in the original or in the new LMM version. This is mainly due to the fact that most LMM parameters lack a final definite setting. Some sub-models are not created with full evidence. On this account, a sensitivity analysis is needed for the LMM_n version. Diversity of model behaviour over the parameter

range will reflect levels of uncertainty in these parameters and reveals areas that should be measured more accurately. The sensitivity of LMM_n is therefore analysed when model parameters are varied within and around empirical ranges of literature.

The response of the LMM to various model settings and an altered data input was investigated for the original model version (Hoshen and Morse 2005; Jones 2007). For this reason, the present study focuses on the model sensitivity with regard to new inserted and most newly set model parameters. Note that b and GF are not used since they exert the same effects as a and c , respectively.

Jones (2007) found that LMM simulations strongly depend on the setting of various model parameters. The model is most sensitive to changes in the p_d -scheme, MMA , n_s , RR_- , and RR_\bullet . In certain situations the modification of single parameters changes the malaria spread from epidemic to endemic or vice versa. Unfortunately, most results focus on changes in PR as well as in the malaria incidence.

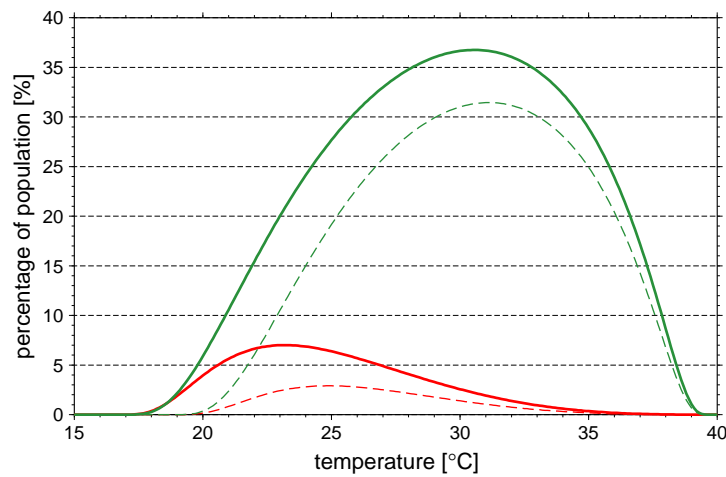


Fig. 6.6: Probability of mosquitoes surviving to the infectious age obtained by combining the daily mosquito survival probability (p_d) of the Martens I (red lines) and Martens II (green lines) schemes with the sporogonic cycle length (n_s). Solid and dashed lines refer to a sporogonic temperature threshold (T_s) of 16 and 18°C, respectively. Note that p_d and n_s both depend on temperature conditions (see Secs. 5.1.5 & 5.1.7).

One important aspect of the model behaviour is the response to different temperature conditions. Various p_d -schemes (Fig. 5.5) reveal a partially strong disparity of the simulations. The comparatively high mortality above 25°C of the Martens I scheme, for example, results only in few mosquitoes surviving to the infectious stage. In contrast, when the LMM is set by Martens II more than 35% of vectors outlive the sporogonic cycle at about 30°C (Fig. 6.6). Running the LMM_n version with a different p_d -scheme makes little sense since various model settings are adjusted to the Martens II scheme (cp. Fig. 6.7g).

Also the setting of T_s largely impacts simulations of the LMM. Malaria transmission already starts at about 18°C for a T_s of 16°C, whereas it is shifted to about 20°C for a threshold of 18°C. Fewer mosquitoes survive to the infectious stage due to the longer

duration of the sporogonic cycle (cp. Fig. 6.6 & Eq. 5.10). These differences are most important for highland areas such as that of East Africa.

The probably most important driver of malaria transmission for most parts of Africa is rainfall. As previously discussed, RR_{\bullet} mainly steers the generation of the mosquito population in the LMM₀ version. Changing the value of RR_{\bullet} therefore has a large effect on the modelled PR . Jones (2007) furthermore alludes to the influence of RR_{-} , which is used as a proxy for varying the degree-days and temperature threshold of the gonotrophic cycle (D_g and T_g). An increase in RR_{-} therefore generates longer gonotrophic cycles (n_g increases) as parameters for dry conditions are more often utilised. As a result, under certain conditions fewer mosquitoes are produced causing a significant lower malaria prevalence.

The following analysis, examines the sensitivity of the LMM_n version by means of 34 station time series (Tab. G.1) including various rainfall and temperature conditions (Fig. 6.1). As previously pointed out, the consideration of the lower temperature limit of malaria transmission is again not possible.

Compared to the original model version various components and parameter settings have been changed in the LMM_n. Dynamics of the mosquito population, for example, are completely revised (Sec. 5.1). The default setting for the following experiment is that of the LMM_n (val_n in Tab. 5.1). A single parameter is then varied at a time to establish the specific response of the model.

Various model settings markedly influence the simulation of malaria transmission in fairly dry areas such as the Sahel (Fig. 6.7). In areas with less than 500 mm of annual rainfall the spread of malaria in the model is only enabled via a proper setting of various parameters. The strongest influence on the spread of malaria in such regions is found for S , r , MMA , $\eta_{d,-RR}$ and $\#E_p$. A somewhat weaker effect is exhibited by $p_{d\downarrow}$, c (GF)¹, and a (b). For example, only low S and high $\#E_p$ values enable an ongoing malaria transmission in the northern part of the Sahel.

Higher transmission rates are simulated when $\eta_{d,-RR}$, $\#E_p$, U_2 , CAP , c (GF), and a (b) are increased and when the setting of MMA , S , HIA , r , as well as $p_{d\downarrow}$ values are reduced. The weakest influences on EIR_a is found for HIA and $p_{d\downarrow}$. In particular, HIA shows a comparatively small influence on the transmission level (Fig. 6.7i). Of course, low HIA values increase the number of mosquitoes becoming infected. $p_{d\downarrow}$ reduces the number of mosquitoes during the start of the rainy season. High absolute $p_{d\downarrow}$ values therefore lead to a smaller size of the mosquito population and reduced level of malaria transmission (Fig. 6.7h).

¹Variables in brackets similar influences the LMM performance.

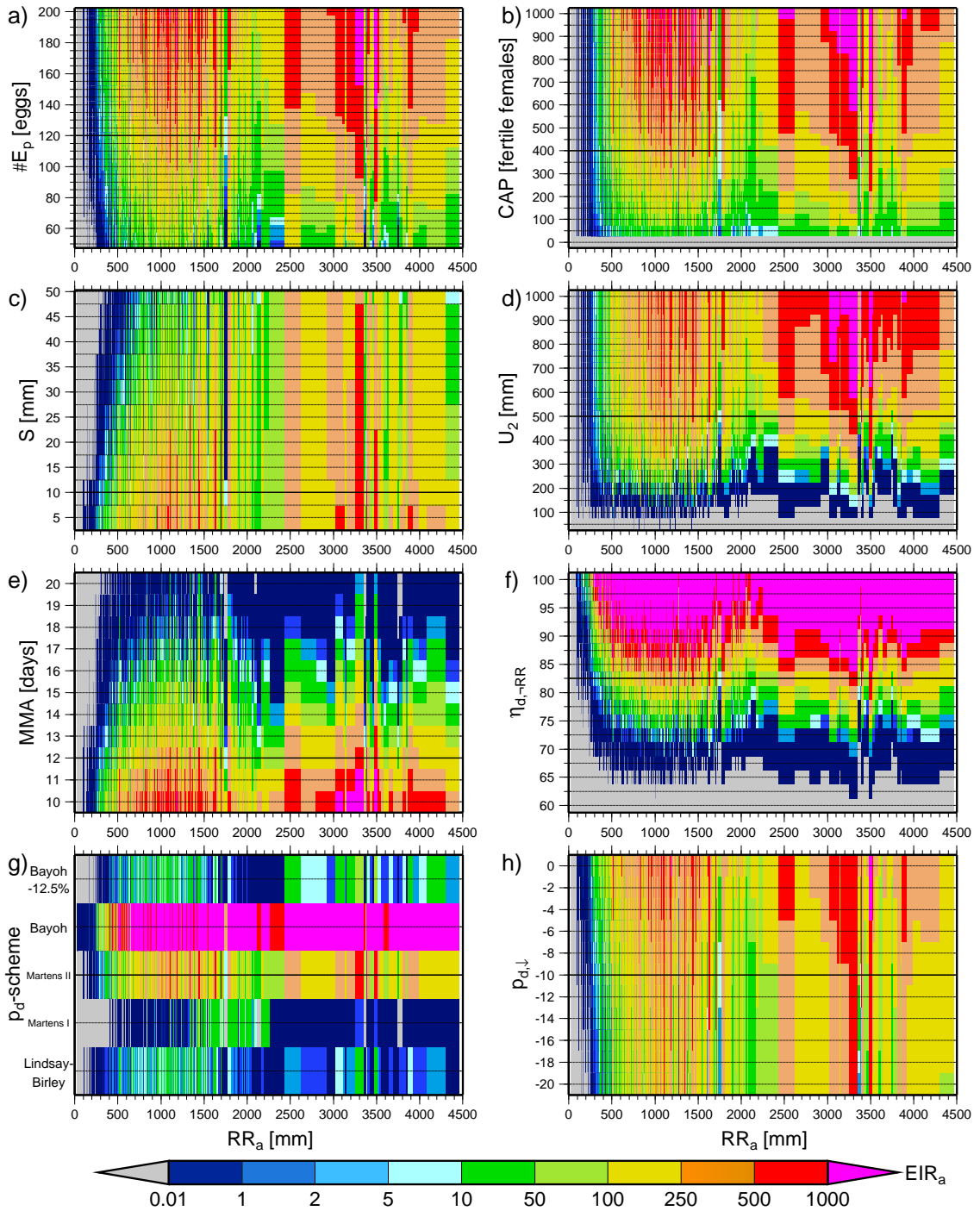


Fig. 6.7: LMM_n sensitivity tests between 1973 and 2006 relative to data from 34 synoptic stations (Tab. G.1) in West Africa and Cameroon (continued on the next page). Simulated EIR_a values are inserted in segments of variable size and are arranged relative to annual rainfall (RR_a). Different settings are indicated via horizontal grid lines and refer to (a) the number of produced eggs per female mosquito ($\#E_p$), (b) the cap on the number of fertile mosquitoes (CAP), parameters (c) S and (d) U_2 of the fuzzy distribution model, (e) the mosquito mature age (MMA), (f) the rainfall independent daily survival probability of immature mosquitoes ($\eta_{d,-RR}$), (g) five different p_d -schemes (cp. Fig. 5.5), (h) the shift off of the dry season mosquito survival probability ($p_{d\downarrow}$), (i) the human infectious age (HIA), (j) the daily human recovery rate (r), (k) the human-to-mosquito transmission efficiency (c), as well as (l) the human blood index (a). Note that (g) includes the Bayoh scheme with an offset of 12.5% that corresponds well to the median p_d value of 84.6% from Kiszewski et al. (2004).

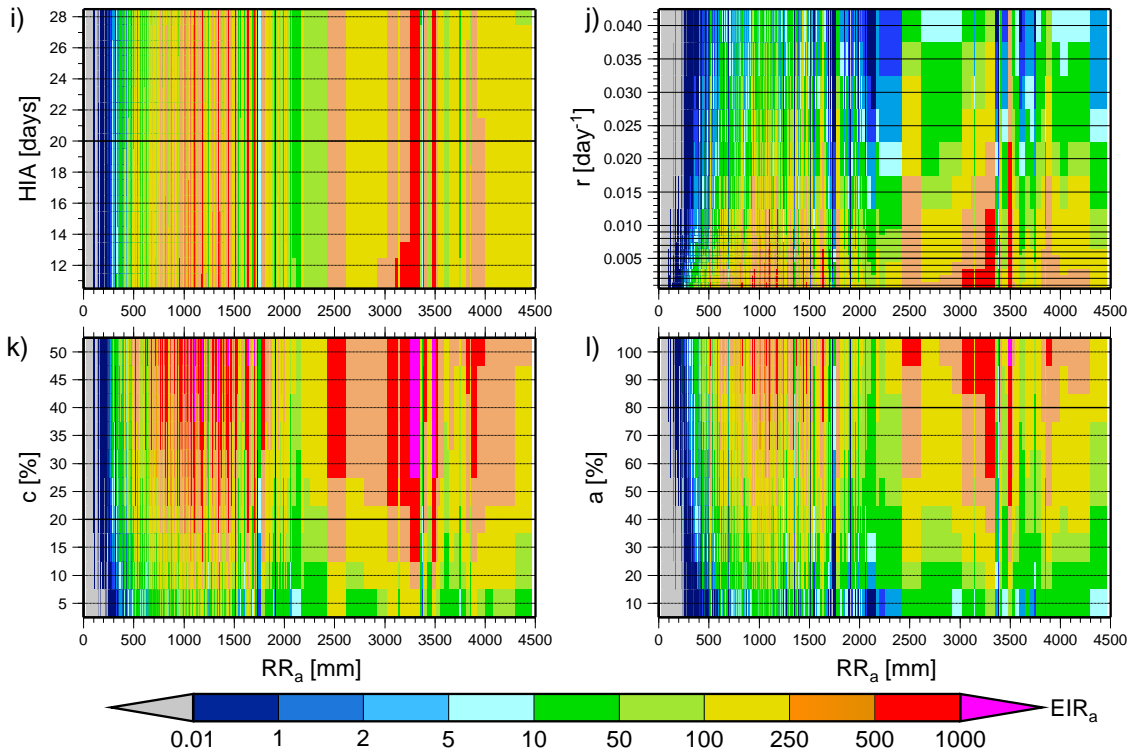


Fig. 6.7: (continued)

The variation of the mosquito population is investigated under different model settings. The growth of the mosquito population basically depends on three factors: mosquito survival (p_d), the length of the gonotrophic cycle (n_g), as well as breeding conditions. The first two factors p_d and n_g have already been considered (see above). The following analysis therefore focuses on effects of the egg deposition as well as aquatic stages on simulations of EIR_a . Various model parameters determine mosquito breeding (Secs. 5.1.2, 5.1.3 & 5.1.4), these are $\#E_p$, CAP , $\eta_{d,-RR}$, MMA , as well as the fuzzy distribution model (expressed via U_1 , S , and U_2).

The strongest impact on the simulation of EIR_a is exerted by MMA and $\eta_{d,-RR}$ (Fig. 6.7e & f). The performance of the LMM_n version is adjusted to the MMA value of 12 days. The combination with the $\eta_{d,-RR}$ value of 82.5% ensures that usually less than 10% of immature mosquitoes survive to the adult stage (Sec. 5.1.4). A smaller MMA value therefore markedly increases the size of the vector population. Malaria transmission is even interrupted for various years under humid conditions when MMA is set to values higher than 15 days. The reason for this behaviour is that a much smaller number of immature mosquitoes reaches the adult mosquito stage when MMA is fixed to such high values. Exactly the opposite holds for the influence of $\eta_{d,-RR}$. Malaria dies out completely in the model when $\eta_{d,-RR}$ is set under about 65%. On the other hand values above about 85% lead to unrealistic high transmission rates.

Also various other malaria variables are sensitive to the setting of the LMM. For example, the duration of the malaria season is strongly influenced by the setting of $p_{d\downarrow}$ (cp. Fig. 6.3). A low absolute value of $p_{d\downarrow}$ markedly increases the frequency of year-

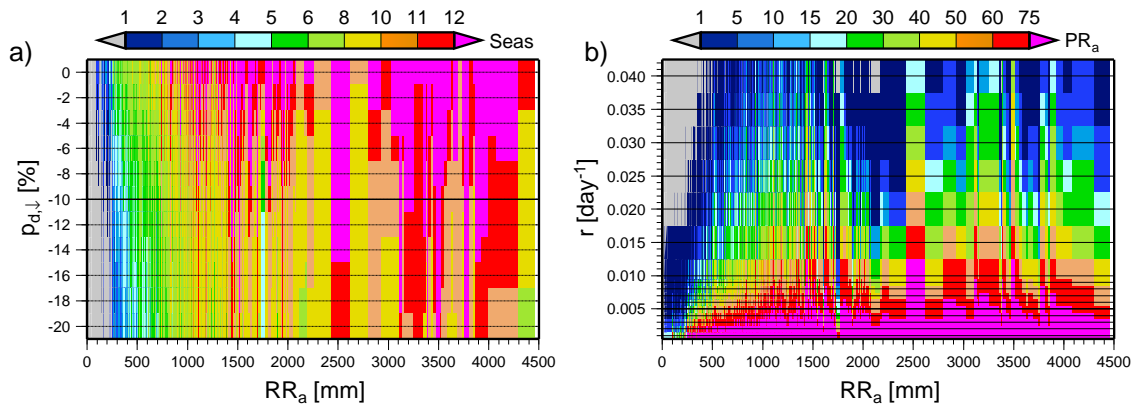


Fig. 6.8: Same as Fig. 6.7, but here for a different setting of (a) $p_{d\downarrow}$ and (b) r . Illustrated are simulated values of (a) $Seas$ and (b) PR_a .

round malaria transmission (Fig. 6.8a). $p_{d\downarrow}$ furthermore determines the length of malaria seasonality in the Sahel.

The value of the recovery rate of the malaria parasite significantly affects the simulation of the malaria prevalence (Fig. 6.8b). As expected low r values lead to high PR_a values. Under such settings the model simulates even for fairly dry areas a holoendemic malaria ($PR_a > 75\%$). For the lowest r settings an abrupt rise in PR_a is found for annual rainfall amounts of about 200 mm. This suggests that even very small transmission rates are able to sustain high PR_a levels. In such situations reductions of the malaria prevalence might not be possible. In contrast, fast recovery rates ($r > 0.03$) result in very low PR_a values. The strong impact of r reveals the importance of a correct determination of r in terms of realistic simulations of the proportion of the population that is carrier of the malaria parasite.

The previous results furthermore show that the simulation of the LMM_n is not only sensitive to rainfall amounts but also strongly depends on its seasonal distribution and intensity. The simulations reveal that large precipitation amounts can lead to a fairly low malaria transmission. Important is not only the amount but also the time period in which precipitation falls. Moderate rainfall amounts support mosquito breeding in the LMM_n , whereas excessive rainfall significantly reduce the number of immatures. Reduced transmission due to high rainfall is, for instance, found for Cotonou, Ziguinchor, Kondja Fouban, and Douala (Fig. 6.4).

Various effects of rainfall in the model can be nicely studied at Cotonou for 1993 and 2005 (Fig. 6.9). In 1993, the LMM_n simulates very low transmission ($EIR_a = 0.5$ infective bites) despite high rainfall amounts ($RR_a = 1727.5$ mm). By contrast, a high EIR_a value (229.5 infective bites) is found for 2005 ($RR_a = 1191.1$ mm). Regarding 2005, the data reveals favourable breeding conditions between the end of February and May. During this period moderate rainfall amounts ($RR_{\Sigma 10d} < 70$ mm) lead to high η_d values ($\simeq 80\%$) and a strong increase in the number of female mosquitoes ($n_f > 250$ females in May). Strong rainfall amounts at the start of June ($RR_{\Sigma 10d} > 200$ mm) subsequently force η_d and hence n_f to decrease ($\eta_d < 60\%$). The rainfall decline at the end of June produces again favourable breeding conditions increasing the vector population until the start of the little

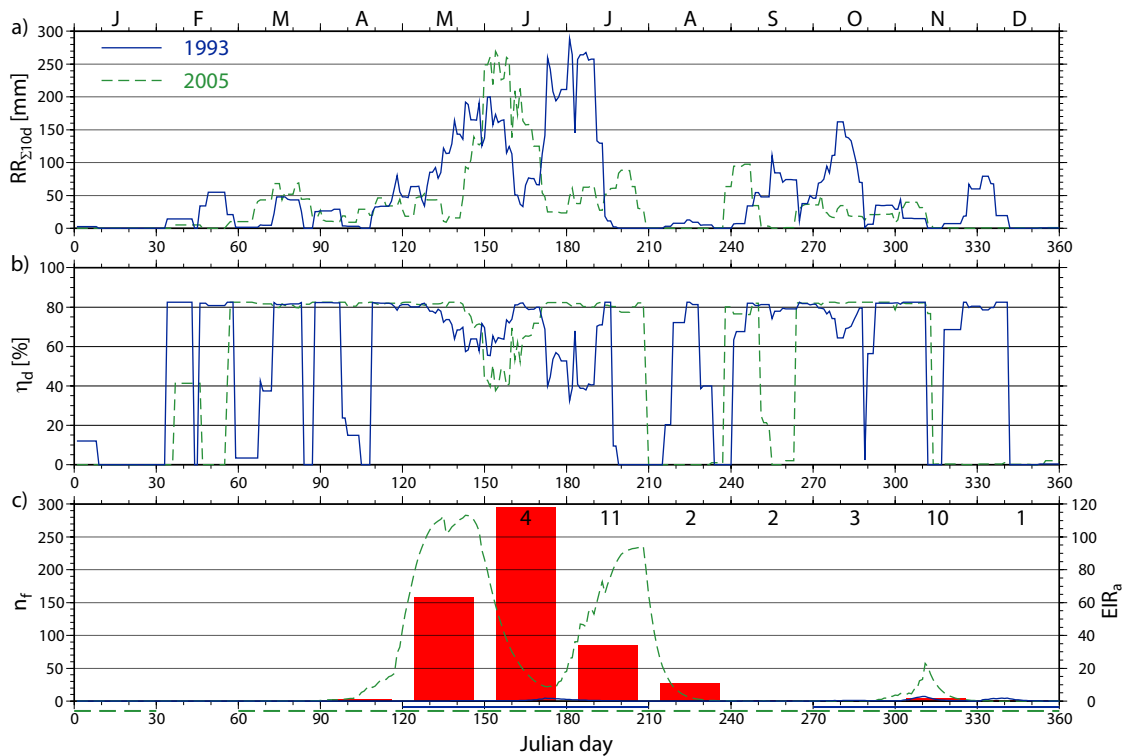


Fig. 6.9: Illustration of daily values of (a) 10-day accumulated precipitation ($RR_{\Sigma 10d}$), (b) the daily survival probabilities of immature mosquitoes (η_d) and (c) the number of female mosquitoes per human (n_f) with regard to the LMM_n simulation of 1993 (blue lines) and 2005 (dashed green lines). In (c) also the monthly entomological inoculation rates (EIR_m) are inserted for 2005 (red bars; right scale). Part (c) additionally indicates the months of the malaria season (lines in the bottom part; $EIR_m > 0.01$ infective bites; cp. Sec. D.5) as well as the frequency of occurrence of $XSeas$ for each month relative to 1973-2006 (one year shows no transmission).

dry season in August. In contrast, breeding in 1993 is inhibited by several dry spells at the start of the rainy season in March and April (η_d decreases to zero). The subsequent excessive rainfall between May and July further reduces η_d and impedes malaria transmission. Therefore, only a fairly small mosquito population is established at the end of June. Also note that in both years the second rainy season in boreal autumn supports development of a comparatively small vector population in November/December. For various other years the maximum of malaria transmission is simulated for the second rainy season. In eleven years out of the 34 years $XSeas$ already occurs in July, but EIR_m peaks in ten years not until November (Fig. 6.9)². In summary, malaria transmission at Cotonou is in the model frequently steered by the more abundant rainy season in boreal spring. During this time, vector breeding is suppressed during dry spells and under excessive rainfall conditions.

In 1993, Akogbéto (1995) conducted entomological measurements at Ganvié (Benin; 6.47N, 2.42E), which is about 40 km to the north of the weather station. At this location HBR already peaked in April one month before the rainfall peak in May. The peak

²Note that due to the duration of the development of gametocytes in humans and due to the length of the sporogonic cycle the EIR maximum lags the peak of the mosquito population.

in April suggests that at Ganvié a larger mosquito population outlived the dry season (e.g., around the lagoon; see also Sec. 5.1.6). In such a situation the population growth is faster in nature than in the model. During the following rain-laden months between May and July ($RR_m > 250$ mm) *HBR* decreased from more than 25 bites in May to about seven mosquito bites per human and per night in July (Fig. 1 in Akogbéto 1995). Similar features were observed by Akogbéto (2000) in a traditional village and in a peri-urban area near Cotonou (cp. Tab. D.3). Here, monthly *HBR* values markedly increased between April and May (comparable to the simulation of 2005), peaked in June, and declined subsequently (Fig. 7 in Akogbéto 2000). In contrast, two less pronounced *HBR* peaks were observed for June and October at the beach of Cotonou. At the Cotonou city centre a primary (secondary) peak was detected for October (July). The observed variety indicates that the LMM_n reproduces a realistic malaria appearance at Benin's coast.

To sum up, in addition to the original version also the LMM_n is fairly sensitive to its parameter settings. Various settings of model parameters result in a markedly altered performance of the model. The mosquito survival scheme, for instance, causes strongly different human biting rates. The level of the parasite prevalence is significantly steered by the recovery rate of humans. It is also found that model simulations are not only sensitive to rainfall amounts but rather depend on its seasonal distribution and intensity.

6.3 LMM_n versus LMM_o

At this point, only the new version of the LMM is validated by entomological and parasitological data from West Africa as well as Cameroon. In this section, also the performance of the LMM_o is analysed. The key feature of this evaluation is that the original version of the model exhibits considerable deficiencies in terms of entomological as well as parasitological observations (see, e.g., Tab. 6.2). The LMM_n represents therefore a significant step forward in the modelling of a weather-driven malaria transmission cycle. The most striking results of the LMM_o simulations at station locations in West Africa and Cameroon as well as from two-dimensional runs are presented.

The comparison of the LMM_o data with field observations reveals two general features. Firstly, the LMM_o fails to simulate malaria transmission in various malarious semi-arid regions and this model version significantly overestimates malaria transmission in humid areas. This feature is the result of the simplified linear relationship between rainfall and the deposition of eggs by female mosquitoes (cp. Sec. 5.1.2). In predominantly dry areas the model is unable to produce reasonable sizes of the mosquito population due to only few simulated deposited eggs. This also leads to a fairly slow increase in numbers of mosquitoes during the onset of the rainy season. Additionally, the mosquito survival of the Martens I scheme is comparatively low at temperatures around 30°C (see Fig. 5.5), which impedes malaria transmission. In contrast, a tremendous number of mosquitoes are generated in humid areas such as Cameroon. The growth of the mosquito population is almost exponential during the course of the rainy sea-

son. Another cause of the increase of the population is the relatively high CAP value (LMM_O (LMM_N): 10,000 (400) fertile females). Secondly, values of the parasite prevalence are flawed in the original model version. Almost the whole population clears the malaria parasite during the dry season due to the high recovery rate (r ; LMM_O (LMM_N): $0.0284 (0.005) \text{ day}^{-1}$). Such a characteristic is, however, not found in parasitological surveys. The strong recovery from infection, moreover, underestimates the maximum level of PR . No more than about 75% of the population are able to be infected in the LMM_O version³.

set	$SC(HBR_a)$	$SC(CSPR_a)$	$SC(EIR_a)$	$SC(Seas)$	$SC(MSeas)$	$SC(XSeas)$	$SC(SSeas)$	$SC(ESeas)$	$SC(PR_a)$	$SC(PR_{max,a})$	$SC(PR_{min,a})$	$SC(all)$
LMM _O	-43 (52)	9 (55)	-20 (54)	27 (42)	18 (41)	22 (37)	16 (41)	22 (37)	8 (29)	12 (25)	4 (27)	75 (440)
LMM _N	37 (52)	33 (55)	41 (54)	31 (42)	23 (41)	28 (37)	28 (41)	18 (37)	16 (29)	16 (25)	8 (27)	279 (440)

Tab. 6.2: Performance of LMM_O and LMM_N relative to entomological and parasitological field studies in West Africa and Cameroon. Numbers in brackets refer to points that could be theoretically achieved. Columns: set: LMM setting; $SC(x)$ denotes the skill score with regard to variable x .

Both features are unveiled by the comparison of LMM_O simulations with entomological and parasitological observations from West Africa and Cameroon. The model completely fails to simulate malaria transmission at the four northernmost locations in the Sahel (Gao, Podor, Rosso, and Saint Louis; e.g., Fig. E.6c; see also Fig. 3.1). Both HBR_a and EIR_a values are clearly lower than observed values in the Sahel (Fig. E.5a & b). In contrast, above RR_a values of about 800 mm the number of mosquito bites increases to unrealistic high values. At Douala, HBR_a partly exceeds 2,000,000 bites per annum. Even in areas with numerous mosquitoes such as irrigated territories, HBR_a is usually limited to values below 50,000 bites. Realistic transmission rates are only found for some medial rainfall conditions between about 400 and 700 mm. These facts clearly demonstrate weaknesses of the linear approximation relative to decadal rainfall of the oviposition process. $CSPR_a$ reveals in general lower values than 1%, likely resulting from the comparatively low mosquito survival of the Martens I scheme (cp. also Fig. 6.6). For this reason, the infectiousness of the mosquito population is underrepresented in the LMM_O. However, this fact is not able to produce realistic EIR_a values at the more humid localities. Besides HBR_a values also values of EIR_a are markedly overestimated by the model at more humid locations (Fig. E.5b). For example, even the lower EIR_a quartile is higher than 4000 infective bites at Yaoundé. In contrast, EIR_a only rarely exceeds 1000 infective bites in entomological field studies (see Tab. S2 in Hay et al. 2005).

³Due to the fact that $(1 - r)^{10} \approx 0.75$ (see also the first footnote in Sec. 7.2.1).

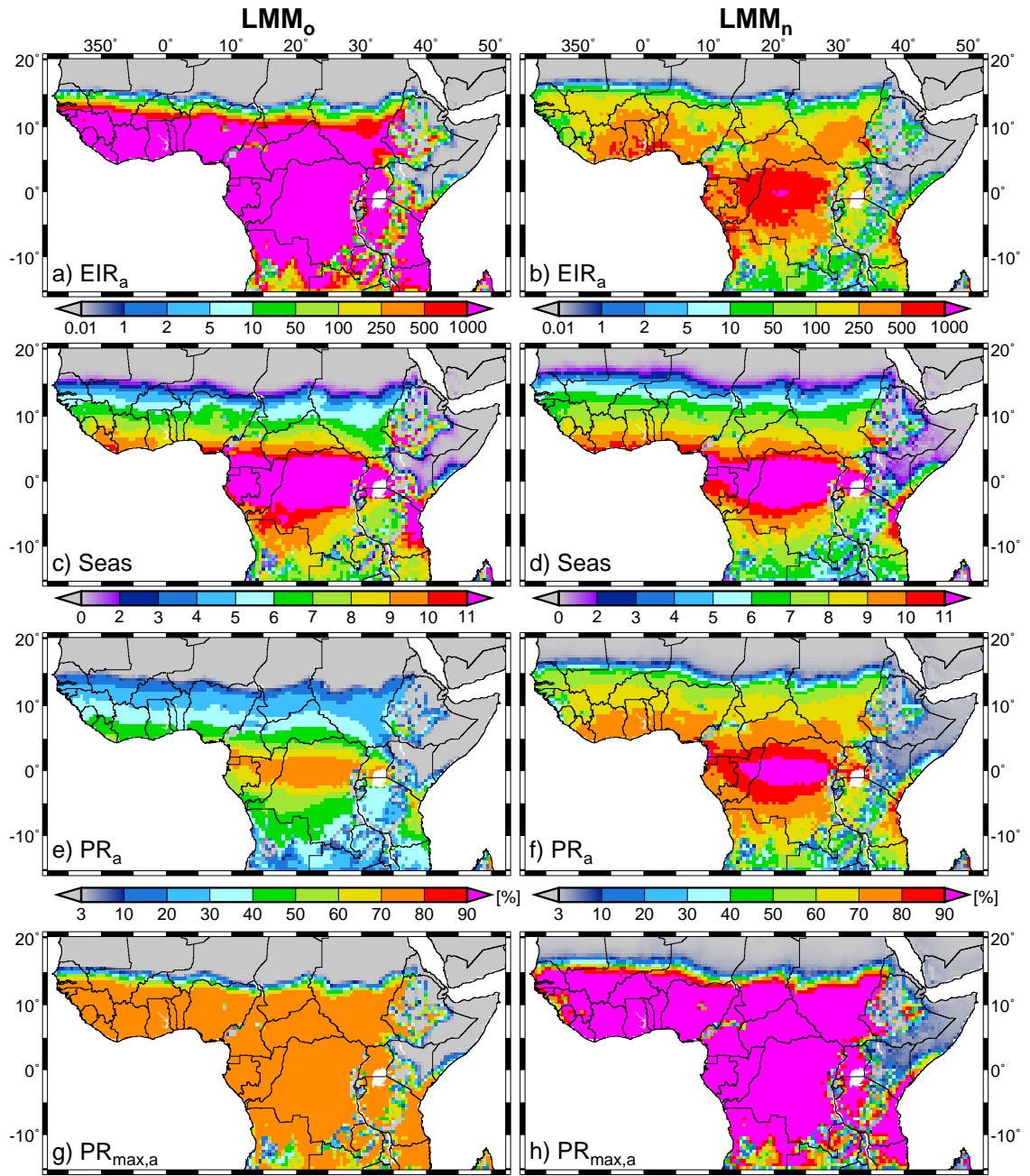


Fig. 6.10: LMM_o and LMM_n simulated present-day (1960-2000) malaria distribution and season length based on REMO(cor) precipitation and temperatures. Displayed are (a & b) EIR_a (in infective bites year⁻¹), (c & d) $Seas$ (in months), (e & f) PR_a , and (g & h) $PR_{max,a}$.

In comparison to observations the malaria season is notably delayed in LMM_o simulations (Fig. E.6). The start of the season occurs about one to two months later under the original than under the new LMM setting (cp. Fig. E.3a). In the West Sahel, for example, transmission starts not until August, whereas transmission begins for various years already in July in the LMM_n runs. In contrast, the simulated end of malaria transmission is somewhat closer to reality. However, due to the large mosquito population at comparatively humid sites, transmission persists frequently longer than observed during the

dry season. The delayed start and somewhat later end of malaria transmission results in a fairly realistic duration of the malaria season. Nevertheless, *Seas* is underestimated in dry areas. The strong growth of the mosquito population causes shorter main transmission seasons in the LMM_O runs. *MSeas* is frequently not as long as in the LMM_N runs (cp. Fig. E.3b). The late onset of the malaria season as well as the slow initial growth of the mosquito population in the LMM_O causes a fairly late occurrence of *XSeas* in the West Sahel. Also for other locations *XSeas* is frequently found later than observed (Fig. E.7a).

The LMM_O simulated parasite prevalence is predominantly influenced by a high recovery rate of humans. For this reason, malaria infection is frequently lower in the LMM_O runs than values from parasitological studies (see Fig. E.7b-d). This is particularly true for the $PR_{min,a}$ value. During the course of the dry season, almost the whole population clears the malaria parasite. In contrast, most observed dry season *PR* data reveals values above 20%. As a direct consequence, also values of PR_a are generally lower than observed. As noted above, the LMM_O is in contrast to the LMM_N not able to reproduce the highest measured $PR_{max,a}$ values.

Also two-dimensional LMM_O simulations confirm the aforementioned statements (Figs. 6.10 & 6.11). The LMM_O simulates much higher transmission rates than observed in endemic malaria areas of Africa. These territories exhibit values higher than 1000 infective bites. The simulations furthermore show that malaria does not penetrate far enough toward the Sahara. The malaria spread stops about 2-4° farther to the south as compared to the distribution of the LMM_N. These facts show that the simulation of the LMM_O is leading to an unrealistic spread of malaria transmission.

The length of the malaria season under the LMM_O simulation is except for areas of Central Africa mostly shorter than in the data of the LMM_N (Fig. 6.10c & d). As aforementioned, the parasite prevalence is comparably low in the LMM_N simulation. The PR_a value barely reaches 60% in Equatorial Africa and $PR_{max,a}$ does not exceed about 75%.

Also results obtained from synoptic stations relative to the malaria season are confirmed by two-dimensional ensemble runs (Fig. 6.11). *MSeas* is somewhat shorter in LMM_O simulations due to extraordinary high transmission rates towards the end of the season. North of about 5°N and 5°S *MSeas* is one to two months shorter than under LMM_N runs. *XSeas* occurs in general later than under LMM_N simulations. In West Africa, *XSeas* is frequently simulated for October than for September. In contrast, for parts of the Guinean coast, *XSeas* is already frequently simulated for July/August. In this zone, the mosquito population is able to grow faster during the first more intense rainy season than in LMM_N simulations. Such a behaviour is not possible in LMM_N runs due to the decreasing pupal and larval survival under high rainfall amounts (cp. Fig. 6.9). As previously mentioned, *SSeas* and *ESeas* occur in general later in LMM_O simulations. Most notable, however, is the strong retardation of the malaria season in highland areas. Strong differences are in particular found for *ESeas* south of the equator and along the Horn of Africa.

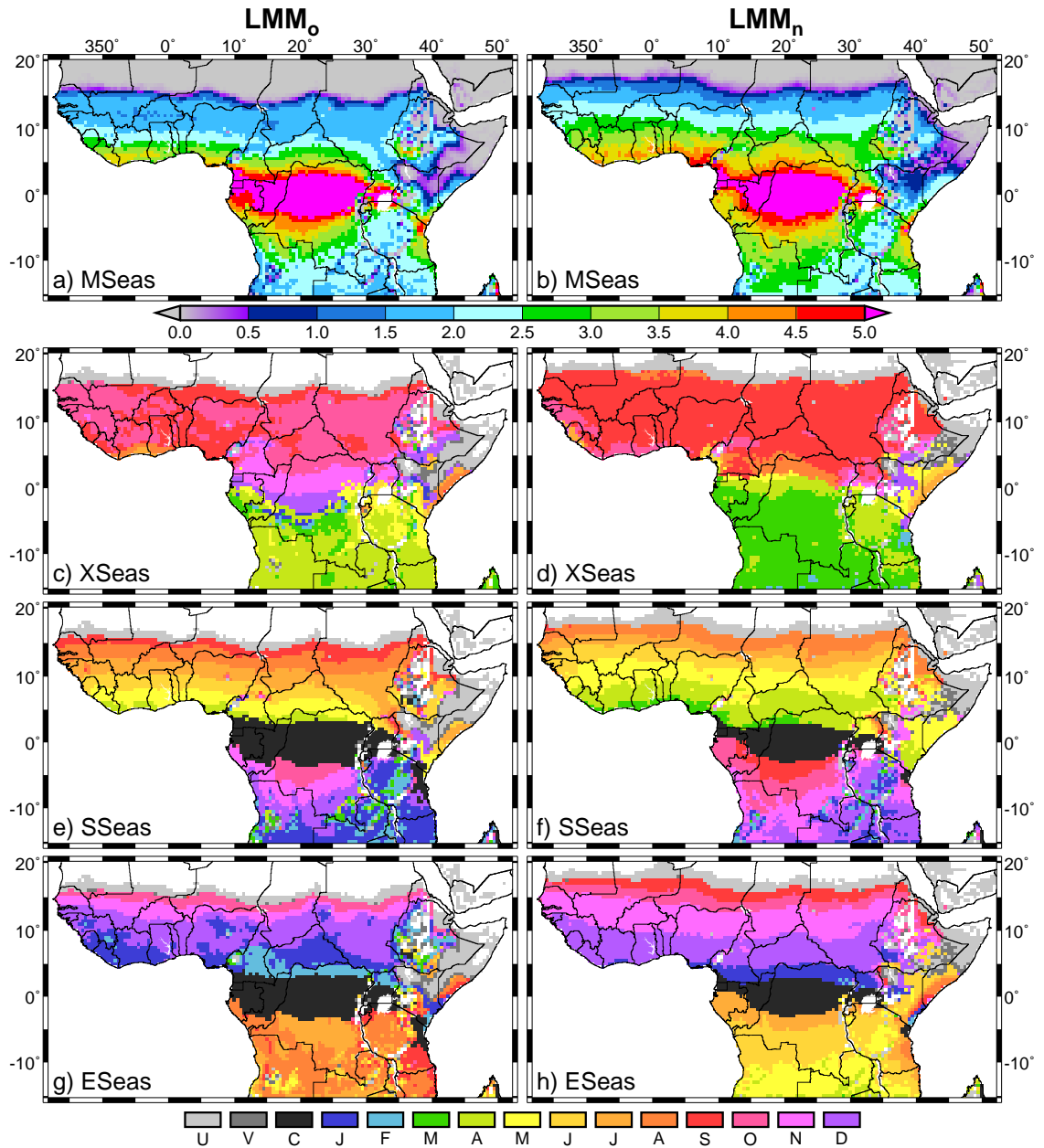


Fig. 6.11: LMM_0 and LMM_n simulated malaria seasonality (in months) for 1960-2000 based on REMO(cor) precipitation and temperatures. Illustrated are (a & b) $MSeas$, (c & d) $XSeas$, (e & f) $SSeas$, and (g & h) $ESeas$. 'U' signs areas of unfrequent malaria transmission; 'V' denotes grid boxes with either rare malaria occurrence or variable seasonality; 'C' identifies year-round malaria transmission (for details see Sec. D.5).

In summary, the LMM_0 shows a markedly too strong (weak) malaria transmission in humid (dry) areas and leads to an unrealistic distribution of malaria. The seasonality is predominantly shifted toward later months. Additionally, the reduced spread of malaria in a couple of highland territories is caused by the comparatively high T_s value of 18°C. It is therefore concluded that the LMM_n version represents a marked improvement of the LMM_0 in terms of the simulation of entomological and parasitological malaria variables. Due to the fact that the LMM_n exhibits realistic transmission rates it is possible to pass EIR data to the Garki model. The LMM_n hence enables more robust projections of the present-day as well as future spread of malaria.

7 Malaria simulations for the present-day and future climate

7.1 REMO climate projections for Africa

The following malaria projections are forced by changes in the bias-corrected REMO temperature and precipitation data. The expected malaria changes therefore can only be understood in connection with altered atmospheric conditions. Knowledge is hence required in terms of future temperatures and rainfall patterns. The REMO ensemble projections were forced by the A1B and B1 emission scenarios (Sec. 2.2) in combination with LUC changes (Sec. 3.10.2). The uncorrected REMO projections were in detail described by Paeth et al. (2009). They further quantified the relative contribution of LUC changes to the total climate change signal. At this point, therefore, only the most important findings are briefly summarised.

Temperatures generally increase in the climate projections within the model domain. The strongest warming signal occurs for the A1B scenario, when LUC changes are considered. The warming is mostly pronounced at the end of the simulation period and is the strongest in tropical Africa, in particular along about 10°N (Fig. 7.1c). This is contrary to the multi-model ensemble of the IPCC-AR4, where the strongest increase is located farther to the north in the western part of the Sahara (cp. Fig. 2.6). Paeth et al. (2009) explained this difference by means of introduced LUC changes which alter the bowen ratio. Note that LUC changes were largely not included in the AOGCMs of the IPCC-AR4. The B1 scenario exhibits similar changes, although, amplitudes are generally 1°C lower than under A1B (Fig. 7.1). In contrast, Paeth et al. (2009) showed that the heating rate is more homogeneous in space and lower when LUC changes are not taken into account. Land degradation accounts for about 35% of the warming signal in tropical Africa (Paeth et al. 2009, their Fig. 7).

Because REMO is not driven by observed SSTs, the model is not able to reproduce the observed drought tendency during the present-day climate (1960-2000). For A1B as well as B1, REMO projects a prominent decrease in rainfall in most parts of West and Central Africa (Fig. 7.2). Annual rainfall decreases by about 100 mm in the southern Sahel and up to 300 mm in the Congo Basin in certain parts reaching more than 20% of

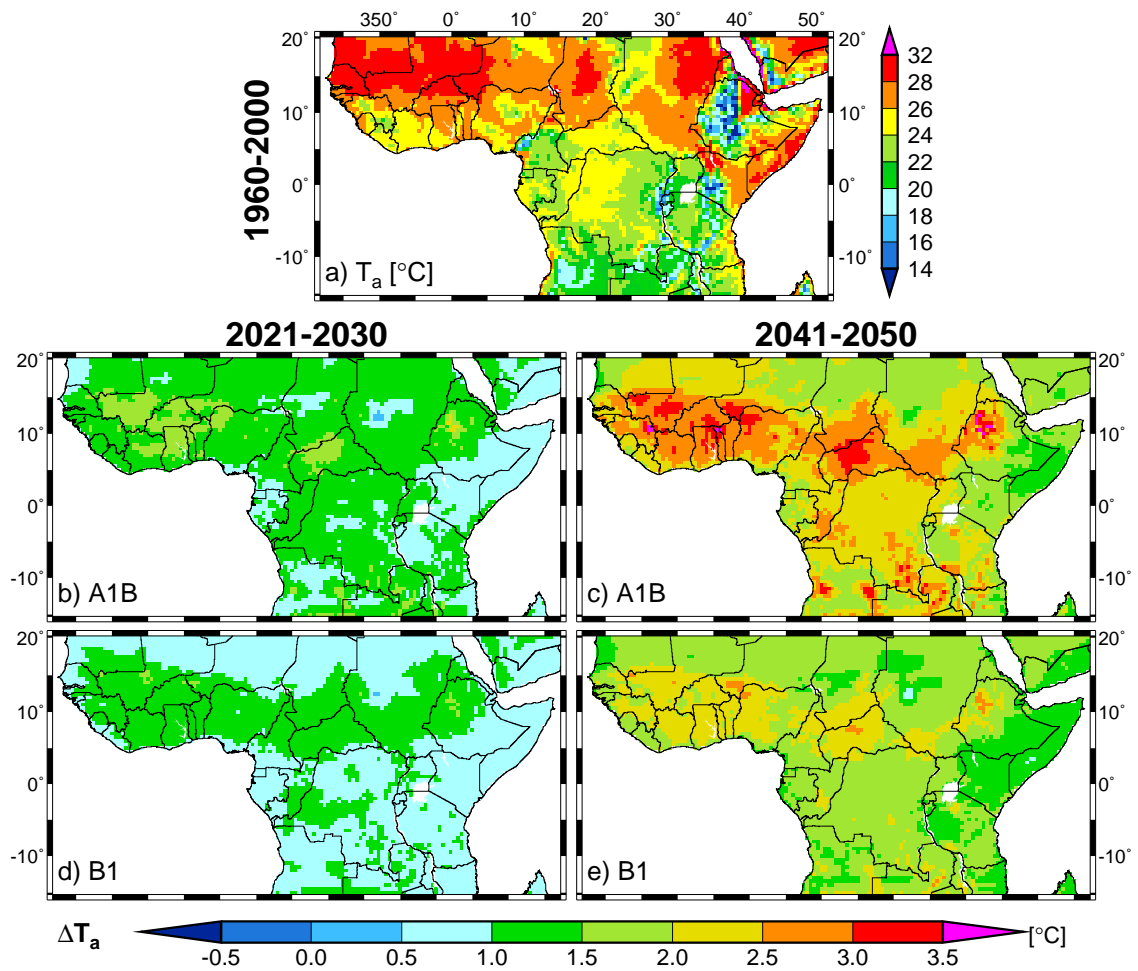


Fig. 7.1: Illustration of the annual mean temperature (T_a in $^{\circ}\text{C}$) of REMO(cor) for (a) 1960-2000 and for (b-e) differences in T_a (ΔT_a) relative to 1960-2000 for 2021-2030 and 2041-2050 of the A1B and B1 scenarios. Note that all displayed grid boxes show statistical significant temperature changes at the 5% level.

the present-day total. In contrast, a positive rainfall trend occurs at the windward side of the Guinean mountains as well as over the Horn of Africa (e.g., Fig. 7.2c). A completely different picture is provided by the A1B scenario without induced LUC changes (Paeth et al. 2009, their Fig. 6). Here, the trend pattern is rather incoherent in space and reveals a lower amplitude. In fact, this pattern is coherent with the projected precipitation trend of the ECHAM5/MPI-OM. Paeth et al. (2009) linked the role of LUC changes to reduced local water recycling due to decreases in evapotranspiration. Except for West Africa, where the GHG forcing contributes up to one-third of the drying, LUC changes are responsible for almost the entire drying signal. The reduced annual precipitation amount leads to longer dry spells reducing water availability.

One result of the warming in tropical Africa is an intensification of the summer monsoon flow. This increases the moisture advection over sub-Saharan Africa and probably causes the rainfall increase in the area of the Guinean mountains. However, in most parts of West and Central Africa this growth is not able to balance the drying trend induced by the reduced local water recycling.

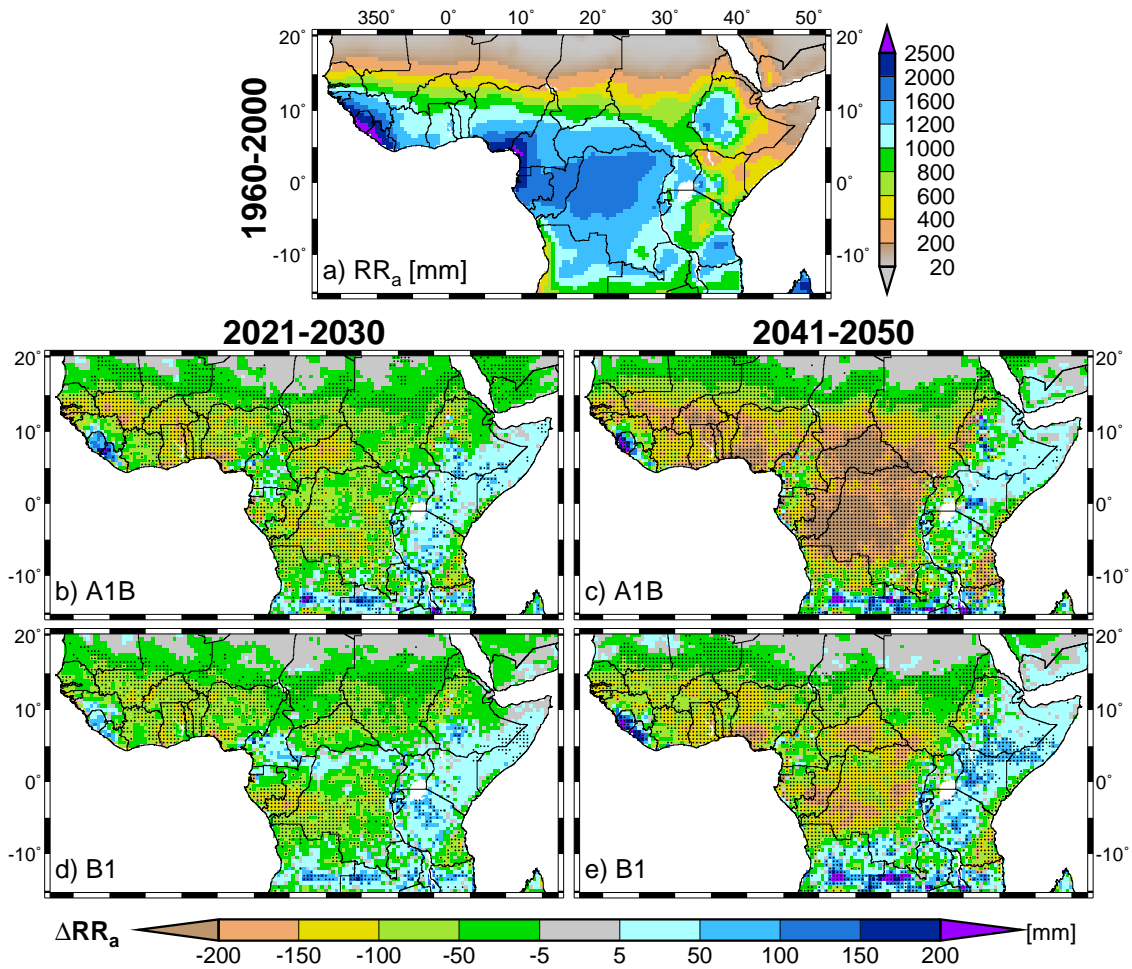


Fig. 7.2: Same as Fig. 7.1, but for the annual precipitation amount (RR_a in mm). Values statistical significant at the 5% level are marked by dots.

7.2 Present-day malaria distribution

7.2.1 LMM_n runs based on IRD/ERA40 (1968-1990)

A realistic simulation of the present-day malaria distribution in Africa is a prerequisite for the projection of the future malaria spread. The skill of the LMM_n in terms of the simulation of various entomological and parasitological variables was shown for single observed rainfall and temperature time series in West Africa and Cameroon (Sec. 6.1). The following two-dimensional malaria runs provide further evidence that the LMM_n version is able to reproduce a realistic malaria distribution.

In order to reduce inherent uncertainties, the LMM_n is first driven on a 1° latitude-longitude grid by IRD rainfall observations and ERA40 temperatures (Secs. 3.6 & 3.9). These runs are restricted to West Africa for the period 1968-1990 and might serve as a reference for subsequent simulations driven by modelled data from REMO.

Apart from the good performance at station locations (Sec. 6.1) the LMM_n also provides realistic entomological data for the West African subcontinent (cp. 7.3). The

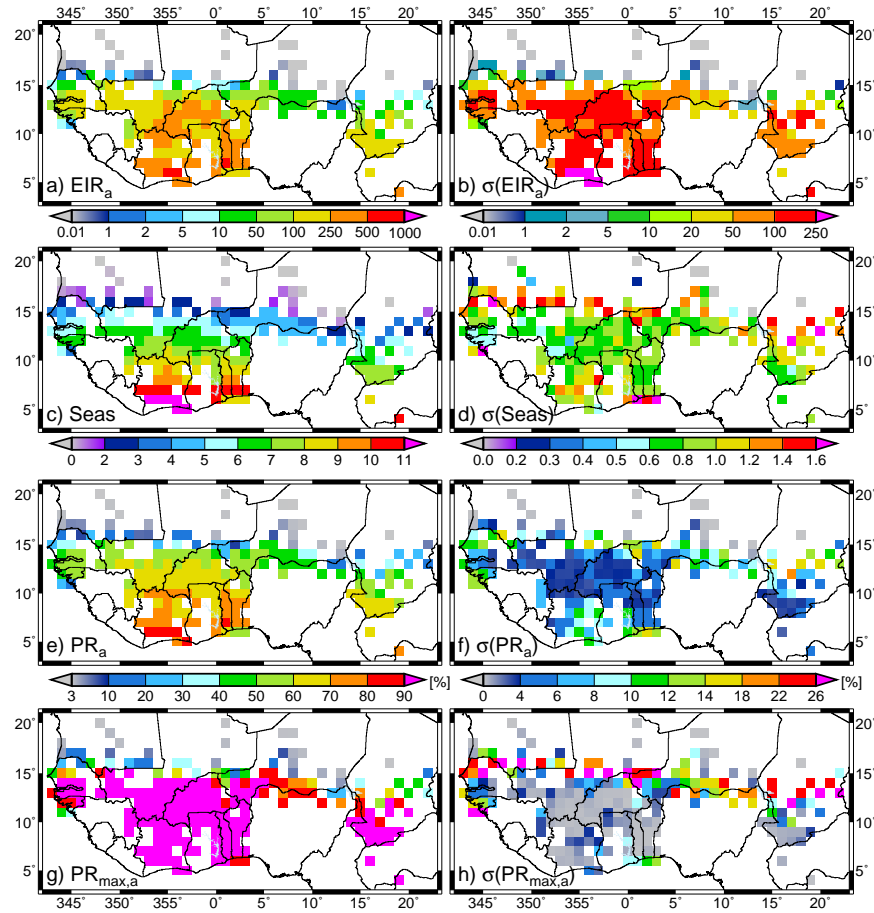


Fig. 7.3: LMM_n simulated present-day (1960-2000) malaria distribution and season length based on IRD precipitation and ERA40 temperatures. Depicted are (a) EIR_a (in infective bites year⁻¹), (b) $\sigma(EIR_a)$ (in infective bites year⁻¹), (c) $Seas$ (in months), (d) $\sigma(Seas)$ (in months), (e) PR_a , (f) $\sigma(PR_a)$, (g) $PR_{max,a}$, and (h) $\sigma(PR_{max,a})$.

largest EIR_a values and the longest malaria seasons are simulated for the southern part of the domain. As expected, transmission is most intense and shows the strongest year-to-year variability along the Guinean coast, the Sudanian zone, and in the southern part of the Sahel. The longest malaria persistence is found for the Guinean coast (Fig. 7.3a-d). South of about 15°N EIR_a usually ranges between 100 and 500 infective bites. A sharp decrease in malaria transmission and in the interannual variability is modelled north of about 15°N. These are areas where the annual rainfall supply falls below 400 mm (average of 1968-1990). Only a marginal malaria transmission is simulated for the fringe of the Sahara desert. Comparatively low are transmission rates at the coast of Togo and Benin. As previously noted, dry spells and excessive rainfall during boreal spring as well as the little dry season can significantly reduce the modelled mosquito population in this area (cp. Sec. 6.2 and Fig. 6.9). In comparison with transmission rates further to the west, southern Chad shows relatively low EIR_a values but reveals an extraordinary year-to-year variability. This might be to a certain extent explained by somewhat lower amounts of precipitation (cp. RR_a in Figs. 4.1 & 4.3a). Excessive rainfall in the frontier border area of Guinea and Guinea-Bissau lead to low simulated EIR_a values (see, e.g.

August in Fig. 4.1). A substantial interannual variability of EIR_a is also simulated. At certain grid points, $\sigma(EIR_a)$ reaches about half or more of the EIR_a value of 1968-1990 (Fig. 7.3b).

The length of the malaria season is closely related to the presence of the monsoon. $Seas$ gradually decreases from about eleven months along the Guinean coast toward less than one month in northern Sahel (Fig. 7.3c). At the coastal area, the season starts around March/April and continues until November/December. Due to the later monsoon onset $SSeas$ is retarded farther in the North. In the Sahel, the transmission is delayed until June to September and the season already ends between September and November (Fig. F.7e & g). In Benin, for example, the average value of $Seas$ decreases in the south-north direction from about ten to six months. $MSeas$ usually adds up to one to five months causing about half of the months of the transmission season to exhibit low transmission rates (Fig. F.7a). North of about 9°N the maximum transmission occurs in general between September and October. However, south of this latitude $XSeas$ is highly variable along the Guinean coastal region. Various years reveal a maximum *monthly Entomological Inoculation Rate* (EIR_m) during boreal spring, whereas for other years the highest EIR_m values occur in boreal autumn (see Figs. F.7c & F.8c). During certain years the presence of the little dry season causes an interruption in the malaria season between August and October/November for various grid points at the coast. This explains the comparatively high value of $\sigma(Seas)$ (Fig. 7.3b).

In agreement with the simulated duration of the malaria season, LMM_n simulations show a decrease in PR_a from the Guinean coast towards the Sahel (Fig. 7.3e). The highest PR_a values of more than 70% are found in the Guinean coastal region. At various grid points south of about 14°N the upper model limit of $PR_{max,a}$ is reached every year (Fig. 7.3g)¹. As observed, PR_a and $PR_{max,a}$ increase strongly in the Sahel from less than 10% to values above 50% (cp. Fig. E.4c)². In this area, $PR_{max,a}$ declines within about three degrees of latitude from values above 90% to values less than 10%. However, the previous validation of the LMM_n already showed (Sec. 6.1) that the simulation of parasitological variables is not as realistic as that of entomological variables (see Sec. 8 for a detailed discussion).

The low and variable transmission intensity and length of the malaria season leads to a strong year-to-year variability of PR in parts of the Sahel. The highest $\sigma(PR_{max,a})$ values are simulated along a latitude band between about 14 and 16°N . Various grid points in the Sahel exhibit a standard deviation above 25%. For the same reasons, $PR_{max,a}$

¹Due to the design of the LMM_n the value of $PR_{max,a}$ is not able to exceed about 95.1%. Under high transmission rates an equilibrium condition is reached in the model, when humans are either in the latent or infectious stage. A fraction of these humans continuously clears their infection. Due to the fixed recovery rate (r) of 0.005 the prepatent period (n_p) of about 10 days is only passed by about 95.1% ($n_p=10$ days $\Rightarrow (1-r)^{n_p} = (1-0.005)^{10} \simeq 0.951$).

²Note that due to the trickle of the number of added infectious mosquitoes (tr_{im}) PR cannot fall to zero in the model (see Sec.5.1.6). A certain level of PR (usually less than 3-4%) is reached by this constant influx even in absence of ‘truly’ simulated transmission. This level is primarily determined by the recovery rate (r) but also depends on atmospheric conditions since mosquito survival in the LMM depends on temperatures and rainfall.

varies significantly at the border area of Guinea and Guinea-Bissau. For most other parts of West Africa the computed standard deviation is fairly low.

7.2.2 Evaluation of LMM_n runs based on REMO (1960-2000)

Subsequent to the modelling of malaria in West Africa forced by observed data, the LMM_n was driven by REMO ensemble runs of the present-day climate of 1960-2000 (see Sec. 3.10). In addition to the presentation of the data, the performance of the model is evaluated using a variety of published malaria maps and additional entomological and parasitological surveys. The modelled spatial and seasonal distribution of the malaria transmission as well as the simulated epidemic risk is also validated.

Present-day malaria runs cover large parts of the African malaria belt (Fig. 7.4). The simulated malaria distribution is comparable to various other published malaria maps (e.g., Fig. 2.8). The spread of malaria is restricted by both, desert areas as well as high-land regions. The pattern of the simulated malaria variables is closely related to runs driven by IRD rainfall and ERA40 temperatures (cp. Figs. 7.3, 7.4, F.7 & F.9). However, malaria transmission reaches higher latitudes in REMO(cor) based LMM_n simulations. This feature is probably related to higher rainfall amounts in the Sahel in REMO(cor) than in IRD (see Sec. 4.1).

The seasonality of malaria in the new simulations also corresponds well to former runs. The largest differences are seen at the Guinean coast. In certain parts, simulations driven by REMO(cor) reveal smaller *Seas* and *MSeas* values. The influence of the little dry season seems to be more pronounced in runs driven by IRD and ERA40. In these runs, malaria transmission is either the strongest between May and July or exhibits a maximum in October-December (Figs. F.7c & F.8a). Such a progression is less frequent in REMO(cor) forced simulations and *XSeas* is only found for September and October (see Figs. F.9c & F.10a). However, the year-to-year variability of *XSeas* is still the largest for certain coastal territories. Large standard deviations are found in particular for the Mount Cameroon region as well as for the coastal zone between Guinea Bissau and Sierra Leone.

The actual runs lead to several new insights into the spread of malaria of West Africa. The additional grid points and the higher spatial resolution show a marked influence of mountainous areas. Compared to nearby plains, temperatures below or around 20°C in the Adamawa and the Jos Plateau (see Fig. 7.1a) lead to lower transmission, shorter and delayed malaria seasons, as well as diminished parasite rates (cp. Figs. 7.4 & F.9). In contrast, the reduced transmission in the Guinean mountains results not from low temperatures but from excessive rainfall. Annual average temperatures in REMO(cor) are above 22°C; however, this region receives large amounts of rainfall (Fig. 7.2a).

The highest *EIR_a* values in the whole model domain are simulated for equatorial Africa and the southwest of Cameroon. These are areas with high annual rainfall but not excessive precipitation like that of the Mount Cameroon (Cameroon; 4°13'N, 9°10'E) area. For the Congo Basin, the LMM_n simulates year-round transmission and the highest

$MSeas$ values, consistent with observations (cp. Carnevale et al. 1992; Bonnet et al. 2002). Additionally, high transmission rates are simulated for grid boxes of the Guinean coast (in particular that of the Dahomey Gap), the southwestern flank of the Ethiopian Highlands, as well as the coast of Tanzania.

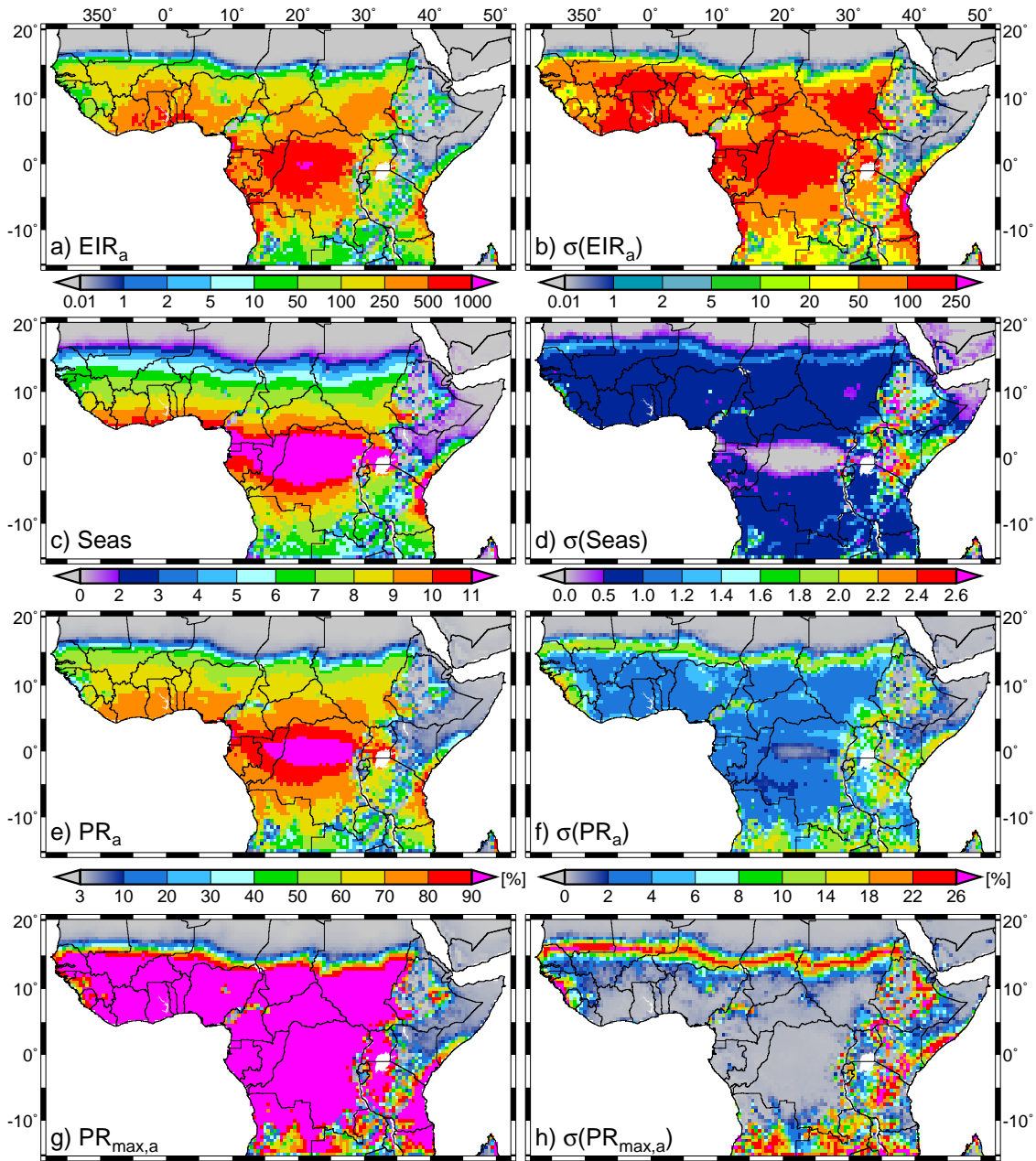


Fig. 7.4: LMM_n simulated present-day (1960-2000) malaria distribution and season length based on REMO(cor) precipitation and temperatures. Displayed are (a) EIR_a (in infective bites year⁻¹), (b) $\sigma(EIR_a)$ (in infective bites year⁻¹), (c) $Seas$ (in months), (d) $\sigma(Seas)$ (in months), (e) PR_a , (f) $\sigma(PR_a)$, (g) $PR_{max,a}$, and (h) $\sigma(PR_{max,a})$.

South of the equator, the onset of transmission is between September and January and malaria usually pauses between April and July, correlating well with MARA maps (cp. Figs. 2.8c & d and F.9e & g). In these territories, the malaria transmission maximises

in the model runs in March or April, which is exactly the opposite of *X Seas* of September or October for areas north of the equator.

The long and short rains in East Africa result in interrupted malaria transmission in certain areas. The LMM_n therefore frequently simulates two malaria seasons (cp. Figs. F.9 & F.10). The first season usually starts in April or May and ends between June and August. The second, shorter malaria season normally starts between November and December with transmission ceasing in December or January (further see App. D.5). The longest malaria season and in parts a year-round transmission is found for the Kenyan and northern Tanzanian coast.

In East Africa, the presence of highlands causes a complex pattern of the malaria distribution. Parts of Ethiopia, Kenya, Tanzania, Rwanda, Burundi, Congo, Zambia, and Angola are covered by highlands (Fig. 2.1b). Atmospheric temperatures (around 20°C or lower; see Fig. 7.1a) in these regions reduce or disrupt the malaria transmission and dry conditions along the Horn of Africa even prohibit the spread of malaria in the model (cp. Fig. 7.2a).

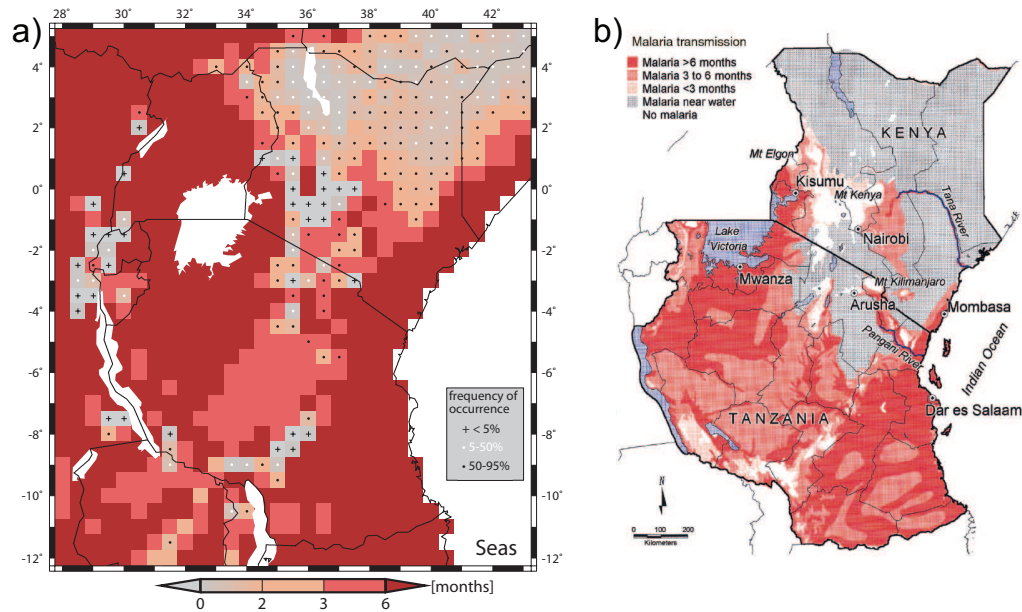


Fig. 7.5: Comparison of (a) the LMM_n simulation with (b) historical Kenyan and Tanzanian malaria maps in terms of the length of the malaria season (*Seas*). The historical analysis of Kenya and Tanzania was performed by Wilson (1956) and Nelson (1959), respectively (see Craig et al. 1999, their Fig. 3b). In (a) black crosses mark grid boxes at which simulated malaria occurs ($EIR_a > 0.01$ infective bites) in less than 5% of the years between 1960 and 2000. In contrast, white (black) dots refer a frequency of occurrence of 5-50 (50-95)%.

Comparison with historical Kenyan and Tanzanian malaria maps enables the verification of model simulations relative to East Africa (see Fig. 7.5). There is a striking resemblance of the simulation with the historical analysis (see also Omumbo et al. 2005, their Fig. 3b). Naturally, some regional details are not captured by the 0.5° latitude-longitude grid. High transmission and parasite rates are both simulated and observed for the northern vicinity of Lake Victoria. In opposition to the model of Omumbo et al.

(2005), the LMM_n simulates a reasonable parasite prevalence and season length south of Lake Victoria. Also, the aforementioned transmission along the coast of Tanzania and southeastern Kenya is included in the historical malaria maps. However, the model seems to overestimate the malaria spread at the coastal zone of Kenya, in particular in the north-eastward direction. The LMM_n exhibits the historically recorded malarious region southeast of Mount Kenya (Kenya; 0°9'S, 37°18'E), which is largely disregarded in the MARA maps (see Fig. 3a in Craig et al. 1999). Here, PR_a ranges between 10 and 40% (Fig. 7.4e) and $Seas$ adds up to 1-5 months in LMM_n runs. There is a close correspondence between modelled and historically recorded malaria free or epidemic-prone areas (see crosses and dots in Fig. 7.5a). As a result of low annual rainfall or low temperatures, the model and historical maps (frequently) lack the malaria transmission in the vicinity of Lake Turkana, in northeastern Kenya, and in Western Kenyan highlands. Also, transmission gaps in the Eastern Arc Mountains of central Tanzania are reflected in the model. However, the LMM_n is, as expected, not able to simulate accurately the malaria spread in the Tana and Pangani river valleys.

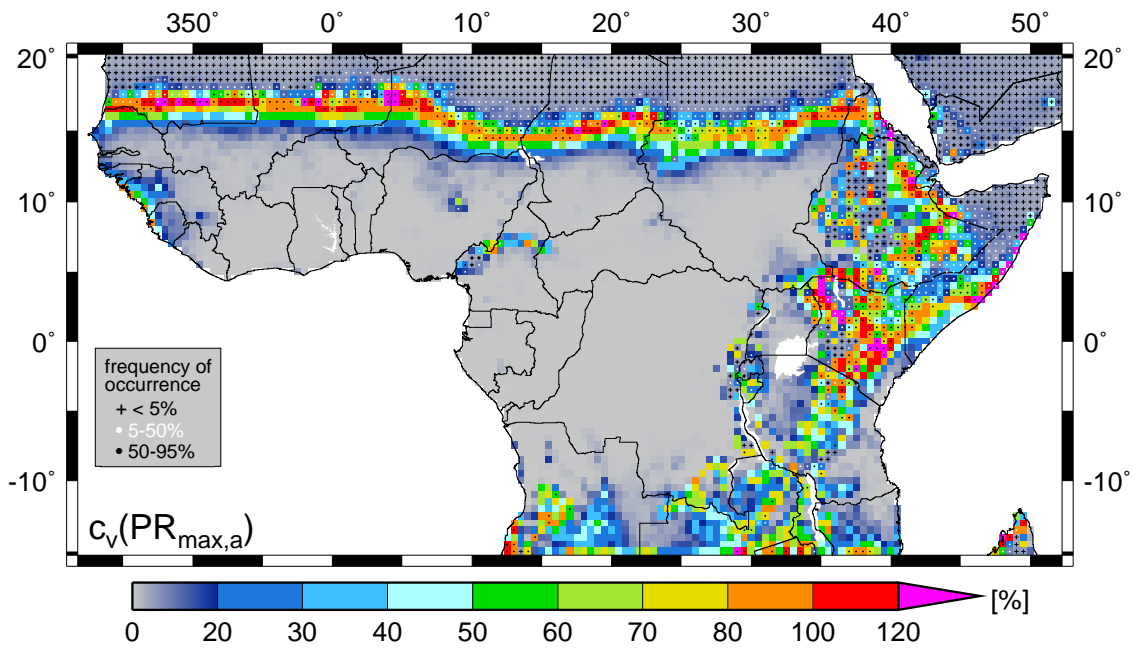


Fig. 7.6: Risk assessment of malaria epidemics with regard to LMM_n runs of the present-day climate (1960-2000) based on REMO(corr). Illustrated is the coefficient of variation (c_v) of $PR_{max,a}$ indicating epidemic risk. Black crosses mark grid boxes at which the simulated malaria occurs ($EIR_a > 0.01$ infective bites) in less than 5% of the years between 1960 and 2000. In contrast, white (black) dots refer to a frequency of occurrence of 5-50 (50-95)%.

Assessment of epidemic malaria risk

The year-to-year variability of the malaria prevalence (Fig. 7.4f & h) is to a certain extent determined by the number of bites humans receive during a certain period. However, once transmission exceeds a certain level no further increase in PR is expected. In fact, the prevalence has been shown to correspond to the logarithm of EIR_a (Beier et al. 1999;

Hay et al. 2005). The approximate saturation level is reached at about 30 infective bites per annum (Smith et al. 1993). On this account, Smith et al. (1993) observed in Kenya no differences in the malaria prevalence despite a tenfold variation in EIR_a . Another factor that determines disease prevalence is its seasonality. Longer transmission seasons likely result in a higher value of PR_a .

Malaria epidemics might be simply defined as an increase in disease prevalence beyond that normally experienced (Macdonald 1957; Connor et al. 1999). Epidemics occur either in usual malaria-free areas or are a result of a significant change in the normally experienced intraseasonal variation of the disease prevalence (cp. Kiszewski and Teklehaimanot 2004). Such events are forced by unusual high seasonal transmission levels and lead to a sharp increase in PR during short time periods. In either case, epidemics lead to a marked increase in $PR_{max,a}$ and are likely to cause a high year-to-year variability of $PR_{max,a}$. Endemic malaria areas with large PR_a values, however, can also reveal high values of $\sigma(PR_{max,a})$. In fact, the interannual variability of $PR_{max,a}$ must be understood in the context of its average value. The *coefficient of variation* (c_v)³ of $PR_{max,a}$ is therefore better suited for the risk assessment of malaria epidemics (Fig. 7.6).

High values of $c_v(PR_{max,a})$ and $\sigma(PR_{max,a})$ are found along a strip within the Sahelian zone between 13 and 18°N (Fig. 7.6), a region well-known for instable malaria transmission. Malaria epidemics have been regularly reported in the arid and semi-arid regions of Senegal, Mauritania, Mali, Niger, Chad, and Sudan (Kiszewski and Teklehaimanot 2004). The band of high $c_v(PR_{max,a})$ values (e.g., >50%) is located about one to two degrees farther to the north than the strip of $\sigma(PR_{max,a})$. Note that transmission rates within the $c_v(PR_{max,a})$ strip are fairly low. During several years the malaria transmission is absent in LMM_n simulations in the northern part of this zone (see the black and white dots in Fig. 7.6). The unstable malaria zone of the LMM_n is about one degree displaced to the south of epidemic malaria areas defined by the climate-suitability of the MDM (cp. Fig. 3 in Snow et al. 1999a).

Various grid points in the Jos Plateau and Adamawa mountains exhibit large coefficients of variation and therefore reveal a potential epidemic risk. However, the malaria transmission seems to be endemic throughout Nigeria, even in the area of the Jos Plateau (e.g., Uneke et al. 2005). Recently, Atangana et al. (2009) performed a *cross-sectional survey* in the Western Cameroon highlands in the area of Mangoum (Cameroon; 5°28'N, 10°33'E) at an *altitude* (z) of about 1100 m with average temperatures of about 22°C. This surveillance showed that the Western Cameroon highlands are characterised by a high malaria transmission intensity ($EIR_a=101$ infectious bites). Also Wanji et al. (2003) found a high EIR_a of 161 infective bites in the Mount Cameroon region. However, no single mosquito was collected and therefore no malaria transmission was observed at

³The coefficient of variation is defined as the ratio of the standard deviation (σ) to the mean (μ): $c_v = \frac{\sigma}{\mu}$. This statistical variable relates the standard deviation of the data to its mean value. The usefulness of c_v is limited when the mean is near zero. In this case, c_v is sensitive to small changes in the mean value. However, due to the structure of the LMM_n the parasite prevalence in sub-Saharan Africa does not fall below 1%.

Vasingi (Cameroon; 4°17'N, 9°15'E) at an altitude of 1200 m. The authors explained the absence of mosquitoes by low temperatures (usually <15°C) and by the lack of appropriate breeding sites due to fast-flowing streams. This finding confirms the unstable or absent malaria transmission in the present-day malaria runs. Due to the orography of REMO (z reaches in parts >1400 m; cp. Fig. 2.1) various grid points of the REMO(cor) data exhibit temperatures below 20°C (Fig. 7.1a).

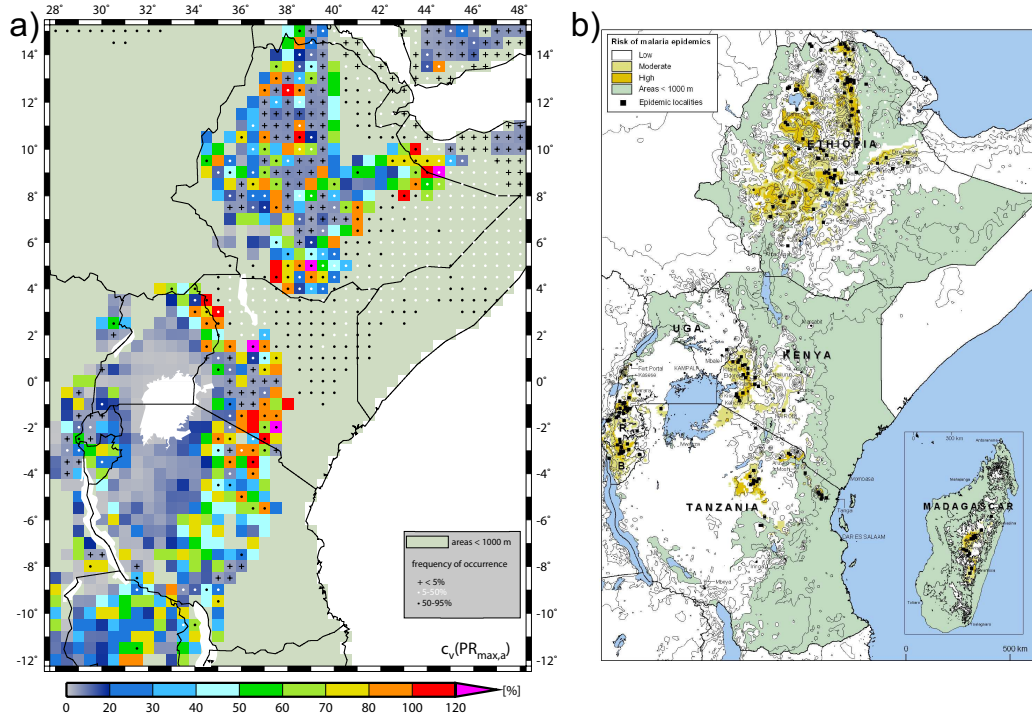


Fig. 7.7: Comparison of (a) $c_v(PR_{max,a})$ as simulated by the LMM_n with (b) epidemic localities and predicted epidemic risk in East African highland areas above 1000 m. The map in (b) has been extracted from Fig. 8.2 in Cox et al. (1999). Crosses and dots in (a) render the same information as in Fig. 7.6.

Also, the southwestern coast of West Africa shows a strong year-to-year variability of the parasite prevalence. These areas might be characterised as epidemic since they also show large values of $c_v(PR_{max,a})$ (>80%). Unfortunately, no malaria data was published for the coast of Guinea-Bissau, Guinea, and Sierra Leone (see Hay et al. 2005, their Tab. S2). Data exists only for the area of Bo in the Southern Province of Sierra Leone (cp. Fig. G.2). An average prevalence of 61% was found by Barnish et al. (1993) for eight villages in 1990 (LMM_n: $50\% \leq PR_{max,a} < 60\%$). During the same time Bockarie et al. (1994) conducted an entomological study. EIR_a ranged from 21.5–36.5 infective bites (LMM_n: $10 \leq EIR_a < 100$). Additionally, measures of the seasonal variation of indoor-resting *Anopheles* females are provided (their Fig. 1). High monthly rainfall from July to September ($RR_m \simeq 500$ mm) is remarkable and the concurrent rapid decline in catches of female mosquitoes. These measurements once again suggest a marked influence of excessive precipitation on the vector population size. It is interesting to note that for this area LMM_n simulations exhibit a secondary maximum of $XSeas$

for July/August (cp. Figs. F.9c & F.10a). Other field studies in the same region detected much higher transmission rates (Bockarie et al. 1993, 1995; Magbity et al. 1997). The highest EIR_a value of 1,235 infective bites was found in the village of Bayama (Sierra Leone; 8°00'N, 11°77'E). However, such values are not simulated by the LMM_n in this region.

The distribution of potential epidemic risk in the Greater Horn of Africa is complex and warrants further investigation. For the present-day climate various areas at high altitudes are unsuitable for the simulated malaria distribution (see Figs. 2.1b, 7.4 & 7.17). A high orography in REMO is found along the East African Rift. Malaria-free areas are simulated for the Eastern Rift Valley comprising the Ethiopian Highlands as well as the Western Kenyan highlands. Malaria is also absent in the Western Rift Valley in the area of southwestern Uganda, Rwanda, and Burundi. The malaria spread is frequently limited along the Udzungwa Mountains to the northeast of Lake Malawi. Also no malaria is modelled for the northern part of Somalia resulting from arid climate conditions (cp. Figs. 2.1b & 7.4).

Marginal malaria areas are either found in arid climates or are located in regions exhibiting temperatures only slightly above the sporogonic temperature threshold. The typology of these areas therefore varies according to whether the transmission is permitted due to exceptional rainfall or whether small temperature increases enable parasite development (Snow et al. 1999a). East African highlands are well known for malaria epidemics. As previously described (Sec. 2.8), various locations in East African highlands experienced a rise in frequencies of epidemics during the 20th century. Unstable highland malaria transmission is concentrated in large parts of Ethiopia, western Kenya, southwestern Uganda, much of Rwanda and Burundi, as well as the northern part of the Eastern Arc Mountains and the Kagera district in Tanzania (Fig. 7.7b).

The LMM_n identifies large parts of East Africa as epidemic-prone areas. The LMM_n simulates a considerable parasite prevalence up to an altitude of about 1900 m (cp. Fig. 7.17), close to the generally considered upper limit of transmission of approximately 2000 m (Kiszewski and Teklehaimanot 2004). The model accurately represents the epidemic risk of various known epidemic highland territories (see Fig. 7.7). However, the results suffer from the horizontal resolution of the model runs. The grid points are not able to represent the variable altitudes at highlands sites. Epidemic risk is underestimated for Western Kenyan highlands⁴. Only few grid points reveal high $c_v(PR_{max,a})$ values. Epidemic-risk in the Eastern Arc Mountains of Tanzania cannot only be explained by altitude. Temperature is not always the significant factor of transmission in this region, which is often limited by the availability of breeding sites for malaria vectors.

⁴Malakooti et al. (1998), for example, described the study site of the tea estate in Kericho (Kenya; 0°22'S, 35°17'E) in Western Kenyan highlands. The altitude of this area ranges from 1,780-2,225 m. By contrast, the REMO background orography abruptly jumps within 1° longitude from Lake Victoria ($z \simeq 1150$ m) to altitudes above about 2000 m. As a result, simulated temperatures in Western Kenyan highlands do not fully reproduce the observed temperature range and hence reduce the likelihood of epidemics in the model. The simulated transmission abruptly decreases from high EIR_a values at the shore of Lake Victoria to almost zero at high altitudes.

This fact likely causes the comparatively low altitude of 1455 m of Tanzania at which epidemic localities were recorded (Cox et al. 1999). Additionally, localised malaria epidemics were monitored at Angola and Zambia (Kiszewski and Teklehaimanot 2004) and the LMM_n simulates a considerable potential epidemic risk for these countries.

Unstable malaria transmission is also found at the Horn of Africa. The MARA project identified arid deserts at the juncture of Kenya, Ethiopia, and Somalia as epidemic-prone areas (see Snow et al. 1999a, their Fig. 3) and the LMM_n identified potential epidemic localities for most parts of these territories (Fig. 7.7a). Unstable malaria transmission areas are both discovered by MARA and the LMM_n for the arid and semi-arid plain areas of Kenya, southeastern Ethiopia, as well as parts of the Afar depression. This is different for almost the whole country of Somalia, which is subject to epidemic risk in the MARA map, whereas only about half of Somalia shows unstable malaria transmission in LMM_n runs (Fig. 7.6). Only a small risk is indicated by the LMM_n for northern Somalia and the southern coast of South Central Somalia.

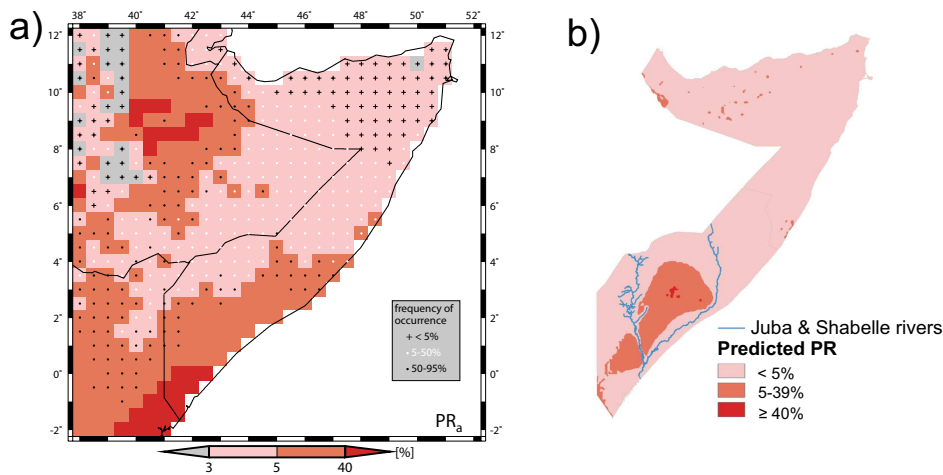


Fig. 7.8: Comparison of parasite prevalence (PR_a) for Somalia between (a) the LMM_n simulation and (b) predicted values from Noor et al. (2008a). Crosses and dots in (a) render the same information as in Fig. 7.6.

Noor et al. (2008a) recently analysed parasitological surveillances from Somalia. According to data from 2005-2007 the parasite prevalence is low in the north (2.8%) and somewhat larger in the south. It is interesting that various observations in northern Somalia reveal no malaria parasites (see Fig. 4 in Guerra et al. 2008). Noor et al. (2008a) additionally performed a spatial prediction of PR for the entire country (Fig. 7.8b). This map shows the largest prevalence (at certain sites >40%) in parts of South Central Somalia with reduced infection rates at coastal regions. In the same area northwest of Mogadishu, Noor et al. (2008b) dissected the *P. falciparum* infection from four cross-sectional surveys in 2007. The prevalence was significantly lower in bed net users and exceeded 20% only in pastoralist communities and in children aged 5-14 years. In the late 1980's, Warsame et al. (1989) additionally found an infection prevalence of 18% among children aged 1-9 years.

Values of the simulated and estimated infection rates in South Central Somalia are comparable to modelled PR_a values (Fig. 7.8). However, the highest prevalence in the model runs is shifted toward the coast underestimating the epidemic risk of this zone. Simulated PR values are hence too low farther inland, which conversely results in an overestimated variability of the malaria transmission (Fig. 7.6). The LMM_n furthermore underestimates the malaria spread in northern Somalia. In contrast to various surveys between 2005 and 2007, almost no transmission is found in model runs for the present-day climate (see crosses in Fig. 7.8a).

In summary, the LMM_n demonstrates a fairly realistic simulation of the malaria spread in Africa. The model correctly reproduces the epidemic potential at fringes of endemic malaria areas. Epidemic-prone areas are found along a band in the northern Sahel, for various highland areas, as well as in arid and semi-arid zones of East Africa. Significant discrepancies are mainly a result of the crude horizontal resolution and likely originate from specific environmental conditions.

7.2.3 Garki model simulations based on LMM_n runs (1960-2000)

The analysis of the present-day malaria situation is supplemented with simulations from the Garki model. This model is driven by 5-day accumulated *EIR* values taken from the LMM_n ensemble runs. Unlike the LMM, the Garki model considers various malaria key features such as immunity (see Sec. 5.2). The application of the Garki model allows an assessment of the age dependence of parasite prevalence and an estimation of the proportion of infectious and immune hosts. The model therefore permits an analysis of changes in the population structure of malaria under future climate conditions. The Garki model furthermore facilitates an assessment of the performance of the LMM_n with regard to simulated parasite prevalence.

The infectious individuals in the Garki model are in the early stages of disease. For this reason, this population group is probably suffering from malaria outbreaks. This group of the human population is therefore likely to be responsible for the largest contribution to morbidity and mortality numbers. The largest annual mean proportions of infectious individuals ($y_{1,a}$) are, for example, found for short seasonal and intense malaria transmission occurring in the Sudanian or southern Sahelian zone (Fig. 7.9a). These regions are characterised by a comparatively slow attainment of immunity in the model. More than one fifth of the human population is infectious in these territories. In fact, these are also areas with a comparatively low proportion of immune individuals (Fig. 7.9g). By contrast, year-round and high transmission rates in the Congo Basin result in fairly low y_1 values due to a rapid immunisation of the population (cp. Fig. 7.20d). Naturally, infectivity is fairly low at fringe malaria areas. In these regions, however, the interannual variability of $y_{1,a}$ is large (Fig. 7.9b). Thus certain atmospheric conditions during particular years lead to a marked increase in infectivity. There is a close correspondence between the standard deviation of $y_{1,a}$ and that of $PR_{max,a}$ from the LMM_n (see Fig. 7.4h). Of course $\sigma(y_{1,a})$ values are much lower than that of $\sigma(PR_{max,a})$ due to the higher level of $PR_{max,a}$.

The Garki model simulates a fairly uniform parasite prevalence in endemic malaria areas. In such regions, the annual mean and maximum malaria positive proportion (y_a & $y_{max,a}$) usually ranges between 50-70% and 60-80%, respectively (Fig. 7.9c & e). The y_a values are more uniform and lower than corresponding LMM_n PR_a values (cp. Fig. 7.4e). Clearly, the considered immunity decreases disease prevalence in the Garki model. Such a condition is found for the Congo Basin leading to a secondary minimum of $y_{max,a}$ (Fig. 7.9e). Due to the design of the model such a feature cannot be simulated by the LMM_n.

It should be noted that malaria transmission in the LMM_n is adjusted to children (see Sec. 5.1.14). For this reason, it is not surprising that the modelled prevalence differs between the two models. The comparison might be more reasonable in terms of child parasite ratios. According to the Garki model, child prevalence in most malaria areas are higher than 70% except for fringe transmission areas (Fig. 7.19a). The *annual mean parasite ratio of children aged 2-10 years* (PR_{2-10}) is larger and again more uniform

than the corresponding LMM_n PR_a value (Fig. 7.9e). In endemic malaria areas, PR_{2-10} ranges between about 70 and 90% whereas PR_a values of the LMM_n fluctuate between about 50 and 90%. This behaviour is not startling since the LMM_n exhibits an about twice as large recovery rate (LMM_n : $r = 0.005 \text{ day}^{-1}$; Garki model: $r = 0.0023 \text{ day}^{-1}$ for non-immune individuals; cp. Sec. 5). Due to high y_a values the transition to non-malaria areas is more abrupt in Garki model simulations. The Garki model also shows strong influences of highlands on malaria prevalence in children.

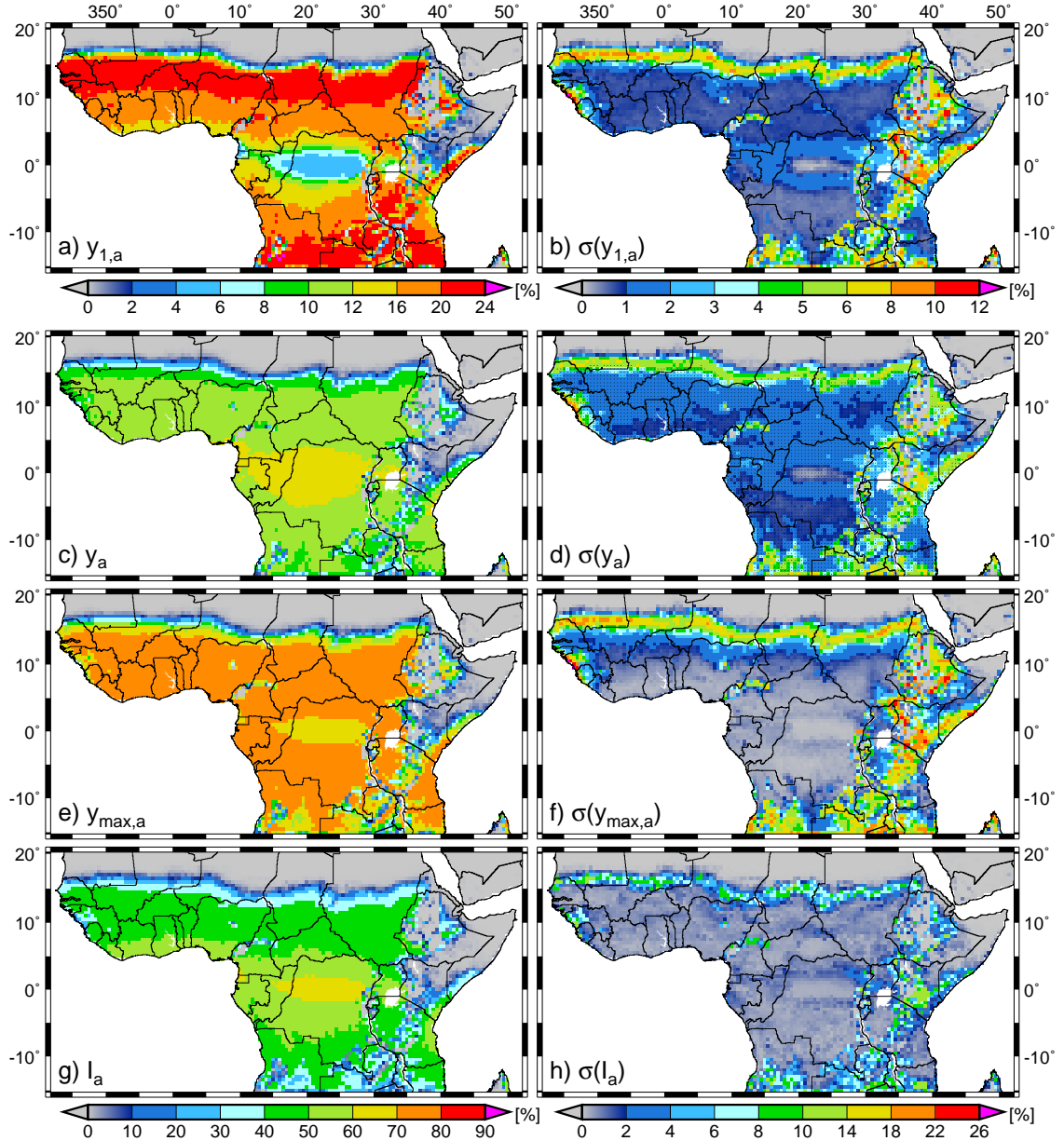


Fig. 7.9: Garki model simulated present-day (1960-2000) malaria variables based on EIR_a values from the LMM_n . Displayed are (a) the annual mean proportion of infectious individuals ($y_{1,a}$), (b) $\sigma(y_{1,a})$, (c) the annual mean proportion of malaria positive individuals (y_a), (d) $\sigma(y_a)$, (e) the annual maximum proportion of malaria positive individuals ($y_{max,a}$), (f) $\sigma(y_{max,a})$, (g) the annual mean proportion of immune individuals (I_a), and (h) $\sigma(I_a)$. Dots in (d) mark areas in which $y_{max,a}$ never falls below 10%.

One expected result are congruent malaria areas between the Garki model and LMM_n (cp. Figs. 7.6 & 7.9b⁵). However, this is more or less obvious since the Garki model is driven by *EIR* data from the LMM_n. More interesting is the fact that both models identify about the same areas with a strong year-to-year variability of the malaria prevalence (Fig. 7.9b, d & f). Nevertheless, values of standard deviations are clearly smaller than the ones of the LMM_n (Fig. 7.9f & h). The reason for this behaviour is likely the fast recovery of infected immune individuals prohibiting a higher number of infections.

The proportion of immune hosts is as expected the largest in the equatorial tropics in the area of year-round malaria transmission (Fig. 7.9g). In the Congo Basin, the *annual mean proportion of immune individuals* (I_a) amounts to about 60-70%. This value is somewhat lower for endemic malaria areas with seasonal transmission. I_a ranges usually from 40-60%. The Garki model simulates a sharp I_a decrease for the northern part of the Sahel as well as for other fringe malaria territories such as highlands. This feature is realistic since unstable malaria transmission does not support development of an adequate immune protection. Note also that I_a only varies from year-to-year in these fringe malaria areas (Fig. 7.9h).

The pattern of patent malaria positives reveals the expected peak in children below an age of about five years (y_a in Fig. 7.20). The transmission level determines whether this peak is attained at an earlier or later age of each child. At very high transmission rates such as in the Congo Basin the y_a maximum is already found at the second year of age (Fig. 7.20d). In epidemic-prone areas no such maximum is found (cp. Fig. 7.20a). The age at which the peak occurs seems not to vary as much with the transmission intensity as is observed in field studies. Additionally, the decline with age in prevalence is not as pronounced as in many field data sets (e.g., Figs. 3 & 4 in Molineaux et al. 1978).

One characteristic of the model for a given overall force of infection is a steeper decline in prevalence with age when transmission is seasonal than when it is not (not shown). Parasite prevalence is reduced when inoculations are delivered seasonally, than when they are evenly distributed throughout the year. This model feature is a result of the way in which superinfections are treated in the model. New infections make less contribution to the prevalence when the host already has a risk of infection. In fact, at certain transmission levels the risk of being infected does not raise anymore.

The simulated age pattern of infectivity seems to correspond reasonably well to gametocyte prevalence data (e.g., Fig. 1 in Dietz et al. 1974). The infectious proportion is again the highest for young children ($y_{1,a}$ in Fig. 7.20). At low transmission levels infectivity declines much slower than at high transmission rates. However, direct feeding or membrane feeding experiments did not revealed as striking age dependencies as is seen in patent gametocytaemia. Muirhead-Thomson (1957), for example, found that adolescents and adults constitute at least 30% of the total reservoir of malaria infection

⁵The coefficient of variation for $y_{max,a}$ was not calculated since various values of $y_{max,a}$ are near to zero. Note also that the model design does not support a computation of the interannual variability of child parasite ratios (cp. Sec. 5.2).

in Liberia. The very steep decline in the Congo Basin hence might be overemphasised in the model.

Another expected result is the rise in the number of immune individuals with age (I_a in Fig. 7.20). Note that hosts do not lose their immunity status in the original version of the Garki model. The increase of the fraction of immune hosts follows in principle a more or less steep saturation curve depending on the transmission level. In the equatorial tropics, already more than 50% of all 15 years olds are immune. Low transmission levels in the northern Sahel and in East African highlands are an example for an almost linear increase with only about 20% of the population are immune at an age of 75 years.

To sum up, the Garki model reproduces fairly realistic features of malaria prevalence. The highest infectivity and prevalence is usually found within the first five years of life due to their low immune status. Children therefore are likely to suffer most from disease outbreaks. A short seasonal and intense malaria transmission causes the largest infectious proportions. The highest immune proportions are found in the oldest age groups. The most rapid immunisation is simulated in areas of year-round and intense malaria transmission.

7.2.4 Malaria seasonality from the MSM (1960-2000)

The malaria seasonality is additionally analysed by MSM simulations (Sec. 5.3). Present-day REMO ensemble runs for 1960-2000 (see Sec. 3.10) were used for calculation of the present-day climate conditions of required two monthly and three yearly climate variables.

The distribution of rainfall and temperatures in space and time determine the simulated malaria seasonality of the MSM. Only a small area in the heart of the African continent exhibits no malaria constraints. For other grid boxes the MSM criteria (Tab. 5.4) are not satisfied at least during parts of the year (see Figs. 7.10 & F.34). The regions north and south of the equator are affected by low precipitation amounts during boreal winter and summer, respectively. Farther north and south also atmospheric temperatures are a crucial factor. During boreal winter (summer) temperatures fall to such low values that the malaria transmission would break north (south) of about 15°N (10°S) under the presence of the parasite. Temperatures further limit the spread of malaria in East African highlands. At few grid points in Ethiopia even the frost criterion impedes malaria transmission in the model.

In Africa, precipitation limits the spread of malaria in various areas. No transmission is hence predicted for regions with low annual precipitation amounts, for example, in the Sahara desert, along the Horn of Africa, and in the vicinity of Lake Turkana (Fig. 7.11a). The catalyst month and the monthly moving precipitation criteria are leading to a variable malaria season length in the simulations. In agreement with the RR_a distribution and LMM_n runs, the MSM reveals a decrease in season length from Equatorial Africa towards the Sahel. Malaria transmission is year-round in the equatorial tropics in the area of the largest precipitation amounts in southern Cameroon, Equatorial Guinea, Gabon,

large parts of Congo, and Uganda, as well as in certain parts of western Kenya and northern Tanzania. Noticeable is the comparatively short malaria transmission in the Eastern Arc Mountains of Tanzania. This feature is again related to low temperatures and rainfall.

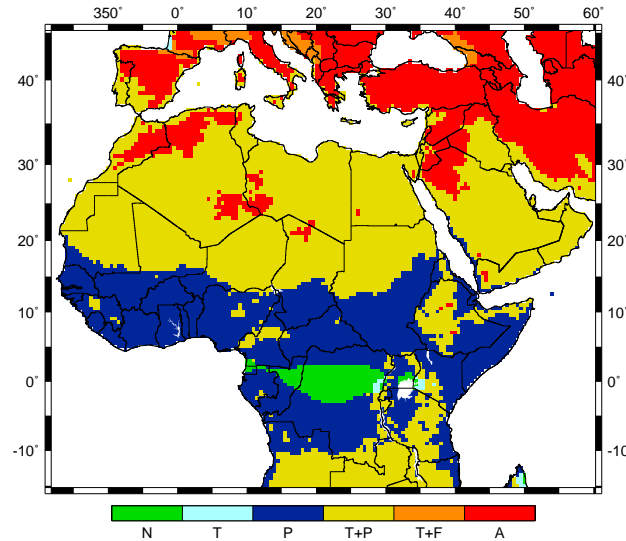


Fig. 7.10: Constraints of malaria transmission for the present-day climate (1960-2000) with regard to MSM criteria (cp. Tab 5.4). Included are criteria that at least once impede malaria transmission during the course of the year. Constraints: T: T_{3m} ; P: RR_{3m} or RR_c ; T+P: T_{3m} & (RR_{3m} or RR_c); T+F: T_{3m} & $T_{min,m}$; A: $T_{min,m}$ & T_{3m} & (RR_{3m} or RR_c); and N: no constraint.

The MSM also correctly reproduces the gap in the malaria spread in East African highlands. The MSM simulates malaria-free areas along the Great Rift Valley, for example, in the Ethiopian Highlands. Also the Fouta Djallon in Guinea, as well as the Jos and Adamawa Plateau in Nigeria and Cameroon markedly reduce the season length or even cause no malaria transmission in the MSM.

Results of MSM simulations compare well with maps provided by MARA (Fig. 2.8b) as well as to results of the LMM_n (see Figs. F.7 & F.9). However, differences relative to MARA maps occur in parts of West Africa as well as in the Greater Horn of Africa. MSM simulations driven by REMO(cor) exhibit a shorter transmission season along the Guinean coast and in the northern Sahel. The MARA map reveals various non-malaria areas in southeastern Ethiopia, the centre of Kenya, and in western Somalia that are not malaria-free in the present MSM simulations. Differences are also found south of the equator in Zambia and Angola. Note that these disagreements are often related to different orographies and an unequal resolution of data sets.

In West Africa, the start of malaria transmission is simulated short after the onset of the rainy season. Comparable to LMM_n simulations the malaria season sets in between March and April and finally ends in November or December at the Guinean coast (Fig. 7.11b & c). Also the MSM reproduces delayed malaria seasonality toward the Sahara. The MSM furthermore depicts two distinct malaria seasons in various parts of East Africa. Two seasons of several grid boxes of the Adamawa Plateau are a result of low

monthly temperatures during boreal summer. It is interesting to note that the LMM_n lacks this feature for most years between 1960 and 2000 (cp. Fig. F.10).

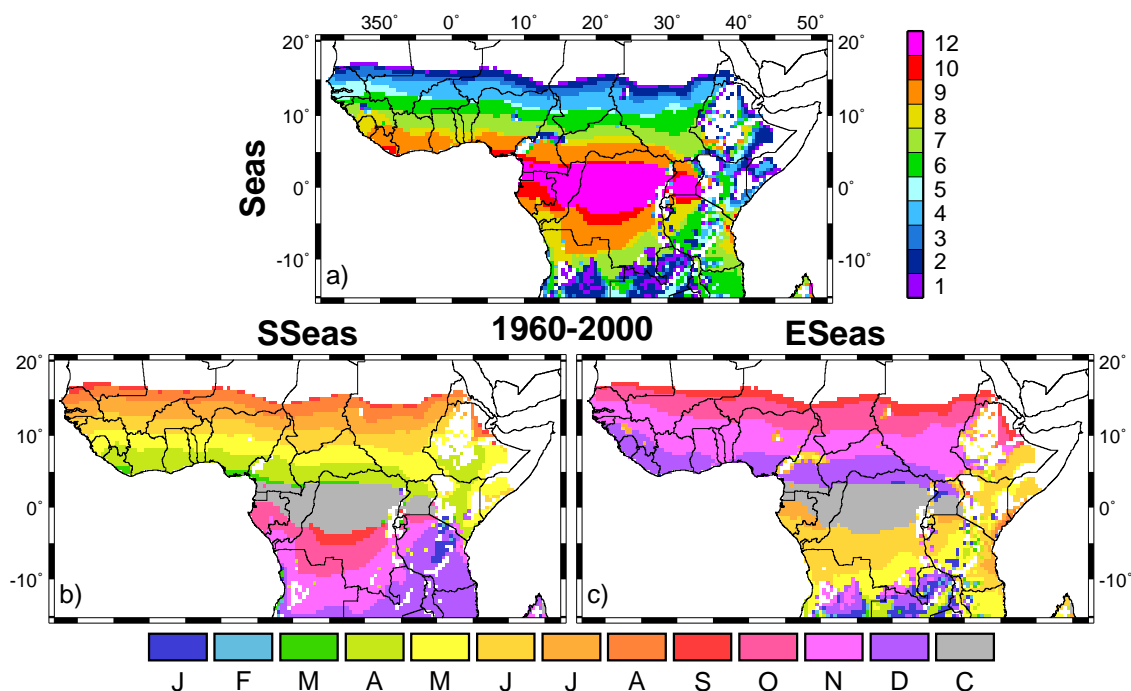


Fig. 7.11: MSM simulations of (a) the length of the malaria season (*Seas*; in months), (b) the start (*SSeas*), and (c) the end month (*ESeas*) of the malaria transmission (C: year-round transmission) for the present-day climate (1960-2000). Regarding *SSeas* and *ESeas* for areas with two seasons only the first malaria season is shown.

For most regions south of the equatorial tropics, malaria transmission is simulated between boreal autumn and early boreal summer. However, due to low temperatures at some grid points in Angola and Zambia seasonality is restricted between November and January. For other parts of this area the malaria season breaks between February and March, which is also detectable in MARA maps (Fig. 2.8b & c). The LMM_n simulates, however, a somewhat reversed pattern (see Fig. F.9). These differences likely result from a different response to comparatively low temperatures of this area (cp. Fig. 7.2a).

In summary, in various African areas precipitation limits the spread of malaria in the MSM. For the equatorial tropics temperature constraints are only found in highland areas. Only a small area in the heart of the African continent exhibits no limitations for malaria transmission. Simulations of the MSM are comparable to MARA maps and reveal only small differences to the LMM_n predicted seasonality.

7.3 Malaria projections for 2001-2050

7.3.1 LMM_n projections based on REMO

Subsequent to the detailed analysis of the present-day malaria distribution the projected future spread of the disease is presented. The analysis of simulated malaria changes focuses on the 2020s and 2040s. These decades are located in the middle and at the end of the future period (2001-2050), respectively. The first time period allows identification of risk areas for improved public health planning in the near future. In contrast, the second decade enables an evaluation of the impact of climate change on malaria in the long run. As previously described (Sec. 7.1), future climate projections foresee in both scenarios a prominent surface warming and a significant reduction of rainfall over several parts of tropical Africa. As a consequence, the simulated spread of malaria and epidemic risk is markedly altered under these future atmospheric conditions.

The Sahel

In the northern part of sub-Saharan Africa, the precipitation decline forces a significant decrease of malaria transmission in the Sahel (Fig. 7.12; see Figs. F.15-F.18 for the projected absolute values). In both scenarios, EIR_a decreases north of about 13°N (Fig. 7.12a & b). The transmission decline is most pronounced in the southern part of the Sahel, that is south of about 15°N. The EIR_a decrease is projected to be the strongest in the northern part of Burkina Faso. In this territory, the simulated transmission approximately halves in comparison to present-day values at the end of the future period (cp. Fig. 7.14b). Also the transmission season markedly shortens in the malaria scenarios. At various grid boxes north of about 10°N $Seas$ decreases by more than 0.5 months (Figs. 7.12c, d & 7.14e). The reduced transmission further translates into a small decrease in the average prevalence (Fig. 7.12e & f). However, south of about 15°N the maximum seasonal parasite prevalence remains on the level of the present-day climate (Fig. 7.12g & h) since EIR_a ranks still above the aforementioned saturation level of about 30 infective bites (cp. Sec. 7.2.2). The slight decrease in PR_a is therefore primarily a result of the shortened malaria season.

In other parts of the Sahel, that is north of about 15°N, the spread of malaria within the human population either fully vanishes (e.g., Fig. 7.16e) or is reduced under the modified future climate. Around of about 16°N, the malaria season is shortened by more than one month (Fig. 7.12c & d). In the 2040s, the malaria transmission is lacking for various grid boxes north of this latitude (see Figs. 7.16c, e & 7.14h). By contrast, south of this latitude transmission is still present but is reduced below the saturation level. This in turn causes the strongly reduced annual maximum of PR between about 14 and 16°N (Fig. 7.12g & h). For example, at about 15°N certain grid boxes reveal a reduced $PR_{max,a}$ from above 80% to values of about 40%.

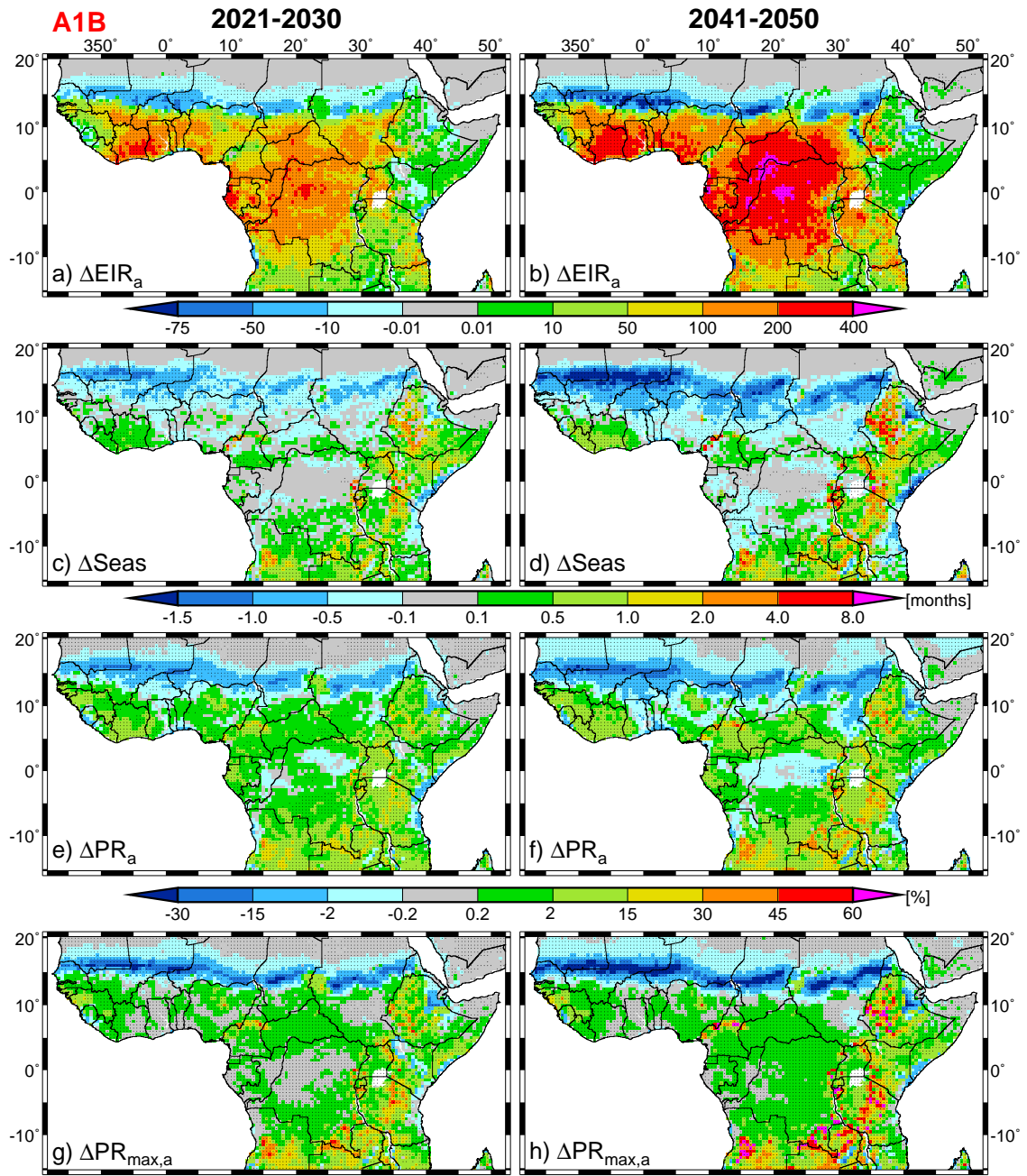


Fig. 7.12: LMM_n projected changes in EIR_a (a & b; in infective bites year⁻¹), $Seas$ (c & d), PR_a (e & f), and $PR_{max,a}$ (g & h) relative to the present-day climate (1960-2000). Illustrated values refer to the A1B scenario (see Fig. F.13 for scenario B1) as well as to 2021-2030 (a, c, e & g) and 2041-2050 (b, d, f & h). Values statistically significant at the 5% level are marked by dots.

Besides the withdrawal of the malaria transmission along the Sahara fringe the change in the year-to-year variability of parasite prevalence is of primary importance. Between about 15-18°N the frequency of the malaria occurrence is reduced (see Fig. 7.16). In comparison to 1960-2000 high $c_v(PR_{max,a})$ values are shifted toward the south by about 1-2° under future climate conditions. North of about 16°N the transmission decline results in lower standard deviations of PR_a and $PR_{max,a}$ (Fig. 7.13c-f). In this zone, malaria epidemics are hence projected to become less likely.

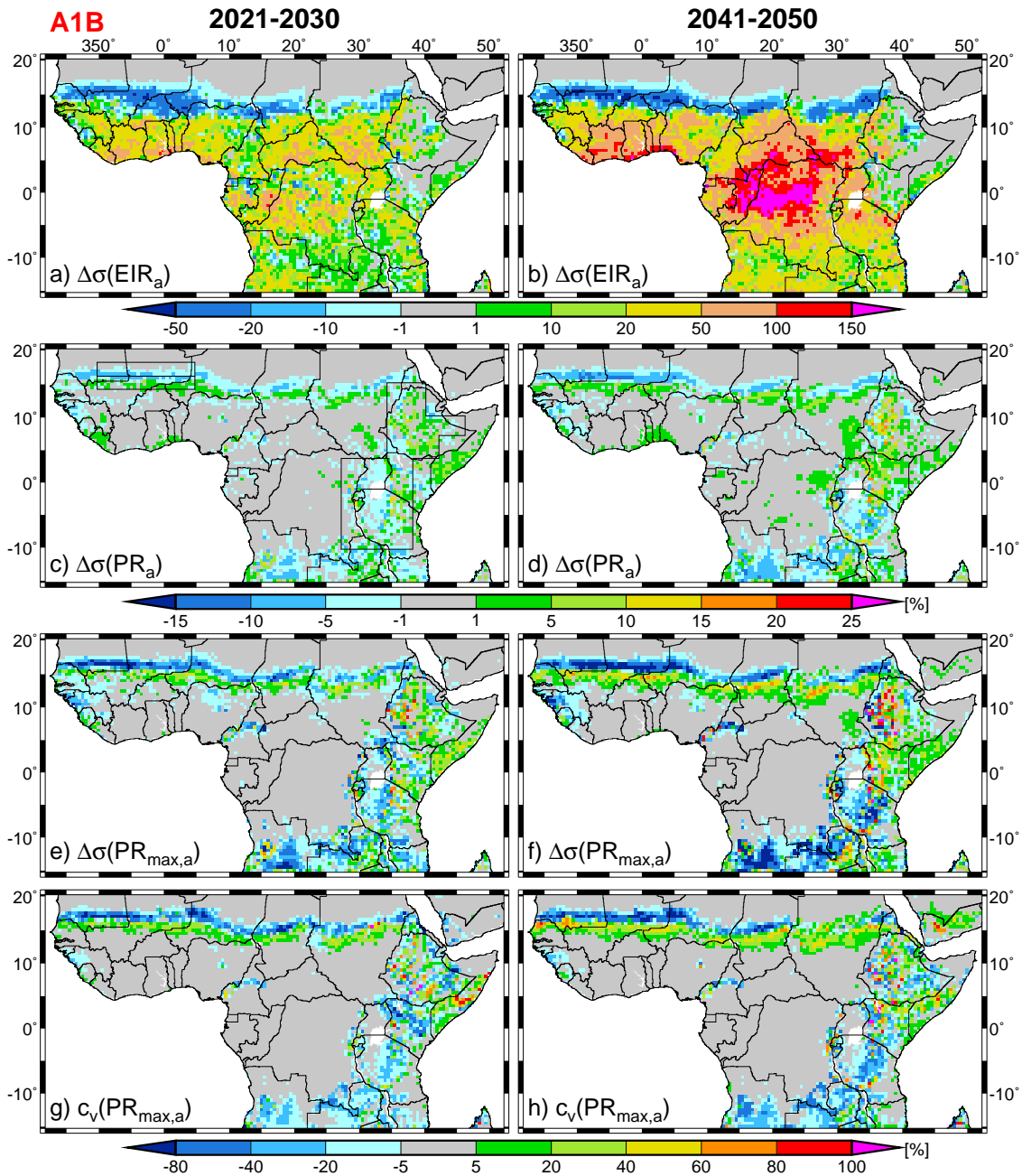


Fig. 7.13: LMM_n projected changes in the standard deviation of EIR_a (a & b; in infective bites year⁻¹), PR_a (c & d), $PR_{max,a}$ (e & f), as well as for $c_v(PR_{max,a})$ (g & h) relative to the present-day climate (1960-2000). Illustrated values refer to the A1B scenario (see Fig. F.14 for scenario B1) as well as to 2021-2030 (a, c, e & g) and 2041-2050 (b, d, f & h). Framed areas in (c) depict the northern and southern Sahel as well as the region of East African highlands.

There is an increase in the interannual variability of PR_a and $PR_{max,a}$ south of about 16°N. The frequency of epidemics therefore is expected to increase in actually denser populated territories. The populous area along the Atlantic coast of Senegal, for example, is projected to become epidemic-prone. More densely populated areas in Mauritania, Mali, Niger, Chad, and Sudan are furthermore projected to extend into a zone of increased epidemic risk (Fig. 7.16). However, the intensity of the year-to-year variability

decreases in general due to the reduced transmission level. In Mali, for example, values of the $c_v(PR_{max,a})$ strip decrease by about 50%. Some large cities like Agadez (Niger) seem to loose their epidemic status. Under the A1B scenario, but not for B1, parts of the dense populated region north of the Sénégal show a markedly reduced epidemic risk in particular in the 2040s.

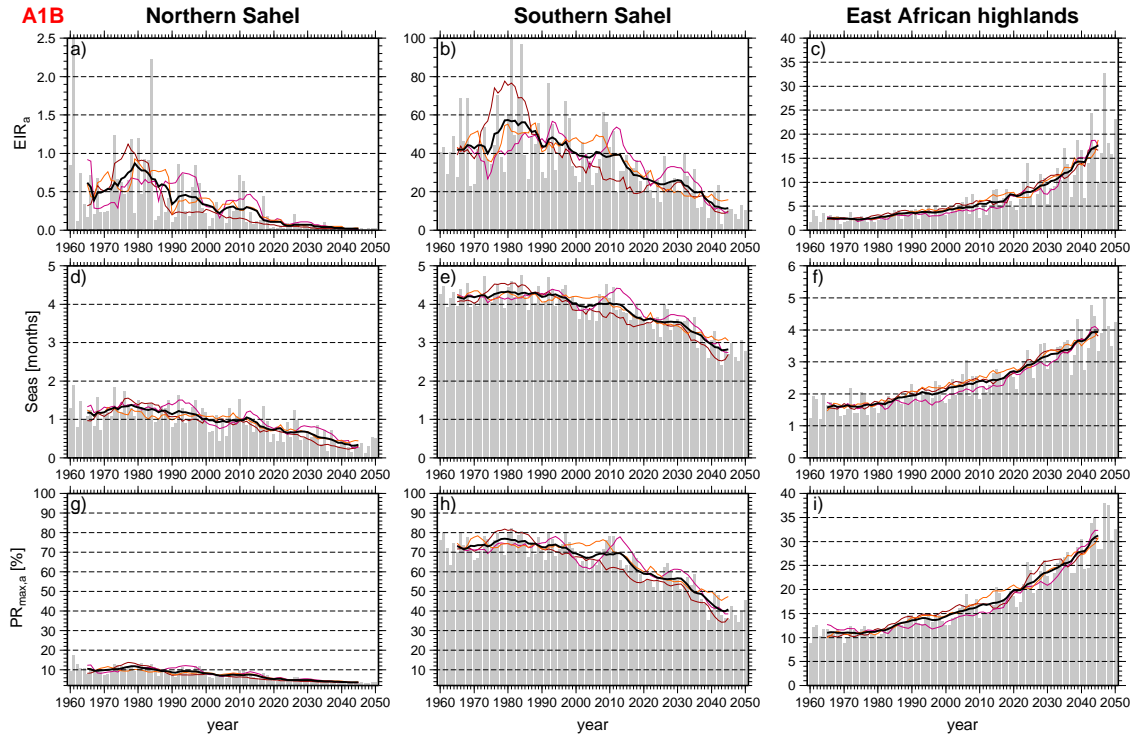


Fig. 7.14: LMM_n simulated time series of entomological and parasitological malaria variables regarding 1960-2050 for the northern Sahel (16.5-18°N, 10°W-5°E; a, d & g; see Fig. 7.13c), southern Sahel (14.5-16°N, 10°W-5°E; b, e & h), and highlands of East Africa (areas ≥ 1500 m; c, f & i). Displayed are yearly anomalies of the ensemble mean (grey bars) relative to 1960-2000 and in terms of EIR_a (a-c; in infective bites year⁻¹), $Seas$ (d-f), and $PR_{max,a}$ (g-i). Further illustrated are 11-year running mean anomalies of three ensemble runs (reddish lines) and the ensemble mean (black line). The data for 2001-2050 refers to the A1B scenario (see Fig. F.24 for scenario B1).

Further parts of West Africa

Farther to the south of West Africa, the decline in precipitation and increase in temperature is beneficial for the growth of the mosquito population. Under these modified atmospheric conditions the flushing of breeding habitats is reduced and the gonotrophic cycle is shortened in the model. Both factors result in a larger number of female mosquitoes under the climate scenarios resulting in a significant increase in EIR_a and its standard deviation (Figs. 7.12a, b & 7.13a, b). For certain parts of the Guinean coastal area EIR_a increases by more than 200 infective bites.

The start of the malaria season is retarded and the transmission ceases earlier under the malaria projections except for areas between Liberia and Ghana (see Figs. F.19-F.22). The slightly shortened malaria season is caused by lower precipitation amounts

at the start and end of the rainy season (see Figs. F.5 & F.6). The shorter transmission period and higher biting rates hence lead to an intensified malaria season. Additionally, maximum transmission occurs somewhat earlier in the year. The longer simulated malaria season for areas around the Ivory Coast is caused by an earlier transmission start in March instead of April resulting from more abundant rainfall in January and February. Higher precipitation amounts reduce biting rates, the length of the malaria season, as well as parasite prevalence at southwestern Sierra Leone.

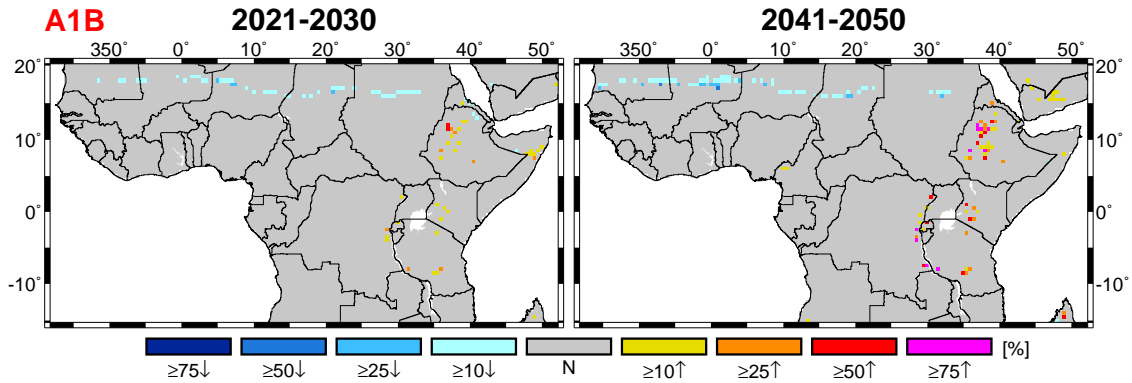


Fig. 7.15: Disappeared and new malaria areas relative to (a) 2021-2030 and (b) 2030-2040 (see Fig. F.26 for scenario B1) projected by LMM_n. Illustrated are areas that either reveal a malaria occurrence of less than 5% for the present-day climate (1960-2000) or during the depicted future decades (cp. Fig. 7.6). Downward arrows indicate a decline in the malaria occurrence from above the specified digit to a value below 5%. In contrast, upward arrows show an increase in the malaria presence from values of less than 5%.

The strongest prevalence increases in West Africa are simulated for the Adamawa and Jos Plateau (see Fig. 7.12e-h) resulting from the marked temperature increase in parts beyond 20°C (see Fig. 7.1). Certain grid boxes in the Adamawa reveal more than 60% higher $PR_{max,a}$ values in the 2040s than between 1960-2000. The comparatively low lying eastern part of the Adamawa is particularly affected. In this territory, the malaria occurrence stabilises due to a sinking interannual variability of $PR_{max,a}$ (Fig. 7.13e-h). A different situation is detected for parts of the Western Cameroon highlands. Formerly malaria-free areas disappear (Fig. 7.15) and $\sigma(PR_{max,a})$ strongly rises at some grid boxes causing a high epidemic potential (cp. Fig. 7.16). Also mountainous areas of Guinea show a relatively strong increase in PR .

Greater Horn of Africa

The most pronounced changes in Africa are found in East Africa particularly at highland areas. Significantly higher temperatures and slightly higher rainfall lead to a small or moderate increase in malaria transmission (rarely exceeding 50 infective bites per annum; cp. Fig. 7.12a & b). However, such an increase in transmission rates leads to a substantial increase in parasite prevalence in formerly epidemic-prone areas. As a result, the spread of malaria is markedly increased in various parts of East Africa. In cer-

tain parts PR_a and $PR_{max,a}$ exhibit 30 and 60% higher values in the 2040s, respectively (Fig. 7.12f & h).

As previously found in other studies (e.g., Lindsay and Martens 1998), the strongest prevalence increase is simulated for highland areas (e.g., Fig. 7.14). Higher temperatures especially affect large parts of the Great Rift Valley (Fig. 7.12e-h). Strongly modified is the spread of malaria transmission at Ethiopian Highlands, the Eastern Arc Mountains, and parts of the Western Rift Valley. In Ethiopia, for example, highland malaria is significantly increased especially westward of the main ridge of the Great Rift Valley. Even some grid boxes of the Western Kenyan highlands are newly affected, despite the fact that these territories are higher than 2000 m in REMO (cp. Fig. 7.16). Also most parts of the Eastern Arc Mountains reveal higher disease frequencies. Changes in this territory not only originate from elevated temperatures but also likely arise from 50-100 mm higher annual rainfall (Fig. 7.2). Atmospheric changes come along with a notable prolongation of the malaria transmission and an earlier (later) start (end) of the season. For example, in certain parts of the Eastern Arc Mountains $SSeas$ already begins in December instead of January/February (Figs. 7.12c-e & F.19-F.22).

In East Africa, also the interannual variability of disease prevalence is markedly modified under the future climate (Fig. 7.13). Whereas the year-to-year variability of EIR_a rises uniformly, there is an irregular change of $\sigma(PR_a)$ and $\sigma(PR_{max,a})$. Areas where the malaria transmission is becoming more stable or instable are often side by side. Such a feature is also valid for changes in the epidemic potential (Fig. 7.16). Various areas show decreasing values of $c_v(PR_{max,a})$, whereas some other grid boxes exhibit a higher coefficient of variation. Highland areas formerly unsuitable for malaria are becoming suitable under the warmer future climate. The simulations clearly indicate changes in the epidemic risk.

The large difference in changes of the year-to-year variability of $PR_{max,a}$ in highlands is a result of elevation. Analysis of disease transmission against height levels illustrates this fact (cp. Fig. 7.17). As expected, the rise in temperatures increases malaria transmission and disease prevalence at all altitudes. Both biting rates as well as the duration of the malaria season increase below 2500 m. This in turn affects parasite prevalence throughout all levels. However, this does not necessarily enhance the epidemic potential. Quite the contrary, at most grid boxes malaria transmission stabilises below about 1900 m, for example, in most parts of the Eastern Arc Mountains. At these altitudes the regular transmission likely improves the partial immunity of the population reducing the mortality of malaria. In contrast, malaria climbs to formerly malaria-free zones above about 2000 m enforcing the probability of malaria epidemics. A comparable situation already took place in Burundi at the end of the 1990s when malaria was first introduced above 1450 m (Bonora et al. 2001). Under both scenarios, various grid boxes in Western Kenyan highlands as well as in the region around the Udzungwa Mountains, for example, are projected to turn into epidemic-prone areas (see Fig. 7.16). The infrequent disease occurrence likely results in higher mortalities above about 2000 m.

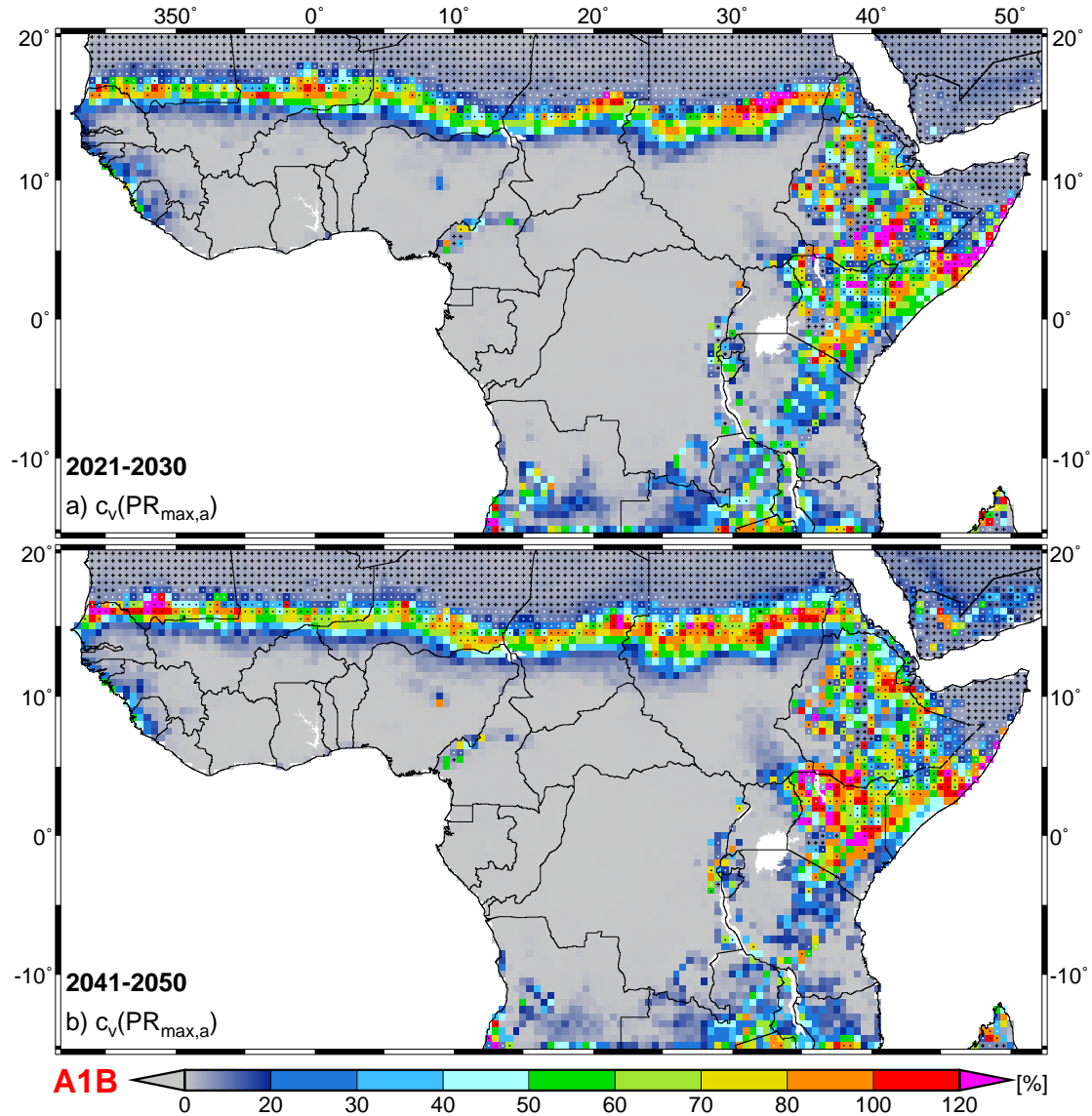


Fig. 7.16: Same as Fig. 7.6, but for malaria projections of $c_v(PR_{max,a})$ for (a) 2021-2030 and (b) 2041-2050 relative to the A1B scenario (see Fig. F.23 for scenario B1).

Changes in malaria transmission are not only restricted to highland territories but are also valid for arid and semi-arid epidemic-prone areas of the Horn of Africa. In such regions, the slightly higher though not significantly rainfall increase results in a small increase in EIR_a values. The malaria transmission in southeastern Ethiopia, southern Somalia, and northeastern Kenya seems to be most prevalent during the 2020s under the A1B scenario (see Fig. 7.16). Changes in the duration of the malaria transmission are the strongest in northern Kenya lengthening by one to two months (Fig. 7.12c-d). Some grid boxes in Ethiopia and Somalia reveal a complete relocation of the malaria season from boreal spring to late boreal autumn (cp. Fig. F.21f). Coastal areas of Kenya and that of southern Somalia reveal lower annual precipitation leading to a decline in the transmission and parasite prevalence. Also the Afar depression exhibits a lower malaria transmission and proportion of infections despite higher rainfall. This modification is

probably a result of temperatures exceeding 35°C around June (see Figs. F.3 & F.4). At such temperatures the mosquito survival probability of the Martens II scheme is slightly reduced (cp. Fig. 5.5).

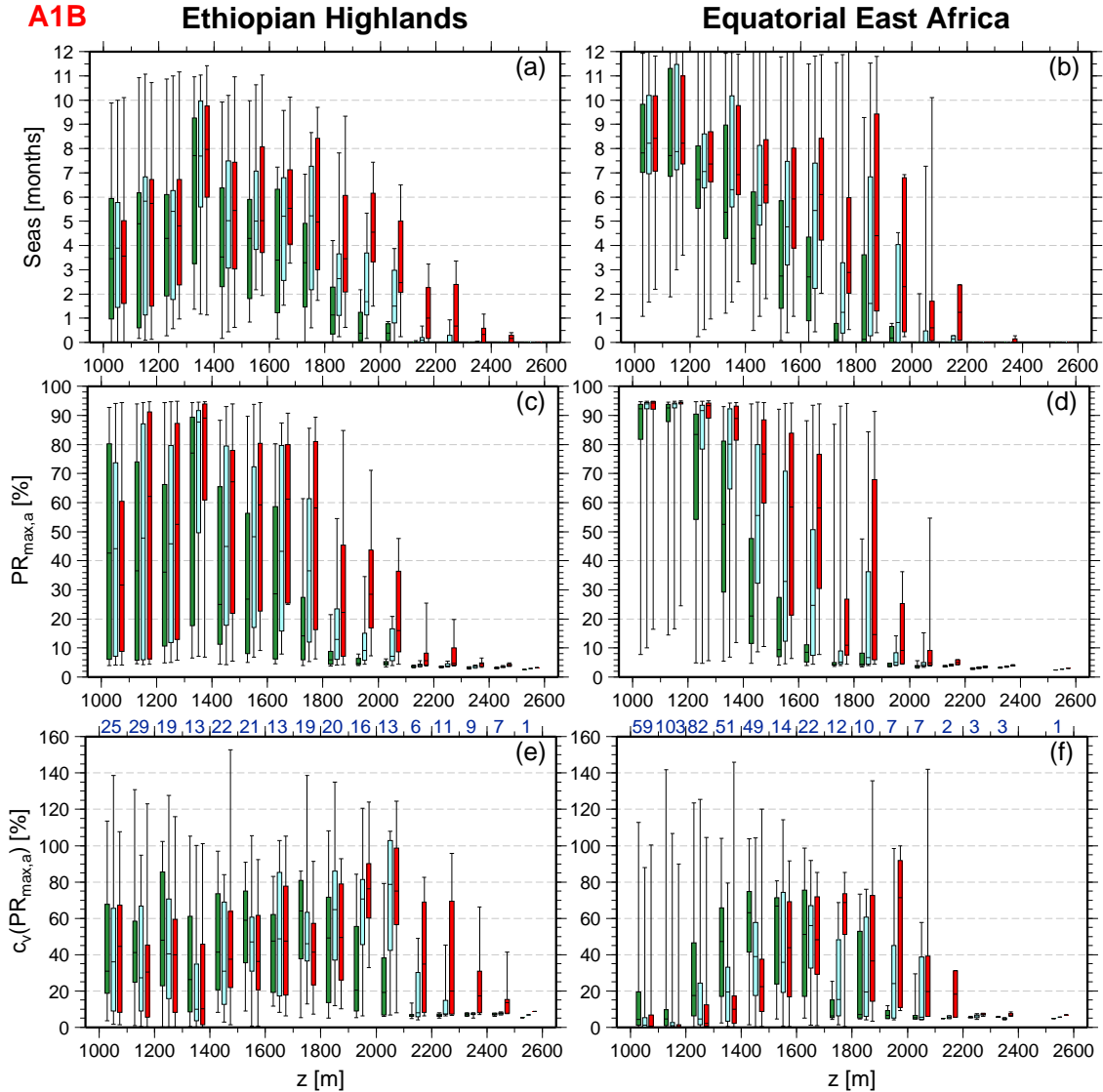


Fig. 7.17: Effect of altitude on LMM_n simulated values of *Seas* (a & b), $PR_{max,a}$ (c & d), as well as $c_v(PR_{max,a})$ (e & f) in the Ethiopian Highlands (cp. the framed area north of 4°N in Fig. 7.13c; a, c & e) and EEA (10°S-4°N, 27-38°E; see Fig. 7.13c; b, d & f) relative to the past period and the A1B scenario (see Fig. F.25 for scenario B1). Data from various grid points between height levels of 1000 and 2600 m is grouped within 100 m altitude segments. Box-and-whisker plots represent ensemble average values of included grid points relative to 1960-2000 (green box plots), 2021-2030 (light blue box plots), and 2041-2050 (red box plots). Blue numbers above (e) and (f) indicate the number of grid points from which the statistic is computed.

Central Africa, Angola, Zambia, and Malawi

The strongest increase in biting rates for the whole model domain is projected for Equatorial Africa. The precipitation decline leads to a pronounced rise in absolute values and

the standard deviation of EIR_a (Figs. 7.12 & 7.13). At the end of the future period in the Congo Basin the modelled EIR_a clearly exceeds 1000 infective bites (Figs. F.15-F.18). However, despite this fact disease prevalence is nearly unchanged. Due to already extremely high transmission levels for the present-day climate nearly no change in parasite prevalence is simulated. Besides a reduction in the length of the main transmission season (cp. Figs. F.19-F.22)⁶, the seasonality is not markedly altered during future decades.

In the southern part of the model domain higher temperatures and unchanged or higher precipitation amounts cause a stronger malaria transmission and an increase in parasite prevalence (Fig. 7.12). Particularly struck are again highland territories like that of the Bié Plateau in Angola, the Muchinga Mountain range of Zambia, as well as elevated locations in southern Congo and west of Lake Malawi. In these regions, particularly in Angola's central highlands, the transmission period is extended by two to four months in the 2040s. At the Bié Plateau and in highlands of southern Congo, $SSeas$ frequently already occurs in November/December instead of January/February (Figs. F.15-F.18). Disease transmission begins about one month earlier in January instead of February at the Muchinga Mountains. For various grid points, $ESeas$ is retarded from April to May. Again some mixed changes are projected for the epidemic potential (Fig. 7.16). The malaria transmission stabilises considerably at various grid boxes, but the epidemic-potential is enhanced for some areas. However, at the end of the future period the malaria spread becomes regular in all of these highland territories since transmission takes place every year.

In summary, according to LMM_n projections the risk of malaria epidemics is becoming lower in the northern Sahelian zone and by contrast a higher risk is projected for the more densely populated areas of the southern Sahelian zone. The malaria transmission in general intensifies along the Greater Horn of Africa. Under the warmer future climate formerly unsuitable highlands turn into epidemic-prone areas. At somewhat lower altitude levels disease transmission stabilises and people likely improve their partial immunity against malaria.

⁶There seems to be an abrupt modification of $XSeas$ in the northern part of Congo. In fact, $XSeas$ jumps from boreal spring to boreal autumn or vice versa. However, in these cases the analysis procedure misses the secondary maximum (cp. App. D.5). About the same is true for coastal areas of Guinea, Sierra Leone, Liberia, Ghana, Nigeria, and Cameroon. The identified pronounced changes are therefore not always statistical significant.

7.3.2 Garki model projections based on LMM_n

So far it has only been speculated that the modified malaria situation induces changes in the immunisation of the human population. The Garki model explicitly enables the analysis of such altered malaria conditions. Additionally, the Garki model provides valuable data in terms of changes in the infectiousness of human hosts. The application of the Garki model is furthermore a way to reduce the uncertainty of the malaria risk assessment. A second set of malaria scenarios is supplied by the Garki model. However, this data set is not fully independent since these projections base on simulated transmission rates from the LMM_n and hence also refer to REMO climate scenarios.

The Garki model provides about the same general picture of the future malaria situation as the LMM_n. Garki model projections indicate fairly similar difference pattern for patent positives (cp. Fig. F.28 with Figs. 7.12 & 7.13), albeit the corresponding amplitude is somewhat lower than that of the LMM_n. Parasite prevalence decreases in the Sahel and is increasing in numerous parts of East Africa. Various grid boxes in endemic areas even reveal a slight decline in y_a and $y_{max,a}$, a feature which is not included in the LMM_n data. Despite the higher transmission both prevalence as well as I_a are slightly reduced in certain areas such as the Congo Basin. This is probably result of the procedure in which superinfection is modelled (cp. Sec. 7.2.3). There is a small disagreement between the data from the Garki model and LMM_n runs around Lake Turkana (in the 2020s), for parts of the Afar depression, as well as coastal areas of Kenya and southern Somalia. For various grid boxes at Guinea, the Garki model predicts decreases in the parasite prevalence, which are not simulated by the LMM_n.

Comparisons of the projected year-to-year variability from the Garki model with that simulated by the LMM_n provide approximately the same change patterns. The interannual variability of y_a and $y_{max,a}$ decreases (increases) in the northern (southern) Sahel and a somewhat mixed picture is found in East Africa. However, a stronger signal is found for some highland territories such as the Ethiopian Highlands and parts of the Adamawa Plateau. These areas therefore reveal a higher epidemic risk in the simulations of the Garki model. By contrast, other areas such as the northern Sahel show a weaker decline in the standard deviation. This is likely a result of the lower base levels of parasite prevalence.

LMM_n simulations enable no statements relative to the proportion of infectious and immune individuals. Runs of the Garki model therefore complete the picture of the future spread of malaria (see Fig. 7.18). The transmission decline in the Sahel considerably reduces the proportion of infectious and immunes in the Sahel. In contrast, intensification of disease transmission leads to a significantly rise in $y_{1,a}$ and I_a for most aforementioned highland areas. Different changes are found for endemic malaria areas. Regions with an increasing immunisation lead to a decline of infectivity and vice versa. That is because immune individuals are not infectious in the Garki model. For example, the extended malaria season (Fig. 7.12c & d) in the southwestern part of West Africa causes higher I_a and lower $y_{1,a}$ values. About the same is true for large parts of the southern

part of the model domain. In contrast, the reduced length of the malaria season leads to a rise in infectivity and a lower immunisation of the population east of the Ivory Coast as well as for the coastal zone of Tanzania and Kenya.

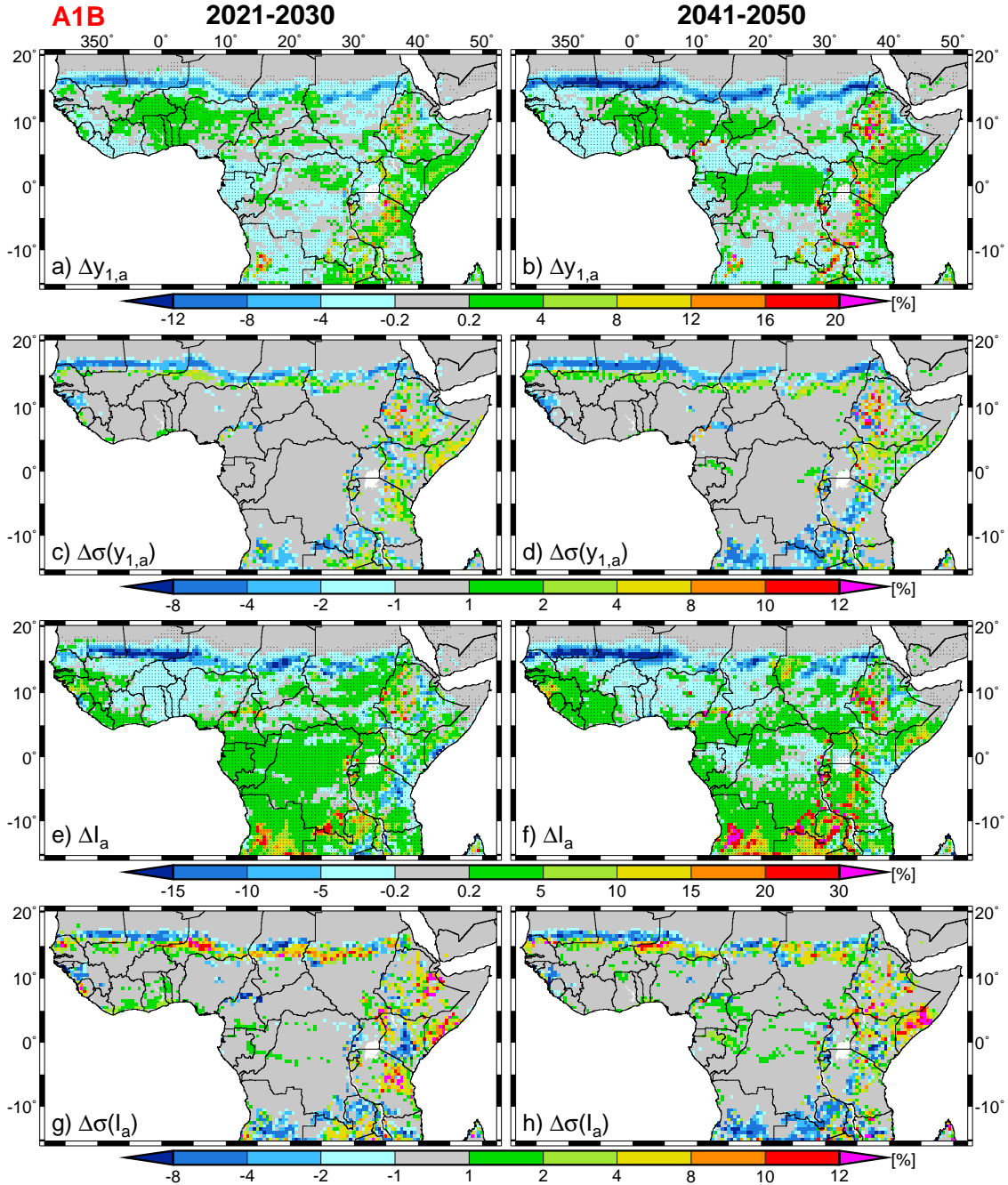


Fig. 7.18: Garki model projected changes in $y_{1,a}$ (a & b), $\sigma(y_{1,a})$ (c & d), I_a (e & f), and $\sigma(I_a)$ (g & h) relative to the present-day climate (1960-2000). Illustrated values refer to the A1B scenario (see Fig. F.27 for scenario B1) as well as to 2021-2030 (a, c, e & g) and 2041-2050 (b, d, f & h). Mean changes statistically significant at the 5% level are marked by dots.

Modification of the interannual variability of $y_{1,a}$ and I_a exhibits again the already noted patterns (Fig. 7.18). The standard deviation decreases (increases) in general in the

northern (southern) part of the Sahel. Mixed changes are again detected for highland territories. However, it is interesting to note for the Sahel that the changes for $\sigma(I_a)$ are the strongest in the 2020s (Fig. 7.18g) and are particularly pronounced for scenario B1 (Fig. F.27g). This is a result of still comparatively high I_a values in the 2020s and under scenario B1 (not shown).

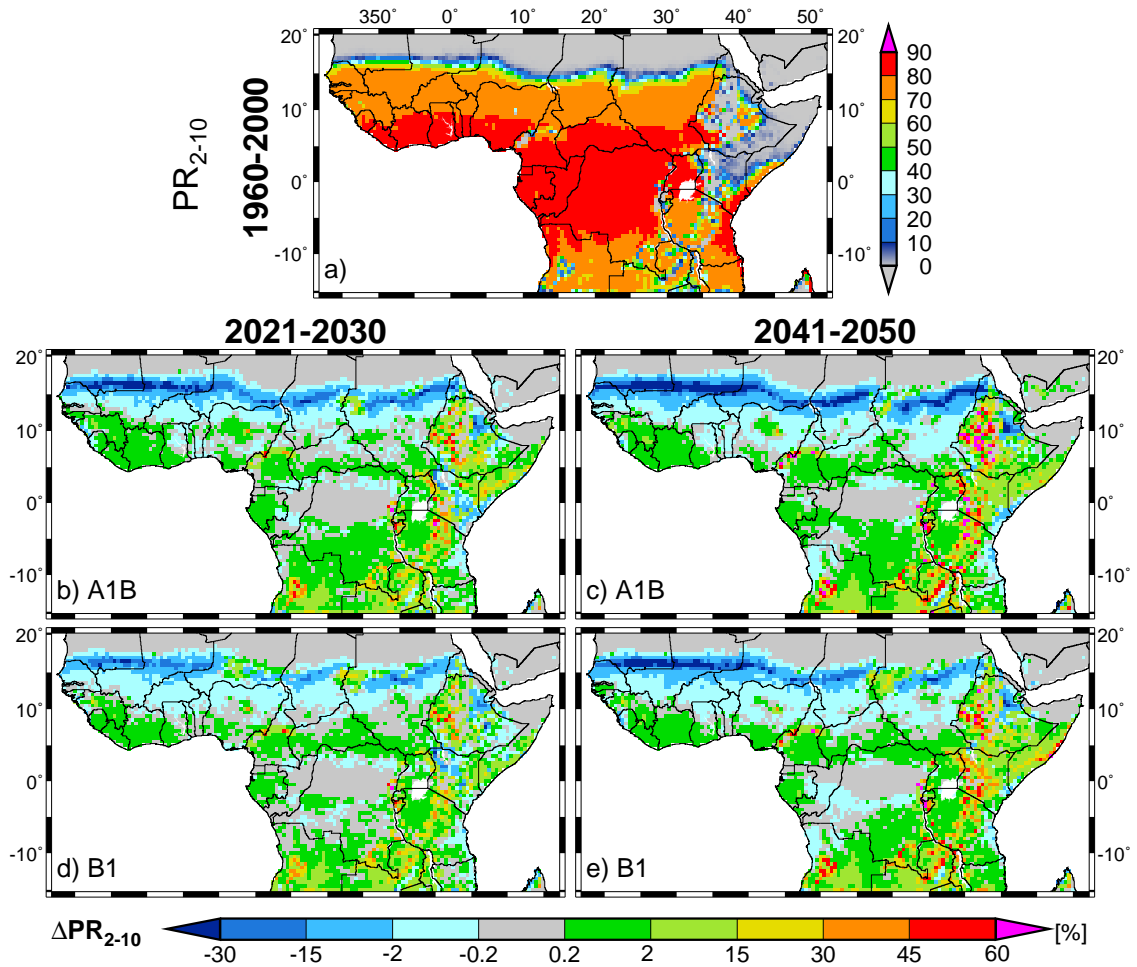


Fig. 7.19: Garki model simulated prevalence in children 2-10 years (PR_{2-10} ; in %) for (a) the present-day climate (1960-2000) as well as for projected changes for (b & c) the A1B and (d & e) B1 scenario. Changed parasite ratios are presented for (b & d) 2021-2030 and (c & e) 2041-2050.

Also the projected change in child prevalence reveals the aforementioned pattern (Fig. 7.19). However, the amplitude of change is considerably stronger than that of the whole population. This is clear since the proportion of infections is usually much higher in children than in adults due to the attainment of immune protection during the course of life. Climate change hence affects mostly the spread of malaria in children.

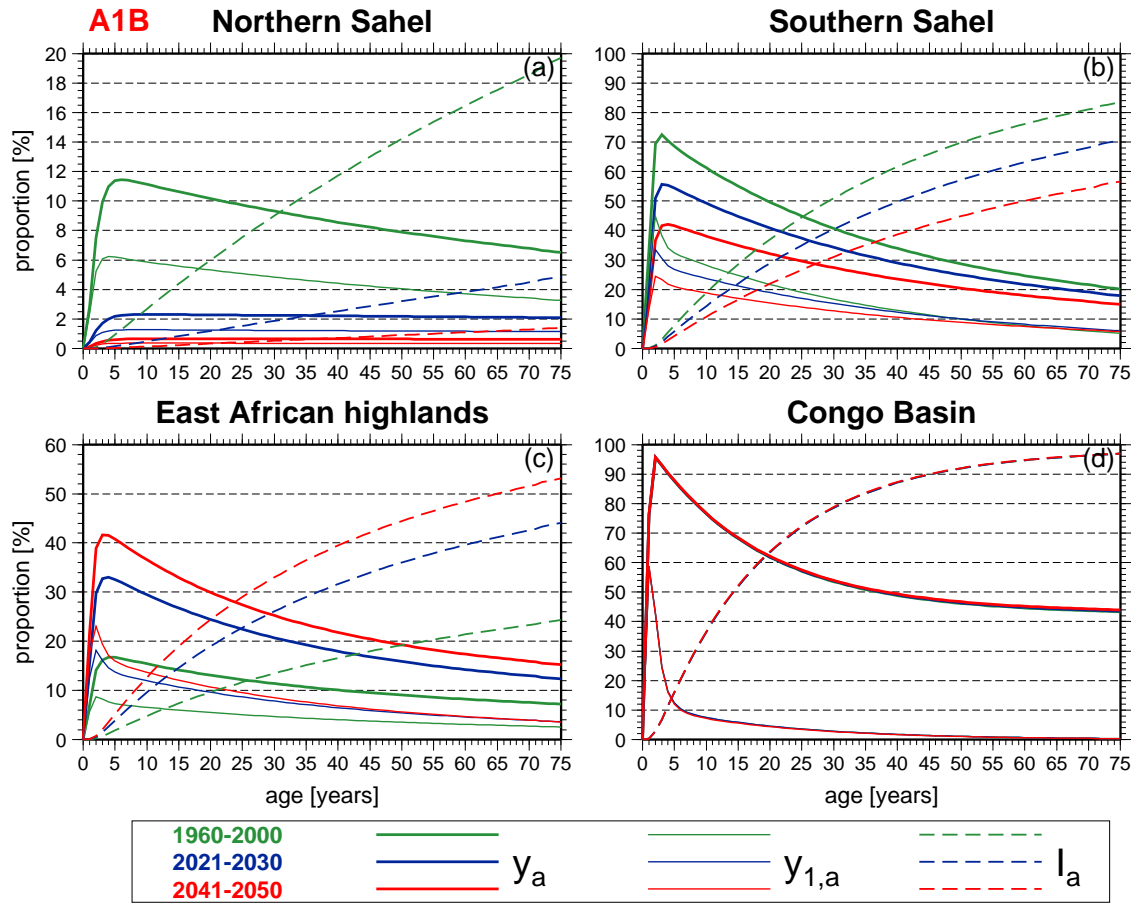


Fig. 7.20: Garki model simulated age distribution of y_a (thick solid lines), $y_{1,a}$ (thin solid lines), and I_a (thin dashed lines) for the present-day climate (1960-2000; green lines) as well as 2021-2030 (blue lines) and 2041-2050 (red lines) of the A1B scenario (see Fig. F.30 for scenario B1). The data shows averaged age dependencies for (a) the northern Sahel (16.5-18°N, 10°W-5°E), (b) the southern Sahel (14.5-16°N, 10°W-5°E), (c) highlands of East Africa (areas ≥ 1500 m), and (d) the Congo Basin (5°S-5°N; 15-28°E; note, the change of present-day values is fairly small). Utilised areas are inserted in Fig. 7.13c.

The projected decline for patent positives in the Sahel concerns all age groups (Fig. 7.20). At the end of the future period less than 1% of the population are infected in the northern Sahel. About the same is true for the immune status of the population. The number of immune hosts is significantly reduced even for the oldest age groups. In this situation a malaria epidemic would not only be restricted to young children and death would occur at every age. The malaria infection and the immune protection also markedly fall in the southern part of the Sahel. Values of y_a and $y_{1,a}$ halve for young children. Only small differences are found for adults. However, in the 2040s the immunisation of adults is reduced by more than 20%. Exact the opposite is true for the East African highlands, where more people are infected in the future scenarios. In these territories proportions of the infected, infectious, and immune human hosts increase in all age groups. The value of y_a , for example, rises from less than 20% to more than 40% for young children. The proportion of the immune population doubles approximately. No markedly change in age-prevalence curves are expected for the Congo Basin.

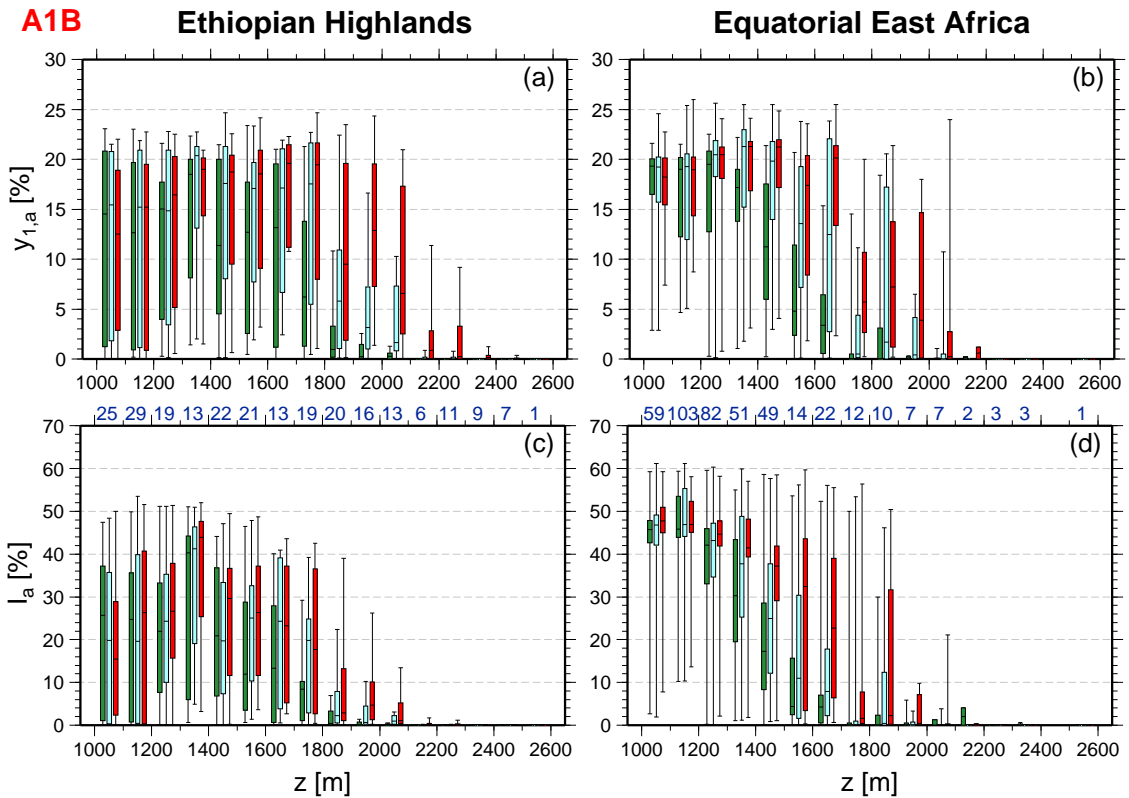


Fig. 7.21: Same as Fig. 7.17, but for the effect of altitude on Garki model simulated values of $y_{1,a}$ (a & b) and I_a (c & d). See Fig. F.31 for scenario B1.

An immune status increase has already been detected for highland areas. Nevertheless, changes strongly depend on altitude in these territories. For this reason, the past and future impact of altitude on the infectiousness and immunity is further analysed for the Ethiopian Highlands as well as elevated locations in EEA. Between levels of about 1300 and 2500 m the infectiousness is generally higher in the future than during the past period. As previously speculated, the higher transmission rates in fact result in a greater immune status of the population below heights of about 2000 m. Most pronounced is the increase of I_a above about 1700 m. In highlands of EEA this level is located much lower at about 1400 m. However, particularly vulnerable future populations are still found. The epidemic risk is significantly raised between approximately 1800 and 2500 m. These are height levels which are at least in parts malaria-free under the present-day climate. In this zone, the pattern for patent positives increases but a marked immune response is lacking in the Garki model.

In summary, the Garki model simulates about the same general patterns of malaria changes than the LMM_n. The Garki model additionally indicates that children will probably be the most affected population group. As expected the transmission decline in the Sahel will cause a reduction in the immune status of all ages. In contrast, highland territories will show an increase in the immunisation of the population. However, changes will strongly depend on altitude.

7.3.3 MSM projection of the malaria seasonality

The impact of climate change on the malaria seasonality is finally additionally analysed by data from the MSM. MSM simulations base on the projected atmospheric conditions of five decades between 2001 and 2050 (cp. App. C.5). MSM projections are furthermore compared with the simulated seasonality of the LMM_n.

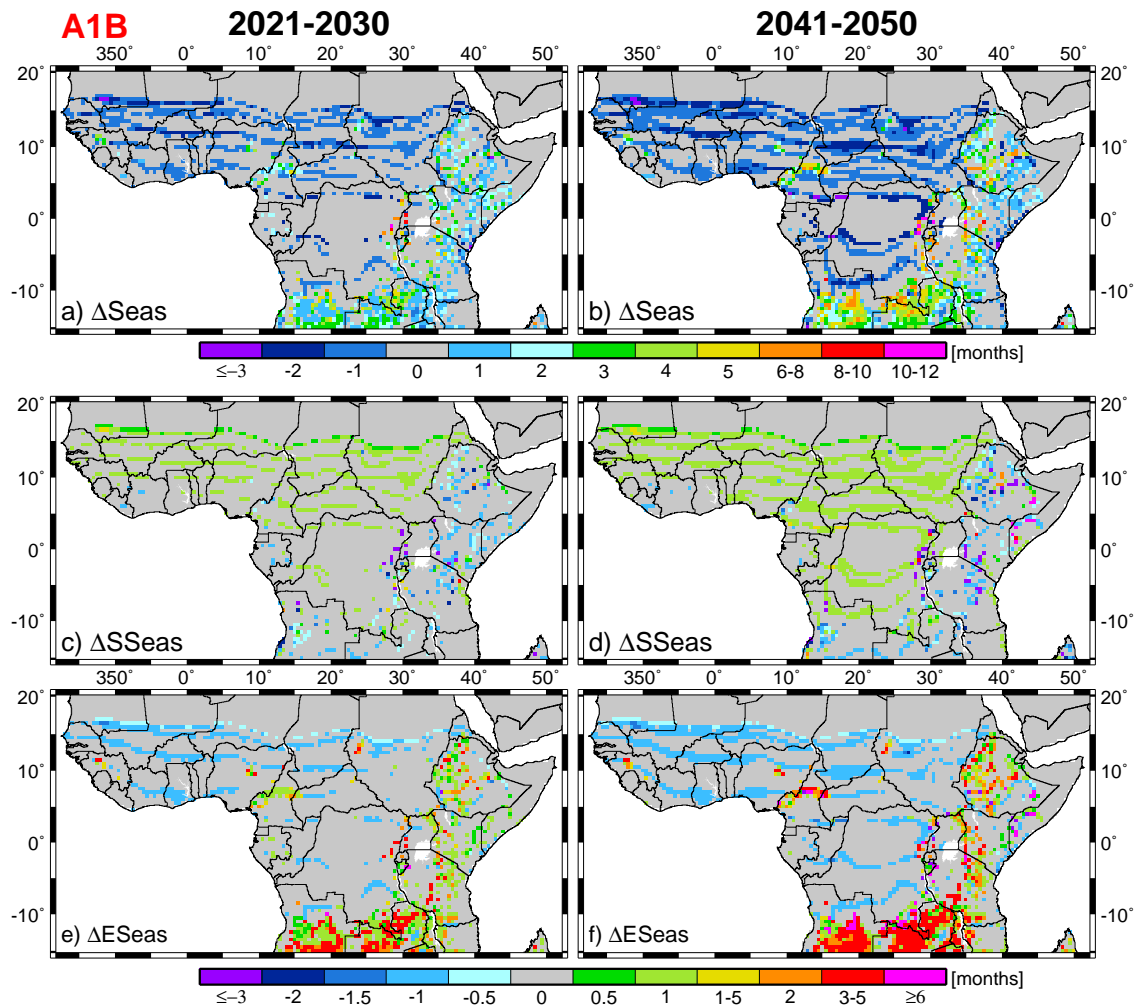


Fig. 7.22: MSM projected changes in *Seas* (a & b), *SSeas* (c & d), and *ESeas* (e & f) relative to the present-day climate (1960-2000). Illustrated values refer to the A1B scenario (see Fig. F.35 for scenario B1) as well as to 2021-2030 (a, c & e) and 2041-2050 (b, d & f). Regarding *SSeas* and *ESeas* for areas with two seasons only differences for the first malaria season are shown. Note that monthly categories prevent an uniform decrease in the length of the malaria season. Due to the predominantly zonal distribution, changes in the malaria season are usually ordered in small broken strips. Changes therefore only occur at fringes of zonal bands.

Reduced precipitation amounts in REMO climate projections are leading to a decrease in the length of the malaria season in most parts of tropical Africa (Fig. 7.22a & b; see also Fig. F.32 for projected absolute values). In contrast, higher temperatures cause an extended transmission period in East Africa as well as in the southern part of the model domain. The comparison with the projected LMM_n seasonality demonstrates a

simpler change pattern (cp. Fig. 7.12). For most parts north of about 16°N a malaria retreat is detected, which is consistent with LMM_n results. MSM and LMM_n simulations also largely agree in the later onset and earlier end of malaria transmission (cp. Figs. 7.22c-f, F.19 & F.21). At central Burkina Faso and along the coast of Benin, for example, the start of transmission is retarded from July to August and from April to May, respectively. In contrast, malaria transmission ceases about one month earlier.

An extended period of malaria transmission is also found in the MSM for the Fouta Djallon as well as the Adamawa and Jos Plateau. At the Adamawa Plateau, for example, for certain grid boxes a five months longer transmission is found (Fig. 7.22a & b) due to the temperature rise of about 2°C (Fig. 7.1c & e).

Higher temperatures and nearly unchanged precipitation amounts likewise cause an increase in the season length for the Greater Horn of Africa as well as for Angola and Zambia. Also in MSM runs the presence of highlands causes a fairly complex change pattern. The MSM projects a reduction of unsuitable malaria areas. The onset (end) of the malaria transmission is projected to be earlier (later) in comparison with the present-day climate. Outstanding is the strong increase in the season length of up to six months at about 12°S, in the Ethiopian Highlands, along the Western Rift Valley, the Western Kenyan highlands, in the Eastern Arc Mountains, on the Bié Plateau, and along the Muchinga Mountains.

To sum up, also in MSM projections the decline in precipitation causes a decrease in season lengths in most parts of tropical Africa. Higher temperatures in highland areas significantly expand the transmission season. Projections from the MSM are fairly consistent with that of the LMM_n.

7.3.4 A1B versus B1

Results regarding runs for scenarios A1B and B1 are similar to each other. However, as expected changes are generally stronger in scenario A1B than in B1 and the amplitude of change is most pronounced at the end of the simulation period in the 2040s. Comparison of change signals with regard to individual decades reveals that scenario B1 lags A1B partly by one to two decades. The reduction or enhancement of the risk of malaria epidemics under the B1 scenario is therefore for most areas somewhat lower. The reader is referred to supplementary figures in App. F for a detailed analysis of projected malaria changes under scenario B1.

8 Summary, discussion, and future prospects

8.1 Summary

Malaria is one of the most serious health problems in the world. The projected climate change will probably alter the range and transmission potential of malaria in Africa. In this study, potential changes in the malaria transmission were assessed by forcing three malaria models with data from ensemble scenario runs of a state-of-the-art regional climate model.

The *Liverpool Malaria Model* (LMM) from the Geography Department of the University of Liverpool was utilised. The LMM simulates the spread of malaria at a daily resolution using daily mean temperature and 10-day accumulated precipitation. Effects of climatic changes on the malaria season were additionally verified by the *MARA Seasonality Model* (MSM). The Garki model finally enabled the completion of the malaria picture in terms of the immune status and the infectiousness of different population groups, as well as relative to the age-dependent prevalence structure.

An extensive literature survey with regard to entomological and parasitological malaria variables provided valuable information for a new parameter setting of the LMM. The simulation of some key processes was changed in order to reflect a more physical relationship. For example, the egg deposition as well as the survival of immature mosquitoes was steered by a fuzzy distribution model. In this sub model mosquito breeding was hampered by dry conditions as well as excessive rainfall. In terms of adult mosquito survival a different survival scheme was applied resulting in a higher malaria risk at temperatures above about 30°C. The recovery rate of humans was furthermore significantly reduced to capture observed values and superinfection.

Calibration of the LMM was performed in West Africa and Cameroon at different atmospheric conditions. Realistic temperature and precipitation time series were reconstructed from various synoptic weather stations. The comparison with observations from eleven entomological and parasitological variables finally defined the new setting of the LMM. Validation of the new model version in the same area revealed that the simulations and defined malaria seasonality compared well with entomological field observations. However, due to limitations of the model and heterogeneous prevalence observations the

performance of the LMM_n was somewhat weaker with regard to parasitological variables. Simulations furthermore captured the spatial and temporal variability of malaria transmission. The LMM_n also demonstrated a fairly realistic two-dimensional simulation of the malaria spread in Africa. The model correctly reproduced the epidemic potential at fringes of endemic malaria areas.

Various sensitivity experiments revealed that the LMM_n is fairly sensitive to values of its internal parameters. For example, EIR_a values strongly depended on the mosquito survival scheme. The recovery rate of humans significantly influenced the size of parasite prevalence. Comparison of LMM_n results with the performance of the original model version exhibited marked improvements. For instance, the distribution of malaria in dry zones as well as transmission rates in humid areas were much more realistic in LMM_n runs.

In every case, three ensemble runs were performed on a 0.5° grid. The LMM was driven for the present-day climate (1960-2000) by bias-corrected data from the *REgional MOdel* (REMO), with land use and land cover according to the *Food and Agriculture Organization* (FAO). Malaria projections were carried out for 2001-2050 according to climate scenarios A1B and B1 as well as FAO land use and land cover changes. Garki model runs were subsequently forced by the *Entomological Inoculation Rate* (EIR) from the LMM. Finally, additional results relative to the malaria season were produced by the MSM.

Comparison of REMO data with gridded rainfall observations, temperature reanalyses, and station time series exhibited considerable deficiencies of the model runs. For example, rainfall was too low at the Sahel and was overrepresented along the Guinean coast. REMO showed a comparatively high frequency of small and excessive rainfall amounts. Also, the amplitude of the seasonal temperature cycle was in general overestimated. REMO temperatures were too low (high) during boreal winter (summer). These deficiencies were markedly reduced by the bias correction of the data set.

For the present climate (1960-2000), the highest biting rates were simulated for Equatorial Africa. The year-round and high transmission rates in the Congo Basin resulted in fairly low infectious proportions due to a rapid immunisation of the population. Malaria simulations showed a decrease in the spread of malaria from Central Africa towards the Sahel. The largest proportions of infectious individuals were found for the short seasonal and intense malaria transmission. These regions were furthermore characterised by a comparatively slow attainment of immunity. The length of the malaria season was closely related to the presence of the monsoon, about half of the months of the transmission season exhibited low transmission rates, and maximum transmission was frequently simulated toward the end of the rainy season. The spread of malaria was limited by extreme dry areas of the Sahara desert and along the Horn of Africa, as well as by low temperatures in highland territories. Model runs showed a marked influence of mountainous areas causing a complex pattern of the spread of malaria in East Africa. Temperatures below or around 20°C led to lower transmission rates, a shorter and delayed malaria season, as well as diminished parasite rates. The pattern of malaria

positives revealed the expected peak in children below an age of about five years. The infectious and immune proportion was the highest for young children and for the oldest age groups, respectively.

Regions of epidemic malaria occurrence, as defined by the coefficient of variation of the annual prevalence maximum, were found along a band in the northern Sahel. Farther south, malaria occurred more regularly and was therefore characterised as endemic. Epidemic-prone areas were additionally identified at various highland territories, as well as in arid and semi-arid zones of the Greater Horn of Africa. No adequate immune protection of the population was found for these areas.

Largely due to land surface degradation, REMO simulated a prominent surface warming and significant reduction in the annual rainfall amount over most of tropical Africa in either scenario. Assuming no future human imposed constraints on malaria transmission, changes in temperature and precipitation will alter the future geographic distribution of malaria. In the northern part of sub-Saharan Africa, the precipitation decline will force a significant decrease of malaria transmission in the Sahel. In addition to the withdrawal of malaria transmission along the Sahara fringe the frequency of malaria occurrence will be reduced for various grid boxes of the Sahel. As a result, epidemics in these more densely populated areas will become more likely, in particular as adults lose their immunity against malaria. Except for highlands of West Africa the level of malaria prevalence farther south will remain stable. However, the start of the malaria season will be delayed and the transmission is expected to cease earlier under malaria projections except for areas between Liberia and Ghana.

The most pronounced changes in Africa were found in both scenarios for East Africa. Significantly higher temperatures and slightly higher rainfall will lead to a small or moderate increase in malaria transmission. However, such an increase in transmission rates will cause a substantial increase in the season length and parasite prevalence in formerly epidemic-prone areas. As a result, the spread of malaria will be markedly increased in various parts of East Africa. Highland areas formerly unsuitable for malaria will become suitable under the warmer future climate. The simulations clearly indicated changes in the highland epidemic risk. At most grid boxes malaria transmission will stabilise below about 2000 m, for example, in most parts of the Eastern Arc Mountains. At these altitudes the more regular transmission will improve the immune status of the population reducing malaria mortality. In contrast, malaria will climb to formerly malaria-free zones above these levels, enhancing the probability of malaria epidemics.

8.2 Discussion and future prospects

The main aim of the present study was to assess the risk of malaria in Africa under the influence of the present and a modified future climate. Ideally a multidisciplinary research program is required for this task. A more complete understanding of the complex ecology of malaria will require integration of research efforts across diverse areas (Col-

well and Patz 1998). At least three basic disciplines (i.e., meteorology, medicine, and entomology) are included in this analysis. Only the combination of meteorological data with the knowledge gathered by entomological and parasitological field research enables the simulation of malaria transmission. A model chain further allowed estimation of different aspects of malaria distribution such as biting rates or the immune status of the population. Despite the known causal links between climate and malaria transmission dynamics, there is still much uncertainty about the potential impact of climate change on malaria (Confalonieri et al. 2007). This study was naturally not able to account for all processes involved in the spread of malaria. Some of these factors might be included in a future extension of the LMM. This section provides a detailed discussion with regard to various aspects of the present study. The used atmospheric data sets and the model calibration are evaluated, as well as the present-day performance and malaria projections of three malaria models are discussed relative to results of former studies.

8.2.1 Calibration and sensitivity of the LMM_n

The data basis for the LMM calibration is far from being optimal. There is a mismatch between scales at which a disease vector responds to hydrologic variability and scales at which hydrological variability is actually observed. Systems must be developed that monitor hydrologic variability at scales corresponding to disease system ecologies (Shaman and Day 2007). More than that, meteorological data from synoptic stations reveals large data gaps in temperature and precipitation reports. However, by means of additional monthly data sets the generation of realistic time series finally succeeded (see Fig. 3.5 & Sec. 4.3). In fact, for certain stations and during various time periods the resulting time series represent realistic atmospheric conditions but do not constitute of real observations. However, the generation of realistic weather conditions was of greater importance since malaria field studies were not conducted directly at the weather stations. These sites therefore in any case exhibit a different temporal variability of rainfall and temperatures. This might be one reason, amongst other factors such as environmental conditions, why year-to-year comparisons between observation and simulation were weakly correlated at single validation locations (not shown).

The required historical entomological and parasitological data is rarely available with sufficient coverage. Most locations show only one, two, or even no field measurements. It is therefore likely that a larger set of observations would have a strong impact on the result of the model calibration. Ideally, model simulations and malaria observations should be compared from year-to-year. However, this would require the simultaneous monitoring of long-term malaria data and meteorological measurements. Such long time series are available for the area of Ndiop (S. Louvet, personal communication, 2007), but these data sets are at present not publicly available.

The close ranking of diverse model runs as well as the lack of sufficient validation data further restricted an objective formal fitting of the model to field data. In fact, various steps of the calibration procedure were subjective. Due to computational demands

it was furthermore not possible to fit all remaining model parameters simultaneously. However, because various settings compensate each other it is likely that the final model formulation conforms as much as possible to reality (cp. Smith et al. 2006b).

Calibration and validation of the model should also be ideally not only restricted to West Africa and Cameroon. However, such an extension to, for example, East Africa would be a time consuming undertaking. The Malaria Atlas Project intends to provide access to various malaria studies (Guerra et al. 2007). This might provide an efficient access to malaria data beyond that of West Africa. Due to the pronounced projected changes such an extension would ideally include East African highlands and an estimation of the sporogonic temperature threshold. However, due to the effect of altitude on malaria it might not be an easy task to find proper malaria and meteorological data.

The diversity of sensitivity tests over the range of adjustable parameter values reflects high levels of uncertainty in the formulation of a final model setting. Those model parameters with a significant impact on simulations are the areas of the model that need to be refined as knowledge of the underlying processes improves (Jones 2007). Until such achievements, a range of model settings could be used. The most thorough way to investigate the considerable uncertainty in the formulation of the model is to run a massive ensemble experiment in which each relevant parameter combination is investigated. This might end up in a set of models that could be used for seasonal ensemble forecasts of malaria (cp. Morse et al. 2005; Hagedorn et al. 2006; Thomson et al. 2006). Due to the computational demand, it was not possible to use different model formulations of the LMM_n in the present study.

8.2.2 Performance of the malaria models

The simulated spread of malaria, the transmission level, and the seasonality seem to be realistically reproduced by the LMM_n. Validation in West Africa and Cameroon clearly showed that modelled features from the new model version compare well with entomological observations. Field studies, for example, also contain the strong decline in EIR_a in the Sahelian zone. Various other published malaria distribution maps (e.g., Figs. 2.8 & 2.9) also correspond well with the simulated spread of malaria by the LMM_n. However, in certain parts the simulated intensity of malaria transmission differs considerably. Rogers et al. (2002), for example, predicted bands of low annual biting rates in West Africa. Such feature are not identifiable in EIR_a values of the LMM_n. The LMM_n in general seems to predict higher transmission rates than the satellite-derived predictions of EIR_a of Rogers et al. (2002) (cp. Figs. 2.9 & 7.4a). Maps of transmission intensity provided by Gemperli et al. (2006b) are fairly spotted. In their analysis the highest transmission intensities in West Africa are found for the southern part of the Sahel. In fact, their prediction likely significantly suffers from the neglected interannual variability of malaria (see also Sec. 2.7.2). Based on available EIR_a observations it is difficult to judge which estimates are closer to reality. However, validation of the LMM_n

under different climatic conditions provides evidence that the present study generated realistic biting rates.

The simulated seasonality corresponds well with observations (cp. Figs. 6.3 & E.3) and with seasonality maps from the MSM (Fig. 2.8b-d). In particular, the patterns of $SSeas$ are almost the same for MSM and LMM_n simulations. LMM_n runs exhibit about a half month later $ESeas$ than modelled by the MSM (cp. Fig. F.32). However, it must be pointed out that MARA results refer to average climate conditions whereas values of the LMM_n are based on single years.

There are many factors that modify transmission that are not accounted for by the used malaria models (see Sec. 8.2.5). The simulation of parasitological malaria variables by the LMM_n is a simplification of real processes. Validation of the LMM_n by means of PR_a , $PR_{max,a}$, and $PR_{min,a}$ measurements in West Africa and Cameroon already revealed major shortcomings of the model (Sec. 6.1). The lowest skill scores were achieved by these parasitological variables.

In addition to the lack of immunity, the LMM_n is not able to account for other malaria factors such as chemoprophylaxis and human activities (see Sec. 2.6.2). Observations suggest a stronger variability in parasite prevalence. At Bobo-Dioulasso, for example, ten observed PR_a values range between 29.1 and 77.5%. In contrast, 34 annual values of the LMM_n only span between 50 and 70% (Fig. E.4c). Unfortunately, for West Africa there seems to be available only one location with two subsequent PR_a observations from different years. Carnevale et al. (1988) provided parasite ratios from a trial of impregnated bed nets at Karangasso (Burkina Faso; 11°13'N, 4°39'W). In the untreated control area (Koko suburb) PR_a in children (1-14 years) decreased from 54.1% in 1985/86 to 39.6% in the second year. This also hints toward a stronger year-to-year variability.

Due to the lack of long-term observations, Kleinschmidt et al. (2001) and Gemperli et al. (2006b) were forced to neglect the interannual variability of PR . This fact might again partly be responsible for the irregular PR pattern in West Africa (cp. Fig. 2.10). Their maps also show a sharp decrease of PR_a north of about 15°N (see also Fig. 6.4). However, in contrast to LMM_n and Garki model simulations, PR_a is frequently lower than 50% south of 15°N. Only few regions exhibit higher PR_a values than 70% as such from the LMM_n and Garki model (Figs. 7.4e & 7.19a). With regard to $PR_{max,a}$ the LMM_n simulated values are often higher than observed. Only Sabatinelli et al. (1986) published a value comparable to the upper limit of $PR_{max,a}$. In 1984 at Koubri (Burkina Faso; 12°09'N, 1°23'W), children between two and five years exhibited a PR value of 94.9% at the peak of the transmission season in August-September. However, as previously mentioned (Sec. 2.4.5) individuals often return a false negative microscopy report when parasite densities fall below sub-microscopic levels.

Different simulated parasite prevalence of the LMM_n and Garki model result in parts from different used recovery rates (r). The value of r for the non-immune population is lower than that used by the LMM_n (r : 0.0023 vs. 0.005 day⁻¹). In fact, the Garki model was only calibrated for one single area in northern Nigeria. Note that Gu et al.

(2003a) found in Kenya a dependence of r on transmission intensity (see Sec.5.1.11). For this reason, it would be more suitable to use recovery rates depending on the exposure history of individuals. However, this would require a different structure of models since individuals must be tracked. Due to the uncertain setting of r the two different used r values can better estimate the uncertainty of the malaria projection. In fact, both models exhibited about the same projected prevalence changes, the influence of different used r values is hence comparatively small.

8.2.3 Uncertainty of the applied climate projections

The atmospheric basis of malaria projections covers only two different climate scenarios from one single regional climate model. Importance of using several climate scenarios to illustrate the range of possible future geographical malaria distributions was, for example, found by Hartman et al. (2002). Ideally, assessment of the malaria risk should therefore be based on projections from different climate models. The applied model chain could be driven by data from the 21 AOGCMs of the IPCC-AR4. However, these data sets suffer from their coarse resolution. Regional climate projections provide a more detailed picture of atmospheric conditions. Unfortunately, for the present study only regional climate projections for large parts of Africa were available from REMO. In the near future, various other regional climate projections will be allocated for the Fifth Assessment Report of the IPCC and will also allow malaria projections beyond 2050. This data basis will enable more robust malaria projections and can provide the basis for a detailed uncertainty analysis of the future spread of malaria.

Of particular interest is, for example, an estimation of precipitation changes in the Sahel. REMO projects a marked reduction of rainfall over most parts of tropical Africa, which are mainly induced by LUC changes. However, as aforementioned (Sec. 2.3.2), it is difficult to identify robust signals in precipitation patterns for West Africa. AOGCMs of the IPCC showed diverse evolutions of the hydrological cycle. In fact, Cook and Vizi (2006) found only four different models exhibiting realistic features of the West African monsoon. Among the six models not reproducing a realistic rainfall pattern was also the ECHAM5/MPI-OM, in which REMO was nested. This might have partially caused systematic errors of the REMO precipitation. Only the bias-correction of rainfall finally enabled the generation of a realistic distribution of precipitation amounts.

The key feature of the REMO scenarios is the induced LUC change. Such changes are at present largely not included in state-of-the-art AOGCMs. REMO simulations strongly indicate that such changes are of particular relevance. In addition to global changes of atmospheric patterns, regional factors like deforestation are also of particular importance for the hydrological cycle. Nevertheless, other climate models have to verify this large impact of land degradation. Results from Paeth et al. (2009) must be confirmed in the light of various other model physics. Inclusion of LUC changes is only a next step towards incorporation of a dynamic vegetation model (e.g., Brücher 2008). Addition-

ally, other physical components of the climate system such as the effect of atmospheric aerosols on the hydrological cycle must be considered (cp. Paeth and Feichter 2006).

A different situation is found for East Africa. In this area, the great majority of AOGCMs agree in the positive sign of the precipitation signal. An increase in the tropics is a plausible hydrological response to a warmer troposphere. However, atmospheric features such as ENSO or IOD might exert a greater influence on future rainfall conditions than presently expected. The IPCC-AR4 found only model dependent changes in the interannual variability of ENSO but no indication of discernible changes. In this context, it should be noted that difficulties still remain in the simulation of ENSO and associated tropical precipitation. Additionally, climate and regional climate models are also not able to simulate all complex features of observed climate dynamics and variability of the Greater Horn of Africa (see Sec. 2.1.2) due to their coarse horizontal resolution.

8.2.4 Evaluation of the malaria projections

In case that humans do not significantly alter malaria transmission, a modified future climate will change the geographic distribution of malaria. The general expectations of the climate change impact on the spread of malaria are confirmed by the present study. The IPCC-AR4 already concluded that climate change will be associated with both geographical expansions and with contractions (Confalonieri et al. 2007). Areas particular vulnerable to future changes were identified as regions of fringe transmission (e.g., McMichael and Haines 1997). Lindsay and Birley (1996) pointed out that usually malaria-free areas and those with an unstable malaria occurrence will be touched. These statements fully apply for projected malaria changes of this analysis. Areas most probably affected are those bordering malaria endemic regions such as parts of the Sahel, the Horn of Africa, or various highland territories. Malaria areas are predicted to disappear in the Sahel and the disease distribution will expand in highlands (Figs. 7.15 & F.26). Jetten et al. (1996) and Reiter (2001) further argued that climate change will have only minor effects on the malaria distribution in endemic areas. This fact is also confirmed by actual malaria runs. Fringe endemic territories are affected and for other endemic areas only changes in the seasonality are expected.

Projected transmission changes in the Sahel are fairly uncertain due to the fact that these mainly depend on changes in rainfall. A pronounced precipitation decline is only one of the plausible scenarios for the Sahel. Martens (1999), for example, predicted a spread of malaria beyond current limits due to a wetter Sahel. Nevertheless, Thomas et al. (2004) also projected a reduction in malaria transmission, although, due to higher daily maximum temperatures. It is interesting to note that Cook and Vizzy (2006) concluded that the MRI model provides the most reasonable scenario of Sahelian precipitation throughout the 21st century. This model projected a doubling of the number of anomalously dry years by the end of the century causing a modest drying in the Sahel.

As previously mentioned, LUC changes are largely not included in AOGCMs. Different REMO scenarios showed that such changes likely cause further drying conditions.

For these reasons, it is concluded that the reduction of transmission in scenarios A1B and B1 is one plausible picture of the future spread of malaria in the Sahel. As Kovats et al. (2001) already argued, these decreasing rainfall amounts have beneficial effects by reducing malaria in the northern part of the Sahel. Although, further to the south endemic zones are projected to turn into epidemic-prone areas with a decreasing immune status of the population. As a result, epidemics in these more densely populated areas will become more likely. However, people are compelled to reside where water is available and therefore might be forced to migrate toward south.

In contrast, that climate change may facilitate the spread of malaria further up some highland areas in Africa is incontestable. Previously, Lindsay and Birley (1996) concluded that climate change probably increases the epidemic risk in highland territories. Lindsay and Martens (1998) and Ebi et al. (2005), for example, projected an increase in malaria suitability of Zimbabwe highlands. Also, Rogers and Randolph (2000) predicted an increase in malaria suitability of East African highlands by 2050. Solely, the timing of changes is somewhat uncertain. Thomas et al. (2004) computed, for instance, only small changes for highland territories in the next 30-40 years. In their scenario, highlands become highly suitable not before 2080. This fact is also shown by the A1B and B1 scenarios of the present study. Changes in scenario A1B in general lead that of B1 by one to two decades. One key result of the actual study is the different response of the population at different height levels under both scenarios. As indicated by Githeko et al. (2000), malaria is projected to become stable below certain elevation levels. In contrast, formerly unsuitable heights lack an immunisation and turn into epidemic-prone areas.

Less certain than the temperature increase in highlands is the expected small rise in annual precipitation. Although, most AOGCMs as well as REMO project somewhat higher rainfall amounts, the influence of ENSO or IOD might be greater than projected. Malaria projections for rather dry areas such as parts of the Eastern Arc Mountains or areas of the Horn of Africa therefore might not be as certain as indicated.

The horizontal resolution of model runs of 0.5 degrees further limits the usefulness of malaria projections, in particular, in East African highlands. The used model orography is not everywhere representative for particular locations. For this reason, the effect of altitude was illustrated (Figs. 7.17 & 7.21). However, such an analysis naturally misses diverse temperature and rainfall conditions at highland territories. Because of dry conditions the Eastern Arc Mountains, for example, show lower parasite prevalence than corresponding height levels of the Ethiopian Highlands. Nevertheless, the provided data might render helpful information for decision makers in terms of malaria control of highland territories.

Projections of the malaria seasonality were provided by the LMM_n and MSM. Both models revealed about the same scenarios of malaria seasonality. Due to decreasing precipitation amounts the length of the malaria season is reduced in most parts of tropical Africa (cp. Martens et al. 1999). In contrast, the temperature increase in highlands causes a marked extension of the malaria season (cp. Martin and Lefebvre 1995). As Kovats et al. (2001) stated, small changes in the seasonality in the Sahel or highland

areas cause strong changes in parasite prevalence. The present results differ from that of Tanser et al. (2003), who predicted an increase in the length of the transmission season. The largest temperature rise and a moderate rainfall reduction under A1FI caused the highest increase in person-months of exposure by 2100.

8.2.5 Neglected factors and future extensions of the LMM

The actual study did not account for various malaria factors (cp. Sec. 2.6.2). Statements from the present analysis are only related to future climatic and land use and land cover scenarios. It should be pointed out here, that climate is rarely the only important driver of malaria. Numerous other studies showed (e.g., Epstein 1998; van Lieshout et al. 2004; Hay et al. 2005; Kelly-Hope and McKenzie 2009) that in particular human activities are crucial for the transmission and prevention of malaria across Africa. For example, modification of the landscape by irrigation (e.g., Briët 2002), forest clearing (e.g., Munga et al. 2006), or urbanisation (e.g., Keiser et al. 2004) can significantly alter malaria transmission. Due to the lack of time and data, the present study assessed only the malaria risk for rural areas without the influence of permanent breeding places. Usefulness of this analysis is therefore limited when permanent streams or urban centres are present.

The collected entomological and parasitological data also provides information for irrigated areas and locations with permanent streams, as well as urban territories. Calibration of the LMM_n therefore could also be performed for such areas. However, this undertaking might be hampered by the lower number of available observations. A systematic, time-consuming screening of literature might provide additional data. In case of permanent streams (e.g., Robert et al. 2003) or seasonal irrigation (e.g., Briët 2002), the LMM_n could be further driven by artificial rainfall amounts representing additional breeding opportunities. Urban areas would rather require a different model setting in order to achieve reduced transmission intensities. In principle, risk assessment is hence also possible for other areas than rural sites.

Species composition of mosquitoes is another neglected factor of malaria transmission. *An. funestus* is, for example, specialised for the extension of the malaria season at the end of the rainy season and at the beginning of the following dry season (cp. Kelly-Hope and McKenzie 2009). Also the degree of the host-vector-pathogen contact depends on the involved vector species. Here, information in terms of anthropophily as well as the presence of animals such as cattle would be needed. In fact, the LMM simply uses only one single setting of the human blood index (a). Such factors require a precise knowledge of the distribution of mosquito species as well as in terms of their behaviour. Kiszewski et al. (2004) as well as Moffett et al. (2007) used such information and constructed risk maps for various mosquito species. Consideration of different mosquito species is, however, beyond the scope of this study and would result in an extensive change of the LMM structure.

The simulation of the development of immature mosquitoes was significantly altered in the LMM_n. Application of a hydrological model might be more appropriate than the

fuzzification of this process. However, hydrological models need detailed information in terms of ground conditions. Such knowledge might only be available for limited areas. Shaman et al. (2002), for example, used a dynamic hydrology model to predict mosquito abundances in flood and swamp water in New Jersey (USA). Gerbaux and Bicout (2008) also applied hydrological features for the impact of rainfall on mosquito production in the Sahel.

The fuzzy distribution model was also applied with regard to immature larvae survival. However, the mosquito mature age (MMA) was fixed to 12 days. A necessity for future improvement of the LMM concerns dependence of immature development on water temperatures (see Bayoh and Lindsay 2003). This would require incorporation of new meteorological variables such as potential evaporation, cloud cover, or sunshine duration (cp. Depinay et al. 2004).

One basic feature of malaria projections is the increase in EIR_a for large parts of tropical Africa, despite a decreasing rainfall supply. This phenomenon is clearly associated with the fuzzy distribution model of egg deposition and immature mosquito survival. It is difficult to judge whether these predicted changes are realistic. In order to answer this question further case studies as such from Paaijmans et al. (2007) should be performed under different rainfall conditions.

A further possible future extension of the LMM includes factors such as immunity, superinfection, and the simulation of age- and transmission-dependent malaria factors. Such factors are essential for state-of-the-art malaria models. The Garki model was used in this study for consideration of superinfection, immunity, as well as the age-structure of parasite prevalence. A suitable approach would be individual-based stochastic malaria modelling. McKenzie et al. (1998, 1999, 2001, 2002) developed discrete-event models of malaria transmission dynamics. In these models, malaria transmission is heterogeneous and characteristic states of humans as well as adult mosquitoes are tracked individually. McKenzie and Bossert (2005) used this discrete-event model and simulated pathogen dynamics within individual hosts and those within interacting host and vector populations. Also Killeen et al. (2000) introduced a malaria model based on life histories of individual mosquitoes. Gu et al. (2003a) considered in addition the life history of human hosts and adult female mosquitoes individually. In their model, immunity is simulated as a function of exposure history representing a reduced susceptibility and an increased recovery rate. Such modelling procedure would have additional benefits for the LMM such as the loss of discretisation effects and would allow for a probabilistic approach in terms of temperature and rainfall thresholds.

The present study also not considers any socio-economic factors. However, economic development of a community is of great importance for the spread of malaria (e.g., Epstein 1998). Villages with irrigation, for example, are sometimes associated with less malaria (Ijumba et al. 2002), probably due to improvement of their living standards. The health impacts will be greatest in low-income countries. Those at greater risk include the urban poor, the elderly and children, traditional societies, farmers, and coastal pop-

ulations (Confalonieri et al. 2007). Socio-economic factors might be integrated into an extended model such as that from Tol and Dowlatabadi (2001).

Studies such as that from Robert and Carnevale (1991) demonstrated that malaria control can significantly reduce malaria transmission. After usage of deltamethrin-treated bed nets EIR_a was reduced by about 94% in an irrigated zone of Burkina Faso. The inclusion of such a factor into the LMM_n would only require a simple reduction of the human blood index (a), the mosquito-to-human (b) as well as the human-to-mosquito transmission efficiency (c). Productivity of breeding habitats under larval control such as environment-friendly biopesticides (e.g., via neem (*Azadirachta indica*) extracts) might also be included in a future extension of the LMM (cp. Gianotti et al. 2008). Such model experiments could illustrate effects of control measures under present-day and future climate conditions.

8.2.6 Final remarks

The present study provides several plausible pictures of the future spread of malaria under the influence of a modified climate. Due to similar atmospheric features of climate scenarios the A1B and B1 malaria scenarios of three different models point into the same direction. Incontestable seem to be expected changes in highland zones. Less uncertain is the change of the malaria situation in the Sahel. Admittedly, the presented scenario is only one realistic picture of the future spread of malaria in the Sahel. However, health planners must be prepared for any possible change.

This study might provide helpful information for decision makers in terms of allocation of resources for malaria control. A clear estimation is provided for policy makers relative to possible consequences of climate change on the disease distribution. Malaria scenarios identified risk areas and may lead to improved public health planning to combat changing malaria risk (Tatem and Hay 2004). Findings of this study might be suitable for strategic planning for malaria control or might form a platform to help target planning tools for long-term control measures. This information can allow international priority setting of malaria control. Disease programs should not only continue their current focus, but should also consider where and when to implement additional surveillance to identify and prevent epidemics if mosquitoes change their geographical range (Confalonieri et al. 2007). High priority should be assigned to improving the public health infrastructure and developing and implementing effective adaptation measures (McCarthy et al. 2001).

This work has further furnished data from various entomological and parasitological field studies. In App. D, the reader has full access to numerous published data that might serve for individual research purposes. Provided references might assist in identifying relevant articles. Note also that all information is available in a digital format in the information system *MalaRis* ('The impact of climate change on Malaria Risk in Africa'; see <http://www.impetus.uni-koeln.de/malaris>) which was developed for IMPETUS (Integrated Approach to the Efficient Management of Scarce Water Resources in West

Africa; German: „Integratives Management Projekt für einen tragfähigen Umgang mit Süßwasser“).

For the risk assessment of possible future malaria occurrence different malaria models were forced by two plausible regional climate projections. This approach focused solely on temperatures and precipitation data and hence assumed no future human imposed constraints on the disease. Under this assumption climate change will cause both increases and decreases in areas suitable for this vector-borne disease. The strongest changes are projected for unstable malaria areas at fringes of endemic disease transmission. However, many other factors such as environmental changes or standards of living will determine vulnerability of individuals in the future. Strategies should be developed to combat projected changes of malaria distribution. Various available resources are urgently required to control malaria under the modified future climate.

Appendices

C Data processing

C.1 Configuration of GSOD time series

The application of temperatures and rainfall from GSOD is hampered by two main problems. Firstly, various entries exhibit erroneous values. A quality check of the data is therefore needed. Secondly, precipitation reports partly overlap requiring a special data processing.

Regarding data quality, the original data undergoes automated quality controls. By means of this control random errors are sorted out from the data input. However, the comparison with, for example, monthly values (cp. Sec. 3.5) showed that errors remain in the summary of day data. Due to remaining errors a time consuming data check was carried out for the period of 1960-2006. Exceptionally high or low temperature values were eliminated (e.g., a temperature drop of more than 10 K from one day to the next).

Due to the more or less random distribution of precipitation in time the correction of precipitation data was complicated:

Precipitation values were principally compared to separately reported monthly precipitation amounts (cp. Sec. 3.5). Regarding months with precipitation, the data is corrected when the monthly GSOD sum exceeds reported monthly precipitation by at least 10 mm. In such cases, precipitation values are eliminated (e.g., unrealistic high 24 hour precipitation) that come up to or exceed the difference between GSOD and reported monthly precipitation. The last case makes sense since rarely all precipitation reports are available. For months without any precipitation (according to monthly reports) all precipitation events were deleted. Sometimes even the correction of transposed digits was possible (e.g., as a result of errors of the SYNOP code, for instance, 31.8 mm were coded as '318' instead of '032' or mixed digits such as '097' instead of '997', which results in 97 mm instead of 0.7 mm). It is also possible that the monthly precipitation data is incorrect (Sec. 3.5). For this reason, the data is not adjusted when several corrections would have been necessary and when there were indications of precipitation (with regard to present and past weather observations). When monthly precipitation data was

not available the monthly GSOD precipitation was compared to PREC/L (cp. Sec. 3.7). Here, only unusual high precipitation amounts (e.g., more than 200 mm) were eliminated in the GSOD data since gridded monthly precipitation is not directly comparable to station observations.

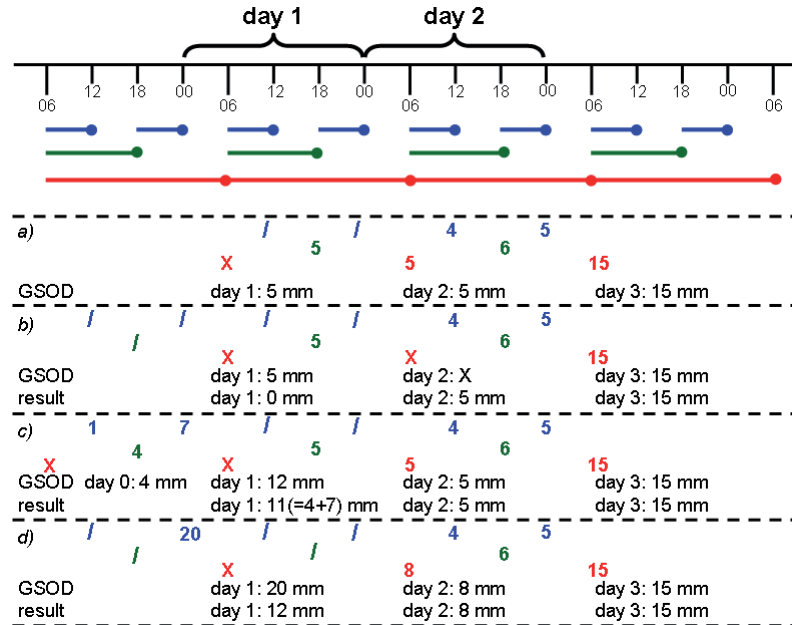


Fig. C.1: Examples in terms of processing of GSOD precipitation data. Blue, green, and red colours indicate 6-, 12-, and 24-hour precipitation, respectively. Dots mark times of SYNOP messages at main synoptic hours. The 'X' characters represent missing reports and '/' symbols stand for messages with no observed precipitation.

The correction of precipitation is exacerbated by the fact that GSOD precipitation does not always refer to 24 hours between 06 UTC of the previous day (day 1) to 06 UTC of the actual day (day 2). Included are also multiple reports of six and twelve-hour periods of precipitation (Fig. C.1). Note that West African weather stations usually report six-hour precipitation at 00 and 12 UTC, twelve-hour precipitation messages are left at 18 UTC, and 24-hour precipitation reports are transmitted at 06 UTC. There is a problem, when 24-hour precipitation is not indicated at day 1. The observation periods of GSOD might partially or completely overlap with the 24-hour precipitation of day 2. This is, for example, true (see Fig. C.1a), when GSOD data indicates 5 mm of precipitation at day 1 (e.g., from the report on 18 UTC) and again 5 mm of rain at 06 UTC day 2 (24-hour rainfall). Except for the six-hour precipitation report at 00 UTC of day 1 all six- and twelve-hour precipitation reports of day 1 are assigned to 24-hour rainfall of day 2 (06 UTC day 1 to 06 UTC day 2). For this reason, incomplete precipitation data of day 1 (i.e., when no 24-hour report is left in GSOD) was transferred to day 2. Of course, only when no 24-hour precipitation report exists for day 2 (cp. Fig. C.1b). However, in such cases some precipitation amounts of day 1 can be omitted, namely that of the 00 UTC day 1 report. For this reason, it was checked if the precipitation value from day 1 was higher than 24-hour precipitation of day 2. In this case, the difference between these two amounts must belong to 24-hour rainfall of day 1 and is therefore added to day 1

precipitation (Fig. C.1c). However, it is obviously still possible that some precipitation is lost (see, e.g., Fig. C.1d).

For some parts of the particular time series the redistribution of the data might lead to a wrong timing of precipitation (one day too late). The precipitation shift causes another problem, when the monthly precipitation sum is compared to monthly reports. Precipitation amounts from a particular month might be assigned to the subsequent month. In this case, the comparison with reported monthly precipitation was performed manually. As a consequence the particular rainfall amount was sometimes set back to the previous day. Note, some doubtful GSOD data after 2000 was additionally checked by SYNOP messages that were archived at the Institute for Geophysics and Meteorology (University of Cologne).

The correction of GSOD precipitation is inevitable since the LMM is fairly sensitive to the data input of precipitation. The raw GSOD precipitation data often includes unrealistically high precipitation values (e.g., Dakar/Yoff: 406.9 mm (04.08.1998) versus an August rainfall of 191 mm). Without this subjective quality check meaningful malaria model runs would have not been possible.

Finally, note that daily mean temperatures from GSOD are only used when they were calculated by at least four observations. That is due to the fact that some synoptic stations only report four observations per day.

C.2 Generation of time series at synoptic stations

The LMM enables the simulation of the spread of malaria only with complete daily temperature and precipitation time series. As previously described, African weather station data suffers from numerous gaps (see Secs. 3.2 & 3.3; cp. Fig. 3.2). The challenge therefore was the reproduction of realistic meteorological time series for 1973-2006. The implemented procedure combines different sources of daily temperature and precipitation time series. Incomplete monthly data sets were, in addition, adjusted by means of monthly and climatic values. The detailed procedure is specified as follows:

Firstly, a complete temperature time series is constructed. Initially, daily mean temperatures are computed from three- or six-hourly SYNOP messages and the number of available hourly reports is noted for a particular day. Daily mean temperatures from SYNOP and GSOD messages are combined to one and a more complete time series. In case of coexistent SYNOP and GSOD data, the value with the higher number of hourly measurements is chosen (in case of equal numbers SYNOPs are preferred). Data gaps or daily mean temperatures based on less than four hourly messages are filled using three iterations. (i) Temperature values are calculated by at least five daily mean temperatures of surrounding days (stepwise iteration from 5-15 days before and after). (ii) If there are not enough values available, monthly mean temperature is instead inserted from GHCN. (iii) If there is no GHCN value available, the averaged temperature of that day of the year is used (i.e., the mean of at least five original temperature values regarding 1973-2006).

As a consequence, the complete reconstructed temperature time series are according to (average) weather conditions of the given space of time.

Secondly, daily precipitation time series are adjusted to monthly precipitation amounts. Initially, various data sources are combined and are chosen in the following order (relative to their assessed reliability): (i) DMN precipitation (Sec. 3.1), (ii) supplementary data source (A. Niang, personal communication, 2008; Sec. 3.1), (iii) SYNOP precipitation reports (Sec. 3.2), and (iv) GSOD data (Sec. 3.3).

In spite of different data sources partially large gaps remain in the data. For the final construction of a realistic daily precipitation time series the available rainfall from SYNOPs are accumulated to monthly precipitation amounts. These values are compared with monthly precipitation provided by the GHCN (Sec. 3.5). When reported values are lower than GHCN monthly rainfall (at least 10 mm), artificial rain events are introduced at days when no or incomplete precipitation reports are available. When there is no GHCN value available monthly precipitation is compared to the gridded PREC/L data set (Sec. 3.7). Artificial precipitation values are by chance firstly fitted into days with missing reports and finally into days with incomplete messages.

The number of introduced monthly precipitation events conforms with the *monthly number of days with at least 1 mm precipitation* ($\#RR_{\geq 1,m}$). Principally, $\#RR_{\geq 1,m}$ is reported in CLIMATE messages. However, CLIMATE messages are often not available for West African weather stations. For these reasons, when possible $\#RR_{\geq 1,m}$ is determined by CLINO data (Sec. 3.4). Unfortunately, such values are not allocated for a lot of stations by the WMO or other sources. In these cases, $\#RR_{\geq 1,m}$ is determined by average values of $\#RR_{\geq 1,m}$ with regard to 1973-2006. $\#RR_{\geq 1,m}$ is itself derived from reported data. However, only those months are used when at least 85% of 24-hour rainfall messages are available or when the amounts of the precipitation messages almost sum up to the GHCN value (maximum difference: 10 mm). After determination of $\#RR_{\geq 1,m}$ missed monthly precipitation is equally distributed onto added rainfall days (e.g.: 40 mm are missing; $\#RR_{\geq 1,m}=12$; eight rainy days are available in the time series composite; four artificial precipitation events of 10 mm are hence introduced).

As noted above (Sec. 3.1) a complete daily precipitation data set was allocated by the DMN. The precipitation time series of six Benin weather stations hence represent real observations. For all the other stations the implementation of artificial precipitation events produces realistic time series. For a particular month when no precipitation messages are available the distribution of precipitation is random and each precipitation event receives the same rainfall. Unknown monthly precipitation amounts (no GHCN data) further introduce uncertainties.

C.3 Bias-correction of REMO precipitation

The simulated REMO precipitation reveals discrepancies relative to IRD (cp. Sec. 4.1). The REMO precipitation therefore was bias-corrected by H. Paeth and R. Girmes (personal communication, 2006). Because the correction procedure was not published and

even no document exists in the grey literature, the bias correction is briefly described at this place:

In order to minimise the REMO model bias with regard to precipitation the rainfall data is corrected relative to CRU (CRU TS 1.1) precipitation (cp. Sec. 3.8). The adjustment is performed relative to the period 1960-1998 representing the maximal intersection between REMO and CRU TS 1.1. Since CRU is only available for land areas the bias correction is only available for REMO land grid points.

Monthly precipitation amounts of REMO and CRU are averaged and compared with each other. In case that averaged REMO precipitation of a month is lower than corresponding CRU values, monthly precipitation is adjusted upwards by the monthly climatological difference. For each concerned month between 1960 and 2000 the particular climatological difference is equally distributed on simulated precipitation events. For this reason, a correction of the precipitation amount of a particular month is not possible when no precipitation event is simulated by REMO. In fact, the introduction of artificial rainfall events is not intended. Furthermore, the correction of only few simulated precipitation events might lead to unusual high precipitation amounts. In order to keep rain events realistic, extreme events in the dry season are artificially limited to 50 mm. Also note that the equal distribution of precipitation is not realistic. However, for the malaria simulation it apparently does not play an important role since the LMM and MSM use 10-day accumulated and monthly rainfall, respectively (see also Fig. 4.2).

In case of higher averaged monthly REMO precipitation in comparison with CRU precipitation, the use of the climatological difference is not possible. This is because the difference might be higher than simulated REMO precipitation of an individual month. An analogue correction as in the first case would therefore lead to undesirable negative precipitation values. As a consequence, a quotient (q) is applied and is defined by the ratio of averaged CRU and REMO precipitation. However, due to the fact that some rainfall amounts are still missing for the monsoon onset the simple usage of q results in too low annual precipitation amounts in the Sahel. On account of this, q was artificially limited to values above or equal to 0.2 (therefore: $0.2 \leq q < 1$). As a result, some too high precipitation amounts are retained after the bias correction during the monsoon retreat, which is somewhat delayed and reveals higher rainfall in the uncorrected data (cp. Sec. 4.1).

The described correction procedure was applied to 1960-2000 and to the whole REMO land area. The same climatological differences and quotients were used for the precipitation bias correction of REMO climate scenarios. It is assumed that the model bias of REMO or rather differences between simulations and reality is still the same under the modified future climate. However, this assumption might not be valid under a strongly changed precipitation regime, for example, a substantial decrease or increase of annual precipitation due to a changed climate.

C.4 Bias-correction of REMO temperatures

The REMO ensemble experiments overestimate the seasonal temperature cycle. REMO temperatures are too low (high) during the dry (rainy) season (Secs. 4.4 & 4.5). A bias correction of REMO temperatures is hence needed. Due to the altitudinal dependence of temperature and different background orographies CRU cannot be used for the rectification of the REMO bias. The bias correction is instead performed by ERA40 (Sec. 3.9). The procedure is the following:

Due to a different horizontal resolution the REMO and ERA40 model are based on different orographies. Since temperatures in general decrease with height, REMO and ERA40 temperatures will differ at locations where there are differences in orographies. Modelled screen level temperatures therefore differ at mountainous areas such as the East African highlands. In order to cope this problem, the *potential temperature* (θ) is computed for a reference level by the modelled surface pressure and the temperature at a height of 2 m. REMO and ERA40 temperatures are taken dry adiabatically to 850 hPa and are compared at this particular level. Note, this procedure is purely a mathematical proceeding and does not mirror a real atmospheric layering.

For comparison of the two data sets the ERA40 data was interpolated to the REMO grid (see App. C.7). The REMO temperature data is compared to ERA40 temperatures by means of θ at 850 hPa (θ_{850}). θ_{850} values are computed by the Poisson equation requiring 2 m temperatures and surface pressure as input variables. The correction of REMO temperatures uses the θ_{850} difference between REMO and ERA40 ($\Delta\theta_{850}$) with regard to the average of 1960-2000. In order to avoid unrealistic jumps in the correction from one day to the other, the $\Delta\theta_{850}$ data is smoothed by means of the eleven-day running mean. Firstly, the correction with smoothed $\Delta\theta_{850}$ is performed on a daily time step and new REMO θ_{850} values are computed. Secondly, the corrected 2 m REMO temperatures are again calculated by the Poisson equation using the new θ_{850} values and the unchanged surface pressure. The result is a REMO temperature that is adjusted to ERA40. With regard to future scenarios it is assumed that the temperature bias of REMO is the same under the changed future climate.

C.5 The ensemble mean

The REMO data consists of twentieth-century simulations (1960-2000) and two climate scenarios (2001-2050). Each period and scenario is represented by three ensemble members in order to obtain a measure of uncertainty. The analysis of data is therefore usually performed by the ensemble mean of a particular variable. The ensemble mean of annual precipitation of the present-day climate (1960-2000), for instance, is computed by means of 123 annual values of three particular simulations (three times 41 annual values). In fact, the ensemble mean of a decade is therefore always the average of 30 values. The standard deviation is also calculated by the corresponding values of three ensemble runs. Daily or monthly values of the seasonal cycle are computed in a comparable way. How-

ever, for certain time series values from every ensemble run are separately presented. That is because the ensemble average of, for instance, single years would considerably reduce the year-to-year variability of time series.

C.6 The 360-day year

The model structure of the LMM is based on a simplification to a 360-day year, consisting of 12 months of 30 days each. The model ‘reality’ utilises a reduced calendar in order to simplify simulations and the data analysis. The input data comprising calendar days must therefore be converted into 30-day months:

A simple method is used for the transformation of data. In case of leap years and non-leap years, five and six days are omitted, respectively. Due to the variable weather conditions during the year the omission of days is quite evenly distributed throughout the year. The 31-day months are simply reduced to 30-day months via the omission of the last day. Since calendar years consist of six 31-day months in case of non-leap years the 31st March is retained. Overall the slightly modified meteorological conditions, for example, the omission of some rainfall amounts, should have only a small effect on the results.

C.7 Grid transformation

Various meteorological data sets exhibit different horizontal resolutions. For example, REMO operates on a 0.5° latitude/longitude grid, whereas IRD precipitation is only available for 1° grid boxes. The comparison of such data sets requires the transformation of one of the data sets.

Due to the fragmentary IRD grid (Fig. 3.4) the REMO data was transformed to the 1° latitude/longitude IRD grid. Only IRD grid boxes with continuous observations between 1968 and 1990 were utilised. The interpolation from the 0.5° to the 1° grid boxes ideally only requires four REMO grid boxes. However, the REMO and IRD grids are displaced to each other. For this reason, eight values from the REMO grid are needed for the calculation of values of the IRD grid. The rainfall field was hence smoothed and the number of rainy days is increased. Note also that only land grid boxes were used for the interpolation.

CRU and REMO exhibit the same horizontal resolution but these data sets are displaced to each other by 0.25° . For this reason, CRU values were interpolated to the REMO grid. When possible the four surrounding land grid boxes of CRU were averaged. As a consequence, CRU values were smoothed.

The varying resolution of REMO and ERA40 represents an issue for the bias correction of REMO temperatures. The resolution of REMO is 0.5° and ERA40 temperatures at screen level are archived on a N80 full Gaussian grid (equivalent to a 1.125° grid). ERA40 temperatures and surface pressures were hence interpolated to the REMO grid

($0.5^\circ \times 0.5^\circ$) using a distance-weighted average of the four nearest neighbour values on the Gaussian grid. Another problem arises from the fact that ERA40 sea grid points were utilised for the interpolation of the REMO land grid point data. The initial masking out of ERA40 sea grid points largely prevents this problem.

REMO and ERA40 were compared with data from synoptic stations in West Africa and Cameroon (Sec. 4.5). Values of observation sites were interpolated from the 0.5° REMO/ERA40 grid using bilinear interpolation. At this step only land grid points were included. Due to the altitudinal dependence of temperature also the difference between altitude of the observation site and that of ERA40 orography was calculated. Sites were not used for composites whose heights differ by more than 300 m from the ERA40 orography (cp. Simmons et al. 2004).

C.8 The Wilcoxon-Mann-Whitney rank-sum test

In this study a test of significance is performed by the *Wilcoxon-Mann-Whitney* (WMW) rank-sum test (also called Mann-Whitney U test, Wilcoxon rank-sum test, etc.). The WMW rank-sum test is a non-parametric test for assessing whether two independent samples of observations come from the same distribution. This test was initially proposed by Wilcoxon (1945), for equal sample sizes, and was later extended to arbitrary sample sizes by Mann and Whitney (1947). It is constructed for changes of obtaining greater values in one sample versus the other. The WMW rank-sum test only requires the two samples to be independent. In fact, no assumptions are made about how the data is distributed in either group. They may be normal, lognormal, exponential, or any other distribution. In contrast, the student t-test can only be applied under special conditions. The data within each group has to be normally distributed and the difference between the groups must be additive. This test strongly depends on the assumption that the mean is a good measure of central tendency for skewed data. These often overlooked problems make the t-test less applicable for general use than the non-parametric rank-sum test (cp. Helsel and Hirsch 2002). However, the student t-test is more powerful at detecting differences between two populations through their means, but the loss of power of the WMW rank-sum test is usually quite small (e.g., Wild and Seber 2000).

The null hypothesis (H_0) of the rank-sum test is that the two samples are drawn from a single population, and therefore that their probability (p) distributions are equal. The alternative hypothesis distinguishes (H_1 , H_2 , and H_3) between one-side and two-sided tests and states that one sample is stochastically greater.

$$H_0 : \text{Prob}[x > y] = 0.5$$

$$H_1 : \text{Prob}[x > y] \neq 0.5 \quad (\text{two-sided test} - x \text{ might be larger or smaller than } y)$$

$$H_2 : \text{Prob}[x > y] > 0.5 \quad (\text{one-sided test} - x \text{ is expected to be larger than } y)$$

$$H_3 : \text{Prob}[x > y] < 0.5 \quad (\text{one-sided test} - x \text{ is expected to be smaller than } y)$$

Computation of the exact test

The test involves calculation of a statistic, usually called the *test statistic* (U), whose distribution under the null hypothesis is known. In case of small samples, the distribution is tabulated, but for larger sample sizes the test statistic approximates the normal distribution. The exact form of the WMW rank-sum test is the only way appropriate to compare groups with small sample sizes (ten or lower). In case that the sample sizes are greater than ten the large-sample approximation (see below) can be utilised.

The WMW rank-sum test is based solely on the order in which two sample groups fall. Sample A and B contain n and m values ($x_i, i = 1, \dots, n; y_j, j = 1, \dots, m$), respectively. The null hypothesis tests if the distribution in sample A is the same as that in sample B ($H_0: A=B$). The alternatives are that sample A is shifted either to the right or left of sample B. The WMW rank-sum test initially ranks $(n+m)$ values of the combined sample. The *test statistic* (W) is the sum of ranks for the group having the smaller sample size¹. The corresponding random variable is designated as \tilde{W} (Gaussian sum formula $\Rightarrow \tilde{W} \in [\frac{n(n+1)}{2}, \frac{(n+m)(n+m+1)}{2} - \frac{n(n+1)}{2}]$). The exact test includes the following steps:

1. The *joint ranks* ($R_k; R_k = 1, \dots, (n+m)$) of single ranked series are computed. All values are ranked without regard to which sample they belong. A median value is used in case of ties.
2. The test statistic (W) is computed for the group having the smaller sample size (e.g., $W = \sum_{k=1}^n R_i$). Either group is used when the sizes are equal ($n=m$).
3. Critical test statistic values (C) for the rank-sum test are specified and the *significance level* (α , e.g., 1%, 5%, or 10%) is chosen. $C_{\frac{\alpha}{2}, n, m}^*$ and $C_{\frac{\alpha}{2}, n, m}$ are determined from a table of critical values of W^2 .
4. H_0 is rejected, if:

$$H_1 : W \leq C_{\frac{\alpha}{2}, n, m}^* \text{ or } W \geq C_{\frac{\alpha}{2}, n, m}$$

$$H_2 : W \geq C_{\alpha, n, m}$$

$$H_3 : W \leq C_{\alpha, n, m}^*$$

¹Variants of the rank-sum test, for example, that proposed by Mann and Whitney (1947), use a different test statistic (U). Note that U is somewhat more clear and accessible ($U = W - \frac{n(n+1)}{2}$). In this case, for each x_i , the y_i 's are counted that are smaller than x_i (a half is counted if $x_i = y_i$). The total of these counts represents U . The minimum value of U is zero (all values of sample A are smaller than those of sample B). Here, the corresponding U value for sample B is the product of sample sizes ($U_{max} = nm$). Tables for the WMW rank-sum test therefore also differ in tabulated critical values of the test statistic. Either data for U or W is provided.

² C^* and C are critical values for the lower and upper tail of the distribution of the random variable of the test statistic \tilde{W} , respectively.

Large Sample Approximation

The large sample approximation of the WMW rank-sum test was applied in the present study. The distribution of the test statistic (W) of the rank-sum test is closely approximating a normal distribution when the sample size for each group is ten or more (see Helsel and Hirsch 2002, their Fig. 5.3). The large sample approximation again does not imply that the data sets are normally distributed. It is rather based on the near normality of the test statistic at large sample sizes. When H_0 is true and if there are no ties, the *average of the test statistic* (μ_W) and the *standard deviation of the test statistic* (σ_W) can be computed by (if $n \leq m$, otherwise exchange n and m in the μ_W equation):

$$\mu_W = \frac{n(n+m+1)}{2}$$

$$\sigma_W = \sqrt{\frac{nm(n+m+1)}{12}}$$

The σ_W value must be reduced in the presence of tied ranks. Conover (2006) provides such a formula ($\sum R_i^2$ refers to the sum of squares of all $(n+m)$ ranks or median ranks actually used in both samples):

$$\sigma_W = \sqrt{\frac{nm}{(n+m)(n+m-1)} \sum_{k=1}^{n+m} R_k^2 - \frac{nm(n+m+1)^2}{4(n+m-1)}}$$

The *test statistic for the large sample approximation* (Z) is computed by standardising the test statistic of the exact test. Due to the fact that the random variable \tilde{W} is discrete a further continuity correction must be applied. The probability of occurrence is adjusted to the normal curve by either adding or subtracting 0.5 (cp. Fig. 5.3 in Helsel and Hirsch 2002), as the test statistic changes by units of one. Z is calculated as follows:

$$Z = \begin{cases} \frac{W+0.5-\mu_W}{\sigma_W} & \text{if } W < \mu_W \\ 0 & \text{if } W = \mu_W \\ \frac{W-0.5-\mu_W}{\sigma_W} & \text{if } W > \mu_W \end{cases}$$

The significance of Z is checked in a table of the standard normal distribution for the final evaluation of the test results. For example, a Z value of -1.96 results in a p -value of about 2.5% for the lower tail of the distribution. For the two-sided rank-sum test ($p = 2 \cdot 0.025$) the null hypothesis is hence rejected at the 10% and 5% significance level (α), but not at a level of 1%.

In the present study, the two-sided WMW rank-sum test identifies areas with significant differences at a 5% significance level. Sample A includes 123 annual values ($n = 3 \cdot 41 = 123$) of three ensemble runs of the present-day climate (1960-2000). Values for projected future conditions of a decade (e.g., 2041-2050) are represented under sample B ($m = 3 \cdot 10 = 30$).

D Entomological and parasitological malaria variables

All across Africa the studies of Hay et al. (2000b, 2005) as well as that of Keiser et al. (2004) already compiled information regarding entomological and parasitological studies undertaken in Africa from 1980 onwards. These articles presented results from various malaria field studies that revealed information regarding different malaria variables. However, not all desirable data is given by review articles of Hay et al. (2000b, 2005) and Keiser et al. (2004), for example, some data with regard to the malaria season is not provided. For this reason and for extension of data, a time-consuming literature research was carried out.

The analysis included references from the three above-mentioned review articles as well as some more recent publications. Due to the availability of meteorological data as well as limitation of time the analysis was restricted to the area of West Africa and Cameroon (cp. Tab. G.1). Moreover, only malaria information from malaria studies with nearby meteorological data (cp. Sec. 3.1-3.5) was used in the present study (cp. Fig. 3.1).

Transmission of malaria depends on environmental conditions (e.g., Hay et al. 2000b). For this reason, it is necessary to divide between rural and urban sites. Additionally, it was checked if permanent streams (e.g., rivers) or irrigation (e.g., rice cultivation) played an important role (see also Sec. 2.6.2). This is of importance since the used malaria models do not include the modelling of, for example, rivers or lakes. However, it was found that most field sites in Cameroon are influenced by the presence of permanent rivers, which is mainly caused by the high annual rainfall amount. Moreover, no significant difference was found in terms of entomological and parasitological data between rural sites and such locations. On this account, also sites with permanent streams were included in the validation procedure of the LMM (Sec. 6). Please also note that it could not be avoided that these analyses rely on subjective definitions by authors of original studies (cp. Hay et al. 2005) as well as the subjective categorisation of the present analysis.

The location of study sites was geo-referenced by four different methods. When possible the geographical position was taken from the particular reference. Otherwise the position was extracted from Hay et al. (2000b, 2005). The remaining positions were deduced from the Heavens-Above web page (<http://www.heavens-above.com/countries.aspx>). When the identification was still impossible the position was graphically derived from published maps. However, for some study sites the determination of the geographical position was not possible. Also note that the exact position was not needed. Only information in terms of the rough distance between the particular location and the next meteorological station was required (e.g., 50 km northwest of Ouagadougou).

A differentiation between the four species of the malaria parasites is not intended by the applied malaria models. As a consequence and against other studies (e.g., Hay et al. 2005) the data collection does not divide between transmission of different malaria

parasites, for example, *P. falciparum*. However, the bulk of malaria transmission is due to *P. falciparum*.

In the following, information is provided for some malaria variables:

D.1 Human biting ratio (*HBR*)

The human bait catch represents a direct sample of human-biting mosquitoes (Le Goff et al. 1997). This involves one or several adults waiting at a given location, mostly indoors or outdoors during night time, and collecting mosquitoes that try to feed on exposed humans. Other sampling techniques are also used such as pyrethrum spray collections (cp. Service 1977a) as well as light (e.g., Lindsay et al. 1993c) and exit traps (e.g., Lindsay et al. 1989). However, these methods depend on the behaviour of mosquitoes and are less directly associated with feeding on humans (e.g., Service 1976). The sampling bias between mainly used human bait catches and light traps was analysed (Lines et al. 1991; Faye et al. 1993; Mbogo et al. 1993; Davis et al. 1995; Smith 1995). There is also a variation in the attractiveness of individuals to mosquitoes (Lindsay et al. 1993a). Due to the difference in body size adults are more attractive to *Anophelines* than children (e.g., Muirhead-Thomson 1951; Port et al. 1980). Some field studies used bait catches performed by children. As proposed by Hay et al. (2000b), in such cases the child *HBR* values were converted to adult *HBR* values via multiplication of 3.57 (Port et al. 1980).

D.2 Circumsporozoite protein rate (*CSPR*)

Only female mosquitoes with sporozoites in their salivary glands are able to infect humans. For this reason, the traditional *CSPR* method is the dissection of salivary glands of caught mosquitoes by microscope. Usually malaria field studies dissect all or at least a representative part of collected mosquitoes. A newer method represents the enzyme-linked immunosorbent assay (ELISA) technique (e.g., Burkot et al. 1984a; Habluetzel et al. 1989; Goldsby et al. 2002), detecting circumsporozoite antigens from mosquito head and/or thorax samples (Hay et al. 2000b). Burkot et al. (1984b) showed that ELISA has a greater sensitivity and species specificity than microscope observations. However, the reliability of microscopy and ELISA varies between studies (Hay et al. 2000b). For this reason, ELISA derived measures of *CSPR* were not adjusted to observations performed by microscopy.

D.3 Entomological inoculation rate (*EIR*)

EIR is a comprehensive indicator and direct measure of the malaria transmission level of a given location (Awolola et al. 2002). This variable is an estimation of the passage of malaria parasites from infectious mosquitoes to humans (Robert et al. 2003). *EIR* is a measurable direct determinant of malaria prevalence, parasite density, incidence, and mortality and therefore represents a testable variable for malaria models (Shililu et al.

2003). *EIR* cannot be measured directly but it can be easily calculated via the above-mentioned standard measures of *HBR* and *CSPR* ($EIR = HBR \cdot CSPR$; cp. Macdonald 1957). However, uncertainty exists when *EIR* is estimated in areas of low mosquito densities (Hay 2000). In such regions, malaria transmission might fall below the limit of detection. Please note, *EIR* is not an exact measure of transmission since not every bite from infectious *Anophelines* results in a human infection (Robert et al. 2003). Above-mentioned diverse entomological methods complicate the comparability of *EIR* values.

D.4 Asexual parasite ratio (*PR*)

The malaria prevalence or asexual parasite ratio is the proportion of the survey population confirmed positive for the malaria parasite. Due to the slow parasite recovery in humans the measure of *PR* is a less suitable indicator of the duration and level of malaria transmission than *EIR* (Reiter et al. 2004; Hay and Snow 2006). As *EIR* rises *PR* rapidly becomes saturated (Kiszewski et al. 2004). However, *PR* is much more easy to access than *EIR* and is therefore a widely available measure of malaria endemicity (e.g., Smith et al. 2005).

In seasonal malaria transmission areas, *PR* values vary considerably (e.g., Sissoko et al. 2004) since they are usually high (low) at the end (start) of the transmission season (e.g., Gazin et al. 1988b). For this reason, when possible minimum and maximum values of *PR* were extracted from literature. However, this is only possible when a sufficient number of surveys were taken place. When monthly data is not available the allocation of data from the temporary survey depends on the related transmission level (e.g., *PR* taken during the end of the low (high) transmission season were assigned to minimum (maximum) *PR* values). Due to the age dependence of *PR* wherever applicable only *PR* from children (usually ≤ 15 years) was extracted.

D.5 Malaria seasonality

Climate change is expected to affect the distribution and seasonality of malaria (e.g., Epstein et al. 1998; WHO 2003; Confalonieri et al. 2007). The detection of the modification of the malaria season is therefore of great importance (Kovats et al. 2001). The malaria transmission in West Africa is usually seasonal and reaches a maximum between the middle of the rainy season and the beginning of the dry season (e.g., Robert et al. 1985).

The analysis of malaria seasonality changes is only possible when the applied malaria models are simulating realistic transmission seasons. A quality check of models in terms of the start, end, and length of the malaria season is hence required by observed data. The definition of the malaria season is usually based on the *monthly Entomological Inoculation Rate* (EIR_m), which is observed by field studies.

The introduction of the malaria disease into the LMM is assured by a constant influx of new infected mosquitoes. As previously discussed, artificial infectious mosquito bites

are excluded by means of two LMM runs (cp. Sec. 5.1.6). The malaria season starts by definition in the first month with an EIR_m value of at least 0.01 infectious bites per human. According to the model structure a value of 0.01 means that during the 30-day month at least one out of the 100 humans is bitten by an infectious mosquito. Consequently, the last month during the transmission period defines the end of the malaria season. Various years also reveal year-round or even no malaria transmission. The length of the malaria season is therefore the number of months with EIR_m reaching at least 0.01 infectious bites. For each site or grid box additionally the length of the main transmission season ($MSeas$) is defined as the number of months in which 75% of EIR_a is transmitted (cp. Hay et al. 2000b)³. Moreover, when possible the month with maximum malaria transmission ($XSeas$) is identified as the month with the highest EIR_m value.

The above chosen threshold ensures attainment of a reasonable transmission level. However, the definition of the malaria season in the model might not be directly comparable to field studies since observations are subject to a certain detection limit. That is due to the fact that field experiments do not continuously measure biting rates (at best, e.g., two times a week) and that these studies do not account for every human of the population.

Analysis	J	F	M	A	M	J	J	A	S	O	N	D
Number of events: $fr(m)$	24	0	0	0	3	10	26	14	1	1	2	72
Criteria A: $fr(m-1) + fr(m)$	96	24	0	0	0	13	36	40	15	2	3	74
Criteria B: $fr(m) + fr(m+1)$	24	0	0	0	13	36	40	15	2	3	74	96
Threshold	25	25	25	25	25	25	25	25	25	25	25	25
Fulfilled criteria (A or B)	1	0	0	0	0	1	1	1	0	0	1	1

Tab. D.1: Artificial example relative to the determination of the season start for a period of 100 years. Within the time frame 153 season starts are identifiable. Criteria A and B require at least 26 events for the considered month and the preceding as well as subsequent month, respectively. In this example, obviously two malaria seasons are present. The first season begins between July and August and the second season starts most frequently in December, but also takes place in January. The periods June-August as well as November-January are selected by the aforementioned procedure (indicated by ‘1’). The average of the first season is hence 7.1 and that for the second season is 12.2.

The definition of the malaria season relative to a long time series is more complex, especially in case of two distinct malaria seasons. The start of malaria transmission usually takes place within a certain period of time. In the Sahel, transmission typically sets in between June and August. However, variable atmospheric conditions might cause unusual transmission seasons. Such events complicate the determination of typical characteristics of the malaria season. In areas of two malaria seasons it is, for instance, possible that the two monthly maxima are not separated. For this reason, only typical periods of

³Note that the computation of $MSeas$ includes only months of the malaria season.

the year are considered. The definition of the start of the malaria season is explained in the following. The determination of *ESeas* as well as *XSeas* is fully analogue:

In a first step, the *frequency* (*fr*) of the season start within a certain month is computed. A month (*m*) is only considered when it either shows or when the preceding or subsequent month reveal a frequent start of the malaria season. The frequency of such events must exceed 25% (criterion A: $fr(m) + fr(m+1) > 0.25 n_y$; criterion B: $fr(m-1) + fr(m) > 0.25 n_y$; n_y : number of years of the period). For the calculation of the mean or standard deviation of the season start only those months are retained that fulfil either criterion A or B (see also the example in Tab. D.1). Note that several periods during the year might have to be considered. These times spans are simply separated by months that do not accomplish criteria A and B. Due to the chosen procedure it is possible that a different number of periods are found for *SSeas*, *ESeas*, and *XSeas*. For example, for some grid boxes in East Africa two malaria seasons are merged or only one season start (end) is found despite most frequently two season ends (starts). Numerous cases exist when transmission occurs infrequently ($\sum fr(m) \leq 0.25 n_y$; denoted as ‘U’ in the figures). In other cases *SSeas*, *ESeas*, or *XSeas* is simulated more often but are not sufficiently clustered. Such a situation might be characterised as a variable malaria season (denoted as ‘V’). Also no *SSeas* and *ESeas* values are found when transmission is often year-round (denoted as ‘C’).

D.6 Data table convention

Tab. D.2: Summary of abbreviations and indices that are generally used in Tabs. D.3- D.15.

abbreviation	explanation
country	country where the study was undertaken
place	location of the study site
long	longitude of the study site (-999.00: position is either unknown or was not sought out)
lat	latitude of the study site (-99.00: position is either unknown or was not sought out)
M1	month, when the study started
YYY1	year of the start of the study
M2	month, when the study ended
YYY2	year of the end of the study
specie	involved mosquito specie(s)
note	notes
ref	reference
U _a	land use classification after Hay et al. (2005): PU=peri-urban (population densities of 250-1,000 persons per km ²), R1=rural 1 (population densities of 100-250 persons per km ²), R2=rural 2 (population densities of <100 persons per km ²), U=urban (population densities of >1,000 persons per km ²).

to be continued

Tab. D.2 – continued

abbreviation	explanation
U _b	as U _a , but as defined by Hay et al. (2000b): R=rural, I=irrigated rice, U=urban area
U _p	as U _a , but as taken from the particular reference: R=rural area, I=irrigation/permanent stream or river, U=urban area (see also Sec. D)
z	altitude of the study site (in m)
-8	special value: data was not available in literature
-9	special value: data has not been checked due to limited access. In such cases some data was taken from Hay et al. (2000b).
a	The position of the study site was taken from Hay et al. 2005.
b	The position of the study site was extracted from Hay et al. 2000b.
c	This value was calculated by using the relationship $EIR = HBR \cdot CSPR$.
d	This value either was already considered or was observed before 1973.
e	time to adult emergence
ē	<i>CSPR</i> was determined by the dissection of salivary glands of caught mosquitoes by microscope.
f	<i>CSPR</i> was determined by the enzyme-linked immunosorbent assay (ELISA) technique.
g	<i>HBR</i> was measured by human bait catches.
h	<i>HBR</i> was measured by pyrethrum spray collections.
ĩ	<i>HBR</i> was measured by using light traps.
i	The position of the study site was taken from http://www.heavens-above.com/countries.aspx .
j	<i>HBR</i> was measured by using exit traps.
k	This value was converted by using a multiplication factor of 3.57 (cp. Port et al. 1980).
m	The position of the study site was derived from a published map.
n	In addition, no malaria transmission was observed during at least one malaria season.
P	time to pupation
r	The position of the study site was found in the reference.
ř	This value is probably not representative (not all field sites could be considered).
s	This value is similar to another value from a different reference regarding the same field site and for about the same period.
y	In addition, a year-round malaria transmission was observed during at least one malaria season.
★	children (the following numbers indicate age classes in years)
★	adults (the following numbers indicate age classes in years)
◆	all ages (the following numbers indicate age classes in years)

D.7 Entomological and parasitological data

Tab. D.3: Data with regard to entomological and parasitological data from malaria field studies. Columns: $CSPR_a$: annual mean circumsporozoite protein rate; HBR_a : annual human biting rate ; EIR_a : annual entomological inoculation rate ; PR_a : annual mean asexual parasite ratio; $PR_{min,a}$: annual minimum asexual parasite ratio; $PR_{max,a}$: annual maximum asexual parasite ratio; $Seas$: length of the malaria season (in months); $MSeas$: length of the main malaria season (in months), that is the number of months in which 75% of EIR_a is recorded; $XSeas$: month of maximum transmission; $SSeas$: start month of the malaria season; $ESeas$: end month of the malaria season; WMO#: WMO station number, which indicates the associated weather station (see Tab. G.1 and Sec. 6; -9999: no WMO station was allocated to the data); for further information see Tab.D.2.

country	place	long [°E]	lat [°N]	M1	YYY1	M2	YYY2	$CSPR_a$	HBR_a	EIR_a	PR_a	$PR_{min,a}$	$PR_{max,a}$	$Seas$	$MSeas$	$XSeas$	$SSeas$	$ESeas$	U_b	U_a	U_p	note	ref	WMO#
Benin	Cotonou- Agabalilamè, Djègbadji, Kétonou	2.43	6.35 ⁱ	-8	-8	-8	-8	0.27 ^{ef}	4502 ^{gh}	12.10	-8.0	-8.0	-8.0	-8	-8	-8	-8	-8	-8	-8	R	rural area in vicinity of a lagoon	Akogbéto 2000	65344
Benin	Cotonou- Centre	2.43	6.35 ^a	-8	-8	-8	-8	1.05 ^{ef}	2768 ^{gh}	29.06	-8.0	-8.0	-8.0	-8	-8	-8	-8	-8	-8	U	U	becomes swampy during the rainy season	Akogbéto 2000	65344
Benin	Cotonou- Fiyégnon Donaten	2.43	6.35 ⁱ	-8	-8	-8	-8	0.48 ^{ef}	1064 ^{gh}	5.10	-8.0	-8.0	-8.0	-8	-8	-8	-8	-8	-8	U	U	at the Atlantic coast	Akogbéto 2000	65344
Benin	Cotonou, Gbégamé quarter	2.45	6.36 ^b	1	1987	12	1987	2.80 ^e	1179 ^{gc}	33.00	-8.0	-8.0	-8.0	2	1	11	11	12	U	U	U	in the heart of Cotonou	Akogbéto et al. 1992	65344
Benin	Cotonou-Ladji, Abomey- Calavi	2.35	6.45 ⁱ	-8	-8	-8	-8	0.80 ^{ef}	5870 ^{gh}	47.00	-8.0	-8.0	-8.0	-8	-8	-8	-8	-8	-8	-8	R	peri-urban area in vicinity of a lagoon	Akogbéto 2000	65344
Benin	Cotonou, Ladji quarter	2.43	6.38 ^b	1	1987	12	1987	1.60 ^e	3625 ^{gc}	58.00	-8.0	-8.0	-8.0	8	4	10	06	13	R	U	R	in the north of Cotonou quarter with lagoons	Akogbéto et al. 1992	65344
Benin	Cotonou, Sainte-Rita Norde quarter	2.42	6.37 ^b	1	1987	12	1987	1.40 ^e	3357 ^{gc}	47.00	-8.0	-8.0	-8.0	6	3	08	07	13	R	U	R	-	Akogbéto et al. 1992	65344
Benin	Ganvié	2.42	6.47 ^b	1	1993	12	1993	0.43 ^e	2555 ^h	11.00	-8.0	-8.0	-8.0	6	-8	-8	03	08	R	PU	R	built on a salt lake	Akogbéto 1995; Akogbéto and Nahum 1996	65344
Benin	Ganvié, near lake Nokoué	2.42	6.42 ^b	1	1994	12	1994	0.36 ^f	2656 ^g	10.60	-8.0	-8.0	-8.0	7	-8	-8	-8	-8	R	U	R	built on a salt lake; reduced EIR after bed net usage	Akogbéto and Nahum 1996	65344
Benin	Ganvié, near lake Nokoué	2.42	6.42 ^b	1	1995	12	1995	0.33 ^f	3540 ^g	11.70	-8.0	-8.0	-8.0	7	-8	-8	-8	-8	R	U	R	Ganvié is built on a salt lake; malaria transmission is reduced in the area with treated mosquito nets	Akogbéto and Nahum 1996	65344
Burkina Faso	Bama	-4.42	11.38 ^b	1	1981	12	1981	-9.00	-9	175.20	-9.0	-9.0	-9.0	-9	3	-9	-9	-9	R	R2	R	-	Carnevale and Robert 1987	65510
Burkina Faso	Baré	-4.10	11.08 ^b	1	1981	12	1981	-9.00	-9	91.24	-9.0	-9.0	-9.0	-9	3	-9	-9	-9	R	R1	R	-	Carnevale and Robert 1987	65510
Burkina Faso	Baré	-4.10	11.08 ^b	-8	-8	-8	-8	-8.00	-8	-8.00	77.5	-8.0	-8.0	-8	-8	-8	-8	-8	-8	-8	R	PR : $\star(5-14)$	Boudin et al. 1993	65510
Burkina Faso	Barkoumbilen and Barkoundouba	-1.23	12.67 ^b	3	1995	10	1995	-8.00 ^f	-8 ^h	>41.00	70.0	56.0	85.0	-8	3	09	-8	-8	R	R2	R	PR : $\star(0-20)$; graphically derived	Modiano et al. 1996	65503

to be continued

Tab. D.3 – continued

country	place	long [°E]	lat [°N]	M1	YYY1	M2	YYY2	$CSPR_a$	HBR_a	EIR_a	PR_a	$PR_{min,a}$	$PR_{max,a}$	$Seas$	$MSeas$	$XSeas$	$SSeas$	$ESeas$	U_b	U_a	U_p	note	ref	WMO#
Burkina Faso	Barkoumbilen and Barkoundouba	-1.23	12.67 ^b	8	1994	11	1994	-8.00 ^f	-8 ^h	>102.00	-8.0	-8.0	86.0	-8	3	09	-8	-8	R	R2	R	$PR: \star(0-20)$; graphically derived	Modiano et al. 1996	65503
Burkina Faso	Bella and Peul Djelgobé camps	-999.00	-99.00	6	1985	3	1986	0.64 ^é	-8 ^g	-8.00	50.7	37.7	71.5	-8	-8	-8	-8	-8	-8	-8	R	$PR: \star(0.5-15)$	Gazin et al. 1988b	65501
Burkina Faso	Bobo-Dioulasso	-4.30	11.20 ^b	11	1991	1	1993	0.11 ^é	2150 ^g	2.37	-8.0	-8.0	-8.0	-8	-8	-8	-8	-8	U	R1	U	-	Lochouarn and Gazin 1993	65510
Burkina Faso	Bobo-Dioulasso, Colma-Nord quarter	-4.30	11.21 ^b	1	1985	12	1985	0.19 ^é	2421 ^g	4.60	29.1	18.0	47.6	2	2	-8	09	10	U/R	R1	R	$PR: \star(0-15)$	Robert et al. 1986, 1989; Gazin et al. 1987	65510
Burkina Faso	Bobo-Dioulasso, Diaradougou quarter	-4.29	11.18 ^b	1	1985	12	1985	0.19 ^{éd}	74 ^g	0.14	6.8	4.6	10.3	1	1	09	09	09	U	R1	U	$PR: \star(0-15)$	Robert et al. 1986, 1989; Gazin et al. 1987	65510
Burkina Faso	Bobo-Dioulasso, Dioulassoba quarter	-4.30	11.19 ^b	1	1985	12	1985	0.19 ^{éd}	289 ^g	0.55	10.9	5.4	13.9	1	1	09	09	09	U	R1	U	$PR: \star(0-15)$	Robert et al. 1986, 1989; Gazin et al. 1987	65510
Burkina Faso	Bobo-Dioulasso, Sarfalao quarter	-4.30	11.20 ^b	6	1993	9	1993	0.46 ^é	870 ^{gc}	4.00	-8.0	-8.0	-8.0	-8	-8	-8	-8	-8	U	-8	U	-	Gazin et al. 1996	65510
Burkina Faso	Bouloy	-0.42	14.70 ⁱ	6	1985	3	1986	0.64 ^{éd}	-8 ^g	-8.00	50.7 ^d	37.7 ^d	71.5 ^d	-8	-8	-8	-8	-8	-8	-8	R	$PR: \star(0.5-15)$	Gazin et al. 1988b	65501
Burkina Faso	Dandé	-4.57	11.58 ⁱ	1	1983	12	1983	-8.00	-8	-8.00	-8.0	-8.0	-8.0	4	3	09	07	10	R	R2	R	-	Robert et al. 1985	65510
Burkina Faso	Dandé	-4.57	11.58 ⁱ	1	1984	12	1984	-8.00	-8	-8.00	-8.0	-8.0	-8.0	4	2	10	07	10	R	R2	R	-	Robert et al. 1985	65510
Burkina Faso	Dandé and Tago	-4.55	11.59 ^b	1	1983	12	1984	4.78 ^{éc}	1380 ^g	55.00	-8.0	-8.0	-8.0	-8	-8	-8	-8	-8	R	R2	R	-	Robert et al. 1985	65510
Burkina Faso	Déou	-0.72	14.60 ⁱ	6	1985	3	1986	0.64 ^{éd}	-8 ^g	-8.00	26.6	16.9	45.5	-8	-8	-8	-8	-8	-8	-8	R	$PR: \star(6-15)$	Gazin et al. 1988b	65501
Burkina Faso	Desso	-4.28	11.35 ^b	1	1981	12	1981	-9.00	-9	208.04	-9.0	-9.0	-9.0	-9	3	-9	-9	-9	R	R2	R	-	Carnevale and Robert 1987	65510
Burkina Faso	Gounghin Nord	-1.55	12.37 ^b	3	1984	12	1984	0.00 ^é	-8 ^h	0.00	-8.0	-8.0	11.8	0	0	-5	-5	-5	U	U	U	$PR: \star(2-5)$	Rossi et al. 1986; Sabatinelli et al. 1986	65503
Burkina Faso	Karangasso	-4.63	11.22 ^b	1	1985	2	1986	4.08 ^é	6441 ^{gc}	262.80	63.0	35.4	82.5	6	3	09	06	11	R	R2	R	$PR: \star(0-4)$	Boudin et al. 1991b, 1992	65510
Burkina Faso	Karangasso	-4.63	11.22 ^b	1	1985	2	1986	4.08 ^{éd}	6441 ^{gdc}	262.80 ^d	59.5	47.0	75.0	6 ^d	3 ^d	09 ^d	06 ^d	11 ^d	R	R2	R	$PR: \star(6-9)$	Boudin et al. 1991b, 1992	65510
Burkina Faso	Karangasso	-4.63	11.22 ^b	1	1985	2	1986	4.08 ^{éd}	6441 ^{gdc}	262.80 ^d	65.3	53.3	78.9	6 ^d	3 ^d	09 ^d	06 ^d	11 ^d	R	R2	R	$PR: \star(10-14)$	Boudin et al. 1991b, 1992	65510
Burkina Faso	Karangasso, Koko suburb	-4.65	11.22 ^b	2	1985	2	1986	2.41 ^é	4805 ^{gc}	116.00	62.0	45.0	75.0	7	4	09	06	12	R	R2	R	$PR: \star$; graphically derived	Robert et al. 1988; Boudin et al. 1991a	65510
Burkina Faso	Karangasso, Koko suburb	-4.65	11.22 ^b	5	1985	4	1986	2.55 ^{és}	4548 ^{ghs}	116.07 ^s	54.1	-8.0	-8.0	5 ^s	3 ^s	10	06 ^d	10 ^s	R	R2	R	-	Carnevale et al. 1988	65510
Burkina Faso	Karangasso, Koko suburb	-4.65	11.22 ^b	5	1986	4	1987	4.56 ^é	4913 ^{gh}	223.75	39.6	-8.0	-8.0	7	5	10	06	12	R	R2	R	-	Carnevale et al. 1988	65510
Burkina Faso	Karangasso, Massasso suburb	-4.64	11.21 ^b	2	1985	2	1986	5.19 ^é	7123 ^{gc}	370.00	62.0 ^d	45.0 ^d	75.0 ^d	7	4	09	06	12	R	R2	R	PR : graphically derived	Robert et al. 1988; Boudin et al. 1991a	65510

to be continued

Tab. D.3 – continued

country	place	long [°E]	lat [°N]	M1	YYY1	M2	YYY2	<i>CSPR_a</i>	<i>HBR_a</i>	<i>EIR_a</i>	<i>PR_a</i>	<i>PR_{min,a}</i>	<i>PR_{max,a}</i>	<i>Seas</i>	<i>MSeas</i>	<i>XSeas</i>	<i>SSeas</i>	<i>ESeas</i>	<i>U_b</i>	<i>U_a</i>	<i>U_p</i>	note	ref	WMO#
Burkina Faso	Karangasso, Massasso suburb	-4.64	11.21 ^b	5	1985	4	1986	5.75 ^{es}	7012 ^{ghs}	403.33 ^s	54.1 ^d	-8.0	-8.0	8 ^s	3 ^s	10 ^s	05 ^s	12 ^d	R	R2	R	reduced <i>EIR</i> after impregnated bed net usage	Carnevale et al. 1988	65510
Burkina Faso	Kolèl	-0.43	14.55 ⁱ	6	1985	3	1986	0.64 ^{ed}	-8 ^g	-8.00	50.7 ^d	37.7 ^d	71.5 ^d	-8	-8	-8	-8	-8	-8	-8	R	<i>PR</i> : *(0.5-15)	Gazin et al. 1988b	65501
Burkina Faso	Kongodjan	-4.45	11.58 ^b	1	1983	12	1983	-8.00	-8	-8.00	59.9	40.5	69.2	7 ^d	3 ^d	08 ^d	06 ^d	12 ^d	R	R2	S	<i>PR</i> : *(0.5-15); area: clay hollows/permanent pond	Gazin et al. 1988a	65510
Burkina Faso	Kongodjan	-4.45	11.58 ^b	1	1983	12	1983	-8.00	-8	-8.00	-8.0	-8.0	-8.0	7	3	08	06	12	R	R2	S	area: clay hollows/permanent pond	Robert et al. 1985	65510
Burkina Faso	Kongodjan	-4.45	11.58 ^b	1	1983	12	1984	1.78 ^{ec}	7480 ^g	133.00	-8.0	-8.0	-8.0	-8	-8	-8	-8	-8	R	R2	S	area: clay hollows/permanent pond	Robert et al. 1985	65510
Burkina Faso	Kongodjan	-4.45	11.58 ^b	1	1984	12	1984	-8.00	-8	-8.00	-8.0	-8.0	-8.0	7	5	10	06	12	R	R2	S	area: clay hollows/permanent	Robert et al. 1985	65510
Burkina Faso	Kongodjan	-4.45	11.58 ^b	1	1984	12	1984	-8.00	-8	-8.00	-8.0	9.1	-8.0	7 ^d	5 ^d	10 ^d	06 ^d	12 ^d	R	R2	S	<i>PR</i> : *(0.5-15); area: clay hollows/permanent pond	Gazin et al. 1988a	65510
Burkina Faso	Koro	-4.20	11.15 ^b	1	1981	12	1981	-9.00	-9	171.60	-9.0	-9.0	-9.0	-9	3	-9	-9	-9	R	R1	R	-	Carnevale and Robert 1987	65510
Burkina Faso	Koubri	-1.38	12.15 ^b	7	1984	12	1984	7.10 ^è	6082 ^{hc}	431.83	-8.0	-8.0	94.9	-8	3	08	-8	-8	R	R2	R	<i>PR</i> : *(2-5)	Rossi et al. 1986; Sabatinelli et al. 1986	65503
Burkina Faso	Ouagadougou, Kologh Naba suburb	-1.54	12.39 ^b	3	1984	12	1984	1.47 ^è	1359 ^{hc}	19.98	-8.0	-8.0	22.1	6	3	10	05	10	U	U	U	<i>PR</i> : *(2-5)	Rossi et al. 1986; Sabatinelli et al. 1986	65503
Burkina Faso	Ouagadougou, Nongremassm suburb	-1.51	12.40 ^b	3	1984	12	1984	0.83 ^è	920 ^{hc}	7.64	-8.0	-8.0	31.5	5	3	10	05	12	U	U	U	<i>PR</i> : *(2-5)	Rossi et al. 1986; Sabatinelli et al. 1986	65503
Burkina Faso	Ouagadougou, Saint Camille suburb	-1.52	12.36 ^b	3	1984	12	1984	1.14 ^è	399 ^{hc}	5.58	-8.0	-8.0	19.7	2	1	08	08	10	U	U	U	<i>PR</i> : *(2-5)	Rossi et al. 1986; Sabatinelli et al. 1986	65503
Burkina Faso	Ouagadougou, Saint Léon suburb	-1.52	12.37 ^b	6	1984	12	1984	0.00 ^è	-8 ^h	0.00	-8.0	-8.0	2.9	0	0	-5	-5	-5	U	U	U	<i>PR</i> : *(2-5)	Rossi et al. 1986; Sabatinelli et al. 1986	65503
Burkina Faso	Ouagadougou, Tanghin suburb	-1.53	12.40 ^m	8	1984	9	1984	-8.00	-8	-8.00	-8.0	-8.0	23.6	-8	-8	-8	-8	-8	-8	-8	U	<i>PR</i> : *(2-5)	Sabatinelli et al. 1986	65503
Burkina Faso	Oursi	-0.45	14.68 ⁱ	6	1985	3	1986	0.64 ^{ed}	-8 ^g	-8.00	26.6 ^d	16.9 ^d	45.5 ^d	-8	-8	-8	-8	-8	-8	-8	R	<i>PR</i> : *(6-15)	Gazin et al. 1988b	65501
Burkina Faso	Pabré	-1.58	12.50 ^b	7	1984	12	1984	6.07 ^è	1673 ^{hc}	101.58	-8.0	-8.0	79.6	-8	3	10	-8	-8	R	PU	R	<i>PR</i> : *(2-5)	Rossi et al. 1986; Sabatinelli et al. 1986	65503
Burkina Faso	six villages, 30 km N/NW of	-999.00	-99.00	4	2003	10	2003	-8.00	-8	-8.00	-8.0	-8.0	-8.0	-8	-8	-8	04	-8	-8	-8	R	<i>PR</i> : *(1-14)	Ouédraogo et al. 2008	65503
Burkina Faso	Ouagadougou six villages, 30 km N/NW of	-999.00	-99.00	6	2002	11	2002	-8.00	-8	-8.00	73.4	63.5	85.0	6	3	09	06	11	-8	-8	R	<i>PR</i> : *(1-14)	Ouédraogo et al. 2008	65503
Burkina Faso	Ouagadougou Soumosso	-4.05	11.02 ^b	1	1981	12	1981	-9.00	-9	200.75	-9.0	-9.0	-9.0	-9	3	-9	-9	-9	R	R2	R	-	Carnevale and Robert 1987	65510
Burkina Faso	Tago	-4.38	11.67 ^b	1	1983	12	1983	-8.00	-8	-8.00	-8.0	-8.0	-8.0	6	3	08 ^d	06	10	R	R2	R	-	Robert et al. 1985	65510
Burkina Faso	Tago	-4.38	11.67 ^b	1	1983	12	1983	-8.00 ^è	-8 ^g	82.00	50.7	30.4	71.1	6 ^d	3 ^d	08	06 ^d	10 ^d	R	R2	R	<i>PR</i> : *(0.5-15)	Gazin et al. 1988a	65510

to be continued

Tab. D.3 – continued

country	place	long [°E]	lat [°N]	M1	YYY1	M2	YYY2	CSPR _a	HBR _a	EIR _a	PR _a	PR _{min,a}	PR _{max,a}	Seas	MSeas	XSeas	SSeas	ESeas	U _b	U _a	U _p	note	ref	WMO#
Burkina Faso	Tago	-4.38	11.67 ^b	1	1984	12	1984	-8.00	-8	-8.00	47.6	14.3	77.6	6	3	08	06	10	R	R2	R	PR: *(0.5-15)	Gazin et al. 1988a	65510
Burkina Faso	Tin Edjar	-0.68	14.69 ^m	6	1985	3	1986	0.64 ^{ed}	-8 ^g	-8.00	33.2	15.0	50.0	-8	-8	-8	-8	-8	-8	-8	R	PR: *(0.5-15)	Gazin et al. 1988b	65501
Burkina Faso	Toukoro	-4.25	11.43 ^b	1	1981	12	1981	-9.00	-9	76.65	-9.0	-9.0	-9.0	-9	3	-9	-9	-9	R	R2	R	-	Carnevale and Robert 1987	65510
Burkina Faso	VK1	-4.41	11.35 ^b	1	1981	12	1981	-9.00	-9	0.00	-9.0	-9.0	-9.0	-9	3	-9	-9	-9	I	R2	I	-	Carnevale and Robert 1987	65510
Burkina Faso	VK2	-4.41	11.37 ^b	1	1981	12	1981	-9.00	-9	21.90	-9.0	-9.0	-9.0	-9	3	-9	-9	-9	I	R2	I	-	Carnevale and Robert 1987	65510
Burkina Faso	VK3	-4.41	11.38 ^b	1	1981	12	1981	-9.00	-9	62.10	-9.0	-9.0	-9.0	-9	3	-9	-9	-9	I	R2	I	-	Carnevale and Robert 1987	65510
Burkina Faso	VK4	-4.42	11.37 ^b	1	1981	12	1981	-9.00	-9	20.10	-9.0	-9.0	-9.0	-9	3	-9	-9	-9	I	R2	I	-	Carnevale and Robert 1987	65510
Burkina Faso	VK4	-4.42	11.37 ^b	1	1985	2	1986	-8.00	-8	-8.00	27.4	16.0	35.7	6 ^d	4	11	05 ^d	12 ^d	I	R2	I	PR: *(0-4)	Boudin et al. 1991b, 1992	65510
Burkina Faso	VK4	-4.42	11.37 ^b	1	1985	2	1986	-8.00	-8	-8.00	33.7	23.9	46.1	6 ^d	4 ^d	11 ^d	05 ^d	12 ^d	I	R2	I	PR: *(10-14)	Boudin et al. 1991b, 1992	65510
Burkina Faso	VK4	-4.42	11.37 ^b	1	1985	2	1986	-8.00	-8	-8.00	41.1	29.4	58.0	6 ^d	4 ^d	11 ^d	05 ^d	12 ^d	I	R2	I	PR: *(5-9)	Boudin et al. 1991b, 1992	65510
Burkina Faso	VK4	-4.42	11.37 ^b	2	1984	12	1984	0.39 ^c	14000	50.00	34.0	25.0	45.0	6	4	10	06	11	I	R2	I	PR: *, graphically derived	Robert et al. 1985; Boudin et al. 1991a	65510
Burkina Faso	VK4	-4.42	11.37 ^b	5	1985	4	1986	0.22 ^{ec}	25490 ^g	54.90	-8.0	-8.0	-8.0	6	-8	-8	05	12	I	R2	I	reduced EIR after bed net usage	Robert and Carnevale 1991	65510
Burkina Faso	VK5	-4.43	11.38 ^b	1	1981	12	1981	-9.00	-9	36.50	-9.0	-9.0	-9.0	-9	3	-9	-9	-9	I	R2	I	-	Carnevale and Robert 1987	65510
Burkina Faso	VK6	-4.44	11.37 ^b	1	1981	12	1981	-9.00	-9	54.80	-9.0	-9.0	-9.0	-9	3	-9	-9	-9	I	R2	I	-	Carnevale and Robert 1987	65510
Burkina Faso	VK6	-4.44	11.37 ^b	1	1983	12	1983	-8.00	-8	-8.00	-8.0	-8.0	-8.0	4	3	06	06	09	I	R2	I	-	Robert et al. 1985	65510
Burkina Faso	VK6	-4.44	11.37 ^b	1	1983	12	1984	0.43 ^{ec}	13900 ^g	60.00	-8.0	-8.0	-8.0	-8	-8	-8	-8	-8	I	R2	I	-	Robert et al. 1985	65510
Burkina Faso	VK6	-4.44	11.37 ^b	1	1984	12	1984	-8.00	-8	-8.00	-8.0	-8.0	-8.0	7	2	07	05	11	I	R2	I	-	Robert et al. 1985	65510
Burkina Faso	Zagtouli	-1.63	12.33 ^b	7	1984	12	1984	8.14 ^ē	1009 ^{hc}	82.11	-8.0	-8.0	57.6	-8	2	08	-8	-8	R/I	U	R	PR: *(2-5)	Rossi et al. 1986; Sabatinelli et al. 1986	65503
Cameroon	Bondi	12.19	3.86 ^m	-8	1998	-8	2000	-8.00	-8	-8.00	50.0	49.3	50.7	-8	-8	-8	-8	-8	-8	-8	R	area: degraded forest; PR: ♦(0.8-77); position from Meunier et al. 1999	Bonnet et al. 2003	64950
Cameroon	Ebogo	11.47	3.40 ^b	4	1991	3	1992	0.84 ^ē	38189 ^g	355.00	-8.0	-8.0	-8.0	12	8	03	-1	-1	R	R2	R/S	area: water drainage	Njan Nloga et al. 1993	64950
Cameroon	Ebolakounou	12.13	3.93 ^a	6	1997	5	1998	4.40 ^{ec}	402 ^g	17.70	61.8	-8.0	-8.0	2	2	05	05	06	-8	R2	R	area: forested; Seas: perennial transmission, but partly below the detection limit; PR: *(0-15)	Meunier et al. 1999; Bonnet et al. 2002	64950
Cameroon	Edea, Bilalang suburb	10.13	3.80 ^b	1	1990	12	1990	1.20 ^ē	317 ^{bc}	3.80	-8.0	-8.0	-8.0	-8	-8	-8	-8	-8	U	R2	R	Seas: few mosquito catches	Robert et al. 1993	64910
Cameroon	Edea, Pongo suburb	10.13	3.80 ^b	1	1990	12	1990	8.24 ^{ec}	368 ^g	30.20	-8.0	-8.0	-8.0	-8	-8	-8	-8	-8	U	R2	R	area: river presence; HBR: large spatial differences; Seas: few mosquito catches	Robert et al. 1993; Manga et al. 1993a	64910
Cameroon	Etoa	11.48	3.77 ^b	2	1996	5	1996	4.10 ^{ec}	11571 ^g	474.50	-8.0	-8.0	-8.0	-8	-8	-8	-8	-8	R	R2	R/S	area: river irrigation; too short study	Manga et al. 1997b	64950

to be continued

Tab. D.3 – continued

country	place	long [°E]	lat [°N]	M1	YYY1	M2	YYY2	CSPR _a	HBR _a	EIR _a	PR _a	PR _{min,a}	PR _{max,a}	Seas	MSeas	XSeas	SSeas	ESeas	U _b	U _a	U _p	note	ref	WMO#	
Cameroon	Etoa	11.48	3.77 ^b	9	1994	2	1995	4.00 ^e	12775 ^{bc}	511.00	54.7	-8.0	-8.0	12	-8	-8	-1	-1	R	R2	R/S	area: river irrigation, rainforest belt; too short study; PR: ★(1-15)	Quakyi et al. 2000	64950	
Cameroon	Koundou	12.12	3.90 ^a	6	1997	5	1998	3.80 ^{bc}	4636 ^g	176.10	69.5	-8.0	-8.0	6	3	05	03	08	-8	R2	R	area: degraded forest; Seas: perennial transmission, but partly the below detection limit; PR: ★(0-15)	Meunier et al. 1999; Bonnet et al. 2002	64950	
Cameroon	Mbalmayo	11.43	3.50 ^f	2	2000	6	2001	3.60 ^f	3588 ^{ghc}	129.00	-8.0	-8.0	-8.0	12	-8	-8	-1	-1	-8	-8	U	area: river presence	Antonio-Nkondjio et al. 2005	64950	
Cameroon	Mbébé	11.00	4.15 ^b	4	1989	3	1990	1.94 ^c	10330 ^g	200.00	72.0	-8.0	-8.0	12	4	02	-1	-1	R	R2	R/S	area: river breeding; reduced EIR after impregnated bed net usage	Le Goff et al. 1992	64950	
Cameroon	Mbébé	11.00	4.15 ^b	4	1989	12	1989	1.23 ^s	>5041 ^{gs}	>62.00 ^s	-8.0	-8.0	-8.0	-8	-8	-8	-8	-8	R	R2	R/S	area: river breeding	Le Goff et al. 1992	64950	
Cameroon	Mengang	12.05	3.88 ⁱ	-8	1998	-8	2000	-8.00	-8	-8.00	70.0	51.2	81.8	-8	-8	-8	-8	-8	-8	-8	R	area: degraded forest; PR: ◆(0.8-77)	Bonnet et al. 2003	64950	
Cameroon	Mutengene, Molyko, Likoko, Vasingi	9.30	4.08 ^a	06/11	1998/1999	09/02	1998/2000	6.97 ^{ef}	2310 ^{ghc}	161.00	71.4	-8.0	-8.0	-8	-8	-8	-8	-8	-8	R1	R	area: Mount Cameroon, RR _a : up to 11,000 mm; no transmission at 1200 m	Wanji et al. 2003	64910	
Cameroon	Nditam	11.26	5.36 ^b	5	1995	3	1996	9.40 ^e	876 ^g	82.34 ^c	-8.0	-8.0	-8.0	12	2	09	-1	-1	R	R2	R	area: in secondary forest/near savannah	Manga et al. 1997a	64893	
Cameroon	Ngoumé	11.40	5.48 ⁱ	5	1995	3	1996	-8.00 ^e	0 ^g	0.00	-8.0	-8.0	-8.0	0	0	-5	-5	-5	-8	-8	R	area: in ancient forest	Manga et al. 1997a	64893	
Cameroon	Nsimalen, Ekoko	12.12	3.82 ^b	4	1991	3	1992	1.16 ^e	8724 ^g	106.00	-8.0	-8.0	-8.0	11	6	15	07	17	R	R2	R/S	area: river breeding, deforested due to airport construction	Manga et al. 1995	64950	
Cameroon	Nsimalen, Nkol Mefou	11.57	3.70 ^b	4	1991	3	1992	2.35 ^e	2920 ^g	68.00	-8.0	-8.0	-8.0	8	6	13	08	15	R	R2	R/S	area: river breeding, forest	Manga et al. 1995	64950	
Cameroon	Olama	11.30	3.40 ^f	2	2000	6	2001	2.18 ^f	14773 ^{ghc}	322.00	-8.0	-8.0	-8.0	12	-8	-8	-1	-1	-8	-8	R/S	area: river presence	Antonio-Nkondjio et al. 2005	64950	
Cameroon	Sanaga river villages	11.00	4.15 ^b	4	1989	3	1990	1.86 ^e	10303 ^g	182.10	-8.0	-8.0	-8.0	12	6	03	-1	-1	R	-8	R/S	area: forested, river breeding (December-June)	Carnevale et al. 1992	64950	
Cameroon	Simbock	11.48	3.82 ^a	2	1999	4	1999	4.80 ^{ef}	-8	-8.00	-8.0	-8.0	-8.0	-8	-8	-8	-8	-8	-8	-8	R/S	area: forested	Fontenille et al. 2001	64950	
Cameroon	Simbock, block 6	11.50	3.83 ^a	10	1998	9	1999	2.71 ^f	10214 ^{bc}	276.80	-8.0	-8.0	-8.0	12	6	01	-1	-1	-8	R1	R/S	area: permanent swamp	Antonio-Nkondjio et al. 2002	64950	
Cameroon	Simbock, block 6	11.50	3.83 ^a	10	1999	9	2000	2.71 ^{fd}	13576 ^{bc}	367.90	-8.0	-8.0	-8.0	12	7	05	-1	-1	-8	R1	R/S	area: permanent swamp	Antonio-Nkondjio et al. 2002	64950	
Cameroon	Simbok	11.47	3.82 ^a	9	1994	2	1995	2.92 ^{bc}	19345 ^g	565.75	60.6	-8.0	-8.0	12	-8	-8	-1	-1	-8	R1	R/S	area: irrigated fields, rainforest; too short study; PR: ★(1-15)	Quakyi et al. 2000	64950	
Cameroon	Yaoundé, Dakar quarter	11.52	3.87 ⁱ	1	2000	12	2000	2.50 ^e	1360 ^{bc}	34.00	-8.0	-8.0	-8.0	-8	-8	-8	-8	-8	-8	-8	U	area: breeding along river	van der Kolk et al. 2003	64950	
Cameroon	Yaoundé, Dakar quarter	11.52	3.87 ⁱ	7	1999	5	2000	-8.00	-8	-8.00	34.0	25.0	40.0	-8	-8	-8	-8	-8	-8	-8	U	area: breeding along river	van der Kolk et al. 2003	64950	
Cameroon	Yaoundé, Essos	11.00	3.00 ^b	6	1989	2	1990	-8.00	-8	-8.00	37.5	14.3	50.5	-8	-8	-8	-8	-8	-8	-9	-9	U	area: near marshy shallows; PR: ★(0-15)	Manga et al. 1993b	64950
Cameroon	Yaoundé, Essos suburb	11.00	3.00 ^b	3	1989	2	1990	20.31 ^{bc}	64 ^g	13.00	-8.0	-8.0	-8.0	-8	-8	-8	-8	-8	-8	U	R2	U	area: marsh breeding; HBR value in the text is different to that given in Tab. 1	Manga et al. 1993a	64950
Cameroon	Yaoundé, Messa quarter	11.52	3.87 ⁱ	10	1990	1	1993	-8.00	-8	-8.00	37.1	-8.0	-8.0	8	-8	-8	-8	-8	-8	-8	U	-	Tchuinkam et al. 1993	64950	
Cameroon	Yaoundé, Nkol Bikok quarter	11.52	3.87 ^b	3	1989	2	1990	5.00 ^e	285 ^g	14.24	-8.0	-8.0	-8.0	1	1	05	05	05	U	-8	U	few mosquito catches	Fondjo et al. 1992	64950	
Cameroon	Yaoundé, Nkol Bisson	11.52	3.87 ⁱ	3	1989	2	1990	6.78 ^{bc}	484 ^g	32.80	-8.0	-8.0	-8.0	-8	-8	01	-8	-8	-8	-8	R/S	area: lake breeding; HBR in text differs from Tab. 1	Manga et al. 1993a	64950	

to be continued

Tab. D.3 – continued

country	place	long [°E]	lat [°N]	M1	YYY1	M2	YYY2	<i>CSPR_a</i>	<i>HBR_a</i>	<i>EIR_a</i>	<i>PR_a</i>	<i>PR_{min,a}</i>	<i>PR_{max,a}</i>	<i>Seas</i>	<i>MSeas</i>	<i>XSeas</i>	<i>SSeas</i>	<i>ESeas</i>	<i>U_b</i>	<i>U_a</i>	<i>U_p</i>	note	ref	WMO#
Cameroon	Yaoundé, Nkol Bissou	11.52	3.87 ⁱ	3	1989	3	1990	1.67 ^e	1814 ^g	30.30	-8.0	-8.0	-8.0	4	3	-8	01/06	02/08	R	-8	R/S	area: near pool; few mosquito catches	Fondjo et al. 1992	64950
Cameroon	Yaoundé, Obili district	11.52	3.87 ⁱ	10	1989	7	1990	-8.00	-8	-8.00	27.8	21.1	45.5	-8	-8	-8	-8	-8	-8	U	U	area: fish breeding ponds; <i>PR</i> : ★(0-15)	Manga et al. 1993b	64950
Cameroon	Yaoundé, Obili district	11.52	3.87 ⁱ	-9	-9	-9	-9	-9.00	-9	3.00	-9.0	-9.0	-9.0	-9	-9	-9	-9	-9	-8	U	U	-	Manga et al. 1992	64950
Congo	Linzolo	15.11	-4.41 ^b	10	1981	1	1984	2.20 ^e	11204 ^{gC}	246.10	-8.0	-8.0	-8.0	12	-8	-8	-1	-1	R	R1	R	-	Trape and Zoulani 1987	-9999
Congo	Linzolo	15.11	-4.41 ^b	11	1981	5	1985	-8.00	-8	-8.00	79.1	78.8	80.9	-8	-8	-8	-8	-8	R	R1	R	-	Trape 1987	-9999
Côte d'Ivoire	Alloukoukro	-5.08	7.80 ^b	1	1991	12	1991	3.15 ^e	8469 ^{gC}	266.50	-8.0	-8.0	-8.0	12	5	09	-1	-1	R	PU	S	-	Dossou-Yovo et al. 1995	65555
Côte d'Ivoire	Alloukoukro	-5.08	7.80 ^b	1	1992	12	1992	3.50 ^e	5612 ^{gC}	196.50	-8.0	-8.0	-8.0	12	5	09	-1	-1	R	PU	S	-	Dossou-Yovo et al. 1995	65555
Côte d'Ivoire	Bouaké, Dar-és-Salam	-5.03	7.68 ⁱ	1	1991	12	1991	0.90 ^e	4889 ^{gC}	44.00	-8.0	-8.0	-8.0	7	5	05	04	11	-8	-8	I	no transmission in August	Dossou-Yovo et al. 1998	65555
Côte d'Ivoire	Bouaké, Dar-és-Salam	-5.03	7.68 ⁱ	1	1992	12	1992	1.10 ^e	4727 ^{gC}	52.00	-8.0	-8.0	-8.0	8	4	05	04	13	-8	-8	I	no transmission in August and November	Dossou-Yovo et al. 1998	65555
Côte d'Ivoire	Bouaké, Kennedy	-5.03	7.68 ⁱ	1	1991	12	1991	2.00 ^e	6700 ^{gC}	134.00	-8.0	-8.0	-8.0	8	4	07	03	11	-8	-8	R	-	Dossou-Yovo et al. 1998	65555
Côte d'Ivoire	Bouaké, Kennedy	-5.03	7.68 ⁱ	1	1992	12	1992	1.80 ^e	5878 ^{gC}	105.80	-8.0	-8.0	-8.0	7	5	09	04	11	-8	-8	R	-	Dossou-Yovo et al. 1998	65555
Côte d'Ivoire	Bouaké, market garden districts	-5.03	7.68 ⁱ	1	1992	12	1992	2.70 ^e	4380 ^g	88.00	-8.0	-8.0	-8.0	8	-8	-8	04	11	R	-8	R	-	Dossou-Yovo et al. 1994	65555
Côte d'Ivoire	Bouaké, rice field district	-5.03	7.68 ⁱ	1	1992	12	1992	0.90 ^e	19467 ^g	126.00	-8.0	-8.0	-8.0	9	-8	-8	04	12	I	-8	I	-	Dossou-Yovo et al. 1994	65555
Côte d'Ivoire	Bouaké, Sokoura	-5.03	7.68 ⁱ	1	1991	12	1991	1.80 ^e	3739 ^{gC}	67.30	-8.0	-8.0	-8.0	8	3	05	03	10	-8	-8	R	-	Dossou-Yovo et al. 1998	65555
Côte d'Ivoire	Bouaké, Sokoura	-5.03	7.68 ⁱ	1	1992	12	1992	2.40 ^e	3708 ^{gC}	89.00	-8.0	-8.0	-8.0	8	5	09	04	11	-8	-8	R	-	Dossou-Yovo et al. 1998	65555
Côte d'Ivoire	Bouaké, Tolak-ouadiokro	-5.03	7.68 ⁱ	1	1991	12	1991	0.80 ^e	13000 ^{gC}	104.00	-8.0	-8.0	-8.0	11	5	08	03	13	-8	-8	I	no transmission in December	Dossou-Yovo et al. 1998	65555
Côte d'Ivoire	Bouaké, Tolak-ouadiokro	-5.03	7.68 ⁱ	1	1992	12	1992	0.70 ^e	22143 ^{gC}	155.00	-8.0	-8.0	-8.0	-8	8	08	02	-8	-8	-8	I	-	Dossou-Yovo et al. 1998	65555
Côte d'Ivoire	Bouaké, Zone	-5.03	7.68 ⁱ	1	1991	12	1991	1.10 ^e	9364 ^{gC}	103.00	-8.0	-8.0	-8.0	11	5	10	03	13	-8	-8	I	no transmission in December	Dossou-Yovo et al. 1998	65555
Côte d'Ivoire	Bouaké, Zone	-5.03	7.68 ⁱ	1	1992	12	1992	0.90 ^e	7000 ^{gC}	63.00	-8.0	-8.0	-8.0	8	5	08	04	11	-8	-8	I	-	Dossou-Yovo et al. 1998	65555
Côte d'Ivoire	Katiola district, 8 villages (no rice cultivation)	-999.00	-99.00	3	1997	1	1998	-8.00	-8	-8.00	87.0	83.0	90.0	8	5	05	04	11	-8	-8	R	<i>PR</i> : ★(0-9); villages are Angolokaha, Doussoulokaha, Folofonkaha, Kabolo, Ounadiékaha, Petionara, Sérigobokaha, and Timorokaha	Henry et al. 2003	65555
Côte d'Ivoire	Korhogo district, 8 villages (rice cultivation during the dry season)	-999.00	-99.00	3	1997	1	1998	-8.00	-8	-8.00	79.0	75.0	81.0	7	-8	05	06	12	-8	-8	I	<i>PR</i> : ★(0-9); villages are Gbahaouakaha, Kohotieri, Koumbolikaha, Lamékaha, Nambékaha, Nombolo, Nongotchénékaha, and Zémongokaha	Henry et al. 2003	65536

to be continued

Tab. D.3 – continued

country	place	long [°E]	lat [°N]	M1	YYY1	M2	YYY2	CSPR _a	HBR _a	EIR _a	PR _a	PR _{min,a}	PR _{max,a}	Seas	MSeas	XSeas	SSeas	ESeas	U _b	U _a	U _p	note	ref	WMO#
Côte d'Ivoire	Korhogo district, 8 villages (rice cultivation during the rainy season)	-999.00	-99.00	3	1997	1	1998	-8.00	-8	-8.00	84.0	80.0	86.0	8	-8	08	04	11	-8	-8	R	PR: *(0-9); villages are Binguebougou, Fapaha, Kombolokoura, Kaforo, Karakpo, Kassoumbarga, Katiorkpo, and Tioro	Henry et al. 2003	65536
Côte d'Ivoire	Tiémélékro	-4.17	6.50 ^f	2	2002	8	2002	3.25 ^f	7662 ^{gc}	249.00	-8.0	-8.0	-8.0	-8	-8	07	04	-8	-8	-8	R	-	Koudou et al. 2005	65562
Côte d'Ivoire	Tiémélékro	-4.17	6.50 ^f	2	2003	8	2003	7.36 ^f	6264 ^{gc}	461.00	-8.0	-8.0	-8.0	-8	-8	08	04	-8	-8	-8	R	-	Koudou et al. 2005	65562
Côte d'Ivoire	Zatta	-5.39	6.88 ^f	2	2002	8	2002	4.58 ^f	17227 ^{gc}	789.00	-8.0	-8.0	-8.0	12	-8	02	-1	-1	-8	-8	I	-	Koudou et al. 2005	65562
Côte d'Ivoire	Zatta	-5.39	6.88 ^f	2	2003	8	2003	1.39 ^f	3453 ^{gc}	48.00	-8.0	-8.0	-8.0	-8	-8	07	06	-8	-8	-8	R	interruption of rice irrigation in 2003	Koudou et al. 2005	65562
Dominican Republic	Calle Duarte, Colonia Japonesa, La Bomba	-999.00	-99.00	7	1987	10	1988	0.03	5731	1.72	-8.0	-8.0	-8.0	-8	-8	-8	-8	-8	-8	-8	-8	-	Mekuria et al. 1991	-9999
Gambia, The	5 villages around Farafenni	-16.57	13.47 ^f	4	2003	5	2003	-8.00 ^f	-8	-8.00	-8.0	19.9	-8.0	-8	-8	-8	-8	-8	-8	-8	R	950 subjects from 5-45	Nwakanma et al. 2008	61701
Gambia, The	Bakau	-16.68	13.48 ^b	6	1988	5	1989	0.98 ^f	104 ^{gbc}	1.02 ^k	2.0	-8.0	-8.0	-8	-8	-8	-8	-8	U	U	U	PR: *(0-9)	Lindsay et al. 1990	61701
Gambia, The	Barokanda	-15.32	13.65 ^b	8	1988	11	1988	2.97 ^{fc}	3701 ⁱ	110.00	-8.0	-8.0	-8.0	5 ^d	-8	09 ^d	08 ^d	12 ^d	R	R2	R	reduced EIR after impregnated bed net usage	Lindsay et al. 1993c,b	61701
Gambia, The	Biran Giddo	-999.00	-99.00	6	1986	12	1986	4.10 ^e	412 ⁱ	16.87 ^c	-8.0	-8.0	-8.0	4	2	09	08	11	-8	-8	R	-	Lindsay et al. 1989	61701
Gambia, The	Bwiam	-16.09	13.23 ^b	7	1991	1	1992	2.47 ^f	37 ^{hj}	0.92	39.5	-8.0	-8.0	-8	-8	-8	-8	-8	R	R2	R	PR: *(1-4)	Thomson et al. 1994, 1995	61701
Gambia, The	Dasilami	-15.23	13.48 ^b	8	1988	11	1988	1.29 ^{fc}	1160 ⁱ	15.00	-8.0	-8.0	-8.0	5 ^d	-8	09 ^d	08 ^d	12 ^d	R	R2	R	reduced EIR after impregnated bed net usage	Lindsay et al. 1993c,b	61701
Gambia, The	Dasilami	-14.27	13.41 ^b	7	1991	1	1992	2.23 ^f	54 ^{hj}	1.21	57.3 ^d	-8.0	-8.0	-8	-8	-8	-8	-8	R	R2	R	PR: *(1-4)	Thomson et al. 1994	61687
Gambia, The	Dongoro Ba	-15.28	13.38 ^b	8	1988	11	1988	17.86 ^{fc}	448 ⁱ	80.00	-8.0	-8.0	-8.0	5 ^d	-8	09 ^d	08 ^d	12 ^d	R	R2	R	reduced EIR after impregnated bed net usage	Lindsay et al. 1993c,b	61701
Gambia, The	4 villages west of Farafenni	-999.00	-99.00	5	2001	6	2001	-8.00	-8	-8.00	-8.0	54.3	-8.0	3	-8	-8	09	11	-8	-8	R	PR: *(0.5-15)	Dunyo et al. 2006	61701
Gambia, The	Jahally	-14.97	13.55 ^b	7	1991	1	1992	0.95 ^f	443 ^{hj}	4.17	34.2 ^d	-8.0	-8.0	-8	-8	-8	-8	-8	R	R2	R	PR: *(1-4)	Thomson et al. 1994, 1995	-9999
Gambia, The	Jalangbereh	-15.40	13.38 ^b	8	1988	11	1988	9.10 ^{fc}	769 ⁱ	70.00	-8.0	-8.0	-8.0	5 ^d	-8	09 ^d	08 ^d	12 ^d	R	R2	R	reduced EIR after impregnated bed net usage	Lindsay et al. 1993c,b	61701
Gambia, The	Jessadi	-15.30	13.63 ^b	8	1988	11	1988	2.68 ^{fc}	2380 ⁱ	64.00	-8.0	-8.0	-8.0	5	-8	09	08	12	R	R2	R	reduced EIR after impregnated bed net usage	Lindsay et al. 1993c,b	61701
Gambia, The	Katamina	-15.28	13.55 ^b	8	1988	11	1988	0.37 ^{fc}	1076 ⁱ	4.00	-8.0	-8.0	-8.0	5 ^d	-8	09 ^d	08 ^d	12 ^d	R	R2	R	reduced EIR after impregnated bed net usage	Lindsay et al. 1993c,b	61701
Gambia, The	Kerewan	-16.09	13.49 ^b	6	1992	11	1992	0.36	217 ^c	0.78	-8.0	-8.0	-8.0	-8	-8	-8	-8	-8	R	R1	R	-	Thomson et al. 1995	61701
Gambia, The	Kerewan	-16.09	13.49 ^b	7	1991	1	1992	0.23 ^f	211 ^{hj}	0.44	28.7 ^d	-8.0	-8.0	-8	-8	-8	-8	-8	R	R1	R	PR: *(1-4)	Thomson et al. 1994, 1995	61701
Gambia, The	Kulari	-14.08	13.40 ^b	7	1991	1	1992	7.65 ^f	102 ^{hj}	7.75	71.2	-8.0	-8.0	-8	-8	-8	-8	-8	R	R1	R	PR: *(1-4)	Thomson et al. 1994, 1995	61687

to be continued

Tab. D.3 – continued

country	place	long [°E]	lat [°N]	M1	YYY1	M2	YYY2	CSPR _a	HBR _a	EIR _a	PR _a	PR _{min,a}	PR _{max,a}	Seas	MSeas	XSeas	SSeas	ESeas	U _b	U _a	U _p	note	ref	WMO#
Gambia, The	Madina	-15.25	13.52 ^b	8	1988	11	1988	7.45 ^{fc}	2376 ⁱ	177.00	-8.0	-8.0	-8.0	5 ^d	-8	09 ^d	08 ^d	12 ^d	R	R2	R	reduced <i>EIR</i> after impregnated bed net usage	Lindsay et al. 1993c,b	61701
Gambia, The	Male Kunda	-15.30	13.55 ^b	8	1988	11	1988	2.60 ^{fc}	2692 ⁱ	70.00	-8.0	-8.0	-8.0	5 ^d	-8	09 ^d	08 ^d	12 ^d	R	R2	R	reduced <i>EIR</i> after impregnated bed net usage	Lindsay et al. 1993c,b	61701
Gambia, The	Niawodurulung	-15.22	13.46 ^b	8	1988	11	1988	0.00 ^{fc}	1481 ⁱ	0.00	-8.0	-8.0	-8.0	5 ^d	-8	09 ^d	08 ^d	12 ^d	R	R2	R	reduced <i>EIR</i> after impregnated bed net usage	Lindsay et al. 1993c,b	61701
Gambia, The	Nyrimba Koyo Ya	-999.00	-99.00	6	1986	12	1986	1.61 ^e	155 ⁱ	2.49 ^c	-8.0	-8.0	-8.0	4	2	09 ^d	08	11	-8	-8	R	untreated bed net usage	Lindsay et al. 1989	-9999
Gambia, The	Pakali Ba	-15.25	13.50 ^b	8	1988	11	1988	3.04 ^{fc}	3253 ⁱ	99.00	-8.0	-8.0	-8.0	5 ^d	-8	09 ^d	08 ^d	12 ^d	R	R2	R	reduced <i>EIR</i> after impregnated bed net usage	Lindsay et al. 1993c,b	61701
Gambia, The	Salikene	-15.97	13.48 ^b	7	1991	1	1992	0.55 ^f	360 ^{hj}	1.94	28.7	-8.0	-8.0	-8	-8	-8	-8	-8	R	R2	R	<i>PR</i> : *(1-4)	Thomson et al. 1994, 1995	61701
Gambia, The	Sare Alpha	-13.98	13.37 ^b	6	1992	11	1992	4.25 ^f	-8 ^{hj}	-8.00	-8.0	-8.0	-8.0	-8	-8	-8	-8	-8	R	R1	R	-	Thomson et al. 1995	61687
Gambia, The	Sare Alpha	-13.98	13.37 ^b	7	1991	1	1992	6.07 ^f	187 ^{hj}	11.15	71.2 ^d	-8.0	-8.0	-8	-8	-8	-8	-8	R	R1	R	<i>PR</i> : *(1-4)	Thomson et al. 1994, 1995	61687
Gambia, The	Saruja	-14.90	13.55 ^b	6	1992	11	1992	0.73 ^f	38 ^{hjc}	2.79	-8.0	-8.0	-8.0	-8	-8	-8	-8	-8	I	R2	R	-	Thomson et al. 1995	-9999
Gambia, The	Saruja	-14.90	13.55 ^b	7	1991	1	1992	2.17 ^f	231 ^{hj}	5.00	34.2	-8.0	-8.0	-8	-8	-8	-8	-8	I	R2	R	<i>PR</i> : *(1-4)	Thomson et al. 1994, 1995	-9999
Gambia, The	Sibanor	-16.20	13.21 ^b	7	1991	1	1992	2.88 ^f	113 ^{hj}	3.24	39.5 ^d	-8.0	-8.0	-8	-8	-8	-8	-8	R	R2	R	<i>PR</i> : *(1-4)	Thomson et al. 1994, 1995	61701
Gambia, The	Sitahuma	-15.40	13.43 ^b	8	1988	11	1988	2.23 ^{fc}	3366 ⁱ	75.00	-8.0	-8.0	-8.0	5 ^d	-8	09 ^d	08 ^d	12 ^d	R	R2	R	reduced <i>EIR</i> after impregnated bed net usage	Lindsay et al. 1993c,b	61701
Gambia, The	Sutukoba	-14.02	13.50 ^b	7	1991	1	1992	2.94 ^f	34 ^{hj}	0.99	57.3	-8.0	-8.0	-8	-8	-8	-8	-8	R	R2	R	<i>PR</i> : *(1-4)	Thomson et al. 1994, 1995	61687
Gambia, The	Tally Ya	-15.72	13.58 ⁱ	6	1986	12	1986	2.31 ^e	682 ⁱ	15.75 ^c	-8.0	-8.0	-8.0	5	3	09 ^d	07	11	-8	-8	R	untreated bed net usage	Lindsay et al. 1989	-9999
Gambia, The	Turan	-15.72	13.58 ⁱ	6	1986	12	1986	2.70 ^e	890 ⁱ	24.04 ^c	-8.0	-8.0	-8.0	5	3	09	07	11	-8	-8	R	-	Lindsay et al. 1989	61701
Gambia, The	Wellingara Ba	-15.26	13.41 ^b	8	1988	11	1988	2.19 ^{fc}	1553 ⁱ	34.00	-8.0	-8.0	-8.0	5 ^d	-8	09 ^d	08 ^d	12 ^d	R	R2	R	reduced <i>EIR</i> after impregnated bed net usage	Lindsay et al. 1993c,b	61701
Ghana	Kassena Nankana district	-1.44	10.76 ^f	5	2001	11	2001	-8.00	-8	-8.00	59.2 ^c	43.6	76.4	-8	-8	-8	-8	-8	-8	R2	I	<i>PR</i> : *(0.5-15)	Koram et al. 2003	65518
Ghana	Kassena Nankana district (irrigated)	-1.44	10.76 ^f	6	2001	5	2002	4.70 ^f	13404 ^{gc}	630.00	-8.0	-8.0	-8.0	8	3	09	06	13	-8	R2	I	-	Appawu et al. 2004	65518
Ghana	Kassena Nankana district (lowland)	-1.44	10.76 ^f	6	2001	5	2002	19.00 ^f	1895 ^{gc}	360.00	-8.0	-8.0	-8.0	5	2	09	07	11	-8	R2	R	-	Appawu et al. 2004	65518
Ghana	Kassena Nankana district (morbidity study)	-1.44	10.76 ^f	10	1990	9	1991	-8.00	-8	-8.00	74.2	53.3	84.5	-8	-8	-8	-8	-8	-8	R2	I	<i>PR</i> : *(0 to 7)	Binka et al. 1994	65518

to be continued

Tab. D.3 – continued

country	place	long [°E]	lat [°N]	M1	YYY1	M2	YYY2	CSPR _a	HBR _a	EIR _a	PR _a	PR _{min,a}	PR _{max,a}	Seas	MSeas	XSeas	SSeas	ESeas	U _b	U _a	U _p	note	ref	WMO#
Ghana	Kassena Nankana district (mortality study)	-1.44	10.76 ^f	10	1990	9	1991	-8.00	-8	-8.00	87.1	76.5	94.2	-8	-8	-8	-8	-8	-8	R2	I	PR: ★(0 to 7)	Binka et al. 1994	65518
Ghana	Kassena Nankana district (rocky highland)	-1.44	10.76 ^f	6	2001	5	2002	10.60 ^f	2151 ^{gc}	228.00	-8.0	-8.0	-8.0	4	3	08	07	10	-8	R2	R	-	Appawu et al. 2004	65518
Kenya	Mumias	0.18	34.49 ^b	5	1995	3	1996	6.79 ^f	700 ^g	47.50	52.3	43.8	60.4	11	7	-8	-8	-8	R	PU	R	PR: ★	Shililu et al. 1998	-9999
Liberia	Yekepa	-8.53	7.58 ^a	11	-8	11	-8	-8.00	-8	-8.00	-8.0	-8.0	13.0	-8	-8	-8	-8	-8	-8	R2	R	PR: ★(2-9)	Björkman et al. 1985	61849
Liberia	Yekepa, close (<3 km)	-8.55	7.56 ^a	11	-8	11	-8	-8.00	-8	-8.00	-8.0	-8.0	22.0	-8	-8	-8	-8	-8	-8	R2	R	PR: ★(2-9); vector control & drug usage	Björkman et al. 1985	61849
Liberia	Yekepa, middle (5-15 km)	-8.63	7.58 ^a	11	-8	11	-8	-8.00	-8	-8.00	-8.0	-8.0	68.0	-8	-8	-8	-8	-8	-8	R2	R	PR: ★(2-9); vector control & sporadic treatment	Björkman et al. 1985	61849
Liberia	Yekepa, far (>15 km)	-8.54	7.58 ⁱ	11	-8	11	-8	-8.00	-8	-8.00	-8.0	-8.0	92.0	-8	-8	-8	-8	-8	-8	R2	R	PR: ★(2-9); vector control & drug usage	Björkman et al. 1985	61849
Mali	Bamako, Sotuba suburb	-7.93	12.65 ^a	6	1998	12	1998	-8.00 ^f	-8 ^g	3.49	-8.0	-8.0	-8.0	7	3	10	06	12	-8	R2	R	-	Sagara et al. 2002	61291
Mali	Dokobougou	-6.13	14.17 ⁱ	8	1995	3	1998	0.59 ^f	-8 ^{gh}	-8.00	48.0	18.0	77.0	-8	-8	-8	-8	-8	-8	-8	R	PR: ★(1-4), partially graphically derived	Dolo et al. 2004; Sissoko et al. 2004	61265
Mali	Kalanampala	-6.87	14.15 ^m	8	1995	3	1998	1.49 ^f	-8 ^{gh}	-8.00	46.0	32.0	57.0	-8	-8	-8	-8	-8	-8	-8	R	PR: ★(1-4), partially graphically derived	Dolo et al. 2004; Sissoko et al. 2004	61265
Mali	Niessoumana	-5.97	14.31 ^m	8	1995	3	1998	0.28 ^f	-8 ^{gh}	-8.00	51.1	24.0	78.0	-8	-8	-8	-8	-8	-8	-8	I	PR: ★(1-4), partially graphically derived	Dolo et al. 2004; Sissoko et al. 2004	61265
Mali	Ténégué	-5.95	14.33 ^m	8	1995	3	1998	0.15 ^f	-8 ^{gh}	-8.00	32.7	18.0	49.0	-8	-8	-8	-8	-8	-8	-8	I	PR: ★(1-4), partially graphically derived	Dolo et al. 2004; Sissoko et al. 2004	61265
Mali	Tissana	-5.92	14.35 ^m	8	1995	3	1998	0.29 ^f	-8 ^{gh}	-8.00	36.7	12.0	52.0	-8	-8	-8	-8	-8	-8	-8	I	PR: ★(1-4), partially graphically derived	Dolo et al. 2004; Sissoko et al. 2004	61265
Mali	Toumakoro	-6.18	14.07 ⁱ	8	1995	3	1998	0.69 ^f	-8 ^{gh}	-8.00	52.3	31.0	71.0	-8	-8	-8	-8	-8	-8	-8	R	PR: ★(1-4), partially graphically derived	Dolo et al. 2004; Sissoko et al. 2004	61265
Nigeria	Garki district, 16 villages	-999.00	-99.00	2	1971	5	1972	-8.00	-8	-8.00	49.0	59.0	42.0	-8	-8	-8	-8	-8	-8	-8	R	graphically derived; ♦	Molineaux et al. 1980	-9999
Nigeria	Lagos, Lemu suburb	3.37	6.47 ^a	1	2000	12	2000	2.54 ^f	1891 ^{ghc}	48.00	-8.0	-8.0	-8.0	12	-8	-8	-1	-1	-8	U	U	<i>Anopheles melas</i> and <i>Anopheles moucheti</i> maintain transmission in dry season	Awolola et al. 2002	65344
Sao and Tomé and Príncipe	Príncipe	7.42	1.53 ^f	5	1999	8	1999	-8.00	-8	-8.00	19.8	-8.0	-8.0	-8	-8	-8	-8	-8	-8	-8	R	PR: ♦	Hagmann et al. 2003	61934
Senegal	Aéré Lao	-14.30	16.40 ^b	5	1982	8	1983	0.24 ^e	1600 ^g	6.40	-8.0	12.0 ^d	17.0 ^d	4	2	11	09	12	R	R2	R	PR: unknown age classes; presence of Senegal river	Vercruysse 1985b	61612
Senegal	Affiniam	-16.37	12.65 ⁱ	1	1985	11	1985	0.03 ^e	66667 ^{gc}	20.00	-8.0	-8.0	-8.0	5	3	09	07	11	R	R2	I	-	Faye et al. 1994	61695
Senegal	Affiniam	-16.37	12.65 ⁱ	1	1986	11	1986	0.30 ^e	13000 ^{gc}	39.00	-8.0	-8.0	-8.0	4	3	09	08 ^d	11 ^d	R	R2	I	-	Faye et al. 1994	61695
Senegal	Barkedji	-14.88	15.28 ^f	6	1994	12	1994	2.19 ^f	5870 ^{ghc}	128.55	-8.0	-8.0	-8.0	4	2	10	09	12	R	R2	R	clay hollows → high HBR _a & EIR _a	Le Masson et al. 1997	61627
Senegal	Barkedji	-14.88	15.28 ^f	7	1995	3	1996	1.52 ^f	6684 ^{ghc}	101.60	-8.0	-8.0	-8.0	6	2	09	08	14	R	R2	R	clay hollows → high HBR _a & EIR _a	Le Masson et al. 1997	61627
Senegal	Boké Diallobé	-14.00	16.10 ^b	5	1982	8	1983	1.20 ^e	200 ^g	0.80	-8.0	12.0	17.0	3	2	09	09	11	R	R2	R	PR: unknown age classes	Vercruysse 1985b	61612
Senegal	Boundoun	-16.47	16.38 ^m	7	1994	11	1994	-8.00	-8	-8.00	0.0	0.0	0.0	0	0	-5	-5	-5	-8	-8	I	PR: ★(0-9)	Faye et al. 1995d	61489
Senegal	Dakar, district Centre	-17.44	14.70 ^a	3	1996	2	1997	0.00 ^e	110 ^h	0.00	1.4	0.4	1.9	0	0	-5	-5	-5	-8	U	U	PR: ★(0-14) ♦	Diallo et al. 2000	61641

to be continued

Tab. D.3 – continued

country	place	long [°E]	lat [°N]	M1	YYY1	M2	YYY2	CSPR _a	HBR _a	EIR _a	PR _a	PR _{min,a}	PR _{max,a}	Seas	MSeas	XSeas	SSeas	ESeas	U _b	U _a	U _p	note	ref	WMO#
Senegal	Dakar, Grande Niaye Mrash	-17.42	14.75 ^f	5	1987	9	1988	0.55 ^e	22 ^{ghc}	0.12	3.7	3.4	4.0	-8	-8	-8	-8	-8	-8	U	U	PR: ♦	Trape et al. 1992	61641
Senegal	Dakar, Grande Niaye Mrash	-17.42	14.75 ^f	6	1987	6	1988	-8.00	-8	-8.00	5.6	3.6	7.5	-8	-8	-8	-8	-8	-8	U	U	PR: *	Trape et al. 1993	61641
Senegal	Diagobél	-16.33	12.70 ⁱ	1	1985	11	1985	0.00 ^e	-8 ^g	0.00	-8.0	-8.0	-8.0	0	0	-5	-5	-5	R	R2	I	-	Faye et al. 1994	61695
Senegal	Diagobél	-16.33	12.70 ⁱ	1	1986	11	1986	0.30 ^e	41000 ^{gc}	123.00	-8.0	-8.0	-8.0	4	3	09 ^d	08 ^d	11 ^d	R	R2	I	-	Faye et al. 1994	61695
Senegal	Diakhanor	-16.77	13.98 ⁱ	6	1995	12	1997	-8.00	-8	-8.00	8.5 ^d	1.9 ^d	15.3 ^d	2	-8	09	08	09	-8	-8	R	PR: unknown age classes	Diop et al. 2002	61679
Senegal	Diakhanor	-16.77	13.98 ⁱ	6	1996	11	1996	-8.00	-8	-8.00	6.5	0.0	14.4	-8	-8	-8	-8	-8	-8	-8	R	PR: *(0-9)	Diop et al. 2006	61679
Senegal	Diamballo	-16.95	15.02 ⁱ	-8	1967	-8	1968	-8.00	-8	-8.00	-8.0	32.0 ^d	50.0 ^d	8 ^d	-8	-8	07 ^d	16 ^d	R	-8	R	-	Faye et al. 1995c	61641
Senegal	Dielmo	-16.42	13.72 ^b	1	1990	12	1990	-8.00	-8	-8.00	85.0	-8.0	-8.0	-8	-8	-8	-8	-8	R	R2	S	PR: *(2-9)	Rogier and Trape 1995	61679
Senegal	Dielmo	-16.42	13.72 ^b	4	1990	3	1991	1.24 ^f	9533 ^{gc}	118.00	-8.0	-8.0	-8.0	12	5	07	-1	-1	R	R2	S	-	Konaté et al. 1994	61679
Senegal	Dielmo	-16.42	13.72 ^b	4	1991	3	1992	1.59 ^f	18462 ^{gc}	294.00	-8.0	-8.0	-8.0	12	5	07	-1	-1	R	R2	S	-	Konaté et al. 1994	61679
Senegal	Dielmo	-16.42	13.72 ^b	4	1992	3	1993	2.77 ^f	8581 ^{ghc}	237.80	-8.0	-8.0	-8.0	12	6	07	-1	-1	R	R2	S	-	Fontenille et al. 1997b	61679
Senegal	Dielmo	-16.42	13.72 ^b	4	1993	3	1994	0.91 ^f	9795 ^{ghc}	88.70	-8.0	-8.0	-8.0	11	4	10	-1	-1	R	R2	S	-	Fontenille et al. 1997b	61679
Senegal	Dielmo	-16.42	13.72 ^b	4	1994	3	1995	0.87 ^f	17322 ^{ghc}	150.10	-8.0	-8.0	-8.0	10	4	14	06	-8	R	R2	S	-	Fontenille et al. 1997b	61679
Senegal	Dielmo	-16.42	13.72 ^b	6	1990	5	1991	1.04 ^e	12500 ^{gc}	130.00	89.3	-8.0	-8.0	12	4	07	-1	-1	R	R2	S	PR: *(0-14)	Trape et al. 1994	61679
Senegal	Dielmo	-16.42	13.72 ^b	6	1991	5	1992	1.57 ^e	22299 ^{gc}	350.10	-8.0	-8.0	-8.0	12	6	09	-1	-1	R	R2	S	-	Trape et al. 1994	61679
Senegal	Diohine	-16.52	14.50 ^b	1	1995	12	1995	1.95 ^f	680 ^{gh}	13.26 ^c	56.7 ^d	41.0 ^d	82.0 ^d	5	-8	09	07	11	R	R1	R	PR: *(0-9)	Robert et al. 1998	61666
Senegal	Diomandou Dieri	-14.65	16.52 ^f	6	1990	11	1991	0.00 ^e	3139 ^g	0.00	-8.0	-8.0	-8.0	0	0	-5	-5	-5	-8	-8	I	-	Faye et al. 1993	61612
Senegal	Diomandou Toulde Galle	-14.71	16.56 ^m	6	1990	11	1991	0.00 ^e	438 ^g	0.00	-8.0	-8.0	-8.0	0	0	-5	-5	-5	-8	-8	R	-	Faye et al. 1993	61612
Senegal	Diomandou Walo	-14.62	16.56 ^m	6	1990	11	1991	0.05 ^e	7483 ^g	1.00	-8.0	-8.0	-8.0	1	1	08	08	08	-8	-8	I	-	Faye et al. 1993	61612
Senegal	Djifère	-16.77	13.93 ⁱ	6	1995	12	1997	2.08 ^f	789 ^{ghc}	16.40	8.5	1.9	15.3	5	-8	11	11	15	-8	-8	S	PR: unknown age classes	Diop et al. 2002	61679
Senegal	Djifère	-16.77	13.93 ⁱ	6	1996	11	1996	-8.00	-8	-8.00	4.9	0.0	14.4	-8	-8	-8	-8	-8	-8	-8	S	PR: *(0-9)	Diop et al. 2006	61679
Senegal	Djilor	-16.33	14.07 ⁱ	6	1995	12	1997	0.39 ^f	2615 ^{ghc}	10.20	12.9	1.1	31.4	6	-8	07	07	12	-8	-8	R	PR: unknown age classes	Diop et al. 2002	61679
Senegal	Kassack-Nord	-16.03	16.40 ^b	9	1992	11	1994	0.00 ^f	-8 ^g	0.00	0.2	0.0	0.4	0	0	-5	-5	-5	R	R2	I	PR: *(0-9)	Faye et al. 1995d	61489
Senegal	Kotiokh	-16.58	14.48 ^b	1	1995	12	1995	1.75 ^f	1558 ^{gh}	26.50	56.7	41.0	82.0	8	-8	09	06	13	R	R1	R	PR: *(0-9); near permanent breeding	Robert et al. 1998	61666
Senegal	Maka-Diama	-16.40	16.20 ^b	9	1992	11	1994	0.00 ^f	-8 ^g	0.00	0.5	0.0	1.0	0	0	-5	-5	-5	R	R2	S	PR: *(0-9)	Faye et al. 1995d	61600
Senegal	Ndiop	-16.42	13.75 ^b	1	1993	12	1993	4.47 ^f	1411 ^{gc}	63.00	-8.0	-8.0	-8.0	4	2	09	07	10	R	R2	R	-	Fontenille et al. 1997a	61679
Senegal	Ndiop	-16.42	13.75 ^b	1	1993	12	1993	-8.00	-8	-8.00	18.0	-8.0	-8.0	-8	-8	-8	-8	-8	R	R2	R	PR: *(2-9)	Rogier and Trape 1995	61679
Senegal	Ndiop	-16.42	13.75 ^b	1	1994	12	1994	3.61 ^f	471 ^{gc}	17.00	-8.0	-8.0	-8.0	3	2	09	08	10	R	R2	R	-	Fontenille et al. 1997a	61679
Senegal	Ndiop	-16.42	13.75 ^b	1	1995	12	1995	4.05 ^f	914 ^{gc}	37.00	-8.0	-8.0	-8.0	3	2	09	08	10	R	R2	R	-	Fontenille et al. 1997a	61679
Senegal	Ndiop	-16.42	13.75 ^b	1	1996	12	1996	4.71 ^f	149 ^{gc}	7.00	-8.0	-8.0	-8.0	1	1	09	09	09	R	R2	R	-	Fontenille et al. 1997a	61679
Senegal	Ngadiaga	-16.95	15.02 ^m	3	1991	11	1991	-8.00	-8	-8.00	6.2	2.0	10.6	-8	-8	-8	-8	-8	R	-8	R	PR: *(0-10)	Faye et al. 1995c	61641
Senegal	Ngadiaga	-16.95	15.02 ^m	8	1993	8	1993	-8.00	-8	-8.00	-8.0	0.0	-8.0	-8	-8	-8	-8	-8	R	-8	R	PR: *(0-10)	Faye et al. 1995c	61641
Senegal	Ngayokhème	-16.43	14.53 ^b	1	1995	12	1995	1.80 ^f	512 ^{gh}	8.96 ^c	56.7 ^d	41.0 ^d	82.0 ^d	5	-8	09	07	11	R	R1	R	PR: *(0-9)	Robert et al. 1998	61666
Senegal	Niakhar	-16.40	14.47 ^f	2	1995	11	1995	-8.00	-8	-8.00	57.0 ^d	41.0 ^d	83.0 ^d	-8	-8	-8	-8	-8	-8	-8	R	PR: *(0-9)	Ndiaye et al. 2001	61666
Senegal	Ousseuk	-16.18	12.84 ^m	1	1985	11	1985	0.36 ^e	3611 ^{gc}	13.00	-8.0	-8.0	-8.0	4	3	09 ^d	07 ^d	10 ^d	-8	R2	I	-	Faye et al. 1994	61695
Senegal	Ousseuk	-16.18	12.84 ^m	1	1986	11	1986	0.46 ^e	3487 ^{gc}	16.00	-8.0	-8.0	-8.0	3	2	09 ^d	08 ^d	10 ^d	-8	R2	I	-	Faye et al. 1994	61695
Senegal	Pikine	-17.40	14.75 ^b	11	1979	1	1981	-8.00	-8	-8.00	8.8 ^d	2.2 ^d	13.5 ^d	-8	-8	-8	-8	-8	U	-8	U	-	Vercruysse et al. 1983	61641
Senegal	Pikine	-17.40	14.75 ^b	12	1979	12	1980	0.55 ^{de}	9145 ^{ghc}	50.30 ^{sk}	-8.0	-8.0	-8.0	12	4	10	-1	-1	U	-8	U	-	Vercruysse et al. 1983	61641
Senegal	Pikine	-17.40	14.75 ^b	12	1979	12	1980	0.55 ^e	7818 ^{gc}	43.00	8.8	2.2	13.5	-9	4	-9	-9	-9	U	-8	U	-	Vercruysse and Jancloes 1981	61641
Senegal	Simal	-16.65	14.15 ⁱ	6	1995	12	1997	2.20 ^f	596 ^{ghc}	13.10	12.9 ^d	1.1 ^d	31.4 ^d	7 ^d	-8	10	06 ^d	12 ^d	-8	-8	R	PR: unknown age classes	Diop et al. 2002	61679
Senegal	Takème	-16.20	12.82 ⁱ	1	1985	11	1985	0.36 ^e	3056 ^{gc}	11.00	-8.0	-8.0	-8.0	4	3	09	07	10	-8	R2	I	-	Faye et al. 1994	61695
Senegal	Takème	-16.20	12.82 ⁱ	1	1986	11	1986	0.46 ^e	4783 ^{gc}	22.00	-8.0	-8.0	-8.0	3	2	09	08	10	-8	R2	I	-	Faye et al. 1994	61695
Senegal	Tendimane	-16.30	12.77 ⁱ	1	1985	11	1985	0.00 ^e	-8 ^g	0.00	-8.0	-8.0	-8.0	0	0	-5	-5	-5	R	R2	I	-	Faye et al. 1994	61695
Senegal	Tendimane	-16.30	12.77 ⁱ	1	1986	11	1986	0.30 ^e	11667 ^{gc}	35.00	-8.0	-8.0	-8.0	4	3	09	08	11	R	R2	I	-	Faye et al. 1994	61695

to be continued

Tab. D.3 – continued

country	place	long [°E]	lat [°N]	M1	YYY1	M2	YYY2	<i>CSPR_a</i>	<i>HBR_a</i>	<i>EIR_a</i>	<i>PR_a</i>	<i>PR_{min,a}</i>	<i>PR_{max,a}</i>	<i>Seas</i>	<i>MSeas</i>	<i>XSeas</i>	<i>SSeas</i>	<i>ESeas</i>	<i>U_b</i>	<i>U_a</i>	<i>U_p</i>	note	ref	WMO#
Senegal	Thiaye	-16.96	14.99 ^m	1	1992	12	1992	0.00 ^f	4540 ^{gh}	0.00	-8.0	3.2	-8.0	0	0	10	-5	-5	R	-8	R	<i>PR</i> : *(0-10); wet depressions → high <i>HBR_a</i>	Faye et al. 1995c	61641
Senegal	Thiaye	-16.96	14.99 ^m	3	1991	12	1991	0.48 ^f	2290 ^{gh}	11.00	-8.0	2.9	5.7	2	2	-5	09	10	R	-8	R	<i>PR</i> : *(0-10); wet depressions → high <i>HBR_a</i>	Faye et al. 1995c	61641
Senegal	Thiaye	-16.96	14.99 ^m	8	1993	8	1993	-8.00	-8	-8.00	-8.0	0.0	-8.0	-8	-8	-8	-8	-8	R	-8	R	<i>PR</i> : *(0-10)	Faye et al. 1995c	61641
Senegal	Thiaye	-17.07	14.92 ^f	9	1992	10	1993	0.00 ^f	1241 ^{gh}	0.00	-8.0	-8.0	-8.0	0	0	-5	-5	-5	-8	-8	R	<i>PR</i> : *(0-10); wet depressions → high <i>HBR_a</i>	Faye et al. 1995c,b	61641
Senegal	Thies	-16.93	14.80 ⁱ	-8	-8	-8	-8	-8.00	-8	-8.00	17.5	-8.0	-8.0	-8	-8	-8	-8	-8	-8	-8	R	<i>PR</i> : *(0-14)	Boudin et al. 2005	61641
Senegal	Wassdou	-13.33	13.35 ^f	9	1992	11	1993	2.75 ^f	7884 ^{gh}	220.00	-8.0	-8.0	-8.0	7	3	09	07	13	-8	-8	R	-	Faye et al. 1995b,a	61687
Sierra Leone	8 villages near Bo	-999.00	-99.00	3	1990	12	1990	-8.00	-8	-8.00	61.0	-8.0	-8.0	-8	-8	-8	-8	-8	-8	-8	R	<i>PR</i> : *(0-7); data exits for single villages	Barnish et al. 1993	-9999
Sierra Leone	Mendewa	-11.48	8.16 ^b	1	1990	4	1991	9.60 ^f	228 ^{bc}	21.90	-8.0	-8.0	-8.0	11 ^d	4 ^d	06 ^d	01 ^d	11 ^d	R	R2	R	-	Bockarie et al. 1994	-9999
Sierra Leone	Nengbema	-11.68	8.13 ^b	1	1990	4	1991	5.25 ^f	410 ^{bc}	21.54	-8.0	-8.0	-8.0	11	4	06	01	11	R	R2	R	-	Bockarie et al. 1994	-9999
Sierra Leone	Njala-Komboya	-11.54	8.20 ^b	1	1990	4	1991	7.63 ^f	349 ^{bc}	26.64	-8.0	-8.0	-8.0	11 ^d	4 ^d	06 ^d	01 ^d	11 ^d	R	R2	R	-	Bockarie et al. 1994	-9999
Sierra Leone	Nyandeyama	-11.66	8.12 ^b	1	1990	4	1991	8.11 ^f	450 ^{bc}	36.50	-8.0	-8.0	-8.0	11 ^d	4 ^d	06 ^d	01 ^d	11 ^d	R	R2	R	-	Bockarie et al. 1994	-9999
Sudan	Asar	13.75	35.25 ^a	10	1998	8	1999	-8.00	-8	-8.00	26.5	1.8	53.2	-8	-8	-8	-8	-8	-8	R2	R	-	Abdel-Wahab et al. 2002	-9999
Uganda	Kampala Mulago III parish	32.58	0.32 ⁱ	11	2004	4	2005	-8.00	-8	-8.00	19.0	-8.0	-8.0	-8	-8	-8	-8	-8	-8	-8	U	<i>PR</i> : *(1-10)	Davis et al. 2006	63608

D.8 Parasitological data assigned to synoptic stations

Tab. D.4: Parasitological data since 1979 assigned to synoptic stations. Columns: WMO#: WMO station number; num: number of included study sites; YYYYs: concerned years. Various meanings of other column titles are the same as that of Tab. D.3. Leading 'l' and 'u' characters indicate the lower and upper range of observed values, respectively. Numbers in brackets represent the number of available observations. For further information see Tab. D.2.

country	place	WMO#	long [°E]	lat [°N]	z	Up	num	YYYYs	<i>l</i> PR _a	<i>u</i> PR _a	<i>l</i> PR _{min,a}	<i>u</i> PR _{min,a}	<i>l</i> PR _{max,a}	<i>u</i> PR _{max,a}
Mali	Mopti Barbe	61265	4°06'W	14°31'N	272	R	3	1995-1998	46.0(3)	52.3	18.0(3)	32.0	57.0(3)	77.0
Mali	Mopti Barbe	61265	4°06'W	14°31'N	272	I	3	1995-1998	32.7(3)	51.1	12.0(3)	24.0	49.0(3)	78.0
Senegal	Rosso	61489	15°49'W	16°30'N	6	I	2	1992-1994	0.0(2)	0.2	0.0(2)	0.0	0.0(2)	0.4
Senegal	Saint Louis	61600	16°27'W	16°03'N	4	S	1	1992-1994	0.5(1)	0.5	0.0(1)	0.0	1.0(1)	1.0
Senegal	Podor	61612	14°58'W	16°39'N	7	R	1	1982-1983	-8.0(-8)	-8.0	12.0(1)	12.0	17.0(1)	17.0
Senegal	Dakar Yoff	61641	17°30'W	14°44'N	24	U	3	1979-1981 1987-1988 1996-1997	1.4(4)	8.8	0.4(4)	3.6	1.9(4)	13.5
Senegal	Dakar Yoff	61641	17°30'W	14°44'N	24	R	1	1991-1993	6.2(2)	17.5	0.0(5)	3.2	5.7(2)	10.6
Senegal	Diourbel	61666	16°14'W	14°39'N	9	R	4	1995	56.7(1)	56.7	41.0(1)	41.0	82.0(1)	82.0
Senegal	Kaolack	61679	16°04'W	14°08'N	7	R	3	1993 1995-1997	6.5(4)	18.0	0.0(3)	1.9	14.4(3)	31.4
Senegal	Kaolack	61679	16°04'W	14°08'N	7	S	2	1990-1991 1995-1997	4.9(4)	89.3	0.0 [‡] (2)	1.9 [‡]	14.4 [‡] (2)	15.3 [‡]
Senegal	Tambacounda	61687	13°41'W	13°46'N	50	R	5	1991-1992	57.3(2)	71.2	-8.0(-8)	-8.0	-8.0(-8)	-8.0
Gambia, The	Banjul Yundum Intl	61701	16°48'W	13°21'N	33	U	1	1988-1989	2.0(1)	2.0	-8.0(-8)	-8.0	-8.0(-8)	-8.0
Gambia, The	Banjul Yundum Intl	61701	16°48'W	13°21'N	33	R	7	1991-1992 2001 2003	28.7(2)	39.5	19.9(2)	54.3	-8.0(-8)	-8.0
Liberia	N [‡] Zerekore Konia	61849	8°50'W	7°44'N	470	R	4	-8	-8.0(-8)	-8.0	-8.0(-8)	-8.0	13.0(4)	92.0
Cameroon	Douala	64910	9°44'E	4°00'N	9	R	1	1998-1999	71.4(1)	71.4	-8.0(-8)	-8.0	-8.0(-8)	-8.0
Cameroon	Yaounde	64950	11°31'E	3°50'N	760	R/S	17	1989-1990 1994-1995 1997-2000	50.0(6)	72.0	49.3 [‡] (2)	51.2 [‡]	50.7 [‡] (2)	81.8 [‡]
Cameroon	Yaounde	64950	11°31'E	3°50'N	760	U	4	1989-1993 1999-2000	27.8(4)	37.5	14.3(3)	25.0	40.0(3)	50.5
Burkina Faso	Dori	65501	0°02'W	14°02'N	277	R	6	1985-1986	26.6(3)	50.7	15.0(3)	37.7	45.5(3)	71.5
Burkina Faso	Ouagadougou	65503	1°31'W	12°21'N	306	R	5	1984 1994-1995 2002-2003	70.0(2)	73.4	56.0(2)	63.5	57.6(6)	94.9
Burkina Faso	Ouagadougou	65503	1°31'W	12°21'N	306	U	6	1984	-8.0(-8)	-8.0	-8.0(-8)	-8.0	2.9(6)	31.5
Burkina Faso	Bobo-Dioulasso	65510	4°19'W	11°10'N	460	R	6	1983-1987	29.1(10)	77.5	14.3(7)	53.3	47.6(7)	82.5
Burkina Faso	Bobo-Dioulasso	65510	4°19'W	11°10'N	460	I	2	1983-1986	33.7(5)	59.9	9.1(6)	40.5	35.7(5)	69.2
Burkina Faso	Bobo-Dioulasso	65510	4°19'W	11°10'N	460	U	4	1985 1991-1993	6.8(2)	10.9	4.6(2)	5.4	10.3(2)	13.9
Burkina Faso	Po	65518	1°09'W	11°09'N	322	I	1	1991 2001	59.2(3)	87.1	43.6(3)	76.5	76.4(3)	94.2
Côte d'Ivoire	Korhogo	65536	5°37'W	9°25'N	381	R	1	1997-1998	84.0(1)	84.0	80.0(2)	80.0	86.0(1)	86.0
Côte d'Ivoire	Korhogo	65536	5°37'W	9°25'N	381	I	1	1997-1998	79.0(1)	79.0	75.0(1)	75.0	81.0(1)	81.0
Côte d'Ivoire	Bouaké	65555	5°04'W	7°44'N	376	R	1	1997-1998	87.0(1)	87.0	83.0(1)	83.0	90.0(1)	90.0

D.9 Entomological data assigned to synoptic stations

Tab. D.5: Entomological data since 1979 assigned to synoptic stations. Columns: WMO#: WMO station number; num: number of included study sites; YYYYs: years that are concerned. Various meanings of other column titles are the same as that of Tab.D.3. Leading 'l' and 'u' characters indicate the lower and upper range of the observed values, respectively. Numbers in brackets represent the number of available observations. Note that with regard to the start and end of the malaria season a transmission break of one month is allowed; values greater than 12 stand for months in the following year (e.g., 13: January); -5: no malaria transmission, -1: year around malaria transmission. For further information see Tab.D.2.

country	place	WMO#	Up	num	YYYYs	lRSPR _a	uRSPR _a	lHBR _a	uHBR _a	lEIR _a	uEIR _a	lSeas	uSeas	lMSeas	uMSeas	lXSeas	uXSeas	lSSeas	uSSeas	lESeas	uESeas
Mali	Mopti Barbe	61265	R	3	1995-1998	0.59(3)	1.49	-8(-8)	-8	-8.00(-8)	-8.00	-8(-8)	-8	-8(-8)	-8	-8(-8)	-8	-8(-8)	-8	-8(-8)	-8
Mali	Mopti Barbe	61265	I	3	1995-1998	0.15(3)	0.29	-8(-8)	-8	-8.00(-8)	-8.00	-8(-8)	-8	-8(-8)	-8	-8(-8)	-8	-8(-8)	-8	-8(-8)	-8
Mali	Bamako Senou	61291	R	1	1998	-8.00(-8)	-8.00	-8(-8)	-8	3.49(1)	3.49	7(1)	7	3(1)	3	10(1)	10	06(1)	06	12(1)	12
Senegal	Rosso	61489	I	1	1992-1994	0.00(2)	0.00	-8(-8)	-8	0.00(2)	0.00	0(2)	0	0(2)	0	-5(2)	-5	-5(2)	-5	-5(2)	-5
Senegal	Saint Louis	61600	S	1	1992-1994	0.00(1)	0.00	-8(-8)	-8	0.00(1)	0.00	0(1)	0	0(1)	0	-5(1)	-5	-5(1)	-5	-5(1)	-5
Senegal	Podor	61612	R	3	1982-1983	0.00(3)	1.20	200(3)	1600	0.00(3)	6.40	0(3)	4	0(3)	2	09 ⁿ (3)	11	09 ⁿ (3)	09	11 ⁿ (3)	12 ⁿ
Senegal	Podor	61612	I	1	1990-1991																
Senegal	Podor	61612	I	1	1982-1983	0.00(2)	0.05	3139(2)	7483	0.00(2)	1.00	0(2)	1	0(2)	1	-5(2)	08	-5(2)	08	-5(2)	08
Senegal	Linguere	61627	R	2	1994-1996	1.52(2)	2.19	5870(2)	6684	101.60(2)	128.55	4(2)	6	2(2)	2	09(2)	10	08(2)	09	12(2)	14
Senegal	Dakar Yoff	61641	U	3	1979-1981	0.00(2)	0.55	22(3)	7818	0.00(3)	43.00	0(2)	12	0(2)	4	-5(2)	10	-5(2)	-1	-5(2)	-1
Senegal	Dakar Yoff	61641	R	3	1987-1988																
Senegal	Dakar Yoff	61641	R	3	1996-1997																
Senegal	Diourbel	61666	R	3	1991-1993	0.00(3)	0.48	1241(3)	4540	0.00(3)	11.00	0(3)	2	0(3)	2	-5(3)	10	-5(3)	09	-5(3)	10
Senegal	Diourbel	61666	R	3	1995	1.75(3)	1.95	512(3)	1558	8.96(1)	26.50	5(3)	8	-8(-8)	-8	09(3)	09	06(3)	07	11(3)	13
Senegal	Kaolack	61679	R	3	1993-1997	0.39(6)	4.71	149(6)	2615	7.00(6)	63.00	1(7)	7	1(4)	2	07(7)	10	06(7)	09	09(7)	12
Senegal	Kaolack	61679	S	2	1990-1997	0.87(8)	2.77	8581(8)	22299	16.40(8)	350.10	5(8)	12	4(7)	6	07(8)	14	06 ^y (8)	11 ^y	15(7)	-1
Senegal	Tambacounda	61687	R	5	1991-1993	2.23(6)	7.65	34(5)	7884	0.99(5)	220.00	7(1)	7	3(1)	3	09(1)	09	07(1)	07	13(1)	13
Senegal	Ziguinchor	61695	I	5	1985-1986	0.00(10)	0.46	3056(10)	66667	0.00(10)	123.00	0(10)	5	0(10)	3	-5(7)	09	07 ⁿ (6)	08 ⁿ	10 ⁿ (6)	11 ⁿ
Gambia, The	Banjul Yundum Intl	61701	U	1	1988-1989	0.98(1)	0.98	104(1)	104	1.02(1)	1.02	-8(-8)	-8	-8(-8)	-8	-8(-8)	-8	-8(-8)	-8	-8(-8)	-8
Gambia, The	Banjul Yundum Intl	61701	R	21	1986 1988-1989	0.23(19)	17.86	37(19)	3701	0.00(19)	177.00	3(4)	5	2(2)	3	09(3)	09	07(4)	09	11(4)	12
Gambia, The	Banjul Yundum Intl	61701	R	21	1991-1992 2001 2003																
Cameroon	Koundja	64893	R	2	1995-1996	9.40(1)	9.40	0(2)	876	0.00(2)	82.34	0(2)	12	0(2)	2	-5(2)	09	-5(2)	-1	-5(2)	-1
Cameroon	Foumban	64910	R	3	1990 1998-1999	1.20(3)	8.24	317(3)	2310	3.80(3)	161.00	-8(-8)	-8	-8(-8)	-8	-8(-8)	-8	-8(-8)	-8	-8(-8)	-8
Cameroon	Douala	64910	R	3	1990 1998-1999	1.20(3)	8.24	317(3)	2310	3.80(3)	161.00	-8(-8)	-8	-8(-8)	-8	-8(-8)	-8	-8(-8)	-8	-8(-8)	-8
Cameroon	Yaounde	64950	R/S	15	1989-1992	0.84(16)	6.78	402(15)	38189	17.70(15)	565.75	2(13)	12	2(10)	8	01(10)	05	01 ^y (13)	08 ^y	06 ^y (13)	17 ^y
Cameroon	Yaounde	64950	U	5	1994-2001																
Cameroon	Yaounde	64950	U	5	1989-1990	2.50(3)	20.31	64(3)	3588	3.00(4)	129.00	1(1)	12	1 ^f (1)	1	05(1)	05	05 ^f (2)	-1	5 ^f (2)	-1
Cameroon	Yaounde	64950	U	5	2000-2001																
Benin	Cotonou	65344	R	6	1987 1993-1995	0.33(6)	1.60	2555(6)	5870	10.60(6)	58.00	6(5)	8	3(2)	4	08(2)	10	03(3)	07	08(3)	13
Benin	Cadjeoun	65344	R	6	1987 1993-1995	0.33(6)	1.60	2555(6)	5870	10.60(6)	58.00	6(5)	8	3(2)	4	08(2)	10	03(3)	07	08(3)	13
Benin	Cotonou	65344	U	4	1987 2000	0.48(4)	2.80	1064(4)	2768	5.10(4)	48.00	2(2)	12	11(1)	11	1 ^f (1)	1 ^f	11(2)	-1 ^f	12(2)	-1
Benin	Cadjeoun	65344	U	4	1987 2000	0.48(4)	2.80	1064(4)	2768	5.10(4)	48.00	2(2)	12	11(1)	11	1 ^f (1)	1 ^f	11(2)	-1 ^f	12(2)	-1
Burkina Faso	Dori	65501	R	6	1985-1986	0.64(1)	0.64	-8(-8)	-8	-8.00(-8)	-8.00	-8(-8)	-8	-8(-8)	-8	-8(-8)	-8	-8(-8)	-8	-8(-8)	-8
Burkina Faso	Ouagadougou	65503	R	5	1984 1994-1995	6.07(3)	8.14	1009(3)	6082	82.11(3)	431.83	6(1)	6	2(6)	3	08(6)	10	04(2)	06	11(1)	11
Burkina Faso	Ouagadougou	65503	U	6	2002-2003																
Burkina Faso	Ouagadougou	65503	U	6	1984	0.00(5)	1.47	399(3)	1359	0.00(5)	19.98	0(5)	6	0(5)	3	08 ⁿ (4)	10	05 ⁿ (5)	08 ⁿ	10 ⁿ (5)	12 ⁿ
Burkina Faso	Bobo-Dioulasso	65510	R	11	1981 1983-1987	0.19(6)	5.75	1380(6)	7123	4.60(13)	370.00	2(9)	7	2(15)	5	08(9)	10	06(9)	09	10(9)	12

to be continued

Tab. D.5 – continued

country	place	WMO#	Up	num	YYYYs	lRSPR _a	uRSPR _a	lHBR _a	uHBR _a	lEIR _a	uEIR _a	lSeas	uSeas	lMSeas	uMSeas	lXSeas	uXSeas	lSSeas	uSSeas	lESeas	uESeas
Burkina Faso	Bobo-Dioulasso	65510	I	7	1981 1983-1986	0.22(4)	1.78	7480(4)	25490	0.00(10)	133.00	4(6)	7	2(12)	5	06(4)	11	05(6)	06	09(6)	12
Burkina Faso	Bobo-Dioulasso	65510	U	5	1985 1991-1993	0.11(3)	0.46	74(4)	2150	0.14(4)	4.00	1(2)	1	1(2)	1	09(2)	09	09(2)	09	09(2)	09
Burkina Faso	Po	65518	R	2	2001-2002	10.60(2)	19.00	1895(2)	2151	228.00(2)	360.00	4(2)	5	2(2)	3	08(2)	09	07(2)	07	10(2)	11
Burkina Faso	Po	65518	I	1	2001-2002	4.70(1)	4.70	13404(1)	13404	630.00(1)	630.00	8(1)	8	3(1)	3	09(1)	09	06(1)	06	13(1)	13
Côte d'Ivoire	Korhogo	65536	R	1	1997-1998	-8.00(-8)	-8.00	-8(-8)	-8	-8.00(-8)	-8.00	8(2)	8	-8(-8)	-8	08(1)	08	04(1)	04	11(1)	11
Côte d'Ivoire	Korhogo	65536	I	1	1997-1998	-8.00(-8)	-8.00	-8(-8)	-8	-8.00(-8)	-8.00	7(1)	7	-8(-8)	-8	05(1)	05	06(1)	06	12(1)	12
Côte d'Ivoire	Bouaké	65555	R	4	1991-1992 1997-1998	1.80(5)	2.70	3708(5)	6700	67.30(5)	134.00	7(6)	8	3(5)	5	05(5)	09	03(6)	04	10(6)	11
Côte d'Ivoire	Bouaké	65555	I/S	5	1991-1992	0.70(9)	3.50	4727(9)	22143	44.00(9)	266.50	7(8)	12	4(8)	8	05(6)	10	02 ^y (9)	04 ^y	11 ^y (8)	13 ^y
Côte d'Ivoire	Dimbokro	65562	R	2	2002-2003	1.39(3)	7.36	3453(3)	7662	48.00(3)	461.00	-8(-8)	-8	-8(-8)	-8	07(3)	08	04(3)	06	-8(-8)	-8
Côte d'Ivoire	Dimbokro	65562	I	1	2002-2003	4.58(1)	4.58	17227(1)	17227	789.00(1)	789.00	12(1)	12	-8(-8)	-8	02(1)	02	-1(1)	-1	-1(1)	-1

D.10 Duration of the gonotrophic cycle (n_g)

Tab. D.6: Information with regard to the duration of the gonotrophic cycle that is the egg development within female mosquitoes. For further information see Tab. D.2.

country	place	long [°E]	lat [°N]	M1	YYY1	M2	YYY2	n_g [days]	specie	note	ref
Ceylon	Peliyagoda	-999.00	-99.00	-8	1962	-8	1964	3.0-4.0	<i>Culex pipiens fatigans</i>	MRR experiments	Samarawickrema 1967
Dominican Republic	Calle Duarte, Colonia Japonesa, La Bomba	-999.00	-99.00	07	1987	10	1988	2.6	<i>An. albimanus</i>	-	Mekuria et al. 1991
Dominican Republic	Calle Duarte, Colonia Japonesa, La Bomba	-999.00	-99.00	07	1987	10	1988	3.2	<i>An. vestitipennis</i>	-	Mekuria et al. 1991
Egypt	Faiyum	-999.00	-99.00	10	1983	-8	-8	2.3-11.8	<i>An. sergentii</i>	laboratory; T : 17-34°C; data for 1st, 2nd, and 3rd cycles	Beier et al. 1987
Egypt	Tersa	-999.00	-99.00	-8	-8	-8	-8	6.1	<i>An. pharoensis</i>	first cycle; observation in laboratory	Kenawy 1991
Egypt	Tersa	-999.00	-99.00	-8	-8	-8	-8	7.4	<i>An. multicolor</i>	first cycle; observation in laboratory	Kenawy 1991
Iran	Zeineddini	-999.00	-99.00	05	1991	05	1991	2.0-3.0	<i>An. culicifacies</i> , <i>An. pulcherrimus</i>	direct observations	Zaim et al. 1993
Mexico	Cosalapa	-92.28	14.63 ^P	06	1993	07	1993	2.0-3.0	<i>An. vestitipennis</i>	autocorrelation time-series analysis	Arredondo-Jimenez et al. 1998
Mexico	Benemérito	-90.65	16.31 ^P	08	1993	09	1993	2.0	<i>An. vestitipennis</i>	autocorrelation time-series analysis	Arredondo-Jimenez et al. 1998
Mexico	Tapachula	-999.00	-99.00	11	1992	12	1992	3.8	<i>An. vestitipennis</i>	cage observations	Arredondo-Jimenez et al. 1998
Mexico	Tapachula foothills	-999.00	-99.00	04	1991	01	1991	3.0	<i>An. pseudopunctipennis</i>	wild-caught females; MRR experiments	Fernandez-Salas et al. 1994
Mexico	Tapachula foothills	-999.00	-99.00	04	1991	04	1991	4.0	<i>An. pseudopunctipennis</i>	insectary-reared females; MRR experiments	Fernandez-Salas et al. 1994
Senegal	Barkedji	-999.00	-99.00	-8	-8	-8	-8	2.2-3.2	<i>Aedes vexans arabiensis</i>	derived from formulas	Kenawy 1991
Sierra Leone	Bayama	-999.00	-99.00	11	1990	10	1991	3.0	<i>An. gambiae s.s.</i>	technique from Birley and Rajagopalan 1981	Bockarie et al. 1995
Tanzania	Namawala	36.40	-8.15 ^P	-8	-8	-8	-8	2.7	<i>An. gambiae s.l.</i> , <i>An. funestus</i> , <i>An. gambiae</i> , <i>An. arabiensis</i>	unpublished data	Charlwood et al. 1995
Tanzania	Muheza	-999.00	-99.00	-8	-8	-8	-8	3.0	<i>An. funestus</i>	different behaviour between cool and hot seasons	Gillies and Wilkes 1963
Tanzania	Muheza	-999.00	-99.00	-8	1963	-8	1964	3.0-5.0	<i>An. gambiae</i>	first cycle; MRR experiments	Gillies and Wilkes 1965
Tanzania	Muheza	-999.00	-99.00	-8	1963	-8	1964	3.0	<i>An. gambiae</i>	second and subsequent cycles; MRR experiments	Gillies and Wilkes 1965

D.11 Produced eggs per female mosquito ($\#E_p$)

Tab. D.7: Data with regard to the number of produced eggs per *Anopheles* female. Columns: $\#E_{p,ave}$: average number of produced eggs per female mosquito; $\#E_{p,min}$: minimum observed number of produced eggs; $\#E_{p,max}$: as $\#E_{p,min}$, but for the maximum; further information see Tab.D.2. The '#' stands for 'number'. y denotes the number of produced eggs and x stands for the wing length (in mm). Minimum and maximum values refer to individual analysed mosquito females.

country	place	long [°E]	lat [°N]	M1	YYY1	M2	YYY2	$\#E_{p,ave}$	$\#E_{p,min}$	$\#E_{p,max}$	specie	note	ref
Egypt	Faiyum	-999.00	-99.00	10	1983	-8	-8	-8.0	11.0	141.0	<i>An. sergentii</i>	laboratory	Beier et al. 1987
Egypt	Tersa	-999.00	-99.00	10	1990	11	1990	73.3	-8.0	-8.0	<i>An. pharoensis</i>	laboratory; # of eggs per female; constant temperatures (25 ± 2°C); $y = 73.3 \pm 16.9$	Kenawy 1991
Egypt	Tersa	-999.00	-99.00	10	1990	11	1990	209.2	-8.0	-8.0	<i>An. pharoensis</i>	laboratory; # of eggs per female; cycling temperatures; $y = 209.2 \pm 36.8$	Kenawy 1991
Egypt	Tersa	-999.00	-99.00	10	1990	11	1990	75.0	-8.0	-8.0	<i>An. multicolor</i>	laboratory; # of eggs per female; constant temperatures (25 ± 2°C); $y = 75.0 \pm 15.8$	Kenawy 1991
Egypt	Tersa	-999.00	-99.00	10	1990	11	1990	164.8	-8.0	-8.0	<i>An. multicolor</i>	laboratory; # of eggs per female; cycling temperatures; $y = 164.8 \pm 61.5$	Kenawy 1991
El Salvador	around Lake Apastepeque	-999.00	-99.00	06	1971	09	1972	120.0	-8.0	-8.0	<i>An. albimanus</i>	-	Weidhaas et al. 1974
Gambia, The	Kaba Kamma	-999.00	-99.00	07	1993	08	1993	-8	20.0	180.0	<i>An. gambiae s.s.</i>	laboratory; # of laid and retained eggs; indoor resting females; $y = 46.67x - 56.7$, x range: 2.5-3.3 mm	Hogg et al. 1996
Gambia, The	Kaba Kamma	-999.00	-99.00	07	1993	08	1993	-8	5.0	160.0	<i>An. arabiensis</i>	laboratory; # of laid and retained eggs; indoor resting females; $y = 66.72x - 125.68$, x range: 2.7-3.3 mm	Hogg et al. 1996
Tanzania	Kilimanjaro region	-999.00	-99.00	-8	-8	-8	-8	12.6	-8.0	-8.0	<i>An. gambiae s.s.</i>	laboratory; # of mature oocytes; small females; blood meal size: 1.0 µl	Takken et al. 1998b
Tanzania	Kilimanjaro region	-999.00	-99.00	-8	-8	-8	-8	108.6	-8.0	-8.0	<i>An. gambiae s.s.</i>	laboratory; # of mature oocytes; large females; blood meal: rat once	Takken et al. 1998b
Tanzania	Michenga	36.63	8.17 ^F	-8	1991	-8	1991	150.0	66.0	290.0	<i>An. gambiae s.l.</i>	laboratory; # of laid and retained eggs; indoor resting females; $y = 133.93x - 187.00$ (note: the value of the y -intercept disagrees with the inserted line in Fig. 3 in the reference); x range: 2.5-3.3 mm	Lyimo and Takken 1993
Tanzania	Michenga	36.63	8.17 ^F	-8	1991	-8	1991	111.0	48.0	178.0	<i>An. gambiae s.l.</i>	laboratory; # of laid and retained eggs; newly emerged females; $y = 89.13x - 152.96$	Lyimo and Takken 1993

D.12 Development of immature mosquitoes

Life tables of developing immature mosquitoes are constructed using either horizontal or vertical methods. Horizontal life table methods are appropriate for distinct cohorts following through time (e.g., in laboratories). By contrast, vertical life table methods are commonly applied for populations with overlapping generations and age distributions remaining stationary during sampling. In this case, larval sampling is usually done in the field using standard dipping techniques. Collected larvae per dip are counted and scored according to their life stage (Mwangangi et al. 2006).

Tab. D.8: Information of immature mosquitoes taken from horizontal life tables as derived under controlled conditions. Columns: $p_{MMA,ave}$: averaged immature survival probability from egg to adult emergence, that is the proportion of immature mosquitoes reaching MMA; $p_{MMA,min}$: as $p_{MMA,ave}$, but for the minimum; $p_{MMA,max}$: as $p_{MMA,ave}$, but for the maximum; MMA_{ave} : average Mosquito Mature Age; MMA_{min} : minimum Mosquito Mature Age; MMA_{max} : maximum Mosquito Mature Age; $\eta_{dc,ave}$: average daily immature mosquito survival probability in protected habitats; $\eta_{dc,min}$: as $\eta_{dc,ave}$, but for the minimum; $\eta_{dc,max}$: as $\eta_{dc,ave}$, but for the maximum; further information see Tab. D.2. Note that minimum and maximum values refer to average values obtained by different experimental settings (T : different temperatures; ρ : different larval densities; DL : different day lengths; \tilde{N} : with additional nutrients; $\neg\tilde{N}$: without added nutrients). Particular applied experimental settings are specified under the 'note' column.

country	place	long [°E]	lat [°N]	M1	YYY1	M2	YYY2	$p_{MMA,ave}$	$p_{MMA,min}$	$p_{MMA,max}$	MMA_{ave}	MMA_{min}	MMA_{max}	$\eta_{dc,ave}$	$\eta_{dc,min}$	$\eta_{dc,max}$	specie	note	ref
Egypt	Faiyum	-999.00	-99.00	10	1983	-8	-8	-8.0	55.8e	72.3e	-8.0	14.2	33.2	-8.0	97.7	98.2	<i>An. sergentii</i>	laboratory; T : 17/(22)/27°C; mud slurry, lower survival in tab/distilled water	Beier et al. 1987
Egypt	Tersa	-999.00	-99.00	10	1990	11	1990	13.0	-8.0	-8.0	16.5 ^p /18.5 ^e	-8.0	-8.0	89.6	-8.0	-8.0	<i>An. pharoensis</i>	laboratory	Kenawy 1991
Egypt	Tersa	-999.00	-99.00	10	1990	11	1990	22.0	-8.0	-8.0	20.0 ^p /21.0 ^e	-8.0	-8.0	93.0	-8.0	-8.0	<i>An. multicolor</i>	laboratory	Kenawy 1991
Kenya	Western Kenyan highland area	-999.00	-99.00	09	2003	09	2003	-8.0	24.0	48.0	-8.0	11.2 ^e	16.5 ^e	-8.0	91.7	94.9	<i>An. gambiae s.l.</i>	farmland; $\rho \neg\tilde{N}$; $z = 1420$ -1580	Munga et al. 2006
Kenya	Western Kenyan highland area	-999.00	-99.00	09	2003	09	2003	0.0	0.0	0.0	-8.0	-8.0	-8.0	-8.0	-8.0	-8.0	<i>An. gambiae s.l.</i>	forest; $\rho \neg\tilde{N}$; $z = 1420$ -1580	Munga et al. 2006
Kenya	Western Kenyan highland area	-999.00	-99.00	09	2003	09	2003	0.0	0.0	0.0	-8.0	-8.0	-8.0	-8.0	-8.0	-8.0	<i>An. gambiae s.l.</i>	swamp; $\rho \neg\tilde{N}$; $z = 1420$ -1580	Munga et al. 2006
Kenya	Western Kenyan highland area	-999.00	-99.00	06	2004	06	2004	-8.0	49.0	65.0	-8.0	12.0 ^e	16.7 ^e	-8.0	95.3	96.5	<i>An. gambiae s.l.</i>	farmland; $\rho \neg\tilde{N}$; $z = 1420$ -1580	Munga et al. 2006
Kenya	Western Kenyan highland area	-999.00	-99.00	06	2004	06	2004	-8.0	0.0	2.0	-8.0	20.1 ^e	27.6 ^e	-8.0	82.3	86.8	<i>An. gambiae s.l.</i>	forest; $\rho \neg\tilde{N}$; $z = 1420$ -1580	Munga et al. 2006
Kenya	Western Kenyan highland area	-999.00	-99.00	06	2004	06	2004	-8.0	6.0	33.0	-8.0	20.1 ^e	27.6 ^e	-8.0	88.7	94.5	<i>An. gambiae s.l.</i>	swamp; $\rho \neg\tilde{N}$; $z = 1420$ -1580	Munga et al. 2006
Kenya	Western Kenyan highland area	-999.00	-99.00	06	2004	06	2004	-8.0	61.0	70.0	-8.0	9.0 ^e	12.1 ^e	-8.0	95.8	96.1	<i>An. gambiae s.l.</i>	farmland; $\rho \tilde{N}$; $z = 1420$ -1580	Munga et al. 2006
Kenya	Western Kenyan highland area	-999.00	-99.00	06	2004	06	2004	-8.0	10.0	23.0	-8.0	18.4 ^e	24.2 ^e	-8.0	90.8	93.0	<i>An. gambiae s.l.</i>	forest; $\rho \tilde{N}$; $z = 1420$ -1580	Munga et al. 2006

to be continued

Tab. D.8 – continued

country	place	long [°E]	lat [°N]	M1	YYY1	M2	YYY2	$PMMA_{ave}$	$PMMA_{min}$	$PMMA_{max}$	MMA_{ave}	MMA_{min}	MMA_{max}	$\eta_{dc,ave}$	$\eta_{dc,min}$	$\eta_{dc,max}$	specie	note	ref
Kenya	Western Kenyan highland area	-999.00	-99.00	06	2004	06	2004	-8.0	24.0	43.0	-8.0	19.3 ^e	23.7 ^e	-8.0	94.2	96.2	<i>An. gambiae s.l.</i>	swamp; ρ \bar{N} ; $z = 1420$ -1580	Munga et al. 2006
Kenya	near Kisumu	-999.00	-99.00	-8	-8	-8	-8	-8.0	53.5	60.6	-8.0	8.5 ^P	9.9 ^P	-8.0	93.9	94.3	<i>An. gambiae</i>	ρ \bar{N} ;	Ginnig et al. 2002
Kenya	near Kisumu	-999.00	-99.00	-8	-8	-8	-8	-8.0	49.4	60.0	-8.0	8.1 ^P	10.3 ^P	-8.0	91.6	95.2	<i>An. gambiae</i>	ρ \bar{N} ;	Ginnig et al. 2002
Kenya	Fort Ternan	35.35	-0.20 ^f	06	2001	08	2001	0.4	-8.0	-8.0	16.5 ^P	-8.0	-8.0	71.6	-8.0	-8.0	<i>An. gambiae s.s.</i> , <i>An. arabiensis</i>	$z = 1550$ -1650	Koenraadt et al. 2006
Liberia	Sua	-999.00	-99.00	-8	-8	-8	-8	-8.0	55.0	80.0	-8.0	10.6 ^P	11.6 ^P	-8.0	94.5	98.1	<i>An. gambiae s.s.</i>	laboratory; ρ	Schneider et al. 2000
Liberia	-	-999.00	-99.00	-8	-8	-8	-8	83.4	72.0	99.0	9.8 ^P	8.0 ^P	13.0	98.2	95.8	99.9	<i>An. gambiae s.s.</i>	laboratory; T ρ	Lyimo et al. 1992
Nigeria	Lagos	-999.00	-99.00	-8	-8	-8	-8	-8.0	-8.0	-8.0	-8.0	-8.0	-8.0	-8.0	88.9	98.9	<i>An. gambiae s.s.</i>	laboratory; T ; no maturation at $T < 18^{\circ}\text{C}$ and $T > 32^{\circ}\text{C}$	Bayoh and Lindsay 2004
Mali	Banambani	-8.05	12.80 ^f	07	2000	08	2000	68.5	-8.0	-8.0	11.8 ^e	-8.0	-8.0	96.8	-8.0	-8.0	<i>An. gambiae s.l.</i>	laboratory	Edillo et al. 2004
Zimbabwe	Zambezi valley	-999.00	-99.00	-8	-8	-8	-8	-8.0	37.0	65.0	-8.0	9.9 ^P	10.4 ^P	-8.0	90.4	96.0	<i>An. arabiensis</i>	laboratory; ρ	Schneider et al. 2000
-	-	-999.00	-99.00	-8	-8	-8	-8	-8.0	35.0	85.0	-8.0	5.4 ^e	30.0 ^e	-8.0	94.8	98.9	<i>Culex pipiens</i> complex	laboratory; T DI	Mogi 1992

Tab. D.9: Information of immature mosquitoes taken from vertical life tables as derived under field conditions. Columns: $PMMA_{ave}$: averaged survival probability of immature mosquitoes from egg to adult emergence, that is the proportion of eggs reaching MMA ; $PMMA_{min}$: as $PMMA_{ave}$, but for the minimum; $PMMA_{max}$: as $PMMA_{ave}$, but for the maximum; MMA : Mosquito Mature Age, that is the duration between egg laying and adult emergence; $\eta_{d,ave}$: average daily survival probability of immature mosquitoes; $\eta_{d,ave}$: as $\eta_{d,min}$, but for the minimum; $\eta_{d,max}$: as $\eta_{d,ave}$, but for the maximum; further information see Tab. D.2.

country	place	long [°E]	lat [°N]	M1	YYY1	M2	YYY2	$PMMA_{ave}$ [%]	$PMMA_{min}$ [%]	$PMMA_{max}$ [%]	MMA [days]	$\eta_{d,ave}$ [%]	$\eta_{d,min}$ [%]	$\eta_{d,max}$ [%]	specie	note	ref
El Salvador	Lake Apastepeque	-999.00	-99.00	06	1971	09	1972	4.8	2.0	15.0	-8.0	-8.0	-8.0	-8.0	<i>An. albimanus</i>	-	Weidhaas et al. 1974
Kenya	Chiga	-999.00	-99.00	-8	-8	-8	-8	-8.0	3.8	4.8	12.5	-8.0	77.0	78.4	<i>An. gambiae</i>	marsh and pool collections	Service 1971
Kenya	Ahero, Rabour, Nduru	34.75	-0.1 ^P	07	1974	07	1974	-8.0	6.6	7.4	11.8	-8.0	79.4	80.2	<i>An. gambiae</i>	rice field, pond, and pool collections; $z = 1000$	Service 1977b
Kenya	Ahero	34.75	-0.1 ^P	07	1974	08	1974	16.5	-8.0	-8.0	11.8	85.8	-8.0	-8.0	<i>An. gambiae</i>	sprayed rice field collections; $z = 1000$	Service 1977b
Kenya	Chiga, Rabour, Kanyamedha, Warthorego	-999.00	-99.00	11	1971	12	1971	-8.0	2.9	3.4	11.8	-8.0	74.0	75.0	<i>An. gambiae</i>	pond collections; $z = 1150$	Service 1973
Kenya	Chiga	-999.00	-99.00	11	1971	12	1971	0.0	-8.0	-8.0	11.8	-8.0	-8.0	-8.0	<i>An. gambiae</i>	ditch collections; $z = 1150$	Service 1973
Kenya	Mwea	-999.00	-99.00	08	2005	04	2006	1.7	0.1	3.4	11.9	69.4	52.7	75.2	<i>An. arabiensis</i>	rice field collections; different rice stages (land preparation, transplanting, and tillering)	Mwangangi et al. 2006
Mali	Banambani	-8.05	12.80 ^P	07	2000	08	2000	17.6	8.0	28.5	11.8	86.3	80.7	89.9	<i>An. gambiae s.l.</i>	rock pool, swamp, and puddle collections	Edillo et al. 2004
Kenya	Baringo	-999.00	-99.00	-9	-9	-9	-9	-9.0	-9.0	-9.0	-9.0	91.9	-9.0	-9.0	<i>An. gambiae</i>	-	Aniedu et al. 1993

D.13 Daily survival probability of adult mosquitoes (p_d)

Tab. D.10: Data with regard to the daily survival probability of adult mosquitoes (p_d) as derived from entomological field studies. Columns: $p_{d,ave}$: average value of p_d ; $p_{d,min}$: minimum of p_d ; $p_{d,max}$: maximum of p_d ; way: determination way of p_d (C: calculated/estimation, see corresponding paper; K: keeping in cages/laboratory; A: age-grading (cp. Gillies 1958); P: parous rate; S: immediate and delayed sporozoite rates (Draper and Davidson 1953); L: ampulla measurements; M: mark-release-recapture method; I: population decline during the dry period (Charlwood et al. 1995); wea: weather conditions during the experiment (R: rainy season; D: dry season; T: transition season between either dry and rainy or rainy and dry season; E: dry and rainy season). For further information see Tab. D.2. Minimum and maximum values refer to annual variations.

country	place	long [°E]	lat [°N]	M1	YYY1	M2	YYY2	$p_{d,ave}$	$p_{d,min}$	$p_{d,max}$	way	species	wea	note	ref
Brasil	Pariquera-Açu county	-47.83	-24.50	01	2000	02	2000	61.0	-8.0	-8.0	M	<i>An. albicansis</i>	R	-	Dos Santos et al. 2004
Burkina Faso	Bobo-Dioulasso	-999.00	-99.00	06	1959	12	1960	88.3	-8.0	-8.0	P	<i>An. gambiae</i>	-	-	Garrett-Jones and Grab 1964
Burkina Faso	Bobo-Dioulasso	-999.00	-99.00	06	1959	12	1960	90.7	-8.0	-8.0	P	<i>An. funestus</i>	-	-	Garrett-Jones and Grab 1964
Burkina Faso	Bobo-Dioulasso	-999.00	-99.00	06	1959	12	1960	84.2	-8.0	-8.0	P	<i>An. nili</i>	-	-	Garrett-Jones and Grab 1964
Burkina Faso	Bobo-Dioulasso	-999.00	-99.00	06	1959	12	1960	88.9	-8.0	-8.0	P	<i>An. coustani</i>	-	-	Garrett-Jones and Grab 1964
Burkina Faso	Bobo-Dioulasso, urban	-999.00	-99.00	01	1985	12	1985	71.0	-8.0	-8.0	P	<i>An. gambiae</i>	R	-	Robert et al. 1989
Burkina Faso	Bobo-Dioulasso, rural	-999.00	-99.00	-8	-8	-8	-8	91.0	-8.0	-8.0	P	<i>An. gambiae</i>	R	-	Robert et al. 1989
Burkina Faso	Goundri	-1.33	12.50 ^f	09	1991	09	1991	73.6	-8.0	-8.0	M	mixture of <i>Anopheles</i>	R	other estimates provide higher values	Costantini et al. 1996
Burkina Faso	Goundri	-1.33	12.50 ^f	09	1992	09	1992	74.3	-8.0	-8.0	M	<i>An. gambiae s.l.</i>	R	other estimates provide higher values	Costantini et al. 1996
Cameroon	Gounougou	-999.00	-99.00	07	1990	09	1990	68.0	-8.0	-8.0	P	<i>An. gambiae s.l.</i>	R	-	Robert et al. 1992
Cameroon	Gounougou	-999.00	-99.00	07	1990	09	1990	79.0	-8.0	-8.0	P	<i>An. funestus</i>	R	-	Robert et al. 1992
Cameroon	Gounougou	-999.00	-99.00	07	1990	09	1990	62.0	-8.0	-8.0	P	<i>An. pharoensis</i>	R	-	Robert et al. 1992
Côte d'Ivoire	Alloukoukro	-5.08	7.80 ^b	01	1991	12	1991	87.0	80.0	97.0	P	<i>An. gambiae s.l.</i>	E	-	Dossou-Yovo et al. 1995
Côte d'Ivoire	Alloukoukro	-5.08	7.80 ^b	01	1992	12	1992	89.0	82.0	95.0	P	<i>An. gambiae s.l.</i>	E	-	Dossou-Yovo et al. 1995
Côte d'Ivoire	Alloukoukro	-5.08	7.80 ^b	01	1992	12	1992	90.0	84.0	100.0	P	<i>An. funestus</i>	E	-	Dossou-Yovo et al. 1995
Côte d'Ivoire	Alloukoukro	-5.08	7.80 ^b	01	1992	12	1992	91.0	87.0	100.0	P	<i>An. funestus</i>	E	-	Dossou-Yovo et al. 1995
Dominican Republic	Calle Duarte, Colonia Japonesa, La Bomba	-999.00	-99.00	07	1987	10	1988	68.4	-8.0	-8.0	P	<i>An. albimanus</i>	-	-	Mekuria et al. 1991
Dominican Republic	Calle Duarte, Colonia Japonesa, La Bomba	-999.00	-99.00	07	1987	10	1988	61.1	-8.0	-8.0	P	<i>An. vestitipennis</i>	-	-	Mekuria et al. 1991
Egypt	Faiyum	-999.00	-99.00	-9	-9	-9	-9	95.0	-8.0	-8.0	K	<i>An. pharoensis</i>	-	-	Kenawy 1991
Egypt	Faiyum	-999.00	-99.00	-9	-9	-9	-9	93.0	-8.0	-8.0	K	<i>An. multicolor</i>	-	-	Kenawy 1991
Egypt	Faiyum	-999.00	-99.00	-9	-9	-9	-9	89.0	-8.0	-8.0	P	<i>An. pharoensis</i>	-	-	Kenawy 1991
Egypt	Faiyum	-999.00	-99.00	-9	-9	-9	-9	80.0	-8.0	-8.0	P	<i>An. multicolor</i>	-	-	Kenawy 1991
Egypt	Faiyum	-999.00	-99.00	10	1983	-8	-8	95.0	-8.0	-8.0	K	<i>An. sergentii</i>	-	laboratory; T: 27 ± 2°C	Beier et al. 1987
El Salvador	around Lake Apastepeque	-999.00	-99.00	01	1972	04	1972	67.5	65.0	70.0	M	<i>An. albimanus</i>	D	MRR/release of sterile females	Weidhaas et al. 1974

to be continued

Tab. D.10 – continued

country	place	long [°E]	lat [°N]	M1	YYYY1	M2	YYYY2	P_d ave	P_d min	P_d max	way	species	wea	note	ref
El Salvador	around Lake Apastepeque	-999.00	-99.00	06	1971	08	1972	82.4	73.0	91.0	M	<i>An. albimanus</i>	R	MRR/release of sterile females; data for May-September	Weidhaas et al. 1974
El Salvador	around Lake Apastepeque	-999.00	-99.00	06	1971	08	1972	77.7	65.0	91.0	M	<i>An. albimanus</i>	R/D	MRR/release of sterile females	Weidhaas et al. 1974
Iran	Arso	-999.00	-99.00	-8	-8	-8	-8	85.5	-8.0	-8.0	P	<i>An. koliensis</i>	-	reduced under DDT	Garrett-Jones and Grab 1964
Iran	Arso	-999.00	-99.00	-8	-8	-8	-8	89.5	-8.0	-8.0	P	<i>An. farauti</i>	-	reduced under DDT	Garrett-Jones and Grab 1964
Iran	Arso	-999.00	-99.00	-8	-8	-8	-8	84.5	-8.0	-8.0	P	<i>An. punctulatus</i>	-	-	Garrett-Jones and Grab 1964
Iran	Baluchistan	-999.00	-99.00	05	1991	10	1991	-8.0	84.0	89.0	-9	<i>An. culicifacies</i> s.l.	-	p_d is lower in sprayed villages	Zaim et al. 1993
Iran	Baluchistan	-999.00	-99.00	05	1991	10	1991	-8.0	80.0	83.0	-9	<i>An. pulcherrimus</i>	-	p_d is lower in sprayed villages	Zaim et al. 1993
Kenya	Mgandini	-999.00	-99.00	10	1972	11	1972	89.0	-8.0	-8.0	M	<i>Aedes aegypti</i>	R	-	McDonald 1977
Kenya	Msihu	39.28	-4.53 ^r	03	1984	04	1984	80.9	-8.0	-8.0	C	<i>An. gambiae</i> s.l.	D	-	Mutero and Birley 1987
Kenya	Msihu	39.28	-4.53 ^r	05	1982	06	1982	71.4	-8.0	-8.0	C	<i>An. gambiae</i> s.l.	R	-	Mutero and Birley 1987
Kenya	Jimbo	39.23	-4.67 ^r	11	1982	12	1982	74.1	-8.0	-8.0	C	<i>An. merus</i>	R	-	Mutero and Birley 1987
Kenya	Mwea	-999.00	-99.00	08	1983	09	1983	81.0	-8.0	-8.0	C	<i>An. arabiensis</i>	R	-	Mutero and Birley 1987
Korea	Paju	-999.00	-99.00	06	2000	08	2000	78.7	70.6	87.2	P	<i>An. sinensis</i>	-	-	Lee et al. 2001
Korea	Kyonggi-do, malarious area	-999.00	-99.00	06	2000	08	2000	86.4	80.4	90.0	P	<i>An. sinensis</i>	-	-	Ree and Hwang 2000
Korea	Kyonggi-do, non-malarious area	-999.00	-99.00	06	2000	08	2000	83.3	80.7	86.6	P	<i>An. sinensis</i>	-	-	Ree and Hwang 2000
Korea	Gyeonggi-do	-999.00	-99.00	06	1999	10	1999	89.0	84.3	92.2	P	<i>An. sinensis</i>	-	large variation	Ree et al. 2001
Korea	Gyeonggi Province	126.83	37.93 ^r	04	1999	10	1999	85.9	80.4	89.5	P	<i>An. sinensis</i>	-	-	Shin et al. 2005
Mexico	Chiapas, coastal plain	-999.00	-99.00	-9	-9	-9	-9	-9.0	45.0	58.0	-9	<i>An. vestitipennis</i>	-	-	Arredondo-Jimenez et al. 1998
Mexico	Chiapas, Lacandon Forest	-999.00	-99.00	-9	-9	-9	-9	68.0	-9.0	-9.0	-9	-	-	<i>An. vestitipennis</i>	Arredondo-Jimenez et al. 1998
Mexico	Tapachula foothills	-999.00	-99.00	-9	-9	-9	-9	-9.0	87.5	88.4	P	<i>An. pseudopunctipennis</i>	D	-	Fernandez-Salas et al. 1994
Nigeria	Kankiya	7.83	12.55	06	1967	10	1967	93.8	-8.0	-8.0	P	<i>An. gambiae</i> species B	R	reduced under DDT	Garrett-Jones and Shidrawi 1969
Nigeria	Kaduna area	-999.00	-99.00	05	1963	08	1963	90.0	-8.0	-8.0	S	<i>An. gambiae</i>	R	-	Service 1965
Nigeria	Kaduna area	-999.00	-99.00	05	1963	08	1963	89.0	-8.0	-8.0	S	<i>An. funestus</i>	R	-	Service 1965
Pakistan	12 villages around Khagrachberi	-999.00	-99.00	07	1966	06	1967	90.0	-8.0	-8.0	P	<i>An. minimus</i>	-	-	Khan and Talibi 1972
Pakistan	12 villages around Khagrachberi	-999.00	-99.00	07	1966	06	1967	86.0	-8.0	-8.0	P	<i>An. vagus</i>	-	-	Khan and Talibi 1972
Pakistan	12 villages around Khagrachberi	-999.00	-99.00	07	1966	06	1967	81.0	-8.0	-8.0	P	<i>An. jeyporiensis</i>	-	-	Khan and Talibi 1972
Pakistan	12 villages around Khagrachberi	-999.00	-99.00	07	1966	06	1967	72.0	-8.0	-8.0	P	<i>An. philippinensis</i>	-	-	Khan and Talibi 1972
Pakistan	Khagrachberi Sattoki	-999.00	-99.00	05	1977	05	1977	80.8	-8.0	-8.0	M	<i>An. stephensi</i>	R	-	Reisen and Aslamkhan 1979
Papua New Guinea	Butelgut	-999.00	-99.00	-8	-8	-8	-8	86.0	-8.0	-8.0	-9	<i>An. punctulatus</i>	-	calculated via a method from Graves et al. 1990	Killeen et al. 2000
Senegal	Aéré Lao	-14.30	16.40 ^b	09	1982	12	1982	-8.0	93.0	97.0	P	<i>An. gambiae</i> s.l.	-	-	Vercruysse 1985b
Senegal	Barkedji	-14.87	15.28 ^b	-8	1993	-8	1993	86.8	-8.0	-8.0	C	<i>Aedes vexans</i> <i>arabiensis</i>	R	-	Ndiaye et al. 2006
Senegal	Boké Diallobé	-14.00	16.10 ^b	09	1982	11	1983	-8.0	90.0	94.0	P	<i>An. gambiae</i> s.l.	-	-	Vercruysse 1985b
Senegal	Pikine	-17.40	14.75 ^b	12	1979	12	1980	82.2	73.8	90.5	P	<i>An. arabiensis</i>	-	p_d (rainy season) > p_d (dry season)	Vercruysse et al. 1983
Senegal	Pikine	-17.40	14.75 ^b	10	1979	12	1980	85.8	-8.0	-8.0	C	-	-	-	Vercruysse 1985a
Senegal	Pikine	-17.40	14.75 ^b	12	1981	12	1982	82.0	77.0	84.0	C	<i>An. arabiensis</i>	-	p_d (rainy season) > p_d (dry season)	Vercruysse 1985a
Sierra Leone	Bayama	-11.77	8.00 ^a	-9	-9	-9	-9	85.0	-9.0	-9.0	-9	<i>An. gambiae</i>	-	-	Bockarie et al. 1995
Sri Lanka	-	-999.00	-99.00	06	1983	05	1984	93.8	-8.0	-8.0	K	<i>An. culicifacies</i>	-	-	De Zoysa et al. 1988

to be continued

Tab. D.10 – continued

country	place	long [°E]	lat [°N]	M1	YYY1	M2	YYY2	<i>Pd_{ave}</i>	<i>Pd_{min}</i>	<i>Pd_{max}</i>	way	species	wea	note	ref
Sudan	Ed dekeinat	-999.00	-99.00	10	1995	12	1996	-8.0	70.7	84.9	P	<i>An. arabiensis</i>	R/T	-	El Sayed et al. 2000
Sudan	El manshial	-999.00	-99.00	10	1995	12	1996	-8.0	69.3	80.6	P	<i>An. arabiensis</i>	R/T	-	El Sayed et al. 2000
Sudan	Ed dekeinat	-999.00	-99.00	10	1995	12	1996	57.4	-8.0	-8.0	P	<i>An. arabiensis</i>	D	-	El Sayed et al. 2000
Sudan	El manshial	-999.00	-99.00	10	1995	12	1996	61.6	-8.0	-8.0	P	<i>An. arabiensis</i>	D	-	El Sayed et al. 2000
Tanzania	Muheza	-999.00	-99.00	02	1963	12	1963	87.6	85.8	90.6	P	<i>An. gambiae</i> species A	-	-	Gillies and Wilkes 1965; Garrett-Jones and Shidrawi 1969
Tanzania	Muheza	-999.00	-99.00	05	1963	08	1963	85.1	82.5	89.4	P	<i>An. gambiae</i> species A	-	-	Gillies and Wilkes 1965; Garrett-Jones and Shidrawi 1969
Tanzania	Muheza	-999.00	-99.00	01	1963	12	1963	86.1	83.9	88.2	P	<i>An. gambiae</i> species A	-	-	Gillies and Wilkes 1965; Garrett-Jones and Shidrawi 1969
Tanzania	Muheza	-999.00	-99.00	11	1962	12	1963	89.4	85.0	92.0	P	<i>An. funestus</i>	-	-	Gillies and Wilkes 1965; Garrett-Jones and Shidrawi 1969
Tanzania	Gonja	-999.00	-99.00	12	1962	01	1964	82.6	77.9	87.3	P	<i>An. gambiae s.l.</i>	-	-	Gillies and Wilkes 1965; Garrett-Jones and Shidrawi 1969
Tanzania	-	-999.00	-99.00	-8	1952	-8	1952	91.0	-8.0	-8.0	P	<i>An. gambiae</i>	-	-	Davidson 1954
Tanzania	-	-999.00	-99.00	-8	1952	-8	1952	93.0	-8.0	-8.0	S	<i>An. gambiae</i>	-	-	Davidson 1954
Tanzania	-	-999.00	-99.00	-8	1952	-8	1952	94.0	-8.0	-8.0	L	<i>An. gambiae</i>	-	-	Davidson 1954
Tanzania	-	-999.00	-99.00	-8	1953	-8	1953	91.0	-8.0	-8.0	P	<i>An. gambiae</i>	-	-	Davidson 1954
Tanzania	-	-999.00	-99.00	-8	1953	-8	1953	90.0	-8.0	-8.0	L	<i>An. gambiae</i>	-	-	Davidson 1954
Tanzania	Namawala	36.40	-8.15°	02	1991	03	1991	82.7	-8.0	-8.0	I	<i>An. arabiensis</i>	D	-	Charlwood et al. 1995
Tanzania	Namawala	36.40	-8.15°	-8	-8	-8	-8	81.3	-8.0	-8.0	M	<i>An. gambiae s.l.</i>	R	-	Charlwood et al. 1997
Tanzania	Namawala	36.40	-8.15°	04	1991	05	1991	83.9	-8.0	-8.0	P	<i>An. gambiae s.l.</i>	R	-	Charlwood et al. 1997
Tanzania	Namawala	36.40	-8.15°	-8	-8	-8	-8	8.0	64.5	73.0	M	<i>An. gambiae s.l.</i>	R	-	Charlwood et al. 1997
Tanzania	Namawala	36.40	-8.15°	-8	1990	-8	1992	81.3	-8.0	-8.0	P	<i>An. gambiae s.l.</i>	R	-	Charlwood et al. 1997
Tanzania	Michenga	36.65	-8.12°	-8	1989	-8	1991	77.0	-8.0	-8.0	P	<i>An. gambiae s.l.</i>	R	-	Charlwood et al. 1997
Tanzania	foothills of the Eastern Usambara Mountains	-999.00	-99.00	03	1956	06	1959	84.1	-8.0	-8.0	M	<i>An. gambiae</i>	-	-	Gillies 1961
Tanzania	Muheza	-999.00	-99.00	11	1962	01	1964	85.4	-8.0	-8.0	M	<i>An. gambiae</i>	-	-	Gillies and Wilkes 1965
Tanzania	Muheza	-999.00	-99.00	11	1962	01	1964	85.0	-8.0	-8.0	M	<i>An. funestus</i>	-	-	Gillies and Wilkes 1965
Tanzania	Gonja	-999.00	-99.00	11	1962	01	1964	79.1	-8.0	-8.0	M	<i>An. gambiae</i>	-	-	Gillies and Wilkes 1965
Tanzania	Ifakara	-999.00	-99.00	-9	-9	-9	-9	78.0	-9.0	-9.0	M	<i>An. gambiae</i>	-	-	Takken et al. 1998a
Tanzania	40 miles west of Tanga	-999.00	-99.00	09	1952	12	1952	-8.0	88.0	93.0	S	<i>An. funestus</i>	R	-	Davidson and Draper 1953
Tanzania	40 miles west of Tanga	-999.00	-99.00	09	1952	12	1952	-8.0	89.0	93.0	S	<i>An. gambiae</i>	R	-	Davidson and Draper 1953
Tanzania	40 miles west of Tanga	-999.00	-99.00	09	1952	12	1952	93.7	83.0	98.5	K	<i>An. funestus</i>	R	kept in cages	Davidson and Draper 1953
Tanzania	40 miles west of Tanga	-999.00	-99.00	09	1952	12	1952	96.3	92.0	99.1	K	<i>An. gambiae</i>	R	kept in cages	Davidson and Draper 1953
Tanzania	coastal region	-999.00	-99.00	-8	-8	-8	-8	-8.0	92.0	93.0	A	<i>An. gambiae</i>	-	-	Gillies 1958
Tanzania	South Pare district	-999.00	-99.00	-8	-8	-8	-8	-8.0	85.0	87.0	A	<i>An. gambiae</i>	-	-	Gillies 1958
Tanzania	Muheza area, 5 villages	-999.00	-99.00	-8	-8	-8	-8	81.9	-8.0	-8.0	A	<i>An. gambiae</i>	-	-	Lines et al. 1991
Thailand	Ban Phluang	-999.00	-99.00	06	1983	05	1984	89.0	-8.0	-8.0	P	<i>An. dirus</i>	D	-	Rosenberg et al. 1990b,b
Thailand	Ban Phluang	-999.00	-99.00	06	1984	05	1985	83.0	-8.0	-8.0	P	<i>An. dirus</i>	D	-	Rosenberg et al. 1990b,b
Thailand	Ban Phluang	-999.00	-99.00	06	1984	05	1985	-8.0	59.0	84.0	P	<i>An. dirus</i>	R/T	-	Rosenberg et al. 1990b
Uganda	-	-999.00	-99.00	-8	-8	-8	-8	93.0	-8.0	-8.0	P	<i>An. gambiae</i>	-	-	Davidson 1954
Uganda	-	-999.00	-99.00	-8	-8	-8	-8	95.0	-8.0	-8.0	L	<i>An. gambiae</i>	-	-	Davidson 1954
Uganda	-	-999.00	-99.00	-8	-8	-8	-8	97.0	-8.0	-8.0	S	<i>An. gambiae</i>	-	-	Davidson 1954
Uganda	Lira	-999.00	-99.00	09	1953	12	1953	95.0	-8.0	-8.0	P	<i>An. gambiae</i>	R	-	Davidson 1955
Uganda	Lira	-999.00	-99.00	09	1953	12	1953	94.0	-8.0	-8.0	P	<i>An. funestus</i>	R	-	Davidson 1955
Uganda	Lira	-999.00	-99.00	09	1953	12	1953	94.5	-8.0	-8.0	K	<i>An. gambiae</i>	R	-	Davidson 1955
Uganda	Lira	-999.00	-99.00	09	1953	12	1953	94.6	-8.0	-8.0	K	<i>An. funestus</i>	R	-	Davidson 1955

to be continued

Tab. D.10 – continued															
country	place	long [°E]	lat [°N]	M1	YYY1	M2	YYY2	<i>P_{d,ave}</i>	<i>P_{d,min}</i>	<i>P_{d,max}</i>	way	species	wea	note	ref
Uganda	Lira	-999.00	-99.00	09	1953	12	1953	97.0	94.0	99.0	S	<i>An. gambiae</i>	R	-	Davidson 1955
Uganda	Lira	-999.00	-99.00	09	1953	12	1953	93.0	88.0	94.0	S	<i>An. gambiae</i>	R	-	Davidson 1955
USA	Sheridan	-999.00	-99.00	08	1984	09	1984	72.0	-9.0	-9.0	-9	<i>An. freeborni</i>	-	unfed	McHugh 1989
USA	Sheridan	-999.00	-99.00	08	1984	09	1984	74.0	-9.0	-9.0	-9	<i>An. freeborni</i>	-	blood-fed	McHugh 1989
USA	Sheridan	-999.00	-99.00	08	1984	09	1984	75.0	-9.0	-9.0	K	<i>An. freeborni</i>	-	-	McHugh 1989

D.14 Sexual Parasite Ratio (*sPR*)

Tab. D.11: Data with regard to the sexual Parasite Ratio (*sPR*), that is the percentage of humans with gametocytes in their blood as well as the Ratio between Sexual and Asexual parasite prevalence (*SAR*), which is the proportion of malaria parasite positive humans that are gametocytaemic. Note that particular values of the asexual Parasite Ratio (*PR*) can be calculated via $PR = \frac{sPR}{SAR}$. Columns: *sPR_a*: annual mean *sPR*; *sPR_{min,a}*: annual minimum *sPR*; *sPR_{max,a}*: annual maximum *sPR*; *SAR_a*: annual mean *SAR*; *SAR_{min,a}*: annual minimum *SAR*; *SAR_{max,a}*: annual maximum *SAR*. For further information see Tab. D.2.

country	place	long [°E]	lat [°N]	M1	YYY1	M2	YYY2	<i>sPR_a</i>	<i>sPR_{min,a}</i>	<i>sPR_{max,a}</i>	<i>SAR_a</i>	<i>SAR_{min,a}</i>	<i>SAR_{max,a}</i>	U _b	U _a	U _p	note	ref
Burkina Faso	Bobo-Dioulasso,	-4.30	11.21 ^b	01	1985	12	1985	10.5	5.6	21.1	36.1	26.7	44.3	U/R	R1	R	*(0-15)	Gazin et al. 1987
	Colma-Nord quarter																	
Burkina Faso	Bobo-Dioulasso,	-4.29	11.18 ^b	01	1985	12	1985	2.3	0.6	4.7	33.3	12.5	45.5	U	R1	U	*(0-15)	Gazin et al. 1987
	Diaradougou quarter																	
Burkina Faso	Bobo-Dioulasso,	-4.30	11.19 ^b	01	1985	12	1985	3.1	2.6	3.4	28.0	19.0	57.1	U	R1	U	*(0-15)	Gazin et al. 1987
	Dioulassoba quarter																	
Burkina Faso	Bouloy, Kodel, Bella and Peul	-999.00	-99.00	06	1985	03	1986	1.7	0.0	5.0	12.9	0.0	16.7	-8	-8	R	★	Gazin et al. 1988b
	Djelgobé camps																	
Burkina Faso	Bouloy, Kodel, Bella and Peul	-999.00	-99.00	06	1985	03	1986	8.6	7.5	9.1	17.0	12.0	24.1	-8	-8	R	*(0.5-15)	Gazin et al. 1988b
	Djelgobé camps																	
Burkina Faso	Karangasso	-4.63	11.22 ^b	02	1985	02	1986	21.3	4.5	30.0	38.3	6.0	52.7	R	R2	R	*(5-9)	Boudin et al. 1991b, 1992
Burkina Faso	Karangasso	-4.63	11.22 ^b	02	1985	02	1986	25.5	9.2	37.3	40.8	24.2	63.9	R	R2	R	*(0-4)	Boudin et al. 1991b, 1992
Burkina Faso	Karangasso	-4.63	11.22 ^b	02	1985	02	1986	29.4	8.5	39.7	47.8	11.8	65.1	R	R2	R	*(10-14)	Boudin et al. 1991b, 1992
Burkina Faso	near Bobo-Dioulasso	-999.00	-99.00	-8	1985	-8	1987	10.9	-8.0	-8.0	-8.0	-8.0	-8.0	R	R2	R	◆	Boudin et al. 1991a
Burkina Faso	Ouagadougou	-999.00	-99.00	08	1984	09	1984	-8.0	-8.0	7.6	25.9	-8.0	-8.0	-8	-8	U	*(0-5); more detailed information is available	Sabatinelli et al. 1986
Burkina Faso	Oursi and Déou	-999.00	-99.00	06	1985	03	1986	4.4	0.0	15.2	16.5	0.0	33.3	-8	-8	R	*(0.5-15)	Gazin et al. 1988b
Burkina Faso	6 villages north of	-999.00	-99.00	12	2003	12	2003	-8.0	21.4	-8.0	-8.0	28.5	-8.0	-8	-8	R	◆; microscope detection	Ouédraogo et al. 2007
	Ouagadougou																	
Burkina Faso	6 villages north of	-999.00	-99.00	12	2003	12	2003	-8.0	70.1	-8.0	-8.0	73.6	-8.0	-8	-8	R	◆; QT-NASBA detection	Ouédraogo et al. 2007
	Ouagadougou																	
Burkina Faso	Tin Edjar	-0.68	14.69 ^m	06	1985	03	1986	0.0	0.0	0.0	0.0	0.0	0.0	-8	-8	R	★	Gazin et al. 1988b
Burkina Faso	Tin Edjar	-0.68	14.69 ^m	06	1985	03	1986	4.2	2.6	5.4	12.5	8.0	26.7	-8	-8	R	*(0.5-15)	Gazin et al. 1988b

to be continued

Tab. D.11 – continued

country	place	long [°E]	lat [°N]	M1	YYY1	M2	YYY2	<i>sPR_a</i>	<i>sPR_{min,a}</i>	<i>sPR_{max,a}</i>	<i>SAR_a</i>	<i>SAR_{min,a}</i>	<i>SAR_{max,a}</i>	U _b	U _a	U _p	note	ref
Burkina Faso	VK4	-4.42	11.37 ^b	01	1985	02	1986	12.0	3.2	16.2	37.2	18.0	56.7	I	R2	I	*(0-4)	Boudin et al. 1992
Burkina Faso	VK4	-4.42	11.37 ^b	01	1985	02	1986	13.9	7.2	23.8	32.2	22.6	48.4	I	R2	I	*(5-9)	Boudin et al. 1992
Burkina Faso	VK4	-4.42	11.37 ^b	01	1985	02	1986	6.2	0.0	19.1	17.0	0.0	56.2	I	R2	I	*(10-14)	Boudin et al. 1992
Cameroon	Bondi	12.19	3.86 ^m	-8	1998	-8	2000	11.8	8.7	15.0	23.7	17.2	30.3	-8	-8	R	♦ (0.8-77); area: degraded forest; position derived from Meunier et al. 1999	Bonnet et al. 2003
Cameroon	Ebolakounou	12.13	3.93 ^a	05	1996	05	1998	4.7	-8.0	-8.0	13.7	-8.0	-8.0	-8	R2	R	★ (>15); forest area	Bonnet et al. 2002
Cameroon	Ebolakounou	12.13	3.93 ^a	05	1996	05	1998	9.1	-8.0	-8.0	14.7	-8.0	-8.0	-8	R2	R	*(0-15); forest area	Bonnet et al. 2002
Cameroon	Koundou	12.12	3.90 ^a	05	1996	05	1998	10.3	-8.0	-8.0	14.8	-8.0	-8.0	-8	R2	R	*(0-15); degraded forest	Bonnet et al. 2002
Cameroon	Koundou	12.12	3.90 ^a	05	1996	05	1998	3.8	-8.0	-8.0	9.6	-8.0	-8.0	-8	R2	R	★ (>15); degraded forest	Bonnet et al. 2002
Cameroon	Mengang	12.05	3.88 ⁱ	-8	1998	-8	2000	23.6	12.9	34.3	33.7	22.1	42.0	-8	-8	R	♦ (0.8-77); area: degraded forest	Bonnet et al. 2003
Cameroon	Mengang and Yaounde	-999.00	-99.00	-8	-8	-8	-8	10.4	-8.0	-8.0	15.6	-8.0	-8.0	-8	-8	R&U	*(0-14)	Boudin et al. 2005
Cameroon	Mengang and Yaounde	-999.00	-99.00	-8	-8	-8	-8	4.8	-8.0	-8.0	11.5	-8.0	-8.0	-8	-8	R&U	★ (>14)	Boudin et al. 2005
Cameroon	Mengang district, 2 villages	-999.00	-99.00	-8	-8	-8	-8	15.7	-8.0	-8.0	27.7	-8.0	-8.0	-8	-8	R	-	Paul et al. 2007
Cameroon	Yaoundé, Messa quarter	-999.00	-99.00	10	1990	01	1993	5.4	-8.0	-8.0	14.6	-8.0	-8.0	-8	-8	U	♦ (4-60)	Tchuinkam et al. 1993
Cameroon	Yaoundé and Mengang	-999.00	-99.00	-8	-8	-8	-8	19.1	-8.0	-8.0	40.2	-8.0	-8.0	-8	-8	-8	detected by quantitative buffy coat tests; patients presenting clinical malaria and	Mulder et al. 1998
																	*(3-15)	
Cameroon	Yaoundé and Mengang	-999.00	-99.00	-8	-8	-8	-8	20.0	-8.0	-8.0	39.8	-8.0	-8.0	-8	-8	-8	detected by thick blood films and quantitative buffy coat tests; patients presenting clinical malaria and	Mulder et al. 1998
																	*(3-15)	
Cameroon	Yaoundé and Mengang	-999.00	-99.00	-8	-8	-8	-8	4.6	-8.0	-8.0	10.1	-8.0	-8.0	-8	-8	-8	detected by thick blood films; patients presenting clinical malaria and	Mulder et al. 1998
																	*(3-15)	
Cameroon	Yaoundé, Dakar quarter	11.52	3.87 ⁱ	07	1999	05	2000	4.3	0.0	7.0	12.6	0.0	21.9	-8	-8	U	♦; microscope; drug influenced	van der Kolk et al. 2003
Cameroon	Yaoundé, Essos	11.00	3.00 ^b	06	1989	02	1990	3.2	2.4	7.4	8.5	0.0	16.7	-8	-8	U	*(0-15)	Manga et al. 1993b
Cameroon	Yaoundé, Obili district	11.52	3.87 ⁱ	10	1989	07	1990	1.1	0.0	3.0	4.0	0.0	7.7	-8	U	U	*(0-15)	Manga et al. 1993b
Côte d'Ivoire	Katiola district, 8 villages (no rice cultivation)	-999.00	-99.00	03	1997	01	1998	13.0	11.0	14.0	14.9	13.3	15.6	-8	-8	R	*(0-9); villages are Angolokaha, Doussoulakaha, Folofonkaha, Kabolo, Ounadiékaha, Petionara, Sérigobokaha, and Timorokaha	Henry et al. 2003
Côte d'Ivoire	Katiola district, 8 villages (no rice cultivation)	-999.00	-99.00	03	1997	01	1998	4.0	3.0	5.0	6.5	5.4	7.6	-8	-8	R	PR: *(≥10); see above	Henry et al. 2003
Côte d'Ivoire	Korhogo district, 8 villages (rice cultivation during the dry season)	-999.00	-99.00	03	1997	01	1998	11.0	10.0	11.0	13.9	13.3	13.6	-8	-8	I	*(0-9); villages are Gbahaouakaha, Kohotieri, Koumbolikaha, Lamékaha, Nambékaha, Nombolo, Nongotchénékaha, and Zémongokaha	Henry et al. 2003
Côte d'Ivoire	Korhogo district, 8 villages (rice cultivation during the dry season)	-999.00	-99.00	03	1997	01	1998	4.0	4.0	5.0	9.2	10.0	10.3	-8	-8	I	subjects (≥10); see above	Henry et al. 2003
Côte d'Ivoire	Korhogo district, 8 villages (rice cultivation during the rainy season)	-999.00	-99.00	03	1997	01	1998	12.0	12.0	12.0	14.3	14.0	15.0	-8	-8	R	*(0-9); villages are Binguebougou, Fapaha, Kombolokoura, Kaforo, Karakpo, Kassoumbarga, Katiorkpo, and Tioro	Henry et al. 2003
Côte d'Ivoire	Korhogo district, 8 villages (rice cultivation during the rainy season)	-999.00	-99.00	03	1997	01	1998	4.0	3.0	5.0	6.1	4.9	7.2	-8	-8	R	*(≥10); see above	Henry et al. 2003
Congo	Linzolo	15.11	-4.41 ^b	11	1981	05	1985	22.5	21.8	27.7	28.5	27.6	34.2	R	R1	R	*(0-14); microscope	Trape 1987
Congo	6 villages near Brazzaville	-999.00	-99.00	11	1981	05	1985	28.4	-8.0	-8.0	34.0	-8.0	-8.0	-8	-8	R	*(5-15) (from school); microscope	Trape 1987
Gambia	4 villages west of Farafenni	-999.00	-99.00	05	2001	06	2001	-8.0	13.5	-8.0	-8.0	24.9	-8.0	-8	-8	R	*(0.5-15)	Dunyo et al. 2006
Gambia, The	5 villages around Farafenni	-16.57	13.47 ^r	04	2003	05	2003	-8.0	-8.0	3.1	-8.0	-8.0	15.3	-8	-8	R	♦ (5-45); detected by microscopy	Nwakanma et al. 2008
Gambia, The	5 villages around Farafenni	-16.57	13.47 ^r	04	2003	05	2003	-8.0	-8.0	3.1	-8.0	-8.0	15.3	-8	-8	R	♦ (5-45); detected by microscopy	Nwakanma et al. 2008
Gambia, The	5 villages around Farafenni	-16.57	13.47 ^r	05	2003	10	2003	24.2	-8.0	-8.0	44.9	-8.0	-8.0	-8	-8	R	♦ (5-45); detected by microscopy	Nwakanma et al. 2008
Gambia, The	5 villages around Farafenni	-16.57	13.47 ^r	05	2003	10	2003	51.6	-8.0	-8.0	62.7	-8.0	-8.0	-8	-8	R	♦ (5-45); PCR/RT-PCR detection	Nwakanma et al. 2008
Gambia, The	near Farafenni, north bank villages	-999.00	-99.00	06/11	1990	06/11	1990	12.3	-8.0	-8.0	-8.0	-8.0	-8.0	-8	-8	-8	*(1-19)	Drakeley et al. 2000

to be continued

Tab. D.11 – continued

country	place	long [°E]	lat [°N]	M1	YYYY1	M2	YYYY2	sPR _a	sPR _{min,a}	sPR _{max,a}	SAR _a	SAR _{min,a}	SAR _{max,a}	U _b	U _a	U _p	note	ref
Gambia, The	near Farafenni, north bank villages	-999.00	-99.00	06/11	1990 1991	06/11	1990 1991	6.1	-8.0	-8.0	-8.0	-8.0	-8.0	-8	-8	-8	★(>20)	Drakeley et al. 2000
Gambia, The	near Farafenni, north bank villages	-999.00	-99.00	-8	-8	-8	-8	-8.0	-8.0	-8.0	-8.0	11.7	31.0	-8	-8	-8	★(>14); graphically derived	Drakeley et al. 2006
Gambia, The	near Farafenni, north bank villages	-999.00	-99.00	-8	-8	-8	-8	-8.0	-8.0	-8.0	-8.0	18.8	43.5	-8	-8	-8	★(0-14); graphically derived	Drakeley et al. 2006
Gambia, The	near Farafenni, south bank villages	-999.00	-99.00	-8	-8	-8	-8	-8.0	-8.0	-8.0	-8.0	15.3	26.0	-8	-8	-8	★(>14); graphically derived	Drakeley et al. 2006
Gambia, The	near Farafenni, south bank villages	-999.00	-99.00	-8	-8	-8	-8	-8.0	-8.0	-8.0	-8.0	16.5	27.0	-8	-8	-8	★(0-14); graphically derived	Drakeley et al. 2006
Ghana	-9	-999.00	-99.00	01	1952	10	1952	20.0	-9.0	-9.0	-9.0	-9.0	-9.0	-8	-8	-9	★(0-14)	Muirhead-Thomson 1954
Ghana	-9	-999.00	-99.00	01	1952	10	1952	6.0	-9.0	-9.0	-9.0	-9.0	-9.0	-8	-8	-9	★(>14)	Muirhead-Thomson 1954
Ghana	Weija	-999.00	-99.00	01	1952	10	1952	20.0	-8.0	-8.0	22.9	-8.0	-8.0	-8	-8	R	★(0.8-10)	Muirhead-Thomson 1954
Kenya	Ahero	-999.00	-99.00	-8	1935	-8	1936	51.6	-8.0	-8.0	61.5	-8.0	-8.0	-8	-8	-8	★(0-4); microscope detection	Garnham 1949
Kenya	Chonyi	-999.00	-99.00	-8	-8	-8	-8	-8.0	-8.0	-8.0	17.3	-8.0	-8.0	-8	-8	-8	★(0-14); graphically derived	Drakeley et al. 2006
Kenya	Chonyi	-999.00	-99.00	-8	-8	-8	-8	-8.0	-8.0	-8.0	3.7	-8.0	-8.0	-8	-8	-8	★(>14); graphically derived	Drakeley et al. 2006
Kenya	Kanyamedha	-999.00	-99.00	-8	1935	-8	1936	24.2	-8.0	-8.0	29.1	-8.0	-8.0	-8	-8	-8	★(0-4); microscope detection	Garnham 1949
Kenya	Kasagam	-999.00	-99.00	-8	1935	-8	1936	9.3	-8.0	-8.0	10.7	-8.0	-8.0	-8	-8	-8	★(0-4); microscope detection	Garnham 1949
Kenya	Kisumu	-999.00	-99.00	-8	1935	-8	1936	17.9	-8.0	-8.0	25.2	-8.0	-8.0	-8	-8	-8	★(0-4); microscope detection	Garnham 1949
Kenya	Ngerenya	-999.00	-99.00	-8	-8	-8	-8	-8.0	-8.0	-8.0	23.8	-8.0	-8.0	-8	-8	-8	★(0-14); graphically derived	Drakeley et al. 2006
Kenya	Ngerenya	-999.00	-99.00	-8	-8	-8	-8	-8.0	-8.0	-8.0	7.3	-8.0	-8.0	-8	-8	-8	★(>14); graphically derived	Drakeley et al. 2006
Kenya	Nyakatch	-999.00	-99.00	-8	1935	-8	1936	37.7	-8.0	-8.0	49.1	-8.0	-8.0	-8	-8	-8	★(0-4); microscope detection	Garnham 1949
Liberia	-9	-999.00	-99.00	-9	-9	-9	-9	15.6	-9.0	-9.0	-9.0	-9.0	-9.0	-8	-8	-9	★(0-14)	Muirhead-Thomson 1957
Liberia	-9	-999.00	-99.00	-9	-9	-9	-9	5.5	-9.0	-9.0	-9.0	-9.0	-9.0	-8	-8	-9	★(>14)	Muirhead-Thomson 1957
Liberia	Marshall Territory	-999.00	-99.00	01	195?	12	195?	6.0	-8.0	-8.0	31.4	-8.0	-8.0	-8	-8	-8	-	Miller 1958
Nigeria	Garki, village 154	-999.00	-99.00	-9	-9	-9	-9	36.5	-8.0	-8.0	-8.0	-8.0	-8.0	-8	-8	-9	★(1-8)	Nedelman 1989
Nigeria	Garki, village 154	-999.00	-99.00	-9	-9	-9	-9	9.8	-8.0	-8.0	-8.0	-8.0	-8.0	-8	-8	-9	◆(>9)	Nedelman 1989
Nigeria	Garki, village 202	-999.00	-99.00	-9	-9	-9	-9	27.0	-8.0	-8.0	-8.0	-8.0	-8.0	-8	-8	-8	★(1-8)	Nedelman 1989
Nigeria	Garki, village 202	-999.00	-99.00	-9	-9	-9	-9	5.5	-8.0	-8.0	-8.0	-8.0	-8.0	-8	-8	-8	◆(>9)	Nedelman 1989
Nigeria	Garki, village 218	-999.00	-99.00	-9	-9	-9	-9	30.0	-8.0	-8.0	-8.0	-8.0	-8.0	-8	-8	-8	★(1-8)	Nedelman 1989
Nigeria	Garki, village 218	-999.00	-99.00	-9	-9	-9	-9	7.8	-8.0	-8.0	-8.0	-8.0	-8.0	-8	-8	-8	◆(>9)	Nedelman 1989
Nigeria	Garki, village 304	-999.00	-99.00	-9	-9	-9	-9	22.5	-8.0	-8.0	-8.0	-8.0	-8.0	-8	-8	-8	★(1-8)	Nedelman 1989
Nigeria	Garki, village 304	-999.00	-99.00	-9	-9	-9	-9	7.3	-8.0	-8.0	-8.0	-8.0	-8.0	-8	-8	-8	◆(>9)	Nedelman 1989
Nigeria	Garki, village 408	-999.00	-99.00	-9	-9	-9	-9	30.5	-8.0	-8.0	-8.0	-8.0	-8.0	-8	-8	-8	★(1-8)	Nedelman 1989
Nigeria	Garki, village 408	-999.00	-99.00	-9	-9	-9	-9	6.3	-8.0	-8.0	-8.0	-8.0	-8.0	-8	-8	-8	◆(>9)	Nedelman 1989
Nigeria	Garki, village 553	-999.00	-99.00	-9	-9	-9	-9	26.0	-8.0	-8.0	-8.0	-8.0	-8.0	-8	-8	-8	★(1-8)	Nedelman 1989
Nigeria	Garki, village 553	-999.00	-99.00	-9	-9	-9	-9	4.5	-8.0	-8.0	-8.0	-8.0	-8.0	-8	-8	-8	◆(>9)	Nedelman 1989
Nigeria	Garki, village 55	-999.00	-99.00	-9	-9	-9	-9	29.5	-8.0	-8.0	-8.0	-8.0	-8.0	-8	-8	-8	◆(>9)	Nedelman 1989
Nigeria	Garki, village 55	-999.00	-99.00	-9	-9	-9	-9	8.8	-8.0	-8.0	-8.0	-8.0	-8.0	-8	-8	-8	◆(>9)	Nedelman 1989
Nigeria	Garki, village 802	-999.00	-99.00	-9	-9	-9	-9	27.5	-8.0	-8.0	-8.0	-8.0	-8.0	-8	-8	-8	★(1-8)	Nedelman 1989
Nigeria	Garki, village 802	-999.00	-99.00	-9	-9	-9	-9	8.3	-8.0	-8.0	-8.0	-8.0	-8.0	-8	-8	-8	◆(>9)	Nedelman 1989
Nigeria	Kaduna area	-999.00	-99.00	05	1963	08	1963	26.5	-8.0	-8.0	-8.0	-8.0	-8.0	-8	-8	-8	-	Service 1965
Nigeria	Lagos	3.40	6.45 ⁱ	-8	1949	-8	1949	11.8	-8.0	-8.0	44.8	-8.0	-8.0	-8	-8	U	★(0-1)	Bruce-Chwatt 1951
Nigeria	Lagos	3.40	6.45 ⁱ	-8	-8	-8	-8	30.2	-8.0	-8.0	38.8	-8.0	-8.0	-8	-8	U	★(1-2)	Bruce-Chwatt 1951
Nigeria	village in Yoruba country	-999.00	-99.00	11	1951	12	1951	-8.0	-8.0	-8.0	-8.0	-8.0	-8.0	-8	-8	R	★(0-15); microscope detection	Draper 1953
Papua New Guinea	72 villages around Madang	-999.00	-99.00	07	1981	01	1983	6.3	5.5	7.0	15.3	14.6	16.0	-8	-8	R	★(0-14)	Cattani et al. 1986
Papua New Guinea	Butelgut	145.75	-5.15 ⁱ	06	1983	09	1985	14.7	-8.0	-8.0	23.3	-8.0	-8.0	-8	-8	R	★(0-20)	Graves et al. 1988
Papua New Guinea	Mebat	145.78	-5.083	06	1983	09	1985	14.3	-8.0	-8.0	25.6	-8.0	-8.0	-8	-8	R	★(0-20)	Graves et al. 1988

to be continued

Tab. D.11 – continued

country	place	long [°E]	lat [°N]	M1	YYY1	M2	YYY2	sPR_a	$sPR_{min,a}$	$sPR_{max,a}$	SAR_a	$SAR_{min,a}$	$SAR_{max,a}$	U_b	U_a	U_p	note	ref
Papua New Guinea	Mebat	145.78	-5.083	06	1983	09	1985	7.9	-8.0	-8.0	15.9	-8.0	-8.0	-8	-8	R	*(0-20)	Graves et al. 1988
Senegal	Aéré Lao and Boké Diallobé	-14.30	16.40 ^b	05	1982	08	1983	-8.0	0.0	4.8	-8.0	0.0	28.2	R	R2	R	-	Vercruyse 1985b
Senegal	Dakar, Grande Niaye Mrash	-17.42	14.75 ^r	05	1987	09	1988	1.3	-8.0	-8.0	34.4	-8.0	-8.0	-8	U	U	◆	Trape et al. 1992
Senegal	Diohine	-16.51	14.48 ^a	10	1996	11	1996	16.7	-8.0	-8.0	25.8	-8.0	-8.0	-8	R1	R	★(19-66)	Sokhna et al. 2001
Senegal	Diohine, Kotiokh and Ngayokhème	-999.00	-99.00	02	1995	11	1995	26.0	15.0	45.0	45.9	36.6	54.9	R	R1	R	*(0-9)	Robert et al. 1998
Senegal	Diohine, Kotiokh and Ngayokhème	-999.00	-99.00	02	1995	11	1995	9.0	3.0	20.0	26.8	18.2	30.8	R	R1	R	★	Robert et al. 1998
Senegal	Thies	-16.93	14.80 ⁱ	-8	-8	-8	-8	4.8	-8.0	-8.0	53.2	-8.0	-8.0	-8	-8	R	★(>14)	Boudin et al. 2005
Senegal	Thies	-16.93	14.80 ⁱ	-8	-8	-8	-8	7.5	-8.0	-8.0	42.9	-8.0	-8.0	-8	-8	R	*(0-14)	Boudin et al. 2005
Sierra Leone	8 villages near Bo	-999.00	-99.00	03	1990	12	1990	10.9	-8.0	-8.0	17.9	-8.0	-8.0	-8	-8	R	*(0.3-7)	Barnish et al. 1993
Sudan	Asar	13.75	35.25 ^a	10	1998	08	1999	29.8	12.2	52.3	-8.0	-8.0	-8.0	-8	R2	R	◆; RT-PCR detection	Abdel-Wahab et al. 2002
Sudan	Asar	13.75	35.25 ^a	10	1998	08	1999	3.5	0.0	6.2	13.2	0.0	-8.0	-8	R2	R	◆; microscope detection	Abdel-Wahab et al. 2002
Sudan	Asar	-999.00	-99.00	10	1999	10	1999	-8.0	-8.0	-8.0	62.0	-8.0	-8.0	-8	R2	R	◆(6-50); RT-PCR detection	Ali et al. 2006
Sudan	Asar	-999.00	-99.00	10	1999	10	1999	-8.0	-8.0	-8.0	6.5	-8.0	-8.0	-8	R2	R	◆(6-50); detection by microscopy	Ali et al. 2006
Tanzania	40 miles west of Tanga	-999.00	-99.00	09	1952	12	1952	7.7	-8.0	-8.0	14.0	-8.0	-8.0	-8	-8	S	◆	Davidson and Draper 1953
Tanzania	Kisegese	-999.00	-99.00	-8	1992	-8	1994	11.6	-8.0	-8.0	-8.0	-8.0	-8.0	-8	-8	-8	*(1-19)	Drakeley et al. 2000
Tanzania	Kisegese	-999.00	-99.00	-8	1992	-8	1994	7.0	-8.0	-8.0	-8.0	-8.0	-8.0	-8	-8	-8	★(>19)	Drakeley et al. 2000
Tanzania	Northeastern Tanzania	-999.00	-99.00	-8	-8	-8	-8	13.5	-8.0	-8.0	28.0	-8.0	-8.0	-8	-8	-8	*(0-14); graphically derived	Drakeley et al. 2006
Tanzania	Northeastern Tanzania	-999.00	-99.00	-8	-8	-8	-8	3.7	-8.0	-8.0	11.2	-8.0	-8.0	-8	-8	-8	★(>14); graphically derived	Drakeley et al. 2006
Thailand	Ban Phluang	-999.00	-99.00	06	1983	05	1985	4.6	1.1	7.7	-8.0	-8.0	-8.0	-8	-8	R	★(>13)	Rosenberg et al. 1990b
Thailand	Ban Phluang	-999.00	-99.00	06	1983	05	1985	6.4	3.2	9.4	-8.0	-8.0	-8.0	-8	-8	R	*(1-14)	Rosenberg et al. 1990b
Uganda	Lira	-999.00	-99.00	09	1953	12	1953	16.9	-8.0	-8.0	28.6	-8.0	-8.0	-8	-8	S	◆; East African plateau	Davidson 1955

D.15 Human-to-mosquito transmission efficiency (c)

Tab. D.12: Data with regard to the human-to-mosquito transmission efficiency (c) that is the proportion of mosquito bites on infectious humans which infect susceptible mosquitoes. For further information see Tab. D.2.

country	place	long [°E]	lat [°N]	M1	YYY1	M2	YYY2	c	U_b	U_a	U_p	note	ref
Burkina Faso	near Bobo-Dioulasso	-999.00	-99.00	-8	1985	-8	1987	37.2	R	R2	R	◆; experimental feeding on heavy carriers of gametocytes	Boudin et al. 1991a
Cameroon	Bondi	12.19	3.86 ^m	-8	1998	-8	2000	11.8	-8	-8	R	★(>14); area: degraded forest	Bonnet et al. 2003
Cameroon	Bondi	12.19	3.86 ^m	-8	1998	-8	2000	36.9	-8	-8	R	★(0-14); area: degraded forest	Bonnet et al. 2003
Cameroon	district of Mengang	-999.00	-99.00	-8	-8	-8	-8	12.1	-8	-8	R	◆(>5); membrane feeding	Bonnet et al. 2002
Cameroon	district of Mengang	-999.00	-99.00	-8	-8	-8	-8	19.4	-8	-8	R	◆(>5); direct skin feeding	Bonnet et al. 2002
Cameroon	Mengang	12.05	3.88 ⁱ	-8	1998	-8	2000	15.5	-8	-8	R	★(0-14); area: degraded forest	Bonnet et al. 2003
Cameroon	Mengang	12.05	3.88 ⁱ	-8	1998	-8	2000	7.7	-8	-8	R	★(>14); area: degraded forest	Bonnet et al. 2003
Cameroon	Mengang district	-999.00	-99.00	-8	-8	-8	-8	33.0	-8	-8	R	◆(>4)	Boudin et al. 2005
Cameroon	Yaoundé, Messa quarter	-999.00	-99.00	10	1990	01	1993	18.6	-8	-8	U	◆(4-60)	Tchuinkam et al. 1993
Cameroon	Yaoundé, Messa quarter	-999.00	-99.00	-8	-8	-8	-8	12.8	-8	-8	U	membrane feeding with blood from 65 gametocyte carriers; ◆(6-36)	Mulder et al. 1994
Cameroon	Yaoundé, Messa quarter	-999.00	-99.00	-8	-8	-8	-8	12.8	-8	-8	U	membrane feeding with blood from 65 gametocyte carriers; ◆(6-36)	Mulder et al. 1994
Cameroon	Yaounde, urban district	-999.00	-99.00	-8	-8	-8	-8	20.0	-8	-8	U	◆(>4)	Boudin et al. 2005
Gambia, The	5 villages around Farafenni	-16.57	13.47 ^f	05	2003	10	2003	43.0	-8	-8	R	membrane feedings on blood following drug treatment	Nwakanma et al. 2008
Gambia, The	5 villages around Farafenni	-16.57	13.47 ^f	05	2003	10	2003	6.4	-8	-8	R	47 trials of membrane feeding on gametocyte carriers; ◆(5-45)	Nwakanma et al. 2008
Gambia, The	near Farafenni, north bank villages	-999.00	-99.00	-8	-8	-8	-8	56.5	-8	-8	-8	★(1-19)	Drakeley et al. 2000
Gambia, The	near Farafenni, north bank villages	-999.00	-99.00	-8	-8	-8	-8	80.0	-8	-8	-8	★(>19)	Drakeley et al. 2000
Ghana	-9	-999.00	-99.00	01	1952	10	1952	0.0	-8	-8	-9	★(>14) (two)	Muirhead-Thomson 1954
Ghana	-9	-999.00	-99.00	01	1952	10	1952	30.0	-8	-8	-9	★(0-14) (40)	Muirhead-Thomson 1954
Ghana	Accra	-999.00	-99.00	-8	-8	-8	-8	50.9	-8	-8	U	◆	Draper 1953
Ghana	Weija	-999.00	-99.00	01	1952	10	1952	26.6	-8	-8	R	★(0.8-10)	Muirhead-Thomson 1954
Liberia	-9	-999.00	-99.00	-9	-9	-9	-9	20.1	-8	-8	-9	★(>14)	Muirhead-Thomson 1957
Liberia	-9	-999.00	-99.00	-9	-9	-9	-9	21.6	-8	-8	-9	★(0-14)	Muirhead-Thomson 1957
Liberia	village	-999.00	-99.00	12	1955	11	1956	19.1	-8	-8	R	★(0-4)	Muirhead-Thomson 1957
Liberia	village	-999.00	-99.00	12	1955	11	1956	20.1	-8	-8	R	★(>14)	Muirhead-Thomson 1957
Liberia	village	-999.00	-99.00	12	1955	11	1956	23.3	-8	-8	R	★(5-14)	Muirhead-Thomson 1957
Nigeria	Kaduna area	-999.00	-99.00	05	1963	08	1963	20.0	-8	-8	R	low gametocyte density	Service 1965
Nigeria	Kaduna area	-999.00	-99.00	05	1963	08	1963	50.0	-8	-8	R	high gametocyte density	Service 1965
Nigeria	Lagos	-999.00	-99.00	-8	-8	-8	-8	46.6	-8	-8	U	*	Draper 1953
Nigeria	village in Yoruba country	-999.00	-99.00	11	1951	12	1951	9.0	-8	-8	R	★(0-10)	Draper 1953
Papua New Guinea	Buksak	-999.00	-99.00	02	1986	12	1986	48.1	-8	-8	R	-	Burkot et al. 1990
Papua New Guinea	Butelgut, Mebat, Sah, Buksak	-999.00	-99.00	-8	1985	-8	1985	37.9	-8	-8	R	◆	Graves et al. 1988
Senegal	Thies	-16.93	14.80 ⁱ	-8	-8	-8	-8	25.0	-8	-8	R	◆(>4)	Boudin et al. 2005
Tanzania	Kisegese	-999.00	-99.00	-8	-8	-8	-8	26.7	-8	-8	-8	★(>19)	Drakeley et al. 2000
Tanzania	Kisegese	-999.00	-99.00	-8	-8	-8	-8	44.1	-8	-8	-8	★(1-19)	Drakeley et al. 2000
Thailand	Phra Phutthabhat	100.8	14.72 ⁱ	06	1965	10	1967	23.2	-8	-8	-8	◆(12-60); rainy season	Rutledge et al. 1969
Thailand	Phra Phutthabhat	100.8	14.72 ⁱ	06	1965	10	1967	37.9	-8	-8	-8	◆(12-60); cool season	Rutledge et al. 1969
Thailand	Phra Phutthabhat	100.8	14.72 ⁱ	06	1965	10	1967	9.7	-8	-8	-8	◆(12-60); hot season	Rutledge et al. 1969

D.16 Mosquito-to-human transmission efficiency (b)

Tab. D.13: Data regarding the mosquito-to-human transmission efficiency (b). Columns: b_{ave} : average mosquito-to-human transmission efficiency; b_{min} : as b_{ave} , but for the minimum; b_{max} : as b_{ave} , but for the maximum; further information see Tab. D.2. Note that minimum and maximum values of b refer to monthly data.

country	place	long [°E]	lat [°N]	M1	YYY1	M2	YYY2	b_{ave} [%]	b_{min} [%]	b_{max} [%]	specie	note	ref
-	-	-999.00	-99.00	-8	-8	-8	-8	44.1	-8.0	-8.0	<i>An. gambiae</i>	in vitro transmitted sporozoites	Beier et al. 1991
-	-	-999.00	-99.00	-8	-8	-8	-8	49.2	-8.0	-8.0	<i>An. stephensi</i>	in vitro transmitted sporozoites	Beier et al. 1991
Kenya	Nyanza Province	-999.00	-99.00	08	1972	07	1973	1.5-2.6	-8.0	-8.0	<i>An. gambiae</i> , <i>An. funestus</i>	infants; neglected HBR age-dependence; ignored superinfection	Pull and Grab 1974
Kenya	Nyanza Province	-999.00	-99.00	08	1972	07	1973	5.4-9.3	-8.0	-8.0	<i>An. gambiae</i> , <i>An. funestus</i>	infants; ignored superinfection	Port et al. 1980
-	-	-999.00	-99.00	-8	-8	-8	-8	33.0	-8.0	-8.0	<i>An. stephensi</i>	★(25-39); without antimalarial immunity	Rickman et al. 1990
Kenya	Saradidi	-999.00	-99.00	02	1986	10	1987	7.5	1.0	28.0	<i>An. gambiae</i> , <i>An. arabiensis</i> , <i>An. funestus</i>	★(0.5-6); neglected HBR age-dependence; ignored superinfection	Beier et al. 1994
Uganda	Lira	-999.00	-99.00	-8	-8	-8	-8	5.0	-8.0	-8.0	<i>An. gambiae</i> , <i>An. funestus</i>	infants; neglected HBR age-dependence; ignored superinfection	Macdonald 1955, 1956
Tanzania	Mngeza	-999.00	-99.00	-8	-8	-8	-8	1.0	-8.0	-8.0	<i>An. gambiae</i> , <i>An. funestus</i>	infants; neglected HBR age-dependence; ignored superinfection	Macdonald 1955, 1956
Ethiopia	Gambela	-999.00	-99.00	12	1967	02	1969	-8.0	6.6	27.3	<i>An. arabiensis</i> , <i>An. funestus</i> , <i>An. nili</i>	★(<15); neglected HBR age-dependence; ignored superinfection; assumption: $r = 0.005$	Krafsur and Armstrong 1978
Ethiopia	Gambela	-999.00	-99.00	12	1967	02	1969	-8.0	4.8	13.3	<i>An. arabiensis</i> , <i>An. funestus</i> , <i>An. nili</i>	★(≥15); neglected HBR age-dependence; ignored superinfection; assumption: $r = 0.005$	Krafsur and Armstrong 1978
Senegal	Pikine	-17.40	14.75 ^b	01	1980	01	1981	-8.0	8.0	46.1	<i>An. arabiensis</i>	★(0.5-6); ignored superinfection	Vercrussse et al. 1983

D.17 Human Blood Index (*a*)

Tab. D.14: Data with regard to the human blood index (*a*). For further information see Tab. D.2.

country	place	long [°E]	lat [°N]	M1	YYY1	M2	YYY2	a [%]	specie	ref
Burkina Faso	Karangasso	-4.65	11.22 ^b	02	1985	02	1986	99.5	<i>An. gambiae</i>	Robert et al. 1988
Burkina Faso	Karangasso	-4.65	11.22 ^b	02	1985	02	1986	98.5	<i>An. funestus</i>	Robert et al. 1988
Burkina Faso	Karangasso	-4.65	11.22 ^b	02	1985	02	1986	0.0	<i>An. rufipes</i>	Robert et al. 1988
Dominican Republic	Calle Duarte, Colonia Japonesa, La Bomba	-999.00	-99.00	07	1987	10	1988	8.0	<i>An. albimanus</i>	Mekuria et al. 1991
Dominican Republic	Calle Duarte, Colonia Japonesa, La Bomba	-999.00	-99.00	07	1987	10	1988	12.0	<i>An. albimanus</i>	Mekuria et al. 1991
Gambia, The	12 villages	-999.00	-99.00	-9	-9	-9	-9	38.3	<i>An. gambiae s.l.</i>	Killeen et al. 2001
Kenya	4 villages in Mumias	-999.00	-99.00	-8	1995	-8	1996	95.9	<i>An. gambiae s.l.</i> , <i>An. funestus</i>	Shililu et al. 1998
Kenya	Nyanza Province	-999.00	-99.00	08	1972	07	1973	95.0	<i>An. gambiae</i>	Pull and Grab 1974
Kenya	Nyanza Province	-999.00	-99.00	08	1972	07	1973	99.0	<i>An. funestus</i>	Pull and Grab 1974
Korea	Baekyeon-ri and Paju	-999.00	-99.00	06	2000	08	2000	0.8	<i>An. sinensis</i>	Lee et al. 2001
Nigeria	Jirima, village	-999.00	-99.00	08	1972	09	1972	100.0	<i>An. gambiae s.s.</i>	Garrett-Jones et al. 1980
Nigeria	Jirima, camp	-999.00	-99.00	08	1972	09	1972	78.6	<i>An. gambiae s.s.</i>	Garrett-Jones et al. 1980
Nigeria	Jirima, village	-999.00	-99.00	08	1972	09	1972	82.9	<i>An. arabiensis</i>	Garrett-Jones et al. 1980
Nigeria	Jirima, camp	-999.00	-99.00	08	1972	09	1972	30.4	<i>An. arabiensis</i>	Garrett-Jones et al. 1980
Nigeria	Lagos, Lemu suburb	3.37	6.47 ^a	01	2000	12	2000	77.6	<i>An. gambiae s.s.</i>	Awolola et al. 2002
Nigeria	Kankiya, sprayed area	-999.00	-99.00	-9	1963	-9	1964	63.0	<i>An. gambiae</i>	Garrett-Jones and Shidrawi 1969
Nigeria	Kankiya, unsprayed area	-999.00	-99.00	-9	1963	-9	1964	75.0	<i>An. gambiae</i>	Garrett-Jones and Shidrawi 1969
Sierra Leone	Njala-Komboya	-11.54	8.20 ^b	01	1990	04	1991	100.0	<i>An. gambiae s.s.</i>	Bockarie et al. 1994
Sierra Leone	Nyandeyama	-11.66	8.12 ^b	01	1990	04	1991	99.0	<i>An. gambiae s.s.</i>	Bockarie et al. 1994
Sierra Leone	Mendewa	-11.48	8.16 ^b	01	1990	04	1991	97.0	<i>An. gambiae s.s.</i>	Bockarie et al. 1994
Sierra Leone	Nengbema	-11.68	8.13 ^b	01	1990	04	1991	100.0	<i>An. gambiae s.s.</i>	Bockarie et al. 1994
Senegal	Dielmo	-16.42	13.72 ^b	07	1997	09	1997	29.6	<i>An. arabiensis</i>	Diatta et al. 1998
Senegal	Dielmo	-16.42	13.72 ^b	07	1997	09	1997	30.3	<i>An. gambiae</i>	Diatta et al. 1998
Senegal	Pikine	-17.40	14.75 ^b	12	1979	12	1980	90.0	<i>An. arabiensis</i>	Vercruysse et al. 1983
Tanzania	Segera	-999.00	-99.00	-8	-8	-8	-8	38.3	<i>An. arabiensis</i>	Killeen et al. 2001
Tanzania	Segera	-999.00	-99.00	-8	-8	-8	-8	99.0	<i>An. funestus</i>	Killeen et al. 2001
Tanzania	Segera	-999.00	-99.00	-8	-8	-8	-8	97.9	<i>An. gambiae s.s.</i>	Killeen et al. 2001
Tanzania	southern slopes of Eastern Usambara Mountains	-999.00	-99.00	09	1952	12	1952	100.0	<i>An. funestus</i>	Davidson and Draper 1953
Tanzania	southern slopes of Eastern Usambara Mountains	-999.00	-99.00	09	1952	12	1952	100.0	<i>An. gambiae</i>	Davidson and Draper 1953
Tanzania	southern slopes of Eastern Usambara Mountains	-999.00	-99.00	09	1952	12	1952	93.3	<i>An. marshalli</i>	Davidson and Draper 1953

D.18 Human Infectious Age (*HIA*)

Tab. D.15: Data with regard to the Human Infectious Age (*HIA*). Columns: PMA: asexual malaria parasite mature age; Pmethod: method of asexual malaria parasite detection; GMA: gametocyte mature age, that is the duration of gametocytogenesis; Gmethod: method of gametocyte detection; further information see Tab.D.2.

PMA [days]	Pmethod	GMA [days]	Gmethod	note	ref
8 (median)	microscope	-8.0	-8	malaria therapy patients	Collins and Jeffery 1999
-9	-9	10.0-14.0	microscope	-	Day et al. 1998
-9	-9	11.0	microscope	GMA: duration between first day of symptoms and gametocyte appearance	Garnham 1949
9.8/10.3/13.0	-9	11.5 (large majority: 10-13)	microscope	PMA: Santee-Cooper/Panama/McLendon strain of <i>P. falciparum</i> ; GMA: duration between the first occurrence of asexual parasites and gametocyte appearance	Jeffery et al. 1959
-9	-9	11.7 (range: 6.0-30.0)	microscope	GMA: duration between first day of symptoms and gametocyte appearance	Miller 1958
9.0-11.0	QBC tube and microscope	-9	-9	PMA: days after infection when tests showed positive results	Rickman et al. 1989
6.5-7.0	presence established in culture	-9	-9	vaccinated and non-vaccinated volunteers	Murphy et al. 1989
14.0-16.5	microscope	-9	-9	patients without antimalarial immunity	Rickman et al. 1990
6.0-7.0	QT-NASBA	-9	-9	experimental infection	Schneider et al. 2005
8.3	microscope	-9	-9	experimental infection	Schneider et al. 2005
-9	-9	10.0	microscope	GMA: duration between first day of fever and gametocyte appearance	Shute and Maryon 1951

E LMM validation and settings

E.1 Definition of the validation

The LMM is validated under weather conditions of meteorological stations in West Africa and Cameroon (Tab. G.1). Malaria simulations are checked against observations of eleven different entomological and parasitological variables. A skill score with regard to every variable as well as to their ensemble ($SC(x)$ and $SC(all)$, respectively) is assigned to every parameter setting of the model.

These comprise the following entomological variables: the human biting ratio (HBR_a), the annual average circumsporozoite protein rate ($CSPR_a$), the annual entomological inoculation rate (EIR_a), and five variables of the malaria season ($SSeas$: season start; $ESeas$: end month; $Seas$: duration of the malaria season; $MSeas$: number of months in which 75% of EIR_a is transmitted; $XSeas$: month of maximum transmission; see App. D.5 for the definition of the simulated malaria seasonality). Also three parasitological variables are included: the annual mean (PR_a), the annual minimum ($PR_{min,a}$), as well as the annual maximum ($PR_{max,a}$) of the asexual parasite ratio.

The evaluation of single model runs is only performed at stations featuring data from malaria field studies. Each simulation at a particular station produces 34 annual values for every considered variable (e.g., EIR_a). On the other hand, entomological data are never measured continuously because of the amount of work required in practice (Chalvet-Monfray et al. 2007). Due to the lack of long time series observations only few data values (if any at all) are available for considered stations (Tabs. D.5, D.4 & D.3). Only data from rural field sites are used for the LMM validation (cp. App. D). Note that field measurements are not performed at the weather stations' location. However, data in the area of the station or from about the same climatic zone is available (Fig. 3.1; see also App. D). In this context, it must be noted that precipitation rates can differ greatly between locations just few kilometres apart, but meteorological stations are much more sparsely distributed (Shaman and Day 2005; Balme et al. 2006; Sec. 4.1.2). Also partially different environmental conditions (e.g., state of ground) make a year-to-year comparison between simulations and field observations impossible. Gerbaux and Bicout (2008), for instance, showed that taking precipitation at some kilometres off the study site can lead to an important error in mosquito production prevision. Shaman and Day (2005) allude to the mismatch between scales at which disease vectors response to hydrologic variability and scales at which hydrologic variability is actually monitored. For all these reasons, a reproduction of the year-to-year variability is not expected. However, the evaluation procedure claims that LMM simulations are comparable to field observations. The following five criteria are applied:

The evaluation of model runs takes the number of available observations into account. Stations with many observations contribute more to the calculated skill score than stations with fewer field measurements (cp. Tab. E.1). The method also makes allowances for the uncertainty of the year-to-year variability. A proper analysis would only

#	name	description	n_{obs}	points
1	overlap	any observation is included in the simulated range	≥ 1	+1
2	enclosure	every observation is included in the simulated range	≥ 2	+1
3a	median enclosure	the observed median is included in the simulated range	≥ 3	+1
4a	median quartile enclosure	the observed median is located within the lower and upper quartile of the simulations	≥ 5	+1
5a	penalty	the simulations exceed the one and a half time maximum of all field observations	≥ 1	-5
3b	frequency	the maximum number of observations and simulations is found in the same month or the observations and simulations reveal most frequently no (year-round) transmission, respectively	≥ 3	+1

Tab. E.1: Criteria in terms of the evaluation of LMM simulations which are based on field observations in the area of synoptic stations. Malaria runs are rated separately for each station. Every fulfilled criterion increases the score of such a model run by one point. The sum of achieved points at all stations and from eleven entomological and parasitological variables finally add to the skill score of a particular LMM setting ($SC(\text{all})$). Note, criteria 1, 2, and 3b are valid for *SSeas*, *ESeas*, and *XSeas*, whereas criteria 1, 2, 3a, and 4a are applied for the rest of the variables. Criterion 5a is only used for the computation of $SC(HBR_a)$ and $SC(EIR_a)$. Columns: #: criteria number; name: short term; description: criteria description; n_{obs} : the lowest number of available observations needed to fulfil the criterion; points: assigned number of points.

be possible for numerous available observations. In fact, an estimate of the frequency distribution is not feasible by few records.

The computed skill score is based on the probability that observations fall into certain ranges of simulations. It is expected that any observation is included in the range of model simulations (1st criterion: overlap). Of course, the model setting performs better when every observation is enclosed in the simulated range (2nd criterion: enclosure). For at least three available records also the observed median is calculated. The confidence in the model setting increases when the observed median is contained in the span of model simulations (criterion 3a: median enclosure). Reliability of the median estimate increases the more field measurements exist. Only for at least five available records the condition is called that the observed median falls within the lower (25th percentile) and upper quartile (75th percentile) of 34 simulated values (criterion 4a: median quartile enclosure).

The hitherto rating system might favour model settings generating unrealistic high values and a strong interannual variation. This fact is inhibited by another criterion that eliminates unrealistic high entomological values (criterion 5a: penalty). Five penalty points are applied to the skill score of HBR_a and EIR_a , when any simulated value ex-

ceeds the one and a half time maximum of all available field measurements. This threshold seems to be a reasonable measure for the restriction of simulated values. Model settings with unrealistic high biting rates (HBR_a and EIR_a values) are rejected.

Due to the possibility of no and year-round transmission the 3rd, 4th, and 5th criteria are not applied for the evaluation of the start ($SSeas$) and end of the malaria season ($ESeas$), as well as the month with maximum transmission ($XSeas$). For these variables, the maximum of the frequency distribution is compared (criterion 3b: frequency). A point is assigned to the model setting when observations and simulations show mostly no (year-round) transmission. In case that the majority of observations exhibits neither a year-round nor no transmission, it was checked if the month with the maximum number of observations agrees with that of the simulation (e.g., $XSeas$ is mostly observed and simulated for August).

E.2 Figures and tables with regard to the LMM calibration

First experiment

rank	CAP	# E_p	S	U_2	$SC(HBR_a)$	$SC(EIR_a)$	$SC(HBR_a, EIR_a)$	$SC(all)$
1	750	50	5	500	34 (52)	39 (54)	73 (106)	251 (440)
2	750	50	10	500	31 (52)	41 (54)	72 (106)	256 (440)
3	500	75	15	500	31 (52)	38 (54)	69 (106)	256 (440)
4	500	100	15	500	36 (52)	32 (54)	68 (106)	246 (440)
5	500	75	10	500	34 (52)	33 (54)	67 (106)	245 (440)
6	250	150	15	500	32 (52)	34 (54)	66 (106)	240 (440)
	250	125	15	500	29 (52)	37 (54)	66 (106)	243 (440)
8	750	75	20	500	31 (52)	34 (54)	65 (106)	255 (440)
	1000	50	10	500	35 (52)	30 (54)	65 (106)	251 (440)
10	500	100	20	500	30 (52)	34 (54)	64 (106)	255 (440)
296	2000	150	5	500	-15 (52)	-57 (54)	-72 (106)	74 (440)
297	2000	125	5	1000	-17 (52)	-56 (54)	-73 (106)	64 (440)
298	2000	150	10	1000	-21 (52)	-53 (54)	-74 (106)	78 (440)
299	2000	150	5	750	-22 (52)	-61 (54)	-83 (106)	54 (440)
300	2000	150	5	1000	-23 (52)	-62 (54)	-85 (106)	50 (440)

Tab. E.2: Top 10 and last 5 of 300 malaria runs from the first calibration experiment according to the skill score relative to HBR_a and EIR_a . Numbers in brackets refer to points that could be theoretically achieved. Note that p_{d_1} is set to zero in initial runs. Columns: rank: ranking with regard to $SC(HBR_a, EIR_a)$; CAP: setting of CAP (in the number of fertile females); # E_p : setting of # E_p (in the number of eggs); S: setting of S (in mm); U_2 : setting of U_2 (in mm). $SC(x)$ denotes the skill score with regard to variable x .

rank	CAP	#E _p	S	U ₂	SC(HBR _a)	SC(CSPR _a)	SC(EIR _a)	SC(Seas)	SC(XSeas)	SC(MSeas)	SC(SSeas)	SC(ESeas)	SC(PR _a)	SC(PR _{max,a})	SC(PR _{min,a})	SC(all)
1	750	75	30	500	27 (52)	27 (55)	34 (54)	33 (42)	19 (41)	33 (37)	26 (41)	24 (37)	13 (29)	16 (25)	7 (27)	259 (440)
2	1000	50	15	500	29 (52)	32 (55)	32 (54)	32 (42)	18 (41)	29 (37)	28 (41)	21 (37)	14 (29)	15 (25)	8 (27)	258 (440)
3	250	150	30	500	23 (52)	32 (55)	35 (54)	30 (42)	21 (41)	30 (37)	29 (41)	21 (37)	13 (29)	15 (25)	8 (27)	257 (440)
4	750	50	10	500	31 (52)	28 (55)	41 (54)	31 (42)	19 (41)	29 (37)	26 (41)	17 (37)	13 (29)	13 (25)	8 (27)	256 (440)
	500	75	15	500	31 (52)	31 (55)	38 (54)	25 (42)	20 (41)	30 (37)	27 (41)	17 (37)	15 (29)	14 (25)	8 (27)	256 (440)
6	750	75	20	500	31 (52)	30 (55)	34 (54)	29 (42)	20 (41)	30 (37)	28 (41)	19 (37)	13 (29)	13 (25)	8 (27)	255 (440)
	750	50	15	500	24 (52)	30 (55)	36 (54)	32 (42)	18 (41)	29 (37)	28 (41)	21 (37)	14 (29)	15 (25)	8 (27)	255 (440)
	500	150	30	500	32 (52)	33 (55)	29 (54)	29 (42)	21 (41)	27 (37)	29 (41)	21 (37)	12 (29)	14 (25)	8 (27)	255 (440)
	500	100	20	500	30 (52)	31 (55)	34 (54)	29 (42)	20 (41)	30 (37)	29 (41)	18 (37)	13 (29)	13 (25)	8 (27)	255 (440)
10	1000	75	30	500	29 (52)	23 (55)	29 (54)	33 (42)	19 (41)	33 (37)	26 (41)	24 (37)	14 (29)	17 (25)	7 (27)	254 (440)

Tab. E.3: As Tab. E.2, but for the skill score of all variables.

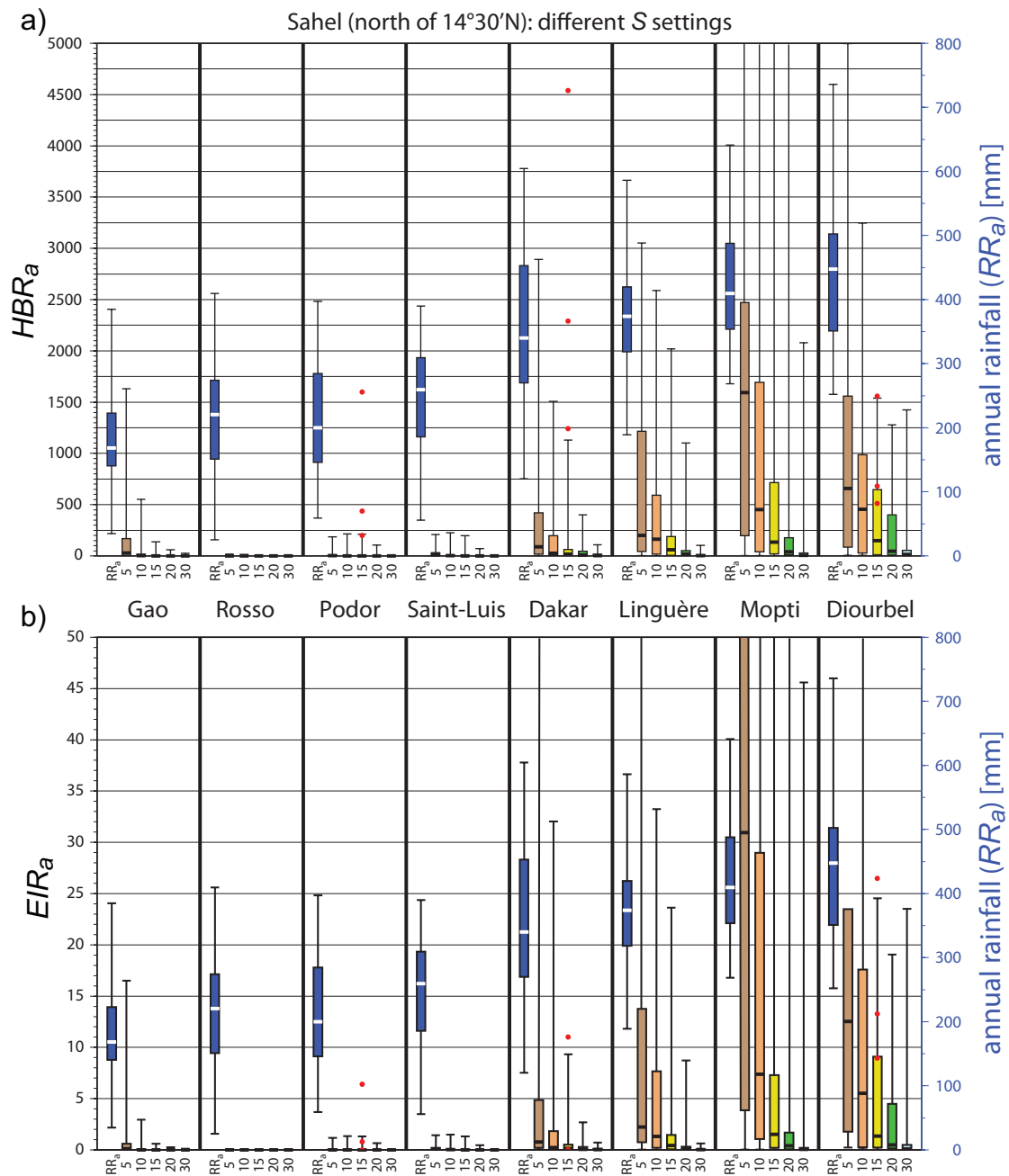
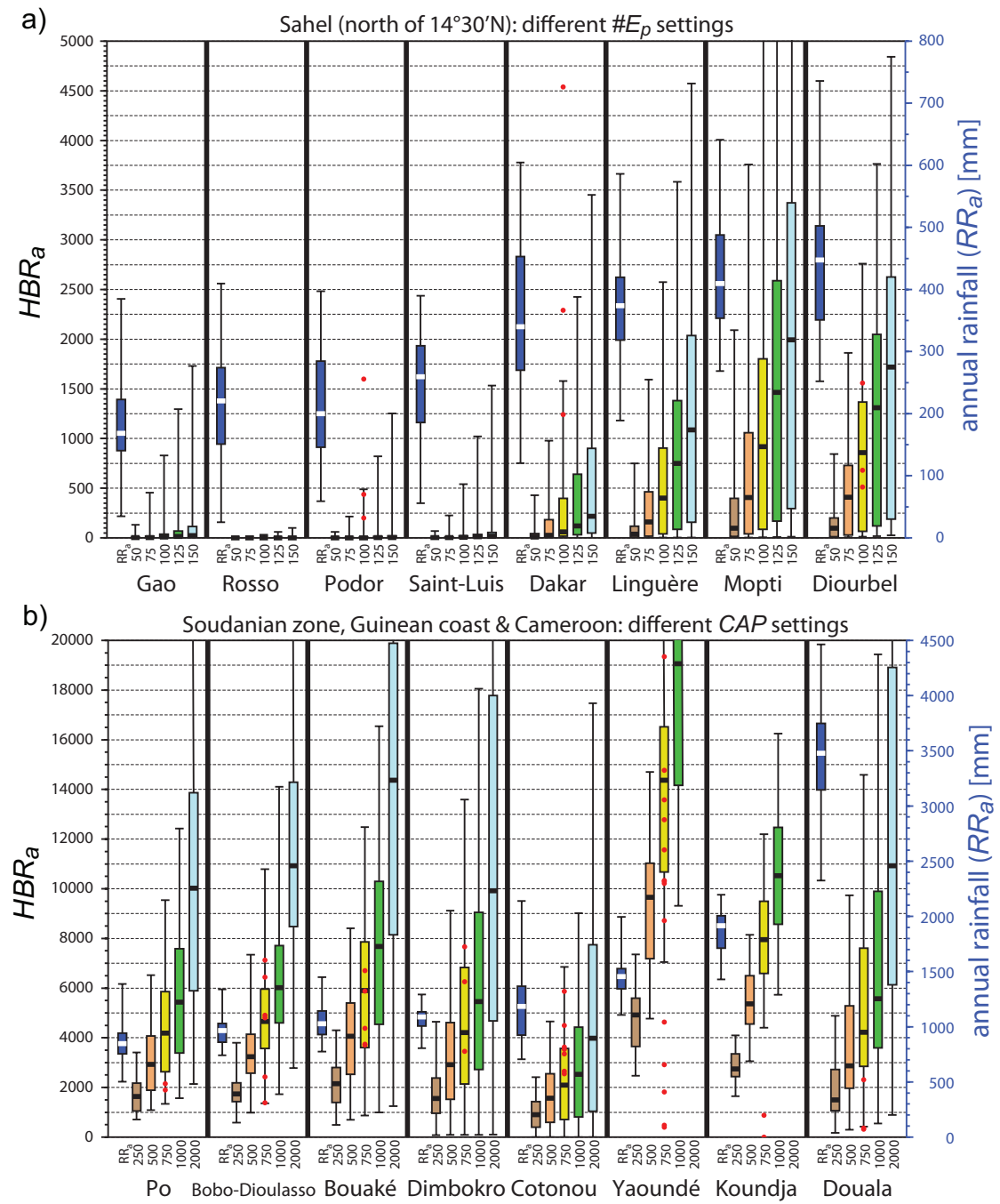


Fig. E.1: Box-and-whisker plots of (a) HBR_a and (b) EIR_a values of five different LMM settings with regard to 34 EIR_a values between 1973 and 2006 relative to eight synoptic stations of the Sahel (north of 14°30'N; cp. Tab.G.1). Different settings of S are represented by varying colours (brown to light blue box plots). Note that various simulated values outrange the scale of the figures. LMM setting: cp. val_n in Tab.5.1, but: $p_{d\downarrow}=0\%$; $CAP=1000$ fertile females; $S=5, 10, 15, 20$, and 30 mm. Red dots depict available field measurements (cp. Tab.D.3). In addition, the statistic relative to RR_a is illustrated for each station (dark blue; right scale).



Second experiment

rank	CAP	$p_{d\downarrow}$	$\#E_p$	$SC(HBR_a)$	$SC(EIR_a)$	$SC(HBR_a, EIR_a)$	$SC(all)$
1	400	-10	120	37 (52)	41 (54)	78 (106)	279 (440)
2	700	-7.5	70	34 (52)	41 (54)	75 (106)	270 (440)
	650	-10	80	34 (52)	41 (54)	75 (106)	268 (440)
	550	-10	90	35 (52)	40 (54)	75 (106)	274 (440)
	500	-10	90	35 (52)	40 (54)	75 (106)	272 (440)
	500	-10	100	35 (52)	40 (54)	75 (106)	272 (440)
	500	-7.5	90	35 (52)	40 (54)	75 (106)	277 (440)
	350	-10	130	35 (52)	40 (54)	75 (106)	281 (440)
9	750	-10	70	34 (52)	40 (54)	74 (106)	266 (440)
	700	-10	70	34 (52)	40 (54)	74 (106)	266 (440)

Tab. E.4: As Tab. E.2, but only for the top 10 of 455 malaria runs from the second calibration experiment. Note that in the second set of runs S and U_2 are set to 10 and 500 mm, respectively. Columns: $p_{d\downarrow}$: setting of $p_{d\downarrow}$ (in %) and see Tab. E.2.

rank	CAP	$p_{d\downarrow}$	$\#E_p$	$SC(HBR_a)$	$SC(CSPR_a)$	$SC(EIR_a)$	$SC(Seas)$	$SC(XSeas)$	$SC(MSeas)$	$SC(SSeas)$	$SC(ESeas)$	$SC(PR_a)$	$SC(PR_{max,a})$	$SC(PR_{min,a})$	$SC(all)$
1	350	-7.5	120	34 (52)	32 (55)	40 (54)	32 (42)	22 (41)	30 (37)	30 (41)	22 (37)	16 (29)	16 (25)	8 (27)	282 (440)
	300	-7.5	130	33 (52)	33 (55)	40 (54)	32 (42)	23 (41)	30 (37)	30 (41)	22 (37)	16 (29)	15 (25)	8 (27)	282 (440)
3	350	-10	130	35 (52)	33 (55)	40 (54)	31 (42)	23 (41)	29 (37)	30 (41)	20 (37)	16 (29)	16 (25)	8 (27)	281 (440)
4	450	-7.5	100	34 (52)	32 (55)	40 (54)	32 (42)	21 (41)	28 (37)	31 (41)	22 (37)	16 (29)	15 (25)	8 (27)	279 (440)
	400	-10	120	37 (52)	33 (55)	41 (54)	31 (42)	23 (41)	28 (37)	28 (41)	18 (37)	16 (29)	16 (25)	8 (27)	279 (440)
	400	-7.5	110	34 (52)	30 (55)	40 (54)	32 (42)	22 (41)	29 (37)	30 (41)	22 (37)	16 (29)	16 (25)	8 (27)	279 (440)
7	800	-7.5	80	35 (52)	32 (55)	36 (54)	34 (42)	20 (41)	27 (37)	31 (41)	22 (37)	17 (29)	16 (25)	8 (27)	278 (440)
	400	-7.5	120	34 (52)	32 (55)	35 (54)	33 (42)	22 (41)	29 (37)	30 (41)	23 (37)	16 (29)	16 (25)	8 (27)	278 (440)
	350	-7.5	130	34 (52)	33 (55)	35 (54)	33 (42)	22 (41)	30 (37)	30 (41)	23 (37)	16 (29)	14 (25)	8 (27)	278 (440)
	350	-5	110	32 (52)	34 (55)	40 (54)	28 (42)	23 (41)	31 (37)	31 (41)	21 (37)	16 (29)	14 (25)	8 (27)	278 (440)

Tab. E.5: As Tab. E.3, but for the top 10 of 455 malaria runs from the second calibration experiment. Note that in the second set of runs S and U_2 are set to 10 and 500 mm, respectively. Columns: $p_{d\downarrow}$: setting of $p_{d\downarrow}$ (in %) and see Tab. E.3

E.3 Figures in terms of the LMM_n validation

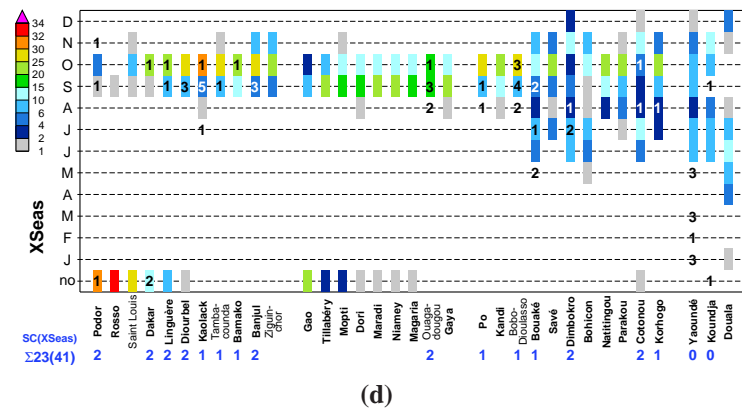
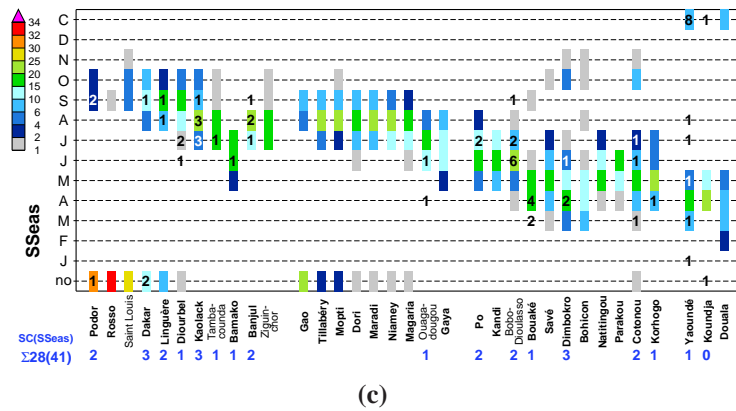
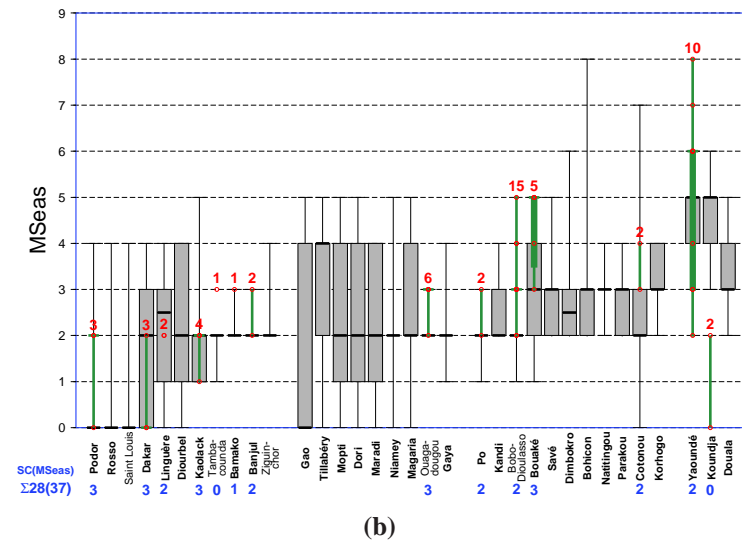
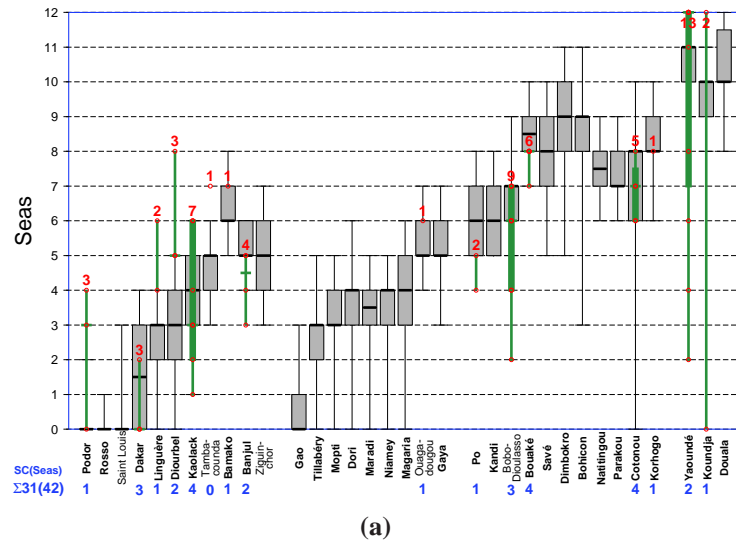


Fig. E.3: Validation of LMM_n simulations in terms of (a) $Seas$, (b) $MSeas$, (c) $SSeas$, and (d) $XSeas$ in West Africa and Cameroon. See Figs. 6.3 & 6.4 for further details.

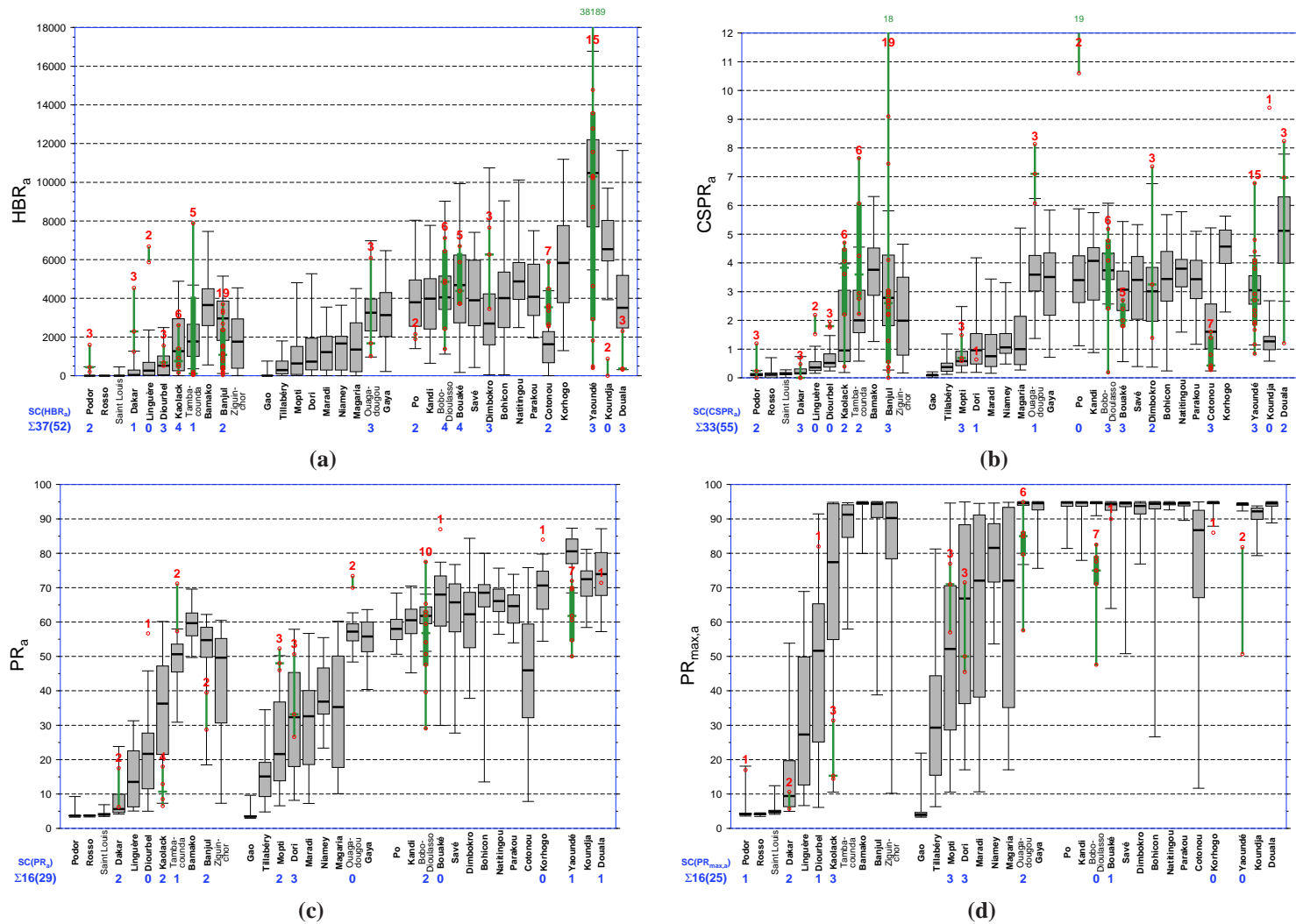


Fig. E.4: Validation of LMM_n simulations in terms of (a) HBR_a , (b) $CSPR_a$, (c) PR_a , and (d) $PR_{max,a}$. See Fig. 6.4 for further details.

E.4 Figures in terms of the LMM_0 validation

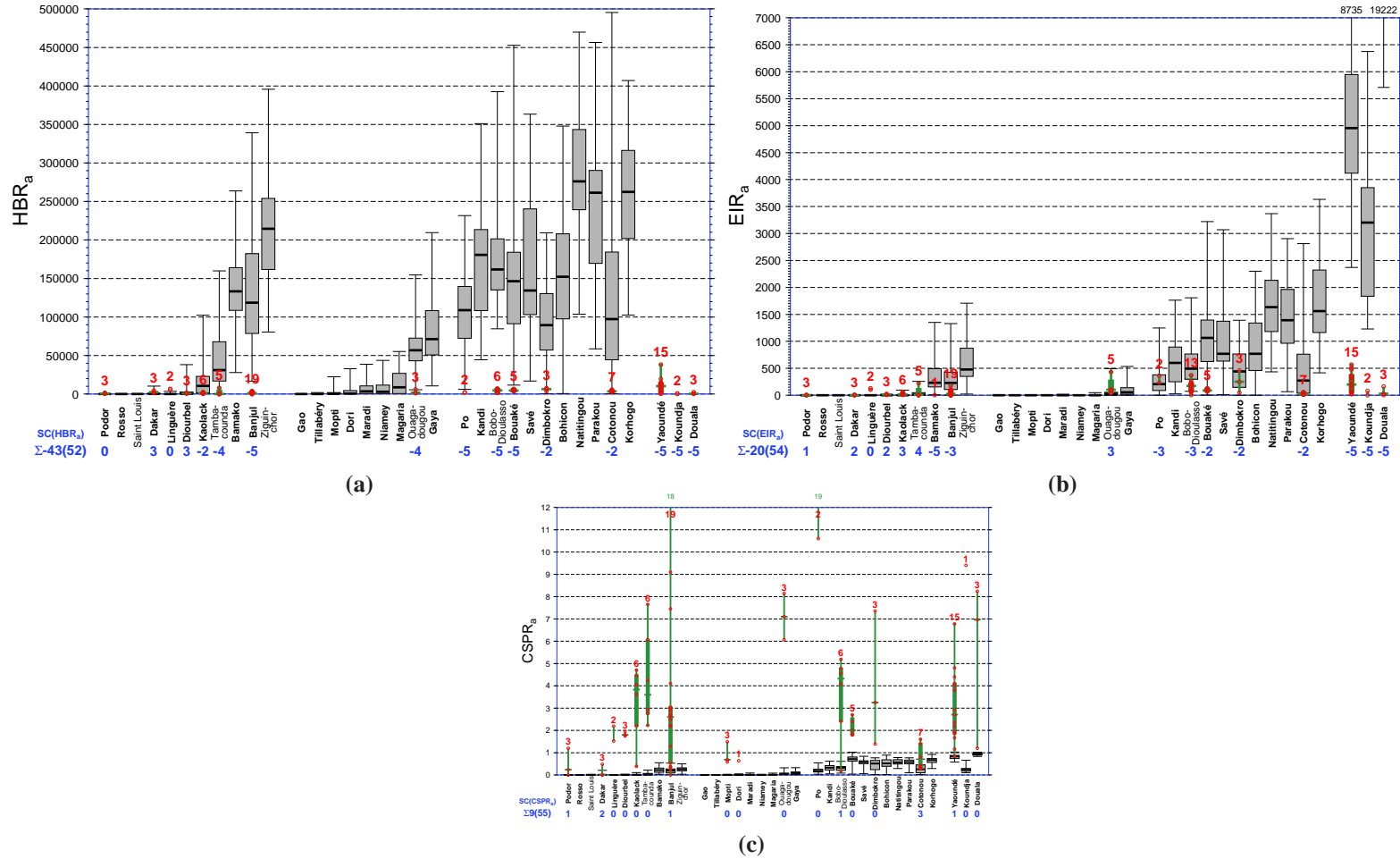


Fig. E.5: Validation of LMM_0 simulations in terms of (a) HBR_a , (b) EIR_a , and (c) $CSPrA$ in West Africa and Cameroon. Note that for HBR_a the box plots of Yaoundé (range: 379,174-1,008,218), Koundja (range: 749,544-1,454,845), and Douala (range: 678395-2,122,510) completely outrange the scale of the figure. See Fig. 6.4 for further details.

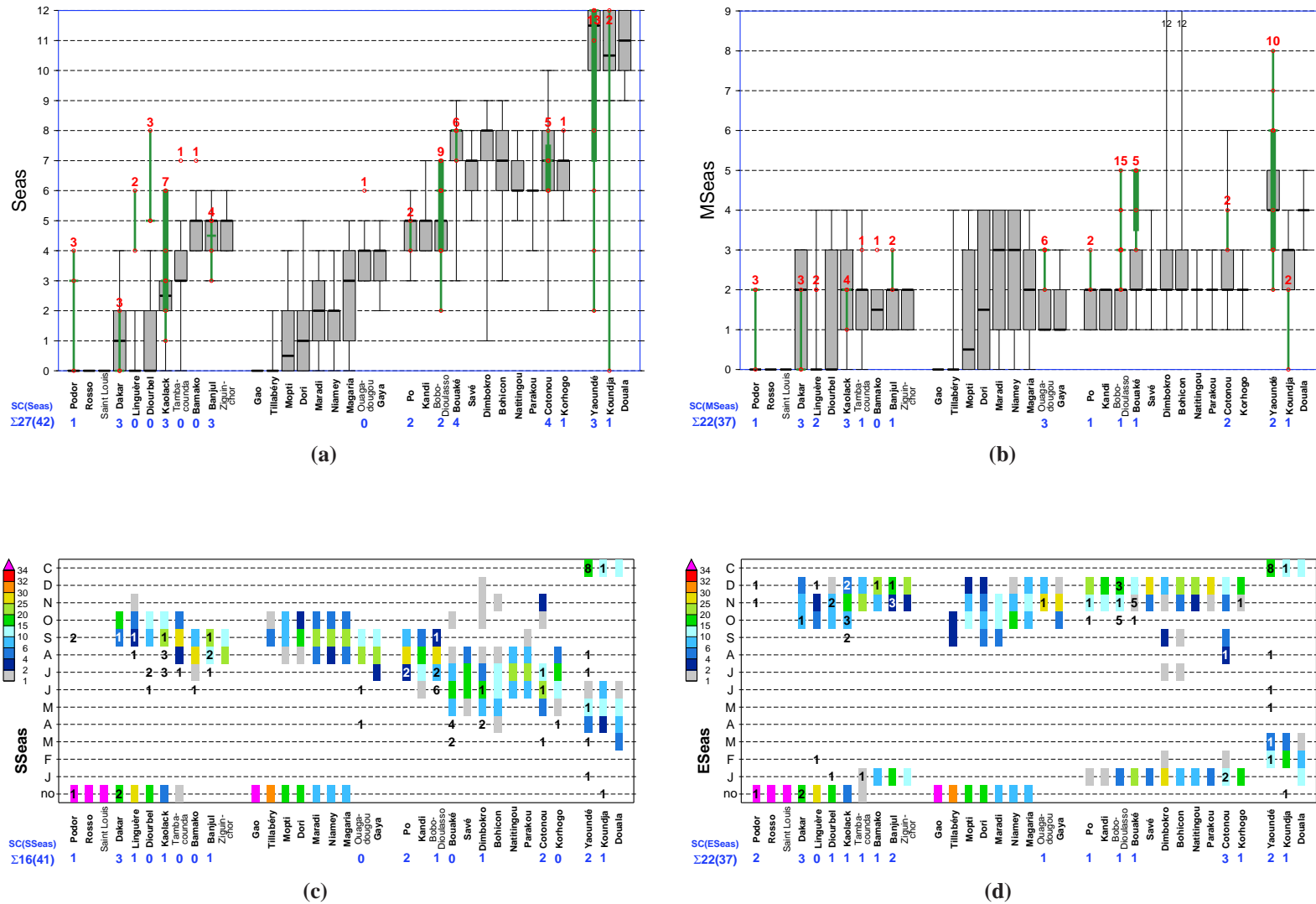


Fig. E.6: Validation of LMM₀ simulations in terms of (a) *Seas*, (b) *MSeas*, (c) *SSeas*, and (d) *ESeas*. See Figs. 6.3 & 6.4 for further details.

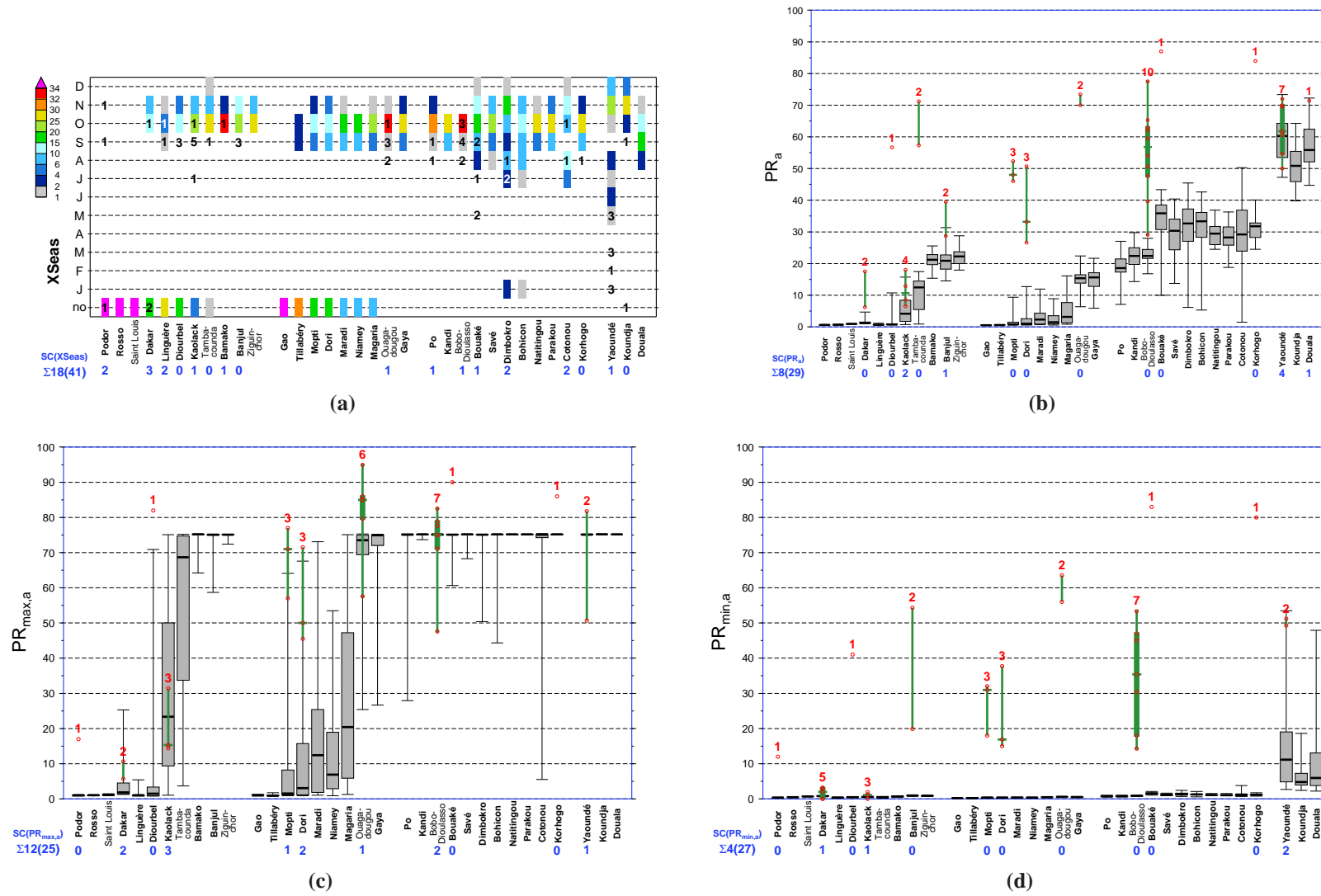


Fig. E.7: Validation of LMM_0 simulations in terms of (a) X_{Seas} , (b) PR_a , (c) $PR_{max,a}$, and (d) $PR_{min,a}$. See Figs. 6.3 & 6.4 for further details.

E.5 Spin-up period of the LMM

The modelling of malaria requires realistic initial conditions. At the beginning of each simulation most state array elements of the LMM are initially empty. For this reason, it is necessary to spin up the model for a simulation period. Jones (2007) found that a running-in period of one to two years achieved suitable starting conditions for the LMM₀. However, the length of the required spin-up depends primarily on the setting of the recovery rate (r). Due to the comparatively large value of r in the original model version almost the entire population clears the malaria parasite during the dry season (Fig. E.7d). This implies that malaria transmission in the following rainy season is basically independent from the history of malaria. Nevertheless, r is significantly reduced in the LMM_n version causing a much higher prevalence at the end of the dry season (cp. Fig. 6.5). The spread of malaria in this model version hence strongly depends on the intensity of former transmission seasons. As a consequence, a longer running-in period is required for the LMM_n version.

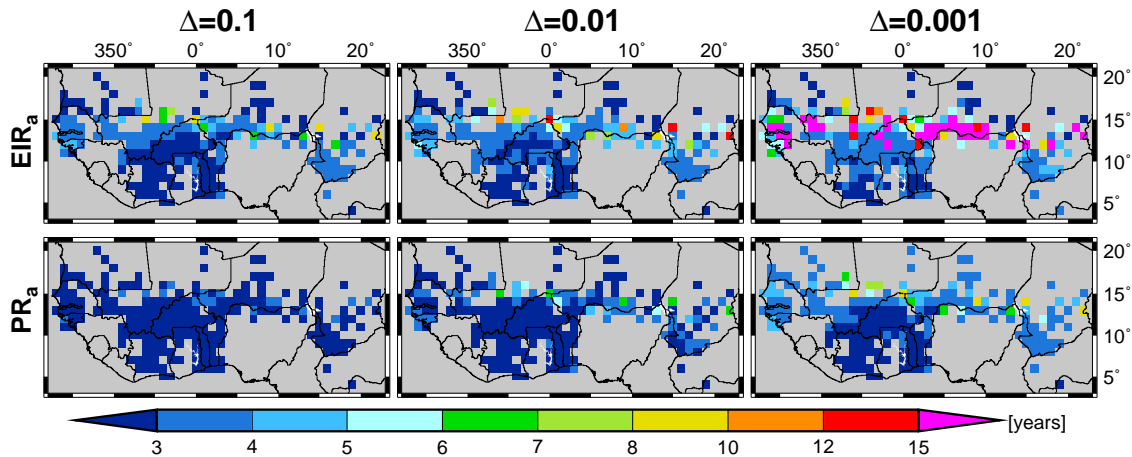


Fig. E.8: Results of the LMM_n spin-up test as driven 30 times by the IRD precipitation and ERA40 temperature data from 1968. Illustrated is the number of years relative to EIR_a (first row; in infective bites day⁻¹) and PR_a (second row; in %) when the yearly difference falls below 0.1, 0.01, or 0.001 for every day of the year.

The length of the proper LMM_n spin-up period was determined via rainfall and temperature data from IRD and ERA40. A LMM_n run was performed using the same daily values of 1968 for 30 years. The suitable running-in period is found when equilibrium is reached in the model. This status is achieved when a yearly pattern repeats itself year after year. The simulated data was evaluated for EIR_a and PR_a values. The experiment shows that south of about 10°N stable oscillation with regard to EIR_a and PR_a is at least reached after three years (Fig. E.8). However, in terms of EIR_a the atmospheric conditions between about 10-16°N require a much longer spin-up. Equilibrium is reached within 15 years for every grid box relative to a threshold of 0.01 infective bites. A numerical oscillation was found around the lowest threshold of 0.001 infective bites day⁻¹. An initial running-in period of 20 years seems hence sufficient for LMM_n simulations⁴.

⁴Note that for the setting and sensitivity tests of the LMM_n a different spin-up period of 13 years was used. In this case, reconstructed time series for 1960-1972 served as running-in data.

F Supplementary figures

F.1 Data from CRU

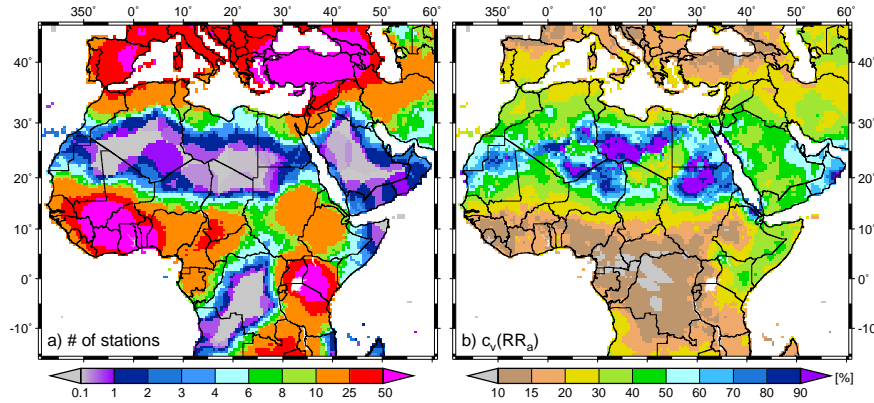


Fig. F.1: (a) Number of stations within the range of grid boxes with regard to CRU precipitation averaged for 1960-2000. The ‘term’ range refers to the correlation decay distance of 450 km assumed for rainfall (New et al. 2000). Note that values do not record the number of stations contributing information to a grid-box, they rather show the number of stations with information upon which the value of the grid box may have been computed, if necessary. (b) Coefficient of variation of RR_a with regard to CRU for 1960-2000.

F.2 Standardised rainfall anomalies

The standardised annual rainfall anomaly ($index(i)$) for a given year i is calculated by dividing the annual rainfall anomaly with respect to the mean of the base period 1960-2000 ($RR_a^{1960-2000}$) by the standard deviation of the base period ($\sigma(RR_a)^{1960-2000}$):

$$index(i) = \frac{RR_a(i) - RR_a^{1960-2000}}{\sigma(RR_a)^{1960-2000}} \quad (8.1)$$

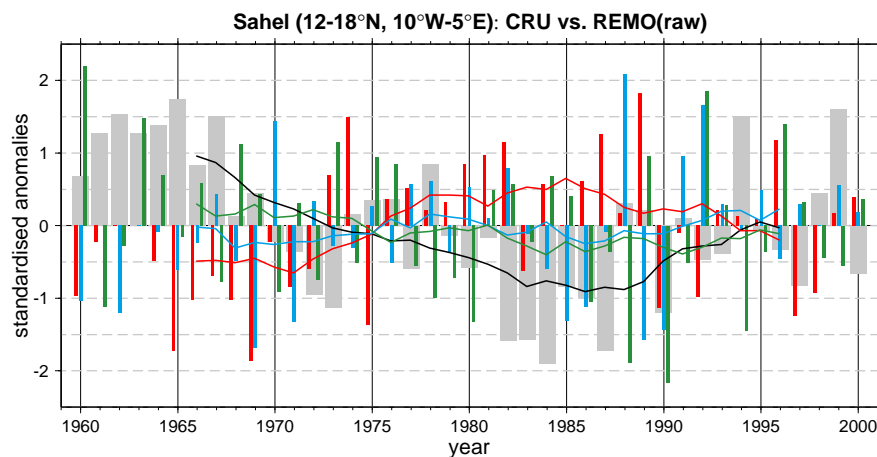


Fig. F.2: Standardised annual precipitation anomalies (Eq. 8.1) with regard to 1960-2000 for CRU (thick black bars) as well as REMO(raw) or REMO(cor) (thin red, green, and blue bars) for the Sahel. For each time series also the 11-year running mean of standardised anomalies is illustrated.

F.3 Monthly REMO temperature and precipitation data

The following two figures provide information that is helpful for the analysis of LMM_n and MSM simulations. The monthly temperature and precipitation data illustrates variable atmospheric conditions in Africa during the course of the year. Additionally, projected atmospheric changes are presented for two decades of the future period. These images enable the understanding of the altered spread of malaria.

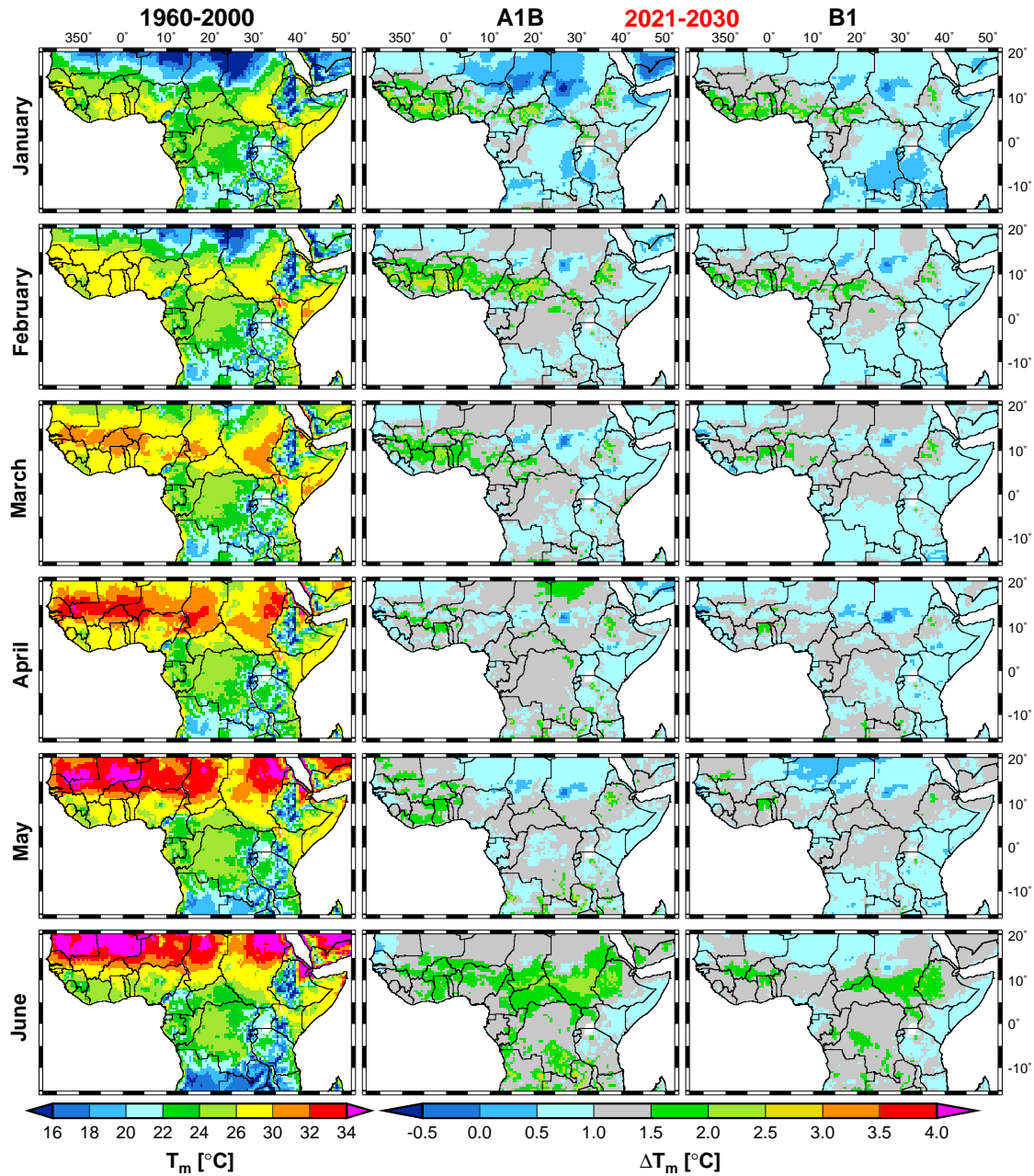


Fig. F.3: Monthly REMO(cor) temperatures (T_m) of the present-day climate (1960-2000) as well as for the difference (ΔT_m) between present-day temperatures and that of 2021-2030 from the A1B as well as B1 scenario (continued on the next page).

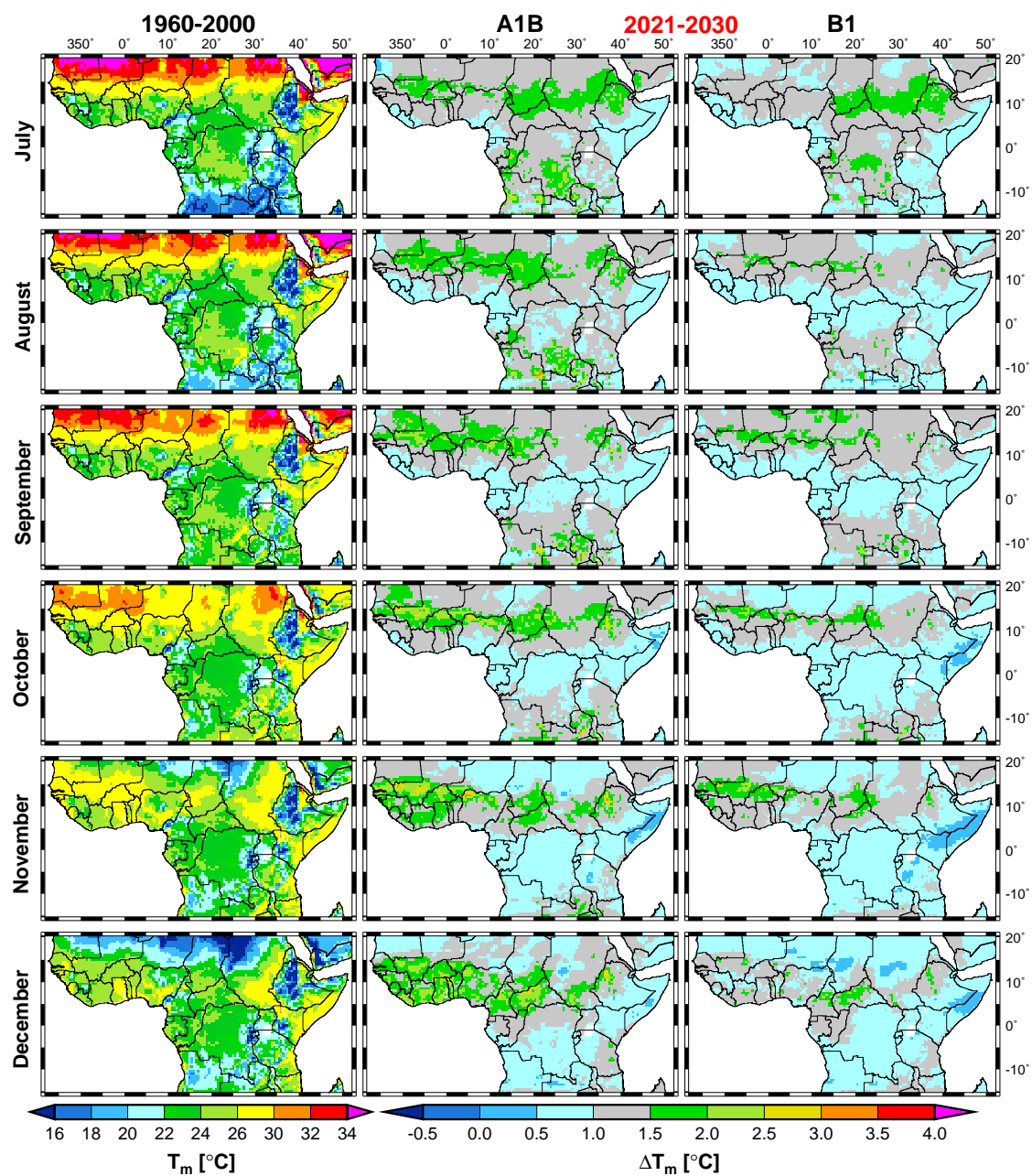


Fig. F.3: (continued)

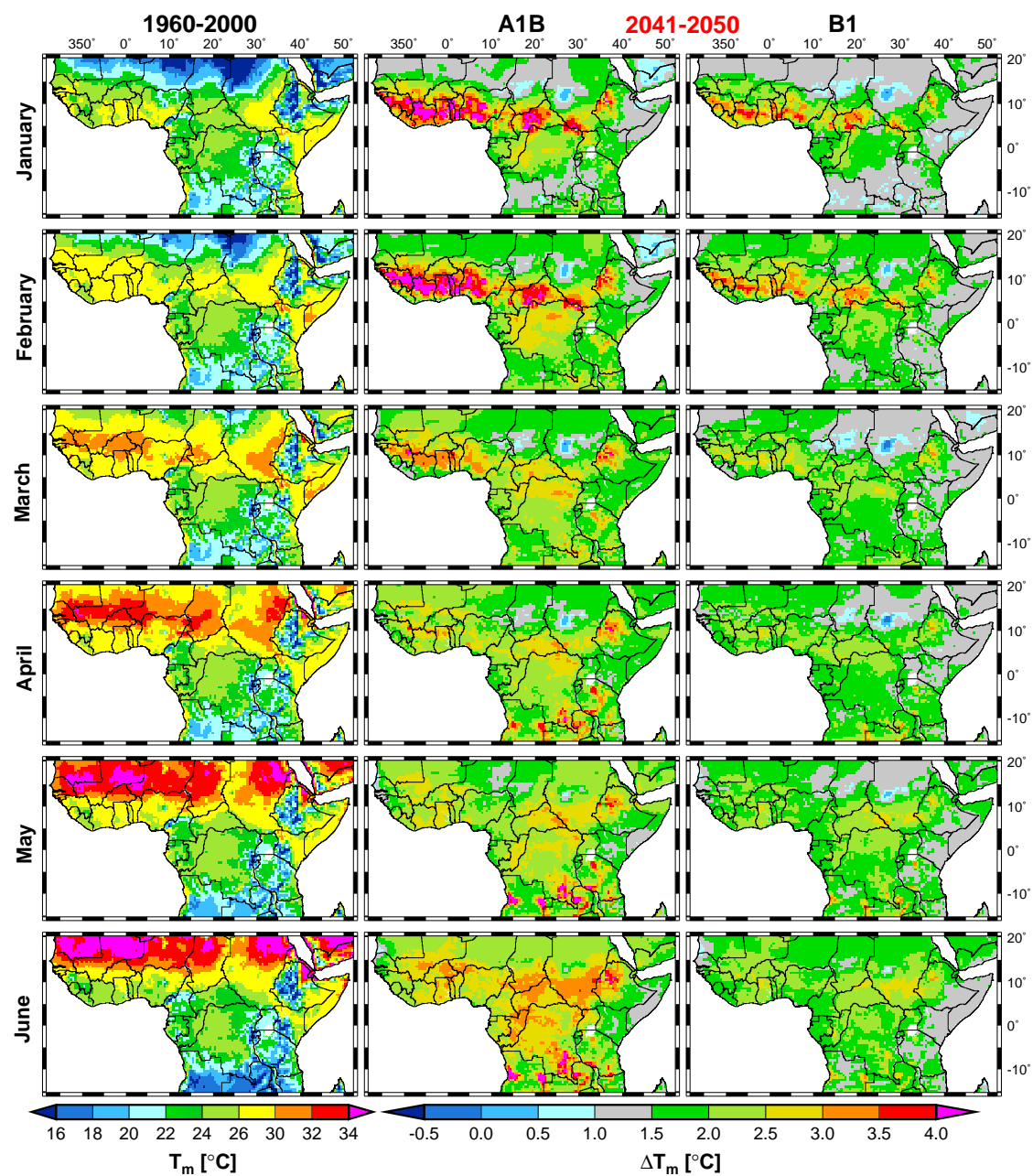


Fig. F.4: Same as Fig. F.3, but for 2041-2050.

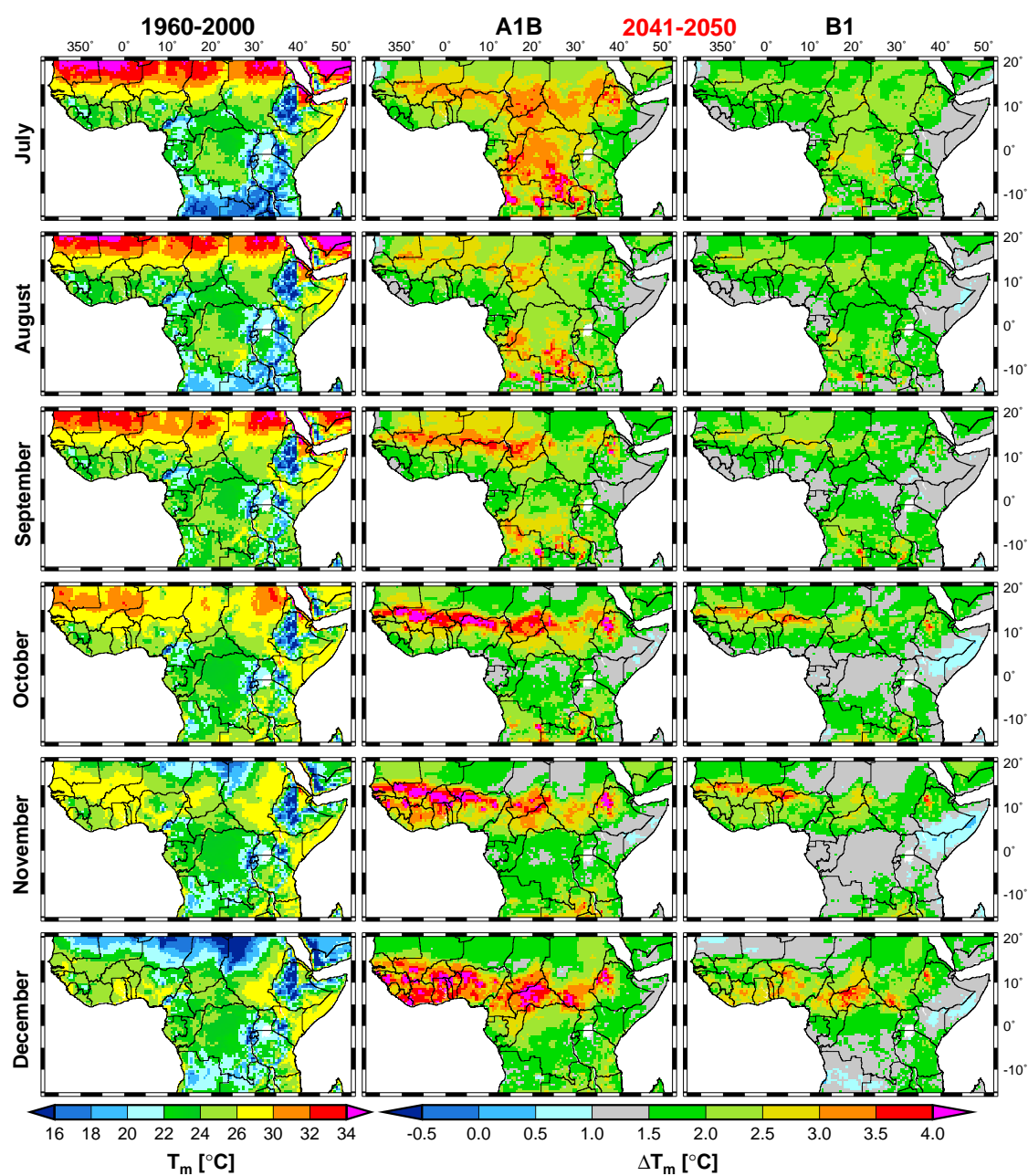


Fig. F.4: (continued)

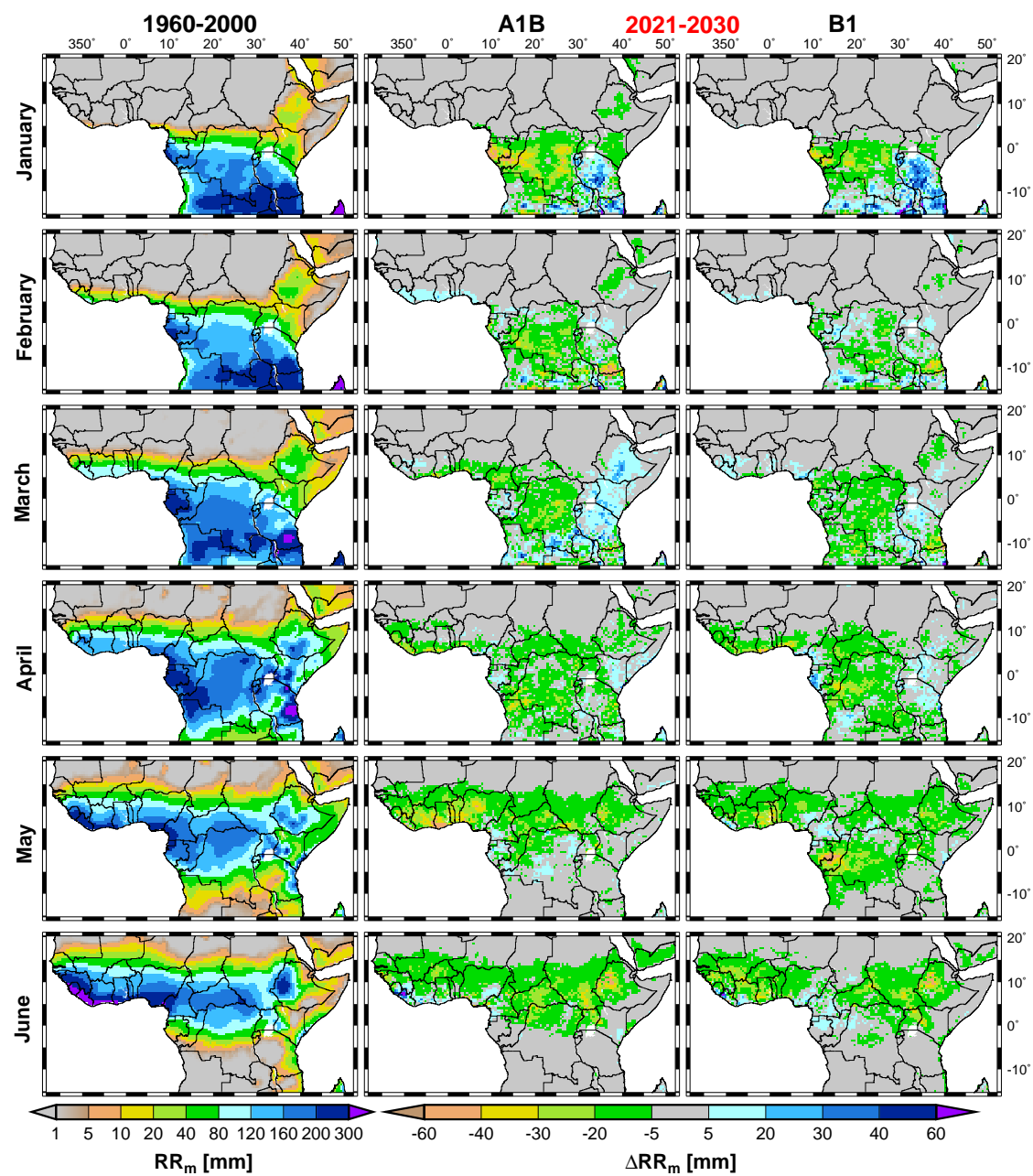


Fig. F.5: Same as Fig. F.3, but for monthly REMO(cor) precipitation (RR_m).

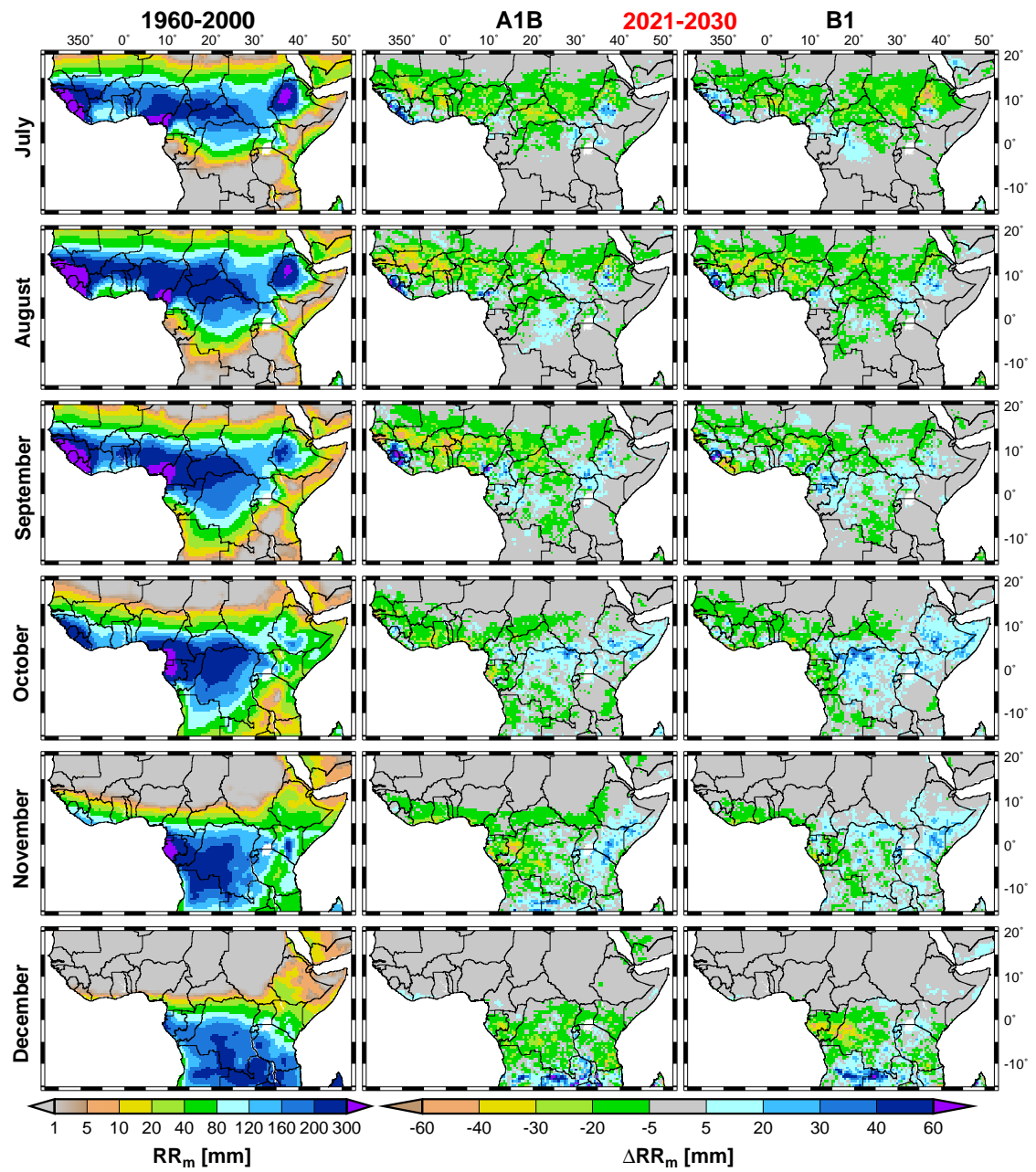


Fig. F.5: (continued)

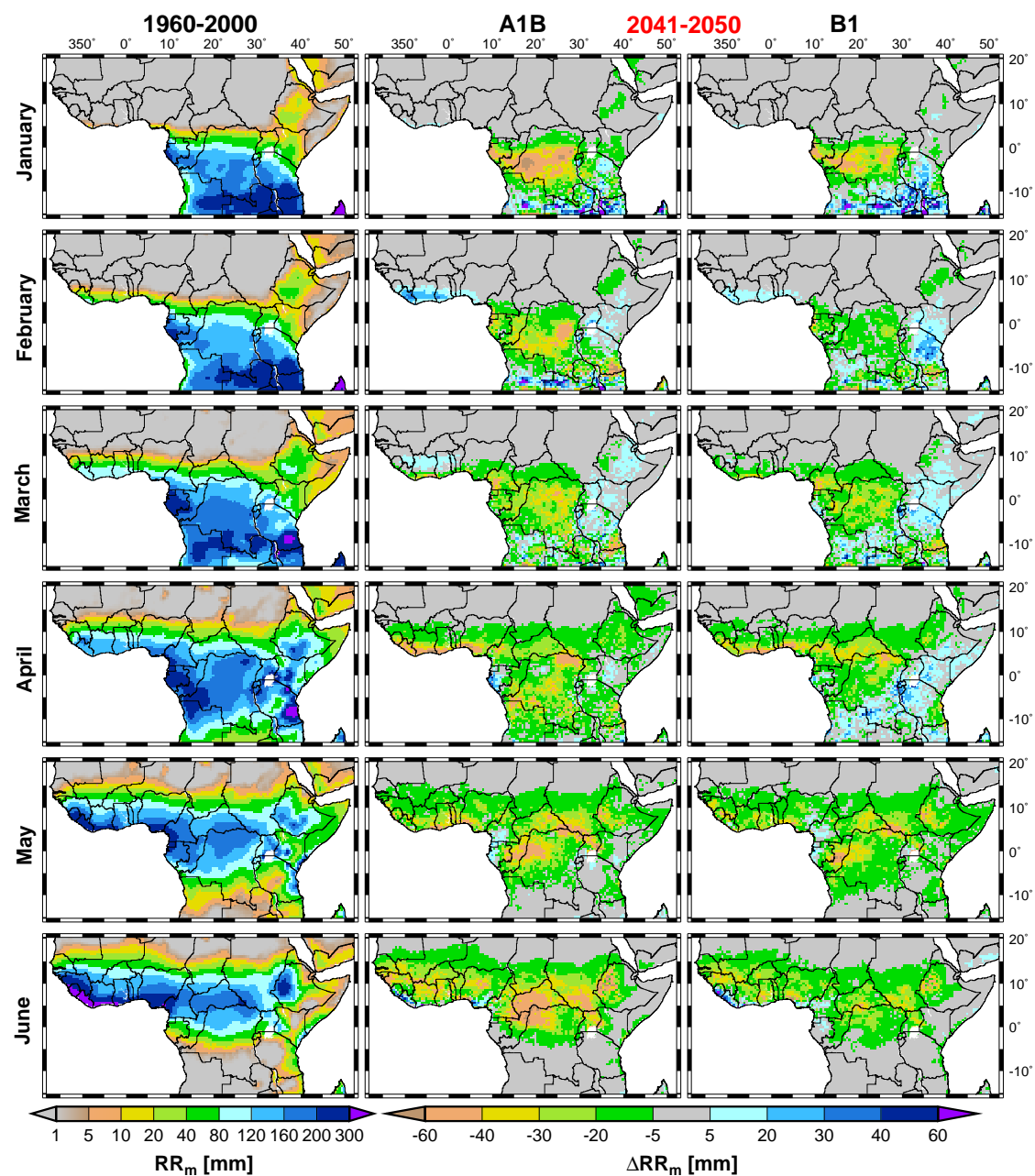


Fig. F.6: Same as Fig. F.5, but for 2041-2050.

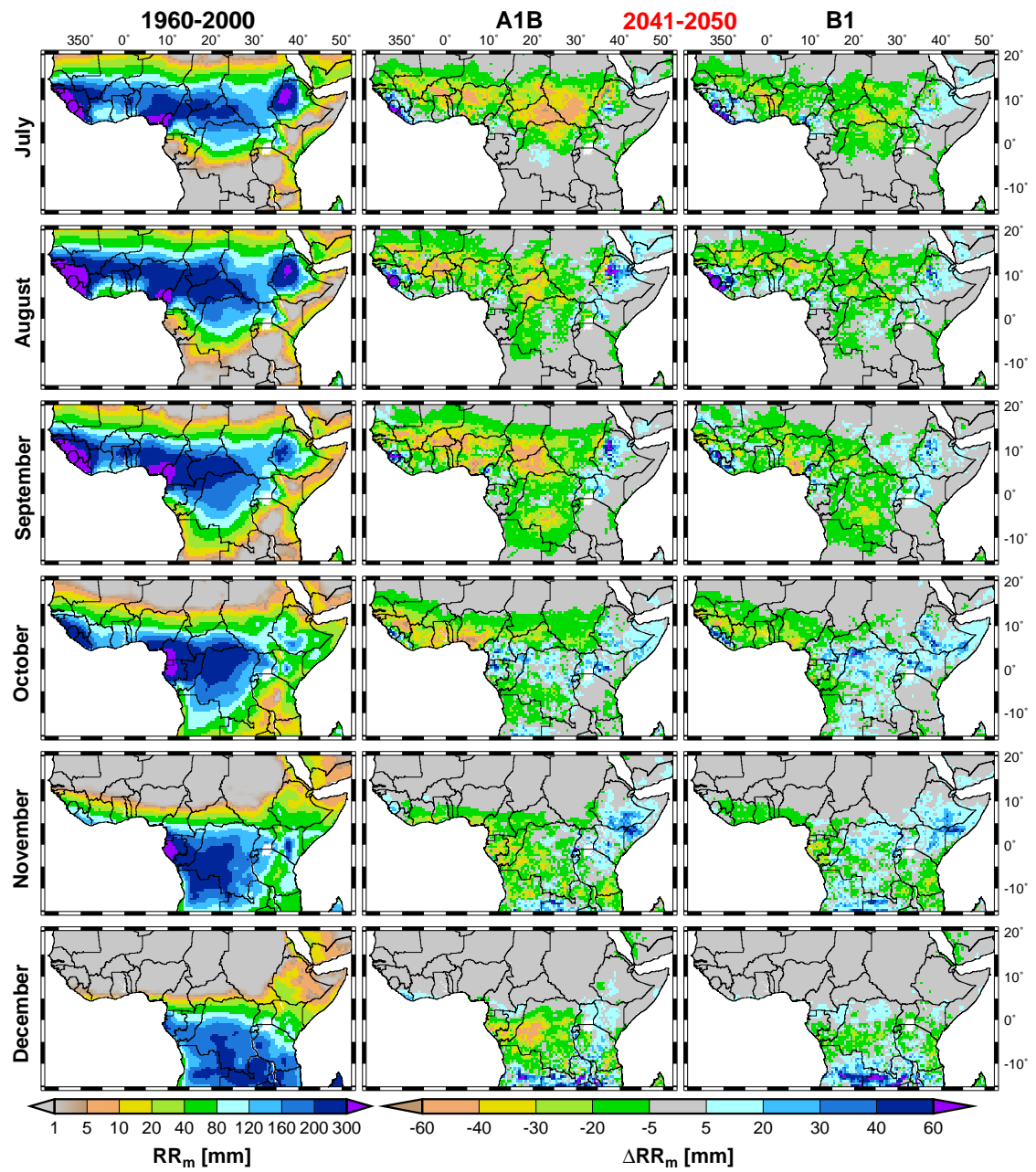


Fig. F.6: (continued)

F.4 Present-day malaria seasonality

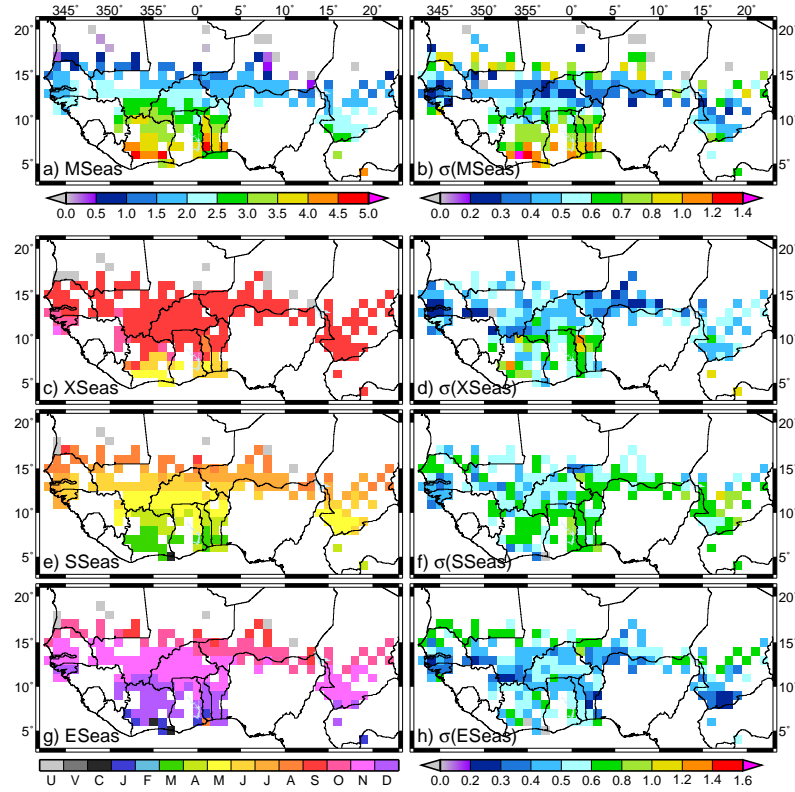


Fig. F.7: LMM_n simulated malaria seasonality (in months) for 1968-1990 based on IRD precipitation and ERA40 temperatures. Depicted are (a) *MSeas*, (b) $\sigma(MSeas)$, (c) *XSeas*, (d) $\sigma(XSeas)$, (e) *SSeas*, (f) $\sigma(SSeas)$, (g) *ESeas*, and (h) $\sigma(ESeas)$. ‘U’ signs areas of unfrequent malaria transmission; ‘V’ denotes grid boxes with either a rare malaria occurrence or a variable seasonality; ‘C’ identifies year-round malaria transmission (for details see App. D.5).

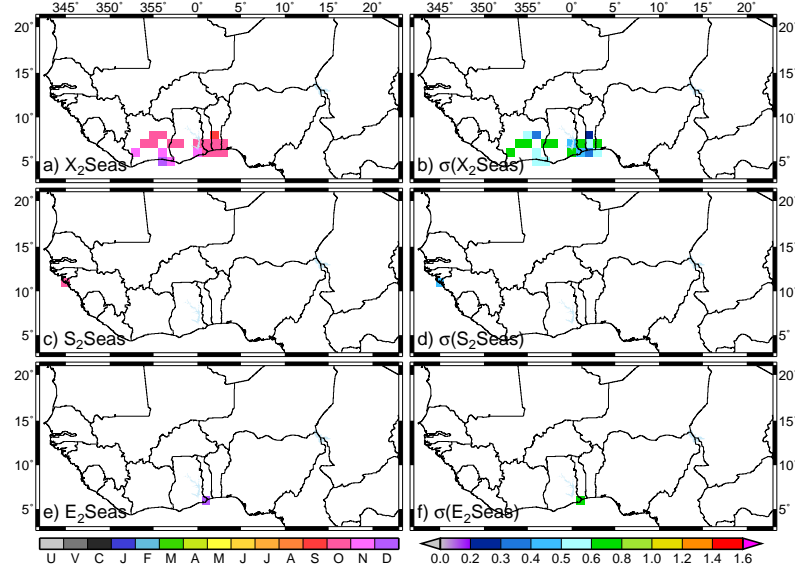


Fig. F.8: Same as Fig. F.7c-h, but for the second identified month of maximum transmission (*X₂Seas*) and values of the second malaria season (*S₂Seas* and *E₂Seas*; see also App. D.5).

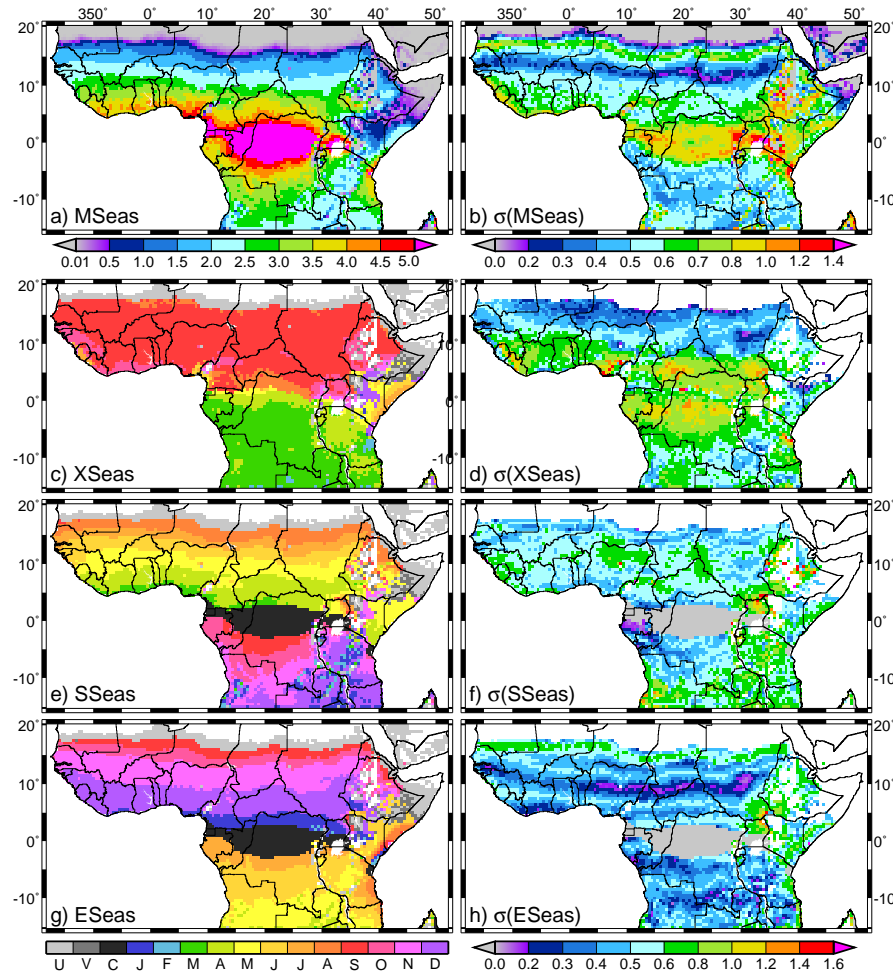


Fig. F.9: Same as Fig. F.7, but for 1960-2000 and for the LMM_n simulation.

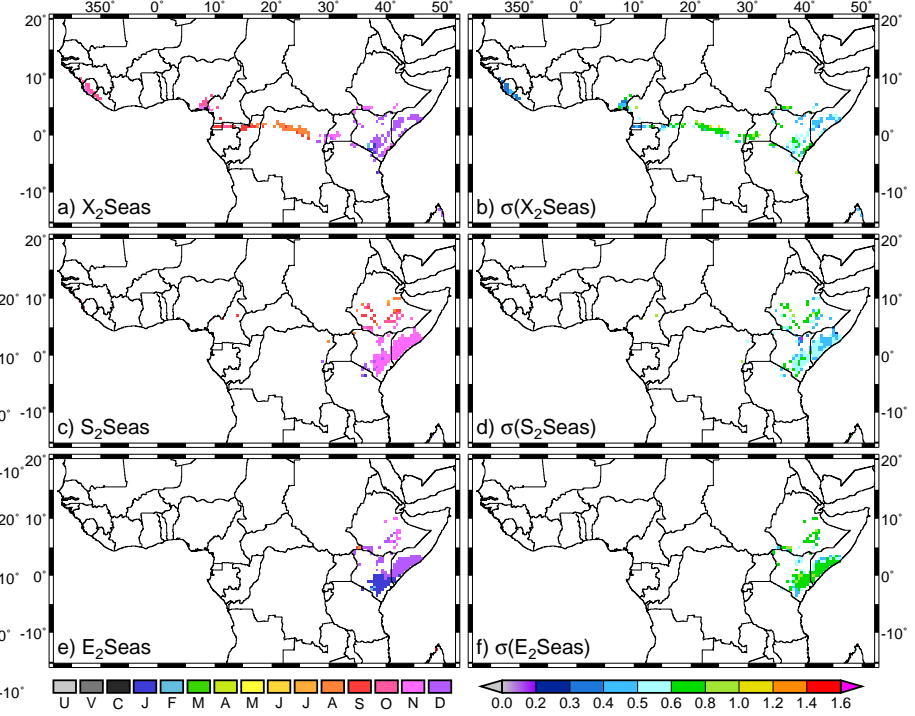


Fig. F.10: Same as Fig. F.8, but based on the present-day climate (1960-2000) from REMO(cor).

F.5 Malaria projections

LMM_n projections

The following figures provide a detailed picture of simulated monthly EIR values. Note that the 5-day accumulated EIR served as data input for the Garki model. The present-day distribution of EIR_m and projected changes hence supply valuable information for the analysis of the Garki model performance.

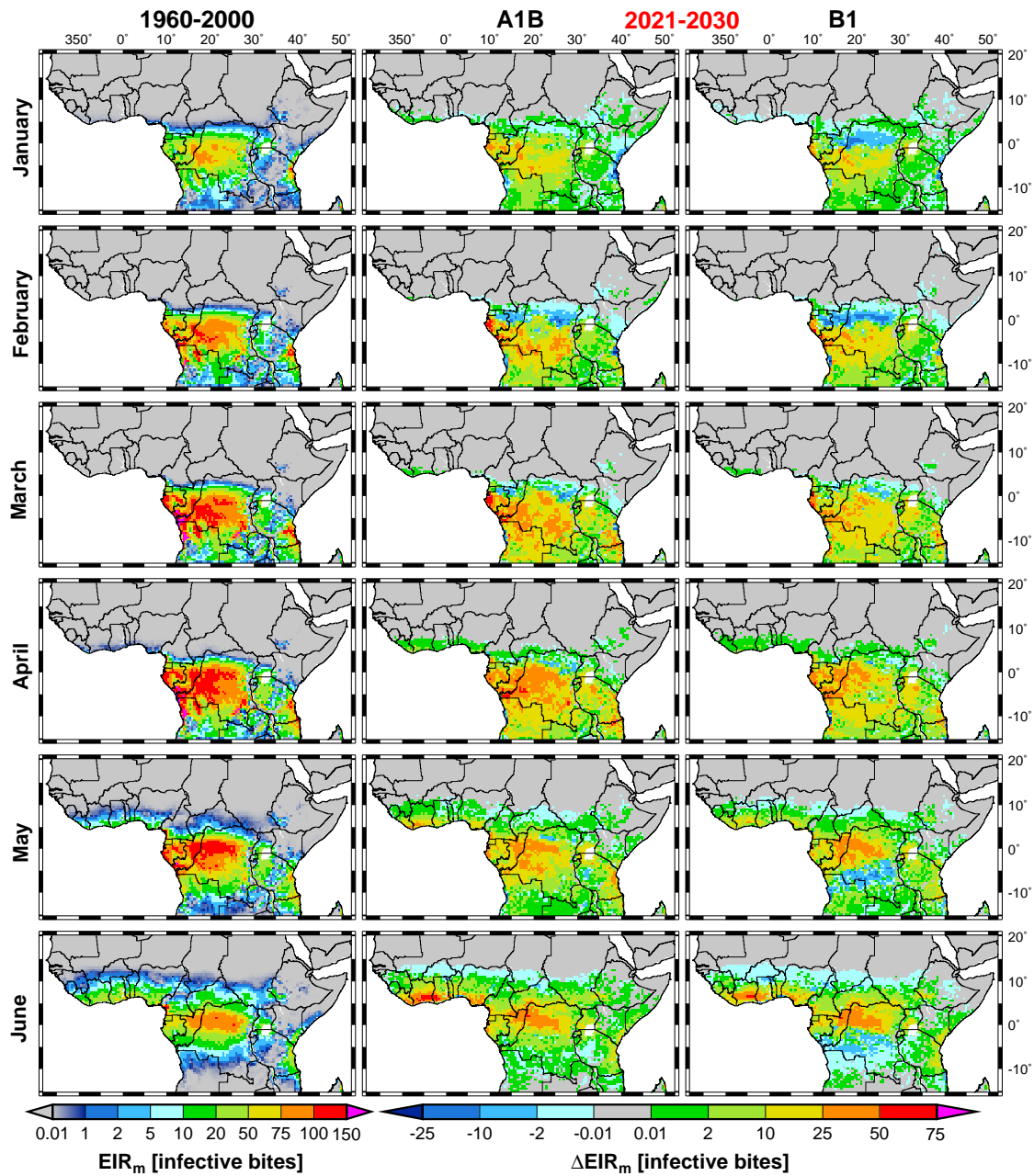


Fig. F.11: Monthly LMM_n entomological inoculation rate (EIR_m) of the present-day climate (1960-2000) as well as for the difference (ΔEIR_m) between the present-day EIR_m and that of 2021-2030 from the A1B as well as B1 scenario (continued on next page).

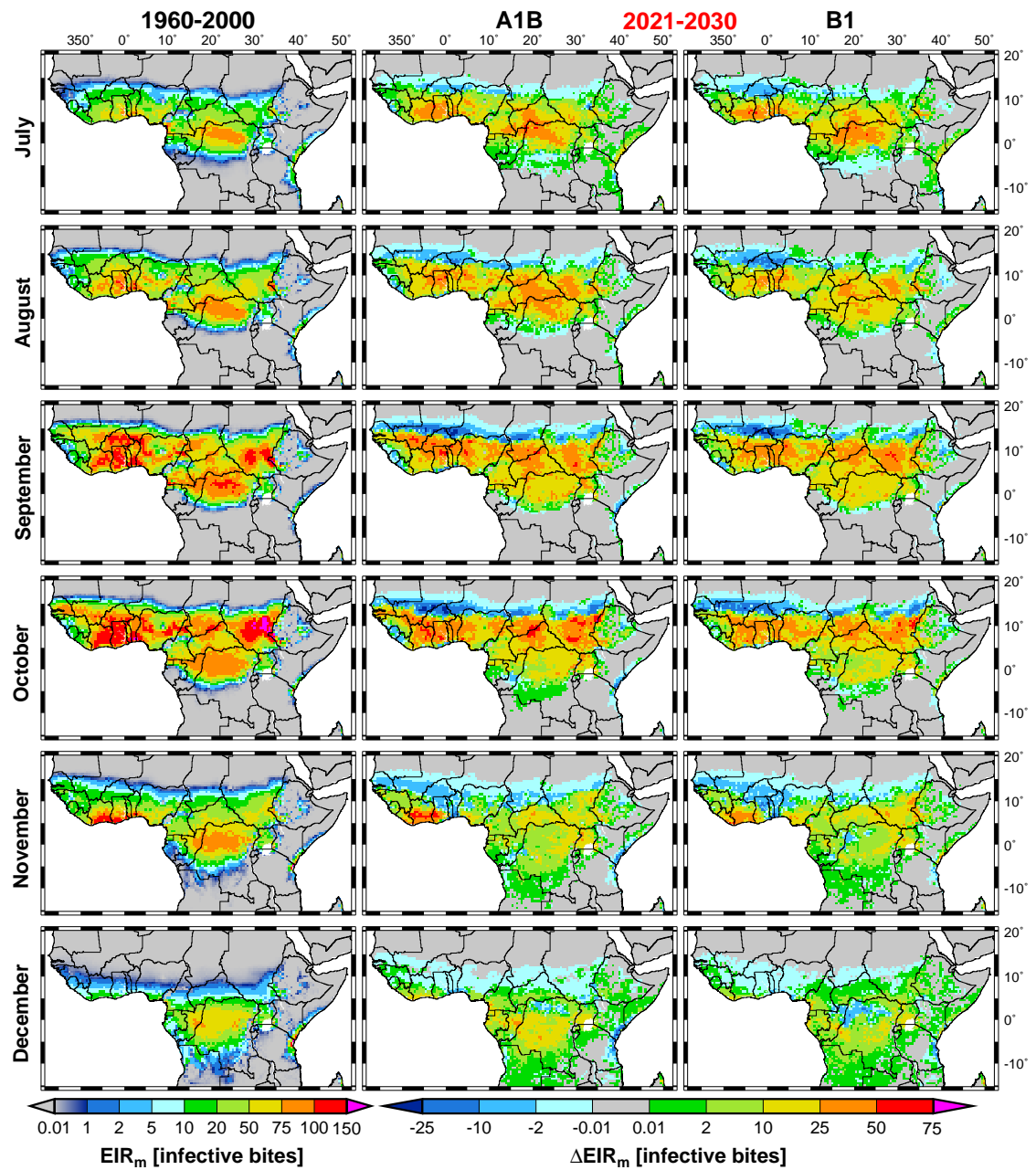


Fig. F.11: (continued)

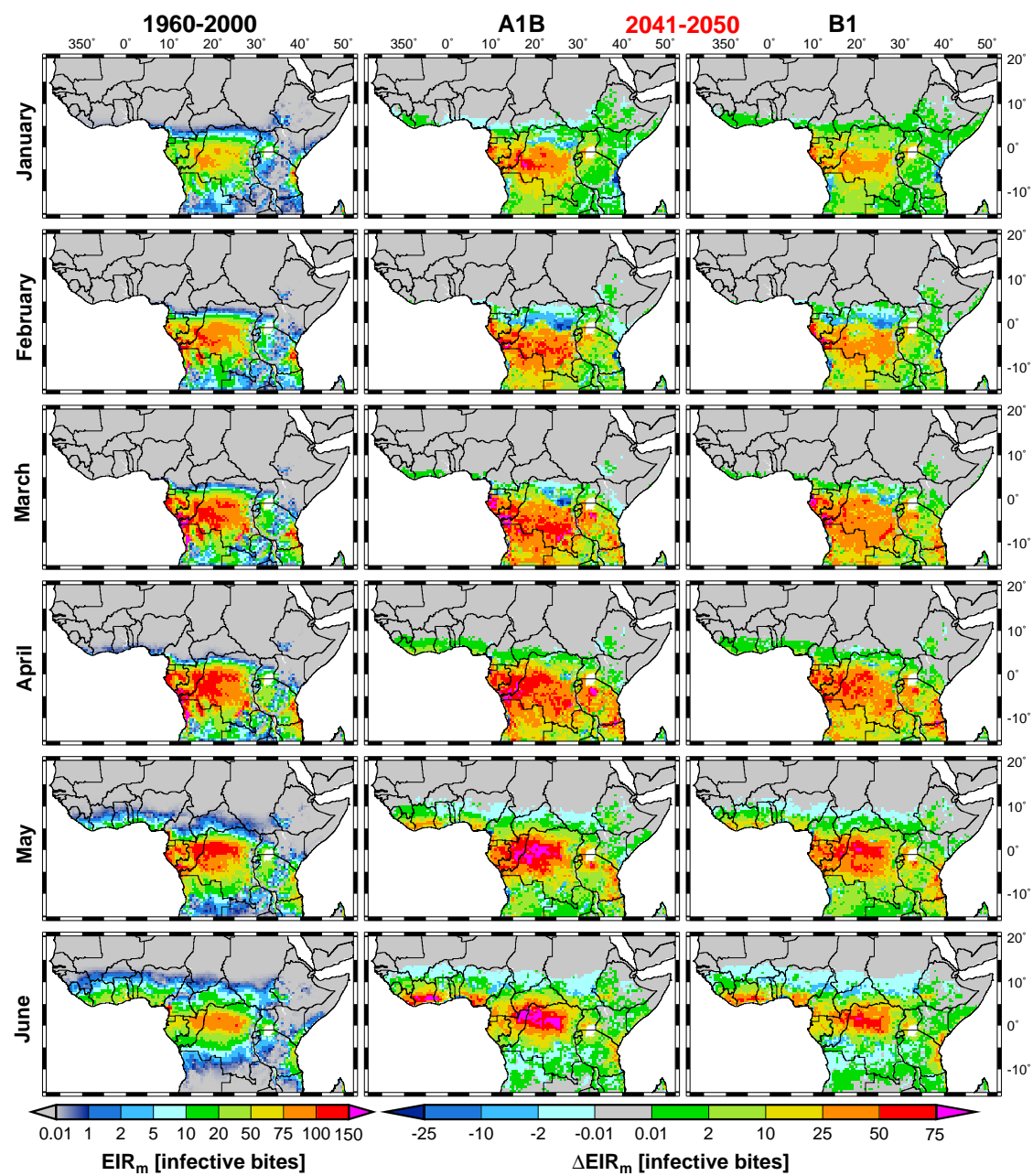


Fig. F.12: Same as Fig. F.11, but for 2041-2050.

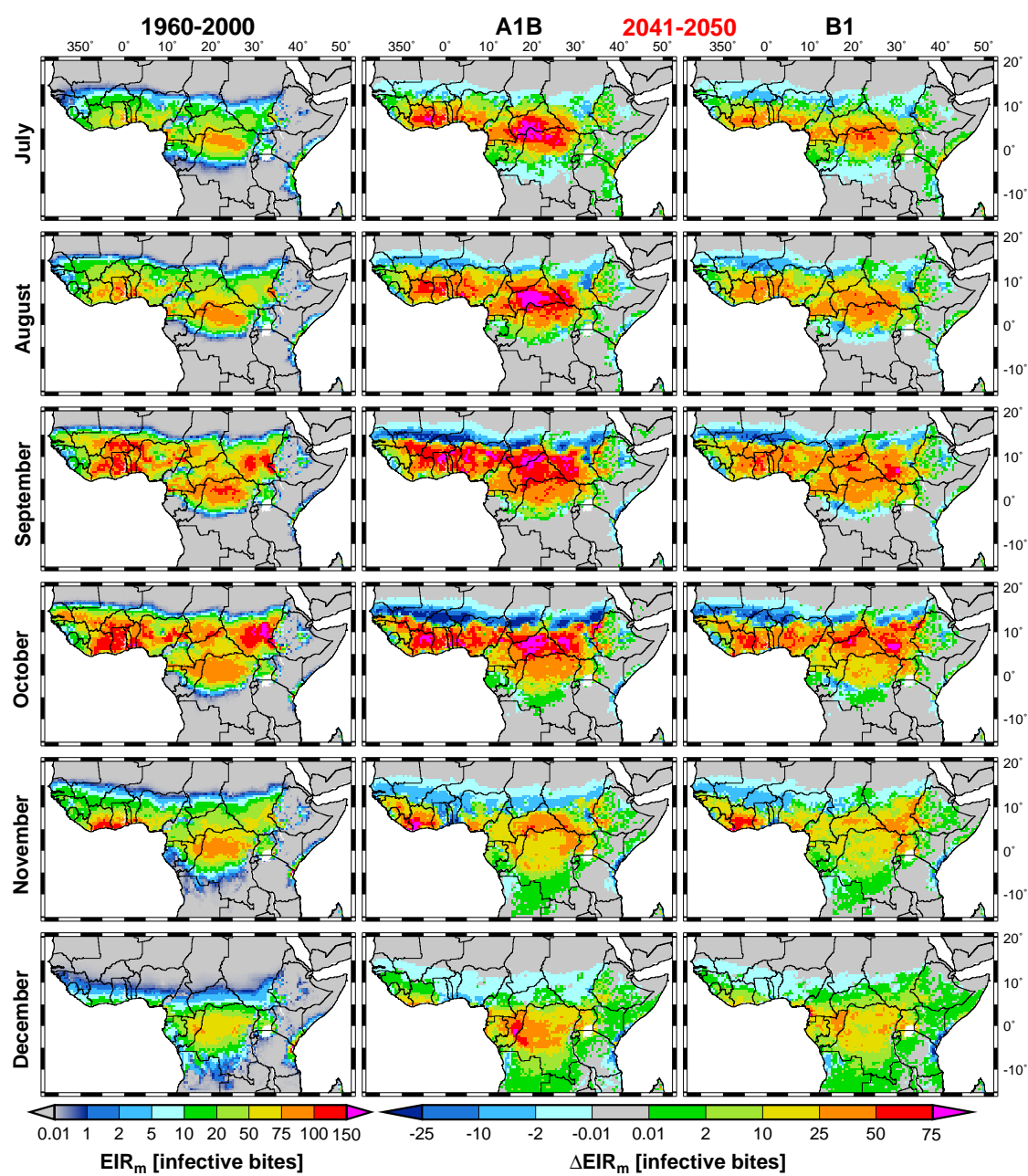


Fig. F.12: (continued)

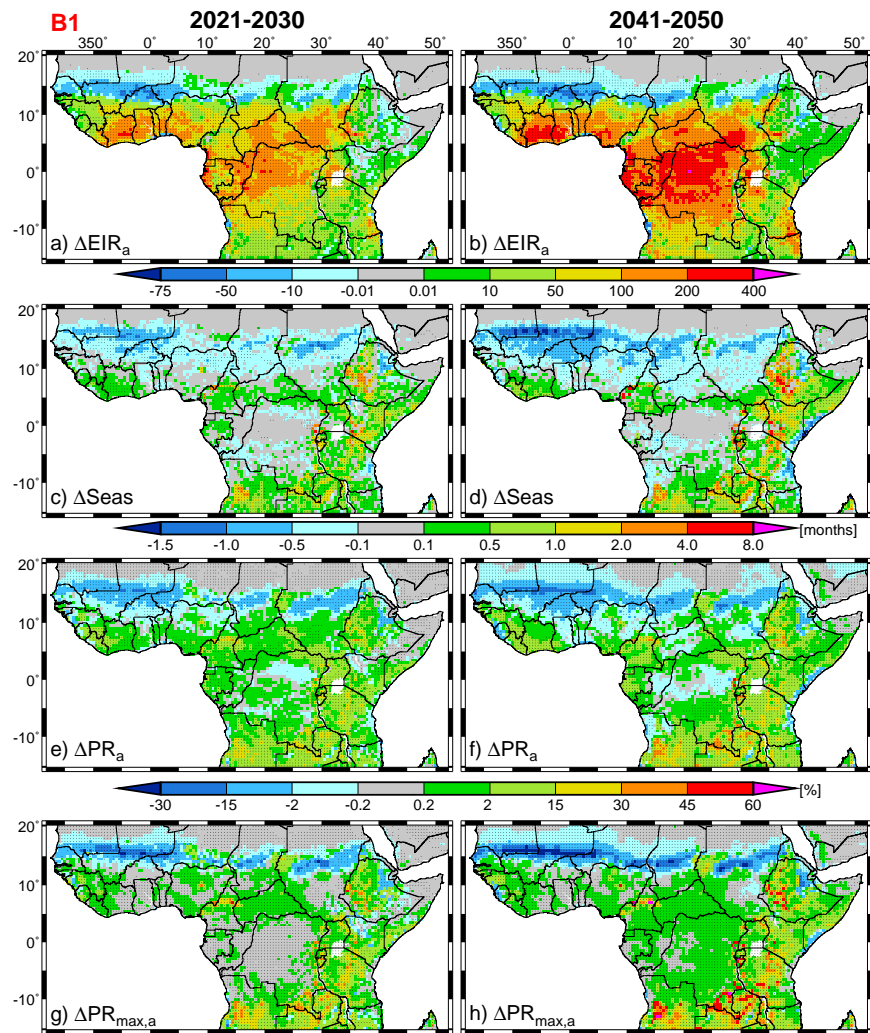


Fig. F.13: Same as Fig. 7.12, but for the B1 scenario.

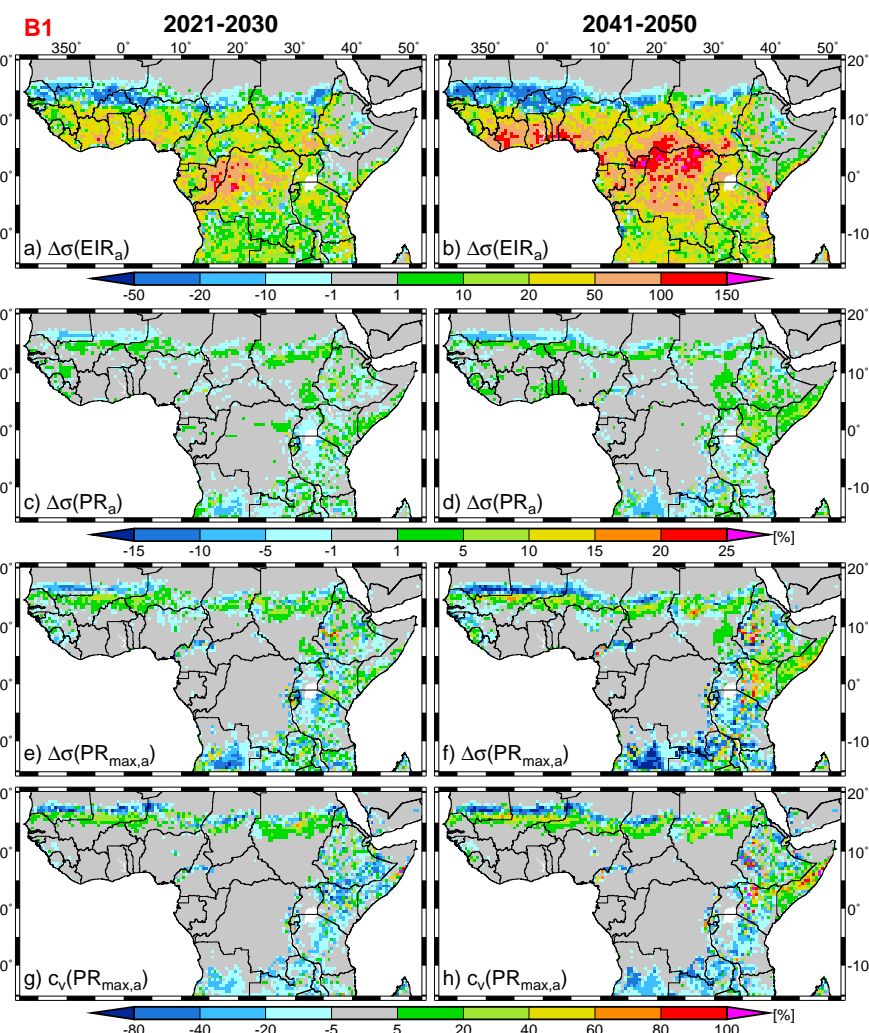


Fig. F.14: Same as Fig. 7.13, but for the B1 scenario.

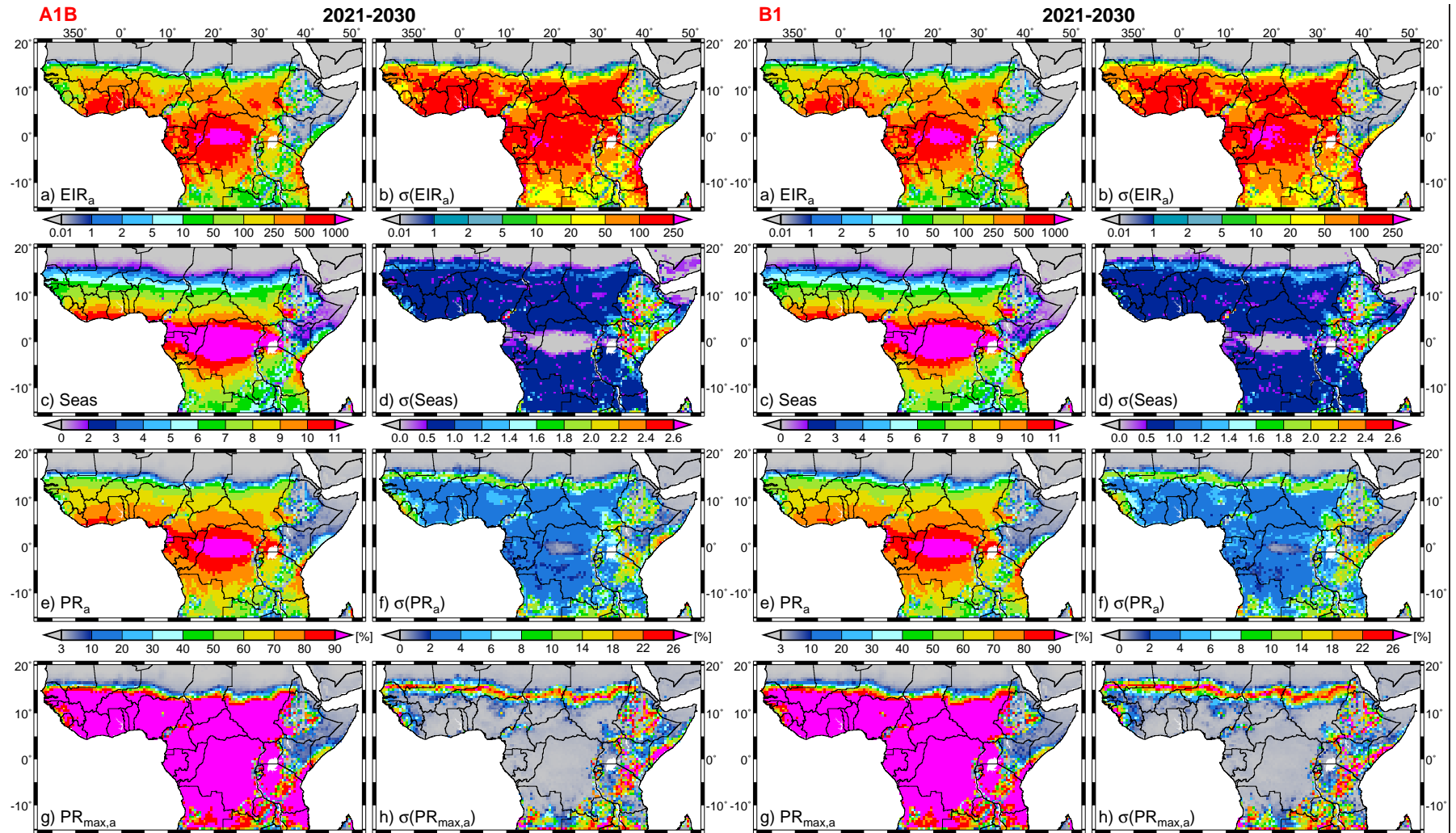


Fig. F.15: Same as Fig. 7.4, but for 2021-2030 and the A1B scenario.

Fig. F.16: Same as Fig. 7.4, but for 2021-2030 and the B1 scenario.

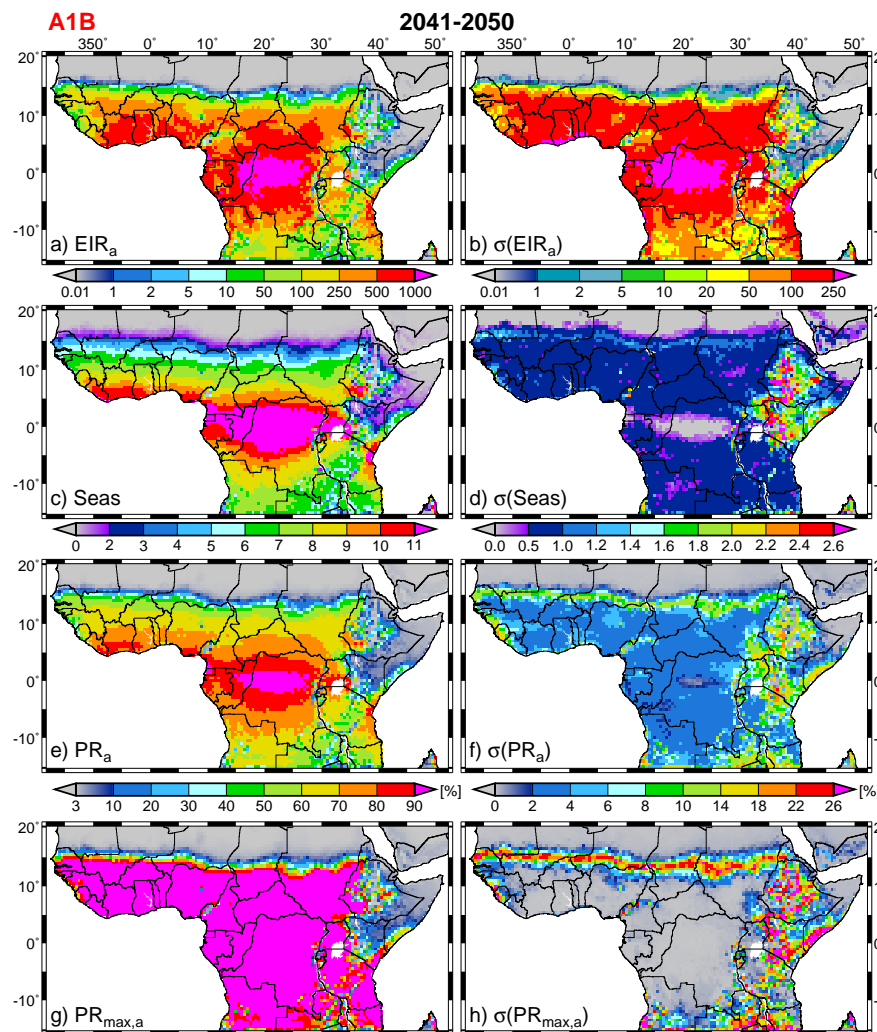


Fig. F.17: Same as Fig. 7.4, but for 2041-2050 and the A1B scenario.

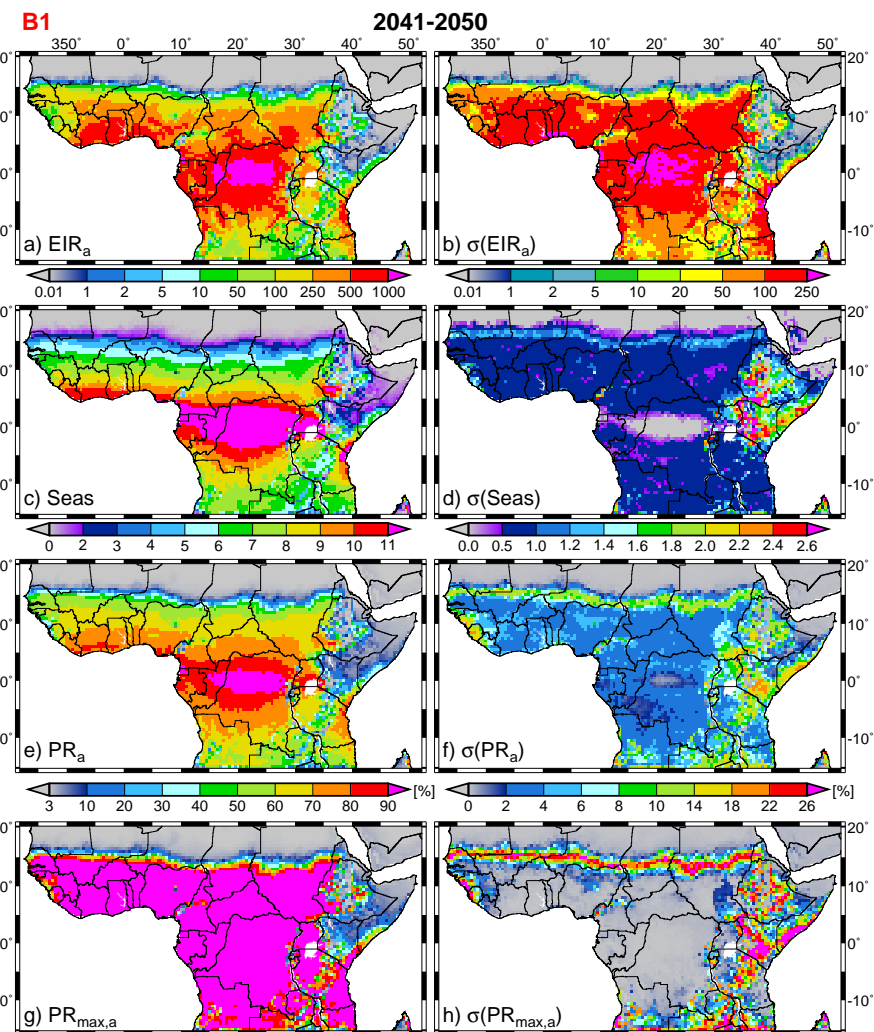


Fig. F.18: Same as Fig. 7.4, but for 2041-2050 and the B1 scenario.

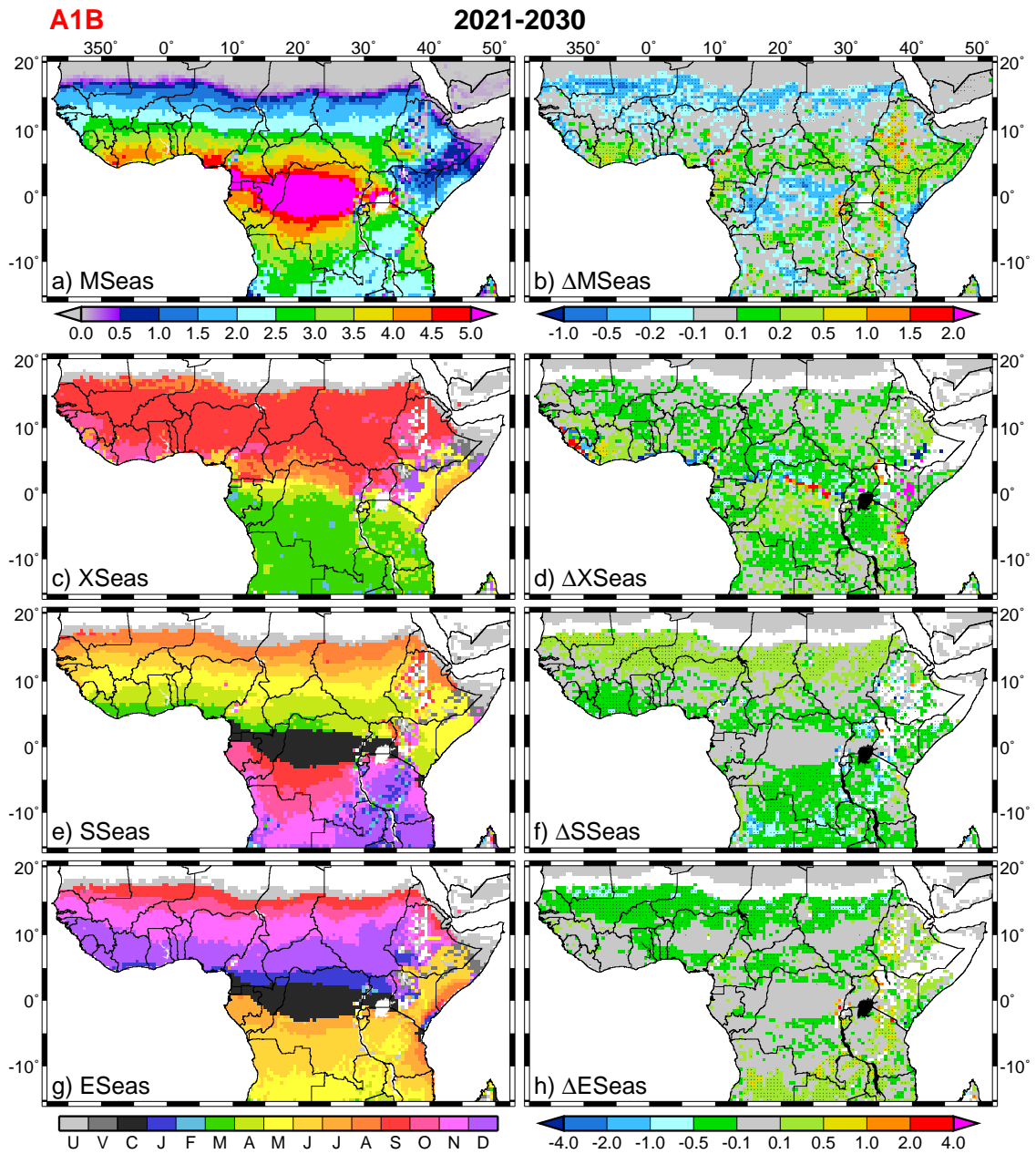


Fig. F.19: LMM_n projected malaria seasonality (in months) for 2021-2030 based on the A1B scenario and REMO(cor). Illustrated are absolute values as well as changes relative to the present-day climate (1960-2000). Depicted are (a) *MSeas*, (b) $\Delta(MSeas)$, (c) *XSeas*, (d) $\Delta(XSeas)$, (e) *SSeas*, (f) $\Delta(SSeas)$, (g) *ESeas*, and (h) $\Delta(ESeas)$. Note that in case of *XSeas*, *SSeas*, *ESeas* positive (negative) values stand for a later (earlier) occurrence. 'U' signs areas of unfrequent malaria transmission, 'V' denotes grid boxes with either a rare malaria occurrence or a variable seasonality, and 'C' identifies year-round malaria transmission (for details see App. D.5). White areas in (d), (f), and (h) refer to areas assigned either for the present-day or future climate to 'U' or 'V'. In the right column, values statistically significant at the 5% level are marked by dots.

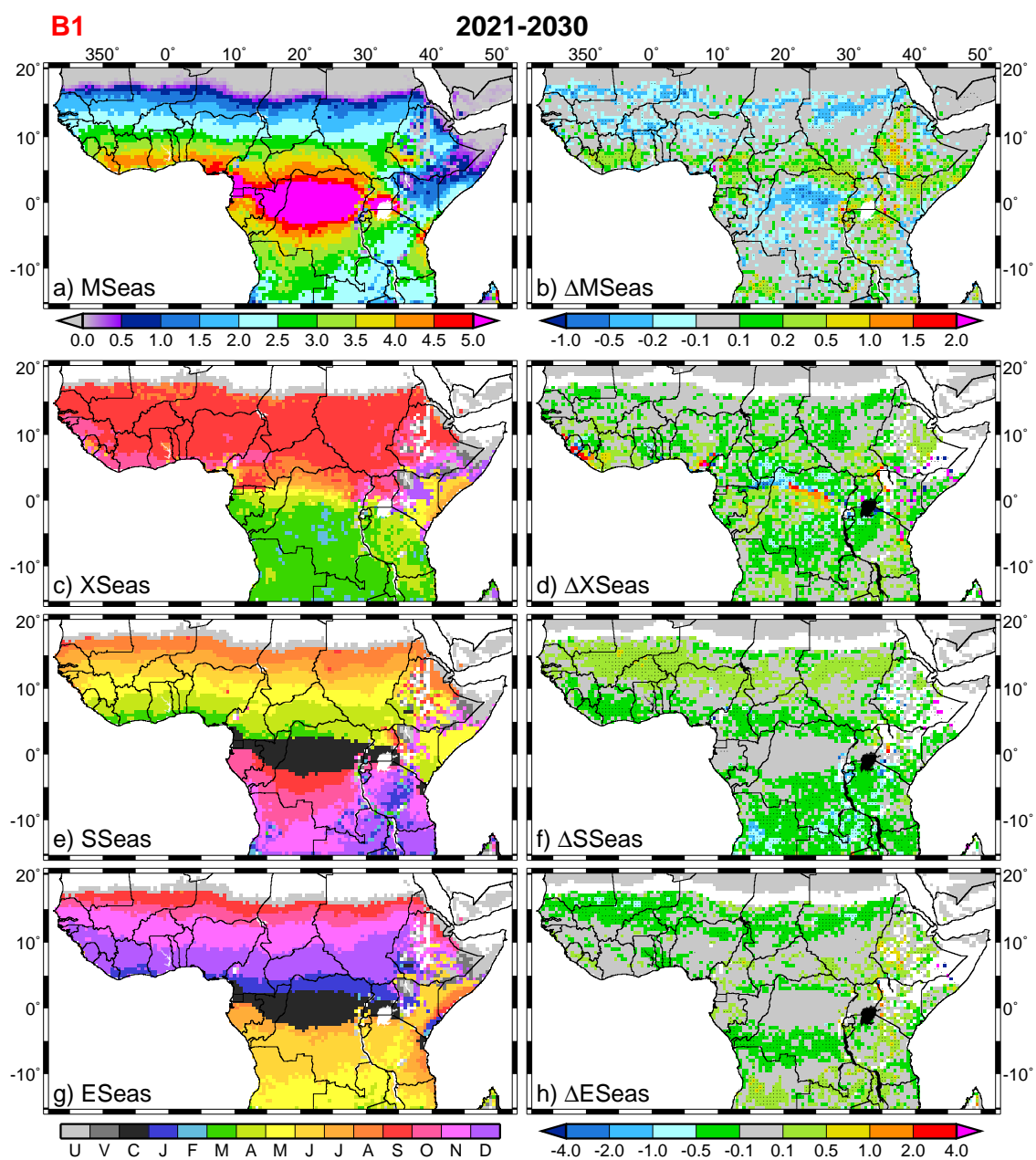


Fig. F.20: Same as Fig. F.19, but for the B1 scenario.

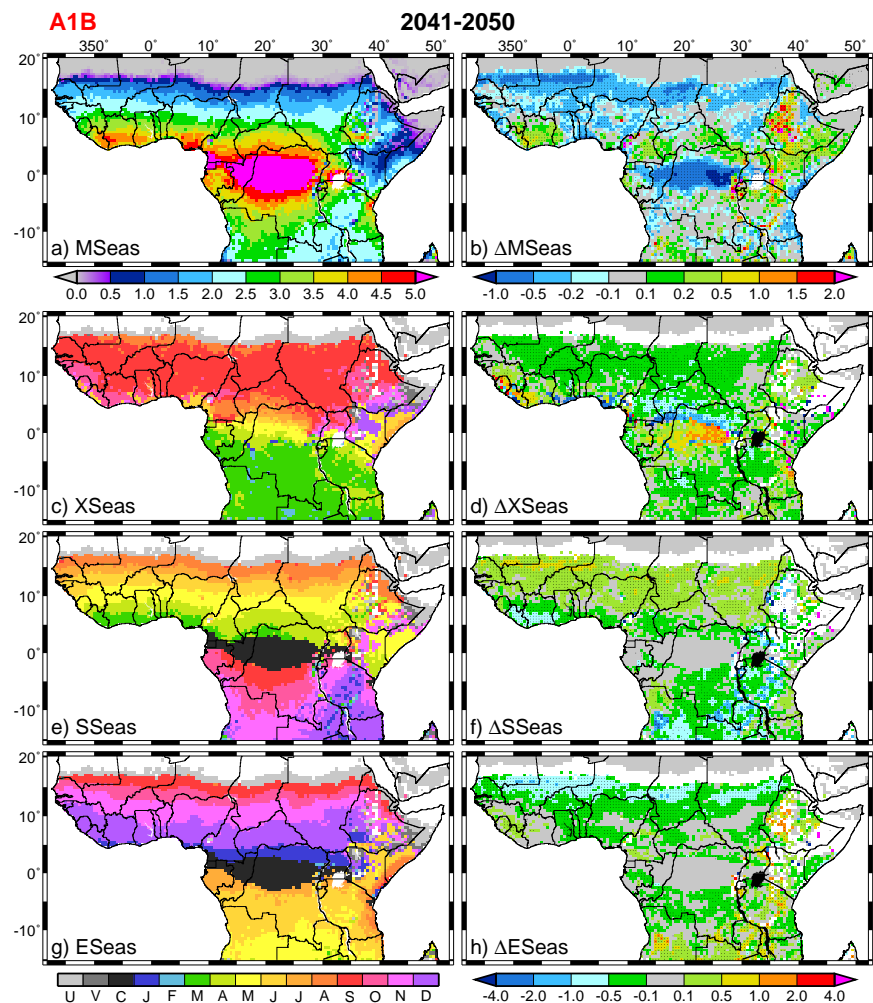


Fig. F.21: Same as Fig. F.19, but for 2041-2050.

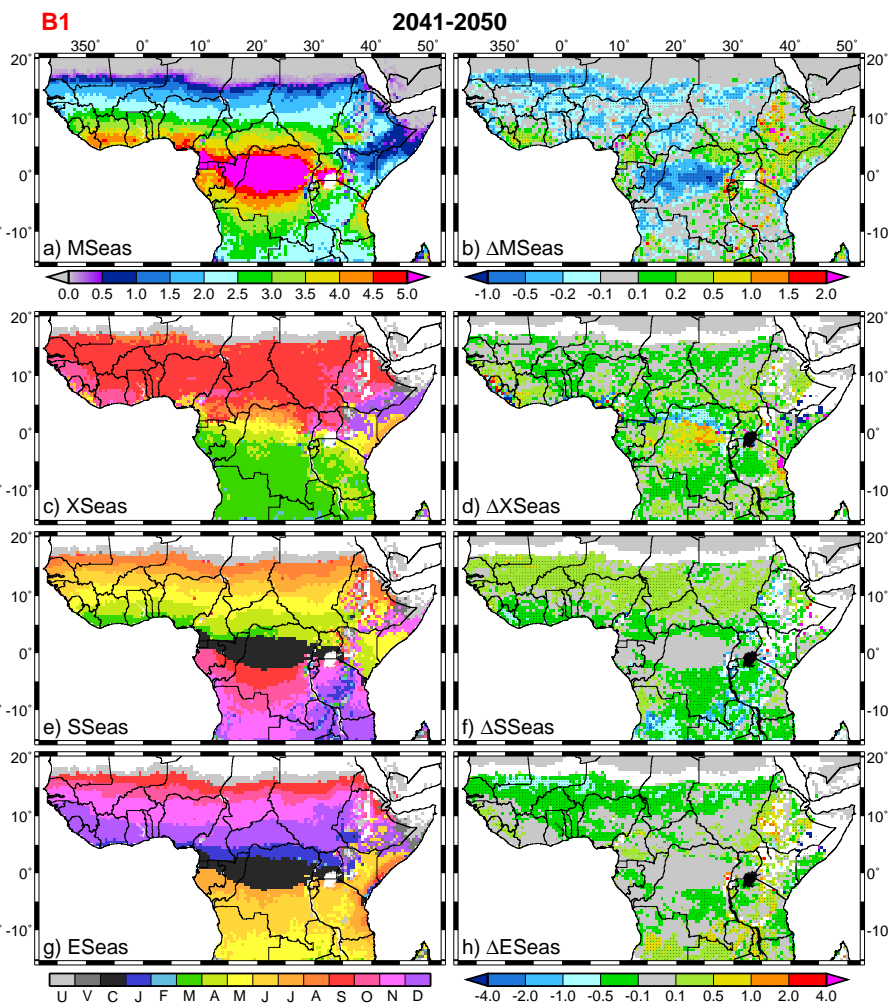


Fig. F.22: Same as Fig. F.19, but for the B1 scenario and for 2041-2050.

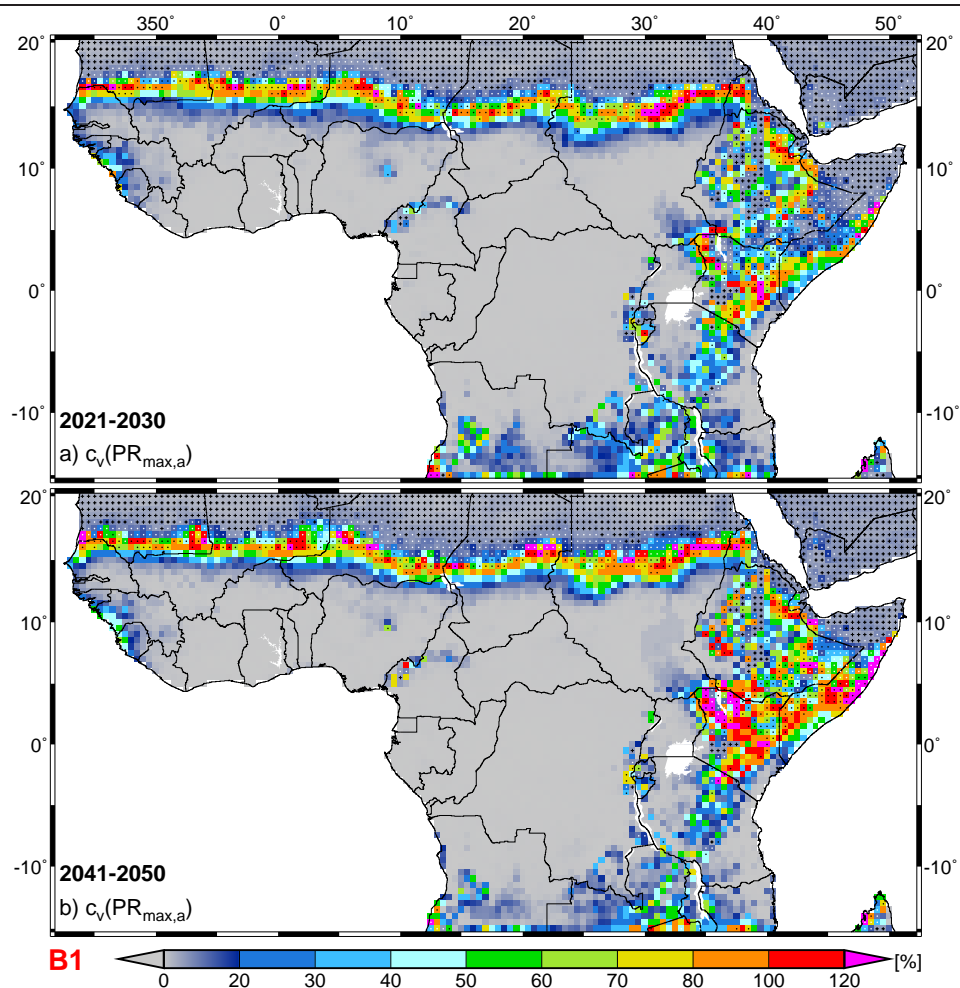


Fig. F.23: Same as Fig. 7.16, but for the B1 scenario.

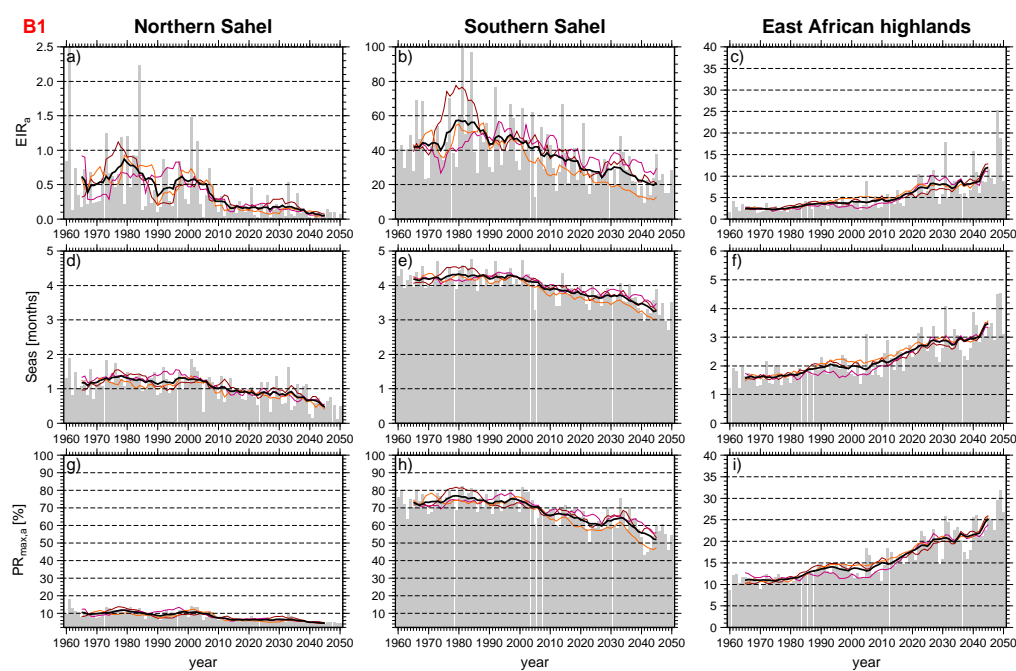


Fig. F.24: Same as Fig. 7.14, but for the B1 scenario.

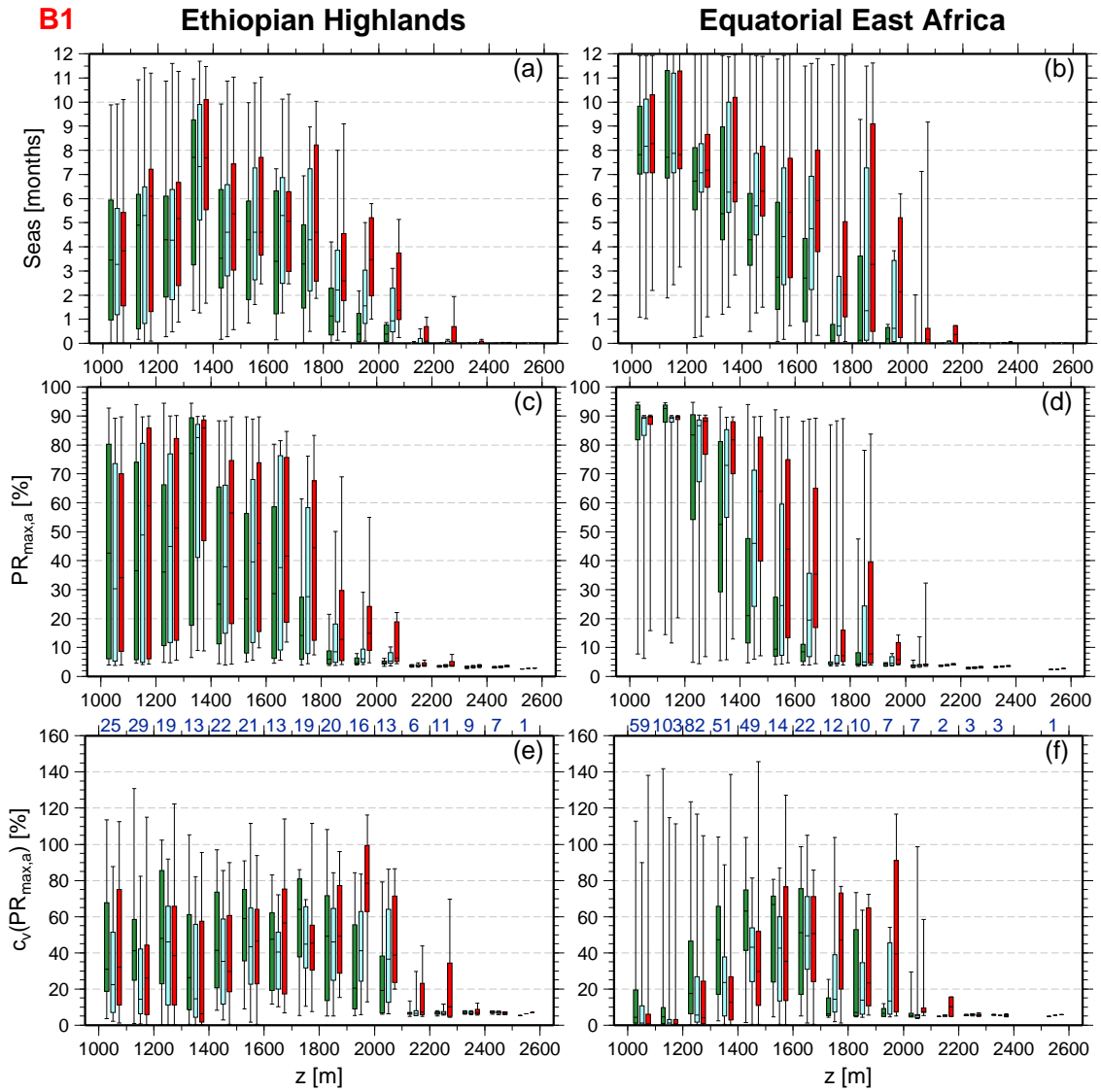


Fig. F.25: Same as Fig. 7.17, but for the B1 scenario.

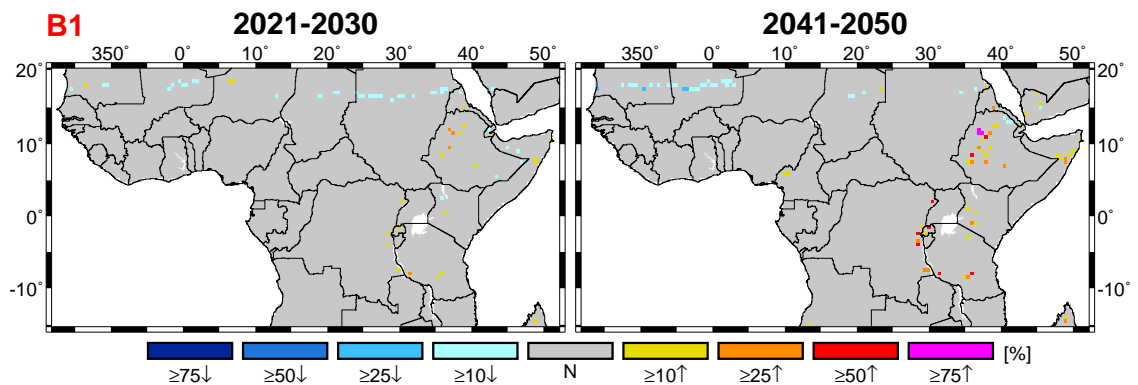


Fig. F.26: Same as Fig. 7.15, but for the B1 scenario.

Garki model projections

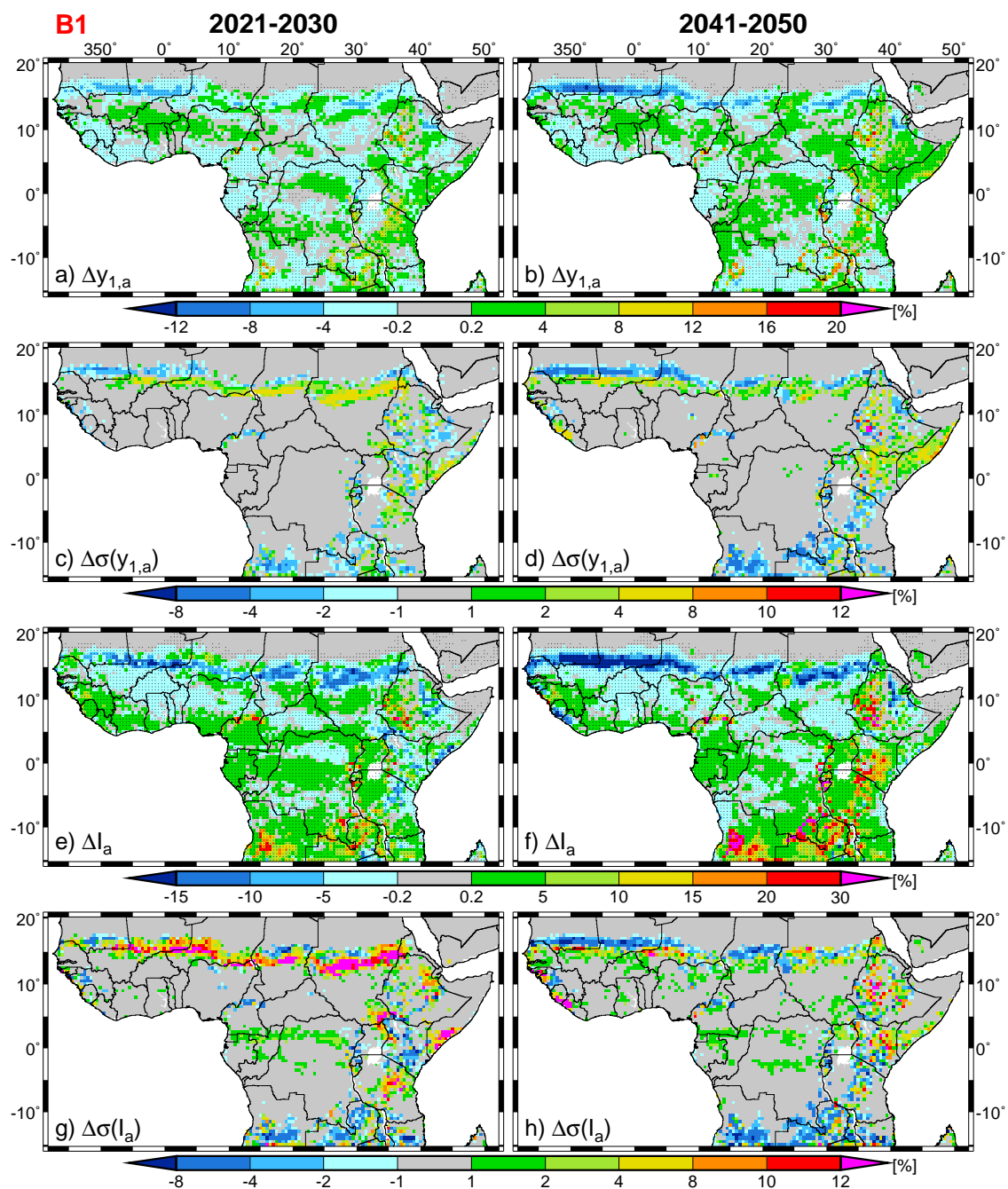


Fig. F.27: Same as Fig. 7.18, but for the B1 scenario.

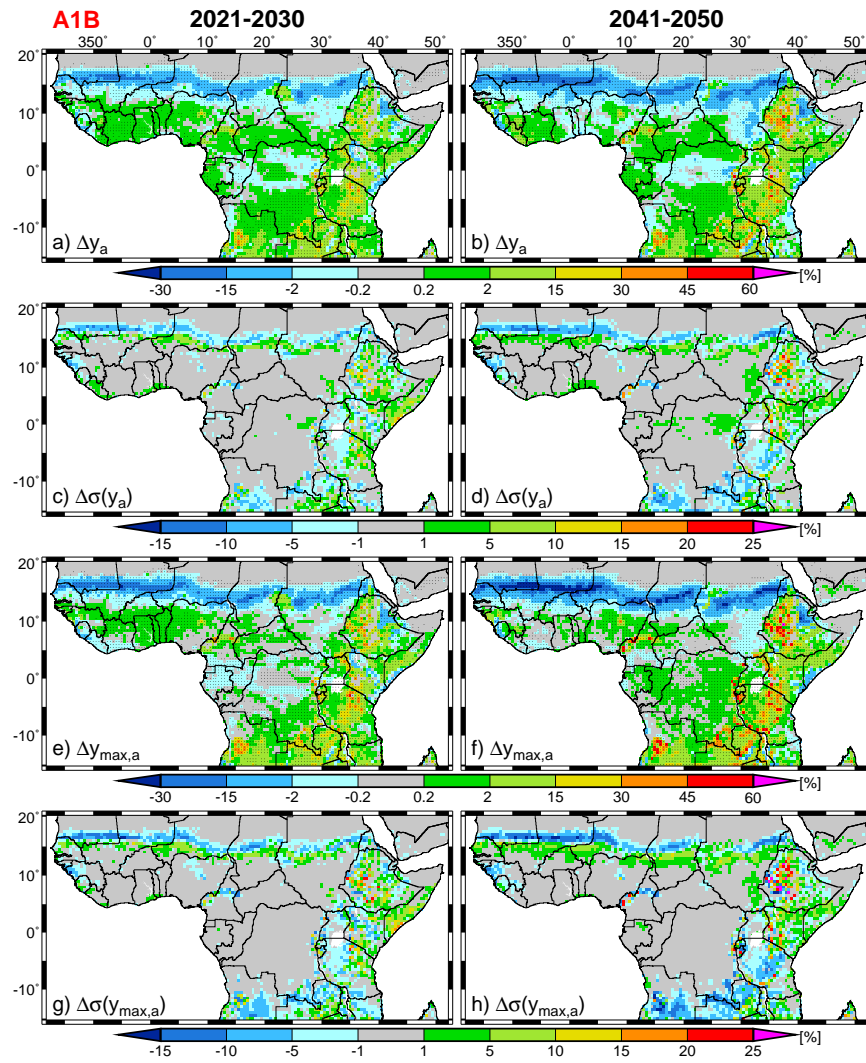


Fig. F.28: Same as Fig. 7.18, but for model variables y_a and $y_{\max,a}$ instead of $y_{1,a}$ and I_a .

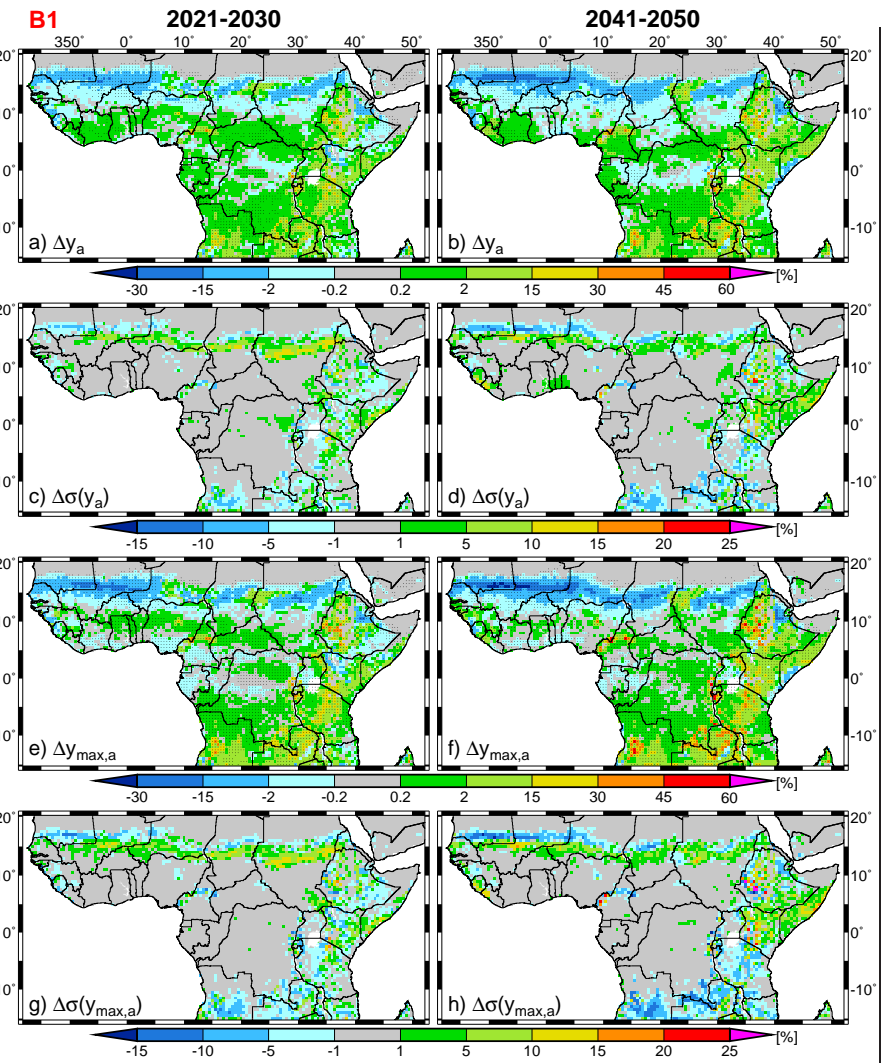


Fig. F.29: Same as Fig. F.28, but for the B1 scenario.

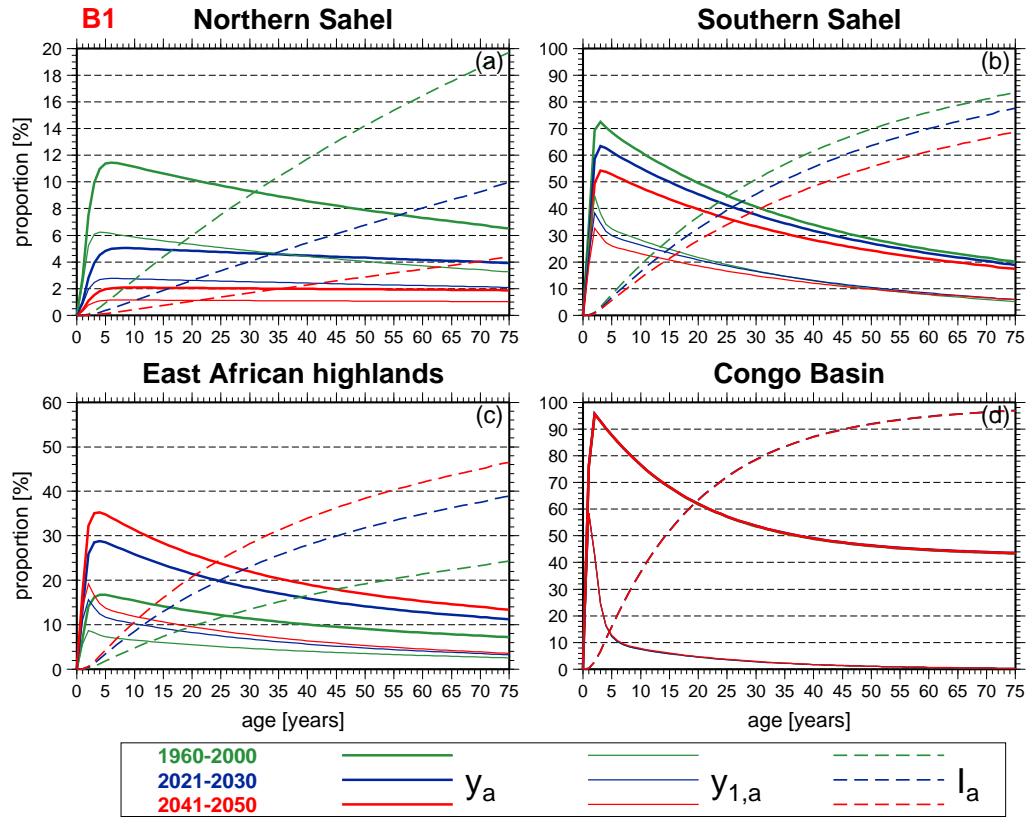


Fig. F.30: Same as Fig. 7.20, but for the B1 scenario.

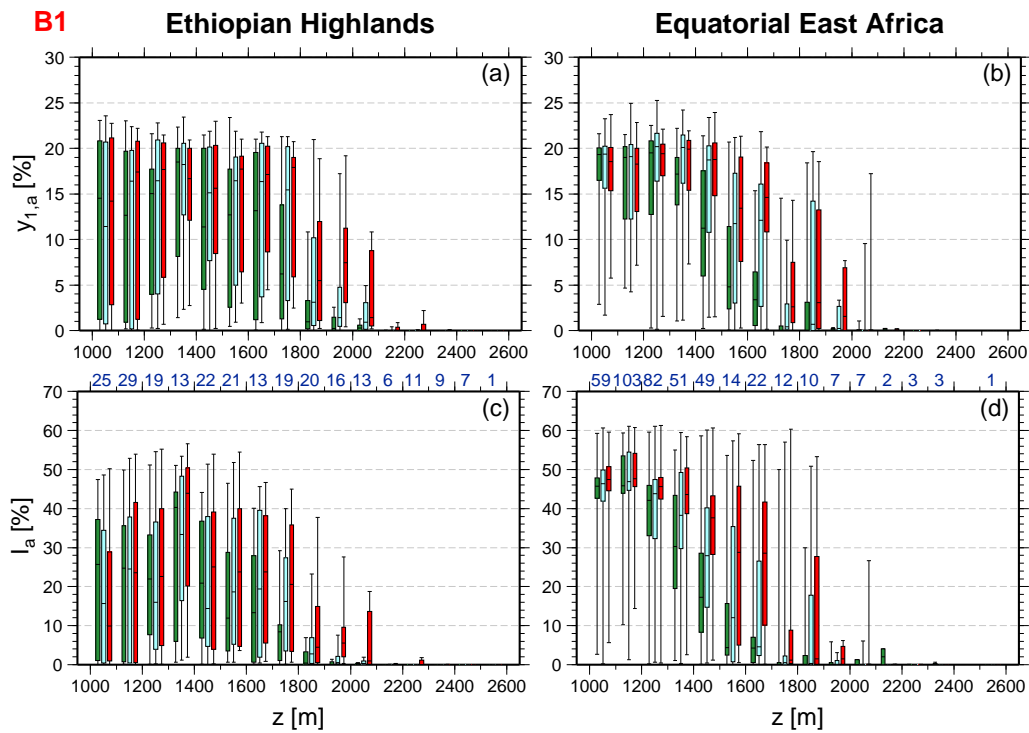


Fig. F.31: Same as Fig. 7.21, but for the B1 scenario.

MSM projections

First malaria season

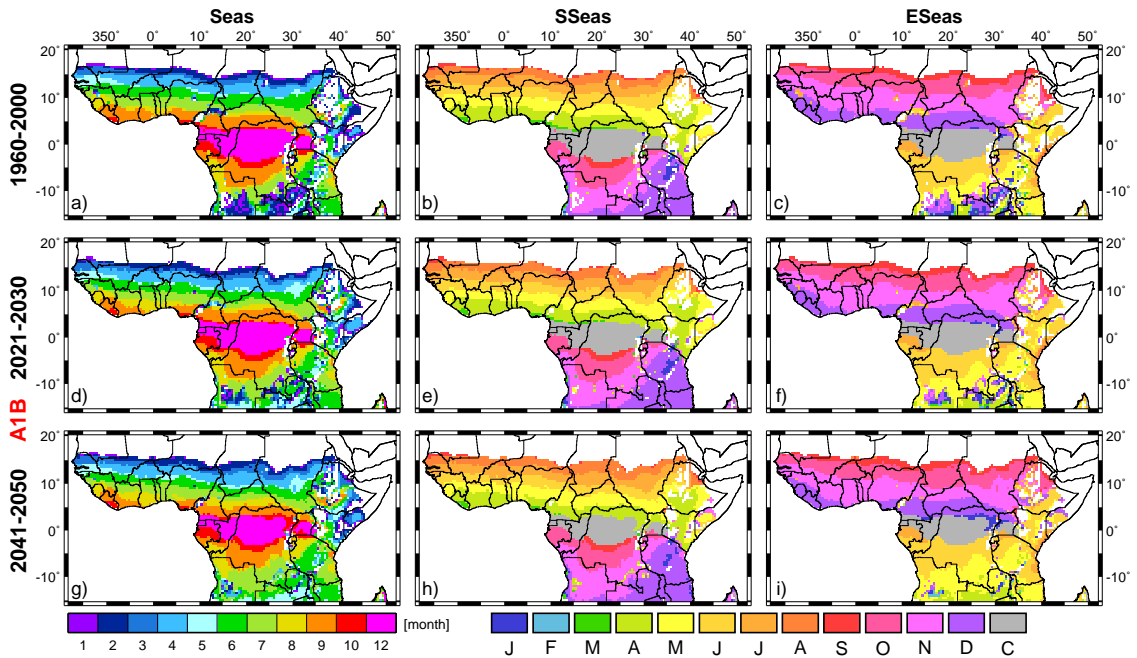


Fig. F.32: MSM simulations of (a, d & g) the length of the malaria season (*Seas*; in months), (b, e & h) the start (*SSeas*), and (c, f & i) the end month (*ESeas*) of malaria transmission (C: year-round transmission). Illustrated are values for (a-c) the present-day climate (1960-2000) as well as for (d-f) 2021-2030 and (g-i) 2041-2050 of the A1B scenario. Regarding *SSeas* and *ESeas* only the first season is shown for areas with two malaria seasons.

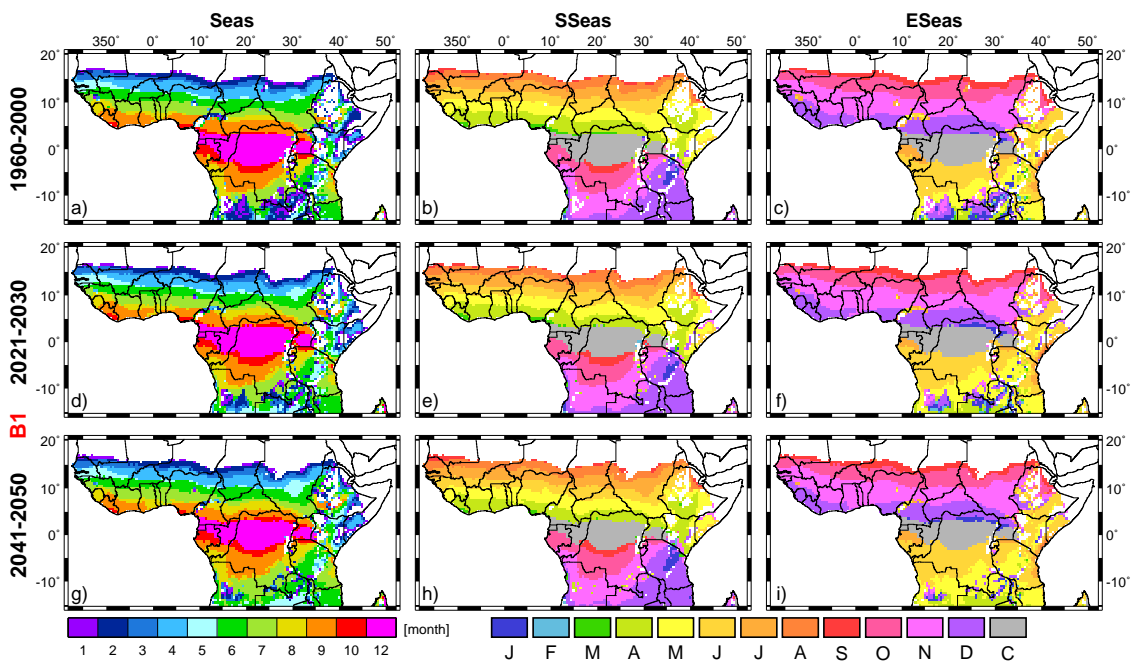


Fig. F.33: Same as Fig. F.32, but here for the B1 scenario.

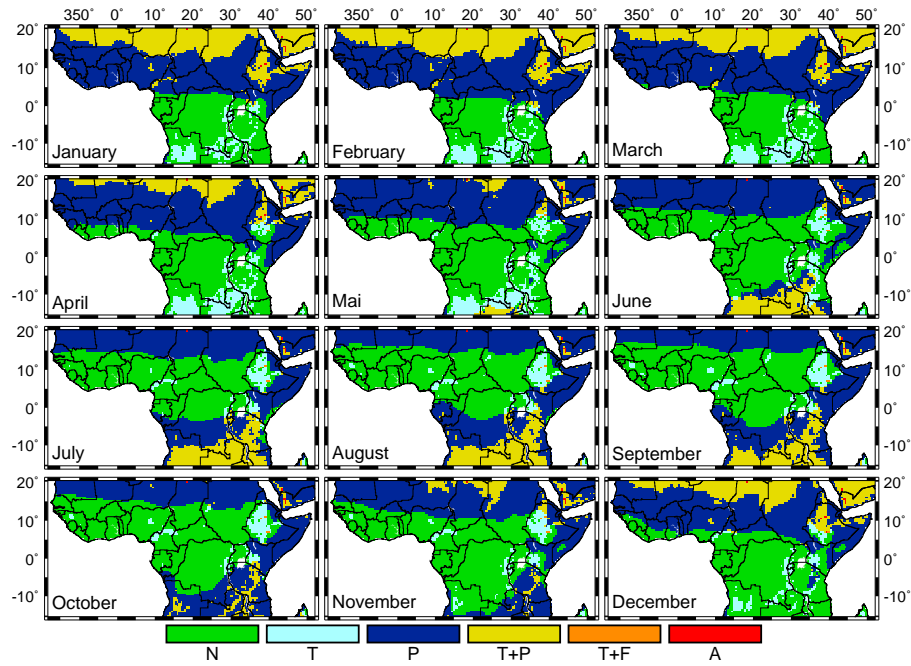


Fig. F.34: Same as Fig. 7.10, but for constraints of malaria transmission of single months.

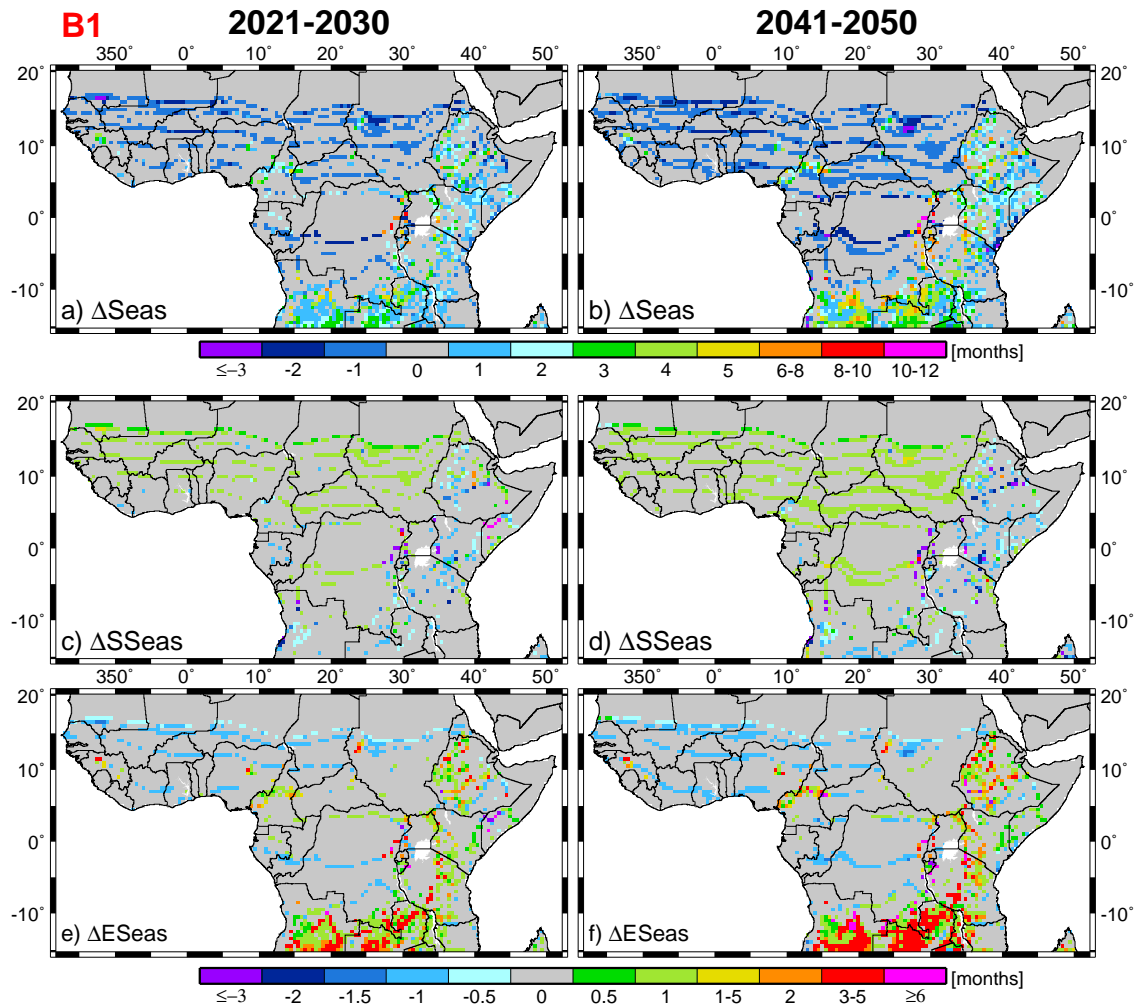


Fig. F.35: Same as Fig. 7.22, but for the B1 scenario.

Second malaria season

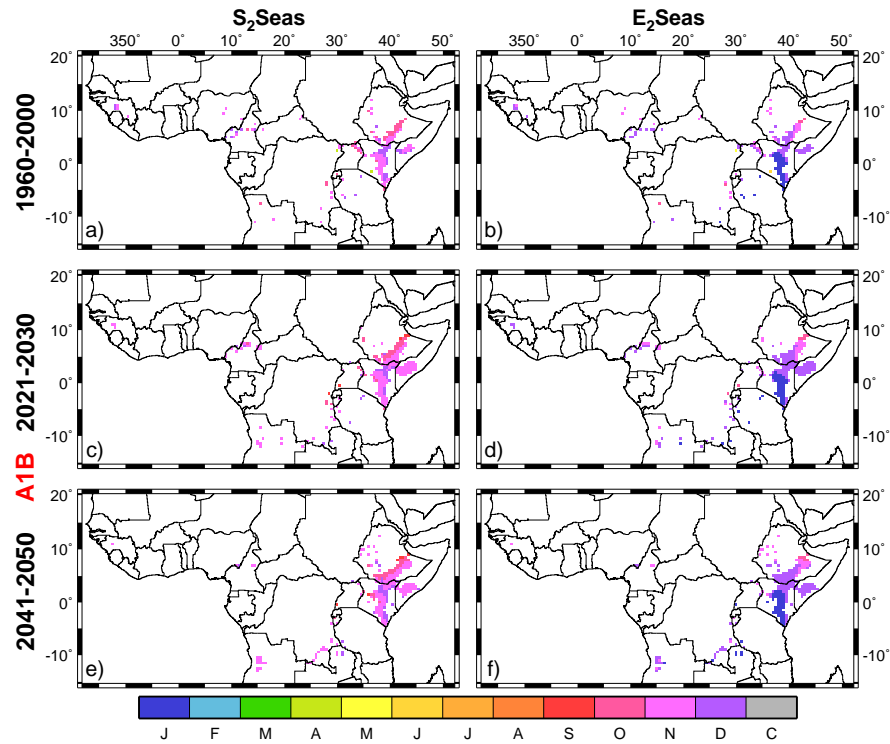


Fig. F.36: MSM simulations of the second malaria season in terms of the present-day climate as well as the A1B scenario. Graphics in (a, c & e) exhibit the start (S_2Seas) and in (b, d & f) the end month (E_2Seas) of the second malaria season. (a & b) represent the period 1960-2000, (c & d) 2021-2030, and (e & f) 2041-2050. Note, only areas with two malaria seasons are considered.

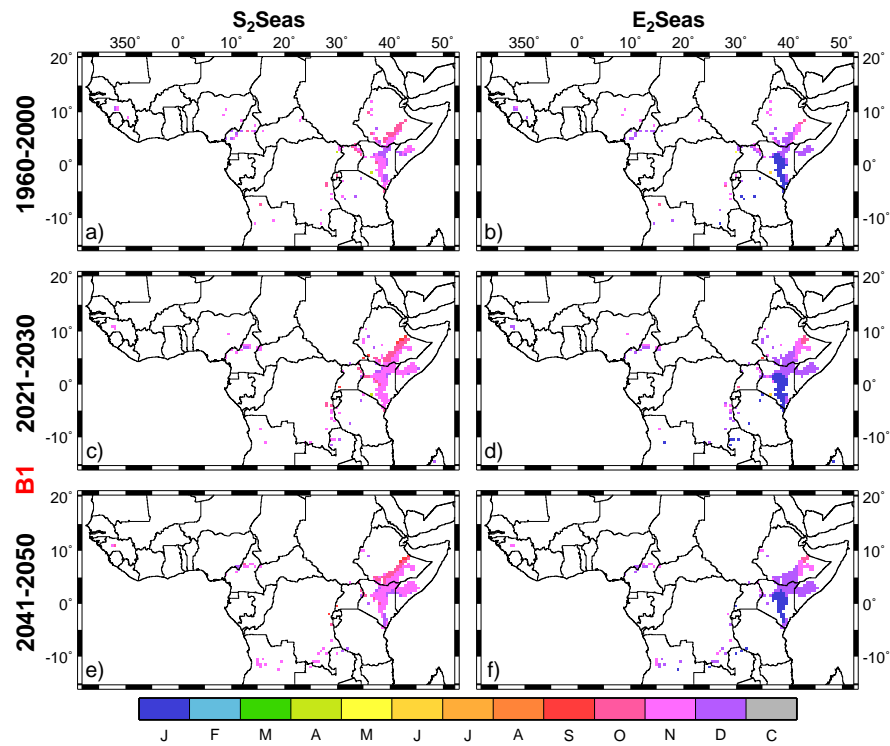


Fig. F.37: Same as Fig. F.36, but here for the B1 emission scenario.

G Geographical information

Tab. G.1: Information relative to synoptic weather stations from West Africa and Cameroon. The country, name, identifier, latitude and longitude positions, as well as the elevation of meteorological stations are given. The LMM was driven by reconstructed temperature and precipitation time series (1973-2006) from these meteorological stations.

country	name	identifier	longitude	latitude	elevation [m]
Niger	Tillabéry	61036	1°27'E	14°12'N	210
Niger	Niamey	61052	2°10'E	13°29'N	227
Niger	Maradi	61080	7°05'E	13°28'N	373
Niger	Magaria	61091	8°56'E	12°59'N	403
Niger	Gaya	61099	3°27'E	11°53'N	203
Mali	Gao	61226	0°03'W	16°16'N	260
Mali	Mopti Barbe	61265	4°06'W	14°31'N	272
Mali	Bamako Senou	61291	7°57'W	12°32'N	381
Mauritania	Rosso	61489	15°49'W	16°30'N	6
Senegal	Saint-Louis	61600	16°27'W	16°03'N	4
Senegal	Podor	61612	14°58'W	16°39'N	7
Senegal	Linguère	61627	15°07'W	15°23'N	21
Senegal	Dakar Yoff	61641	17°30'W	14°44'N	24
Senegal	Diourbel	61666	16°14'W	14°39'N	9
Senegal	Kaolack	61679	16°04'W	14°08'N	7
Senegal	Tambacounda	61687	13°41'W	13°46'N	50
Senegal	Ziguinchor	61695	16°16'W	12°33'N	23
Gambia, The	Banjul Yundum	61701	16°48'W	13°21'N	33
Cameroon	Koundja Foumban	64893	10°45'E	5°39'N	1210
Cameroon	Douala	64910	9°44'E	4°00'N	9
Cameroon	Yaoundé	64950	11°31'E	3°50'N	760
Benin	Kandi	65306	2°56'E	11°08'N	292
Benin	Natitingou	65319	1°23'E	10°19'N	461
Benin	Parakou	65330	2°37'E	9°21'N	393
Benin	Savé	65335	2°29'E	8°02'N	200
Benin	Bohicon	65338	2°04'E	7°10'N	166
Benin	Cotonou	65344	2°23'E	6°21'N	9
Burkina Faso	Dori	65501	0°02'W	14°02'N	277
Burkina Faso	Ouagadougou	65503	1°31'W	12°21'N	306
Burkina Faso	Bobo-Dioulasso	65510	4°19'W	11°10'N	460
Burkina Faso	Po	65518	1°09'W	11°09'N	322
Burkina Faso	Korhogo	65536	5°37'W	9°25'N	381
Côte d'Ivoire	Bouaké	65555	5°04'W	7°44'N	376
Côte d'Ivoire	Dimbokro	65562	4°42'W	6°39'N	92

Glossary

An. gambiae s.l.

The term *Anopheles gambiae sensu lato* comprises six morphologically hardly distinguishable *Anopheles* species: *Anopheles gambiae sensu stricto* Giles (1902), *Anopheles arabiensis* Patton (1905), *Anopheles quadriannulatus* Theobald (1911), *Anopheles bwambiae* White (1985), *Anopheles merus* Dönitz (1902), and *Anopheles melas* Theobald (1903). 2

Anopheles

Anopheles is a genus of mosquito from the family Culicidae. Several hundred *Anopheles* species are recognised. About 100 of these species are able to transmit human malaria, while commonly only a few tens are vectors of malaria. 2

aestivation

Aestivation is a physical state of adult mosquitoes, when mosquitoes remain inactive, except for sporadic journeys to obtain blood-meals to sustain themselves. Aestivating females can be distinguished because they become gonotrophically discordant and do not develop eggs after taking a blood meal (Charlwood et al. 2000). 29

anthropophilic

Preferring human beings to other animals, such as a mosquito. An anthropophilic mosquito hence predominantly takes blood meals on humans. 84

anthropophily

Anthropophily describes mosquitoes that are *anthropophilic*. 2

asexual parasite ratio

The asexual parasite ratio is the proportion of the survey population that is confirmed positive for the malaria parasite. Naturally, it is determined by taking standard thick and thin blood smears from volunteers, staining slides with Giemsa, and examining slides by a microscope (Beier et al. 1999). Malaria parasites are

identified and counted canonically by immature ring stage trophozoites (Hay and Snow 2006). 23

asymptomatic

In medicine, a disease is asymptomatic while the patient does not experience symptoms. Asymptomatic diseases may not be discovered until the patient undergoes medical tests. 23

box-and-whisker plot

A box-and-whisker plot (sometimes called simply box plot) is a histogram-like method of displaying data. Box-and-whisker plots provide information relative to lower and upper extremes, lower and upper quartiles, as well as the median of the considered data. 47

climate

Climate represents an averaged weather, which is observed over a long lasting period. In meteorology, climate is defined via the 30 year climate normal period (e.g., 1961-1990). 47

climate change

The term climate change refers to a statistically significant variation of the mean state of climate or of its variability. This variation must hold on for an extended period (e.g., 30 years). 1

control run

During a control run it is tested if a model is able to produce a realistic statistic. 53

cross-sectional survey

A cross-sectional survey provides a ‘snapshot’ of the frequency and characteristics of a disease in a population at a particular point in time. 126

degree-day

The time needed to complete a temperature dependent process can be expressed in the term $\frac{dd}{T-T_-}$. Here the degree-day (dd) represents accumulation of temperature units ($T - T_-$) over time (e.g., if $dd=110$ K and $T - T_-=10$ K, the process would last 11 days). At temperatures below the temperature threshold (T_-) the process is not accomplished. 73

endemic

Malaria transmission is endemic, when the disease can persist/survive in a region for any length of time. 23

endophilic

Mosquitoes are endophilic when they prefer to rest indoors after feeding on humans (endophilic). 84

endophily

Endophily describes mosquitoes that are *endophilic*. 85

ensemble runs

Climate projections are in general performed by ensemble runs. Every run of an atmospheric model can only produce a certain statistic of weather conditions that determines the model climate. Confidence is therefore improved in a larger universal set that is when several runs are performed by using the same forcing but different starting conditions. The output from several simulations therefore samples uncertainty in the initial state. Such a group of runs is termed 'ensemble' and represents a more robust statistical set than the output from any ensemble member. 16

epidemic

A disease is epidemic, when occasional disease outbreaks occur in normally disease-free areas. Studies might also relate the term epidemic to unusual high seasonal transmission levels. 9

epidemiology

Epidemiology is the investigation of factors affecting the health and illness of populations. 25

exophilic

An exophilic mosquito tends to inhabit/rest outdoors. An exophilic animal is ecologically independent of humans and their domestic environment. 84

gametocytaemia

Presence of gametocytes in the peripheral blood is called gametocytaemia. 87

gametocyte

A gametocyte, either male or female, is a cell that is specialised in the transmission of the malaria parasite between humans and mosquitoes. Five different maturation stages of *P. falciparum* gametocytes are known (Talman et al. 2004). 22

gametocytogenesis

Production of mature male and female gametocytes is termed gametocytogenesis. 86

gonotrophic cycle

The gonotrophic cycle denotes the time for preparation of a brood in female *Anopheles*. It includes development of eggs within the mosquito female as well as the time between the egg deposition and the blood meal of the mosquito female. 28

greenhouse gas

Greenhouse gases absorb and emit infrared terrestrial radiation at special given wavelengths. Primary greenhouse gases of the atmosphere are carbon dioxide, water vapour, nitrous oxide, methane, and ozone. 1

horizontal life table

Horizontal life tables provide information of distinct cohorts following through time. 77

host

A host is a human, animal, or plant on which or in which another organism lives. 2

incidence

Incidence is usually a measure of risk of developing some new condition within a specified period of time. However, incidence often loosely expresses simply the number of new cases during a particular time period. 31

incubation period

The incubation period is the time between infection and appearance of symptoms of disease. 28

infection

Infection is the detrimental colonization of a host organism by foreign species. In the present study, malaria infected hosts are not infectious. 22

infectious

A necessary condition for disease transmission from one host to another is the presence of pathogenic microbial agents. Regarding malaria the term infectious relates either to humans harbouring mature gametocytes or to mosquitoes carrying sporozoites in their salivary glands. 21

inoculation

Inoculation is the placement of something to where it will grow or reproduce. It is, for example, used in respect of the communication of a disease to a living organism by transferring its causative agent into an organism. In case of malaria, the malaria parasite is introduced into the human host. 24

merozoite

A merozoite is a daughter cell of a protozoan parasite. Merozoites are result of asexual reproduction (e.g., schizogony). In malaria, merozoites infect red blood cells and rapidly reproduce asexually. They break and destroy red blood cells and subsequently infect others. 21

morbidity

Morbidity is defined as the rate of occurrence of disease within a population and given time period. 3

mortality

Mortality is the rate of occurrence of death due to a disease within a population and time period. 2

mosquito

A mosquito is an insect of the family Culicidae and order Diptera (two-winged flies) population. About 3,500 mosquito species are known. Mosquito females deposit their eggs into or in the vicinity of standing water. Egg, larvae, and pupal stages are entirely aquatic. 1

multi-model

Data from several models is the basis for multi-model data sets. Uncertainties and weaknesses of single models are partially overcome by analysing data from the multi-model. Assuming that simulation errors in different models are independent, the average of the multi-model is expected to outperform individual ensemble members. Such a multi-model ensemble is, for example, instrumental in analysing probabilistic projections of the future climate. 16

nulliparous

In entomology, nulliparous refers to the parity of females. A female mosquito that never produced eggs is termed nulliparous. 79

ovariole

An ovariole is one of the tubes of which ovaries of most insects are composed. 78

parous

In entomology, parous refers to the parity of females. A female mosquito already producing eggs is termed parous. 78

potential evaporation

Potential evaporation is a measure of the degree to which the weather or climate of a region is favourable to the process of evaporation (Glickman 2000). It is defined

as the amount of evaporation that would occur if a sufficient water source would be available. 100

prepatent period

The so-called prepatent period is the time needed for the detection of asexual parasites in blood after infection of a human via a female mosquito. 86

prevalence

In epidemiology, the prevalence of a disease in a population is defined as the total number of cases of disease in the population, divided by the number of individuals in the population. In case of malaria the term prevalence denotes the proportion of the population that is carrier of the malaria parasite. 23

protozoa

The protozoa are one-celled animals, they breathe, move, and reproduce like multi-celled animals. Some protozoans are harmful to man as they cause serious diseases. However, others are helpful because they eat, for example, harmful bacteria. 1

scenario

Scenarios are descriptions of the future state of, for example, climate or land cover. Scenarios are based upon observations of the past and they extrapolate actual trends into the future. 12

sequestration

During sequestration a fraction of asexual parasites develops into gametocytes (gamete precursors) while sequestered in deep tissues (Eichner et al. 2001). 22

sporogonic cycle

The sporogonic cycle denotes the development of the malaria parasite in female mosquitoes. The cycle starts when mosquitoes receive gametocytes from human blood and is terminating when sporozoites reach the salivary glands. The sporogonic cycle is governed by temperature and requires temperatures above a certain minimum temperature, the so-called sporogonic temperature threshold. 23

sporogonic temperature threshold

The sporogonic temperature threshold is the minimum temperature needed to start the sporogonic cycle. 28

sporozoite

In case of malaria, sporozoites are cells that develop in the mosquito's salivary glands, leave the mosquito during a blood meal, and enter the liver where they multiply. Sporozoites are formed by sporogony, a type of sexual or asexual reproduction. 21

superinfection

Superinfection is the process by which a cell, that has previously been infected, gets coinfecting with a different parasite strain. An individual can receive more than one infective inoculation of parasites via multiple infectious bites. 25

transmission blocking immunity

Transmission-blocking immunity is a form of immunity, which is largely antibody mediated and operates in the mosquito midgut to block either fertilization of female gametes by male gametes or subsequent zygote development (Wizel and Kumar 1991). 24

trophozoite

A trophozoite is the activated, feeding stage in the life cycle of protozoan parasites such as the malaria-causing *P. falciparum*. The trophozoite undergoes schizogony (asexual reproduction) and develops into a schizont containing merozoites. 21

vector

In biology, the term vector denotes an organism transmitting disease, infections, or foreign living material. Vector control is hence a method limiting or eradicating vectors. 1

vectorial capacity

Vectorial Capacity (VC) is the number of potentially contacts an individual human makes, through the vector population, per unit time (Dietz et al. 1974). VC is computed by means of the following equation (cp. Garrett-Jones 1964), where n_f is the number of female mosquitoes per human, a is the human blood index, n_s is the duration of the extrinsic incubation period, and p_d is the daily survival probability of mosquitoes: $VC = \frac{n_f a^2 p_d^{n_s}}{-\ln(p_d)}$. 35

vertical life table

Vertical life tables provide information for populations with overlapping generations and age distributions remaining stationary during a sampling period. 77

zoophilic

Zoophilic mosquitoes tend to feed on animals. 84

zoophily

Zoophily describes mosquitoes that are *zoophilic*. 2

References

- Abdel-Wahab, A., A.-M. A. Abdel-Muhsin, E. Ali, S. Suleiman, S. Ahmed, D. Walliker, and H. A. Babiker, 2002: Dynamics of Gametocytes among *Plasmodium falciparum* Clones in Natural Infections in an Area of Highly Seasonal Transmission. *The Journal of Infectious Diseases*, **185**, 1838–1842.
- Ahumada, J. A., D. Lapointe, and M. D. Samuel, 2004: Modeling the Population Dynamics of *Culex quinquefasciatus* (Diptera: Culicidae), along an Elevational Gradient in Hawaii. *Journal of Medical Entomology*, **41**, 1157–1170.
- Akogbeto, M., 1995: Étude entomologique sur la transmission du paludisme côtier lagunaire: cas d'un village construit sur un lac d'eau saumâtre. *Annales de la Société Belge de Médecine Tropicale*, **75**, 219–227.
- Akogbeto, M., 2000: Le paludisme côtier lagunaire à Cotonou: données entomologiques. *Cahiers Santé*, **10**, 267–275.
- Akogbeto, M., J. P. Chippaux, and M. Coluzzi, 1992: Le paludisme urbain côtier à Cotonou (République du Bénin). Étude entomologique. *Revue d'Epidémiologie et de Santé Publique*, **40**, 233–239.
- Akogbeto, M. and A. Nahum, 1996: Impact des moustiquaires imprégnées de deltaméthrine sur la transmission du paludisme dans un milieu côtier lagunaire, Bénin. *Bulletin de la Société de Pathologie Exotique*, **89**, 291–298.
- Ali, A. and T. Lebel, 2009: The Sahelian standardized rainfall index revisited. *International Journal of Climatology*, **29**, 1705–1714.
- Ali, E., M. J. Mackinnon, A. A. Abdel-Muhsin, S. Ahmed, D. Walliker, and H. A. Babiker, 2006: Increased density but not prevalence of gametocytes following drug treatment of *Plasmodium falciparum*. *Transactions of the Royal Society of Tropical Medicine and Hygiene*, **100**, 176–183.
- Allard, P., 2000: Der Einfluß von 'African Easterly Waves'-Ereignissen auf den Niederschlag und die Feuchtetransporte für ausgewählte Gebiete in Westafrika. M.S. thesis, Institute for Geophysics and Meteorology, University of Cologne, 79 pp., Cologne, Germany.
- Anderson, R. M. and R. M. May, 1991: *Infectious Diseases of Humans: Transmission and Control*. Oxford University Press, 757 pp.
- Aniedu, I., M. J. Mutinga, and C. M. Muteru, 1993: Vertical estimates of survivorship of larvae and pupae of *Anopheles gambiae* Giles complex in Baringo district, Kenya. *Insect Science and its Application*, **14**, 39–48.
- Antonio-Nkondjio, C., P. Awono-Ambene, J. C. Toto, M. Y. Meunier, S. Z.-K. R. Nyambam, C. S. Wondji, T. Tchuinkam, and D. Fontenille, 2002: High malaria transmission intensity in a village close to Yaounde, the capital city of Cameroon. *Journal of Medical Entomology*, **39**, 350–355.
- Antonio-Nkondjio, C., F. Simard, P. Awono-Ambene, P. Ngassam, J. C. Toto, T. Tchuinkam, and D. Fontenille, 2005: Malaria vectors and urbanization in the equatorial forest region of south Cameroon. *Transactions of the Royal Society of Tropical Medicine and Hygiene*, **99**, 347–354.
- Appawu, M., S. Owusu-Agyei, S. Dadzie, V. Asola, F. Anto, K. Koram, W. Rogers, F. Nkrumah, S. L. Hoffman, and D. J. Fryauff, 2004: Malaria transmission dynamics at a site in northern Ghana proposed for testing malaria vaccines. *Tropical medicine and international health*, **9**, 164–170.
- Aron, J. L., 1988: Mathematical modelling of immunity to malaria. *Mathematical Biosciences*, **90**, 385–396.
- Aron, J. L. and R. May, 1982: The population dynamics of malaria. *Population dynamics of infectious diseases*, R. M. Anderson, Ed., Chapman and Hall, London, United Kingdom, 139–179.
- Arredondo-Jimenez, J. I., M. H. Rodriguez, and R. K. Washino, 1998: Gonotrophic cycle and survivorship of *Anopheles vestitipennis* (Diptera: Culicidae) in two different ecological areas of southern Mexico. *Journal of Medical Entomology*, **35**, 937–942.
- Atangana, J., E. Fondjo, A. Fomena, J. L. Tamesse, S. Patchoké, H. N. M. Ndjemai, and P. A. B. Ndong, 2009: Seasonal variations of malaria transmission in Western Cameroon highlands: Entomological, parasitological and clinical investigations. *Journal of Cell and Animal Biology*, **3**, 33–38.
- Awolola, T. S., O. Okwa, R. H. Hunt, A. F. Ogunrinade, and M. Coetzee, 2002: Dynamics of the malaria-vector populations in coastal Lagos, south-western Nigeria. *Annals of Tropical Medicine and Parasitology*, **96**, 75–82.
- Ba, M. B. and S. E. Nicholson, 1998: Analysis of Convective Activity and its Relationship to the Rainfall over the Rift Valley Lakes of East Africa during 1983-90 Using the Meteosat Infrared Channel. *Journal of Applied Meteorology*, **37**, 1250–1264.
- Babiker, H. A., A.-M. A. Abdel-Muhsin, L. C. Ranford-Cartwright, G. Satti, and D. Walliker, 1998: Characteristics of *Plasmodium falciparum* parasites that survive the lengthy dry season in eastern Sudan where malaria transmission is markedly seasonal. *The American Journal of Tropical Medicine and Hygiene*, **59**, 582–590.
- Babiker, H. A., A. Abdel-Wahab, S. Ahmed, S. Suleiman, L. Ranford-Cartwright, R. Carter, and D. Walliker, 1999: Detection of low level *Plasmodium falciparum* gametocytes using reverse transcriptase polymerase chain reaction. *Molecular and Biochemical Parasitology*, **99**, 143–148.
- Bader, J. and M. Latif, 2003: The impact of decadal-scale Indian Ocean sea surface temperature anomalies on Sahelian rainfall and the North Atlantic Oscillation. *Geophysical Research Letters*, **30**, 2169, doi:10.1029/2003GL018426.
- Balas, N., S. E. Nicholson, and D. Klotter, 2007: The relationship of rainfall variability in West Central Africa to sea-surface temperature fluctuations. *International Journal of Climatology*, **27**, 1335–1349.
- Balls, M. J., R. Bødker, C. J. Thomas, W. Kisinza, H. A. Msangeni, and S. W. Lindsay, 2004: Effect of topography on the risk of malaria infection in the Usambara Mountains, Tanzania. *Transactions of the Royal Society of Tropical Medicine and Hygiene*, **98**, 400–408.
- Balme, M., T. Vischel, T. Lebel, C. Peugeot, and S. Galle, 2006: Assessing the water balance in the Sahel: Impact of small scale rainfall variability on runoff. Part 1: Rainfall variability analysis. *Journal of Hydrology*, **331**, 336–348.
- Barnish, G., G. H. Maude, M. J. Bockarie, O. A. Erunkulu, M. S. Dumbuya, and B. M. Greenwood, 1993: Malaria in a rural area of Sierra Leone. II. Parasitological and related results from pre- and post-rains clinical surveys. *Annals of Tropical Medicine and Parasitology*, **87**, 137–148.
- Bayoh, M. N., 2001: Studies on the development and survival of *Anopheles gambiae sensu stricto* at various temperatures and relative humidities. Ph.D. thesis, University of Durham, Durham, South Africa.
- Bayoh, M. N. and S. W. Lindsay, 2003: Effect of temperature on the development of the aquatic stages of *Anopheles gambiae sensu stricto* (Diptera: Culicidae). *Bulletin of Entomological Research*, **93**, 375–381.
- Bayoh, M. N. and S. W. Lindsay, 2004: Temperature-related duration of aquatic stages of the Afrotropical malaria vector mosquito *Anopheles gambiae* in the laboratory. *Medical and Veterinary Entomology*, **18**, 174–179.
- Behera, S. K., J.-J. Luo, S. Masson, P. Delecluse, S. Gualdi, A. Navarra, and T. Yamagata, 2005: Paramount Impact of the Indian Ocean Dipole on the East African Short Rains: A CGCM Study. *Journal of Climate*, **18**, 4514–4530.
- Beier, J. C., R. Copeland, C. Oyaro, A. Masinya, W. O. Odago, S. Oduor, D. K. Koech, and C. R. Roberts, 1990: *Anopheles gambiae* complex egg-stage survival in dry soil from larval development sites in western Kenya. *Journal of the American Mosquito Control Association*, **6**, 105–109.
- Beier, J. C., J. R. Davis, J. A. Vaughan, B. H. Noden, and M. S. Beier, 1991: Quantitation of *Plasmodium falciparum* Sporozoites Transmitted In Vitro by Experimentally Infected *Anopheles gambiae* and *Anopheles stephensi*. *The American Journal of Tropical Medicine and Hygiene*, **44**, 564–570.
- Beier, J. C., G. F. Killen, and J. I. Githure, 1999: Entomologic inoculation rates and *Plasmodium falciparum* malaria prevalence in Africa. *The American Journal of Tropical Medicine and Hygiene*, **61**, 109–113.

- Beier, J. C., C. N. Oster, F. K. Onyango, J. D. Bales, J. A. Sherwood, P. V. Perkins, D. K. Chumo, D. V. Koech, R. E. Whitmire, C. R. Roberts, C. L. Diggs, and S. L. Hoffman, 1994: *Plasmodium falciparum* incidence relative to entomologic inoculation rates at a site proposed for testing malaria vaccines in western Kenya. *The American Journal of Tropical Medicine and Hygiene*, **50**, 529–536.
- Beier, M. S., J. C. Beier, A. A. Merdan, B. M. E. Sawaf, and M. A. Kadder, 1987: Laboratory rearing techniques and adult life table parameters for *Anopheles gambiae* from Egypt. *Journal of the American Mosquito Control Association*, **3**, 266–270.
- Bekessy, A., L. Molineaux, and Y. Storey, 1976: Estimation of incidence and recovery rates of *Plasmodium falciparum* parasitaemia, from longitudinal data. *Bulletin of the World Health Organization*, **54**, 685–693.
- Beltrando, G. and P. Camberlin, 1993: Interannual variability of rainfall in the eastern Horn of Africa and indicators of atmospheric circulation. *International Journal of Climatology*, **13**, 533–546.
- Besancenot, J.-P., P. Handschumacher, J.-A. Ndione, I. Mbaye, and K. Laaidi, 2004: Climat, eau et santé au Sahel ouest-africain. *Sécheresse*, **15**, 233–241.
- Biasutti, M. and A. Giannini, 2006: Robust Sahel drying in response to late 20th century forcings. *Geophysical Research Letters*, **33**, L11 706, doi:10.1029/2006GL026067.
- Binka, F. N., S. S. Morris, D. A. Ross, P. Arthur, and M. E. Aryeetey, 1994: Patterns of malaria morbidity and mortality in children in northern Ghana. *Transactions of the Royal Society of Tropical Medicine and Hygiene*, **88**, 381–385.
- Birley, M. H. and P. K. Rajagopalan, 1981: Estimation of the survival and biting rates of *Culex quinquefasciatus* (Diptera: Culicidae). *Journal of Medical Entomology*, **18**, 181–186.
- Björkman, A., P. Hedman, J. Brohult, M. Willcox, I. Diamant, P. O. Pehrsson, L. Rombo, and E. Bengtsson, 1985: Different malaria control activities in an area of Liberia - effects on malarial metrics parameters. *Annals of Tropical Medicine and Parasitology*, **79**, 239–246.
- Black, E., J. Slingo, and K. R. Sperber, 2003: An Observational Study of the Relationship between Excessively Strong Short Rains in Coastal East Africa and Indian Ocean SST. *Monthly Weather Review*, **131**, 74–94.
- Block, P. and B. Rajagopalan, 2007: Interannual Variability and Ensemble Forecast of Upper Blue Nile Basin *Kiremt* Season Precipitation. *Journal of Hydrometeorology*, **8**, 327–343.
- Bockarie, M. J., M. W. Service, G. Barnish, G. H. Maude, and B. M. Greenwood, 1994: Malaria in a rural area of Sierra Leone. III. Vector ecology and disease transmission. *Annals of Tropical Medicine and Parasitology*, **88**, 251–262.
- Bockarie, M. J., M. W. Service, G. Barnish, and Y. T. Touré, 1995: Vectorial capacity and entomological inoculation rates of *Anopheles gambiae* in a high rainfall forested area of southern Sierra Leone. *Tropical Medicine and Parasitology*, **46**, 164–171.
- Bockarie, M. J., M. W. Service, Y. T. Touré, S. Traoré, G. Barnish, and B. M. Greenwood, 1993: The ecology and behaviour of the forest form of *Anopheles gambiae*. *Parassitologia*, **35** (Suppl.), 5–8.
- Bödker, R., 2000: Malaria in the Usambara mountains, Tanzania. Ph.D. thesis, Danish Bilharziasis Laboratory, University of Copenhagen, Copenhagen, Denmark.
- Bonnet, S., L. C. Gouagna, R. E. Paul, I. Safeukui, J.-Y. Meunier, and C. Boudin, 2003: Estimation of malaria transmission from humans to mosquitoes in two neighbouring villages in south Cameroon: evaluation and comparison of several indices. *Transactions of the Royal Society of Tropical Medicine and Hygiene*, **97**, 53–59.
- Bonnet, S., R. E. Paul, C. Gouagna, I. Safeukui, J. Y. Meunier, R. Gounoue, and C. Boudin, 2002: Level and dynamics of malaria transmission and morbidity in an equatorial area of South Cameroon. *Tropical Medicine and International Health*, **7**, 249–256.
- Bonora, S., F. G. D. Rosa, M. Boffito, G. D. Perri, and A. Rossati, 2001: Rising temperature and the malaria epidemic in Burundi. *Trends in Parasitology*, **17**, 572–573.
- Boudin, C., A. Diop, A. Gaye, L. Gadiaga, C. Gouagna, I. Safeukui, and S. Bonnet, 2005: *Plasmodium falciparum* transmission blocking immunity in three areas with perennial or seasonal endemicity and different levels of transmission. *The American Journal of Tropical Medicine and Hygiene*, **73**, 1090–1095.
- Boudin, C., M. Olivier, J.-F. Molez, J.-P. Chiron, and P. Ambroise-Thomas, 1993: High human malarial infectivity to laboratory-bred *Anopheles gambiae* in a village in Burkina Faso. *The American Journal of Tropical Medicine and Hygiene*, **48**, 700–706.
- Boudin, C., V. Robert, P. Carnevale, and T. P. Ambroise, 1991a: Epidemiology of *Plasmodium falciparum* in a rice field and a savanna area in Burkina Faso: seasonal fluctuations of gametocytaemia and malaria infectivity. *Annals of Tropical medicine and Parasitology*, **85**, 377–385.
- Boudin, C., V. Robert, P. Carnevale, and P. Ambroise-Thomas, 1992: Epidemiology of *Plasmodium falciparum* in a rice field and a savanna area in Burkina Faso. Comparative study on the acquired immunoprotection in native populations. *Acta Tropica*, **51**, 103–111.
- Boudin, C., V. Robert, J. P. Verhave, P. Carnevale, and P. Ambroise-Thomas, 1991b: *Plasmodium falciparum* and *P. malariae* epidemiology in a West African village. *Bulletin of the World Health Organization*, **69**, 199–205.
- Bouma, M. J., H. E. Soudrop, and H. J. van der Kaay, 1994: Health and climate change. *The Lancet*, **343**, 302.
- Bousema, J. T., L. C. Gouagna, C. J. Drakeley, A. M. Meutstege, B. A. Okech, I. N. J. Akim, J. C. Beier, J. I. Githure, and R. W. Sauerwein, 2004: *Plasmodium falciparum* gametocyte carriage in asymptomatic children in western Kenya. *Malaria Journal*, **3**, 18.
- Boyd, M. F., 1949: *Malariaology*, Vol. 1. WB Saunders Co., Philadelphia, USA, 787 pp.
- Breman, J. G., A. Egan, and G. T. Keusch, 2001: Introduction and summary: The intolerable burden of malaria: A new look at the numbers. *The American Journal of Tropical Medicine and Hygiene*, **64** (Suppl. 1-2), iv–vii.
- Briët, O. J. T., 2002: A simple method for calculating mosquito mortality rates, correcting for seasonal variations in recruitment. *Medical and Veterinary Entomology*, **16**, 22–27.
- Briët, O. J. T., J. Dossou-Yovo, E. Akodo, N. van de Giesen, and T. M. Teuscher, 2003: The relationship between *Anopheles gambiae* density and rice cultivation in the savannah zone and forest zone of Côte d'Ivoire. *Tropical Medicine and International Health*, **8**, 439–448.
- Brinkmann, U. and A. Brinkmann, 1991: Malaria and health in Africa: the present situation and epidemiological trends. *Tropical Medicine and Parasitology*, **42**, 204–213.
- Brown, V., M. A. Issak, M. Rossi, P. Barboza, and A. Paugam, 1998: Epidemic of malaria in north-eastern Kenya. *The Lancet*, **352**, 1356–1357.
- Bruce-Chwatt, L. J., 1951: Gametocyte rates. *Transactions of the Royal Society of Tropical Medicine and Hygiene*, **44**, 761–763.
- Brücher, T., 2008: Verbesserung der Simulation des westafrikanischen Klimas durch die Implementierung eines einfachen dynamischen Vegetationsmodells (SVege) in das Klimamodell ECHAM5. Ph.D. thesis, University of Cologne, 168 pp., Cologne, Germany.
- Buckle, C., 1996: *Weather and Climate in Africa*. Longman Publishing Group, United Kingdom, 320 pp.
- Buckling, A., L. Crooks, and A. F. Read, 1999: *Plasmodium chabaudi*: Effect of Antimalarial Drugs on Gametocytogenesis. *Experimental Parasitology*, **93**, 45–54.
- Buckling, A. and A. F. Read, 2001: The effect of partial host immunity on the transmission of malaria parasites. *Proceedings of the Royal Society of London, Series B*, **268**, 2325–2330.
- Burkot, T. R., W. G. Goodman, and G. R. DeFoliart, 1984a: Identification of mosquito blood meals by enzyme-linked immunosorbent assay. *American Society of Tropical Medicine and Hygiene*, **30**, 1336–1341.
- Burkot, T. R., P. M. Graves, R. Paru, D. Battistutta, A. Barnes, and A. Saul, 1990: Variations in malaria transmission rates are not related to anophelines survivorship per feeding cycle. *The American Journal of Tropical Medicine and Hygiene*, **43**, 321–327.
- Burkot, T. R., P. M. Graves, R. Paru, R. A. Wirtz, and P. F. Heywood, 1988: Human malaria transmission studies in the *Anopheles punctulatus* complex in Papua New Guinea: Sporozoite rates, inoculation rates, and sporozoite densities. *The American Journal of Tropical Medicine and Hygiene*, **39**, 135–144.
- Burkot, T. R., J. L. Williams, and I. Schneider, 1984b: Identification of *Plasmodium falciparum*-infected mosquitoes by a double antibody enzyme-linked immunosorbent assay. *The American Journal of Tropical Medicine and Hygiene*, **33**, 783–788.
- Burpee, R. W., 1972: The Origin and Structure of Easterly Waves in the Lower Troposphere of North Africa. *Journal of Atmospheric Sciences*, **29**, 77–90.
- Cadet, D. L. and N. O. Nnoli, 1987: Water vapor transport over Africa and the Atlantic Ocean during summer 1979. *The Quarterly Journal of the Royal Meteorological Society*, **113**, 581–602.
- Camberlin, P., 1995: June–September rainfall in North-Eastern Africa and atmospheric signals over the tropics: a zonal perspective. *International Journal of Climatology*, **15**, 773–783.
- Camberlin, P., 1997: Rainfall Anomalies in the Source Region of the Nile and Their Connection with the Indian Summer Monsoon. *Journal of Climate*, **10**, 1380–1392.
- Caminade, C., L. Teray, and E. Maconnave, 2006: West African monsoon system response to greenhouse gas and sulphate aerosol forcing under two emission scenarios. *Climate Dynamics*, **26**, 531–547.
- Cancré, N., A. Tall, C. Rogier, J. Faye, O. Sarr, J.-F. Trape, A. Spiegel, and F. Bois, 2000: Bayesian Analysis of an Epidemiologic Model of *Plasmodium falciparum* Malaria Infection in Ndio, Senegal. *American Journal of Epidemiology*, **152**, 760–770.
- Carlson, T. N., 1969a: Some remarks on African disturbances and their progress over the tropical Atlantic. *Monthly Weather Review*, **97**, 716–726.
- Carlson, T. N., 1969b: Synoptic histories of three African disturbances that developed into Atlantic hurricanes. *Monthly Weather Review*, **97**, 256–276.
- Carnevale, P., J. L. Frézil, M. F. Bosseno, F. le Pont, and J. Lancien, 1978: Etude de l'agressivité d'*Anopheles gambiae* A en fonction de l'âge et du sexe des sujets humains. *Bulletin of the World Health Organization*, **56**, 147–154.
- Carnevale, P., P. Guillet, V. Robert, D. Fontenille, J. Doannio, M. Coosemans, and J. Mouchet, 1999: Diversity of malaria in rice growing areas of the Afrotropical region. *Parassitologia*, **41**, 273–276.
- Carnevale, P., G. Le Goff, J.-C. Toto, and V. Robert, 1992: *Anopheles nili* as the main vector of human malaria in villages of southern Cameroon. *Medical and Veterinary Entomology*, **6**, 135–138.

- Carnevale, P. and V. Robert, 1987: Introduction of irrigation in Burkina Faso and its effect on malaria transmission. *Effects of Agricultural Development on Vector-borne Diseases*, FAO, Ed., FAO, Rome, Italy, 57–67.
- Carnevale, P., V. Robert, C. Boudin, J.-M. Halna, L. Pazart, P. Gazin, A. Richard, and J. Mouchet, 1988: La lutte contre le paludisme par des moustiquaires imprégnées de pyréthrinoides au Burkina Faso. *Bulletin de la Société de Pathologie Exotique*, **81**, 832–846.
- Cattani, J. A., J. L. Tulloch, H. Vrbova, D. Jolley, F. D. Gibson, J. S. Moir, P. F. Heywood, M. P. Alpers, A. Stevenson, and R. Clancy, 1986: The Epidemiology of Malaria in a Population Surrounding Madang, Papua New Guinea. *The American Journal of Tropical Medicine and Hygiene*, **35**, 3–15.
- Chalvet-Monfray, K., P. Sabatier, and D. J. Bicot, 2007: Downscaling modeling of the aggressiveness of mosquitoes vectors of diseases. *Ecological Modelling*, **204**, 540–546.
- Charlwood, J. D. and W. A. Alecrim, 1989: Capture-recapture studies with the South American malaria vector *Anopheles darlingi*, Root. *Annals of Tropical Medicine and Parasitology*, **83**, 569–576.
- Charlwood, J. D., T. Smith, P. F. Billingsley, W. Takken, E. O. K. Lyimo, and J. H. E. T. Meuwissen, 1997: Survival and infection probabilities of anthropophagic *anophelines* from an area of high prevalence of *Plasmodium falciparum* in humans. *Bulletin of Entomological Research*, **87**, 445–453.
- Charlwood, J. D., R. Vij, and P. F. Billingsley, 2000: Dry season refugia of Malaria-transmitting mosquitoes in a dry savannah zone of East Africa. *The American Journal of Tropical Medicine and Hygiene*, **62**, 726–732.
- Charlwood, J. D., J. Kihonda, S. Sama, P. F. Billingsley, H. Hadji, J. P. Verhave, E. Lyimo, P. C. Luttikhuisen, and T. Smith, 1995: The rise and fall of *Anopheles arabiensis* (Diptera: Culicidae) in a Tanzanian village. *Bulletin of Entomological Research*, **85**, 37–44.
- Charney, J., 1975: Dynamics of deserts and drought in the Sahel. *The Quarterly Journal of the Royal Meteorological Society*, **101**, 193–202.
- Chen, M., P. Xie, J. E. Janowiak, and P. A. Arkin, 2002: Global Land Precipitation: A 50-yr Monthly Analysis Based on Gauge Observations. *Journal of Hydrometeorology*, **3**, 249–266.
- Cherubini, T., S. Businger, C. Velden, and R. Ogasawara, 2006: Assimilation of satellite derived winds in mesoscale forecasts over Hawaii. *Monthly Weather Review*, **134**, 2009–2020.
- Christensen, J. H., B. Hewitson, A. Busuioac, A. Chen, X. Gao, I. Held, R. Jones, R. K. Kolli, W. T. Kwon, R. Laprise, V. M. na Rueda, L. Mearns, C. G. Menéndez, J. Räisänen, A. Rinke, A. Sarr, and P. Whetton, 2007a: Regional Climate Projections. *Climate Change 2007: The Physical Science Basis*, S. Solomon, D. Qin, M. Manning, Z. Chen, M. Marquis, K. B. Averyt, M. Tignor, and H. L. Miller, Eds., Cambridge University Press, Cambridge, United Kingdom and New York, USA, 847–940, contribution of Working Group I to the Fourth Assessment Report of the Intergovernmental Panel on Climate Change.
- Christensen, T., B. M. Knudsen, J.-P. Pommereau, G. Letrenne, A. Hertzog, F. Vial, J. Ovarlez, and M. Piot, 2007b: Evaluation of ECMWF ERA-40 temperature and wind in the lower tropical stratosphere since 1988 from past long-duration balloon measurements. *Atmospheric Chemistry and Physics*, **7**, 3399–3409.
- Clark, C. O., P. J. Webster, and J. E. Cole, 2003: Interdecadal Variability of the Relationship between the Indian Ocean Zonal Mode and East African Coastal Rainfall Anomalies. *Journal of Climate*, **16**, 548–554.
- Clements, A. N. and G. D. Paterson, 1981: The analysis of mortality and survival rates in wild populations of mosquitoes. *The journal of applied ecology*, **18**, 373–399.
- Coetzee, M., 2004: Distribution of the African malaria vectors of the *Anopheles gambiae* complex. *The American Journal of Tropical Medicine and Hygiene*, **70**, 103–104.
- Cole-Tobian, J. L., P. A. Zimmerman, and C. L. King, 2007: High-throughput identification of the predominant malaria parasite clone in complex blood stage infections using a multi-SNP molecular haplotyping assay. *The American Society of Tropical Medicine and Hygiene*, **76**, 12–19.
- Collins, W. E. and G. M. Jeffery, 1999: A retrospective examination of the patterns of recrudescence in patients infected with *Plasmodium falciparum*. *The American Journal of Tropical Medicine and Hygiene*, **61**, 44–48.
- Colwell, R. R. and J. A. Patz, 1998: Climate, Infectious Disease and Health: An Interdisciplinary Perspective. Tech. rep., American Academy of Microbiology, 23 pp., Washington, USA.
- Confalonieri, U., B. Menne, R. Akhtar, K. L. Ebi, M. Hauengue, R. S. Kovats, B. Revich, and A. Woodward, 2007: Human health. *Climate Change 2007: Impacts, Adaptation and Vulnerability*, M. L. Parry, O. F. Canziani, J. P. Palutikof, P. J. van der Linden, and C. E. Hanson, Eds., Cambridge University Press, Cambridge, United Kingdom, 391–431, contribution of Working Group II to the Fourth Assessment Report of the Intergovernmental Panel on Climate Change.
- Connor, S. J., M. C. Thomson, S. P. Flasse, and A. H. Perryman, 1998: Environmental Information Systems in Malaria Risk Mapping and Epidemic Forecasting. *Disasters*, **22**, 39–56.
- Connor, S. J., M. C. Thomson, and D. H. Molyneux, 1999: Forecasting and prevention of epidemic malaria: new perspectives on an old problem. *Parasitologia*, **41**, 439–446.
- Conover, W. J., 2006: *Practical Nonparametric Statistics*. 3d ed., Wiley-India edition, 595 pp.
- Conway, D., 2000: The Climate and Hydrology of the Upper Blue Nile River. *The Geographical Journal*, **166**, 49–62.
- Cook, G. C., 1992: Effect of global warming on the distribution of parasitic and other infectious diseases: a review. *Journal of the Royal Society of Medicine*, **85**, 688–691.
- Cook, K. H. and E. K. Vizy, 2006: Coupled Model Simulations of the West African Monsoon System: Twentieth and Twenty-First-Century Simulations. *Journal of Climate*, **19**, 3681–3703.
- Coppola, E. and F. Giorgi, 2005: Climate change in tropical regions from high-resolution time-slice AGCM experiments. *The Quarterly Journal of the Royal Meteorological Society*, **131**, 3123–3145.
- Costantini, C., L. Song-Gang, A. della Torre, N. Sagnon, M. Coluzzi, and C. E. Taylor, 1996: Density, survival and dispersal of *Anopheles gambiae* complex mosquitoes in a West African Sudan savanna village. *Medical and Veterinary Entomology*, **10**, 203–219.
- Cox, J., M. Craig, D. le Sueur, and B. Sharp, 1999: Mapping malaria risk in the highlands of Africa. Tech. rep., MARA/HIMAL, 96 pp., London, United Kingdom, Durban, South Africa. Available online at <http://www.lshtm.ac.uk/dcvbu/himal/Documents.html>.
- Cox, J., S. I. Hay, T. A. Abeku, F. Checchi, and R. W. Snow, 2007: The uncertain burden of *Plasmodium falciparum* epidemics in Africa. *Trends in Parasitology*, **23**, 142–148.
- Craig, M. H., R. W. Snow, and D. le Sueur, 1999: A Climate-based Distribution Model of Malaria Transmission in Sub-Saharan Africa. *Parasitology Today*, **15**, 105–111.
- Cuzin-Quattara, N., A. H. van den Broek, A. Habluetzel, A. Diabate, E. Sanogo-Ilboudo, D. A. Diallo, S. N. Cousens, and F. Esposito, 1999: Wide-scale installation of insecticide-treated curtains confers high levels of protection against malaria transmission in a hyperendemic area of Burkina Faso. *Transactions of the Royal Society of Tropical Medicine and Hygiene*, **93**, 473–479.
- D'Alessandro, U., 1999: Malaria in Pregnancy. *Annals of Tropical Medicine and Parasitology*, **93**(Suppl.1), S5–S6.
- Davidson, G., 1954: Estimation of the Survival-Rate of Anopheline Mosquitoes in Nature. *Nature*, **174**, 792–793.
- Davidson, G., 1955: Further studies of the basic factors concerned in the transmission of malaria. *Transactions of the Royal Society of Tropical Medicine and Hygiene*, **49**, 339–350.
- Davidson, G. and C. C. Draper, 1953: Field studies of some of the basic factors concerned in the transmission of malaria. *Transactions of the Royal Society of Tropical Medicine and Hygiene*, **47**, 522–535.
- Davies, T. D., C. E. Vincent, and A. K. C. Beresford, 1985: July-August rainfall in West-Central Kenya. *Journal of Climatology*, **5**, 17–33.
- Davis, J. C., T. D. Clark, S. K. Kemble, N. Talemwa, D. Njama-Meya, S. G. Staedke, and G. Dorsey, 2006: Longitudinal study of urban malaria in a cohort of Ugandan children: description of study site, census and recruitment. *Malaria Journal*, **5**, 18.
- Davis, J. R., T. Hall, E. M. Chee, A. Majala, J. Minjas, and C. J. Shiff, 1995: Comparison of sampling anopheline mosquitoes by light-trap and human-bait collection indoors at Baramoyo, Tanzania. *Medical and Veterinary Entomology*, **9**, 249–255.
- Day, K. P., R. E. Hayward, and M. Dyer, 1998: The biology of *Plasmodium falciparum* transmission stages. *Parasitology*, **116**(Suppl.), S95–S109.
- De Roode, J. C., R. Cullen, A. S. Bell, and A. F. Read, 2004: Competitive release of drug resistance following drug treatment of mixed *Plasmodium chabaudi* infections. *Malaria Journal*, **3**, 33.
- De Savigny, D. and F. Binka, 2004: Monitoring future impact on malaria burden in sub-Saharan Africa. *The American Journal of Tropical Medicine and Hygiene*, **71**(Suppl.2), 224–231.
- De Zoysa, A. P. K., P. R. J. Herath, T. A. Abhayawardana, U. K. G. K. Padmalal, and K. N. Mendis, 1988: Modulation of human malaria transmission by anti-gamete transmission blocking immunity. *Transactions of the Royal Society of Tropical Medicine and Hygiene*, **82**, 548–553.
- Defries, R., L. Bounoua, and G. Collatz, 2002: Human modification of the landscape and surface climate in the next fifty years. *Global Change Biology*, **8**, 438–458.
- Depinay, J.-M. O., C. M. Mbogo, G. Killeen, B. Knols, J. Beier, J. Carlson, J. Dushoff, P. Billingsley, H. Mwambi, J. Githure, A. M. Toure, and F. E. McKenzie, 2004: A simulation model of African *Anopheles* ecology and population dynamics for the analysis of malaria transmission. *Malaria Journal*, **3**, 29.
- Detinova, T. S., 1962: *Age-grouping methods in Diptera of medical importance with special reference to some vectors of malaria*. No. 47 in Monograph Series, WHO, 216 pp.
- Diallo, S., L. Konaté, O. Ndir, T. Dieng, Y. Dieng, I. B. Bah, O. Faye, and O. Gaye, 2000: Le paludisme dans le district sanitaire centre de Dakar (Sénégal). Données entomologiques, parasitologiques et cliniques. *Cahiers Santé*, **10**, 221–229.
- Diatta, M., A. Spiegel, L. Lochouart, and D. Fontenille, 1998: Similar feeding preferences of *Anopheles gambiae* and *A. arabiensis* in Senegal. *Transactions of the Royal Society of Tropical Medicine and Hygiene*, **92**, 270–272.
- Diebner, H. H., M. Eichner, L. Molineaux, W. E. Collins, G. M. Jeffery, and K. Dietz, 2000: Modelling the Transition of Asexual Blood Stages of *Plasmodium falciparum* to Gametocytes. *Journal of Theoretical Biology*, **202**, 113–127.
- Dietz, K., 1988: Mathematical models for transmission and control of malaria. *Malaria, principles and practice of malariology*, W. H. Wernsdorfer and I. McGregor, Eds., Churchill Livingstone, Edinburgh, London, Melbourne, and New York, 1091–1133.

- Dietz, K., L. Molineaux, and A. Thomas, 1974: A malaria model tested in the African savannah. *Bulletin of the World Health Organization*, **50**, 347–357.
- Diggle, P., R. Moyeed, B. Rowlingson, and M. Thomson, 2002: Childhood Malaria in the Gambia: A Case-Study in Model-Based Geostatistics. *Journal of Applied Statistics*, **51**, 493–506.
- Diop, A., L. Konaté, J.-F. Molez, M. Diouf, O. Gaye, D. Fontenille, M. Diagne, and O. Faye, 2006: Le paludisme en zone de mangrove du delta du Saloum (Sénégal). *Cahiers Santé*, **16**, 253–257.
- Diop, A., J. F. Molez, L. Konate, D. Fontenille, O. Gaye, M. Diouf, M. Diagne, and O. Faye, 2002: Rôle d'*Anopheles melas* Theobald (1903) dans la transmission du paludisme dans la mangrove du Saloum au Sénégal. *Parasite*, **9**, 239–246.
- Diro, G. T., D. I. F. Grimes, E. Balck, A. O'Neill, and E. Pardo-Iguzquiza, 2009: Evaluation of reanalysis rainfall estimates over Ethiopia. *International Journal of Climatology*, **29**, 67–78.
- Diuk-Wasser, M. A., M. B. Toure, G. Dolo, M. Bagayoko, N. Sogoba, S. F. Traore, N. Manoukis, and C. E. Taylor, 2005: Vector abundance and malaria transmission in rice-growing villages in Mali. *The American Journal of Tropical Medicine and Hygiene*, **72**, 725–731.
- Dolo, G., O. J. Briët, A. Dao, S. F. Traoré, M. Bouaré, N. Sogoba, O. Niaré, M. Bagayogo, D. Sangaré, T. Teuscher, and Y. T. Touré, 2004: Malaria transmission in relation to rice cultivation in the irrigated Sahel of Mali. *Acta Tropica*, **89**, 147–159.
- Dos Santos, R. I. C., O. P. Forattini, and M. N. Burattini, 2004: *Anopheles albittarsis s.l.* (Diptera: Culicidae) Survivorship and Density in a Rice Irrigation Area of the State of São Paulo, Brazil. *Journal of Medical Entomology*, **41**, 997–1000.
- Dossou-Yovo, J., J. Doannio, F. Rivière, and J. Duval, 1994: Rice cultivation and malaria transmission in Bouaké city (Côte d'Ivoire). *Acta Tropica*, **57**, 91–94.
- Dossou-Yovo, J., J. M. C. Doannio, S. Diarrassouba, and G. Chauvancy, 1995: Malaria in Côte d'Ivoire wet savannah region: The entomological input. *Tropical Medicine and Parasitology*, **46**, 263–269.
- Dossou-Yovo, J., J. M. C. Doannio, S. Diarrassouba, and G. Chauvancy, 1998: Impact d'aménagements de rizières sur la transmission du paludisme dans la ville de Bouaké, Côte d'Ivoire. *Bulletin de la Société de pathologie exotique*, **91**, 327–333.
- Douville, H., P. Viterbo, J.-F. Mahfouf, and A. C. M. Beljaars, 2000: Evaluation of the Optimum Interpolation and Nudging Techniques for Soil Moisture Analysis Using FIFE Data. *Monthly Weather Review*, **128**, 1733–1756.
- Drakeley, C., C. Sutherland, J. T. Bousema, R. W. Sauerwein, and G. A. Targett, 2006: The epidemiology of *Plasmodium falciparum* gametocytes: weapons of mass dispersion. *Trends in Parasitology*, **22**, 424–430.
- Drakeley, C. J., N. I. J. Akim, R. W. Sauerwein, B. M. Greenwood, and G. A. T. Targett, 2000: Estimates of the infectious reservoir of *Plasmodium falciparum* malaria in The Gambia and in Tanzania. *Transactions of the Royal Society of Tropical Medicine and Hygiene*, **94**, 472–476.
- Drakeley, C. J., I. Carneiro, H. Reyburn, R. Malima, J. P. A. Lusingu, J. Cox, T. G. Theander, W. M. M. M. Nkya, M. M. Lemnge, and E. M. Riley, 2005: Altitude-Dependent and -Independent Variations in *Plasmodium falciparum* Prevalence in Northeastern Tanzania. *The Journal of Infectious Diseases*, **191**, 1589–1598.
- Draper, C. C., 1953: Observations on the infectiousness of gametocytes in hyperendemic malaria. *Transactions of the Royal Society of Tropical Medicine and Hygiene*, **47**, 160–165.
- Draper, C. C. and G. Davidson, 1953: A New Method of Estimating the Survival-Rate of Anopheline Mosquitoes in Nature. *Nature*, **172**, 503.
- Dunyo, S., P. Milligan, T. Edwards, C. Sutherland, G. Targett, and M. Pinder, 2006: Gametocytaemia after Drug Treatment of Asymptomatic *Plasmodium falciparum*. *Public Library of Science Clinical Trials*, **1**, e20.
- Ebi, K. L., J. Hartman, N. Chan, J. McConnell, M. Schlesinger, and J. Weyant, 2005: Climate suitability for stable malaria transmission in Zimbabwe under different climate change scenarios. *Climatic Change*, **73**, 375–393.
- Edillo, F. E., Y. T. Touré, G. C. Lanzaro, G. Dolo, and C. E. Taylor, 2004: Survivorship and Distribution of Immature *Anopheles gambiae s.l.* (Diptera: Culicidae) in Banambani Village, Mali. *Journal of Medical Entomology*, **41**, 333–339.
- Eichner, M., H. H. Diebner, L. Molineaux, W. E. Collins, G. M. Jeffery, and K. Dietz, 2001: Genesis, sequestration and survival of *Plasmodium falciparum* gametocytes: parameter estimates from fitting a model to malariatherapy data. *Transactions of the Royal Society of Tropical Medicine and Hygiene*, **95**, 497–501.
- El Sayed, B. B., D. E. Arnot, M. M. Mukhtar, O. Z. Baraka, A. A. Dafalla, D. E. A. Elnaiem, and A. H. D. Nugud, 2000: A study of the urban malaria transmission problem in Khartoum. *Acta Tropica*, **75**, 163–171.
- Eltahir, E. and C. Gong, 1996: Dynamics of Wet and Dry Years in West Africa. *Journal of Climate*, **9**, 1030–1042.
- Epstein, P. R., 1998: Global warming and vector-borne disease. *The Lancet*, **351**, 1737.
- Epstein, P. R., H. F. Diaz, S. Elias, G. Grabherr, N. E. Graham, W. J. M. Martens, E. Moseley-Thompson, and J. Susskind, 1998: Biological and Physical signs of Climate Change: Focus on Mosquito-borne Diseases. *Bulletin of the American Meteorological Society*, **79**, 409–417.
- Ermert, V. and T. Brücher, 2008: The Climate of Benin (1961 to 1990). *IMPETUS Atlas Benin. Research results 2000-2007*, M. Judex and H.-P. Thamm, Eds., IMPETUS, 2d ed., 17–18.
- Fall, S., D. Niyogi, and F. H. M. Semazzi, 2006: Analysis of mean climate conditions in Senegal (1971-1998). *Earth Interactions*, **10**, 1–40.
- FAO, 2006: Global forest resources assessment 2005. Progress towards sustainable forest management. Forestry Paper 147, FAO, 348 pp., Rome, Italy.
- Faye, O., D. Fontenille, J. P. Herve, P. A. Diack, and S. D. J. Mouchet, 1993: Le paludisme en zone sahélienne du Sénégal. 1. Données entomologiques sur la transmission. *Annales de la Société Belge de Médecine Tropicale*, **73**, 21–30.
- Faye, O., O. Gaye, O. Faye, and S. Diallo, 1994: La transmission du paludisme dans des villages éloignés ou situés en bordure de la mangrove au Sénégal. *Bulletin de la Société de Pathologie Exotique*, **87**, 157–163.
- Faye, O., L. Konaté, D. Fontenille, O. Gaye, N. Sy, G. Hébrard, J. P. Hervé, and Y. T. Touré, 1995a: Variations saisonnières des populations d'*Anopheles gambiae s.l.* et transmission du paludisme dans un village de savane soudanienne du sud-est du Sénégal. *Bulletin Institut Fondamental d'Afrique Noire: Série A*, **48**, 57–66.
- Faye, O., O. Gaye, D. Fontenille, N. Sy, L. Konaté, G. Hébrard, J.-P. Hervé, J. Trouillet, S. Diallo, and J. Mouchet, 1995b: Comparaison de la transmission du paludisme dans deux faciès épidémiologiques au Sénégal: la zone côtière sahélienne et la zone méridionale soudanienne. *Dakar Médical*, **40**, 201–207.
- Faye, O., O. Gaye, D. Fontenille, G. Hébrard, L. Konaté, N. Sy, J.-P. Hervé, Y. Touré, S. Diallo, J.-F. Molez, and J. Mouchet, 1995c: La sécheresse et la baisse du paludisme dans les Niayes du Sénégal. *Cahiers Santé*, **5**, 299–305.
- Faye, O., D. Fontenille, O. Gaye, N. Sy, J. F. Molez, L. Konaté, G. Hébrard, J. P. Herve, J. Trouillet, S. Diallo, and J. Mouchet, 1995d: Paludisme et riziculture dans le delta du fleuve Sénégal (Sénégal). *Annales de la Société Belge de Médecine Tropicale*, **75**, 179–189.
- Fernandez-Salas, I., M. H. Rodriguez, and D. R. Roberts, 1994: Gonotrophic cycle and survivorship of *Anopheles pseudopunctipennis* (Diptera: Culicidae) in the Tapachula foothills of southern Mexico. *Journal of Medical Entomology*, **31**, 340–347.
- Filion, G. J. P., R. E. L. Paul, and V. Robert, 2006: Transmission and immunity: the importance of heterogeneity in the fight against malaria. *Trends in Parasitology*, **22**, 345–348.
- Fink, A. H., 2006: Das westafrikanische Monsunsystem (The West African monsoon system). *Promet*, **32**, 114–122.
- Fink, A. H., S. Kottlaus, and S. Pohle, 2008: Rainfall Variability in West Africa. *IMPETUS Atlas Benin. Research results 2000-2007*, M. Judex and H.-P. Thamm, Eds., IMPETUS, 2d ed., 11–12.
- Fink, A. H. and A. Reiner, 2003: Spatio-temporal Variability of the Relation between African Easterly Waves and West African Squall Lines in 1998 and 1999. *Journal of Geophysical Research*, **108**, 4332–4348.
- Fink, A. H., D. G. Vincent, and V. Ermert, 2006: Rainfall Types in the West African Soudanian Zone during the Summer Monsoon 2002. *Monthly Weather Review*, **134**, 2143–2164.
- Flohn, H., 1965: Equatorial westerlies over Africa, their extension and significance. *Bonner Meteorologische Abhandlungen*, **5**, 36–48.
- Fondjo, E., V. Robert, G. Le Goff, J. C. Toto, and P. Carnevale, 1992: Le paludisme urbain à Yaoundé (Cameroun). 2. Etude entomologique dans deux quartiers peu urbanisés. *Bulletin de la Société de Pathologie Exotique*, **85**, 57–63.
- Fontenille, D., J.-Y. Meunier, C. A. Nkondjio, and T. Tchuinkam, 2001: Use of Circumsporozoite Protein Enzyme-Linked Immunosorbent Assay Compared with Microscopic Examination of Salivary Glands for Calculation of Malaria Infectivity Rates in Mosquitoes (Diptera: Culicidae) from Cameroon. *Journal of Medical Entomology*, **38**, 451–454.
- Fontenille, D., L. Lochouart, M. Diatta, C. Sokhna, I. Dia, N. Diagne, J. J. Lemasson, K. Ba, A. Tall, C. Rogier, and J.-F. Trape, 1997a: Four years' entomological study of the transmission of seasonal malaria in Senegal and the bionomics of *Anopheles gambiae* and *A. arabiensis*. *Transactions of the Royal Society of Tropical Medicine and Hygiene*, **91**, 647–652.
- Fontenille, D., L. Lochouart, N. Diagne, C. Sokhna, J. J. Lemasson, M. Diatta, L. Konaté, F. Faye, C. Rogier, and J.-F. Trape, 1997b: High annual and seasonal variations in malaria transmission by *anophelines* and vector species composition in Dielmo, a holoendemic area in Senegal. *The American Journal of Tropical Medicine and Hygiene*, **56**, 247–253.
- Gallup, J. L. and J. D. Sachs, 2001: The economic burden of malaria. *The American Journal of Tropical Medicine and Hygiene*, **64**(Suppl. 1-2), 85–96.
- Garnham, P. C. C., 1949: Malarial immunity in Africans: effects in infancy and early childhood. *Annals of Tropical Medicine and Parasitology*, **43**, 47–61.
- Garrett-Jones, C., 1964: The human blood index of malaria vectors in relation to epidemiological assessment. *Bulletin of the World Health Organization*, **30**, 241–261.
- Garrett-Jones, C., P. F. L. Boreham, and C. P. Pant, 1980: Feeding habits of anophelines (Diptera: Culicidae) in 1971-78, with reference to the human blood index: a review. *Bulletin of Entomological Research*, **70**, 165–185.

- Garrett-Jones, C. and B. Grab, 1964: The Assessment of Insecticidal Impact on the Malaria Mosquito's Vectorial Capacity, from Data on the Proportion of Parous Females. *Bulletin of the World Health Organization*, **31**, 71–86.
- Garrett-Jones, C. and G. R. Shidrawi, 1969: Malaria Vectorial Capacity of a Population of *Anopheles gambiae*: An Exercise in Epidemiological Entomology. *Bulletin of the World Health Organization*, **40**, 531–545.
- Gatebe, C. K., P. D. Tyson, H. Annegarn, S. Piketh, and G. Helas, 1999: A seasonal air transport climatology for Kenya. *Journal of Geophysical Research*, **104**, 14 237–14 244.
- Gay-Andrieu, F., E. Adehossi, V. Lacroix, M. Gagara, M. L. Ibrahim, H. Kourna, and H. Boureima, 2005: Epidemiological, clinical and biological features of malaria among children in Niamey, Niger. *Malaria Journal*, **4**, 10.
- Gazin, P., K. Goncalves., B. Koné, and L. Lochouam, 1996: Incidence des accès palustres dans un quartier de la ville de Bobo-Dioulasso (Burkina Faso). *Bulletin de la Société de Pathologie Exotique*, **89**, 200–203.
- Gazin, P., V. Robert, and P. Carnevale, 1987: Le paludisme urbain à Bobo-Dioulasso (Burkina Faso). 2. Les indices paludologiques. *Cahiers O.R.S.T.O.M. Série Entomologie Médicale et Parasitologie*, **25**, 27–31.
- Gazin, P., V. Robert, M. Cot, and P. Carnevale, 1988a: *Plasmodium falciparum* incidence and patency in a high seasonal transmission area of Burkina Faso. *Transactions of the Royal Society of Tropical Medicine and Hygiene*, **82**, 50–55.
- Gazin, P., V. Robert, M. Cot, J. Simon, J. M. Halna, F. Darriet, D. Legrand, P. Carnevale, and P. Ambroise-Thomas, 1988b: Le paludisme dans l'Oudalan, région sahélienne du Burkina Faso. *Annales de la Société Belge de Médecine Tropicale*, **68**, 255–264.
- Gemperli, A., P. Vounatsou, N. Sogoba, and T. Smith, 2006a: Malaria Mapping Using Transmission Models: Application to Survey Data from Mali. *American Journal of Epidemiology*, **163**, 289–297.
- Gemperli, A., N. Sogoba, E. Fondjo, M. Mabaso, M. Bagayoko, O. J. T. Brit, D. Anderegg, J. Liebe, T. Smith, and P. Vounatsou, 2006b: Mapping malaria transmission in West and Central Africa. *Tropical Medicine and International Health*, **11**, 1032–1046.
- Gerbaux, M. and D. Bicot, 2008: Impact of rainfall spatial variability on mosquito production in Sahel, submitted to Journal of Theoretical Biology.
- Giannini, A., R. Saravanan, and P. Chang, 2003: Oceanic Forcing of Sahel Rainfall on Interannual to Interdecadal Time Scales. *Science*, **302**, 1027–1030.
- Gianotti, R. L., A. Bombliès, M. Dafalla, I. Issa-Arzika, J.-B. Duchemin, and E. A. B. Eltahir, 2008: Efficacy of local neem extracts for sustainable malaria vector control in an African village. *Malaria Journal*, **7**, 138.
- Gillies, M. T., 1958: A modified Technique for the age-grading of populations of *Anopheles gambiae*. *Annals of Tropical Medicine and Parasitology*, **52**, 261–273.
- Gillies, M. T., 1961: Studies on the dispersion and survival of *Anopheles gambiae* Giles in East Africa, by means of marking and release experiments. *Bulletin of Entomological Research*, **52**, 99–127.
- Gillies, M. T. and T. J. Wilkes, 1963: Observations on nulliparous and parous rates in a population of *Anopheles funestus* in East Africa. *Annals of Tropical Medicine and Parasitology*, **57**, 204–213.
- Gillies, M. T. and T. J. Wilkes, 1965: A study on the age-composition of populations of *Anopheles gambiae* Giles and *A. funestus* Giles in north-eastern Tanzania. *Bulletin of Entomological Research*, **56**, 237–262.
- Gimnig, J. E., M. Ombok, L. Kamau, and W. A. Hawley, 2001: Characteristics of Larval Anopheline (Diptera: Culicidae) Habitats in Western Kenya. *Journal of Medical Entomology*, **38**, 282–288.
- Gimnig, J. E., M. Ombok, S. Otieno, M. G. Kaufman, J. M. Vulule, and E. D. Walker, 2002: Density-dependent development of *Anopheles gambiae* (Diptera: Culicidae) larvae in artificial habitats. *Journal of Medical Entomology*, **39**, 162–172.
- Gin, L. S., 1965: *Objective Analysis of Meteorological Fields*. Israel Program for Scientific Translations, Jerusalem, Israel, 242 pp.
- Githeko, A. K., S. W. Lindsay, U. E. Confalonieri, and J. A. Patz, 2000: Climate change and vector-borne diseases: a regional analysis. *Bulletin of the World Health Organization*, **78**, 1136–1147.
- Glickman, T. S., 2000: *Glossary of Meteorology*: 2d ed., American Meteorological Society, Boston, USA, 855 pp.
- Goetz, S. J., S. D. Prince, and J. Small, 2000: Advances in satellite remote sensing of environmental variables for epidemiological applications. *Advances in Parasitology*, **47**, 289–307.
- Goldsbey, R. A., T. J. Kindt, B. A. Osborne, and J. Kuby, 2002: Enzyme-Linked Immunosorbent Assay. *Immunology*, W. H. Freeman, Ed., Basingstoke: Palgrave Macmillan, New York, USA, 5th ed., 148–150.
- Graves, P. M., T. R. Burkot, A. J. Saul, R. J. Hayes, and R. Carter, 1990: Estimation of anopheline survival rate, vectorial capacity and mosquito infection probability from malaria vector infection rates in villages near Madang, Papua New Guinea. *Journal of Applied Ecology*, **27**, 134–147.
- Graves, P. M., T. R. Burkot, R. Carter, J. A. Cattani, M. Lagog, J. Parker, B. J. Brabin, F. D. Gibson, D. J. Bradley, and M. P. Alders, 1988: Measurement of malarial infectivity of human populations to mosquitoes in the Madang area, Papua New Guinea. *Parasitology*, **96**, 251–263.
- Greenwood, B. and T. Mutabingwa, 2002: Malaria in 2002. *Nature*, **415**, 670–672.
- Greenwood, B. M., K. Bojang, C. J. M. Whitty, and G. A. T. Targett, 2005: Malaria. *The Lancet*, **365**, 1487–1498.
- Grover-Kopce, E. K., M. B. Blumenthal, P. Ceccato, T. Dinku, J. A. Omumbo, and S. J. Connor, 2006: Web-based climate information resources for malaria control in Africa. *Malaria Journal*, **5**, 38.
- Gu, W., G. F. Killeen, C. M. Mbogo, J. L. Regens, J. I. Githure, and J. C. Beier, 2003a: An individual-based model of *Plasmodium falciparum* malaria transmission on the coast of Kenya. *Transactions of the Royal Society of Tropical Medicine and Hygiene*, **97**, 43–50.
- Gu, W., C. M. Mbogo, J. I. Githure, J. L. Regens, G. F. Killeen, C. M. Swalm, G. Yan, and J. C. Beier, 2003b: Low recovery rates stabilize malaria endemicity in areas of low transmission in coastal Kenya. *Acta Tropica*, **86**, 71–81.
- Gubler, D. J., 1998: Resurgent Vector-Borne Diseases as a Global Health Problem. *Emerging Infectious Diseases*, **4**, 442–450.
- Guerra, C. A., P. W. Gikandi, A. J. Tatem, A. M. Noor, D. L. Smith, S. I. Hay, and R. W. Snow, 2008: The Limits and Intensity of *Plasmodium falciparum* Transmission: Implications for Malaria Control and Elimination Worldwide. *Public Library of Science Medicine*, **5**, e38.
- Guerra, C. A., S. I. Hay, L. S. Lucioparades, P. W. Gikandi, A. J. Tatem, A. M. Noor, and R. W. Snow, 2007: Assembling a global database of malaria parasite prevalence for the Malaria Atlas Project. *Malaria Journal*, **6**, 17.
- Guerra, C. A., R. W. Snow, and S. I. Hay, 2006: A global assessment of closed forests, deforestation and malaria risk. *Annals of Tropical Medicine and Parasitology*, **100**, 189–204.
- Gupta, S., R. W. Snow, C. A. Donnelly, K. Marsh, and C. Newbold, 1999: Immunity to non-cerebral severe malaria is acquired after one or two infections. *Nature Medicine*, **5**, 340–343.
- Haarsma, R., F. Selten, S. Weber, and M. Kliphuis, 2005: Sahel rainfall variability and response to greenhouse warming. *Geophysical Research Letters*, **32**, doi:10.1029/2005GL023232.
- Habluetzel, A., F. Esposito, and S. Lombardi, 1989: New methods in epidemiology and diagnosis of malaria and babesiosis: Immunotechniques for epidemiology of malaria: appropriate tools for integration of primary health care with malaria research and control. *Transactions of the Royal Society of Tropical Medicine and Hygiene*, **83**, 15–19.
- Hagedorn, R., F. Doblas-Reyes, and T. Palmer, 2006: A real application of seasonal forecasts - malaria early warnings. *ECMWF Newsletter*, **107**, 3–4.
- Hagedorn, R., F. J. Doblas-Reyes, and T. N. Palmer, 2005: The rationale behind the success of multi-model ensembles in seasonal forecasting. Part I: Basic concept. *Tellus*, **57A**, 219–233.
- Hagemann, S., M. Botzet, L. Dümenil, and B. Machenhauer, 1999: Derivation of global GCM boundary conditions from 1 km land use satellite data. Report 289, Max Planck Institute for Meteorology, 34 pp., Hamburg, Germany.
- Hagmann, R., J. D. Charlwood, V. Gil, C. Ferreira, V. do Rosário, and T. A. Smith, 2003: Malaria and its possible control on the island of Príncipe. *Malaria Journal*, **2**, 15.
- Haines, A. and C. Fuchs, 1991: Potential impacts on health of atmospheric change. *Journal of Public Health Medicine*, **13**, 69–80.
- Haines, A., R. S. Kovats, D. Campbell-Lendrum, and C. Corvalan, 2006: Climate change and human health: impacts, vulnerability, and mitigation. *The Lancet*, **367**, 2101–2109.
- Halpern, D. and P. M. Woiceshyn, 1999: Onset of the Somali Jet in the Arabian Sea during June 1997. *Journal of Geophysical Research*, **104**, 18 041–18 046.
- Hamad, A. A., A. E. H. D. Nugud, D. E. Arnot, H. A. Gihai, A.-M. A. Abdel-Muhsin, G. M. H. Satti, T. G. Theander, A. M. Creasey, H. A. Babiker, and D.-E. A. Elnaei, 2002: A marked seasonality of malaria transmission in two rural sites in eastern Sudan. *Acta Tropica*, **83**, 71–82.
- Hamilton, R. A. and J. W. Archbold, 1945: Meteorology of Nigeria and adjacent territories. *The Quarterly Journal of the Royal Meteorological Society*, **71**, 231–265.
- Hartman, J., K. Ebi, K. J. McConnell, N. Chang, and J. Weyant, 2002: Climate suitability: For stable malaria transmission in Zimbabwe under different climate change scenarios. *Global Change and Human Health*, **3**, 42–54.
- Hastenrath, S., 2000: Zonal Circulations over the Equatorial Indian Ocean. *Journal of Climate*, **13**, 2746–2756.
- Hastenrath, S., 2001: Variations of East African climate during the past two centuries. *Climatic Change*, **50**, 209–217.
- Hastenrath, S., A. Nicklis, and L. Greischar, 1993: Atmospheric-Hydrospheric Mechanisms of Climate Anomalies in the Western Equatorial Indian Ocean. *Journal of Geophysical Research*, **98**, 20 219–20 235.
- Hawking, F., M. E. Wilson, and K. Gammage, 1971: Evidence for cyclic development and short-lived maturity in the gametocytes of *Plasmodium falciparum*. *Transactions of the Royal Society of Tropical Medicine and Hygiene*, **65**, 549–555.
- Hay, S. I., 2000: An overview of remote sensing and geodesy for epidemiology and public health application. *Advances in Parasitology*, **47**, 1–35.

- Hay, S. I., J. Cox, D. J. Rogers, S. E. Randolph, D. I. Stern, G. D. Shanks, M. F. Myers, and R. W. Snow, 2002a: Climate change and the resurgence of malaria in the East African highlands. *Nature*, **415**, 905–909.
- Hay, S. I., J. Cox, D. J. Rogers, S. E. Randolph, D. I. Stern, G. D. Shanks, M. F. Myers, and R. W. Snow, 2002b: Regional warming and malaria resurgence. *Nature*, **420**, 628.
- Hay, S. I., C. A. Guerra, A. J. Tatem, P. M. Atkinson, and R. W. Snow, 2005: Urbanization, malaria transmission and disease burden in Africa. *Nature reviews. Microbiology*, **3**, 81–90.
- Hay, S. I., C. A. Guerra, A. J. Tatem, A. M. Noor, and R. W. Snow, 2004: The global distribution and population at risk of malaria: past, present, and future. *The Lancet Infectious Diseases*, **4**, 327–336.
- Hay, S. I., J. A. Omumbo, M. H. Craig, and R. W. Snow, 2000a: Earth Observation, Geographic Information Systems and *Plasmodium falciparum* Malaria in Sub-Saharan Africa. *Advances in Parasitology*, **47**, 173–215.
- Hay, S. I., M. J. Packer, and D. J. Rogers, 1997: The impact of remote sensing of the study and control of invertebrate intermediate hosts and vectors of disease. *International Journal of Remote Sensing*, **18**, 2899–2930.
- Hay, S. I., D. J. Rogers, S. E. Randolph, D. I. Stern, J. Cox, G. D. Shanks, and R. W. Snow, 2002c: Hot topic or hot air? Climate change and malaria resurgence in East African highlands. *Trends in Parasitology*, **18**, 530–534.
- Hay, S. I., D. J. Rogers, G. D. Shanks, M. F. Myers, and R. W. Snow, 2001: Malaria early warning in Kenya. *Trends in Parasitology*, **17**, 95–99.
- Hay, S. I., D. J. Rogers, J. F. Toomer, and R. W. Snow, 2000b: Annual *Plasmodium falciparum* entomological inoculation rates (EIR) across Africa: literature survey, Internet access and review. *Transactions of the Royal Society of Tropical Medicine and Hygiene*, **94**, 113–127.
- Hay, S. I., M. Simba, A. M. Noor, M. Busolo, H. L. Guyatt, S. A. Ochola, and R. W. Snow, 2002d: Defining and Detecting Malaria Epidemics in the Highlands of Western Kenya. *Emerging Infectious Diseases*, **8**, 555–562.
- Hay, S. I. and R. W. Snow, 2006: The Malaria Atlas Project: Developing Global Maps of Malaria Risk. *Public Library of Science Medicine*, **3**, e473.
- Hay, S. I., R. W. Snow, and D. J. Rogers, 1998: Predicting malaria seasons in Kenya using multitemporal meteorological satellite sensor data. *Transactions of the Royal Society of Tropical Medicine and Hygiene*, **92**, 12–20.
- Hay, S. I., C. J. Tucker, D. J. Rogers, and M. J. Packer, 1996: Remotely sensed surrogates of meteorological data for the study of the distribution and abundance of arthropod vectors of disease. *Annals of Tropical Medicine and Parasitology*, **90**, 1–19.
- Hegerl, G. C., F. W. Zwiers, P. Braconnot, N. P. Gillett, Y. Luo, J. A. M. Orsini, N. Nicholls, J. E. Penner, and P. A. Stott, 2007: Understanding and Attributing Climate Change. *Climate Change 2007: The Physical Science Basis*, S. Solomon, D. Qin, M. Manning, Z. Chen, M. Marquis, K. B. Averyt, M. Tignor, and H. L. Miller, Eds., Cambridge University Press, Cambridge, United Kingdom and New York, USA, 663–745, contribution of Working Group I to the Fourth Assessment Report of the Intergovernmental Panel on Climate Change.
- Helsel, D. R. and R. M. Hirsch, 2002: *Statistical Methods in Water Resources*. Book 4, US Geological Survey, 522 pp., techniques of Water-Resources Investigations.
- Henry, M.-C., C. Rogier, I. Nzeyimana, S. B. Assi, J. Dossou-Yovo, M. Audibert, J. Mathonnat, A. Keundjian, E. Akodo, T. Teuscher, and P. Carnevale, 2003: Inland valley rice production systems and malaria infection and disease in the savannah of Côte d'Ivoire. *Tropical Medicine and International Health*, **8**, 449–458.
- Hewitson, B. C. and R. G. Crane, 2006: Consensus between GCM climate change projections with empirical downscaling: precipitation downscaling over South Africa. *International Journal of Climatology*, **26**, 1315–1337.
- Hodges, K. I., 1998: Feature-Point Detection Using Distance Transforms: Application to Tracking Tropical Convective Complexes. *Monthly Weather Review*, **126**, 785–795.
- Hoerling, M. P., J. W. Hurrell, J. Eischeid, and A. Phillips, 2006: Detection and Attribution of Twentieth-Century Northern and Southern African Rainfall Change. *Journal of Climate*, **19**, 3989–4008.
- Hogg, J. C., M. C. Thompson, and H. Hurd, 1996: Comparative fecundity and associated factors for two sibling species of the *Anopheles gambiae* complex occurring sympatrically in The Gambia. *Medical and Veterinary Entomology*, **10**, 385–391.
- Horsfall, W. R., 1955: *Mosquitoes: Their Bionomics and Relation to Disease*. Ronald Press, New York, USA, 723 pp.
- Hoshen, M. B. and A. P. Morse, 2004: A weather-driven model of malaria transmission. *Malaria Journal*, **3**, 32.
- Hoshen, M. B. and A. P. Morse, 2005: A model structure for estimating malaria risk. *Environmental Change and Malaria Risk - Global and Local Implications*, W. Takken, P. Martens, and R. J. Bogers, Eds., Springer, Wageningen, Netherlands, No. 9 in UR Frontis Series, 41–50.
- Houghton, J. T., B. A. Caller, and S. K. Varney, 1992: *Climate Change 1992: The Supplementary Report to the IPCC Scientific Assessment*. Cambridge University Press, Cambridge, United Kingdom, 205 pp.
- Ijumba, J. N. and S. W. Lindsay, 2001: Impact of irrigation on malaria in Africa: paddies paradox. *Medical and Veterinary Entomology*, **15**, 1–11.
- Ijumba, J. N., F. C. Shenton, S. E. Clarke, F. W. Moshia, and S. W. Lindsay, 2002: Irrigated crop production is associated with less malaria than traditional agricultural practices in Tanzania. *Transactions of The Royal Society of Tropical Medicine and Hygiene*, **96**, 476–480.
- Ikemoto, T. and K. Takai, 2000: A New Linearized Formula for the Law of Total Effective Temperature and the Evaluation of Line-Fitting Methods with Both Variables Subject to Error. *Environmental Entomology*, **29**, 671–682.
- Jacob, D., 2001: A note to the simulation of the annual and inter-annual variability of the water budget. *Meteorology and Atmospheric Physics*, **77**, 61–73.
- Jacob, D., B. J. J. M. van den Hurk, U. Andrae, G. Elgered, C. Fortelius, L. P. Graham, S. D. Jackson, U. Karstens, C. Koepken, R. Lindau, R. Podzun, B. Rockel, F. Rubel, B. H. Sass, R. Smith, and X. Yang, 2001: A comprehensive model intercomparison study investigating the water budget during the PIDCAP period. *Meteorology and Atmospheric Physics*, **77**, 19–44.
- Janicot, S., V. Moron, and B. Fontaine, 1996: Sahel droughts and ENSO dynamics. *Geophysical Research Letters*, **23**, 515–518.
- Janicot, S., S. Trzaska, and I. Poccard, 2001: Summer Sahel-ENSO teleconnection and decadal time scale SST variations. *Climate Dynamics*, **18**, 303–320.
- Jeffery, G. M., M. D. Young, R. W. Burgess, and D. E. Eyles, 1959: Early activity in sporozoite-induced *Plasmodium falciparum* infections. *Annals of Tropical Medicine and Parasitology*, **53**, 51–58.
- Jepson, W. F., A. Moutia, and C. Courtois, 1947: The malaria problem in Mauritius: The binomics of Mauritian anophelines. *Bulletin of Entomological Research*, **38**, 177–208.
- Jetten, T. H., P. Martens, and W. Takken, 1996: Model simulations To Estimate Malaria Risk Under Climate Change. *Journal of Medical Entomology*, **33**, 361–371.
- Jones, A. E., 2007: Seasonal ensemble prediction of malaria in Africa. Ph.D. thesis, University of Liverpool, 312 pp., Liverpool, United Kingdom.
- Jones, A. E., U. U. Wort, A. P. Morse, I. M. Hastings, and A. S. Gagnon, 2007: Climate prediction of El Niño malaria epidemics in north-west Tanzania. *Malaria Journal*, **6**, 162.
- Julvez, J., J. Mouchet, A. Michault, A. Fouta, and M. Hamidine, 1997a: Eco-épidémiologie du paludisme à Niamey et dans la vallée du fleuve, République du Niger, 1992-1995. *Bulletin de la Société de pathologie exotique*, **90**, 94–100.
- Julvez, J., J. Mouchet, A. Michault, A. Fouta, and M. Hamidine, 1997b: Evolution du paludisme dans l'est sahélien du Niger. Une zone écologiquement sinistrée. *Bulletin de la Société de pathologie exotique*, **90**, 101–104.
- Jung, G., 2006: Regional climate change and the impact on hydrology in the volta basin of West Africa. *Wissenschaftliche Berichte Forschungszentrum Karlsruhe*, **7240**, 1–147.
- Jury, M. R., D. B. Enfield, and J.-L. Mélice, 2002: Tropical monsoons around Africa: Stability of El Niño–Southern Oscillation associations and links with continental climate. *Journal of Geophysical Research*, **107**, C10, doi:10.1029/2000JC000507.
- Kamga, A. F., G. S. Jenkins, A. T. Gaye, A. Garba, A. Sarr, and A. Adedoyin, 2005: Evaluating the National Center for Atmospheric Research climate system model over West Africa: Present-day and the 21st century A1 scenario. *Journal of Geophysical Research*, **110**, D03 106, doi:10.1029/2004JD004689.
- Keiser, J., M. C. D. Castro, M. F. Maltese, R. Bos, M. Tanner, B. H. Singer, and J. Utzinger, 2005: Effect of Irrigation and Large Dams on the Burden of Malaria on a Global and Regional Scale. *The American Journal of Tropical Medicine and Hygiene*, **74**, 392–406.
- Keiser, J., J. Utzinger, M. C. de Castro, T. A. Smith, M. Tanner, and B. H. Singer, 2004: Urbanization in sub-Saharan Africa and malaria control. *The American Journal of Tropical Medicine and Hygiene*, **71** (Suppl. 2), 118–127.
- Kelly-Hope, L. A. and F. E. McKenzie, 2009: The multiplicity of malaria transmission: a review of entomological inoculation rate measurements and methods across sub-Saharan Africa. *Malaria Journal*, **8**, 19.
- Kenawy, M. A., 1991: Development and survival of *Anopheles pharoensis* and *An. multicolor* from Faiyum, Egypt. *Journal of the American Mosquito Control Association*, **7**, 551–555.
- Khan, A. Q. and S. A. Talibi, 1972: Epidemiological assessment of malaria transmission in an endemic area of East Pakistan and the significance of congenital immunity. *Bulletin of the World Health Organization*, **46**, 783–792.
- Kilian, A. H. D., P. Langi, A. Talisuna, and G. Kabagambe, 1999: Rainfall pattern, El Niño and malaria in Uganda. *Transactions of the Royal Society of Tropical Medicine and Hygiene*, **93**, 22–23.
- Killeen, G. F., F. E. McKenzie, B. D. Foy, C. Bøgh, and J. C. Beier, 2001: The availability of potential hosts as a determinant of feeding behaviours and malaria transmission by African mosquito populations. *Transactions of the Royal Society of Tropical Medicine and Hygiene*, **95**, 469–476.
- Killeen, G. F., F. E. McKenzie, B. D. Foy, C. Schieffelin, P. F. Billingsley, and J. C. Beier, 2000: A simplified model for predicting malaria entomologic inoculation rates based on entomologic and parasitologic parameters relevant to control. *The American Journal of Tropical Medicine and Hygiene*, **62**, 535–544.
- Killeen, G. F., A. Ross, and T. Smith, 2006: Infectiousness of malaria-endemic human populations to vectors. *The American Journal of Tropical Medicine and Hygiene*, **75** (Suppl. 2), 38–45.

- Kinuthia, J. H., 1992: Horizontal and Vertical Structure of the Lake Turkana Jet. *Journal of Applied Meteorology*, **31**, 1248–1274.
- Kirby, M. J. and S. W. Lindsay, 2004: Responses of adult mosquitoes of two sibling species, *Anopheles arabiensis* and *A. gambiae* s.s. (Diptera: Culicidae), to high temperatures. *Bulletin of Entomological Research*, **94**, 441–448.
- Kiszewski, A., A. Mellinger, A. Spielman, P. Malaney, S. E. Sachs, and J. Sachs, 2004: A Global Index Representing the Stability of Malaria Transmission. *The American Journal of Tropical Medicine and Hygiene*, **70**, 486–498.
- Kiszewski, A. and A. Teklehaimanot, 2004: A review of the clinical and epidemiological burdens of epidemic malaria. *The American Journal of Tropical Medicine and Hygiene*, **71** (Suppl. 2), 128–135.
- Kleinschmidt, I., M. Bagayoko, G. P. Y. Clarke, M. Craig, and D. le Sueur, 2000: A spatial statistical approach to malaria mapping. *International Journal of Epidemiology*, **29**, 355–361.
- Kleinschmidt, I., J. Oumumbo, O. Briët, N. van de Giesen, N. Sogoba, N. K. Mensah, P. Windmeijer, M. Moussa, and T. Teuscher, 2001: An empirical malaria distribution map for West Africa. *Tropical Medicine and International Health*, **6**, 779–786.
- Klinkenberg, E., F. Huibers, W. Takken, and Y. T. Touré, 2002: Water management as a tool for malaria mosquito control? *Irrigation and Drainage Systems*, **16**, 201–212.
- Koenraadt, C. J. M., K. P. Paaijmans, P. Schneider, A. K. Githeko, and W. Takken, 2006: Low larval vector survival explains unstable malaria in the western Kenya highlands. *Tropical Medicine and International Health*, **11**, 1195–1205.
- Koenraadt, C. J. M. and W. Takken, 2003: Cannibalism and predation among larvae of the *Anopheles gambiae* complex. *Medical and Veterinary Entomology*, **17**, 61–66.
- Konaté, L., N. Diagne, K. Brahimi, O. Faye, F. Legros, C. Rogier, V. Petrarca, and J.-F. Trape, 1994: Biologie des vecteurs et transmission de *Plasmodium falciparum*, *P. malariae* and *P. ovale* dans un village de savane d'Afrique de l'ouest (Dielmo, Sénégal). *Parasite*, **1**, 325–333.
- Konaté, L., A. Diop, N. Sy, M. N. Faye, Y. Deng, A. Izri, O. Faye, and J. Mouchet, 2001: Comeback of *Anopheles funestus* in Sahelian Senegal. *The Lancet*, **358**, 336.
- Koram, K. A., S. Owusu-Agyei, D. J. Fryauff, F. Anto, F. Atuguba, A. Hodgson, S. L. Hoffmann, and F. K. Nkrumah, 2003: Seasonal profiles of malaria infection, anaemia, and bednet use among age groups and communities in northern Ghana. *Tropical Medicine and International Health*, **8**, 793–802.
- Korecha, D. and A. Barnston, 2007: Predictability of June–September Rainfall in Ethiopia. *Monthly Weather Review*, **135**, 628–650.
- Koudou, B. G., Y. Tano, M. Doumbia, C. Nsanzabana, G. Cissé, O. Girardin, D. Dao, E. K. N'Goran, P. Vounatsou, G. Bordmann, J. Keiser, M. Tanner, and J. Utzinger, 2005: Malaria transmission dynamics in central Côte d'Ivoire: the influence of changing patterns of irrigated rice agriculture. *Medical and Veterinary Entomology*, **19**, 27–37.
- Kovats, R. S., D. H. Campbell-Lendrum, A. J. McMichael, A. Woodward, and J. S. Cox, 2001: Early effects of climate change: do they include changes in vector-borne disease? *Philosophical transactions of the Royal Society of London, Series B, Biological sciences*, **356**, 1057–1068.
- Kovats, S. and A. Haines, 1995: The Potential Health Impacts of Climate Change: An Overview. *Medicine and War*, **11**, 168–178.
- Krafsur, E. S. and J. C. Armstrong, 1978: An integrated view of entomological and parasitological observations on falciparum malaria in Gambela, Western Ethiopian Lowlands. *Transactions of the Royal Society of Tropical Medicine and Hygiene*, **72**, 348–356.
- Kuhn, K. G., D. H. Campbell-Lendrum, and O. R. Davies, 2002: A continental risk map for malaria mosquito (Diptera: Culicidae) vectors in Europe. *Journal of Medical Entomology*, **39**, 621–630.
- Kun, J. F., M. A. Missinou, B. Lell, M. Sovric, H. Knoop, B. Bojowald, O. Dangelmaier, and P. G. Kremsner, 2002: New emerging *Plasmodium falciparum* genotypes in children during the transition phase from asymptomatic parasitemia to malaria. *The American Journal of Tropical Medicine and Hygiene*, **66**, 653–658.
- Kunstmann, H. and G. Jung, 2005: Impact of regional climate change on water availability in the Volta basin of West Africa. *Regional Hydrological Impacts of Climatic Variability and Change*, IAHS Press, Wallingford, United Kingdom, IAHS-AISH publication, 75–86.
- Lamb, P., 1978: Large-scale tropical Atlantic surface circulation patterns associated with sub-Saharan weather anomalies. *Tellus*, **30**, 240–251.
- Le Barbé, L. and T. Lebel, 1997: Rainfall climatology of the HAPEX-Sahel region during the years 1950–1990. *Journal of Hydrology*, **188–189**, 43–73.
- Le Barbé, L., T. Lebel, and D. Tapsoba, 2002: Rainfall Variability in West Africa during the Years 1950–90. *Journal of Climate*, **15**, 187–202.
- Le Goff, G., P. Carnevale, E. Fondjo, and V. Robert, 1997: Comparison of three sampling methods of man-biting anophelines in order to estimate the malaria transmission in a village of south Cameroon. *Parasite*, **4**, 75–80.
- Le Goff, G., V. Robert, E. Fondjo, and P. Carnevale, 1992: Efficacy of insecticide impregnated bed-nets to control malaria in a rural forested area in southern Cameroon. *Memorias do Instituto Oswaldo Cruz*, **87** (Suppl. 3), 355–359.
- Le Masson, J. J., D. Fontenille, L. Louchouart, I. Dia, F. Simard, K. Ba, A. Diop, M. Diatta, and J.-F. Molez, 1997: Comparison of behavior and vector efficiency of *Anopheles gambiae* and *An. arabiensis* (Diptera: Culicidae) in Barkedji, a Sahelian area of Senegal. *Journal of Medical Entomology*, **34**, 396–403.
- Lebel, T. and A. Ali, 2009: Recent trends in the Central and Western Sahel rainfall regime (1990–2007). *Journal of Hydrology*, doi:10.1016/j.jhydrol.2008.11.03.
- Lee, H. I., J. S. Lee, E. H. Shin, W. J. Lee, Y. Y. Kim, and K. R. Lee, 2001: Malaria transmission potential by *Anopheles sinensis* in the Republic of Korea. *The Korean journal of parasitology*, **39**, 185–192.
- Léong Pock Tsy, J. M., J. B. Duchemin, L. Marrama, P. Rabarison, G. Le Goff, V. Rajaonarivelo, and V. Robert, 2003: Distribution of the species of the *Anopheles gambiae* complex and first evidence of *Anopheles merus* as a malaria vector in Madagascar. *Malaria Journal*, **2**, 33.
- Leroux, M., 1983: *The Climate of Tropical Africa - Atlas*. Champion, Paris, France, 250 maps.
- Lindblade, K. A., E. D. Walker, A. W. Onapa, J. Katungu, and M. L. Wilson, 1999: Highland malaria in Uganda: prospective analysis of an epidemic associated with El Niño. *Transactions of the Royal Society of Tropical Medicine and Hygiene*, **93**, 480–487.
- Lindsay, S. W., J. H. Adiamah, J. E. Miller, R. J. Pleass, and J. R. M. Armstrong, 1993a: Variation in Attractiveness of Human Subjects to Malaria Mosquitoes (Diptera: Culicidae) in The Gambia. *Journal of Medical Entomology*, **30**, 638–673.
- Lindsay, S. W., P. L. Alonso, J. R. M. A. Schellenberg, J. Hemingway, J. H. Adiamah, F. C. Shenton, M. Jawara, and B. M. Greenwood, 1993b: A malaria control trial using insecticide-treated bed nets and targeted chemoprophylaxis in a rural area of The Gambia, West Africa: 7. Impact of permethrin-impregnated bed nets on malaria vectors. *Transactions of the Royal Society of Tropical Medicine and Hygiene*, **87** (Suppl. 2), 45–51.
- Lindsay, S. W., P. L. Alonso, J. R. M. A. Schellenberg, J. Hemingway, P. J. Thomas, F. C. Shenton, and B. M. Greenwood, 1993c: A malaria control trial using insecticide-treated bed nets and targeted chemoprophylaxis in a rural area of The Gambia, West Africa: 3. Entomological characteristics of the study area. *Transactions of the Royal Society of Tropical Medicine and Hygiene*, **87** (Suppl. 2), 19–23.
- Lindsay, S. W. and M. Birley, 2004: Rural Development and Malaria Control in Sub-Saharan Africa. *EcoHealth*, **1**, 129–137.
- Lindsay, S. W. and M. H. Birley, 1996: Climate change and malaria transmission. *Annals of Tropical Medicine and Parasitology*, **90**, 573–588.
- Lindsay, S. W., R. Bødker, R. Malima, H. A. Msangeni, and W. Kinsinza, 2000: The effect of the 1997–98 El Niño on highland malaria in Tanzania. *Lancet*, **355**, 989–990.
- Lindsay, S. W., H. Campbell, J. H. Adiamah, A. M. Greenwood, J. E. Bangali, and B. M. Greenwood, 1990: Malaria in a peri-urban area of The Gambia. *Annals of Tropical Medicine and Parasitology*, **84**, 553–562.
- Lindsay, S. W. and W. J. M. Martens, 1998: Malaria in the African highlands: past, present and future. *Bulletin of the World Health Organization*, **76**, 33–45.
- Lindsay, S. W., L. Parson, and C. J. Thomas, 1998: Mapping the ranges and relative abundance of the two principal African malaria vectors, *Anopheles gambiae sensu stricto* and *An. arabiensis*, using climate data. *Proceedings of the Royal Society of London. Series B*, **265**, 847–854.
- Lindsay, S. W., F. C. Shenton, R. W. Snow, and B. M. Greenwood, 1989: Responses of *Anopheles gambiae* complex mosquitoes to the use of untreated bednets in The Gambia. *Medical and Veterinary Entomology*, **3**, 253–262.
- Lines, J. D., T. J. Wilkes, and E. O. Lyimo, 1991: Human malaria infectiousness measured by age-specific sporozoite rates in *Anopheles gambiae* in Tanzania. *Parasitology*, **102** (Suppl.), 167–177.
- Lochouart, L. and I. Gazin, 1993: La transmission du paludisme dans la ville de Bobo-Dioulasso (Burkina Faso). *Annales de la Société Belge de Médecine Tropicale*, **73**, 287–296.
- Loevinsohn, M. E., 1994: Climatic warming and increased malaria incidence in Rwanda. *The Lancet*, **343**, 714–718.
- Lu, J. and T. Delworth, 2005: Oceanic forcing of late 20th century Sahel drought. *Geophysical Research Letters*, **32**, doi:10.1029/2005GL023316.
- Luyten, J. R., M. Fieuz, and J. Gonella, 1980: Equatorial Currents in the Western Indian Ocean. *Science*, **209**, 600–603.
- Lyimo, E. O. and W. Takken, 1993: Effects of adult body size on fecundity and the pre-gravid rate of *Anopheles gambiae* females in Tanzania. *Medical and Veterinary Entomology*, **7**, 328–332.
- Lyimo, E. O., W. Takken, and J. Koella, 1992: Effect of rearing temperature and larval density on larval survival, age at pupation and adult size of *Anopheles gambiae*. *Entomologia Experimentalis et Applicata*, **63**, 265–271.
- Macdonald, G., 1955: The measurement of malaria transmission. *Proceedings of the Royal Society of Medicine*, **48**, 295–301.
- Macdonald, G., 1956: Epidemiological basis of malaria control. *Bulletin of the World Health Organisation*, **15**, 613–626.
- Macdonald, G., 1957: *The epidemiology and control of malaria*. Oxford University Press, London, United Kingdom.
- Macdonald, G., C. B. Cuellar, and C. V. Foll, 1968: The dynamics of malaria. *Bulletin of the World Health Organisation*, **38**, 743–755.
- Macdonald, G. and G. W. Göckel, 1964: The Malaria Parasite Rate and Interruption of Transmission. *Bulletin of the World Health Organisation*, **31**, 365–377.
- MacPherson, G. G., M. J. Warrell, N. J. White, S. Loareesuwan, and D. A. Warrell, 1985: Human cerebral malaria. A quantitative ultrastructural analysis of parasitized erythrocyte sequestration. *American Journal of Pathology*, **119**, 385–401.
- Madden, R. A. and P. R. Julian, 1971: Detection of a 40–50 day oscillation in the zonal wind in the tropical Pacific. *Journal of Atmospheric Sciences*, **28**, 702–708.

- Magbity, E. B., N. T. Marbiah, G. Maude, C. F. Curtis, D. J. Bradley, B. M. Greenwood, E. Petersen, and J. D. Lines, 1997: Effects of community-wide use of lambda-deltacyhalothrin-impregnated bednets on malaria vectors in rural Sierra Leone. *Medical and Veterinary Entomology*, **11**, 79–86.
- Mahfouf, J.-F., P. Viterbo, H. Douville, A. C. M. Beljaars, and S. Saarinen, 2000: A revised land-surface analysis scheme in the Integrated Forecasting Systems. *ECMWF Newsletter*, **88**, 8–13.
- Majewski, D., 1991: The Europa-Modell of the Deutscher Wetterdienst. *ECMWF Seminar on Numerical Methods in Atmospheric Models*, **2**, 147–191.
- Malakooti, M. A., K. Biomndo, and G. D. Shanks, 1998: Reemergence of Epidemic Malaria in the Highlands of Western Kenya. *Emerging Infectious Diseases*, **4**, 671–676.
- Manga, L., B. Bouchite, J. C. Toto, and A. Froment, 1997a: La faune anophélienne et la transmission du paludisme dans une zone de transition forêt/savane au centre de Cameroun. *Bulletin de la Société de Pathologie Exotique*, **90**, 128–130.
- Manga, L., E. Fondjo, P. Carnevale, and V. Robert, 1993a: Importance of Low Dispersion of *Anopheles gambiae* (Diptera: Culicidae) on Malaria Transmission in Hilly Towns in South Cameroon. *Journal of Medical Entomology*, **30**, 936–938.
- Manga, L., V. Robert, J. Messi, M. A. Desfontaine, and P. Carnevale, 1992: Le paludisme urbain à Yaoundé (Cameroun). 1. Éntomologique dans deux quartiers centraux. *Mémoires de la Société Royale Belge d'Entomologie*, **35**, 155–162.
- Manga, L., J. C. Toto, and P. Carnevale, 1995: Malaria vectors and transmission in an area deforested for a new international airport in southern Cameroon. *Annales de la Société Belge de Medecine Tropicale*, **75**, 43–49.
- Manga, L., J. C. Toto, G. Le Goff, and J. Brunhes, 1997b: The bionomics of *Anopheles funestus* and its role in malaria transmission in a forested area of southern Cameroon. *Transactions of the Royal Society of Tropical Medicine and Hygiene*, **91**, 387–388.
- Manga, L., O. Traore, M. Cot, E. Mooh, and P. Carnevale, 1993b: Le Paludisme dans la ville de Yaoundé (Cameroun). 3. - Étude parasitologique dans deux quartiers centraux. *Bulletin de la Société de Pathologie Exotique*, **86**, 56–61.
- Mann, H. B. and D. R. Whitney, 1947: On a test of whether one of two random variables is stochastically larger than the other. *Annals of Mathematical Statistics*, **18**, 50–60.
- MARA, 1998: Towards an Atlas of Malaria Risk in Africa: First Technical Report of the MARA/ARMA Collaboration. Tech. rep., MARA/ARMA, 32 pp., Durban, South Africa.
- Marchant, R., C. Mumbi, S. Behera, and T. Yamagata, 2006: The Indian Ocean dipole - the unsung driver of climatic variability in East Africa. *African Journal of Ecology*, **45**, 4–16.
- Marimbu, J., A. Ndayiragije, M. L. Bras, and J. Chaperon, 1993: Environment and malaria in Burundi. Apropos of a malaria epidemic in a non-endemic mountainous region. *Bulletin de la Société de Pathologie Exotique*, **86**, 399–401.
- Martens, P., 1999: How Will Climate Change Affect Human Health? *American Scientist*, **87**, 534–541.
- Martens, P., R. S. Kovats, S. Nijhof, P. de Vries, M. T. J. Livermore, D. J. Bradley, J. Cox, and A. J. McMichael, 1999: Climate change and future populations at risk of malaria. *Global Environmental Change*, **9**, S98–S107.
- Martens, W. J. M., 1997: Health Impacts of Climate Change and Ozone Depletion: an Eco-epidemiological Modelling Approach. Ph.D. thesis, Maastricht University, Maastricht, Netherlands.
- Martens, W. J. M., T. H. Jetten, and D. A. Focks, 1997: Sensitivity of Malaria, Schistosomiasis and Dengue to Global Warming. *Climatic Change*, **35**, 145–156.
- Martens, W. J. M., T. H. Jetten, J. Rottmans, and L. W. Niessen, 1995a: Climate change and vector-borne diseases: A global modelling perspective. *Global Environmental Change*, **5**, 195–209.
- Martens, W. J. M., L. W. Niessen, J. Rotmans, T. H. Jetten, and A. J. McMichael, 1995b: Potential Impact of Global Climate Change on Malaria Risk. *Environmental Health Perspectives*, **103**, 458–464.
- Martin, P. H. and M. Lefebvre, 1995: Malaria and Climate: Sensitivity of Malaria. Potential Transmission to Climate. *Ambio*, **24**, 200–207.
- Matola, Y. G., G. B. White, and S. A. Magayuka, 1987: The changed pattern of malaria endemicity and transmission at Amani in the eastern Usambara Mountains, northeastern Tanzania. *Journal of Tropical Medicine and Hygiene*, **90**, 127–134.
- Maynard, K. and J.-F. Royer, 2004: Effects of realistic land-cover change on a greenhouse-warmed African climate. *Climate Dynamics*, **22**, 343–358.
- Mbogo, C. N. M., G. E. Glass, D. Forster, E. W. Kabiru, J. I. Githure, J. H. Ouma, and J. C. Beier, 1993: Evaluation of light traps for sampling anopheline mosquitoes in Kilifi, Kenya. *Journal of the American Mosquito Control Association*, **9**, 260–263.
- McCarthy, J. J., O. F. Canziani, N. A. Leary, and D. J. Dokken, 2001: *Climate Change 2001: Impacts, Adaptation and Vulnerability*. Cambridge University Press, Cambridge, United Kingdom, 1032 pp.
- McDonald, P. T., 1977: Population characteristics of domestic *Aedes aegypti* (Diptera: Culicidae) in villages on the Kenya Coast. I. Adult survivorship and population size. *Journal of Medical Entomology*, **14**, 42–48.
- McHugh, C. P., 1989: Ecology of a Semi-Isolated Population of Adult *Anopheles Freeborni*: Abundance, Trophic Status, Parity, Survivorship, Gonotrophic Cycle Length, and Host Selection. *The American Society of Tropical Medicine and Hygiene*, **41**, 169–176.
- McKenzie, F. E., J. K. Baird, J. C. Beier, A. A. Lal, and W. H. Bossert, 2002: A biologic basis for integrated malaria control. *The American Journal of Tropical Medicine and Hygiene*, **67**, 571–577.
- McKenzie, F. E. and W. H. Bossert, 2005: An integrated model of *Plasmodium falciparum* dynamics. *Journal of Theoretical Biology*, **232**, 411–426.
- McKenzie, F. E., G. F. Killeen, J. C. Beier, and W. H. Bossert, 2001: Seasonality, parasite diversity, and local extinctions in *Plasmodium falciparum* malaria. *Ecology*, **82**, 2673–2681.
- McKenzie, F. E., R. C. Wong, and W. H. Bossert, 1998: Discrete-event simulation models of *Plasmodium falciparum* malaria. *Simulation*, **71**, 250–261.
- McKenzie, F. E., R. C. Wong, and W. H. Bossert, 1999: Discrete-event models of mixed-phenotype *Plasmodium falciparum* malaria. *Simulation*, **73**, 213–217.
- McMichael, A. J., 1997: Integrated assessment of potential health impact of global environmental change: Prospects and limitations. *Environmental Modeling Assessment*, **2**, 129–137.
- McMichael, A. J., 2000: The urban environment and health in a world of increasing globalization: issues for developing countries. *Bulletin of the World Health Organization*, **78**, 1117–1126.
- McMichael, A. J. and A. Haines, 1997: Global climate change: the potential effects on health. *British Medical Journal*, **315**, 805–809.
- Meehl, G. A., T. F. Stocker, W. D. Collins, P. Friedlingstein, A. T. Gaye, J. M. Gregory, A. Kitoh, R. Knutti, J. M. Murphy, A. Noda, S. C. B. Raper, I. G. Watterson, A. J. Weaver, and Z. C. Zhao, 2007: Global Climate Projections. *Climate Change 2007: The Physical Science Basis*, S. Solomon, D. Qin, M. Manning, Z. Chen, M. Marquis, K. B. Averyt, M. Tignor, and H. L. Miller, Eds., Cambridge University Press, Cambridge, United Kingdom and New York, USA, 747–845, contribution of Working Group I to the Fourth Assessment Report of the Intergovernmental Panel on Climate Change.
- Mekuria, Y. R., R. Granados, M. A. Tidwell, D. C. Williams, R. A. Wirtz, and D. R. Roberts, 1991: Malaria transmission potential by *Anopheles* mosquitoes of Dajabon, Dominican Republic. *Journal of the American Mosquito Control Association*, **7**, 456–461.
- Menegon, M., C. Severini, A. Sannella, M. G. Paglia, D. Sangaré, A. Abdel-Wahab, A.-M. A. Abdel-Muhsin, H. Babiker, D. Walliker, and P. Alano, 2000: Genotyping of *Plasmodium falciparum* gametocytes by reverse transcriptase polymerase chain reaction. *Molecular and Biochemical Parasitology*, **111**, 153–161.
- Menendez, C., 1999: Priority areas for current research on malaria during pregnancy. *Annals of Tropical Medicine and Parasitology*, **93**, S71–S74.
- Meunier, J. Y., I. Safeukui, D. Fontenille, and C. Boudin, 1999: Etude de la transmission du paludisme dans une future zone d'essai vaccinal en forêt équatoriale du sud Cameroun. *Bulletin de la Société de Pathologie Exotique*, **92**, 309–312.
- Miller, M. J., 1958: Observations on the natural history of malaria in the semi-resistant West African. *Transactions of the Royal Society of Tropical Medicine and Hygiene*, **52**, 152–168.
- Minakawa, N., S. Munga, F. Atieli, E. Mushinzimana, G. Zou, A. K. Githeko, and G. Yan, 2005: Spatial distribution of anopheline larval habitats in western Kenyan highlands: effects of land cover types and topography. *The American Journal of Tropical Medicine and Hygiene*, **73**, 157–165.
- Minakawa, N., G. Sonye, N. Mogi, A. K. Githeko, and G. Yan, 2002: The Effects of Climatic Factors on the Distribution and Abundance of Malaria Vectors in Kenya. *Journal of Medical Entomology*, **39**, 833–841.
- Mitchell, T. D. and P. D. Jones, 2005: An improved method of constructing a database of monthly climate observations and associated high-resolution grids. *International Journal of Climatology*, **25**, 693–712.
- Modiano, D., V. Petrarca, B. S. Sirima, I. Nebie, D. Diallo, F. Esposito, and M. Coluzzi, 1996: Different response to *Plasmodium falciparum* malaria in West African sympatric ethnic groups. *Proceedings of the National Academy of Sciences USA*, **93**, 13 206–13 211.
- Moffett, A., N. Shackelford, and S. Sarkar, 2007: Malaria in Africa: Vector Niche Models and Relative Risk Maps. *Public Library of Science ONE*, **2**, e824.
- Mogi, M., 1992: Temperature and Photoperiod Effects on Larval Ovarian Development of New Zealand Strains of *Culex quinquefasciatus* (Diptera: Culicidae). *Annals of the Entomological Society of America*, **85**, 58–66.
- Molez, J. F., A. Diop, O. Gaye, J. J. Lemasson, and D. Fontenille, 2006: Malaria morbidity in Barkedji, village of Ferlo, in Senegal Sahelian area. *Bulletin de la Société de Pathologie Exotique*, **99**, 187–190.
- Molineaux, L., 1988: The epidemiology of human malaria as an explanation of its distribution, including some implications for its control. *Malaria, principles and practice of malariology*, W. H. Wernsdorfer and I. McGregor, Eds., Churchill Livingstone, Edinburgh, London, Melbourne, and New York, 913–998.
- Molineaux, L., K. Dietz, and A. Thomas, 1978: Further epidemiological evaluation of a malaria model. *Bulletin of the World Health Organization*, **56**, 565–571.

- Molineaux, L. and G. Gramiccia, 1980: *The Garki Project, Research on the Epidemiology and Control of Malaria in the Sudan Savanna of West Africa*. WHO, Geneva, Switzerland, 311 pp.
- Molineaux, L., J. Storey, J. E. Cohen, and A. Thomas, 1980: A longitudinal study of human malaria in the West African savanna in the absence of control measures: Relationship between different *Plasmodium* species, in particular *P. falciparum* and *P. malariae*. *The American Journal of Tropical Medicine and Hygiene*, **29**, 725–737.
- Morse, A. P., F. J. Doblas-Reyes, M. B. Hoshen, R. Hagedorn, and T. N. Palmer, 2005: A forecast quality assessment of an end-to-end probabilistic multi-model seasonal forecast system using a malaria model. *Tellus*, **57A**, 464–475.
- Mouchet, J., 2000: Airport malaria: a rare disease still poorly understood. *Euro surveillance*, **5**, 75–76.
- Mouchet, J., O. Faye, J. Julvez, and S. Manguin, 1996: Drought and malaria retreat in the Sahel, West Africa. *The Lancet*, **348**, 1735–1736.
- Mouchet, J., S. Manguin, K. Sircoulon, S. Lavnevale, O. Faye, A. W. Onapa, P. Carnevale, J. Julvez, and D. Fontenille, 1998: Evolution of malaria in Africa for the past 40 years: impact of climatic and human factors. *Journal of the American Mosquito Control Association*, **14**, 121–130.
- Muirhead-Thomson, R. C., 1951: The distribution of anopheline mosquito bites among different age groups. *British Medical Journal*, **1**, 1114–1117.
- Muirhead-Thomson, R. C., 1954: Factors determining the true reservoir of infection of *Plasmodium falciparum* and *Wuchereria bancrofti* in a West African village. *Transactions of the Royal Society of Tropical Medicine and Hygiene*, **48**, 208–225.
- Muirhead-Thomson, R. C., 1957: The Malarial Infectivity of an African Village Population to Mosquitoes (*Anopheles Gambiae*): A Random Xenodiagnostic Survey. *The American Journal of Tropical Medicine and Hygiene*, **6**, 971–979.
- Mulder, B., T. Tchuinkam, K. Decherig, J. P. Verhave, P. Carnevale, J. H. E. T. Meuwissen, and V. Robert, 1994: Malaria transmission-blocking activity in experimental infections of *Anopheles gambiae* from naturally infected *Plasmodium falciparum* gametocyte carriers. *Transactions of the Royal Society of Tropical Medicine and Hygiene*, **88**, 121–125.
- Mulder, B., W. van der Ligt, R. Sauerwein, and J. P. Verhave, 1998: Detection of *Plasmodium falciparum* gametocytes with the QBC® test and Giemsa-stained thick blood films for malaria transmission studies in Cameroon. *Transactions of the Royal Society of Tropical Medicine and Hygiene*, **92**, 395–396.
- Munga, S., N. Minakawa, G. Zhou, E. Mushinzimana, O.-O. J. Barrack, A. K. Githeko, and G. Yan, 2006: Association between land cover and habitat productivity of malaria vectors in western Kenyan highlands. *The American Journal of Tropical Medicine and Hygiene*, **74**, 69–75.
- Muriu, S. M., E. J. Muturi, J. I. Shililu, C. M. Mbogo, J. M. Mwangangi, B. G. Jacob, L. W. Irungu, R. W. Mukabana, J. I. Githure, and R. J. Novak, 2008: Host choice and multiple blood feeding behaviour of malaria vectors and other anophelines in Mwea rice scheme, Kenya. *Malaria Journal*, **7**, 43.
- Murphy, J. R., S. Baqar, J. R. Davis, D. A. Herrington, and D. F. Clyde, 1989: Evidence for a 6.5-day minimum exoerythrocytic cycle for *Plasmodium falciparum* in humans and confirmation that immunization with a synthetic peptide representative of a region of the circumsporozoite protein retards infection. *Journal of Clinical Microbiology*, **27**, 1434–1437.
- Mutero, C. M. and M. H. Birley, 1987: Estimation of the Survival Rate and Oviposition Cycle of Field Populations of Malaria Vectors in Kenya. *The Journal of Applied Ecology*, **24**, 853–863.
- Mwangangi, J. M., E. J. Muturi, J. Shililu, S. M. Muriu, B. Jacob, E. W. Kabiru, C. M. Mbogo, J. Githure, and R. Novak, 2006: Survival of immature *Anopheles arabiensis* (Diptera: Culicidae) in aquatic habitats in Mwea rice irrigation scheme, central Kenya. *Malaria Journal*, **5**, 114.
- Nabarro, D. N. and E. M. Tayle, 1998: The "Roll Back Malaria" Campaign. *Science*, **280**, 2067–2068.
- Nájera, J. A., 1974: A critical review of the field application of a mathematical model of malaria eradication. *Bulletin of the World Health Organization*, **50**, 449–457.
- Nakićenović, N., J. Alcamo, G. Davis, B. de Vries, J. Fenhann, S. Gaffin, K. Gregory, A. Grübler, T. Y. Jung, T. Kram, E. L. L. Rovere, L. Michaelis, S. Mori, T. Morita, W. Pepper, H. Pitcher, L. Price, K. Riahi, A. Roehrl, H. H. Rogner, A. Sankovski, M. Schlesinger, P. Shukla, S. Smith, R. Swart, S. van Rooijen, N. Victor, and Z. Dadi, 2000: Special Report on Emissions Scenarios. Tech. rep., Working Group III of the Intergovernmental Panel on Climate Change, 599 pp., New York, USA.
- Nassir, E., A.-M. A. Abdel-Muhsin, S. Suliaman, F. Kenyon, A. Kheir, H. Geha, H. M. Ferguson, D. Walliker, and H. A. Babiker, 2005: Impact of genetic complexity on longevity and gametocytogenesis of *Plasmodium falciparum* during the dry and transmission-free season of eastern Sudan. *International Journal for Parasitology*, **35**, 49–55.
- Ndiaye, O., J.-Y. L. Hesran, J.-F. Etard, A. Diallo, F. Simondon, M. N. Ward, and V. Robert, 2001: Variations climatique et mortalité attribuée au paludisme dans la zone de Niakhar, Sénégal, de 1984 à 1996. *Santé*, **11**, 25–33.
- Ndiaye, P. I., D. J. Bicut, B. Mondet, and P. Sabatier, 2006: Rainfall triggered dynamics of *Aedes* mosquito aggressiveness. *Journal of Theoretical Biology*, **243**, 222–229.
- Nedelman, J., 1984: Inoculation and recovery rates in the malaria model of Dietz, Molineaux, and Thomas. *Mathematical Biosciences*, **69**, 209–233.
- Nedelman, J., 1985: Some New thoughts about Some Old Malaria Models. *Mathematical Biosciences*, **73**, 159–182.
- Nedelman, J., 1989: Gametocitaemia and Infectiousness in *Falciparum* malaria: Observations and Models. *Advances in Disease Vector Research*, **6**, 59–89.
- Nelson, G. S., 1959: *Atlas of Kenya*. 1st ed., Crown Printers, Nairobi, Kenya.
- New, M., M. Hulme, and P. Jones, 1999: Representing Twentieth-Century Space-Time Climate Variability. Part I: Development of a 1961–1990 Mean Monthly Terrestrial Climatology. *Journal of Climate*, **12**, 829–856.
- New, M., M. Hulme, and P. Jones, 2000: Representing Twentieth-Century Space-Time Climate Variability. Part II: Development of a 1901–1996 Monthly Grids of Terrestrial Surface Climate. *Journal of Climate*, **13**, 2217–2238.
- New, M., D. Lister, M. Hulme, and I. Makin, 2002: A high-resolution data set of surface climate over global land areas. *Climate Research*, **21**, 1–25.
- Nicholson, S., 2005: On the question of the "recovery" of the rains in the West African Sahel. *Journal of Arid Environments*, **63**, 615–641.
- Nicholson, S. E., 1996: A Review of Climate Dynamics and Climate Variability in Eastern Africa. *The Limnology, Climatology, and Paleoclimatology of the East African Lakes*, T. C. Johnson and E. O. Odada, Eds., Gordon and Breach Publishers, Amsterdam, Netherlands, 24–56.
- Nicholson, S. E. and B. S. Nyenzi, 1990: Temporal and Spatial Variability of SSTs in the Tropical Atlantic and Indian Oceans. *Meteorology and Atmospheric Physics*, **42**, 1–17.
- Nikolaev, B. P., 1935: On the influence of temperature on the development of malaria plasmodia in the mosquito. *Leningrad Pasteur Institute of Epidemiology and Bacteriology*, **2**, 108–109.
- Njan Nloga, A., V. Robert, J. C. Toto, and P. Carnevale, 1993: *Anopheles moucheti*, vecteur principal du paludisme au sud Cameroun. *Bulletin de Liaison et de Documentation de l'OCEAC*, **26**, 63–67.
- Noor, A. M., A. C. Clements, P. W. Gething, G. Moloney, M. Borle, T. Shewchuk, S. I. Hay, and R. W. Snow, 2008a: Spatial prediction of *Plasmodium falciparum* prevalence in Somalia. *Malaria Journal*, **7**, 159.
- Noor, A. M., G. Moloney, M. Borle, G. W. Fegan, T. Shewchuk, and R. W. Snow, 2008b: The use of mosquito nets and the prevalence of *Plasmodium falciparum* infection in rural South Central Somalia. *Public Library of Science ONE*, **3**, e2081.
- Nwakanma, D., A. Kheir, M. Sowa, S. Dunyo, M. Jawara, M. Pinder, P. Milligan, D. Walliker, and H. A. Babiker, 2008: High gametocyte complexity and mosquito infectivity of *Plasmodium falciparum* in the Gambia. *International Journal for Parasitology*, **38**, 219–227.
- Ogallal, L. J., 1989: The spatial and temporal patterns of the East African seasonal rainfall derived from principal component analysis. *International Journal of Climatology*, **9**, 145–167.
- Omer, S. M. and J. L. Cloudsley-Thompson, 1970: Survival of Female *Anopheles gambiae* Giles Through a 9-Month Dry Season in Sudan. *Bulletin of the World Health Organization*, **42**, 319–330.
- Omotsho, J. B., 1985: The separate contribution of line squalls, thunderstorms and the monsoon to the total rainfall in Nigeria. *Journal of Climatology*, **5**, 543–552.
- Omumbo, J. A., S. I. Hay, R. W. Snow, A. J. Tatem, and D. J. Rogers, 2005: Modelling malaria risk in East Africa at high-spatial resolution. *Tropical Medicine and International Health*, **10**, 557–566.
- Oouchi, K., J. Yoshimura, H. Yoshimura, R. Mizuta, S. Kusunoki, and A. Noda, 2006: Tropical Cyclone Climatology in a Global Warming Climate as Simulated in a 20 km-Mesh Global Atmospheric Model: Frequency and Wind Intensity Analyses. *Journal of the Meteorological Society of Japan*, **84**, 259–276.
- Ouédraogo, A. L., P. Schneider, M. de Kruijff, I. Nébé, J. P. Verhave, N. Cuzin-Ouattara, and R. W. Sauerwein, 2007: Age-dependent distribution of *Plasmodium falciparum* gametocytes quantified by PfS25 real-time QT-NASBA in a cross-sectional study in Burkina Faso. *The American Journal of Tropical Medicine and Hygiene*, **76**, 626–630.
- Ouédraogo, A. L., S. J. de Vlas, I. Nébé, E. Ilboudo-Sanogo, J. T. Bousema, A. S. Ouattara, J. P. Verhave, N. Cuzin-Ouattara, and R. W. Sauerwein, 2008: Seasonal patterns of *Plasmodium falciparum* gametocyte prevalence and density in a rural population of Burkina Faso. *Acta Tropica*, **105**, 28–34.
- Paaajmans, K. P., M. O. Wandago, A. K. Githeko, and W. Takken, 2007: Unexpected High Losses of *Anopheles gambiae* Larvae Due to Rainfall. *Public Library of Science ONE*, **2**, e1146.
- Paeth, H., 2005: The climate of tropical and northern Africa - a statistical-dynamical analysis of the key factors in climate variability and the role of human activity in future climate change. Bonner meteorologische Abhandlungen, 61, Meteorologisches Institut Bonn, 320 pp., Bonn, Germany.
- Paeth, H., K. Born, R. Girmes, R. Podzun, and D. Jacob, 2009: Regional Climate Change in Tropical and Northern Africa due to Greenhouse Forcing and Land Use Changes. *Journal of Climate*, **22**, 114–132.
- Paeth, H. and J. Feichter, 2006: Greenhouse-gas versus aerosol forcing and African climate response. *Climate Dynamics*, **26**, 35–54.
- Palmer, T. N., 1986: The influence of the Atlantic, Pacific and Indian oceans on Sahel rainfall. *Nature*, **322**, 251–253.
- Palmer, T. N., A. Alessandri, U. Andersen, P. Cantelaube, M. Davey, P. Décluse, M. Déqué, E. Diez, F. J. Doblas-Reyes, H. Feddersen, R. Graham, S. Gualdi, J.-F. Guérémy, R. Hagedorn, M. Hoshen, N. Keenlyside, M. Latif, A. Lazar, E. Maisonneuve, V. Marletto, A. P. Morse, B. Orfila, P. Rogel, J.-M. Terres, and M. C. Thomson, 2004a:

- Development of a european multi-model ensemble system for seasonal to inter-annual prediction (DEMETER). *Bulletin of the American Meteorological Society*, **85**, 853–872.
- Palmer, T. N., A. Alessri, U. Andersen, P. Cantelaupe, M. Davey, P. Délécluse, M. Déqué, E. Diez, F. J. Doblas-Reyes, H. Feddersen, R. Graham, S. Gualdi, J.-F. Guérémy, R. Hagedorn, M. Hoshen, N. Keenlyside, M. Latif, A. Lazar, E. Maisonnave, V. Marletto, A. P. Morse, B. Orfila, P. Rogel, J.-M. Terres, and M. C. Thomson, 2004b: Development of a european multi-model ensemble system for seasonal to inter-annual prediction (DEMETER). ECMWF Technical Memorandum, 434, ECMWF, 25 pp., Reading, United Kingdom.
- Parker, D. J., D. J. Thorncroft, R. R. Burton, and A. Diongue-Niang, 2005: Analysis of the African Easterly Jet using aircraft observations from the JET2000 experiment. *The Quarterly Journal of the Royal Meteorological Society*, **131**, 1461–1482.
- Pascual, M., J. A. Ahumada, L. F. Chaves, X. Rodó, and M. Bouma, 2006: Malaria resurgence in the East African highlands: Temperature trends revisited. *Proceedings of the National Academy of Sciences USA*, **103**, 5829–5834.
- Pascual, M., B. Cazelles, M. J. Bouma, L. F. Chaves, and K. Koelle, 2008: Shifting patterns: malaria dynamics and rainfall variability in an African highland. *Proceedings of the Royal Society of London, Series B*, **275**, 123–132.
- Patz, J. A., D. Campbell-Lendrum, T. Holloway, and J. A. Foley, 2005: Impact of regional climate change on human health. *Nature*, **438**, 310–317.
- Patz, J. A., P. R. Epstein, T. A. Burke, and J. M. Balbus, 1996: Global Climate Change and Emerging Infectious Diseases. *Journal of American Medical Association*, **275**, 217–223.
- Patz, J. A. and S. W. Lindsay, 1999: New challenges, new tools: the impact of climate change on infectious diseases. *Current opinion in microbiology*, **2**, 445–451.
- Patz, J. A. and S. H. Olson, 2006: Climate change and health: global to local influences on disease risk. *Annals of Tropical Medicine and Parasitology*, **100**, 535–549.
- Patz, J. A. and W. K. Reisen, 2001: Immunology, climate change and vector-borne disease. *Trends in Immunology*, **22**, 171–172.
- Patz, J. A., K. Strzepec, S. Lele, M. Hedden, S. Green, B. Noden, S. I. Hay, L. Kalkstein, and J. C. Beier, 1998: Predicting key malaria transmission factors, biting and entomological inoculation rates, using modelled soil moisture in Kenya. *Tropical Medicine and International Health*, **3**, 818–827.
- Paul, R. E. L., S. Bonnet, C. Boudin, T. Tchuinkam, and V. Robert, 2007: Aggregation in malaria parasites places limits on mosquito infection rates. *Infection, Genetics and Evolution*, **7**, 577–586.
- Payne, S. W. and M. M. McGarry, 1977: The relationship of satellite inferred convective activity to easterly waves over West Africa and the adjacent ocean during phase III of GATE. *Monthly Weather Review*, **105**, 413–420.
- Pedgley, D. E., 1972: Desert depressions over north-east Africa. *Meteorological Magazine*, **101**, 228–244.
- Peel, M. C., B. L. Finlayson, and T. A. McMahon, 2007: Updated world map of the Köppen-Geiger climate classification. *Hydrology and Earth System Sciences*, **11**, 1633–1644.
- Peters, M. and G. Tetzlaff, 1988: The Structure of West African Squall Lines and Their Environmental Moisture Budget. *Meteorology and Atmospheric Physics*, **39**, 74–84.
- Peterson, T. C., R. Vose, R. Schmoyer, and V. Razuvayev, 1998: Global Historical Climatology Network (GHCN) quality control of monthly temperature data. *International Journal of Climatology*, **18**, 1169–1179.
- Peterson, T. C. and R. S. Vose, 1997: An overview of the Global Historical Climatology Network temperature database. *Bulletin of the American Meteorological Society*, **78**, 2837–2849.
- Phillips, D. R., 1993: Urbanization and human health. *Parasitology*, **106** (Suppl.), S93–S107.
- Phillips, R. S., 2001: Current Status of Malaria and Potential for Control. *Clinical Microbiology Reviews*, **14**, 208–226.
- Port, G. R., P. F. L. Boreham, and J. H. Bryan, 1980: The relationship of host size to feeding by mosquitoes of the *Anopheles gambiae* Giles complex (Diptera: Culicidae). *Bulletin of Entomological Research*, **70**, 133–144.
- Price, R. N., F. Nosten, C. Luxemburger, F. O. ter Kuile, L. Paiphun, T. Chongsuphajaisiddhi, and N. J. White, 1996: Effects of artemisinin derivatives on malaria transmissibility. *The Lancet*, **347**, 1654–1658.
- Pull, J. H. and B. Grab, 1974: A simple epidemiological model for evaluating the malaria inoculation rate and the risk of infection in infants. *Bulletin of the World Health Organization*, **51**, 507–516.
- Pytharoulis, I. and C. Thorncroft, 1999: The Low-Level Structure of African Easterly Waves in 1995. *Monthly Weather Review*, **127**, 2266–2280.
- Quakyi, I. A., R. G. F. Leke, R. Befidi-Mengue, M. Tsafack, D. Bomba-Nkolo, L. Manga, V. Tchinda, E. Njeungue, S. Kouontchou, J. Fogako, P. Nyonglema, L. T. Harun, R. Djokam, G. Sama, A. Eno, R. Megnekou, S. Metenou, L. Ndountse, A. Same-Ekobo, G. Alake, J. Meli, J. Ngu, F. Tietche, J. Lohoue, J. L. Mvondo, E. Wansi, R. Leke, A. Folefack, J. Bigoga, C. Bomba-Nkolo, V. Titanji, A. Walker-Abbey, M. A. Hickey, A. H. Johnson, and D. W. Taylor, 2000: The epidemiology of *Plasmodium falciparum* malaria in two Cameroonian villages: Simbok and Etoa. *The American Journal of Tropical Medicine and Hygiene*, **63**, 222–230.
- Rall, D. A., R. A. Wood, S. Bony, R. Colman, T. Fichefet, J. Pyfe, V. Kattsov, A. Pitman, J. Shukla, J. Srinivasan, R. J. Stouffer, A. Sumi, and K. E. Taylor, 2007: Climate Models and Their Evaluation. *Climate Change 2007: The Physical Science Basis*, S. Solomon, D. Qin, M. Manning, Z. Chen, M. Marquis, K. B. Averyt, M. Tignor, and H. L. Miller, Eds., Cambridge University Press, Cambridge, United Kingdom and New York, USA, 589–662, contribution of Working Group I to the Fourth Assessment Report of the Intergovernmental Panel on Climate Change.
- Ree, H. I. and U. W. Hwang, 2000: Comparative study on longevity of *Anopheles sinensis* in malarious and non-malarious areas in Korea. *The Korean Journal of Parasitology*, **38**, 263–266.
- Ree, H. I., U. W. Hwang, I. Y. Lee, and T. E. Kim, 2001: Daily survival and human blood index of *Anopheles sinensis*, the vector species of malaria in Korea. *Journal of the American Mosquito Control Association*, **17**, 67–72.
- Reed, R. J., D. C. Norquist, and E. E. Recker, 1977: The structure and properties of African wave disturbances as observed during phase III of GATE. *Monthly Weather Review*, **105**, 317–333.
- Reisen, W. K. and M. Aslamkhan, 1979: A release-recapture experiment with the malaria vector, *Anopheles stephensi* Liston, with observations on dispersal, survivorship, population size, gonotrophic rhythm and mating behaviour. *Annals of Tropical Medicine and Parasitology*, **73**, 251–269.
- Reiter, P., 2000: From Shakespeare to Defoe: Malaria in England in the Little Ice age. *Emerging Infectious Diseases*, **6**, 1–11.
- Reiter, P., 2001: Climate Change and Mosquito-Borne Disease. *Environmental Health Perspectives*, **109**, 141–161.
- Reiter, P., C. J. Thomas, P. M. Atkinson, S. I. Hay, S. E. Randolph, D. J. Rogers, G. D. Shanks, R. W. Snow, and A. Spielman, 2004: Global warming and malaria: a call for accuracy. *The Lancet Infectious Diseases*, **4**, 323–324.
- Rickman, L., T. R. Jones, G. W. Long, S. Paparello, I. Schneider, C. F. Paul, R. L. Beaudoin, and S. L. Hoffman, 1990: *Plasmodium falciparum*-infected *Anopheles stephensi* inconsistently transmit malaria to humans. *The American Journal of Tropical Medicine and Hygiene*, **43**, 441–445.
- Rickman, L. S., G. W. Long, R. Oberst, A. Cabanban, R. Sangalang, J. I. Smith, J. D. Chulay, and S. L. Hoffman, 1989: Rapid diagnosis of malaria by acridine orange staining of centrifuged parasites. *The Lancet*, **333**, 68–71.
- Robert, V. and P. Carnevale, 1991: Influence of deltamethrin treatment of bed nets on malaria transmission in the Kou valley, Burkina Faso. *Bulletin of the World Health Organization*, **69**, 735–740.
- Robert, V., P. Carnevale, V. Ouédraogo, V. Petrarca, and M. Coluzzi, 1988: La transmission du paludisme humain dans un village de savane du sud-ouest du Burkina Faso. *Annales de la Société Belge de Médecine Tropicale*, **68**, 107–121.
- Robert, V., H. Dieng, L. Lochouart, S. F. Traoré, J.-F. Trape, F. Simondon, and D. Fontenille, 1998: La transmission du paludisme dans la zone de Niakhar, Sénégal. *Tropical Medicine and International Health*, **3**, 667–677.
- Robert, V., I. Gazin, V. Ouédraogo, and I. Carnevale, 1986: Le paludisme urbain à Bobo-Dioulasso (Burkina Faso). 1. Etude entomologique de la transmission. *Cahiers O.R.S.T.O.M. Série Entomologie Médicale et Parasitologie*, **24**, 121–128.
- Robert, V., P. Gazin, R. Benasseni, and P. Carnevale, 1989: Le paludisme urbain à Bobo-Dioulasso (Burkina Faso). *Urbanisation et santé dans le Tiers Monde: transition épidémiologique, changement social et soins de santé primaires*, G. Salem and J. Emile, Eds., ORSTROM, Paris, France, 181–185.
- Robert, V., P. Gazin, C. Boudin, J. F. Molez, V. Ouédraogo, and P. Carnevale, 1985: La transmission du paludisme en zone de savane arborée et en zone rizicole des Bobo Dioulasso (Burkina Faso). *Annales de la Société Belge de Médecine Tropicale*, **65**, 201–214.
- Robert, V., G. Le Goff, J.-C. Toto, L. Mulder, E. Fondjo, L. Manga, and P. Carnevale, 1993: Anthropophilic mosquitoes and malaria transmission at Edea, Cameroon. *Tropical Medicine and Parasitology*, **44**, 14–18.
- Robert, V., K. Macintyre, J. Keating, W. McWilson, J. P. Trappe, J. B. Duchemin, and J. C. Beier, 2003: Malaria transmission in urban sub-Saharan Africa. *The American Society of Tropical Medicine and Hygiene*, **68**, 169–176.
- Robert, V., A. van den Broek, P. Stevens, R. Slootweg, V. Petrarca, M. Coluzzi, G. Le Goff, M. A. D. Deco, and P. Carnevale, 1992: Mosquitoes and malaria transmission in irrigated rice-fields in the Benoue Valley of northern Cameroon. *Acta Tropica*, **52**, 201–204.
- Roberts, D. R., S. Mangun, and J. Mouchet, 2000: DDT house spraying and re-emerging malaria. *The Lancet*, **356**, 330–332.
- Roeckner, E., 2004a: IPCC-AR4 MPI-ECHAM5_T63L31 MPI-OM_GR1.5L40_20C3M run no.2: atmosphere 6 HOUR values MPImet/MaD Germany. DKRZ, World Data Center for Climate, CERA-DB "EH5-T63L31_OM-GR1.5L40_20C_2_6H", http://cera-www.dkrz.de/WDCC/ui/Compact.jsp?acronym=EH5-T63L31_OM-GR1.5L40_20C_2_6H.
- Roeckner, E., 2004b: IPCC-AR4 MPI-ECHAM5_T63L31 MPI-OM_GR1.5L40_SRESA1B run no.2: atmosphere 6 HOUR values MPImet/MaD Germany. DKRZ, World Data Center for Climate, CERA-DB "EH5-T63L31_OM-GR1.5L40_A1B_2_6H", http://cera-www.dkrz.de/WDCC/ui/Compact.jsp?acronym=EH5-T63L31_OM-GR1.5L40_A1B_2_6H.

- GR1.5L40_A1B_2_6H.
- Roeckner, E., 2004c: IPCC-AR4 MPI-ECHAM5_T63L31 MPI-OM_GR1.5L40 SRESB1 run no.2: atmosphere 6 HOUR values MPImet/MaD Germany. DKRZ, World Data Center for Climate, CERA-DB "EH5-T63L31_OM-GR1.5L40_B1_2_6H", http://cera-www.dkrz.de/WDCC/ui/Compact.jsp?acronym=EH5-T63L31_OM-GR1.5L40_B1_2_6H.
- Roeckner, E., M. Lautenschlager, and H. Schneider, 2006a: IPCC-AR4 MPI-ECHAM5_T63L31 MPI-OM_GR1.5L40 20C3M run no.1: atmosphere 6 HOUR values MPImet/MaD Germany. DKRZ, World Data Center for Climate, doi:10.1594/WDCC/EH5-T63L31_OM-GR1.5L40_20C_1_6H.
- Roeckner, E., M. Lautenschlager, and H. Schneider, 2006b: IPCC-AR4 MPI-ECHAM5_T63L31 MPI-OM_GR1.5L40 20C3M run no.3: atmosphere 6 HOUR values MPImet/MaD Germany. DKRZ, World Data Center for Climate, doi:10.1594/WDCC/EH5-T63L31_OM-GR1.5L40_20C_3_6H.
- Roeckner, E., M. Lautenschlager, and H. Schneider, 2006c: IPCC-AR4 MPI-ECHAM5_T63L31 MPI-OM_GR1.5L40 SRESA1B run no.1: atmosphere 6 HOUR values MPImet/MaD Germany. DKRZ, World Data Center for Climate, doi:10.1594/WDCC/EH5-T63L31_OM-GR1.5L40_A1B_1_6H.
- Roeckner, E., M. Lautenschlager, and H. Schneider, 2006d: IPCC-AR4 MPI-ECHAM5_T63L31 MPI-OM_GR1.5L40 SRESA1B run no.3: atmosphere 6 HOUR values MPImet/MaD Germany. DKRZ, World Data Center for Climate, doi:10.1594/WDCC/EH5-T63L31_OM-GR1.5L40_A1B_3_6H.
- Roeckner, E., M. Lautenschlager, and H. Schneider, 2006e: IPCC-AR4 MPI-ECHAM5_T63L31 MPI-OM_GR1.5L40 SRESB1 run no.1: atmosphere 6 HOUR values MPImet/MaD Germany. DKRZ, World Data Center for Climate, doi:10.1594/WDCC/EH5-T63L31_OM-GR1.5L40_B1_1_6H.
- Roeckner, E., M. Lautenschlager, and H. Schneider, 2006f: IPCC-AR4 MPI-ECHAM5_T63L31 MPI-OM_GR1.5L40 SRESB1 run no.3: atmosphere 6 HOUR values MPImet/MaD Germany. DKRZ, World Data Center for Climate, doi:10.1594/WDCC/EH5-T63L31_OM-GR1.5L40_B1_3_6H.
- Roeckner, E., K. Arpe, L. Bengtsson, M. Christoph, M. Claussen, L. Dümenil, M. Esch, M. Giorgetta, U. Schlese, and U. Schulzweida, 1996: The atmospheric general circulation model ECHAM-4: model description and simulation of present-day climate. Report, 218, Max Planck Institute for Meteorology, 90 pp., Hamburg, Germany.
- Rogers, D. J. and S. E. Randolph, 2000: The Global Spread of Malaria in a Future, Warmer World. *Science*, **289**, 1763–1766 (Corrected in print, 29 Sept. 2000, p. 2283.).
- Rogers, D. J., S. E. Randolph, R. W. Snow, and S. I. Hay, 2002: Satellite imagery in the study and forecast of malaria. *Nature*, **415**, 710–715.
- Rogier, C. and J.-F. Trape, 1995: Etude de l'acquisition de la prémunition en zone d'holo- et de méso-endémie palustre à Dielmo et à Nidiop (Senegal): Résultats préliminaires, 1990-1994. *Médecine Tropicale*, **55**, 71–76.
- Rosenberg, R., R. G. Andre, and S. Ketragsee, 1990a: Seasonal fluctuation of *Plasmodium falciparum* gametocytaemia. *Transactions of the Royal Society of Tropical Medicine and Hygiene*, **84**, 29–33.
- Rosenberg, R., R. G. Andre, and L. Somchit, 1990b: Highly efficient dry season transmission of malaria in Thailand. *Transactions of the Royal Society of Tropical Medicine and Hygiene*, **84**, 22–28.
- Ross, A., G. Killeen, and T. Smith, 2006: Relationships between host infectivity to mosquitoes and asexual parasite density in *Plasmodium falciparum*. *The American Journal of Tropical Medicine and Hygiene*, **75** (Suppl. 2), 32–37.
- Ross, R., 1911: *The Prevention of Malaria*. 2d ed., John Murray, London, United Kingdom, 669 pp.
- Ross, R., 1928: *Studies on malaria*. John Murray, London, United Kingdom, 196 pp.
- Rossi, P., A. Belli, L. Mancini, and G. Sabatinelli, 1986: Enquête entomologique longitudinale sur la transmission du paludisme à Ouagadougou (Burkina Faso). *Parassitologia*, **28**, 1–15.
- Rotstayn, L. D. and U. Lohmann, 2002: Tropical Rainfall Trends and the Indirect Aerosol Effect. *Journal of Climate*, **15**, 2103–2116.
- Rowell, D. P., 2001: Teleconnections between the tropical Pacific and the Sahel. *The Quarterly Journal of the Royal Meteorological Society*, **127**, 1683–1706.
- Rowell, D. P., 2003: The Impact of Mediterranean SSTs on the Sahelian Rainfall Season. *Journal of Climate*, **16**, 849–862.
- Ruiz-Barradas, A., J. A. Carton, and S. Nigam, 2000: Structure of Interannual-to-Decadal Climate Variability in the Tropical Atlantic Sector. *Journal of Climate*, **13**, 3285–3297.
- Rutledge, L. C., D. J. Gould, and B. Tantiachareon, 1969: Factors affecting the infection of anophelines with human malaria in Thailand. *Transactions of the Royal Society of Tropical Medicine and Hygiene*, **63**, 613–619.
- Sabatinelli, G., A. Bosman, L. Lamizana, and P. Rossi, 1986: Prévalence du paludisme à Ouagadougou et dans le milieu rural limitrophe en période de transmission maximale. *Parassitologia*, **28**, 17–31.
- Sachs, J. and P. Malaney, 2002: The economic and social burden of malaria. *Nature*, **415**, 680–685.
- Sagara, I., D. Sangaré, G. Dolo, A. Guindo, M. Sissoko, M. Sogoba, M. B. Niambélé, D. Yalcoué, D. C. Kaslow, A. Dicko, A. D. Klion, D. Diallo, L. H. Miller, Y. Touré, and O. Doumbo, 2002: A high malaria reinfection rate in children and young adults living under a low entomological inoculation rate in a periurban area of Bamako, Mali. *The American Journal of Tropical Medicine and Hygiene*, **66**, 310–313.
- Saji, N. H., B. N. Goswami, P. N. Vinayachandran, and T. Yamagata, 1999: A dipole mode in the tropical Indian Ocean. *Nature*, **401**, 360–363.
- Saji, N. H. and T. Yamagata, 2003a: Possible impacts of Indian Ocean Dipole mode events on global climate. *Climate Research*, **25**, 151–169.
- Saji, N. H. and T. Yamagata, 2003b: Structure of SST and Surface Wind Variability during Indian Ocean Dipole Mode Events: COADS Observations. *Journal of Climate*, **16**, 2735–2751.
- Samarawickrema, W. A., 1967: A Study of the Age-composition of Natural Populations of *Culex pipiens fatigans* Wiedemann in Relation to the Transmission of Filariasis due to *Wuchereria bancrofti* (Cobbold) in Ceylon. *Bulletin of the World Health Organization*, **37**, 117–137.
- Schneider, P., W. Takken, and P. J. McCall, 2000: Interspecific competition between sibling species larvae of *Anopheles arabiensis* and *An. gambiae*. *Medical and Veterinary Entomology*, **14**, 165–170.
- Schneider, P., L. Wolters, G. Schoone, H. Schallig, P. Sillekens, R. Hermesen, and R. Sauerwein, 2005: Real-Time Nucleic Acid Sequence-Based Amplification Is More Convenient than Real-Time PCR for Quantification of *Plasmodium falciparum*. *Journal of Clinical Microbiology*, **43**, 402–405.
- Scholte, E.-J., B. N. Njiru, R. C. Smallegang, W. Takken, and B. G. J. Knols, 2003: Infection of malaria (*Anopheles gambiae* s.s.) and filariasis (*Culex quinquefasciatus*) vectors with the entomopathogenic fungus *Metarhizium anisopliae*. *Malaria Journal*, **2**, 29.
- Segele, Z. T. and P. J. Lamb, 2003: Interannual variability of growing season over drought-prone areas of Ethiopia. *CLIVAR Exchanges*, **27**, 36–39.
- Segele, Z. T. and P. J. Lamb, 2005: Characterization and variability of Kiremt rainy season over Ethiopia. *Meteorology and Atmospheric Physics*, **89**, 153–180.
- Segele, Z. T., P. J. Lamb, and L. M. Leslie, 2008: Large-scale atmospheric circulation and global sea surface temperature associations with Horn of Africa June–September rainfall. *International Journal of Climatology*, doi:10.1002/joc.1751.
- Seleshi, Y. and U. Zanke, 2004: Recent changes in rainfall and rainy days in Ethiopia. *International Journal of Climatology*, **24**, 973–983.
- Service, M. W., 1965: Some basic entomological factors concerned with the transmission and control of malaria in northern Nigeria. *Transactions of the Royal Society of Tropical Medicine and Hygiene*, **59**, 292–296.
- Service, M. W., 1971: Studies on Sampling Larval Populations of the *Anopheles gambiae* complex. *Bulletin of the World Health Organization*, **45**, 169–180.
- Service, M. W., 1973: Mortalities of the larvae of the *Anopheles gambiae* Giles complex and detection of predators by the precipitin test. *Bulletin of Entomological Research*, **62**, 359–369.
- Service, M. W., 1976: *Mosquito ecology: Field Sampling Methods*. Elsevier Applied Science, London, United Kingdom, 583 pp.
- Service, M. W., 1977a: A critical review of procedures for sampling populations of adult mosquitoes. *Bulletin of Entomological Research*, **67**, 343–382.
- Service, M. W., 1977b: Mortalities of the immature stages of species B of the *Anopheles gambiae* complex in Kenya: comparison between rice fields and temporary pools, identification of predators, and effects of insecticidal spraying. *Journal of Medical Entomology*, **13**, 535–545.
- Shaman, J. and J. F. Day, 2005: Achieving Operational Hydrologic Monitoring of Mosquitoborne Disease. *Emerging Infectious Diseases*, **11**, 1343–1350.
- Shaman, J. and J. F. Day, 2007: Reproductive Phase Locking of Mosquito Populations in Response to Rainfall Frequency. *Public Library of Science ONE*, **3**, e331.
- Shaman, J., M. Stieglitz, C. Stark, S. L. Blanco, and M. Cane, 2002: Using a Dynamic Hydrology Model to Predict Mosquito Abundances in Flood and Swamp Water. *Emerging Infectious Diseases*, **8**, 6–13.
- Shanko, D. and P. Camberlin, 1998: The effects of the Southwest Indian Ocean tropical cyclones on Ethiopian drought. *International Journal of Climatology*, **18**, 1373–1388.
- Shanks, G. D., K. Biomndo, S. I. Hay, and R. W. Snow, 2000: Changing patterns of clinical malaria since 1965 among a tea estate population located in the Kenyan highlands. *Transactions of the Royal Society of Tropical Medicine and Hygiene*, **94**, 253–255.
- Shanks, G. D., S. I. Hay, D. I. Stern, K. Biomndo, and R. W. Snow, 2002: Meteorologic Influences on *Plasmodium falciparum* Malaria in the Highland Tea Estates of Kericho, Western Kenya. *Emerging Infectious Diseases*, **8**, 1404–1408.
- Sharpe, P. J. H. and D. W. DeMichele, 1977: Reaction Kinetics of Poikilotherm Development. *Journal of Theoretical Biology*, **64**, 649–670.
- Shililu, J., W. A. Maier, H. M. Seitz, and A. S. Orago, 1998: Seasonal density, sporozoite rates and entomological inoculation rates of *Anopheles gambiae* and *Anopheles funestus* in a high-altitude sugarcane growing zone in western Kenya. *Tropical Medicine and International Health*, **3**, 706–710.
- Shililu, J., T. Ghebremeskel, S. Mengistu, H. Fekadu, M. Zerom, C. Mbogo, J. Githure, R. Novak, E. Brantly, and J. C. Beier, 2003: High seasonal variation in entomologic inoculation rates in Eritrea, a semi-arid region of unstable malaria in Africa. *The American Journal of Tropical Medicine and Hygiene*, **69**, 607–613.
- Shin, E.-H., W. J. Lee, H. I. Lee, D. K. Lee, and T. A. Klein, 2005: Seasonal population density and daily survival of anopheline mosquitoes (Diptera: Culicidae) in a malaria endemic area, Republic of Korea. *Journal of Vector Ecology*, **30**, 33–40.
- Shinoda, M., T. Okatani, and M. Saloum, 1999: Diurnal variations of rainfall over Niger in the West African Sahel: A comparison between wet and drought years. *International Journal of Climatology*, **19**, 81–94.

- Shlenova, M. F., 1938: The speed of blood digestion in female *A. maculipennis* messae at stable effective temperature [in Russian]. *Medicinskaja parazitologija i parazitarnye bolezni*, **7**, 716–735.
- Shute, P. G. and M. Maryon, 1951: A study of gametocytes in a West African strain of *Plasmodium falciparum*. *Transactions of the Royal Society of Tropical Medicine and Hygiene*, **44**, 421–438.
- Simmons, A. J., P. D. Jones, V. da Costa Bechtold, A. C. M. Beljaars, P. W. Källberg, S. Saarinen, S. M. Uppala, P. Viterbo, and N. Wedi, 2004: Comparison of trends and low-frequency variability in CRU, ERA-40, and NCEP/NCAR analyses of surface air temperature. *Journal of Geophysical Research*, **109**, D24 115, doi:10.1029/2004JD005 306.
- Sinden, R., 1983: Sexual Development of Malarial Parasites. *Advances in Parasitology*, **22**, 153–216.
- Sissoko, M. S., A. Dicko, O. J. Briët, M. Sissoko, I. Sagara, H. D. Keita, M. Sogoba, C. Rogier, Y. T. Touré, and O. K. Doumbo, 2004: Malaria incidence in relation to rice cultivation in the irrigated Sahel of Mali. *Acta Tropica*, **89**, 161–170.
- Small, J., S. J. Goetz, and S. I. Hay, 2003: Climatic suitability for malaria transmission in Africa, 1911–1995. *Proceedings of the National Academy of Sciences of the United States of America*, **100**, 15 341–15 345.
- Smalley, M. E., S. Abdalla, and J. Brown, 1981: The distribution of *Plasmodium falciparum* in the peripheral blood and bone marrow of Gambian children. *Transactions of the Royal Society of Tropical Medicine and Hygiene*, **75**, 103–105.
- Smith, D. L., J. Dushoff, R. W. Snow, and S. I. Hay, 2005: The entomological inoculation rate and *Plasmodium falciparum* infection in African children. *Nature*, **438**, 492–495.
- Smith, D. L., F. E. McKenzie, R. W. Snow, and S. I. Hay, 2007: Revisiting the Basic Reproductive Number for Malaria and Its Implications for Malaria Control. *Public Library of Science Biology*, **5**, e42.
- Smith, T., 1995: Proportionality between light trap catches and biting densities of malaria vectors. *Journal of the American Mosquito Control Association*, **11**, 377–378.
- Smith, T., N. Maire, K. Dietz, G. F. Killeen, P. Vounatsou, L. Molineaux, and M. Tanner, 2006a: Relationship between the entomologic inoculation rate and the force of infection for *Plasmodium falciparum* malaria. *The American Journal of Tropical Medicine and Hygiene*, **75** (Suppl. 2), 11–18.
- Smith, T., J. D. Charlwood, J. Kihonda, S. Mwankusye, P. Billingsley, J. Meuwissen, E. Lyimo, W. Takken, T. Teuscher, and M. Tanner, 1993: Absence of seasonal variation in malaria parasitaemia in an area of intense seasonal transmission. *Acta Tropica*, **54**, 55–72.
- Smith, T., G. F. Killeen, N. Maire, A. Ross, L. Molineaux, F. Tediosi, G. Hutton, J. Utzinger, K. Dietz, and M. Tanner, 2006b: Mathematical modeling of the impact of malaria vaccines on the clinical epidemiology and natural history of *Plasmodium falciparum* malaria: Overview. *The American Journal of Tropical Medicine and Hygiene*, **75** (Suppl. 2), 1–10.
- Snow, R. W., M. Craig, U. Deichmann, and K. Marsh, 1999a: Estimating mortality, morbidity and disability due to malaria among Africa's non-pregnant population. *Bulletin World Health Organization*, **77**, 624–640.
- Snow, R. W., M. H. Craig, U. Deichmann, and D. le Sueur, 1999b: A Preliminary Continental Risk Map for Malaria Mortality among African Children. *Parasitology Today*, **15**, 99–104.
- Snow, R. W., J. A. Omumbo, B. Lowe, C. S. Molyneux, J. O. Obiero, A. Palmer, M. W. Weber, M. Pinder, B. Nahlen, C. Obonyo, C. Newbold, S. Gupta, and K. Marsh, 1997: Relation between severe malaria morbidity in children and level of *Plasmodium falciparum* transmission in Africa. *The Lancet*, **349**, 1650–1654.
- Sokhna, C. S., F. B. K. Faye, A. Spiegel, H. Dieng, and J.-F. Trape, 2001: Rapid reappearance of *Plasmodium falciparum* after drug treatment among Senegalese adults exposed to moderate seasonal transmission. *The American Journal of Tropical Medicine and Hygiene*, **65**, 167–170.
- Solomon, S., D. Qin, M. Manning, Z. Chen, M. Marquis, K. B. Averyt, M. Tignor, and H. L. Miller, 2007: *Climate Change 2007: The Physical Science Basis*. Cambridge University Press, Cambridge, United Kingdom and New York, USA, 996 pp., contribution of Working Group I to the Fourth Assessment Report of the Intergovernmental Panel on Climate Change.
- Song, Y., F. H. M. Semazzi, L. Xie, and L. J. Ogallo, 2004: A coupled regional climate model for the Lake Victoria basin of East Africa. *International Journal of Climatology*, **24**, 57–75.
- Stafford Smith, D. M., 1981: Mosquito records from the Republic of Niger, with reference to the construction of the new 'Trans-Sahara Highway'. *Journal of Tropical Medicine and Hygiene*, **84**, 95–100.
- Steketee, R. W. and T. K. Mutabingwa, 1999: Malaria in pregnant women: research, epidemiology, policy and practice. *Annals of Tropical Medicine and Parasitology*, **93**, S7–S9.
- Struchiner, C. J., M. E. Halloran, and A. Spielman, 1989: Modeling malaria vaccines. I: New uses for old ideas. *Mathematical Biosciences*, **94**, 87–113.
- Styler, L. M., J. R. Carey, J.-L. Wang, and T. W. Scott, 2007: Mosquitoes do senesce: departure from the paradigm of constant mortality. *The American Journal of Tropical Medicine and Hygiene*, **76**, 111–117.
- Sultan, B. and S. Janicot, 2003: The West African Monsoon Dynamics. Part II: The „Preonset“ and „Onset“ of the Summer Monsoon. *Journal of Climate*, **16**, 3407–3427.
- Sultan, B., S. Janicot, and A. Diedhiou, 2003: The West African Monsoon Dynamics. Part I: Documentation of Intraseasonal Variability. *Journal of Climate*, **16**, 3389–3406.
- Sun, L., F. H. M. Semazzi, F. Giorgi, and L. Ogallo, 1999: Application of the NCAR regional climate model to eastern Africa 1. Simulation of the short rains of 1988. *Journal of Geophysical Research*, **104**, 6529–6548.
- Sutherst, R. W., 1993: Arthropods as disease vectors in a changing environment. *Environmental change and human health*, J. V. Lake, G. R. Bock, and K. Ackrill, Eds., John Wiley and Sons, Chichester, United Kingdom, 124–145.
- Sutherst, R. W., 1998: Implications of global change and climate variability for vector-borne diseases: generic approaches to impact assessments. *International Journal for Parasitology*, **28**, 935–945.
- Sutherst, R. W., 2004: Global Change and Human Vulnerability to Vector-Borne Diseases. *Clinical Microbiology Reviews*, **17**, 136–173.
- Sutherst, R. W. and G. F. Maywald, 1985: A computerised system for matching climates in ecology. *Agriculture, Ecosystems and Environment*, **13**, 281–299.
- Takken, W., J. D. Charlwood, P. F. Billingsley, and G. Gort, 1998a: Dispersal and survival of *Anopheles funestus* and *A. gambiae* s. l. (Diptera: Culicidae) during the rainy season in southeast Tanzania. *Bulletin of Entomological Research*, **88**, 561–566.
- Takken, W., M. J. Klowden, and G. M. Chambers, 1998b: Effect of Body Size on Host Seeking and Blood meal Utilization in *Anopheles gambiae* sensu stricto (Diptera: Culicidae): The Disadvantage of Being Small. *Journal of Medical Entomology*, **35**, 639–645.
- Talman, A. M., O. Domarle, F. E. McKenzie, F. Ariey, and V. Robert, 2004: Gametocytogenesis: the puberty of *Plasmodium falciparum*. *Malaria Journal*, **3**, 24.
- Tanner, M. and D. de Savigny, 2008: Malaria eradication back on the table. *Bulletin of the World Health Organization*, **86**, 82–83.
- Tanser, F. C., B. Sharp, and D. le Sueur, 2003: Potential effect of climate change on malaria transmission in Africa. *The Lancet*, **362**, 1792–1798.
- Tatem, A. J. and S. I. Hay, 2004: Measuring Urbanization Pattern and Extent for Malaria Research: A Review of Remote Sensing Approaches. *Journal of Urban Health*, **81**, 363–376.
- Taylor, C. E., Y. T. Touré, M. Coluzzi, and V. Petrarca, 1993: Effective population size and persistence of *Anopheles arabiensis* during the dry season in west Africa. *Medical and Veterinary Entomology*, **7**, 351–357.
- Taylor, C. M., E. F. Lambin, N. Stephenne, R. J. Harding, and R. L. H. Essery, 2002: The Influence of Land Use Change on Climate in the Sahel. *Journal of Climate*, **15**, 3615–3629.
- Tchuinkam, T., B. Mulder, K. Dechering, H. Stoffels, J.-P. Verhave, M. Cot, P. Carnevale, J. H. E. T. Meuwissen, and V. Robert, 1993: Experimental infections of *Anopheles gambiae* with *Plasmodium falciparum* of naturally infected gametocyte carriers in Cameroon: factors influencing the infectivity to mosquitoes. *Tropical Medicine and Parasitology*, **44**, 271–276.
- Thomas, C., 2004: Malaria: A changed climate in Africa? *Nature*, **427**, 690–691.
- Thomas, C. J., G. Davies, and C. E. Dunn, 2004: Mixed picture for changes in stable malaria distribution with future climate in Africa. *Trends in Parasitology*, **20**, 216–220.
- Thomson, J. G. and A. Robertson, 1935: The structure and development of *Plasmodium falciparum* gametocytes in the internal organs and peripheral circulation. *Transactions of the Royal Society of Tropical Medicine and Hygiene*, **29**, 31–40.
- Thomson, M. C., S. J. Connor, U. D'Alessandro, B. Rowlingson, P. Diggle, M. Creswell, and B. Greenwood, 1999: Predicting malaria infection in Gambian children from satellite data and bed net use surveys: the importance of spatial correlation in the interpretation of results. *The American Journal of Tropical Medicine and Hygiene*, **61**, 2–8.
- Thomson, M. C., S. J. Connor, P. Milligan, and S. P. Flasse, 1997: Mapping Malaria Risk in Africa: What can Satellite Data Contribute? *Parasitology Today*, **13**, 313–318.
- Thomson, M. C., S. J. Connor, P. J. M. Milligan, and S. P. Flasse, 1996: The ecology of malaria - as seen from Earth-observation satellites. *Annals of Tropical Medicine and Parasitology*, **90**, 243–264.
- Thomson, M. C., U. D'Alessandro, S. Bennett, S. J. Connor, P. Langerock, M. Jawara, J. Todd, and B. M. Greenwood, 1994: Malaria prevalence is inversely related to vector density in The Gambia, West Africa. *Transactions of the Royal Society of Tropical Medicine and Hygiene*, **88**, 638–643.
- Thomson, M. C., F. J. Doblas-Reyes, S. J. Mason, R. Hagedorn, S. J. Connor, T. Phindela, A. P. Morse, and T. N. Palmer, 2006: Malaria early warnings based on seasonal climate forecasts from multi-model ensembles. *Nature*, **439**, 576–579.
- Thomson, M. C., T. Palmer, A. P. Morse, M. Creswell, and S. J. Connor, 2000: Forecasting disease risk with seasonal climate predictions. *The Lancet*, **355**, 1559–1560.
- Thomson, M. C., J. H. Adiamah, S. J. Connor, M. Jawara, S. Bennett, U. D'Alessandro, M. Quinones, P. Langerock, and B. M. Greenwood, 1995: Entomological evaluation of The Gambia's national impregnated bednet programme. *Annals of Tropical Medicine and Parasitology*, **89**, 229–241.

- Thorncroft, C. D. and B. J. Hoskins, 1994: An idealized study of African easterly waves. Part I: A linear view. *The Quarterly Journal of the Royal Meteorological Society*, **120**, 953–982.
- Thorncroft, C. D., D. J. Parker, R. R. Burton, M. Diop, J. H. Ayers, H. Barjat, S. Devereau, A. Diongue, R. Dumelow, D. R. Kindred, N. M. Price, M. Saloum, C. M. Taylor, and A. M. Tompkins, 2003: The JET2000 Project - Aircraft Observations of the African Easterly Jet and African Easterly Waves. *Bulletin of the American Meteorological Society*, **84**, 337–351.
- Tiedtke, M., 1989: A comprehensive mass flux scheme for cumulus parameterization in large scale models. *Monthly Weather Review*, **117**, 1779–1800.
- Tol, R. S. J. and H. Dowlatabadi, 2001: Vector-borne diseases, development & climate change. *Integrated Assessment*, **2**, 173–181.
- Touré, Y. T., G. Dolo, V. Petrarca, S. F. Traoré, M. Bouaré, A. Dao, J. Carnahan, and C. E. Taylor, 1998: Mark-release-recapture experiments with *Anopheles gambiae* s.l. in Banambani village, Mali, to determine population size and structure. *Medical and Veterinary Entomology*, **12**, 74–83.
- Touré, Y. T. and A. Oduola, 2004: Focus: Malaria. *Nature reviews. Microbiology*, **2**, 276–277.
- Trape, J. F., 1987: Études sur le paludisme dans une zone de mosaïque forêt-savane d’Afrique centrale, la région de Brazzaville. II. Densités parasitaires. *Bulletin de la Société de Pathologie Exotique*, **80**, 520–531.
- Trape, J.-F., E. Lefebvre-Zante, F. Legros, P. Druilhe, C. Rogier, H. Bouganali, and G. Salem, 1993: Malaria morbidity among children exposed to low seasonal transmission in Dakar, Senegal and its implications for malaria control in tropical Africa. *The American Journal of Tropical Medicine and Hygiene*, **48**, 748–756.
- Trape, J.-F., E. Lefebvre-Zante, F. Legros, G. Ndiaye, H. Bouganali, P. Druilhe, and G. Salem, 1992: Vector density gradients and the epidemiology of urban malaria in Dakar, Senegal. *The American Journal of Tropical Medicine and Hygiene*, **47**, 181–189.
- Trape, J. F. and A. Zoulani, 1987: Études sur le paludisme dans une zone de mosaïque forêt-savane d’Afrique centrale, la région de Brazzaville. I. Résultats des enquêtes entomologiques. *Bulletin de la Société de Pathologie Exotique*, **80**, 84–99.
- Trape, J.-F., C. Rogier, L. Konaté, N. Diagne, H. Bouganali, B. Canque, F. Legros, A. Badji, G. Ndiaye, P. Ndiaye, K. Brahimi, O. Faye, P. Druilhe, and L. P. D. Silva, 1994: The Dielmo Project: a Longitudinal Study of Natural Malaria Infection and the Mechanisms of Protective Immunity in a Community Living in a Holoendemic Area of Senegal. *The American Journal of Tropical Medicine and Hygiene*, **51**, 123–137.
- Trenberth, K. E., P. D. Jones, P. Ambenje, R. Bojariu, D. Easterling, A. K. Tank, D. Parker, F. Rahimzadeh, J. A. Renwick, M. Rusticucci, B. Soden, and P. Zhai, 2007: Observations: Surface and Atmospheric Climate Change. *Climate Change 2007: The Physical Science Basis*, S. Solomon, D. Qin, M. Manning, Z. Chen, M. Marquis, K. B. Averyt, M. Tignor, and H. L. Miller, Eds., Cambridge University Press, Cambridge, United Kingdom and New York, USA, 235–336, contribution of Working Group I to the Fourth Assessment Report of the Intergovernmental Panel on Climate Change.
- UN, 2006: *World Population Prospects: The 2004 Revision*. United Nations Publications, New York, USA, 91 pp., population Database, <http://esa.un.org/unpp/>.
- Uneke, C. J., O. Ogbu, P. U. Inyama, and G. I. Anyanwu, 2005: Malaria infection in HIV-seropositive and HIV-seronegative individuals in Jos-Nigeria. *Journal of Vector Borne Diseases*, **42**, 151–154.
- Uppala, S. M., P. W. Kållberg, A. J. Simmons, U. Andrae, V. da Costa Bechtold, M. Fiorino, J. K. Gibson, J. Haseler, A. Hernandez, G. A. Kelly, X. Li, K. Onogi, S. Saarinen, N. Sokka, R. P. Allan, E. Andersson, K. Arpe, M. A. Balmaseda, A. C. M. Beljaars, L. van de Berg, J. Bidlot, N. Bormann, S. Caires, F. Chevallier, A. Dethof, M. Dragosavac, M. Fisher, M. Fuentes, S. Hagemann, E. Höltn, B. J. Hoskins, L. Isaksen, P. A. E. M. Janssen, R. Jenne, A. P. McNally, J.-F. Mahfouf, J.-J. Morcrette, N. A. Rayner, R. W. Saunders, P. Simon, A. Sterl, K. E. Trenberth, A. Untch, D. Vasiljevic, P. Viterbo, and J. Woollen, 2005: The ERA-40 reanalysis. *Quarterly Journal of the Royal Meteorological Society*, **131**, 2961–3012.
- van der Kolk, M., A. E. Tebo, H. Nimpaye, D. N. Ndongol, R. W. Sauerwein, and W. M. C. Eling, 2003: Transmission of *Plasmodium falciparum* in urban Yaoundé, Cameroon, is seasonal and age-dependent. *Transactions of the Royal Society of Tropical Medicine and Hygiene*, **97**, 375–379.
- van Lieshout, M., R. S. Kovats, M. T. J. Livermore, and P. Martens, 2004: Climate change and malaria: analysis of the SRES climate and socio-economic scenarios. *Global Environmental Change*, **14**, 87–99.
- Velema, J. P., E. M. Alihonou, J. P. Chippaux, Y. van Boxel, E. Gbedji, and R. Adegbin, 1991: Malaria morbidity and mortality in children under three years of age on the coast of Benin, West Africa. *Transactions of the Royal Society of Tropical Medicine and Hygiene*, **85**, 430–435.
- Vercruysee, J., 1985a: Estimation of the Survival Rate of *Anopheles arabiensis* in an Urban Area (Pikine-Senegal). *The Journal of Animal Ecology*, **54**, 343–350.
- Vercruysee, J., 1985b: Étude entomologique sur la transmission du paludisme humain dans le bassin du fleuve Sénégal (Senegal). *Annales de la Société Belge de Médecine Tropicale*, **65** (Suppl. 2), 171–179.
- Vercruysee, J. and M. Jancloes, 1981: Etude entomologique sur la transmission du paludisme humain dans la zone urbaine de Pikine (Senegal). *Cahiers O.R.S.T.O.M. Série Entomologie Médicale et Parasitologie*, **19**, 165–178.
- Vercruysee, J., M. Jancloes, and L. van de Velden, 1983: Epidemiology of seasonal falciparum malaria in an urban area of Senegal. *Bulletin of the World Health Organization*, **61**, 821–831.
- Vollmert, P., A. H. Fink, and H. Besler, 2003: “Ghana Dry Zone” and “Dahomey Gap”: Ursachen für eine Niederschlagsanomalie im tropischen Westafrika. *Erde*, **134**, 375–393.
- Walter, A., K. Keuler, D. Jacob, R. Knoche, A. Block, S. Kotlarski, G. Moller-Westermeier, D. Rechid, and W. Ahrens, 2006: A high resolution reference data set of German wind velocity 1951–2001 and comparison with regional climate model results. *Meteorologische Zeitschrift*, **15**, 585–596.
- Wanji, S., T. Tanke, S. N. Atanga, C. Ajonina, T. Nicholas, and D. Fontenille, 2003: *Anopheles* species of the mount Cameroon region: biting habits, feeding behaviour and entomological inoculation rates. *Tropical Medicine and International Health*, **8**, 643–649.
- Warsame, M., H. Perlmann, S. Ali, H. Hagi, S. Farah, M. Lebbad, and A. Björkman, 1989: The seroreactivity against Pf155 (RESA) antigen in villagers from a mesoendemic area in Somalia. *Tropical Medicine and Parasitology*, **40**, 412–414.
- Washington, R., M. Harrison, D. Conway, E. Black, A. Challinor, D. Grimes, R. Jones, A. Morse, G. Kay, and M. Todd, 2006: African Climate Change: Taking the Shorter Route. *Bulletin of the American Meteorological Society*, **87**, 1355–1366.
- Washino, R. K. and B. L. Wood, 1994: Application of Remote Sensing to Arthropod Vector Surveillance and Control. *The American Journal of Tropical Medicine and Hygiene*, **50**, 134–144.
- Webster, P. J., A. M. Moore, J. P. Loschnigg, and R. R. Leben, 1999: Coupled ocean-atmosphere dynamics in the Indian Ocean during 1997–98. *Nature*, **401**, 356–360.
- Weidhaas, D. E., S. G. Breeland, C. S. Lofgren, D. A. Dame, and R. Kaiser, 1974: Release of Chemosterilized Males for the Control of *Anopheles Albimanus* in El Salvador. IV. Dynamics of the Test Population. *The American Society of Tropical Medicine and Hygiene*, **23**, 298–308.
- Wernsdorfer, W. H. and S. I. McGregor, 1988: *Malaria - Principles and Practice of Malariology*. Churchill Livingstone, Edinburgh, London, Melbourne, and New York, 1818 pp.
- WHO, 1997: World malaria situation in 1994. *Weekly epidemiological record*, **72**, 269–276.
- WHO, 2003: Climate change and human health - risks and responses. Summary. Report, WHO, 37 pp., Geneva, Switzerland.
- Wijesundera, M., 1988: Malaria outbreaks in new foci in Sri Lanka. *Parasitology Today*, **4**, 147–150.
- Wilcoxon, F., 1945: Individual comparisons by ranking methods. *Biometrics Bulletin*, **1**, 80–83.
- Wild, C. and G. Seber, 2000: *Chance Encounters: a First Course in Data Analysis and Inference*. John Wiley and Sons, New York, USA, 632 pp.
- Williams, K. D., A. Jones, D. L. Roberts, C. A. Senior, and M. J. Woodage, 2001: The response of the climate system to the indirect effects of anthropogenic aerosol. *Climate Dynamics*, **17**, 845–856.
- Wilson, D. B., 1956: *Atlas of Tanzania*. 3d ed., Government Printers, Dar es Salam, Tanzania, survey Division, Department of Lands and Surveys.
- Wizel, B. and N. Kumar, 1991: Identification of a continuous and cross-reacting epitope for *Plasmodium falciparum* transmission-blocking immunity. *Proceedings of the National Academy of Sciences USA*, **88**, 9533–9537.
- WMO, 1996: *Climatological Normals (CLINO) for the Period 1961–1990*. No. 847, WMO, Geneva, Switzerland, 768 pp.
- Worrall, E., A. Rietveld, and C. Delacollette, 2004: The Burden of Malaria Epidemics and Cost-Effectiveness of Interventions in Epidemic Situations in Africa. *The American Journal of Tropical Medicine and Hygiene*, **71** (Suppl. 2), 136–140.
- Wyrtki, K., 1973: An Equatorial Jet in the Indian Ocean. *Science*, **181**, 262–264.
- Zaim, M., A. H. Zahirmia, and A. V. Manouchehri, 1993: Survival rates of *Anopheles culicifacies* s.l. and *Anopheles pulcherrimus* in sprayed and unsprayed villages in Ghassreghand district, Baluchistan, Iran, 1991. *Journal of the American Mosquito Control Association*, **9**, 421–425.

Acknowledgements

This work would not have been completed without the help and support of many individuals. At this point I would like to express my thanks to all people that contributed to the present study.

First of all I wish to thank Prof. Dr. A. H. Fink for supervising this study. I'm thankful for his expertise and various ideas. He provided contacts for my stay abroad in Liverpool. A further thank is devoted to Prof. Dr. P. Speth, who was lining up the IMPETUS project and who had the initial idea of this study. I'm also grateful for the second reviewer Prof. Dr. M. K. Kerschgens.

I'm deeply grateful for the support of the third reviewer Dr. A. P. Morse and his colleague Dr. A. E. Jones. Without the collaboration with the University of Liverpool the study would not have been possible in the described way. Dr. A. P. Morse kindly provided the LMM and significantly contributed to the setting up of the present study. Dr. A. E. Jones introduced me into the application of the LMM. She modified the structure of the LMM for several times, which finally enabled the development of the new LMM version. Additionally, I like to thank Dr. A. P. Morse for his support in terms of my stay at the University of Liverpool.

A special thank goes to Prof. Dr. H. Paeth, who performed the REMO consortial runs at the German Climate Computing Centre (German: „Deutsches Klimarechenzentrum“) in Hamburg. He kindly provided precipitation, temperature, surface pressure, and orography data of REMO. Furthermore, he and Dipl.-Geogr. R. Girmes bias-corrected REMO precipitation data, which greatly improves the reliability of malaria projections. I'm also grateful to Dipl.-Met. K.-O. Heuer and Stud.-Geogr. V. Aich for their assistance in the analysis of REMO data.

I wish to thank Dr. M. Christoph and Dr. J. Verheyen, who contributed to the concept of the IMPETUS problem cluster Be-G.4. They likewise supported the preparation of my stay in Great Britain.

In addition, I'm grateful to numerous people who kindly provided useful data, literature references, or special knowledge. These are: Dipl.-Met. C. Baugirdis from DWD/Offenbach (synoptic station data for West Africa), Dr. A. Bomblies from the College of Engineering and Mathematical Sciences (CEMS)/University of Vermont (*Anopheles gambiae s.l.* larvae and female photos; malaria literature), Dr. M. Chen

from Climate Prediction Center (CPC)/Camp Springs (PREC/L data), Dr. M. Craig from the Medical Research Council/Durban (p_d literature), Prof. Dr. K. Dietz from the Department of Medical Biometry/Tübingen (Garki model), Dr. J.-B. Duchemin from the 'Centre de Recherche Médicale et Sanitaire (CERMES)'/Niamey (construction of the MalaRis logo and Fig. 5.1), Dr. C. Drakeley from the London School of Hygiene and Tropical Medicine (gametocytogenesis and c), Prof. Dr. M. Eichner from the Department of Medical Biometry/Tübingen (maturation of gametocytes), Dr. A. Niang Fall from the 'Ecole doctorale Eau, Qualité, Usage de l'Eau'/Dakar (daily rainfall data for Senegal; monthly precipitation values for West Africa), Dr. C. Favier from the 'Laboratoire d'Océanographie et du Climat: Expérimentations et Approches Numériques (LOCEAN)'/Paris (p_d discussion), Dr. C. Guerra from the Malaria Atlas Project (PR information), Dr. A. Kiszewski from the Department of Immunology and Infectious Diseases/Harvard University (p_d data and $p_{d\downarrow}$ discussion), Dr. S. Louvet from the 'Centre de Recherches de Climatologie (CRC)'/Dijon (malaria literature), Prof. Dr. T. A. Smith from the Swiss Tropical Institute/Zürich (Garki model), Prof. Dr. R. Steffen and M. Funk-Baumann from the Institute of Social and Preventive Medicine/Zürich (references), S. Stephens and N. Lott as well as Dr. R. S. Vose from US National Climatic Data Center (GSOD precipitation and GHCN data, respectively).

Furthermore, I like to thank the staff of the Institute of Geophysics and Meteorology; the collegueship provided a pleasant working atmosphere. Fruitful discussions and the existing knowledge helped to overcome various difficulties. A special thank goes to these colleagues: Dr. T. Brücher (amongst others: provision and processing of ECMWF data), Dr. K. Born (data analysis), Dipl.-Geogr. R. Hoffmann (data processing; construction of MalaRis), Dr. A. Krueger (discussions), Stud.-Met. R. Haas (Generic Mapping Tool), Dr. J. Pinto (statistical significance), as well as a team (Dipl.-Met. L. Kirchhübel, Dipl.-Met. S. Kotthaus, Dipl.-Met. S. Pohle, Stud.-Met. R. Schuster) that prepared and supervised the provision of synoptic station data from 2006 for Benin.

I also like to thank Dr. C. Bain, Dipl.-Psych. S. Dutson, Dr. A. E. Jones, Dipl.-Biol. K. Kreppel, Dipl.-Chem. V. Laumann, and Dr. J. Schrage for their tireless proof-reading of parts of the manuscript.

This study was part of the IMPETUS West-Africa project and was supported by the Federal German Ministry of Education and Research (BMBF) under grant No. 01 LW 06001A in the GLOWA programme and by the Ministry of Innovation, Science, Research and Technology (MIWFT) of the federal state of North Rhine-Westphalia under grant No. 313-21200200.

Finally, a special thank is devoted to my parents who supported me for my whole life. Last but not least I would like to thank all my friends for their great support.

Erklärung

Ich versichere, dass ich die von mir vorgelegte Dissertation selbstständig angefertigt, die benutzten Quellen und Hilfsmittel vollständig angegeben und die Stellen der Arbeit - einschließlich Tabellen, Karten und Abbildungen -, die anderen Werken im Wortlaut oder dem Sinn nach entnommen sind, in jedem Einzelfall als Entlehnung kenntlich gemacht habe; dass diese Dissertation noch keiner anderen Fakultät oder Universität zur Prüfung vorgelegen hat; dass sie noch nicht teilweise bzw. ganz veröffentlicht worden ist sowie, dass ich eine solche Veröffentlichung vor Abschluss des Promotionsverfahrens nicht vornehmen werde. Die Bestimmungen dieser Promotionsordnung sind mir bekannt. Die von mir vorgelegte Dissertation ist von Prof. Dr. A. H. Fink betreut worden.

Köln, 20. Mai 2010

(Volker Ermert)

Lebenslauf

Persönliche Angaben

Name:	Volker Ermert
Anschrift:	Luxemburger Str. 83 50674 Köln
Geburtstag:	12.11.1976
Geburtsort:	Kirchen/Sieg
Familienstand:	ledig
Staatsangehörigkeit:	deutsch

Schulbildung

08/1983-07/1987	Martin-Luther-Grundschule in Betzdorf
09/1987-06/1993	Bertha-von-Suttner-Realschule in Betzdorf Abschluss: Mittlere Reife
08/1993-06/1996	Freiherr-vom-Stein-Gymnasium in Betzdorf Abschluss: Abitur

Grundwehrdienst

07/1996-04/1997	Wehrdienst in der Heeresfliegerbrigade 3 der Gunter-Plüschow-Kaserne in Mendig
-----------------	---

Studium

04/1997-09/2004	Studium der Meteorologie an der Universität zu Köln Abschluss: Diplom-Meteorologe
seit 12/2005	Promotionsstudium in Meteorologie an der Mathe- matisch-Naturwissenschaftlichen Fakultät der Universität zu Köln

Berufliche Tätigkeiten

01/2000-09/2004	Studentische Hilfskraft am Institut für Geophysik und Meteorologie der Universität zu Köln
seit 10/2004	Wissenschaftlicher Angestellter am Institut für Geophysik und Meteorologie der Universität zu Köln